frontiers | Research Topics

Fungal secondary metabolites as valuable chemical entities for medicines and agrochemicals

Edited by
Peng Zhang, Weiyi Wang and Siti Aisyah Alias

Published in
Frontiers in Microbiology

ISSN 1664-8714
ISBN 978-2-83251-709-3
DOI 10.3389/978-2-83251-709-3

About Frontiers

Frontiers is more than just an open access publisher of scholarly articles: it is a pioneering approach to the world of academia, radically improving the way scholarly research is managed. The grand vision of Frontiers is a world where all people have an equal opportunity to seek, share and generate knowledge. Frontiers provides immediate and permanent online open access to all its publications, but this alone is not enough to realize our grand goals.

Frontiers journal series

The Frontiers journal series is a multi-tier and interdisciplinary set of open-access, online journals, promising a paradigm shift from the current review, selection and dissemination processes in academic publishing. All Frontiers journals are driven by researchers for researchers; therefore, they constitute a service to the scholarly community. At the same time, the *Frontiers journal series* operates on a revolutionary invention, the tiered publishing system, initially addressing specific communities of scholars, and gradually climbing up to broader public understanding, thus serving the interests of the lay society, too.

Dedication to quality

Each Frontiers article is a landmark of the highest quality, thanks to genuinely collaborative interactions between authors and review editors, who include some of the world's best academicians. Research must be certified by peers before entering a stream of knowledge that may eventually reach the public - and shape society; therefore, Frontiers only applies the most rigorous and unbiased reviews. Frontiers revolutionizes research publishing by freely delivering the most outstanding research, evaluated with no bias from both the academic and social point of view. By applying the most advanced information technologies, Frontiers is catapulting scholarly publishing into a new generation.

What are Frontiers Research Topics?

Frontiers Research Topics are very popular trademarks of the *Frontiers journals series*: they are collections of at least ten articles, all centered on a particular subject. With their unique mix of varied contributions from Original Research to Review Articles, Frontiers Research Topics unify the most influential researchers, the latest key findings and historical advances in a hot research area.

Find out more on how to host your own Frontiers Research Topic or contribute to one as an author by contacting the Frontiers editorial office: frontiersin.org/about/contact

Fungal secondary metabolites as valuable chemical entities for medicines and agrochemicals

Topic editors

Peng Zhang — Tobacco Research Institute, Chinese Academy of Agricultural Sciences, China

Weiyi Wang — Third Institute of Oceanography, State Oceanic Administration, China

Siti Aisyah Alias — University of Malaya, Malaysia

Topic coordinators

Tingting Wang — Ningbo University, China

Jiao Xiao — Shenyang Pharmaceutical University, China

Citation

Zhang, P., Wang, W., Alias, S. A., eds. (2023). *Fungal secondary metabolites as valuable chemical entities for medicines and agrochemicals*.

Lausanne: Frontiers Media SA. doi: 10.3389/978-2-83251-709-3

Table of contents

frontiers | Frontiers in Microbiology

TYPE Editorial
PUBLISHED 06 February 2023
DOI 10.3389/fmicb.2023.1150023

OPEN ACCESS

EDITED AND REVIEWED BY
Rustam Aminov,
University of Aberdeen, United Kingdom

*CORRESPONDENCE
Weiyi Wang
✉ wywang@tio.org.cn
Ting-Ting Wang
✉ wangtingting1@nbu.edu.cn

SPECIALTY SECTION
This article was submitted to Antimicrobials, Resistance and Chemotherapy, a section of the journal Frontiers in Microbiology

RECEIVED 23 January 2023
ACCEPTED 24 January 2023
PUBLISHED 06 February 2023

CITATION
Wang W and Wang T-T (2023) Editorial: Fungal secondary metabolites as valuable chemical entities for medicines and agrochemicals. *Front. Microbiol.* 14:1150023. doi: 10.3389/fmicb.2023.1150023

Editorial: Fungal secondary metabolites as valuable chemical entities for medicines and agrochemicals

Weiyi Wang[1]* and Ting-Ting Wang[2]*

[1]Key Laboratory of Marine Biogenetic Resources, Third Institute of Oceanography, Ministry of Natural Resources, Xiamen, China, [2]Li Dak Sum Marine Biopharmaceutical Research Center, Department of Marine Pharmacy, College of Food and Pharmaceutical Sciences, Ningbo University, Ningbo, China

KEYWORDS

fungal secondary metabolites, biological activities, chemodiversity, polyketides, alkaloids

Editorial on the Research Topic
Fungal secondary metabolites as valuable chemical entities for medicines and agrochemicals

Natural products, metabolites derived from animals, plants, and microorganisms have a long history as sources of medical and agricultural chemicals. Fungi are a rich source of bioactive natural products. They produce large amounts of compounds with very diverse structural types, such as polyketides, alkaloids, terpenes, and peptides. These metabolites were proven to possess various biological activities, such as antibacterial, antiviral, antitumor, anti-inflammatory, and antiparasitic activities. Some chemicals have already been developed into medicines or pesticides. Examples include penicillin (a β-lactam antibiotic) and lovastatin (a cholesterol-lowering drug). However, the emergence and development of drug resistance in the fields of medicine and agriculture makes it necessary to constantly search for molecules with new mechanisms of action or better activities.

This Research Topic aims to present research progresses and review papers focusing on novel fungal secondary metabolites with high medical and/or agricultural potentials. In this Research Topic, 11 papers have been published: three review papers and eight original research articles.

Some review papers have already discussed secondary metabolites from certain genera of fungi, such as cytotoxic metabolites from *Penicillium* (Koul and Singh, 2017) and bioactive metabolites from marine *Aspergillus* (Wang and Ding, 2018). In this Research Topic, two review papers summarized the secondary metabolites of the *Talaromyces* and the *Alternaria* species. Lei et al. reviewed the chemical constituents of the genus *Talaromyces,* which yield diverse secondary metabolites with various biological activities. Zhao et al. reviewed the products of the genus *Alternaria* focusing mainly on their structural features, various bioactivities, and possible biosynthetic pathways.

In addition to focusing on different genera of fungi, some review articles focused on certain types of metabolites. Diterpenes from marine-derived fungi (Qiu et al., 2022) and alkaloids from endophytic fungi (Daley and Cordell, 2021) are two examples. Chen et al. reviewed the chemodiversity and bioactivities of halometabolites from marine-derived fungi. It was discovered that many brominated and iodinated compounds were generated by the substitution of bromide and iodide ions for the chloride ion during the cultivation process. This confirms the importance of culture conditions on the final products of fungi.

In this Research Topic, we also included some articles reporting the isolation, structure elucidation, and bioactivity evaluation of metabolites derived from different fungi. Three papers were about *Penicillium* strains and two papers were about the genus of *Aspergillus* and *Trichoderma*, respectively. There were reports on different types of metabolites, such as polyketides and alkaloids, with various bioactivities, namely cytotoxic, antimicrobial, anti-inflammatory, and anti-pulmonary fibrosis activities.

Weng et al. found ten metabolites from *Penicillium oxalicum* 2021CDF-3, an endophyte of the marine red algae. The new polyketide oxalihexane A showed a remarkable inhibitory effect on the human pancreatic cancer PATU8988T cell line. The treatment with oxalihexane A down-regulated the expression level of Cyclin D1. Shi et al. isolated seven spirooxindole alkaloids from a terrestrial strain of *Penicillium brefeldianum* and evaluated their antimicrobial activities toward several pathogenic strains. The compound 12α-hydroxyverruculogen TR-2 displayed moderate inhibitory activity toward the dimorphic switch of pathogenic smut fungi *Sporisorium scitamineum*. Weng et al. obtained eight compounds from *Penicillium* sp. YT2019-3321, an endophytic fungus of Lonicera japonica. A new polyketide, penicidone E, showed cytotoxicity against the human pancreatic tumor cells PATU8988T. Xu et al. obtained four indole alkaloids and four polyketides from the deep-sea-derived fungus *Aspergillus flavipes* DS720. The compound flavonoid A showed broad-spectrum cytotoxicities against HeLa, 5637, CAL-62, PATU8988T, A-375, and A-673 cell lines. Hao et al. isolated 25 compounds from the deep-sea fungus *Trichoderma* sp. MCCC 3A01244. The newly identified β-carboline alkaloid trichocarboline A was found to decrease pulmonary fibrosis by inhibiting the TGF-β/Smad signaling pathway.

Although more and more secondary metabolites were obtained from fungi, the exploitation of their biosynthetic potential is far from sufficient. It is believed that by changing the cultivation conditions and growth media composition we can trigger the secondary metabolic pathways. In this Research Topic, Sequeira et al. tried to activate the production of fungal secondary metabolites by supplementing cholinium-based ionic liquids to the growth media of *Neurospora crassa*, *Aspergillus nidulans*, and *Aspergillus fumigatus*. Both the diversity of metabolites and the levels of certain compounds were increased. Also, the change in bioactivities of the organic extracts was observed. Their work proved that the altering of media components can lead to the changing of fungal products.

In addition to newly discovered compounds, the activity evaluation using different cell lines or models also contributes to the development of leads and drugs, as does the further study of activity mechanisms of the "old" compounds. This Research Topic included two articles reporting the activity evaluation of certain compounds from the genus *Trichoderma*. Huo et al. evaluated the anti-inflammatory activity of trichodimerol, which was first isolated from *Trichoderma longibraciatum*. Trichodimerol was found to reduce the production of NO, ROS, interleukin (IL)-6, and the tumor necrosis factor (TNF)-α. It could also inhibit the production of some inflammatory mediators as well as the expression of some proteins. It was thus concluded that trichodimerol may inhibit inflammation through the NF-κB and NLRP3 pathways. Zhang et al. evaluated the antibacterial effects of TKA, peptaibols produced by *Trichoderma longibrachiatum* SMF2, against the pathogen *Xanthomonas oryzae* pv. *oryzae* (*Xoo*). They found that TKA could significantly inhibit the growth of *Xoo*. The lesion length on the rice leaf was significantly reduced when treated with TKA. Mechanism analyses revealed that TKA treatments resulted in the damage of *Xoo* cell morphology and the release of intracellular substances.

It is expected that this Research Topic will promote interest in the research of agricultural and medical active metabolites derived from fungi.

Author contributions

WW wrote the manuscript. T-TW revised the manuscript. The final draft of the manuscript was finalized and approved for publication by all authors.

Acknowledgments

We thank the Frontiers editorial staff for assistance in putting together this Research Topic collection.

Conflict of interest

The authors declare that the research was conducted in the absence of any commercial or financial relationships that could be construed as a potential conflict of interest.

Publisher's note

References

Daley, S., and Cordell, G. A. (2021). Biologically significant and recently isolated alkaloids from endophytic fungi. *J. Nat. Prod.* 84, 871–897. doi: 10.1021/acs.jnatprod.0c01195

Koul, M., and Singh, S. (2017). Penicillium spp.: prolific producer for harnessing cytotoxic secondary metabolites. *Antican. Drugs.* 28, 11–30. doi: 10.1097/cad.0000000000000423

Qiu, P., Xia, J., Zhang, H., Lin, D., and Shao, Z. (2022). A review of diterpenes from marine-derived fungi: 2009–2021. *Molecules.* 27, 8303. doi: 10.3390/molecules27238303

Wang, K. W., and Ding, P. (2018). New bioactive metabolites from the marine-derived fungi aspergillus. *Mini-Rev. Med. Chem.* 18, 1072–1094. doi: 10.2174/1389557518666180305160856

frontiers | Frontiers in Microbiology

TYPE Original Research
PUBLISHED 22 July 2022
DOI 10.3389/fmicb.2022.959754

OPEN ACCESS

EDITED BY
Peng Zhang,
Tobacco Research Institute (CAAS), China

REVIEWED BY
Sherif S. Ebada,
Ain Shams University, Egypt
Weaam Ebrahim,
Mansoura University, Egypt

*CORRESPONDENCE
De-Yuan Fu
fdy1003@163.com

†These authors have contributed equally to this work

SPECIALTY SECTION
This article was submitted to Antimicrobials, Resistance and Chemotherapy, a section of the journal Frontiers in Microbiology

RECEIVED 02 June 2022
ACCEPTED 30 June 2022
PUBLISHED 22 July 2022

CITATION
Xu A, Xu X-N, Zhang M, Li C-L, Liu L and Fu D-Y (2022) Cytotoxic indole alkaloids and polyketides produced by a marine-derived fungus *Aspergillus flavipes* DS720. *Front. Microbiol.* 13:959754. doi: 10.3389/fmicb.2022.959754

Cytotoxic indole alkaloids and polyketides produced by a marine-derived fungus *Aspergillus flavipes* DS720

An Xu[1†], Xiang-Nan Xu[2†], Mi Zhang[3], Chun-Lian Li[2], Li Liu[4] and De-Yuan Fu[2*]

[1]Clinical Medical College, Yangzhou University, Yangzhou, China, [2]Department of Thyroid and Breast Surgery, Northern Jiangsu People's Hospital, Yangzhou, China, [3]The School of Basic Medical Sciences, Fujian Medical University, Fuzhou, China, [4]Department of General Surgery, Suqian First People's Hospital, Suqian, China

Marine-derived microorganisms possess the unique metabolic pathways to produce structurally novel secondary metabolites with potent biological activities. In this study, bioactivity-guided isolation of the marine deep-sea-derived fungus *Aspergillus flavipes* DS720 led to the characterization of four indole alkaloids (compounds **1**–**4**) and four polyketides (compounds **5**–**8**), such as two new indoles, flavonoids A (**1**) and B (**2**) with a C-6 reversed prenylation, and a new azaphilone, flaviazaphilone A (**5**). Their chemical structures were unambiguously established by an extensive interpretation of spectroscopic data, such as 1D/2D NMR and HRESIMS data. The absolute configurations of the new compound **5** were solved by comparing the experimental and calculated Electronic Circular Dichroism (ECD) spectra. Since sufficient amount of flavonoids A (**1**) was obtained, **1** was subjected to a large-scale cytotoxic activity screening against 20 different human tumor cell lines. The results revealed that **1** showed broad-spectrum cytotoxicities against HeLa, 5637, CAL-62, PATU8988T, A-375, and A-673 cell lines, with the inhibition rates of more than 90%. This study indicated that the newly discovered indole alkaloid **1** may possess certain potential for the development of lead compounds in the future.

KEYWORDS

indole alkaloids, polyketides, marine fungus, *Aspergillus flavipes*, cytotoxic activity

Introduction

Marine-derived microorganisms are widely distributed in the marine ecosystem. Marine microorganisms are subjected to various extreme environmental stresses, and therefore, they have evolved unique metabolic pathways to synthesize structurally novel secondary metabolites with potent biological activities (Jiang et al., 2020). Marine microorganisms are one of the most notable and prolific sources of bioactive natural products (Carroll et al., 2021). Although a large number of natural products have been discovered from marine microorganisms (Rateb and Ebel, 2011; Zhang et al., 2020), it is a matter of fact that, the trend toward finding new natural products is

approaching saturation due to the redundancy of the isolation and characterization of microorganisms. Therefore, the discovery of new compounds from unexplored environments has proven to be an alternative strategy to search for microbial novelty. Extremophiles, which were isolated from the deep-sea, hydrothermal vents, cold water, and polar region, are largely unexplored (Soldatou and Baker, 2017). These microorganisms are extraordinarily adapted and metabolically active under extreme environmental conditions, which promote them to produce abundant novel secondary metabolites (Obulisamy and Mehariya, 2021).

Marine-derived fungi belonging to the genus *Aspergillus* have been widely studied for their biosynthetic potential for generating bioactive secondary metabolites, such as diverse polyketides (macrolides, phenols, quinines, and lactones), heterocyclic alkaloids, terpenoids, steroids, and other miscellaneous compounds (Xu et al., 2020). In our ongoing research on bioactive secondary metabolites from the deep-sea-derived fungi, an *Aspergillus flavipes* DS720 (Figure 1) was isolated from a deep seawater sample, which was collected from the Mariana Trench at a depth of 2,000 m. Preliminary cytotoxic screening indicated that the extracts of this fungal strain possessed considerable inhibitory effects on various human tumor cell lines. Especially, the extracts showed strong activities against HeLa, PATU8988T, A-375, and A-673 cell lines at the concentration of 40 mg/ml, with inhibition rates of 75, 82, 83, and 86%, respectively. Based on prescreening results, a large fermentation was performed. Subsequent chromatographic purification of the ethyl acetate extracts yielded eight compounds, such as four indole alkaloids (compounds **1**–**4**) and four polyketides (compounds **5**–**8**) (Figure 2). Among them, flavonoids A (**1**) and B (**2**) with a C-6 reversed prenylation, and an azaphilone, flavia azaphilone A (**5**), are new compounds. Since a sufficient amount of flavonoids A (**1**) was obtained (45 mg/20 g, pure compound/crude extract), a large-scale cytotoxic activity screening of **1** against 20 different human tumor cell lines was performed. Interestingly, **1** showed broad-spectrum cytotoxicities against HeLa, 5637, CAL-62, PATU8988T, A-375, and A-673 cell lines, with the inhibition rates of more than 90%. In this study, the isolation, structural elucidation, and cytotoxic activities of the new compound **1** are discussed herein.

Materials and methods

General

Specific rotation values were recorded on a JASCO P-1020 digital polarimeter (Tokyo, Japan). UV spectra were obtained with a Lambda 35 UV/Vis spectrophotometer (Perkin Elmer, Waltham, United States). Scientific LTQ Orbitrap XL spectrometer (Thermo Scientific, Waltham) was applied to measure the mass spectra of the new compounds. The 1D and 2D NMR spectra were measured with an Agilent DD2 spectrometer (Agilent Technologies, Santa Clara, United States, 500 MHz for ^{1}H and 125 MHz for ^{13}C). Chemical shifts (δ) were referenced to DMSO-d_6 at 2.50 for ^{1}H and 39.5 for ^{13}C. Open column chromatography (CC) was performed by silica gel (200–300 mesh, Qingdao Marine Chemical Factory, Qingdao, China), octadecylsilyl (ODS) reversed-phase gel (30–50 μm, YMC CO., LTD., Japan), and Sephadex LH-20 (GE Healthcare, United States). All solvents used were of either analytical grade or filtered prior to use.

Fungal material

The fungal strain DS720 used in this study was isolated from a deep seawater sample, which was collected from the Mariana Trench at a depth of 2,000 m (N 11°21.738′, E 142°29.307′). This fungus was preliminarily identified as *Aspergillus flavipes* by a standard molecular biological protocol. The sequence analysis of the internal transcribed spacer (ITS) region of the rDNA shared a 99% match to *A. flavipes* NRRL 5175 (Accession No. EF661428) in the BLASTn search. Then, sequences of the ITS (GenBank Accession No. ON340751) and β-tubulin genes from *Aspergillus* species were aligned by MEGA version 6.0 and manually improved when necessary. Subsequently, the phylogenetic tree of the combined dataset was made on the basis of maximum-likelihood (ML) analysis with MEGA version 6.0 with 1,000-generation bootstrap values, for which a value $\geq$ 50% was considered significantly (Figure 1). A voucher strain of this fungus was deposited at School of Life Sciences, Nanjing University.

Cultivation and extraction

The cultivation of the fungal strain DS720 was performed in 1 L Erlenmeyer flasks containing commercially available PDB medium (potato dextrose broth, Solarbio Life Sciences CO., LTD., Beijing, China). The mycelium from each culture plate was inoculated in a 500 ml Erlenmeyer flask, which was filled with 200 ml of PDB medium supplemented with 3% sea salt. Then, the flask culture was subjected to a rotary shaker at 200 rpm as seed cultures. Following cultivation for 5 days, the seed cultures were transferred into autoclaved 1 L Erlenmeyer flasks with PDB medium. The fermentation process was carried out under static conditions and daylight for 30 days. After the fermentation, the cultures (~30 L) were filtered to separate the broth and mycelia layer. The broth was extracted adequately with EtOAc for three times, while the mycelia were crushed and extracted with EtOAc. The combined EtOAc extracts were evaporated under reduced pressure to yield 20 g of a crude gum.

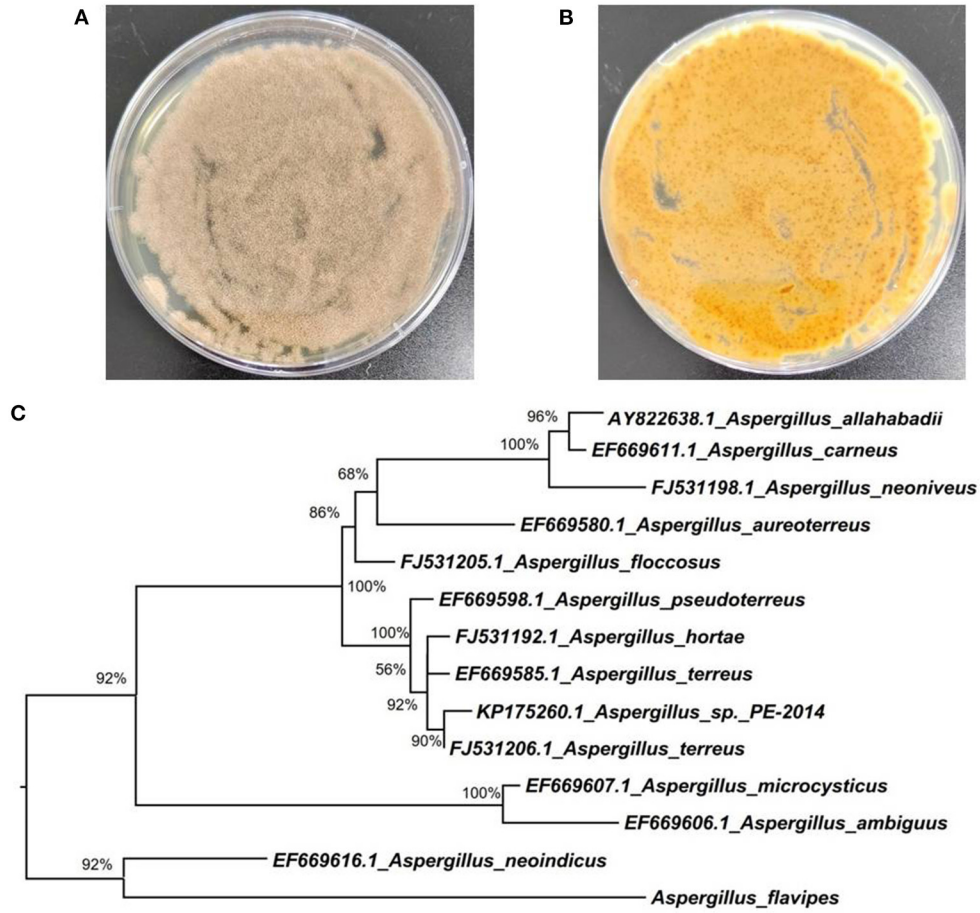

FIGURE 1
Morphology of *Aspergillus flavipes* DS720 cultured on PDA medium [**(A)**, front view; **(B)** reverse view]; **(C)** Neighbor-joining tree based on ITS and β-tubulin sequences.

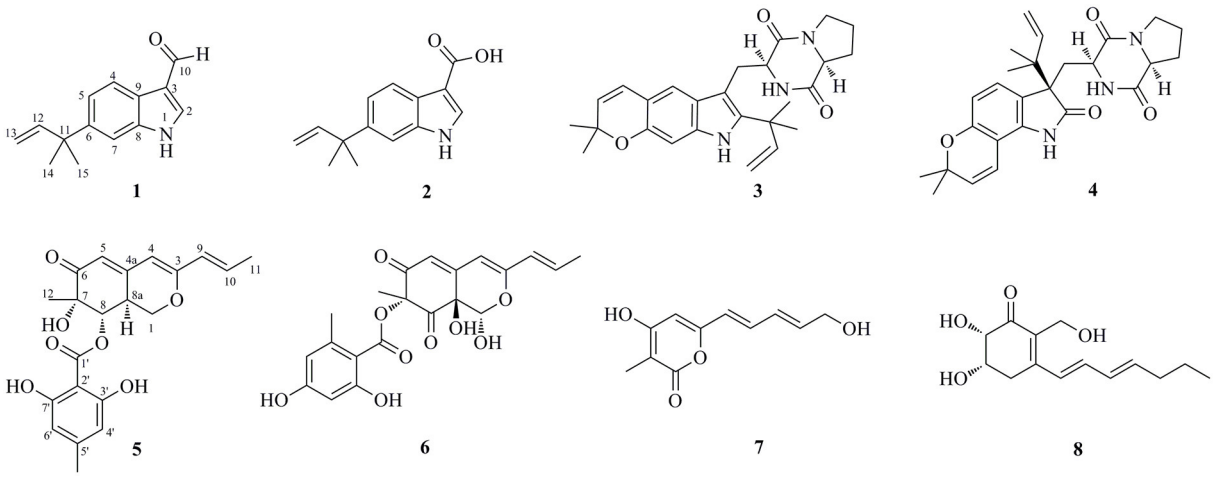

FIGURE 2
Chemical structures of the isolated compounds **1**–**8**.

Isolation and purification

The obtained crude gum was subjected to open silica gel CC with a stepwise mixed CH_2Cl_2/MeOH solvent system with the ratios of 100:1, 50:1, 25:1, 10:1, 5:1, and 1:1 (v/v) to yield six fractions (Fr.1–6). Fr.2, eluted with CH_2Cl_2/MeOH 50:1, was fractionated by ODS reversed-phase gel column with a stepwise solvent system of MeOH/H_2O (from 20 to 90%) to give subfractions Fr.2.1–2.6. The Fr.2.2 was purified by semi-preparative HPLC eluting with 50% MeOH–H_2O to obtain compound **3** (t_R 12.6 min; 2.1 mg), while Fr.2.4 was applied to a Sephadex LH-20 (MeOH) to give compound **4** (1.8 mg). Fr.3, eluted with CH_2Cl_2/MeOH 25:1, was afforded to silica gel CC (CH_2Cl_2/MeOH, from 30:1 to 5:1) to give two subfractions, Fr.3.1 and Fr.3.2. Compound **1** (t_R 16.0 min; 45 mg) was isolated from Fr.3.1 as the main ingredient components by semi-preparative HPLC (60% MeOH–H_2O). Purification of Fr.3.2 by semi-preparative HPLC using 55% MeOH–H_2O obtained compound **2** (t_R 10.5 min; 3.2 mg). Fr.4 (eluted with CH_2Cl_2/MeOH 10:1) and Fr.5 (eluted with CH_2Cl_2/MeOH 5:1) were combined and then fractionated with silica gel CC (CH_2Cl_2/MeOH, from 20:1 to 1:1) to obtain three subfractions Fr.4.1–4.3. Compound **7** (2.6 mg) was isolated from Fr.4.1 by preparative TLC (pTLC) eluting with MeOH/H_2O 20:1, whereas compound **8** (2.0 mg) was obtained from Fr.4.2 by pTLC eluting with CH_2Cl_2/MeOH/acetic acid 20:1:0.5. Fr.4.3 was subjected to semi-preparative HPLC (55% MeOH–H_2O) to give compounds **5** (t_R 10.0 min; 1.9 mg) and **6** (t_R 15.2 min; 1.2 mg).

Flavonoid A [**1**, 6-(2-methylbut-3-en-2-yl)-1*H*-indole-3-carbaldehyde]: colorless oil; UV (MeOH) λ_{max} (log ε) 204 (4.28), 229 (4.24), 292 (3.54) nm; ^{1}H and ^{13}C NMR data, see Table 1; HRESIMS *m/z* 214.1223 $[M + H]^+$ (calcd for $C_{14}H_{16}NO$, 214.1226); *m/z* 236.1044 $[M + Na]^+$ (calcd for $C_{14}H_{15}NONa$, 236.1046).

Flavonoid B [**2**, 6-(2-methylbut-3-en-2-yl)-1*H*-indole-3-carboxylic acid]: colorless oil; UV (MeOH) λ_{max} (log ε) 203 (4.32), 231 (4.22), 296 (3.49) nm; ^{1}H and ^{13}C NMR data, see Table 1; HRESIMS *m/z* 230.1179 $[M + H]^+$ (calcd for $C_{14}H_{16}NO_2$, 230.1176).

Flaviazaphilone A [**5**, (7*S*,8*S*,8a*S*)-7-hydroxy-7-methyl-6-oxo-3-((*E*)-prop-1-en-1-yl)-6,7,8,8a-tetrahydro-1*H*-isochromen-8-yl 2,6-dihydroxy-4-methylbenzoate]: colorless oil; $[\alpha]_D^{20}$ + 72.5 (*c* 0.05, MeOH); UV (MeOH) λ_{max} (log ε) 211 (4.36), 268 (3.96), 317 (3.85), 340 (3.84) nm; ^{1}H and ^{13}C NMR data, see Table 2; HRESIMS *m/z* 387.1433 $[M + H]^+$ (calcd for $C_{21}H_{23}O_7$, 387.1438).

Computational section

The conformer rotamer ensemble sampling tool (crest) was utilized to generate candidate conformers and DFT calculations were performed using the Gaussian 16 program (Frisch et al., 2016). The conformers within an energy window of 10 kcal/mol were optimized at B3LYP/6-31G(d) level of theory with Grimme's D3 dispersion correction ("EmpiricalDispersion = GD3" key words in input files). Frequency analysis of all optimized conformations was undertaken at the same level of theory to ensure they were true local minima on the potential energy surface. Then, energies of all optimized conformations were evaluated by M062X/6-311+G(2d,p) with D3 dispersion correction. Gibbs free energies of each conformer were calculated by adding "Thermal correction to Gibbs Free Energy" obtained by frequency analysis to electronic energies obtained at M062X/6-311+G(2d,p). Room-temperature (298.15 K) equilibrium populations were calculated according to the Boltzmann distribution law. Those conformers accounting for over 2% population were subjected to subsequent calculations. Time-dependent density-functional theory (TDDFT) ECD calculations were run at Cam-B3LYP/TZVP level of theory in MeOH with IEFPCM solvent model, respectively. For each conformer, 30 excited states were calculated. The calculated ECD curves were generated using Multiwfn 3.6 software.

Cytotoxic assay

Cytotoxic activities of the crude exacts and the new compound **1** against 20 different human tumor cells (human lung cancer cells A549, human breast cancer cells MCF7, human gastric carcinoma cells MKN-45, human colon cancer cells HCT 116, human hepatoma cell lines HepG2, human cervical carcinoma cells HeLa, human chronic myelogenous leukemia cells K-562, human brain tumor stem cells SF126, human ovarian teratoma cells PA-1, human renal clear cell adenocarcinoma cells 786-O, human esophageal cancer cells TE-1, human bladder cancer cells 5,637, human prostatic cancer cells DU 145, human thyroid cancer cells CAL-62, human pancreatic cancer cells PATU8988T, human osteosarcoma cells HOS, human malignant melanoma cells A-375, human rhabdomyosarcoma cells A-673, human pharyngeal squamous cells FaDu, and human gallbladder carcinoma cells GBC-SD) were evaluated by the CCK-8 method (Chen et al., 2021). The tested cells were treated with 40 mg/ml of compound samples. A total of 10 μl of 5 g/L CCK-8 solutions were added to each well at 48 h. The cell lines were then incubated at 37°C for 1.5 h. Absorbance data were obtained with a microplate spectrophotometer reader at 490 nm. Commercial doxorubicin was used as the positive control.

Statistical analysis

The data were statistically analyzed using SPSS software (Version 18.0, Chicago, IL, USA) and were expressed as the means ± *SD*.

TABLE 1 ^{1}H NMR (500 MHz, δ in ppm) and ^{13}C NMR Data (125 MHz, δ in ppm) for 1 and 2 (measured in DMSO-d_6).

Postion	Compound 1		Compound 2	
	δ_H (*J* in Hz)	δ_C, type	δ_H (*J* in Hz)	δ_C, type
1-NH	11.25, br s	–	10.84, br s	–
2	8.17, s	138.1, CH	7.83, d (2.1)	131.6, CH
3		117.8, C		107.5, C
4	7.18, d (8.5)	120.5, CH	7.09, s	119.4, CH
5	8.05, dd (8.5, 1.8)	119.5, CH	7.96, dd (8.4, 1.9)	119.1, CH
6		132.1, C		131.7, C
7	7.18, br s (overlapped)	122.2, CH	7.10, s	120.9, CH
8		134.2, C		133.5, C
9		125.2, C		127.1, C
10	9.95, s	185.0, CH		166.1, C
11		40.2, C		40.2, C
12	6.15, dd (17.5, 10.6)	146.3, CH	6.12, dd (17.5, 10.6)	146.4, CH
13	5.08, d (10.6) 4.98, d (17.5)	112.4, CH_2	5.07, d (10.6) 5.00, d (17.5)	112.2, CH_2
14	1.50, s	27.5, CH_3	1.48, s	27.4, CH_3
15	1.50, s	27.5, CH_3	1.48, s	27.4, CH_3

Results and discussion

Structural elucidation of the new compounds

Flavonoid A (**1**) was obtained as colorless oil. The molecular formula of **1** was deduced as $C_{14}H_{15}NO$ by the observation of $[M + H]^+$ and $[M + Na]^+$ ion peaks in the HRESIMS spectrum at *m/z* 214.1223 and 236.1044, respectively. The ^{1}H NMR spectroscopic data (Table 1) exhibited the presence of one isolated NH signal at δ_H 11.25 (1H, br s, 1-NH), two overlapped methyl groups at δ_H 1.50 (6H, s, H_3-14, and H_3-15), a set of terminal methylene signal at δ_H 5.08 (1H, d, J = 10.6 Hz, H-13α) and 4.98 (1H, d, J = 17.5 Hz, H-13β), six methines such as three aromatic at δ_H 7.18 (1H, d, J = 8.5 Hz, H-4), 8.05 (1H, dd, J = 8.5, 1.8 Hz, H-5), and 7.18 (1H, br s, H-7), two olefinic at δ_H 8.17 (1H, s, H-2) and 6.15 (1H, dd, J = 17.5, 10.6 Hz, H-12), and one aldehyde group at δ_H 9.95 (1H, s, H-10). The ^{13}C NMR combined with DEPT spectra revealed 14 carbon signals, which were classified into one aldehyde carbon at δ_C 185.0 (C-10), one terminal methylene group at δ_C 112.4 (C-13), five aromatic/olefinic methines, five quaternary carbons, and two methyl groups. Eight characteristic aromatic/olefinic carbons (C-2–C-9) along with the NH signal (1-NH) hinted at the presence of an indole moiety containing a 1,2,5-trisubstituted benzene ring. The key eteronuclear Multiple-Bond Correlation (HMBC) correlations from H_2-13 to C-11 and C-12, from H-12 to C-6, and from H_3-14 to C-12 revealed a *trans*-isopentene group. The definite HMBC correlations from the two *gem*-methyl groups of the isopentene (H_3-14 and H_3-15) to C-6 as well as correlations from H-5 and H-7 to C-11 indicated that the prenylation was occurred at C-6 of the benzene (Figure 3). Moreover, the aldehyde group was attached to C-3 as evidenced from the HMBC correlation from H-2 to C-10 (Figure 3). Accordingly, the structure of compound **1** was established.

Flavonoid B (**2**) was also obtained as colorless oil and its molecular formula was determined by HRESIMS data. The HRESIMS spectrum of **2** showed a prominent pseudomolecular ion peak at *m/z* 230.1179 $[M + H]^+$, which was attributed to the molecular formula of $C_{14}H_{15}NO_2$. With compound **1** in hand, the structural elucidation of **2** was straightforward. Investigation of the 1D NMR data (Table 1) confirmed that **2** possessed high structural similarity with **1**. Compared with the ^{1}H and ^{13}C NMR data of **1**, the main difference was that **2** had an additional ester carbonyl at δ_C 166.1 (C-10), rather than the aldehyde group in **1**. In addition, the chemical shifts at C-2 (δ_C 131.6) and C-3 (δ_C 107.5) in **2** were changed significantly. The ester carbonyl group was deduced to be located at C-2 based on the HMBC correlation from H-2 to C-10 (Figure 3). With the aid of detailed analysis of 1D and 2D NMR data, compound **2** was characterized as a new indole with a C-6 reversed prenylation.

Flaviazaphilone A (**5**) was isolated as colorless oil. The HRESIMS of **5** gave a molecular formula of $C_{21}H_{22}O_7$ (*m/z* 387.1433 $[M + H]^+$, calcd for $C_{21}H_{23}O_7$, 387.1438). The NMR data of **5** (Table 2) indicated the presence of one ketone carbonyl at δ_C 195.1 (C-6), one ester carbonyl at δ_C 169.2 (C-1'), seven quaternary carbons such as six sp^2 and one oxygenated sp^3 at δ_C 73.8 (C-7), six aromatic/olefinic methines at δ_C 133.4 (C-10), 126.0 (C-9), 116.7 (C-5), 110.1 (C-6'), 103.4 (C-4), and 100.9 (C-4'), two sp^3 methines such as one oxymethine at δ_C 75.5

(C-8), one oxygenated methylene at δ_C 68.0 (C-1), and three methyl groups at δ_C 21.8 (C-8'), 19.8 (C-12), and 18.6 (C-11). The ^1H–^1H COSY correlations indicated the presence of two spin systems, CHO–CH–CH_2O and CH=CH–CH_3 (Figure 3). The mutual HMBC correlations shown in Figure 3 revealed that **5** possessed an azaphilone skeleton. These spectroscopic features suggested the presence of a similar azaphilone skeleton with that of berkazaphilone C, which was previously isolated from an extremophilic fungus *Penicillium rubrum* (Stierle et al., 2012).

TABLE 2 ^1H NMR (500 MHz, δ in ppm) and ^{13}C NMR Data (125 MHz, δ in ppm) for **5** (measured in DMSO-d_6).

Postion	δ_H (*J* in Hz)	δ_C, type
1	4.62, dd (10.6, 5.2)	68.0, CH_2
3		159.7, C
4	5.74, s	103.4, CH
4a		150.8, C
5	5.68, d (1.5)	116.7, CH
6		195.1, C
7		73.8, C
8	5.02, d (10.0)	75.5, CH
8a	3.18, m	35.1, CH
9	6.00, d (15.9)	126.0, CH
10	6.29, m	133.4, CH
11	1.79, d (7.4)	18.6, CH_3
12	1.10, s	19.8, CH_3
1'		169.2, C
2'		109.9, C
3'		161.1, C
4'	6.16, d (2.3)	100.9, CH
5'		140.1, C
6'	6.14 d (2.3)	110.1, CH
7'		159.6, C
8'	2.25, s	21.8, CH_3

The main differences were the substituents of the benzene ring. Key HMBC correlations from H-8' to C-4' and C-5', from H-6' to C-7', from H-4' to C-2' and C-3' constructed the substructure of 1,2,3,5-tetrasubstituted benzene ring.

The relative stereochemistry of **5** was established by interpretation of NOESY spectrum and ^3J-coupling data. The NOE correlation between H_3-12 and H-8 indicated a cofacial relationship between H_3-12 and H-8 (Figure 3). In addition, ^3J-coupling data showed *ax*/*ax* interactions between H-8 and H-8a (J = 10.0 Hz) (Stierle et al., 2012). Furthermore, the large coupling constant between H-9 and H-10 (J = 15.9 Hz) illustrated that the double bond at C-9 and C-10 was in the *E* configuration. To determine the absolute configurations of **5**, ECD computations for B3LYP/6-311+G(d)-optimized conformers were carried out at Cam-B3LYP/TZVP level. The experimental and calculated ECD spectra of **5** exhibited high consistency (Figure 4), and thus finally determined the absolute configurations of **5** as 7*S*, 8*S*, 8a*S*.

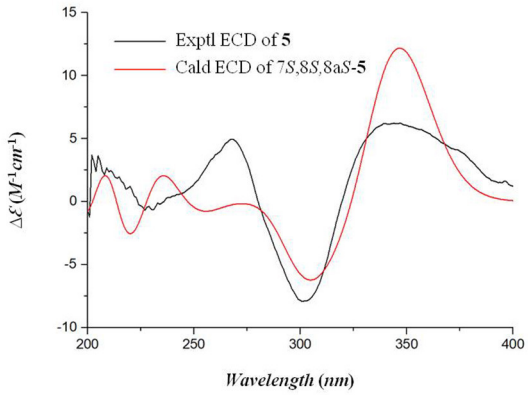

FIGURE 4
The experimental and calculated ECD spectra of compound **5**.

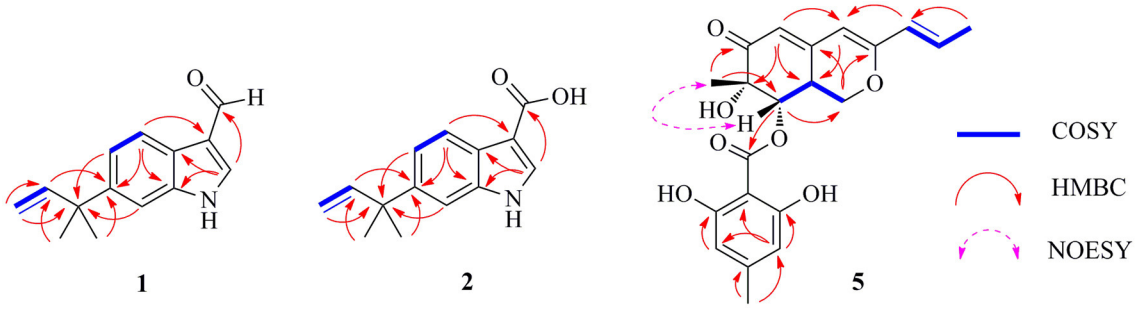

FIGURE 3
Selected Homonuclear chemical shift Correlation Spectroscopy (COSY), eteronuclear Multiple-Bond Correlation (HMBC), and Nuclear Overhauser Effect Spectroscopy (NOESY) correlations of **1**, **2**, and **5**.

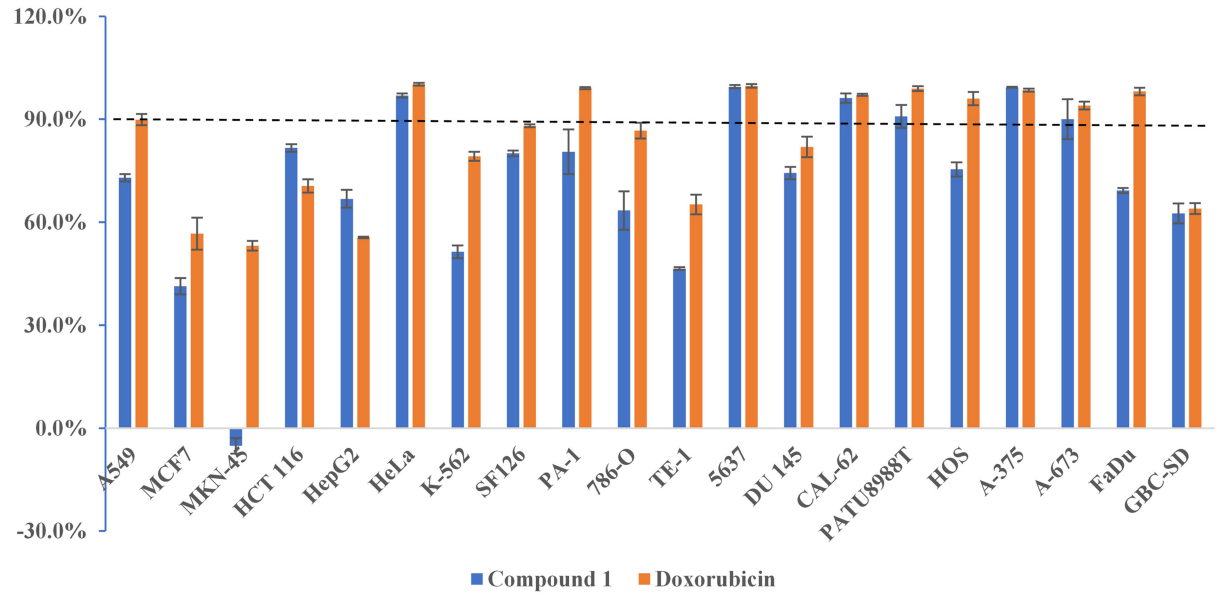

FIGURE 5
Cytotoxicities of compound **1** against 20 different human tumor cell lines.

In addition to the new compounds **1**, **2**, and **5**, five related known compounds (**3**, **4**, **6**–**8**) were obtained from this fungal strain. Based on comparison of their spectroscopic data with those in the literatures, they were identified as dihydrocarneamide A (**3**) (Zhang et al., 2015), notoamide C (**4**) (Kato et al., 2007), purpurquinone A (**6**) (Wang et al., 2011), saturnispol G (**7**) (Meng et al., 2018), and palitantin B (**8**) (Yang et al., 2020), respectively.

Cytotoxic activity

The new compounds **1**, **2**, and **5** were evaluated to determine their cytotoxic activity against HeLa cell lines. Compound **1** exhibited obvious cytotoxicity with the inhibition rate of (96.94 ± 0.62) % at the concentration of 20 μM. Since sufficient amount of **1** was obtained (45 mg/20 g, pure compound/crude extract), a large-scale cytotoxic activity screening of **1** against 20 different human tumor cell lines was performed. As a result, **1** showed high and broad-spectrum cytotoxicities against HeLa, 5637, CAL-62, PATU8988T, A-375, and A-673 cell lines, with the inhibition rates of (96.94 ± 0.62) %, (99.49 ± 0.50) %, (96.16 ± 1.34) %, (90.83 ± 3.31) %, (99.32 ± 0.11) %, and (90.01 ± 5.81) %, respectively (Figure 5). In particularly, since thyroid cancer is one of the leading cancers worldwide, chemotherapy is currently needed. Compound **1** showed strong activity against human thyroid cancer cells CAL-62 (96.16%), with an IC_{50} value of 10.4 μM, indicating that it may possess certain potential for the development of antitumor lead compounds. Moreover, further studies should focus on cytotoxicity assay on normal cell lines to check the specificity of the cytotoxicity. The safety index for cytotoxicity assay will reveal the true cytotoxic potential of the isolated compounds.

Conclusions

In conclusion, four indole alkaloids (compounds **1**–**4**) and four polyketides (compounds **5**–**8**) were isolated and identified from the deep-sea-derived fungus *Aspergillus flavipes* DS720. Among them, the indoles flavonoids A (**1**) and B (**2**) and the azaphilone flaviazaphilone A (**5**) are new compounds. Flavonoids A (**1**) and B (**2**) represent rare examples with a C-6 reversed prenylation. The structures of the new compounds were determined by analysis of NMR data, HRESIMS, and TDDFT ECD calculations. In the screening of cytotoxicities of **1** against 20 different human tumor cell lines, **1** showed high and broad-spectrum cytotoxicity against HeLa, 5637, CAL-62, PATU8988T, A-375, and A-673 cell lines. This study indicated that the deep-sea-derived microbes were considered to be valuable resources for the development of new drugs. Meanwhile, the newly discovered indole alkaloid **1** may be a promising antitumor lead compound.

Data availability statement

The original contributions presented in the study are included in the article/supplementary material, further inquiries can be directed to the corresponding author.

Author contributions

AX and X-NX: conceptualization and writing—original draft preparation. AX, X-NX, MZ, and C-LL: experiment implementation. LL: data processing. D-YF: writing—review and editing. All authors have read and approved the final manuscript.

Funding

This work was supported by the National Natural Science Foundation of China (82072909).

Conflict of interest

The authors declare that the research was conducted in the absence of any commercial or financial relationships that could be construed as a potential conflict of interest.

Publisher's note

All claims expressed in this article are solely those of the authors and do not necessarily represent those of their affiliated organizations, or those of the publisher, the editors and the reviewers. Any product that may be evaluated in this article, or claim that may be made by its manufacturer, is not guaranteed or endorsed by the publisher.

Supplementary material

The Supplementary Material for this article can be found online at: https://www.frontiersin.org/articles/10.3389/fmicb.2022.959754/full#supplementary-material

References

Carroll, A. R., Copp, B. R., Davis, R. A., Keyzers, R. A., and Prinsep, M. R. (2021). Marine natural products. *Nat. Prod. Rep.* 38, 362–413. doi: 10.1039/D0NP00089B

Chen, Y., Zhu, H. Y., Xu, L. C., Wang, S. P., Liu, S., Liu, G. D., et al. (2021). Antimicrobial and cytotoxic phenolic bisabolane sesquiterpenoids from the fungus *Aspergillus flavipes* 297. *Fitoterapia* 155, 105038. doi: 10.1016/j.fitote.2021.105038

Frisch, M. J., Trucks, G. W., Schlegel, H. B., Scuseria, G. E., Robb, M. A., Cheeseman, J. R., et al. (2016). *Gaussian 16 Rev. C.01*. Wallingford, CT: Gaussian Inc.

Jiang, L. L., Tang, J. X., Bo, Y. H., Li, Y. Z., Feng, T., Zhu, H. W., et al. (2020). Cytotoxic secondary metabolites isolated from the marine alga-associated fungus *Penicillium chrysogenum* LD-201810. *Mar. Drugs* 18, 276. doi: 10.3390/md18050276

Kato, H., Yoshida, T., Tokue, T., Nojiri, Y., Hirota, H., Ohta, T., et al. (2007). Notoamides A–D: prenylated indole alkaloids isolated from a marine-derived fungus, *Aspergillus* sp. *Angew Chem. Int. Ed.* 46, 2254–2256. doi: 10.1002/anie.200604381

Meng, J., Cheng, W., Heydari, H., Wang, B., Zhu, K., Konuklugil, B., et al. (2018). Sorbicillinoid-based metabolites from a sponge-derived fungus *Trichoderma saturnisporum*. *Mar. Drugs* 16, 226. doi: 10.3390/md16070226

Obulisamy, P. K., and Mehariya, S. (2021). Polyhydroxyalkanoates from extremophiles: a review. *Bioresour. Technol.* 325, 124653. doi: 10.1016/j.biortech.2020.124653

Rateb, M. E. M., and Ebel, R. (2011). Secondary metabolites of fungi from marine habitats. *Nat. Prod. Rep.* 28, 290. doi: 10.1039/c0np00061b

Soldatou, S., and Baker, B. J. (2017). Cold-water marine natural products, 2006 to 2016. *Nat. Prod. Rep.* 34, 585–626. doi: 10.1039/C6NP00127K

Stierle, A. A., Stierle, D. B., and Girtsman, T. (2012). Caspase-1 inhibitors from an extremophilic fungus that target specific leukemia cell lines. *J. Nat. Prod.* 75, 344–350. doi: 10.1021/np200414c

Wang, H., Wang, Y., Wang, W., Fu, P., Liu, P., and Zhu, W. (2011). Anti-influenza virus polyketides from the acid-tolerant fungus *Penicillium purpurogenum* JS03-21. *J. Nat. Prod.* 74, 2014–2018. doi: 10.1021/np2004769

Xu, K., Yuan, X. L., Li, C., and Li, X. D. (2020). Recent discovery of heterocyclic alkaloids from marine-derived *Aspergillus* species. *Mar. Drugs* 18, 54. doi: 10.3390/md18010054

Yang, L. J., Peng, X. Y., Zhang, Y. H., Liu, Z. Q., Li, X., Gu, Y. C., et al. (2020). Antimicrobial and antioxidant polyketides from a deep-sea-derived fungus *Aspergillus versicolor* SH0105. *Mar. Drugs* 18, 636. doi: 10.3390/md18120636

Zhang, P., Li, X. M., Wang, J. N., Li, X., and Wang, B. G. (2015). Prenylated indole alkaloids from the marine-derived fungus *Paecilomyces variotii*. *Chin. Chem. Lett.* 26, 313–316. doi: 10.1016/j.cclet.2014.11.020

Zhang, P., Wei, Q., Yuan, X., and Xu, K. (2020). Newly reported alkaloids produced by marine-derived *Penicillium* species (covering 2014–2018). *Bioorg. Chem.* 99, 103840. doi: 10.1016/j.bioorg.2020.103840

frontiers | Frontiers in Microbiology

ORIGINAL RESEARCH
published: 25 July 2022
doi: 10.3389/fmicb.2022.946286

Untargeted Metabolomics Sheds Light on the Secondary Metabolism of Fungi Triggered by Choline-Based Ionic Liquids

*Patrícia Sequeira[1†], Maika Rothkegel[1†], Patrícia Domingos[1], Isabel Martins[1], Céline C. Leclercq[2], Jenny Renaut[2], Gustavo H. Goldman[1,3] and Cristina Silva Pereira[1]**

[1] Applied and Environmental Mycology Laboratory, Instituto de Tecnologia Química e Biológica António Xavier, Universidade Nova de Lisboa (ITQB-NOVA), Oeiras, Portugal, [2] Integrative Biology Platform, Environmental Research and Technology Platform, Luxembourg Institute of Science and Technology, Belvaux, Luxembourg, [3] Faculdade de Ciências Farmacêuticas de Ribeirão Preto, Universidade de São Paulo, Ribeirão Preto, Brazil

OPEN ACCESS

Edited by:
Peng Zhang,
Tobacco Research Institute (CAAS), China

Reviewed by:
Arsa Thammahong, Chulalongkorn University, Thailand
Rosa Estela Quiroz Castañeda, Instituto Nacional de Investigaciones Forestales, Agrícolas y Pecuarias (INIFAP), Mexico

***Correspondence:**
Cristina Silva Pereira
spereira@itqb.unl.pt

[†] These authors have contributed equally to this work and share first authorship

Specialty section:
This article was submitted to Antimicrobials, Resistance and Chemotherapy, a section of the journal Frontiers in Microbiology

Received: 17 May 2022
Accepted: 20 June 2022
Published: 25 July 2022

Citation:
Sequeira P, Rothkegel M, Domingos P, Martins I, Leclercq CC, Renaut J, Goldman GH and Silva Pereira C (2022) Untargeted Metabolomics Sheds Light on the Secondary Metabolism of Fungi Triggered by Choline-Based Ionic Liquids. Front. Microbiol. 13:946286. doi: 10.3389/fmicb.2022.946286

Fungal secondary metabolites constitute a rich source of yet undiscovered bioactive compounds. Their production is often silent under standard laboratory conditions, but the production of some compounds can be triggered simply by altering the cultivation conditions. The usage of an organic salt – ionic liquid – as growth medium supplement can greatly impact the biosynthesis of secondary metabolites, leading to higher diversity of compounds accumulating extracellularly. This study examines if such supplements, specifically cholinium-based ionic liquids, can support the discovery of bioactive secondary metabolites across three model species: *Neurospora crassa, Aspergillus nidulans*, and *Aspergillus fumigatus*. Enriched organic extracts obtained from medium supernatant revealed high diversity in metabolites. The supplementation led apparently to increased levels of either 1-aminocyclopropane-1-carboxylate or α-aminoisobutyric acid. The extracts where bioactive against two major foodborne bacterial strains: *Staphylococcus aureus* and *Escherichia coli*. In particular, those retrieved from *N. crassa* cultures showed greater bactericidal potential compared to control extracts derived from non-supplemented cultures. An untargeted mass spectrometry analysis using the Global Natural Product Social Molecular Networking tool enabled to capture the chemical diversity driven by the ionic liquid stimuli. Diverse macrolides, among other compounds, were putatively associated with *A. fumigatus*; whereas an unexpected richness of cyclic (depsi)peptides with *N. crassa*. Further studies are required to understand if the identified peptides are the major players of the bioactivity of *N. crassa* extracts, and to decode their biosynthesis pathways as well.

Keywords: ***Neurospora crassa*, *Aspergillus nidulans*, *Aspergillus fumigatus*, non-proteinogenic amino acids, antimicrobial compounds, peptidome**

INTRODUCTION

Microbial infections and antimicrobial resistance constitute globally a major threat to human health. The last was recognized by the World Health Organization, in 2019, as one of the top 10 global public health threats facing humanity. It is estimated that *ca.* 700,000 people die every year from drug-resistant infections (World Health Organization [WHO], 2021). To fight this threat, the

development of new drugs that target microbial virulence and/or pathogenicity is a priority (Meyer et al., 2016). Microorganisms constitute a diverse and resourceful source for bioactive natural products discovery, which can be used as drug leads or therapeutics itself (Newman and Cragg, 2020). In particular, filamentous fungi are considered gifted producers of structurally diverse low-molecular weight secondary metabolites. These compounds are synthesized by using precursors derived from primary metabolism and, generally, are not essential for the growth and development of the producer organism (Fox and Howlett, 2008; Brakhage, 2012; Netzker et al., 2015). Secondary metabolites are, however, often critical for the survival and growth of the fungus in its ecological niche (Fox and Howlett, 2008; Rodrigues, 2016), with roles identified for example in nutrient acquisition, interaction with other organisms and growth inhibition of competitors (Calvo et al., 2002; Khaldi et al., 2010; Brakhage, 2012; Macheleidt et al., 2016).

Fungal secondary metabolites classes comprise polyketides (PKs), non-ribosomal peptides (NRPs), PK-NRPs hybrids, indole alkaloids, and terpenes (Pusztahelyi et al., 2015; Bills and Gloer, 2016). PKs, the most abundant class, use acetyl-CoA and malonyl-CoA units, and biosynthesis is simply achieved by the elongation of carboxylic acid building blocks. The scaffold is further modified by oxygenases, glycosyltransferase and other transferases leading to a high degree of structural diversity (Hertweck, 2009; Brakhage, 2012). NRPs, the second largest class, are synthesized by the modular assembly of short carboxylic acids and/or amino acids (El Maddah et al., 2017). They are constituted of both proteinogenic and non-proteinogenic amino acids and show high diversity in terms of length, variation in their functional domains and whether they are cyclized or not (Keller et al., 2005). Other units such as fatty acids, α-hydroxy acids, α-keto acids, heterocycles, and others, can also be incorporated (McErlean et al., 2019). Terpenes(oids) are made up of several C5 isoprene units, which are synthesized from acetyl-CoA through the mevalonate pathway. They are found to be linear or cyclic, saturated or unsaturated. Their classification is based on the number of isoprene units, among others, triterpenes (steroids) and tetraterpenes (carotenoids) (Bhattarai et al., 2021). Compounds of pharmacological interest are for example griseofulvin – PKS (Cacho et al., 2013) and echinocandin B – NRP (Cacho et al., 2012), both with antibiotic properties, and fumagillin – terpenoid, with potential antifungal and antitumoral properties (Lin et al., 2013).

The first biosynthesis step is catalyzed by a multidomain (backbone) enzyme that defines the produced class: PKs synthases, NRP synthases, hybrid NRP–PK synthases, prenyltransferases (or dimethylallyl tryptophan synthases), or terpene cyclases (Keller, 2019). Genes encoding for biosynthesis of a secondary metabolite are often arranged in gene clusters that are co-regulated under certain conditions; usually silent under standard laboratory conditions (Brakhage, 2012). Many backbone genes already identified have not yet been matched to the produced compound, and *vice versa* (Bergmann et al., 2007; Brakhage, 2012). To stimulate the production of a rich diversity of secondary metabolites, several strategies have been used, for example co-cultivation with other fungi/bacteria or genome engineering (Netzker et al., 2015; Begani et al., 2018; Liu et al., 2021). As illustrative examples, temperature modulates the production of trypacidin and endocrocin in *A. fumigatus* germinating spores, whereas white light represses the production of aflatoxin and sterigmatocystin in *A. fumigatus* (Hagiwara et al., 2017) and of the later metabolite in *A. nidulans* (Bayram et al., 2008). The simplest is, however, the one strain-many compounds (OSMAC) approach that explores modification of the cultivation conditions to activate those metabolic pathways (Bode et al., 2002). Ionic liquids, organic salts with a melting point below 100°C, represent a promising class of chemical stimuli that can profoundly impact fungi metabolism (Petkovic et al., 2009; Martins et al., 2013; Alves et al., 2016; Hartmann et al., 2019). When used as growth media supplements, many backbone genes underwent upregulation and a higher diversity of secondary metabolites, including cryptic ones, were biosynthesized (Martins et al., 2013; Alves et al., 2016). The stimuli caused by the ionic liquid supplements differ from that of a simple inorganic salt (Petkovic et al., 2010). As an example, in *A. nidulans*, orselinic acid, which has been identified in ionic liquid supplemented cultures (Alves et al., 2016), is also produced during co-cultivation with *Streptomyces* spp. that modulates the epigenetic machinery of the fungus (Bayram et al., 2019).

This study examines if ionic liquids supplements can support discovery of bioactive secondary metabolites in fungi. Three model fungi – *Neurospora crassa, Aspergillus nidulans*, and *Aspergillus fumigatus*, and two choline-based ionic liquids – choline chloride (ChoCl) and choline decanoate (ChoDec), were tested. Specifically, we focused on compounds accumulating extracellularly. The antibacterial activity of the ensuing crude extracts was evaluated against two major foodborne bacterial strains, *Staphylococcus aureus* and *Escherichia coli*. To characterize the chemical landscape of the extracts, their amino acid composition and an untargeted mass spectrometry analysis using the online platform Global Natural Product Social Molecular Networking – GNPS – were applied. An unexpected richness of peptide-based structures could be putatively associated with *N. crassa*.

MATERIALS AND METHODS

Chemicals

Compounds used in preparation of minimal media were purchased from Sigma-Aldrich, except for NaCl and $MgSO_4{\cdot}7H_2O$ (Panreac), phosphoric acid (Fisher Scientific) and $NaNO_3$ (ACROS organics). The standard chemicals [1-aminocyclopropane-1-carboxylate (ACC) and α-aminoisobutyric acid (Aib)] and chromatographic solvents were of highest analytical grade and purchased from Sigma Aldrich and Fisher Scientific, respectively. Water was obtained from a Milli-Q system (Millipore). Choline Chloride (>98%; ChoCl) was purchased from Sigma Aldrich and Choline Decanoate (>95%; ChoDec) from Iolitec.

Fungal Strains

Aspergillus fumigatus AF293 (FGSC A1100), *A. nidulans* (FGSC A4) and *N. crassa* (FGSC 2489) were obtained from the Fungal Genetics Stock Center. All strains were cultivated on DG18 (Oxoid) agar plates. Cultures were incubated in the dark, for 6–7 days, at 30°C (*A. nidulans* and *N. crassa*) or 37°C (*A. fumigatus*). Asexual spores (conidia) were harvested using a NaCl (0.85% w/v) and Tween-20 (0.1% w/v) sterile solution and collected after passing through three layers of miracloth. The harvested spores were washed twice with a sterile NaCl solution (0.85% w/v) and finally resuspended in the NaCl solution (0.85% w/v), to be used immediately, or in a cryoprotective saline solution containing 10% (v/v) glycerol, to be stored at −20°C or −80°C.

Growth Media

Aspergillus fumigatus and *A. nidulans* were cultivated in liquid minimal medium containing glucose (10.0 $g{\cdot}L^{-1}$), thiamine (0.01 $g{\cdot}L^{-1}$), 5% (v/v) nitrate salts solution [$NaNO_3$ (120.0 $g{\cdot}L^{-1}$), KCl (10.4 $g{\cdot}L^{-1}$), $MgSO_4{\cdot}7H_2O$ (10.4 $g{\cdot}L^{-1}$) and KH_2PO_4 (30.4 $g{\cdot}L^{-1}$)] and 0.1% (v/v) trace elements solution [$ZnSO_4{\cdot}7H_2O$ (22.0 $g{\cdot}L^{-1}$), H_3BO_3 (11.0 $g{\cdot}L^{-1}$), $MnCl_2{\cdot}4H_2O$ (5.0 $g{\cdot}L^{-1}$), $FeSO_4{\cdot}7H_2O$ (5.0 $g{\cdot}L^{-1}$), $CoCl_2{\cdot}6H_2O$ (1.7 $g{\cdot}L^{-1}$), $CuSO_4{\cdot}5H_2O$ (1.6 $g{\cdot}L^{-1}$), $Na_2MoO_4{\cdot}2H_2O$ (1.5 $g{\cdot}L^{-1}$) and Na_4EDTA (50.0 $g{\cdot}L^{-1}$)]. The pH was adjusted to 6.5 with NaOH and the medium sterilized in an autoclave (15 min; 110°C).

Neurospora crassa was cultivated in liquid minimal medium containing K_2PO_4 (1 $g{\cdot}L^{-1}$) and glucose (10 $g{\cdot}L^{-1}$) dissolved in distilled water. The pH was adjusted to 7 with 10% phosphoric acid and the medium sterilized in an autoclave (10 min; 110°C). Filter sterilized salts solution [1% (v/v), *per* 100 mL: $NaNO_3$ (30 g), $MgSO_4.7H_2O$ (5 g), KCl (5 g), $ZnSO_4.H_2O$ (100 mg), $CuSO_4.5H_2O$ (50 mg), HCl 37% (10 μL) and $FeSO_4.7H_2O$ (100 mg)] was added after autoclaving.

Minimal Inhibitory Concentrations (MICs) of Ionic Liquids

The minimal inhibitory concentrations (MICs) were determined as described previously (Petkovic et al., 2010). Final concentrations of ionic liquids in growth media ranged from 100 μM up to maximum solubility. Each liquid medium (1 mL) was inoculated with 10^6 spores and divided into four wells (0.2 mL each) of a 96 well microtiter plate. Cultures were incubated in the dark, at 30°C (*A. nidulans* and *N. crassa*) or 37°C (*A. fumigatus*) for 7 days. Fungal growth (or lack thereof) was determined at the end of incubation gauging by eye the formation of mycelium (turbidity). The lowest concentration that inhibited the formation of mycelium was defined as the MIC. Values should not be interpreted as absolute ones, but as an indication of the inhibitory and the fungicidal upper concentration limits.

Metabolite Production

Fungal cultures (100 mL) were initiated from 10^6 spores *per* mL in the respective minimal medium. Liquid cultures were incubated in the dark at 30°C (*N. crassa*, *A. nidulans*) or 37°C (*A. fumigatus*) with orbital agitation of 200 rpm. After 24 h, the ionic liquid supplement was added at 50% (i.e., 1.7 mM ChoDec for *A. fumigatus*) or 80% of the MIC (i.e., 0.96 M and 1.76 M ChoCl for *N. crassa* and *A. nidulans*, respectively, and 2.7 mM ChoDec for *A. fumigatus*). Negative conditions (without ionic liquid supplement) were prepared in parallel. Cultures were grown for 10 more days under agitation (100 rpm). At the end of incubation, the media supernatants were separated from mycelia using vacuum assisted filtration with miracloth (Merck Millipore Calbiochem). *Neurospora crassa* filtrates required the use of protease inhibitors (cOmplete Protease Inhibitor Cocktail, Waters) as preliminary tests showed degradation of untreated extracts (data not shown). The mycelia and filtrates were frozen immediately in liquid nitrogen and lyophilized.

Metabolite Extraction

Lyophilized filtrates were homogenized in 10 mL Milli-Q water, extracted three times with ethyl acetate (1:1) and the combined ethyl acetate fractions dried under soft nitrogen flow. Peptide enrichment was achieved using the Sep-Pak plus C18 cartridge (Waters) as previously described (Krause et al., 2006). The samples were re-dissolved in 10 mL of MeOH/H_2O (1/2, v/v) and loaded with a syringe into a conditioned cartridge. The cartridge was washed with 10 mL of Milli-Q water and 10 mL MeOH/H_2O (1/2, v/v). The retained compounds were eluted with 10 mL of MeOH to a pre-weighed glass tube and dried under soft nitrogen flow; crude extracts. Conditioning of the cartridge was done successively with 10 mL of MeOH, Milli-Q water and MeOH/H_2O (1/2, v/v).

Chromatographic Analysis

The crude extracts in 10% (w/v) MeOH, were chromatographically separated using a Waters Acquity chromatographer with Photodiode Array detector, cooling auto-sampler and column oven. A Symmetry C18 column (250 × 4.6 mm), packed with end-capped particles (5 μm, pore size 100 Å) (Waters Corporation), was used at 26°C. Data were acquired using Empower 2 software, 2006 (Waters Corporation). Samples were injected using a 10 μL loop operated in full loop mode. The mobile phase, at a flow rate of 0.9 $mL{\cdot}min^{-1}$, consisted of a solution of 0.1% trifluoracetic acid in water (v/v) (TFA, solvent A) and Acetonitrile (ACN, solvent B), set to a linear gradient of 99.5 to 0% of solvent A during 30 min, followed by 100% of solvent B for 10 min, 2 min to return to the initial conditions, and additional 10 min to re-equilibrate the column. The chromatographic profiles of the samples were obtained at the wavelength of 205 nm. Sample fractionation was performed with a Fraction collector III (Waters) connected to the Acquity chromatographer (Waters) using the same conditions described above. The collected fractions were dried under nitrogen flow and kept at 4°C (short term) or −20°C (long term) until further analysis.

Total Amino Acid Hydrolysis and Analysis

Total hydrolysis of the crude extracts (approximately 100 μg) was performed using 6 N HCl for 24 h at 110°C under

inert atmosphere (nitrogen flushed). The fractions were also hydrolyzed for 1 h at 150°C under inert atmosphere (nitrogen/vacuum cycles) in a Workstation Pico-Tag (Waters). Hydrolyzed samples were further analyzed using the AccQTag Ultra Amino Acid Analysis Method (eluent concentrates, derivatization kit and standard mixture of amino acid hydrolyzates, Waters) (Penrose et al., 2001; Armenta et al., 2010). Briefly, the hydrolyzed samples, the standards of Aib and ACC, and the standard mixture of amino acid hydrolyzates were derivatized following the manufacturer's instructions. The obtained derivatives were separated on an AccQTag Ultra column (100 mm × 2.1 mm, 1.7 μm) by reversed phase ultra-performance liquid chromatography (UPLC), and detected by fluorescence (FLR), according to the following details. The column heater was set at 55°C, and the mobile phase flow rate was maintained at 0.7 mL·min^{-1}. Eluent A was 5% AccQTag Ultra concentrate solvent A and eluent B was 100% AccQTag Ultra solvent B. The separation gradient was 0–0.54 min (99.9% A), 5.74 min (90.9% A), 7.74 min (78.8% A), 8.04 min (40.4% A), 8.05–8.64 min (10.0% A) and 8.73–10.50 min (99.9% A). Two microliters (2 μL) of sample were injected for analysis using a 10 μL loop. The FLR detector was set at 266 and 473 nm of excitation and emission wavelengths, respectively. Data were acquired using Empower 2 software, 2006 (Waters). Calibration curves of each standard were used to quantify amino acids, the values are represented as the relative % of total amount of amino acids. The total area of peaks was used to determine the overall % of identification.

Antibiotic Evaluation of Peptide-Based Metabolites

The extracts were assessed for their antimicrobial activity against gram-positive bacteria *Staphylococcus aureus* NCTC8325 and gram-negative bacteria *Escherichia coli* TOP 10, following the standard methodology implemented by the Clinical and Laboratory Standards Institute (Clinical and Laboratory Standards Institute [CLSI], 2018). First, bacteria were grown until approximately 1 to 2 × 10^8 CFU·mL^{-1} in Mueller Hinton Broth (MHB, Panreac). Then, two-fold serial dilutions were performed to obtain final extracts concentrations between 1,000 and 62.5 μg·mL^{-1}. Plates were incubated at 37°C for 24 h in a Bioscreen C analyzer (Oy Growth Curves Ab Ltd), taking hourly absorbance measurements (600 nm). All tests were done in triplicate; abiotic (medium alone) and biotic controls (each bacterium without extract) were included for each replicate.

After incubation with the crude extracts, 100 μL of each sample were mixed with 10 μL of 5 mg·mL^{-1} 3-(4,5-dimethylthiazol-2-yl)-2,5-diphenyl tetrazolium bromide (MTT) (Sigma Aldrich) in PBS (96-well microtiter plates) and incubated (dark, 37°C, 30 min). Then, 100 μL 10% SDS in 0.01 M HCl were added to each well and plates incubated for 2 h in the dark at room temperature. Absorbance was measured at 560 and 700 nm using Tecan Infinite 200 Microplate (Männedorf, Switzerland). For quantification, values at 560 nm were subtracted from the values at 700 nm. A second aliquot of 50 μL was used to label the cells with propidium iodide (20 μM PI, Biotium) and SYTO9 (3 μM; Alfagene) and further incubated for 15 min at room temperature with agitation. Fluorescence intensity was measured with a FLUOstar OPTIMA Microplate Reader (BMG·Labtech) using a 488/20 nm excitation filter (for both SYTO9 and PI), and a 528/20 nm (SYTO9 emission wavelength) and 645/40 nm (PI emission wavelength) emission filter. The signal from the staining solution (SYTO9/PI) was subtracted from all data to minimize cross-signal background. Microscopy assessment of the live/dead staining was done on a Leica DM 6000B upright microscope equipped with an Andor iXon 885 EMCCD camera and controlled with the MetaMorph V5.8 software, using the 100 × 1.4 NA oil immersion objective plus a 1.6× optovar, the fluorescence filter sets FTIC + TX2 and Contrast Phase optics. Images were analyzed by FIJI software (Fiji Is Just ImageJ). IC_{50} (half maximal inhibitory concentration of a compound) values were calculated from dose response curves constructed by plotting cell viability (MTT data) versus extract concentration (μg·mL^{-1}) using the Logit regression model (dose effect analysis tool of XLSTAT).

LC-MS/MS Analysis

NanoLC-MS/MS analysis was performed using an Eksigent Nano-LC 425 System (Eksigent, SCIEX) coupled TripleTOF 6600 + mass spectrometer (SCIEX). Samples (<1 μg·mL^{-1}; 4 μL each) were analyzed as follows. *N. crassa* samples were loaded on a C18 PepMap trap column (5 μm, 300 μm × 5 mm) (Thermo Scientific) at a flow rate of 2 μL min^{-1} for 10 min using 2% (v/v) ACN + 0.05% (v/v) TFA as mobile phase (Ribeiro et al., 2020); then peptides were separated at a flow rate of 300 nL·min^{-1} into a C18 PepMap 100 column (75 μm × 150 mm, 3 μm, 100 Å) (Thermo Scientific) using a linear binary gradient of 0.1% formic acid (v/v) in water (solvent A) and 0.1% formic acid (v/v) in ACN (solvent B) for a total running time of 100 min. Gradient program was 3–60% B in 60 min, then 40% B from 60 to 70 min, increasing again to 80% B to wash the column and finally re-equilibrating to the initial conditions (3% B) for 20 min. For *A. fumigatus* samples, the initial step of pre-concentration was the same as for *N. crassa*. Running gradient was different and adapted from Marik et al. (2018). Briefly, samples were separated at a flow rate of 300 nL·min^{-1} using a linear gradient of 0.05% (v/v) TFA in water (Solvent A) and 0.05% (v/v) TFA in ACN/MeOH (1:1, v/v) (solvent B). Gradient program for solvent B was 65% for 5 min, 65–80% from 5 to 45 min, then 100% until 75 min and last 65% from 76 to 81 min. MS data was acquired in positive mode over a mass range 300–1,250 m/z (for *N. crassa*) and 100–2,000 m/z (for *A. fumigatus*), with 250 ms of accumulation time. The 30 most intense ions were selected to perform fragmentation with high sensitivity mode using the automatically adjusted system of rolling collision energy. MS/MS scans were acquired over a mass range 100–1500 m/z with an accumulation time set at 50 ms; raw data files.

Molecular Networking and Compound Dereplication Using GNPS Platform

Raw data files (.wiff) were converted to open format mzXML using ProteoWizard MSConvert version 3.0.10051 (Kessner et al., 2008) to transform spectra from profile to centroid mode.[1] Data files were uploaded on GNPS through WinSCP (version 5.17.3) to generate a molecular network according to guidelines (Aron et al., 2020), which can be openly accessed.[2] To create the network, first all MS/MS spectra were aligned. Data were then filtered by removing all MS/MS peaks within ± 17 Da of the precursor m/z. MS/MS spectra were window filtered by choosing only the top six peaks in the ± 50 Da window throughout the spectrum. The precursor ion mass tolerance was set to 2.0 Da and a MS/MS fragment ion tolerance of 0.5 Da. A network was then created where edges were filtered to have a cosine score >0.7 and more than 6 matched peaks. Cosine score ranges from 0 (different parent ions) to 1 (structurally similar compounds) (Watrous et al., 2012). Edges between two nodes were kept in the network only if each of the nodes appeared in each other's respective top 10 most similar nodes. The maximum size of a molecular family was set to 100, and the lowest scoring edges were removed until the size was below this threshold. Self-loop nodes indicate that there is no structurally related molecule present in the sample. The spectra in the network were then searched against GNPS' spectral libraries (e.g., MassBank, ReSpect, and NIST) to assign a putative identification (Wang et al., 2016). The library spectra were filtered in the same manner as the input data. All matches kept between network spectra and library spectra were again required to have a score >0.7 and at least 6 matched peaks. The resulting molecular network was visualized using Cytoscape software v3.7.2 (Shannon et al., 2003). The molecular network is comprised by nodes (specific consensus spectrum) connected with edges (significant pairwise alignment between nodes). Nodes were labeled with putative identification and colored according to the group where the precursor was detected; edges thickness is proportional to cosine score. Complementary to library matching, DEREPLICATOR + workflow allow to predict fragmentation spectra *in silico* from known structures and to search for candidate structures in chemical databases (Mohimani et al., 2018). MS/MS data were used as input. The output table with potential candidates was integrated into the molecular network using Cytoscape. Manual validation of putative identifications was done through removal of hits from negative mode MS (not acquired herein) or after mirror plots (library compounds vs. input spectra) inspection. According to Sumner et al. (2007), putative annotations of compound and molecular families based on GNPS correspond to level 2 (Sumner et al., 2007). Herein, no standards were used to validate identifications. Complementary analysis of the MS spectra of the fractions was done using the NRPro tool[3] which includes databases not represented in GNPS, namely NORINE and NPAtlas (Ricart et al., 2020). Input data (MS/MS spectra in .mgf format) were uploaded, and search parameters were set as follows: peptide tolerance of 0.02 Da and fragment mass tolerance of 0.01 Da with M + H ionization with a charge up to 2. Decoy was activated; generates *p*-values associated with the identifications. Hits were validated (p-value < 0.05) upon further inspection of the number of scored peaks vs. annotated peaks.

[1] http://proteowizard.sourceforge.net

[2] http://gnps.ucsd.edu

[3] https://web.expasy.org/nrpro/

Statistical Analysis

Data were analyzed using standard statistical software (Origin v8.5 Software, San Diego, CA, United States, and GraphPad Software Prism v7, San Diego, CA, United States). Three biological replicates were executed. Results are expressed as mean value ± standard deviation. The statistical significance of values between conditions was evaluated by One-Way ANOVA test. Differences were considered significant when the p-value ≤ 0.05.

RESULTS AND DISCUSSION

Ionic Liquid Supplements Triggered a Metabolic Shift in the Fungal Cultures

It has been observed that culture conditions greatly impact secondary metabolism (Mathew Valayil, 2016). This explains the rationale behind the OSMAC approach to alter secondary metabolism in fungi (Chiang et al., 2009), and the usage of ionic liquids supplements as well (Petkovic et al., 2009; Alves et al., 2016). In the present study, two choline based ionic liquids were chosen, namely ChoCl and ChoDec. The first one has been previously reported to boost differential metabolic responses in fungi (Martins et al., 2013; Alves et al., 2016). ChoDec because longer alkyl chains in the anion have higher toxicity toward fungi and accordingly, less amounts are needed to induce stress (Petkovic et al., 2010; Hartmann et al., 2015). The MIC values for each fungus – *A. nidulans*, *A. fumigatus*, and *N. crassa* – are listed in **Table 1**. Choline based ionic liquids have been shown to be biodegradable, specifically the choline cation was observed to be partially degraded after 15 days of incubation with either *A. nidulans* and *N. crassa* (Martins et al., 2013). The decanoate anion was herein undetectable in the medium supernatant (chromatographic analysis) after 5 days of incubation (data not shown). Similar degradation yields have been previously reported for other filamentous fungi (Boethling et al., 2007; Petkovic et al., 2010).

Upon 10 days of incubation, fungal cultures were harvested, and the cultivation media were extracted. Secondary metabolites were enriched by liquid-liquid extraction with ethyl acetate, followed by solid-phase extraction resulting in peptide enriched

TABLE 1 | Minimal inhibitory concentrations of the cholinium-based ionic liquids (choline chloride, ChoCl and choline decanoate, ChoDec) used as media supplements for each fungal strain.

	ChoCl [M]	ChoDec [mM]
A. fumigatus	1.7	3.4
A. nidulans	2.2	2.6
N. crassa	1.2	–

fractions (Krause et al., 2006). The metabolic footprints (i.e., pool of metabolites produced at a given point under certain culture conditions) of the crude extracts were investigated by liquid chromatography (**Figure 1**). *A. nidulans* and *A. fumigatus,* in contrast to *N. crassa,* show high basal diversity of metabolites. In general, the profiles are distinct in cultures grown in the supplemented media compared to the negative control (without supplementation). The observed metabolic footprints depend on the ionic liquid supplement (**Figure 1A**) and of its concentration as well (*viz,* 50 and 80% of the MIC of ChoDec) (**Figure 1B**). This result corroborates preceding observations that distinct ionic liquids induced distinct metabolic alterations on the fungal metabolism, increasing, in general, the diversity of synthesized low molecular-weight molecules (Petkovic et al., 2009; Martins et al., 2013; Alves et al., 2016). Using a similar approach, monodictyphenone and orsellinic acid, otherwise cryptic metabolites, accumulated (in a pool of *ca.* 40 ion masses) in cultures of *A. nidulans* grown in medium supplemented with 1-ethyl-3-methylimidazolium chloride (Alves et al., 2016). Orsellinic acid had been also identified in *A. nidulans* during co-cultivation with *Streptomyces* spp. (Fischer et al., 2018). Proteomic analyses of *A. nidulans* and *N. crassa* cultures, showed that several biological processes and pathways were affected upon supplementation with ChoCl, provoking also an accumulation of stress-responsive proteins and osmolytes (Martins et al., 2013).

Total Amino Acid Hydrolysis Discloses the Presence of Non-proteinogenic Residues in *Neurospora crassa* and *Aspergillus fumigatus* Extracts

Fungi are able to use both proteogenic and non-proteinogenic amino acids (NPAAs) for incorporation in NRPs; NPAAs may positively impact the stability, potency, permeability, oral bioavailability, and immunogenicity of peptides as they do not occur naturally in humans (Ding et al., 2020). In fact, an important feature of many fungal antimicrobial peptides is the presence of NPAAs or other α-hydroxy and carboxylic acids (Mootz et al., 2002). A previous study has shown that ChoCl supplementation of *N. crassa* growth medium led to the increased expression of the 1-aminocyclopropane-1-carboxylate (ACC) deaminase, which mediates the formation of ACC (Martins et al., 2013). In some fungi, the presence of ACC has been linked to the peptaibiotics neofrapeptins and acretocins, isolated from *Geotrichum candidum* SID 22780 and *Acremonium crotocinigenum* cultures, respectively (Fredenhagen et al., 2006; Brückner et al., 2019). Peptaibiotics show a unique structure varying from 5 to 21 amino acid residues, including numerous NPAAs, mainly α-aminoisobutyric acid (Aib), and/or lipoamino acids (Degenkolb et al., 2003; Degenkolb and Brückner, 2008). Aib has been found to correlate to specific types of secondary structures, namely helical structures, improving peptide functioning and increasing enzymatic resistance (Niu et al., 2020).

To verify if the ionic liquid-supplements have induced the production of peptides containing NPAAs, specifically ACC and Aib, the total amino acid content of extracts (upon hydrolysis) were chromatographically analyzed. Both NPAAs could be detected, most evident in *N. crassa* and *A. fumigatus* (**Figure 2**). Specifically, in *N. crassa* ACC levels show increasing trend upon ChoCl supplementation, consistent with the accumulated levels of ACC deaminase described before (Martins et al., 2013). *A. fumigatus* control extracts show low levels of Aib with a slight, but not statistically significant, increase when the culture is supplemented with ChoDec (at 80% of MIC). In *A. nidulans*, an increasing trend in either NPAAs upon ChoDec supplementation was observed, but the overall amounts of Aib and ACC are substantially lower compared to the other two fungi.

Ionic liquid-exposure altered the pattern of the overall amino acid content, suggestive of an altered peptidome profile (**Supplementary Table 1**). Nonetheless, no meaningful alterations were found (pair-wise ANOVA) in the detected amounts of each amino acid with or without media supplementation, possibly consequence of high variability between the biological replicates. For *A. fumigatus* around 30% and for *N. crassa* 45–65% of the peaks could not be assigned to any of the amino acid standards. For *A. nidulans*, the values were lower: 4–7% (negative and ChoCl supplemented extracts) and 27% (ChoDec supplemented extracts). Despite these inherent technical fragilities, this analysis provides an estimation of the amino acid profiles of each sample, and excitingly point to the existence of peptides containing ACC and/or Aib in either crude extract from ionic liquid supplemented cultures. Based on these results, *N. crassa* and *A. fumigatus* extracts were selected for subsequent analyses focusing antibacterial efficacy and compositional signature (LC-MS/MS).

Neurospora crassa and *Aspergillus fumigatus* Crude Extracts Depict Antibacterial Activity

The antibacterial activity of *N. crassa* and *A. fumigatus* extracts against *S. aureus* and *E. coli* was assessed using the broth dilution method. For each crude extract, two-fold dilutions of an initial concentration of 1,000 $\mu g \cdot mL^{-1}$ were performed. Bacterial growth, inferred by the medium turbidity (600 nm), was measured for 24 h. After growth, bacterial viability was evaluated via measurements of the metabolic activity (MTT) and the live/dead cell ratio obtained from fluorescent staining quantifications. After 24 h, cell viability decreased significantly relative to the bacterial control, reflected in the MTT and live/dead cell ratio quantifications (**Figure 3** and **Supplementary Table 2**). Microscopic snapshots show major cell lysis upon exposure to extracts derived from ionic liquid-supplemented cultures compared to the bacterial control (no extract) (**Figure 4**). Based on the estimated IC_{50} values (**Table 2**), the supplementation compared to control conditions, increased greatly the bactericidal activity of the derived *N. crassa* extracts, but not those of *A. fumigatus*. At this stage, the observed activity cannot be linked to a specific compound. To pinpoint potential candidates, untargeted

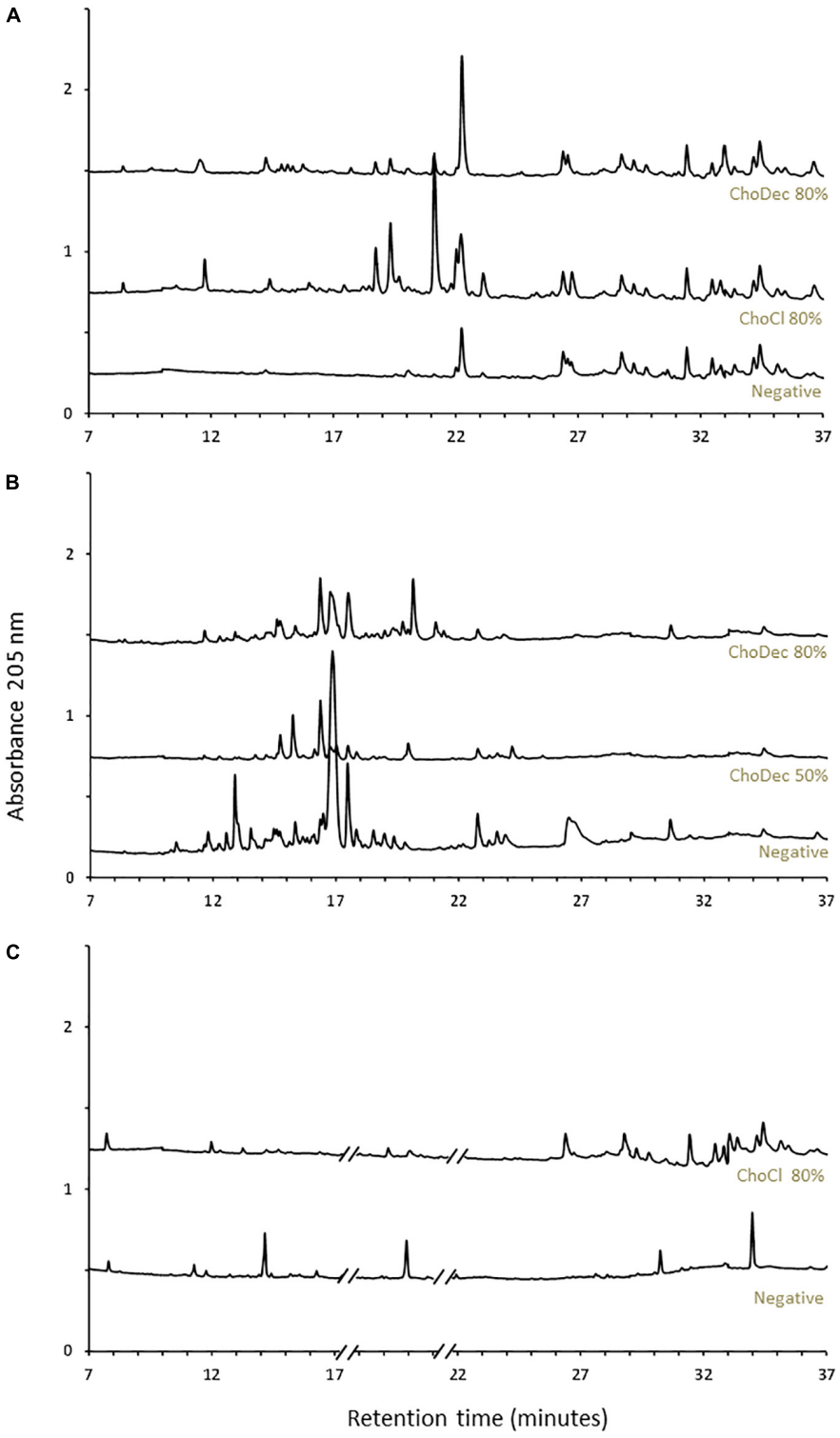

FIGURE 1 | Ionic liquid supplements triggered a metabolic shift in the fungal cultures. Chromatographic analyses of the metabolic footprint of *A. nidulans* **(A)**, *A. fumigatus* **(B)**, and *N. crassa* **(C)** crude extracts. Crude extracts are from cultures grown for 10 days in either choline chloride (ChoCl) or choline decanoate (ChoDec) supplemented media, at 50 or 80% of the MIC, and from cultures without ionic liquid supplementation (i.e., negative controls). Truncated parts of the chromatogram from *N. crassa* cultures **(C)** correspond to the elution of protease inhibitors. The *y*-axis scale represents the base peak intensity, where units are arbitrary.

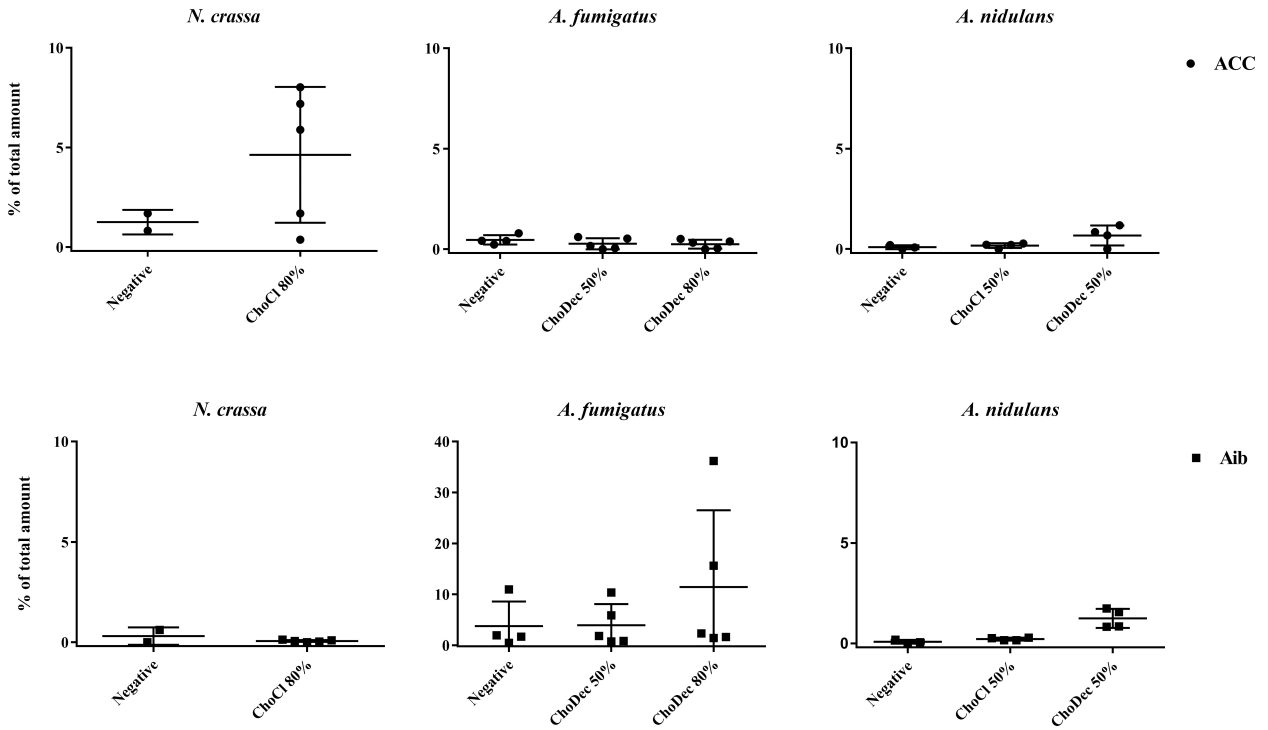

FIGURE 2 | Total amino acid hydrolysis discloses the presence of two non-proteinogenic residues in *N. crassa* and *A. fumigatus* extracts. Scatter plot depicting individual values of percentage (%) of total amount of 1-aminocyclopropane-1-carboxylate, ACC (●) and α-aminoisobutyric acid, Aib (■) obtained from total hydrolysis of the crude extracts derived from cultures grown in media with or without (i.e., negative) supplementation. The *y*-axis scales are not normalized to allow easier visualization of the amount of either non-proteinogenic amino acid in each condition.

MS analyses using the GNPS platform were applied. A total of 52 and 18 compounds were identified in *N. crassa* and *A. fumigatus* extracts derived from the ionic-liquid supplemented cultures, respectively (**Figure 5** and **Supplementary Tables 3, 4**). By eliminating compounds of low signal intensity, the most promising candidates potentially produced by *A. fumigatus* are macrolides and terpenes, whereas for *N. crassa* are cyclic peptides, including five depsipeptides; structurally of high pharmacological interest (**Table 3**). Fractionation of the later, added another cyclic peptide to the pool of compounds annotated through the GNPS tool; likely of low abundance in the crude extract. Analysis of their whole chemical landscape highlighted, however, a weak sample deconvolution with many compounds present in the three fractions. Through their direct query in the NRPro database, five additional hits of cyclic peptides (including one depsipeptide) were found (**Supplementary Table 5**).

The results show the production of antimicrobial compounds in *N. crassa* cultures under ionic liquid supplementation, likely associated to production of metabolites otherwise cryptic. The hypothesis that these antimicrobial compounds support *N. crassa* competitiveness in specific niches deserves further consideration. However, contrary to that observed for *N. crassa*, the supplementation did not increase the antibacterial activity of *A. fumigatus* derived extracts. Regardless of these contrasting results, the chemical landscape of either extract was further analyzed using an untargeted MS metabolomics approach.

LC-MS/MS Analyses of *Aspergillus fumigatus* Extracts Derived From Ionic Liquid Supplemented Cultures, Suggests the Accumulation of Macrolides, Among Other Metabolites

The MS spectra collected for the *A. fumigatus* extracts derived from the ionic liquid supplemented cultures were subjected to a molecular networking analysis on the web-based platform GNPS. This platform relies on the principle that structurally similar compounds will have similar MS/MS fragmentation patterns, and hence allows deconvolution of large MS datasets, annotation, and discovery of novel and/or analog compounds. This automated annotation belongs to a class 2 classification (Sumner et al., 2007), therefore all compounds identification discussed below remain putative, requiring, for targeted compounds, further validation in the near future.

The metabolic footprints of *A. fumigatus* extracts grown in media supplemented with 50% (G1) or 80% (G2) of the ChoDec MIC concentration were analyzed. In this case, of 1471 nodes, 684 nodes were clustered into 135 molecular families and the remaining 787 did not share any connection (full dataset hyperlink in **Supplementary Table 3**). In total, 18 metabolites were putatively identified, 9 by spectral match in GNPS databases (black border nodes) and 9 by *in silico* DEREPLICATOR + tool (red border nodes) (**Figure 5A**, full

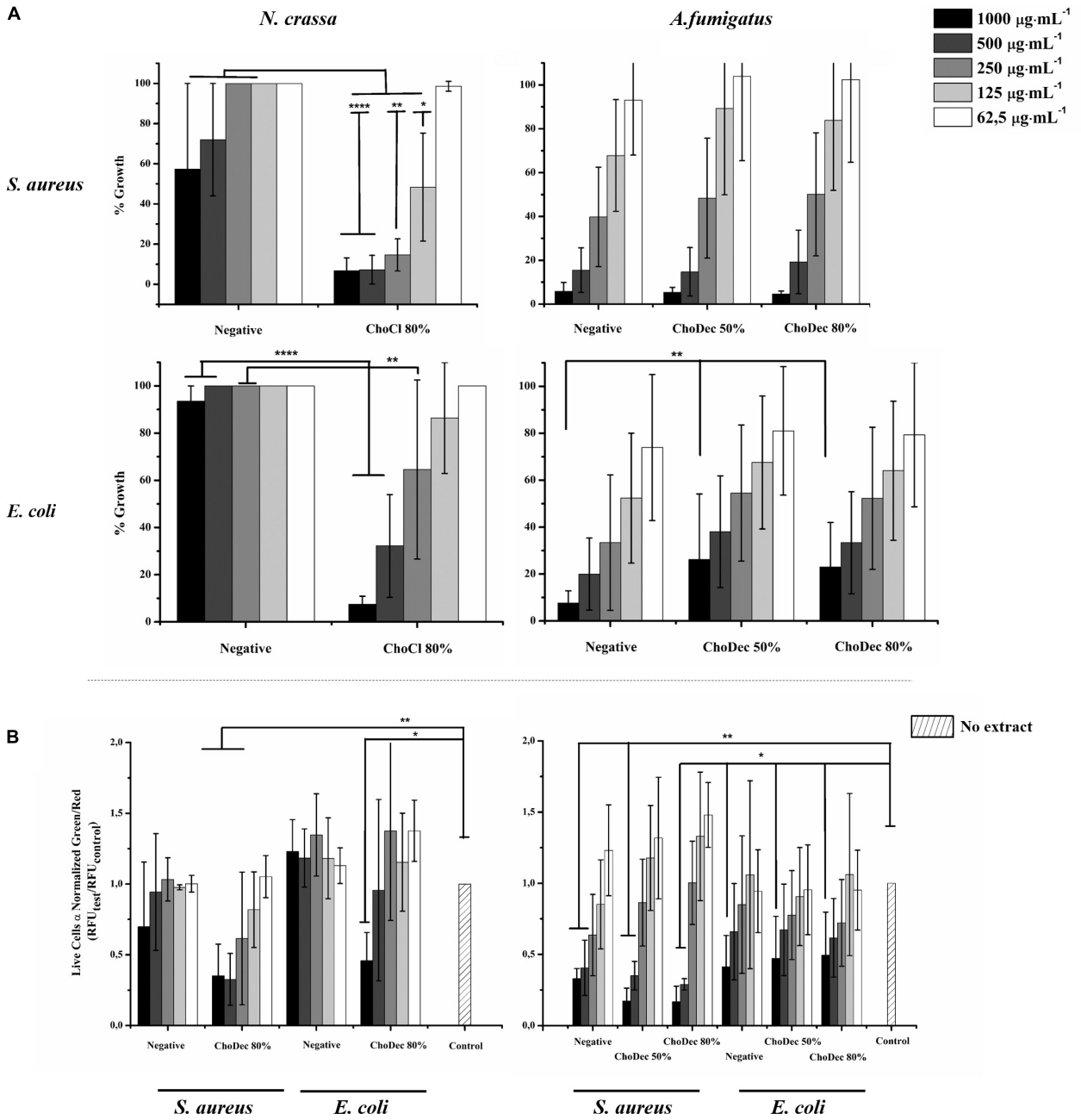

FIGURE 3 | *N. crassa* and *A. fumigatus* crude extracts depict antibacterial activity against *S. aureus* and *E. coli*. Cell viability measured by MTT assay of extracts derived from cultures grown in media with or without (i.e., negative) supplementation **(A)**. Quantification of bacterial viability through the normalized green/red ratio (i.e., SYTO9 (green, live cells)/PI (red, dead cells) staining) **(B)**. Statistically significant differences are depicted; $^{*}p \leq 0.05$, $^{**}p \leq 0.01$, $^{****}p \leq 0.0001$.

list in **Supplementary Table 4**). Most of the nodes correspond to metabolites produced in both conditions. Only compounds with signal intensity $>1.5{\cdot}10^{7}$ in the total ion chromatogram (with a clear separation from baseline values) will be discussed in greater detail (**Table 3**, bottom panel in **Figure 5A**). Half of these compounds belong to the class of polyketides, some of which were found only in G2 (80% MIC). In either sample, G1 and G2, the most frequently found polyketide compounds are macrolides; class of antibiotics composed of a large lactone ring with a sugar attached. The macrolides putatively identified were dolabelide C, efomycin G, roflamycoin, and antibiotic A 59770A. The first has been reported in a sea hare (Suenaga et al., 1997), while the last three are known as bacterial metabolites (Schlegel et al., 1981; Hoehn et al., 1990; Klassen et al., 2019). Macrolides production in fungi has been, however, reported before; e.g., phaeospelide A in *Aspergillus oryzae* (Morishita et al.,

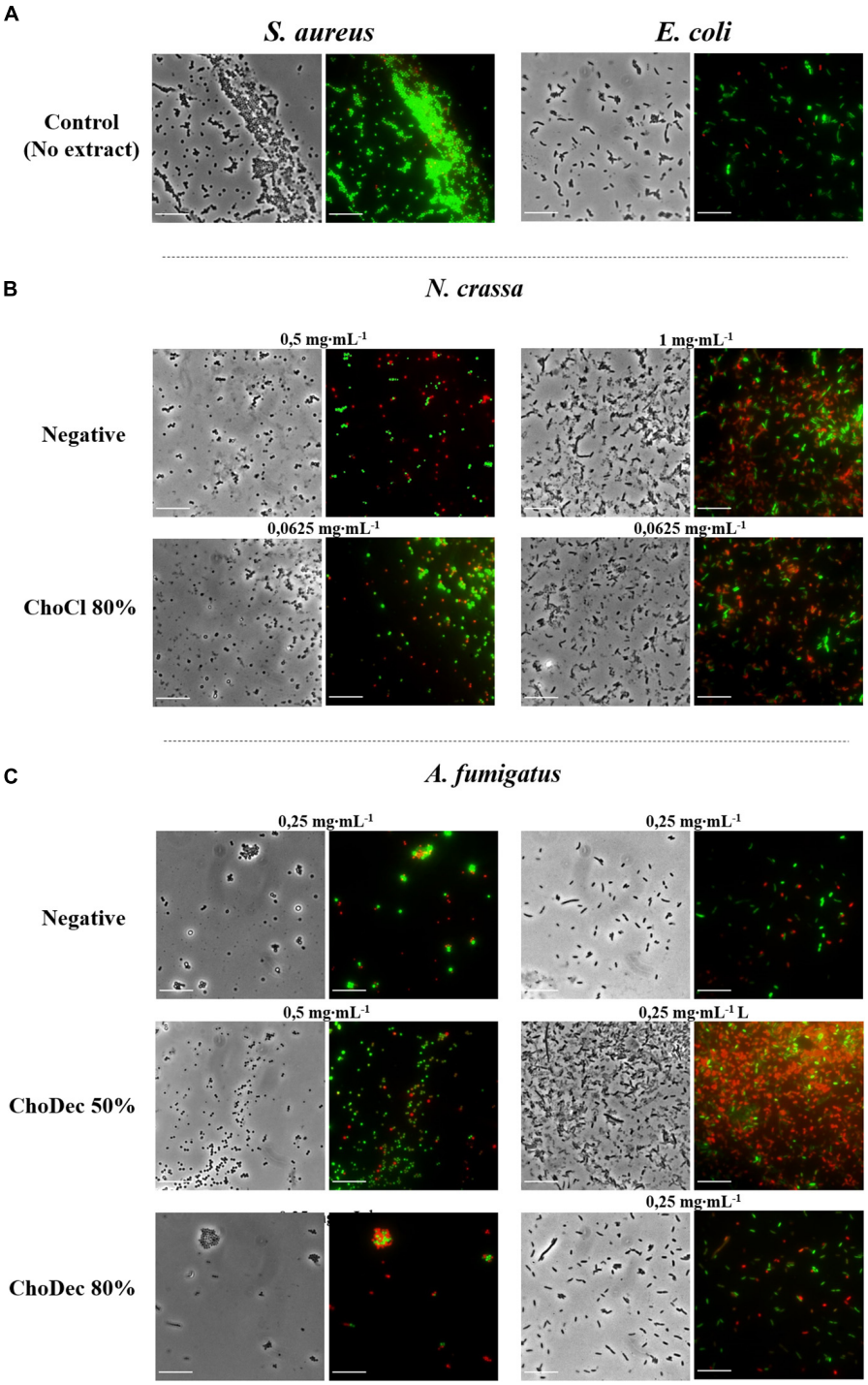

FIGURE 4 | *N. crassa* and *A. fumigatus* crude extracts led to significant lysis of *S. aureus* and *E. coli* cells, which is denoted by the red labeling. Microscopic snapshots of *E. coli* and *S. aureus* grown in the absence of extract **(A)** and in the presence of crude extracts derived from cultures grown in media with or without (*i.e.,* negative) supplementation: *N. crassa* **(B)** and *A. fumigatus* **(C)**. Images of bacteria at concentrations near the measured IC_{50} for each crude extract are shown. Cells were stained with SYTO9 (green) and PI (red) denoting live and dead cells, respectively. Scale bar, 10 μm.

2019). These extracts showed a more pronounced effect over *S. aureus* (**Figure 3**), consistent with the putative identification of macrolides. This class of compounds is usually bacteriostatic, most efficient against Gram-positive bacteria but can also be active against several Gram-negative bacteria (Arslan, 2022). In particular, efomycin is active against a number of drug-resistant

pathogens (e.g., methicillin-resistant *S. aureus*) (Wu et al., 2013), and roflamycoin exerts activity against a broad spectrum of organisms (Han et al., 2021).

Apart from macrolides, in either sample, 7α,27-dihydroxycholesterol was identified, which belongs to the terpen(oid) class. It derives from cholesterol, and has been reported before in *A. fumigatus* metabolome (Gil-De-la-fuente et al., 2021). It is functionally relevant, helping the fungus to bypass the effects of ergosterol inhibitor class of antifungals (Xiong et al., 2005); a potential new drug target. Finally, PKs-terpenes hybrids (Keller, 2019), namely two pregnane glycosides were identified in either extract. They show broad spectrum activity (e.g., anticancer, analgesic, anti-inflammatory and antimicrobial) and to date only few have been reported in fungi, for example in *Aspergillus versicolor* cultures grown in rich medium for 15 days (Ding et al., 2019) and *Cladosporium* sp. grown in rice-based medium for 45 days (Yu et al., 2018). A single peptide was putatively identified, namely the cyclohexapeptide aerucyclamide D, a ribosomal metabolite that has been previous described in a cyanobacterium as a new antiparasitic compound (Portmann et al., 2008).

LC-MS/MS Analyses of *Neurospora crassa* Extracts Derived From Ionic Liquid Supplemented Cultures, Suggests the Accumulation of Several Cyclic (Depsi)peptides, Among Other Metabolites

Neurospora crassa extracts derived from ChoCl supplemented cultures were chromatographically fractionated at the retention times of 15.6, 17.3, 19.6 min, corresponding to G1, G2, and G3, respectively. The peptidome of each fraction was analyzed as previously described (including the NPAAs ACC and Aib) (**Supplementary Figure 1**). G1 contains ACC; G2 contains Aib and ACC, and G3 contains none. Accordingly, G2 might comprise peptaibiotics. To determine the complete amino acid sequence of these fractions, Edman sequencing was attempted but failed, possibly due to a blocked N-terminal (Mootz et al., 2002). Overall, these observations further support the hypothesis that growth medium supplementation with ChoCl triggered production of peptaibiotics in *N. crassa*, otherwise cryptic.

The chemical landscape of these three samples and of the corresponding crude extract (G4) were analyzed, similarly to that done for *A. fumigatus*. A total of 5,249 nodes were obtained, 1,514 nodes clustered into 247 molecular families, and the remaining are self-loop nodes (full dataset hyperlink in **Supplementary Table 3**). To simplify, only clusters with putative hits are shown. In total, 10 compounds were putatively identified by comparison against GNPS databases (black border nodes) and 42 compounds by using the DEREPLICATOR + tool (red border nodes) (**Figure 5B**, full list in **Supplementary Table 4**). To focus the discussion, for G4 only the compounds presenting signal intensity $>3.0{\cdot}10^7$ in the total ion chromatogram are further considered, whereas for G1–G3 the two highest intensity signals are detailed if absent in G4 (**Table 3**, bottom panel in **Figure 5B**). G4 shows, as expected, the highest diversity of compounds. Similar to that found in *A. fumigatus* extracts, macrolides were the only polyketide compounds identified, specifically aldgamycin K and levorin A3. A single terpene, corticosterone, and one lipid-based metabolite, leukotriene E4 methyl ester, were putatively identified as well. Leukotrienes are eicosanoids produced by pathogenic fungi, suggested to act as virulence factors (Noverr et al., 2002). They are a subset of oxylipins, a class of metabolites that act mainly as lipid mediators, signaling spore development, metabolites production and virulence in fungi (Tsitsigiannis and Keller, 2007).

Remarkably, *N. crassa* seems to be an abundant producer of NRP, including peptides (linear and cyclic, 7 distinct compounds) and depsipeptides (5 distinct compounds) when grown in medium supplemented with ChoCl. Specially, two cyclic peptides were identified: pseudostellarin C and mollamide B, and five linear peptides: pepsin S 735A, halo-toxin, two tripeptides (Fru-Leu-Ile and Ile-Pro-Ile) and one hexapeptide (Val-Val-Pro-Val-Pro-Asn). Pepsin is the only linear peptide identified in all samples, possibly an artifact of the protease inhibitors herein used. The tri/hexapeptides identified here have never been reported before, questioning if these compounds are hydrolyzed products or are precursors of larger peptides. Besides, four cyclic depsipeptides were also putatively identified: discokiolide A, dideoxy-sandramycin, chlorodestruxin and chaiyaphumine D, all of which, expect the last, have been reported before and related to either antitumor or anti-insecticidal activities. Syringostatin A, a lipodepsinonapeptide, reported antifungal activity (Sorensen et al., 1996). In cyclic depsipeptides at least one amino acid is replaced by a hydroxylated carboxylic acid (α-hydroxy acid), resulting in a mix of amide and ester bonds in the core ring, conferring high stability (Taevernier et al., 2017; Wang et al., 2018). α-Hydroxy acids structural similarity to α-amino acids, ensures that depsipeptides can interact with numerous proteins yet showing higher resistance against hydrolyzing enzymes due

TABLE 2 | IC_{50} values determined for *A. fumigatus* and *N. crassa* crude extracts from media supplemented or not (negative control) with choline chloride (ChoCl) or choline decanoate (ChoDec), at 50 or 80% of the MICs.

Fungal strain	Bacterial strain	Extract tested	IC_{50} ($\mu g{\cdot}mL^{-1}$)
N. crassa	*E. coli*	Negative	1,280
		ChoCl 80%	103
	S. aureus	Negative	310
		ChoCl 80%	70
A. fumigatus	*E. coli*	Negative	120
		ChoDec 50%	310
		ChoDec 80%	350
	S. aureus	Negative	310
		ChoDec 50%	260
		ChoDec 80%	470

IC_{50} represents the crude extract concentration that inhibits bacterial activity by 50% and were calculated from curves constructed by plotting cell viability (MTT data) vs. extract concentration ($\mu g{\cdot}mL^{-1}$).

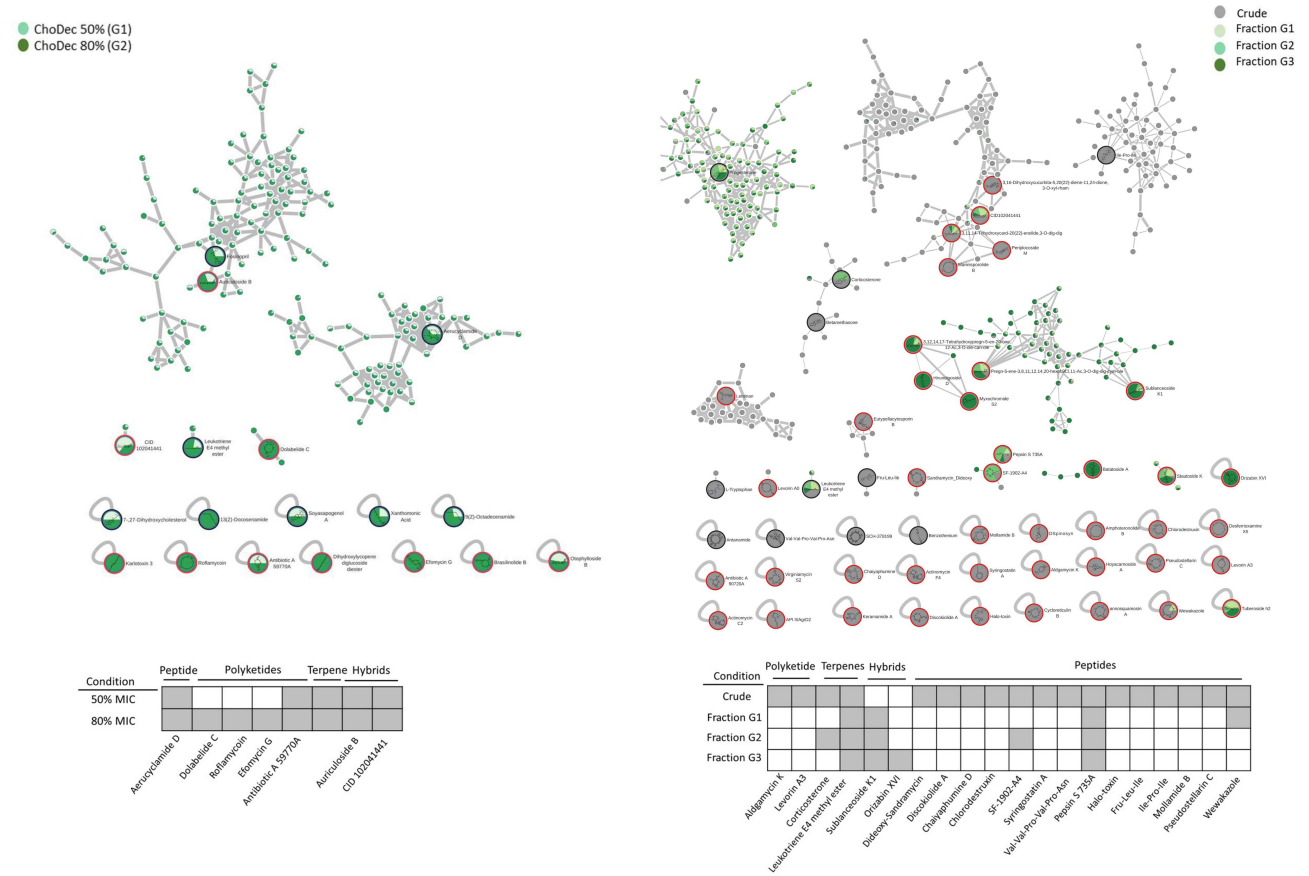

FIGURE 5 | The molecular network generated by the GNPS tool using the MS data acquired for *A. fumigatus* **(A)** and *N. crassa* **(B)** extracts derived from ionic liquid supplemented cultures, considering the putatively identified compounds the accumulation, among other metabolites of macrolides and peptides, respectively. Putative identifications retrieved by using molecular networking analysis and compound dereplication in GNPS, from spectral match (*) and *in silico* tool DEREPLICATOR + . For *N. crassa*, isolated fractions (G1, G2, and G3) as well as crude (G4) extracts were analyzed; whereas for *A. fumigatus*, extracts from cultures supplemented with choline decanoate at 50% (G1) and 80% (G2) of the MIC. Only peaks with signal intensity $>1.5{\cdot}10^7$ (for *A. fumigatus*: G1 and G2) and $>3{\cdot}10^7$ (for *N. crassa*: G4) in the total ion chromatogram are depicted (Full list in **Supplementary Table 3**). For *N. crassa* fractions, G1 to G3, the two most intense peaks in the total ion chromatogram are depicted.

to cyclization (Gentilucci et al., 2010; Stone and Deber, 2017). The higher resistance is expected to result in enhanced oral bioavailability (Sivanathan and Scherkenbeck, 2014). Several known depsipeptides contain NPAAs, for example 2-hydroxy-3-methyl-pentanoic acid, tiglic acid, α-aminobutyric acid, picolinic acid; constituents of compounds putatively identified in the extracts yet below the defined threshold of peak intensity, e.g., SCH-378199 and virginiamycin S5 (**Supplementary Table 4**). This observation is consistent with the presence of many non-identified amino acids in the *N. crassa* extracts (nearly half of the chromatographic peak area could not be assigned, **Supplementary Table 1**). The presence of Aib in this class of compounds remains to be seen. On the contrary, ACC is known to be a building block of depsipeptides, for example of BZR-cotoxin II, a metabolite of *Bipolaris zeicola*, and of CBS 154-94A, a metabolite of *Streptomyces* sp. (Fredenhagen et al., 2006). The last has antibiotic activity, acting as protein farnesyl transferase inhibitor. Finally, the cyclic lipodepsipeptide SF-1902-A4 was also identified (present also in G2); previous reported as antibacterial (Omoto et al., 1981). As above mentioned, most compounds were only found in the crude extract, except in the denoted cases. Looking to the two most intense peaks of G1–G3 fractions revealed the presence of wewakazole (G1, also in G4 but below the defined intensity threshold), orizabin XIV (G3), and sublanceoside K1 (in all fractions). The first compound, a cyclic dodecapeptide, has been reported to exhibit cytotoxicity against H460 human lung cancer cell line (Gogineni and Hamann, 2018). The second, is a glycolipid that inhibits the activity of 1,3-β-glucan synthase, required for cell wall synthesis in fungi (Castelli et al., 2002); a target of clinically approved antifungal drugs (Lima et al., 2019). The last, a terpene glucoside, has no reported bioactivity to date. Apart from these compounds, the remaining hits correspond to clusters containing spectra from

all samples (G1 to G3), and include compounds belonging to resin glycosides, fatty acids, terpenoids and cyclic peptides. The chromatographic elution of the fractions (with close retention times) did not result in a clean separation, explaining why these clustered together in the molecular network. Since that NRPro tool (see text footnote 3) that is specific for NRPs is not included in the GNPS platform, the MS/MS spectra of the fractions were also queried in this database. Putative identifications were found only for G1 and G2 (**Supplementary Figure 2** and **Supplementary Table 5**) revealing five additional cyclic peptides candidates. Specifically, G1 showed matches to guangomide A (depsipeptide), arbumelin and a cyclohexapeptide. The first two compounds have been previously identified in fungal strains, namely in *Trichothecium sympodiale* (Sy-Cordero et al., 2011) and *Calcarisporium arbuscular* (upon target inactivation of H3 deacetylase) (Mao et al., 2015), respectively. In G2, cyclotheonamide E3 and nostophycin were found, compounds identified before in a marine sponge (Nakao et al., 1998) and in a cyanobacterium (Fujii et al., 1999), respectively. In addition, the fractions were analyzed by NMR but their chemical complexity and low abundance of each constituent of the mixture hindered stringent spectral assignments (data not shown).

CONCLUSION AND FUTURE PERSPECTIVES

The aim of this study was to examine if ionic liquids supplements, specifically choline-based ones, can support discovery of bioactive secondary metabolites in three distinct fungi – *N. crassa, A. nidulans*, and *A. fumigatus*. The usage of ionic liquid-based supplements has been shown before to greatly impact fungal metabolism, leading to upregulation of the expression of genes coding in secondary metabolism, including some backbone genes, and altering the ensuing extracellular metabolic footprint. Building on this past evidence, choline-based ionic liquids were used as growth media supplements (at concentrations below their MIC, **Table 1**), testing different anions and concentrations as well. In either fungus, the media supplementation altered the diversity of compounds accumulating extracellularly (**Figure 1**). The peptidome composition of the obtained crude extracts (inferred by the abundance/diversity of amino acids in the corresponding hydrolyzates) was also impacted by the supplementation (**Supplementary Table 1**). Specifically, ACC and Aib levels showed increasing trend in *N. crassa* and *A. fumigatus*, respectively (**Figure 2**). Moreover, these metabolite extracts reduced the metabolic activity of bacterial cells, in some cases leading to cell lysis (**Figures 3**, **4**). Based on the estimated IC_{50} values (**Table 2**), the supplementation compared to control conditions, increased greatly the bactericidal activity of the derived *N. crassa* extracts, but not those of *A. fumigatus*. At this stage, the observed activity cannot be linked to a specific compound. To pinpoint potential candidates, untargeted MS analyses using the GNPS platform were applied. A total of 52 and 18 compounds were identified in *N. crassa* and *A. fumigatus* extracts derived from the ionic-liquid supplemented cultures, respectively (**Figure 5** and **Supplementary Table 4**). By eliminating compounds of low signal intensity, the most promising candidates potentially produced by *A. fumigatus* are macrolides and terpenes, whereas for *N. crassa* are cyclic peptides, including five depsipeptides; structurally of high pharmacological interest (**Table 3**). Fractionation of the later, added another cyclic peptide to the pool of compounds annotated through the GNPS tool; likely of low abundance in the crude extract. Analysis of their whole chemical landscape highlighted, however, a weak sample deconvolution with many compounds present in the three fractions. Through their direct query in the NRPro database, five additional hits of cyclic peptides (including one depsipeptide) were found (**Supplementary Table 4**).

The usage of GNPS as a dereplication strategy clearly showed that a rich diversity of structures can be generated under an ionic liquid stimulus. It allowed for a rapid comparison of the collected MS data, to obtain a "holistic" view of the chemical space of the fungal extracts, getting one step closer to the identification of novel bioactive metabolites. Its effectiveness can be illustrated by two related examples: diversity of secondary metabolites in *Botryosphaeria mamani* upon medium supplementation with histone deacetylase inhibitors (Triastuti et al., 2019), and in *Penicillium nordicum*, which completed with isotope labeling analyses, led to identification of 69 unknown metabolites (Hautbergue et al., 2019). The tool is subjected to the availability of similar structures in the GNPS databases (as highlighted by additional identifications in the fractions when using NRPro); all the identifications proposed herein remain putative and further confirmation is therefore required. Database search tools, e.g., Mascot, usually used for the MS/MS identification of linear peptides are not directly applicable to cyclopeptides or depsipeptides that generate very complex fragmentation patterns. In addition, >300 NPAAs can be incorporated into fungal NRPs, further enlarging the associated chemical space. None of the compounds putatively identified (**Supplementary Tables 4**, **5**) contains either ACC or Aib, irrespectively of their detection in the hydrolyzates of the crude extracts/fractions. This is likely due to the lack of similar structures in the GNPS and NRPro databases. Besides, it reveals that the chemical space of either extract remains to be fully disclosed. Despite these limitations, specifically the GNPS tool exposed the most promising candidates – cyclic (depsi)peptides of *N. crassa*, setting foundations for their isolation and identification in the near future.

The data attained highlight the capacity of *N. crassa* to generate a rich portfolio of cyclic peptide-based metabolites, with high pharmacological interest. In the genome of *N. crassa*, only four putative NRPS genes have been assigned, none, however, has been linked to the produced metabolite to date. Preliminary tests suggest that three of these genes suffered upregulation in the supplemented medium compared to control (data not shown). Due to the scarcity of NRPS genes in *N. crassa* genome, ionic-liquid supplementation shows matchless potential to link each NRPS to its peptide-product(s), deserving focused analysis soon.

TABLE 3 | Untargeted LC-MS/MS analyses of *A. fumigatus* and *N. crassa* extracts derived from ionic liquid supplemented cultures suggests the accumulation, among other metabolites of macrolides and peptides, respectively.

Putative identification	Exact mass	Condition	Class	Reported activity	References
Aspergillus fumigatus					
Dolabelide C	796.497	G2	Macrolide	Antitumor	Suenaga et al., 1997
Roflamycoin	738.455	G2	Macrolide	Antifungal; antiprotozoalc	Schlegel and Thrum, 1971; Han et al., 2021
Efomycin G	1010.58	G2	Macrolide	Antibacterial; antitumor	Wu et al., 2013; Supong et al., 2016; Gui et al., 2019
Antibiotic A 59770A	1000.63	G1, G2	Macrolide	Pesticidal agents	Hoehn et al., 1990
Aerucyclamide D*	603.06	G1, G2	Cyclic peptide	Antiparasitic	Portmann et al., 2008
7α,27-Dihydroxycholesterol*	401.342	G1, G2	Steroid	Not reported	Brown and Jessup, 1999
Auriculoside B	1214.64	G1, G2	Pregnane glycoside	Antitumor	Zhang et al.
CID 102041441	810.477	G1, G2	Pregnane glycoside	Not reported	Deng et al., 2010
Neurospora crassa					
Levorin A3	1092.58	G4	Macrolide	Antifungal	Pawlak et al., 2005; Szczeblewski et al., 2017
Dideoxy-Sandramycin	1188.56	G4	Cyclic depsipeptide	Antitumor	Boger and Chen, 1997
Discokiolide A	1026.51		Cyclic depsipeptide	Antitumor	Tada et al., 1992
Chaiyaphumine D	644.296	G4	Cyclic depsipeptide	Not reported	Grundmann et al., 2014
Chlorodestruxin	629.319	G4	Cyclic depsipeptide	Anti-insecticidal	Gupta et al., 1989
SF-1902-A4	667.452	G2, G4	Cyclic lipodepsipeptide	Antibacterial	
Syringostatin A	1178.59	G4	Cyclic lipodepsipeptide	Antifungal	Sorensen et al., 1996
Val-Val-Pro-Val-Pro-Asn*	651.396	G4	Peptide	Not reported	In-house library from GNPS
Pepsin S 735A	685.463	All samples	Peptide	Protease inhibitor	Morishima et al., 1970; OMURA et al., 1986
Halo-toxin	626.343	G4	Peptide	Not reported	Kajimoto et al., 1989
Fru-Leu-Ile*	407.239		Peptide	Not reported	In-house library from GNPS
Ile-Pro-Ile*	342.239	G4	Peptide	Not reported	In-house library from GNPS
Mollamide B	696.367	G4	Cyclic peptide	Antimalarial, antivirus, antitumor	Donia et al., 2008
Pseudostellarin C	812.443	G4	Cyclic peptide	Tyrosinase inhibitor; antitumor	Morita et al., 1994
Wewakazole	1140.54	G1, G4	Cyclic peptide	Antitumor	Nogle et al., 2003; Gogineni and Hamann, 2018
Corticosterone*	347.222	G2, G4	Terpene	Not reported	Steiger and Reichstein, 1938
Leukotriene E4 methyl ester*	459.22	All samples	Lipid	Immunomodulation	Cohen et al., 2002
Orizabin XIV	1120.6	G3	Glycolipid	Antitumor; β-1-3-glucan synthase inhibitor; antibacterial	Pereda-Miranda and Hernández-Carlos, 2002
Sublanceoside K1	1082.57	G1, G2, G3	Terpene glycoside	Not reported	Warashina and Noro, 2006

Putative identifications retrieved by using molecular networking analysis and compound dereplication in GNPS, from spectral match (*) and in silico tool DEREPLICATOR+. For N. crassa, isolated fractions (G1, G2, and G3) as well as crude (G4) extracts were analyzed; whereas for A. fumigatus, extracts from cultures supplemented with choline decanoate at 50% (G1) and 80% (G2) of the MIC. Only peaks with signal intensity $>1.5{\cdot}10^7$ (for A. fumigatus: G1 and G2) and $>3{\cdot}10^7$ (for N. crassa: G4) in the total ion chromatogram are depicted (Full list in ***Supplementary Table 3****). For N. crassa fractions, G1 to G3, the two most intense peaks in the total ion chromatogram are depicted.*

DATA AVAILABILITY STATEMENT

The datasets presented in this study can be found in online repositories. The names of the repository/repositories and accession number(s) can be found below: EBI – MTBLS5072.

AUTHOR CONTRIBUTIONS

CSP and GG supervised the project. CSP supervised the interpretation of data and prepared the final version of the manuscript. All authors have made substantial contributions to the acquisition, analysis and interpretation of data, and contributed to the drafting of the manuscript.

FUNDING

This work was supported by the FCT – Fundação para a Ciência e a Tecnologia, I.P., through MOSTMICRO-ITQB R&D Unit (UIDB/04612/2020) and LS4FUTURE Associated Laboratory (LA/P/0087/2020), as well as the projects PTDC/CTA-AMB/6587/2020 and AAC 01/SAICT/2016 (CERMAX, ITQB-NOVA, Oeiras, Portugal). This work was also partially supported by the Portuguese Platform of BioImaging (PPBI) (PPBI-POCI-01-0145-FEDER-022122), co-funded by national funds from Orçamento de Estado (OE), and by European funds from Fundo Europeu de Desenvolvimento Regional (FEDER). MR, PS, and IM are grateful to FCT for the fellowship PD/BD/113989/2015, PD/BD/135481/2018 and for the working contract financed by national funds under Norma Transitória D.L. no. 57/2016, respectively.

ACKNOWLEDGMENTS

We acknowledge the use of microscope at the Bacterial Imaging Cluster (ITQB-NOVA). We are thankful to Pedro Lamosa and Maria C. Leitão (ITQB NOVA) for support with the NMR and chromatographic analyses, respectively. Finally, we acknowledge Paula Alves (ITQB alumni) for collection of preliminary data that inspired this study.

SUPPLEMENTARY MATERIAL

The Supplementary Material for this article can be found online at: https://www.frontiersin.org/articles/10.3389/fmicb.2022.946286/full#supplementary-material

REFERENCES

Alves, P. C., Hartmann, D. O., Nunez, O., Martins, I., Gomes, T. L., Garcia, H., et al. (2016). Transcriptomic and metabolomic profiling of ionic liquid stimuli unveils enhanced secondary metabolism in Aspergillus nidulans. *BMC Genomics* 17:284. doi: 10.1186/s12864-016-2577-6

Armenta, J. M., Cortes, D. F., Pisciotta, J. M., Shuman, J. L., Blakeslee, K., Rasoloson, D., et al. (2010). Sensitive and rapid method for amino acid quantitation in malaria biological samples using AccQ Tag ultra performance liquid chromatography-electrospray ionization-MS/MS with multiple reaction monitoring. *Anal. Chem.* 82, 548–558. doi: 10.1021/ac901790q

Aron, A. T., Gentry, E. C., McPhail, K. L., Nothias, L. F., Nothias-Esposito, M., Bouslimani, A., et al. (2020). Reproducible molecular networking of untargeted mass spectrometry data using GNPS. *Nat. Protoc.* 15, 1954–1991. doi: 10.1038/S41596-020-0317-5

Arslan, I. (2022). "Trends in antimicrobial resistance in healthcare-associated infections: a global concern," in *Encyclopedia of Infection and Immunity,* ed. N. Rezaei (Amsterdam: Elsevier), 652–661. doi: 10.1016/B978-0-12-818731-9.00111-7

Bayram, O., Krappmann, S., Ni, M., Bok, J. W., Helmstaedt, K., Valerius, O., et al. (2008). VelB/VeA/LaeA complex coordinates light signal with fungal development and secondary metabolism. *Science* 320, 1504–1506. doi: 10.1126/science.1155888

Bayram, ÖS., Dettmann, A., Karahoda, B., Moloney, N. M., Ormsby, T., McGowan, J., et al. (2019). Control of development, secondary metabolism and light-dependent carotenoid biosynthesis by the velvet complex of Neurospora crassa. *Genetics* 212, 691–710.

Begani, J., Lakhani, J., and Harwani, D. (2018). Current strategies to induce secondary metabolites from microbial biosynthetic cryptic gene clusters. *Ann. Microbiol.* 68, 419–432. doi: 10.1007/S13213-018-1351-1

Bergmann, S., Schümann, J., Scherlach, K., Lange, C., Brakhage, A. A., and Hertweck, C. (2007). Genomics-driven discovery of PKS-NRPS hybrid metabolites from Aspergillus nidulans. *Nat. Chem. Biol.* 3, 213–217. doi: 10.1038/nchembio869

Bhattarai, K., Kabir, M. E., Bastola, R., and Baral, B. (2021). Fungal natural products galaxy: biochemistry and molecular genetics toward blockbuster drugs discovery. *Adv. Genet.* 107, 193–284. doi: 10.1016/bs.adgen.2020.11.006

Bills, G. F., and Gloer, J. B. (2016). Biologically Active Secondary Metabolites from the Fungi. *Microbiol. Spectr.* 4, 1–32. doi: 10.1128/microbiolspec.funk-0009-2016

Bode, H. B., Bethe, B., Höfs, R., and Zeeck, A. (2002). Big effects from small changes: possible ways to explore nature's chemical diversity. *Chembiochem* 3, 619–627. doi: 10.1002/1439-7633(20020703)3:7<619::AID-CBIC619>3.0.CO;2-9

Boethling, R. S., Sommer, E., and DiFiore, D. (2007). Designing Small Molecules for Biodegradability. *Chem. Rev.* 107, 2207–2227. doi: 10.1021/cr050952t

Brakhage, A. A. (2012). Regulation of fungal secondary metabolism. *Nat. Rev. Microbiol.* 11, 21–32. doi: 10.1038/nrmicro2916

Brückner, H., Fox, S., and Degenkolb, T. (2019). Sequences of acretocins, peptaibiotics Containing the rare 1-aminocyclopropanecarboxylic acid, from Acremonium crotocinigenum CBS 217.70. *Chem. Biodivers.* 16:e1900276. doi: 10.1002/cbdv.201900276

Cacho, R. A., Chooi, Y. H., Zhou, H., and Tang, Y. (2013). Complexity generation in fungal polyketide biosynthesis: a spirocycle-forming P450 in the concise pathway to the antifungal drug griseofulvin. *ACS Chem. Biol.* 8, 2322–2330. doi: 10.1021/cb400541z

Cacho, R. A., Jiang, W., Chooi, Y. H., Walsh, C. T., and Tang, Y. (2012). Identification and characterization of the echinocandin b biosynthetic gene cluster from Emericella rugulosa NRRL 11440. *J. Am. Chem. Soc.* 134, 16781–16790. doi: 10.1021/ja307220z

Calvo, A. M., Wilson, R. A., Bok, J. W., and Keller, N. P. (2002). Relationship between secondary metabolism and fungal development. *Microbiol. Mol. Biol. Rev.* 66, 447–459. doi: 10.1128/MMBR.66.3.447-459.2002

Castelli, M. V., Cortés, J. C. G., Escalante, A. M., Bah, M., Pereda-Miranda, R., Ribas, J. C., et al. (2002). In vitro inhibition of 1,3-β-Glucan synthase by glycolipids from convolvulaceous species. *Planta Med.* 68, 739–742. doi: 10.1055/S-2002-33791

Chiang, Y.-M., Lee, K.-H., Sanchez, J., Keller, N. P., and Wang, C. C. (2009). Unlocking Fungal Cryptic Natural Produts. *Nat. Prod. Commun.* 11, 1505–1510. doi: 10.1038/jid.2014.371

Clinical and Laboratory Standards Institute [CLSI] (2018). *Performance Standards for Antimicrobial Susceptibility Testing*, 28th Edn. Wayne, PA: Clinical and Laboratory Standards Institute.

Degenkolb, T., and Brückner, H. (2008). Peptaibiomics: towards a myriad of bioactive peptides containing C(alpha)-dialkylamino acids? *Chem. Biodivers.* 5, 1817–1843. doi: 10.1002/cbdv.200890171

Degenkolb, T., Berg, A., Gams, W., Schlegel, B., and Gräfe, U. (2003). The occurrence of peptaibols and structurally related peptaibiotics in fungi and their mass spectrometric identification via diagnostic fragment ions. *J. Pept. Sci.* 9, 666–678. doi: 10.1002/psc.497

Ding, J.-H., Ding, Z.-G., Zhao, J.-Y., Li, M.-G., Hu, D.-B., Jiang, X.-J., et al. (2019). A new pregnane steroid from cultures of Aspergillus versicolor. *Nat. Prod. Res.* 33, 1885–1890. doi: 10.1080/14786419.2018.1478828

Ding, Y., Ting, J. P., Liu, J., Al-Azzam, S., Pandya, P., and Afshar, S. (2020). Impact of non-proteinogenic amino acids in the discovery and development of peptide therapeutics. *Amino Acids* 52, 1207–1226. doi: 10.1007/S00726-020-02890-9

El Maddah, F., Nazir, M., and König, G. M. (2017). The Rare Amino Acid Building Block 3-(3-furyl)-Alanine in the Formation of Non-ribosomal Peptides. *Nat. Prod. Commun.* 12, 147–150. doi: 10.1177/1934578X1701200140

Fischer, J., Müller, S. Y., Netzker, T., Jäger, N., Gacek-Matthews, A., Scherlach, K., et al. (2018). Chromatin mapping identifies BasR, a key regulator of bacteria-triggered production of fungal secondary metabolites. *eLife* 7:e40969. doi: 10.7554/eLife.40969

Fox, E. M., and Howlett, B. J. (2008). Secondary metabolism: regulation and role in fungal biology. *Curr. Opin. Microbiol.* 11, 481–487. doi: 10.1016/j.mib.2008.10.007

Fredenhagen, A., Molleyres, L.-P., Böhlendorf, B., and Laue, G. (2006). Structure determination of neoefrapeptins A to N: peptides with insecticidal activity produced by the fungus Geotrichum candidum. *J. Antibiot.* 59, 267–280. doi: 10.1038/ja.2006.38

Fujii, K., Sivonen, K., Kashiwagi, T., Hirayama, K., and Harada, K. (1999). Nostophycin, a Novel Cyclic Peptide from the Toxic Cyanobacterium Nostoc sp. 152. *J. Org. Chem.* 64, 5777–5782. doi: 10.1021/jo982306i

Gentilucci, L., De Marco, R., and Cerisoli, L. (2010). Chemical Modifications Designed to Improve Peptide Stability: Incorporation of Non-Natural Amino Acids, Pseudo-Peptide Bonds, and Cyclization. *Curr. Pharm. Des.* 16, 3185–3203. doi: 10.2174/138161210793292555

Gil-De-la-fuente, A., Mamani-Huanca, M., Stroe, M. C., Saugar, S., Garcia-Alvarez, A., Brakhage, A. A., et al. (2021). Aspergillus Metabolome Database for Mass Spectrometry Metabolomics. *J. Fungi* 7:387. doi: 10.3390/JOF7050387

Gogineni, V., and Hamann, M. T. (2018). Marine natural product peptides with therapeutic potential: chemistry, biosynthesis, and pharmacology. *Biochim. Biophys. Acta Gen. Subj.* 1862, 81–196. doi: 10.1016/j.bbagen.2017.08.014

Hagiwara, D., Sakai, K., Suzuki, S., Umemura, M., Nogawa, T., Kato, N., et al. (2017). Temperature during conidiation affects stress tolerance, pigmentation, and trypacidin accumulation in the conidia of the airborne pathogen Aspergillus fumigatus. *PLoS One* 12:e0177050. doi: 10.1371/journal.pone.0177050

Han, X., Wang, J., Liu, L., Shen, F., Meng, Q., Li, X., et al. (2021). Identification and predictions regarding the biosynthesis pathway of polyene macrolides produced by Streptomyces roseoflavus Men-myco-93-63. *Appl. Environ. Microbiol.* 87, 1–13. doi: 10.1128/AEM.03157-20

Hartmann, D. O., Piontkivska, D., Moreira, C. J. S., and Pereira, C. S. (2019). Ionic liquids chemical stress triggers sphingoid base accumulation in aspergillus nidulans. *Front. Microbiol.* 10:864. doi: 10.3389/fmicb.2019.00864

Hartmann, D. O., Shimizu, K., Siopa, F., Leitão, M. C., Afonso, C. A. M., Canongia Lopes, J. N., et al. (2015). Plasma membrane permeabilisation by ionic liquids: a matter of charge. *Green Chem.* 17, 4587–4598. doi: 10.1039/C5GC01472G

Hautbergue, T., Jamin, E. L., Costantino, R., Tadrist, S., Meneghetti, L., Tabet, J. C., et al. (2019). Combination of isotope labeling and molecular networking of tandem mass spectrometry data to reveal 69 unknown metabolites produced by Penicillium nordicum. *Anal. Chem.* 91, 12191–12202. doi: 10.1021/acs.analchem.9b01634

Hertweck, C. (2009). The biosynthetic logic of polyketide diversity. *Angew. Chem. Int. Ed.* 48, 4688–4716. doi: 10.1002/anie.200806121

Hoehn, M. M., Michel, K. H., and Yao, R. C.-F. (1990). *Macrolide Antibiotics. European Patent No 0 398 588 A1*. Munich: European Patent Office.

Keller, N. P. (2019). Fungal secondary metabolism: regulation, function and drug discovery. *Nat. Rev. Microbiol.* 17, 167–180. doi: 10.1038/s41579-018-0121-1

Keller, N. P., Turner, G., and Bennett, J. W. (2005). Fungal Secondary Metabolism - From Biochemistry to Genomics. *Nat. Rev. Microbiol.* 3, 937–947. doi: 10.1038/nrmicro1286

Kessner, D., Chambers, M., Burke, R., Agus, D., and Mallick, P. (2008). ProteoWizard: open source software for rapid proteomics tools development. *Bioinformatics* 24, 2534–2536. doi: 10.1093/bioinformatics/btn323

Khaldi, N., Seifuddin, F. T., Turner, G., Haft, D., Nierman, W. C., Wolfe, K. H., et al. (2010). SMURF: genomic mapping of fungal secondary metabolite clusters. *Fungal Genet. Biol.* 47, 736–741. doi: 10.1016/j.fgb.2010.06.003

Klassen, J. L., Lee, S. R., Poulsen, M., Beemelmanns, C., and Kim, K. H. (2019). Efomycins K and L from a termite-associated Streptomyces sp. M56 and their putative biosynthetic origin. *Front. Microbiol.* 10:1739. doi: 10.3389/fmicb.2019.01739

Krause, C., Kirschbaum, J., and Brückner, H. (2006). Peptaibiomics: an advanced, rapid and selective analysis of peptaibiotics/peptaibols by SPE/LC-ES-MS. *Amino Acids* 30, 435–443. doi: 10.1007/s00726-005-0275-9

Lima, S. L., Colombo, A. L., and de Almeida Junior, J. N. (2019). Fungal cell wall: emerging antifungals and drug resistance. *Front. Microbiol.* 10:2573. doi: 10.3389/fmicb.2019.02573

Lin, H. C., Chooi, Y. H., Dhingra, S., Xu, W., Calvo, A. M., and Tang, Y. (2013). The fumagillin biosynthetic gene cluster in Aspergillus fumigatus encodes a cryptic terpene cyclase involved in the formation of β-trans-bergamotene. *J. Am. Chem. Soc.* 135, 4616–4619. doi: 10.1021/ja312503y

Liu, Z., Zhao, Y., Huang, C., and Luo, Y. (2021). Recent advances in silent gene cluster activation in Streptomyces. *Front. Bioeng. Biotechnol.* 9:632230. doi: 10.3389/fbioe.2021.632230

Macheleidt, J., Mattern, D. J., Fischer, J., Netzker, T., Weber, J., Schroeckh, V., et al. (2016). Regulation and Role of Fungal Secondary Metabolites. *Annu. Rev. Genet.* 50, 371–392. doi: 10.1146/annurev-genet-120215-035203

Mao, X.-M., Xu, W., Li, D., Yin, W.-B., Chooi, Y.-H., Li, Y.-Q., et al. (2015). Epigenetic genome mining of an endophytic fungus leads to the pleiotropic biosynthesis of natural products. *Angew. Chem. Int. Ed.* 54, 7592–7596. doi: 10.1002/anie.201502452

Marik, T., Tyagi, C., Racić, G., Rakk, D., Szekeres, A., Vágvölgyi, C., et al. (2018). New 19-Residue Peptaibols from Trichoderma Clade Viride. *Microorganisms* 6:85. doi: 10.3390/microorganisms6030085

Martins, I., Hartmann, D. O., Alves, P. C., Planchon, S., Renaut, J., Leitão, M. C., et al. (2013). Proteomic alterations induced by ionic liquids in Aspergillus nidulans and Neurospora crassa. *J. Proteomics* 94, 262–278. doi: 10.1016/j.jprot.2013.09.015

Mathew Valayil, J. (2016). Activation of Microbial Silent Gene Clusters: Genomics Driven Drug Discovery Approaches. *Biochem. Anal. Biochem.* 5, 2–5. doi: 10.4172/2161-1009.1000276

McErlean, M., Overbay, J., and Van Lanen, S. (2019). Refining and expanding nonribosomal peptide synthetase function and mechanism. *J. Ind. Microbiol. Biotechnol.* 46, 493–513. doi: 10.1007/S10295-018-02130-W

Meyer, V., Andersen, M. R., Brakhage, A. A., Braus, G. H., Caddick, M. X., Cairns, T. C., et al. (2016). Current challenges of research on filamentous fungi in relation to human welfare and a sustainable bio-economy: a white paper. *Fungal Biol. Biotechnol.* 3:6. doi: 10.1186/s40694-016-0024-8

Mohimani, H., Gurevich, A., Shlemov, A., Mikheenko, A., Korobeynikov, A., Cao, L., et al. (2018). Dereplication of microbial metabolites through database search of mass spectra. *Nat. Commun.* 9, 1–12. doi: 10.1038/s41467-018-06082-8

Mootz, H. D., Schwarzer, D., and Marahiel, M. A. (2002). Ways of assembling complex natural products on modular nonribosomal peptide synthetases. *ChemBioChem* 3, 490–504. doi: 10.1002/1439-7633(20020603)3:6<490::AID-CBIC490<3.0.CO;2-N

Morishita, Y., Zhang, H., Taniguchi, T., Mori, K., and Asai, T. (2019). The discovery of fungal polyene macrolides via a postgenomic approach reveals a polyketide macrocyclization by trans-acting thioesterase in fungi. *Org. Lett.* 21, 4788–4792. doi: 10.1021/acs.orglett.9b01674

Nakao, Y., Oku, N., Matsunaga, S., and Fusetani, N. (1998). Cyclotheonamides E2 and E3, New Potent Serine Protease Inhibitors from the Marine Sponge of the Genus Theonella. *J. Nat. Prod.* 61, 667–670. doi: 10.1021/np970544n

Netzker, T., Fischer, J., Weber, J., Mattern, D. J., König, C. C., Valiante, V., et al. (2015). Microbial communication leading to the activation of silent fungal secondary metabolite gene clusters. *Front. Microbiol.* 6:299. doi: 10.3389/fmicb.2015.00299

Newman, D. J., and Cragg, G. M. (2020). Natural Products as Sources of New Drugs over the Nearly Four Decades from 01/1981 to 09/2019. *J. Nat. Prod.* 83, 770–803. doi: 10.1021/acs.jnatprod.9b01285

Niu, X., Thaochan, N., and Hu, Q. (2020). Diversity of linear non-ribosomal peptide in biocontrol fungi. *J. Fungi* 6:61. doi: 10.3390/jof6020061

Noverr, M. C., Toews, G. B., and Huffnagle, G. B. (2002). Production of prostaglandins and leukotrienes by pathogenic fungi. *Infect. Immun.* 70, 400–402. doi: 10.1128/IAI.70.1.400-402.2002

Omoto, S., Ogino, H., and Inouye, S. (1981). Studies on SF=1902 A2 A5, minor components of SF-1902 (globomycin). *J. Antibiot.* 34, 1416–1423. doi: 10.7164/antibiotics.34.1416

Penrose, D. M., Moffatt, B. A., and Glick, B. R. (2001). Determination of 1-aminocyclopropane-1-carboxylic acid (ACC) to assess the effects of ACC deaminase-containing bacteria on roots of canola seedlings. *Can. J. Microbiol.* 47, 77–80. doi: 10.1139/w00-128

Petkovic, M., Ferguson, J. L., Gunaratne, H. Q. N., Ferreira, R., Leitão, M. C., Seddon, K. R., et al. (2010). Novel biocompatible cholinium-based ionic liquids—toxicity and biodegradability. *Green Chem.* 12, 643–649. doi: 10.1039/B922247B

Petkovic, M., Ferguson, J., Bohn, A., Trindade, J., Martins, I., Carvalho, M. B., et al. (2009). Exploring fungal activity in the presence of ionic liquids. *Green Chem.* 11, 889–894. doi: 10.1039/b823225c

Portmann, C., Blom, J. F., Kaiser, M., Brun, R., Jüttner, F., and Gademann, K. (2008). Isolation of aerucyclamides C and D and structure revision of microcyclamide 7806A: Heterocyclic ribosomal peptides from Microcystis aeruginosa PCC 7806 and their antiparasite evaluation. *J. Nat. Prod.* 71, 1891–1896. doi: 10.1021/np800409z

Pusztahelyi, T., Holb, I. J., and Pócsi, I. (2015). Secondary metabolites in fungus-plant interactions. *Front. Plant Sci.* 6:573. doi: 10.3389/fpls.2015.00573

Ribeiro, D. M., Planchon, S., Leclercq, C. C., Dentinho, M. T. P., Bessa, R. J. B., Santos-Silva, J., et al. (2020). The effects of improving low dietary protein utilization on the proteome of lamb tissues. *J. Proteomics* 223:103798. doi: 10.1016/j.jprot.2020.103798

Ricart, E., Pupin, M., Müller, M., and Lisacek, F. (2020). Automatic Annotation and Dereplication of Tandem Mass Spectra of Peptidic Natural Products. *Anal. Chem.* 92, 15862–15871. doi: 10.1021/acs.analchem.0c03208

Rodrigues, A. G. (2016). "Secondary Metabolism and Antimicrobial Metabolites of Aspergillus," in *New and Future Developments in Microbial Biotechnology and Bioengineering: Aspergillus System Properties and Applications*, ed. V. K. Gupta (Amsterdam: Elsevier), 81–93. doi: 10.1016/B978-0-444-63505-1.00006-3

Schlegel, R., Thrum, H., Zielinski, J., and Borowski, E. (1981). The structure of roflamycoin, a new polyene macrolide antifungal antibiotic. *J. Antibiot.* 34, 122–123. doi: 10.7164/antibiotics.34.122

Shannon, P., Markiel, A., Ozier, O., Baliga, N. S., Wang, J. T., Ramage, D., et al. (2003). Cytoscape: a software environment for integrated models of biomolecular interaction networks. *Genome Res.* 13, 2498–2504. doi: 10.1101/gr.1239303

Sivanathan, S., and Scherkenbeck, J. (2014). Cyclodepsipeptides: A Rich Source of Biologically Active Compounds for Drug Research. *Molecules* 19, 12368–12420. doi: 10.3390/molecules190812368

Sorensen, K. N., Kim, K. H., and Takemoto, J. Y. (1996). In vitro antifungal and fungicidal activities and erythrocyte toxicities of cyclic lipodepsinonapeptides produced by *Pseudomonas* syringae pv. syringae. *Antimicrob. Agents Chemother.* 40, 2710–2713. doi: 10.1128/aac.40.12.2710

Stone, T. A., and Deber, C. M. (2017). Therapeutic design of peptide modulators of protein-protein interactions in membranes. *Biochim. Biophys. Acta Biomembr.* 1859, 577–585. doi: 10.1016/j.bbamem.2016.08.013

Suenaga, K., Nagoya, T., Shibata, T., Kigoshi, H., and Yamada, K. (1997). Dolabelides C and D, cytotoxic macrolides isolated from the sea hare Dolabella auricularia. *J. Nat. Prod.* 60, 155–157. doi: 10.1021/np960612q

Sumner, L. W., Amberg, A., Barrett, D., Beale, M. H., Beger, R., Daykin, C. A., et al. (2007). Proposed minimum reporting standards for chemical analysis Chemical Analysis Working Group (CAWG) Metabolomics Standards Initiative (MSI). *Metabolomics* 3, 211–221. doi: 10.1007/S11306-007-0082-2

Sy-Cordero, A. A., Graf, T. N., Adcock, A. F., Kroll, D. J., Shen, Q., Swanson, S. M., et al. (2011). Cyclodepsipeptides, Sesquiterpenoids, and Other Cytotoxic Metabolites from the Filamentous Fungus Trichothecium sp. (MSX 51320). *J. Nat. Prod.* 74, 2137–2142. doi: 10.1021/np2004243

Taevernier, L., Wynendaele, E., Gevaert, B., and De Spiegeleer, B. (2017). Chemical classification of cyclic depsipeptides. *Curr. Protein Pept. Sci.* 18, 425–452. doi: 10.2174/1389203717666161128141438

Triastuti, A., Vansteelandt, M., Barakat, F., Trinel, M., Jargeat, P., Fabre, N., et al. (2019). How histone deacetylase inhibitors alter the secondary metabolites of Botryosphaeria mamane, an endophytic fungus isolated from Bixa orellana. *Chem. Biodivers.* 16:e1800485. doi: 10.1002/cbdv.201800485

Tsitsigiannis, D. I., and Keller, N. P. (2007). Oxylipins as developmental and host–fungal communication signals. *Trends Microbiol.* 15, 109–118. doi: 10.1016/j.tim.2007.01.005

Wang, M., Carver, J. J., Phelan, V. V., Sanchez, L. M., Garg, N., Peng, Y., et al. (2016). Sharing and community curation of mass spectrometry data with Global Natural Products Social Molecular Networking. *Nat. Biotechnol.* 34, 828–837. doi: 10.1038/nbt.3597

Wang, X., Gong, X., Li, P., Lai, D., and Zhou, L. (2018). Structural Diversity and Biological Activities of Cyclic Depsipeptides from Fungi. *Molecules* 23:169. doi: 10.3390/molecules23010169

Watrous, J., Roach, P., Alexandrov, T., Heath, B. S., Yang, J. Y., Kersten, R. D., et al. (2012). Mass spectral molecular networking of living microbial colonies. *Proc. Natl. Acad. Sci. U.S.A.* 109, E1743–E1752. doi: 10.1073/pnas.1203689109

World Health Organization [WHO] (2021). *Global Antimicrobial Resistance and Use Surveillance System (GLASS) Report: 2021*. Geneva: World Health Organization.

Wu, C., Tan, Y., Gan, M., Wang, Y., Guan, Y., Hu, X., et al. (2013). Identification of elaiophylin derivatives from the marine-derived actinomycete Streptomyces sp. 7-145 using PCR-based screening. *J. Nat. Prod.* 76, 2153–2157. doi: 10.1021/NP4006794

Xiong, Q., Hassan, S. A., Wilson, W. K., Han, X. Y., May, G. S., Tarrand, J. J., et al. (2005). Cholesterol import by Aspergillus fumigatus and its influence on antifungal potency of sterol biosynthesis inhibitors. *Antimicrob. Agents Chemother.* 49, 518–524. doi: 10.1128/AAC.49.2.518-524.2005

Yu, M. L., Guan, F. F., Cao, F., Jia, Y. L., and Wang, C. Y. (2018). A new antiviral pregnane from a gorgonian-derived Cladosporium sp. fungus. *Nat. Prod. Res.* 32, 1260–1266. doi: 10.1080/14786419.2017.1342086

Conflict of Interest: The authors declare that the research was conducted in the absence of any commercial or financial relationships that could be construed as a potential conflict of interest.

Publisher's Note: All claims expressed in this article are solely those of the authors and do not necessarily represent those of their affiliated organizations, or those of the publisher, the editors and the reviewers. Any product that may be evaluated in this article, or claim that may be made by its manufacturer, is not guaranteed or endorsed by the publisher.

frontiers | Frontiers in Microbiology

ORIGINAL RESEARCH
published: 28 July 2022
doi: 10.3389/fmicb.2022.947226

β-Carboline Alkaloids From the Deep-Sea Fungus *Trichoderma* sp. MCCC 3A01244 as a New Type of Anti-pulmonary Fibrosis Agent That Inhibits TGF-β/Smad Signaling Pathway

*Meng-Jiao Hao[1], Pei-Nan Chen[1], Hou-Jin Li[2], Feng Wu[1], Guang-Yu Zhang[1], Zong-Ze Shao[3], Xiu-Pian Liu[3], Wen-Zhe Ma[4], Jun Xu[1], Taifo Mahmud[5] and Wen-Jian Lan[1]**

[1] School of Pharmaceutical Sciences, Sun Yat-sen University, Guangzhou, China, [2] School of Chemistry, Sun Yat-sen University, Guangzhou, China, [3] Key Laboratory of Marine Biogenetic Resources, Third Institute of Oceanography, Ministry of Natural Resources, Xiamen, China, [4] State Key Laboratory of Quality Research in Chinese Medicine, Macau University of Science and Technology, Macau, Macau SAR, China, [5] Department of Pharmaceutical Sciences, Oregon State University, Corvallis, OR, United States

OPEN ACCESS

Edited by:
Peng Zhang,
Tobacco Research Institute (CAAS), China

Reviewed by:
Bin Wu,
Zhejiang University, China
Guoqiang Li,
Ocean University of China, China

***Correspondence:**
Wen-Jian Lan
lanwj@mail.sysu.edu.cn

Specialty section:
This article was submitted to Antimicrobials, Resistance and Chemotherapy, a section of the journal Frontiers in Microbiology

Received: *18 May 2022*
Accepted: *23 June 2022*
Published: *28 July 2022*

Citation:
Hao M-J, Chen P-N, Li H-J, Wu F, Zhang G-Y, Shao Z-Z, Liu X-P, Ma W-Z, Xu J, Mahmud T and Lan W-J (2022) β-Carboline Alkaloids From the Deep-Sea Fungus Trichoderma sp. MCCC 3A01244 as a New Type of Anti-pulmonary Fibrosis Agent That Inhibits TGF-β/Smad Signaling Pathway. Front. Microbiol. 13:947226. doi: 10.3389/fmicb.2022.947226

Pulmonary fibrosis is a scarring disease of lung tissue, which seriously threatens human health. Treatment options are currently limited, and effective strategies are still lacking. In the present study, 25 compounds were isolated from the deep-sea fungus *Trichoderma* sp. MCCC 3A01244. Among them, two β-carboline alkaloids, trichocarbolines A (**1**) and C (**4**) are new compounds. The chemical structures of these compounds were elucidated based on their HRESIMS, 1D and 2D NMR spectra, optical rotation calculation, and comparisons with data reported in the literature. Trichocarboline B [(+)- and (–)-enantiomers] had previously been synthesized, and this is its first report as a natural product. Their anti-pulmonary fibrosis (PF) activity and cytotoxicity were investigated. Compounds **1**, **11**, and **13** strongly inhibited TGF-β1-induced total collagen accumulation and showed low cytotoxicity against the HFL1 cell line. Further studies revealed compound **1** inhibited extracellular matrix (ECM) deposition by downregulating the expression of protein fibronectin (FN), proliferating cell nuclear antigen (PCNA), and α-smooth muscle actin (α-SMA). Mechanistic study revealed that compound **1** decreased pulmonary fibrosis by inhibiting the TGF-β/Smad signaling pathway. As a newly identified β-carboline alkaloid, compound **1** may be used as a lead compound for developing more efficient anti-pulmonary fibrosis agents.

Keywords: β-carboline alkaloids, *Trichoderma*, amino acid–directed strategy, anti-pulmonary fibrosis, TGF-β/Smad

INTRODUCTION

Damage to alveolar epithelial cells, excessive proliferation of fibroblasts, and inappropriate deposition of extracellular matrix (ECM) produce pulmonary fibrosis (PF), which leads to scarring, impaired lung function, and ultimately lung failure (Herrera et al., 2018). At least five million people are affected by pulmonary fibrosis globally, and the average life expectancy for people with

pulmonary fibrosis is less than 5 years (Lynch and Belperio, 2012). Pulmonary fibrosis is the main manifestation of the sequelae of COVID-19 (Zhou et al., 2021). PF is estimated to occur in about one-third of patients hospitalized with COVID-19 as of July 2020 (Vasarmidi et al., 2020). To date, two available antifibrotic drugs, pirfenidone and nintedanib have been approved by FDA for treating idiopathic pulmonary fibrosis (IPF). However, clinical application of nintedanib is limited due to poor oral bioavailability, metabolic instability, and off-target side effects (Roth et al., 2015). Treatment with pirfenidone can produce skin and gastrointestinal-related adverse effects (Cottin and Maher, 2015). Hence, more effective and safer drugs for pulmonary fibrosis treatment are urgently needed.

The master target for antifibrotic therapies is the TGF-β pathway. TGF-β is upregulated and activated in fibrotic diseases. TGF-β1 triggers a pro-fibrotic response *via* activation of the Smad-2/3 cascade, which regulates fibroblast phenotype and function, induces myofibroblast transdifferentiation, and promotes ECM deposition (Biernacka et al., 2011). The intervention of the intracellular phosphorylation of Smad-2/3 protein can reduce TGF-β-induced fibrosis (Walton et al., 2017). Thus, exogenous compounds that disrupt TGF-β/Smad signaling and inhibit myofibroblast activation are likely to be potential anti-pulmonary fibrosis drugs.

As part of our efforts to discover new natural products with anti-pulmonary fibrosis activity, we investigated the chemical constituents of a fungal strain, *Trichoderma* sp. MCCC 3A01244, collected at the 3300 m depth in the Northern Basin of the South China Sea. *Trichoderma* species are commonly found in diverse environments (Reino et al., 2008). Fungi from this genus can produce a variety of structurally intriguing compounds, including terpenoids, polyphenols, pyrones, cyclopeptides, and polyketides (Tchameni et al., 2020). Many of them showed various biological activities, including antimicrobial (Shi et al., 2020), antimicroalgal (Zou et al., 2021a), antioxidant (Miyano et al., 2020), antifouling (Yu et al., 2021), anti-hepatitis C virus (HCV) (Li B. et al., 2019), and cytotoxic activities (Liu et al., 2020), implying the potential of *Trichoderma* species as a source of drugs for agricultural and/or human uses. Some *Trichoderma* species have been commercialized as agents to control phytopathogenic fungi or stimulate plant growth (Morán-Diez et al., 2021; Zou et al., 2021b). Here, we report the isolation, structure characterization, anti-PF activity, and cytotoxicity of secondary metabolites isolated from the deep-sea fungus *Trichoderma* sp. MCCC 3A01244. Among them, trichocarboline A (**1**), a β-carboline alkaloid, is potentially anti-pulmonary fibrosis by inhibiting TGF-β/Smad signaling pathway.

MATERIALS AND METHODS

General Experimental Procedures

Optical rotations were measured on an Anton Paar MCP500 polarimeter. IR spectra were obtained on a Bruker Tensor-27 spectrophotometer. UV spectra were measured by a Shimadzu UV-vis-NIR spectrophotometer. NMR spectra were acquired on Bruker Avance II 400 and 500 spectrometers (Bruker Bio Spin AG, Industriestrasse 26, Fallanden, Switzerland). The chemical shifts are referred to the residual solvent signals (acetone-d_6: δ_H 2.05, δ_C 29.8; $CDCl_3$: δ_H 7.26, δ_C 77.2; CD_3OD: δ_H 3.30, δ_C 49.0; DMSO-d_6: δ_H 2.50, δ_C 39.5). HRESIMS data were recorded on Thermo DSQ EI low-resolution and Thermo MAT95XP EI high-resolution mass spectrometers (Thermo Fisher Scientific Inc.). Silica gel (200-300 mesh, Qingdao Marine Chemical Factory) and Sephadex LH-20 (GE Healthcare) were used for column chromatography. Preparative HPLC adopted a Shimadzu LC-20AT HPLC pump (Shimadzu Corporation, Nakagyo-Ku, Kyoto, Japan) with an SPD-20A dual λ absorbance detector (Shimadzu Corporation, Nakagyo-Ku, Kyoto, Japan), as well as a Shim-pack PRC-ODS HPLC column (250 × 20 mm, Shimadzu Corporation, Nakagyo-Ku, Kyoto, Japan) and a Chiral CD-Ph HPLC column (250 × 10 mm, Shimadzu Corporation, Nakagyo-Ku, Kyoto, Japan).

Fungal Material and Fermentation

The deep-sea fungus *Trichoderma* sp. MCCC 3A01244 was obtained from the Marine Culture Collection of China (MCCC). It was originally separated from seawater at the depth of 3300 m in the northern basin of the South China Sea. It was persevered in the School of Pharmaceutical Sciences, Sun Yat-sen University, Guangzhou, China. This fungal strain was identified according to the morphological characteristics and analysis of internal transcribed spacer (ITS) rDNA. The ITS gene sequence was deposited in NCBI's GenBank with the accession number MW581838. The fermentation medium consists of glucose 10 g/L, peptone 5 g/L, yeast extract 2 g/L, L-Trp 3 g/L, L-Ser 2 g/L, L-Thr 2 g/L, L-Lys 2 g/L, L-Phe 2 g/L, L-Val 2 g/L, L-Met 2 g/L, sea salt 20 g/L and water 1 L (pH adjusted to 7.0). Fungal mycelia were crumbled and transferred aseptically to Erlenmeyer flasks. The flasks, each containing 400 mL sterilized liquid medium, were statically incubated at 28 °C for 30 days.

Extraction and Isolation

After 30 days of fermentation, the culture broth and the mycelia (200 L) were separated by filtration and extracted exhaustively with EtOAc and MeOH, respectively. The EtOAc extract was evaporated to afford a crude extract (69 g). The MeOH extract was concentrated *in vacuo* to yield an oily brown residue (19 g). The EtOAc extract was then subjected to column chromatography (CC) over silica gel with a gradient of petroleum ether–EtOAc (10:0-0:10) to EtOAc–MeOH (10:0-0:10) to afford 7 fractions (Fr.1–Fr.7). Fr.3 was subsequently separated by Sephadex LH-20 (MeOH) to provide five subfractions (Fr.3.1–Fr.3.5). Fr.3.2 was further fractionated by preparative HPLC with MeOH–H_2O (65:35 v/v) to yield compounds **14** (37.1 mg) and **23** (26.9 mg). Fr.3.4 was chromatographed by preparative HPLC with MeOH–H_2O (43:57 v/v) to afford **8** (16.4 mg) and **16** (10.5 mg). Compounds **10** (3.0 mg) and **11** (5.0 mg) were obtained from Fr.4 by chromatography on a Sephadex LH-20 column (MeOH) and then on a preparative HPLC column (MeOH–H_2O, 78:22 v/v). Compounds **6** (8.7 mg), **20** (7.8 mg) and **22** (30.1 mg) were also purified from Fr.4 using preparative HPLC with MeOH–H_2O (55:45 v/v). Fr.5 was subdivided to five subfractions (Fr.5.1–Fr.5.5) using a silica gel column with a

stepwise gradient of petroleum ether–EtOAc (10:0–0:10). Fr.5.2 was separated by Sephadex LH-20 CC (MeOH) to give compound **15** (20.8 mg). Compounds **1** (3.0 mg) and **13** (1.0 mg) were isolated from Fr.5.4 by Sephadex LH-20 CC (MeOH). Fr.5.3 was fractionated by a silica gel column and a preparative HPLC to give compounds **19** (8.9 mg), **21** (21.0 mg), **5** (2.0 mg), **7** (10.0 mg) and the mixture of **2** and **3** (10 mg). Fr.6 was separated by repeated CC on a silica gel column and Sephadex LH-20 (MeOH) to afford compounds **4** (0.8 mg) and **17** (2.4 mg).

On the other hand, the MeOH extract was subjected to a silica gel column with a gradient of petroleum ether–EtOAc (10:0–0:10) to EtOAc–MeOH (10:0–0:10) to afford 12 fractions (Fr.M-1–Fr.M-12). Compound **12** (22.5 mg) was obtained from Fr.M-7 by chromatography on a Sephadex LH-20 column (MeOH) followed by a preparative HPLC column (MeOH–H_2O, 75:25 v/v). Fr.M-11 was subjected to Sephadex LH-20 CC (MeOH) and subsequently separated by preparative HPLC (MeOH–H_2O, 60:40 v/v) to obtain **24** (2.0 mg) and **25** (2.0 mg). Similarly, Fr.M-12 was separated by Sephadex LH-20 CC (MeOH) and purified by preparative HPLC (MeOH–H_2O, 33:67 v/v) to give compounds **9** (5.3 mg) and **18** (1.3 mg).

Spectroscopic Data

*Trichocarboline A (**1**)*: a light yellow powder, [α]20 D -29.0 (*c* 0.05, MeOH); UV (MeOH) λ_{max} (log ε) 283 (4.33), 305 (4.05), 378 (3.99); IR: ν_{max} 3326, 2918, 2849, 1671, 1646, 1626, 1469, 1433, 1322, 1204, 1128, 1062, 1015 cm^{-1}; ^1H and ^{13}C NMR data see **Table 1**; HR(-)ESIMS *m/z* 283.1089 $[M - H]^-$ (calcd for $C_{16}H_{15}N_2O_3$, 283.1088).

(–)-*Trichocarboline B (**2**)*: a light yellow powder, [α]20 D -106.0 (*c* 0.10, MeOH); UV (MeOH) λ_{max} (log ε) 235 (4.84), 289 (4.49), 339 (4.02), 349 (4.01) nm; IR: ν_{max} 3557, 2962, 2925, 2873, 1627, 1567, 1494, 1456, 1430, 1323, 1238, 1045 cm^{-1}; ^1H and ^{13}C NMR data see **Table 1**; HR(-)ESIMS *m/z* 225.1034 $[M - H]^-$ (calcd for $C_{14}H_{13}N_2O$, 225.1033).

(+)-*Trichocarboline B (**3**)*: a light yellow powder, [α]20 D + 100.0 (*c* 0.08, MeOH); UV (MeOH) λ_{max} (log ε) 235 (4.84), 289 (4.49), 339 (4.02), 349 (4.01) nm; IR: ν_{max} 3557, 2962, 2925, 2873, 1627, 1567, 1494, 1456, 1430, 1323, 1238, 1045 cm^{-1}; ^1H and ^{13}C NMR data see **Table 1**; HR(-)ESIMS *m/z* 225.1034 $[M - H]^-$ (calcd for $C_{14}H_{13}N_2O$, 225.1033).

*Trichocarboline C (**4**)*: a red solid; UV (MeOH) λ_{max} (log ε) 217 (2.37) nm; IR: ν_{max} 3398, 2946, 1726, 1446, 1354, 1320, 1185, 1024, 958, 875 cm^{-1}; ^1H and ^{13}C NMR data see **Table 1**; HR(+)ESIMS *m/z* 241.0978 $[M + H]^+$ (calcd for $C_{14}H_{13}N_2O_2$, 241.0972).

Chiral Separation of 2 and 3

By using a Chiral CD-Ph column (MeOH/H_2O 60:40; flow rate 1.0 mL/min), the mixture of enantiomers **2** and **3** was resolved to afford **2** (3.0 mg, t_R = 32.5 min) and **3** (3.0 mg, t_R = 40.0 min).

Specific Optical Rotation Calculation

The specific optical rotation values of compounds **1**-**3** were calculated by quantum chemical calculations using Gaussian 09 software (Li et al., 2012). They were further optimized by the density functional theory method at the B3LYP/6-311G (2d, p) level and calculations were made at the PBE1PBE/6-311 + + G (d, p) level in MeOH with a PCM model. The calculated specific optical rotation was averaged according to the Boltzmann distribution theory and their relative Gibbs free energy.

Cell Culture and Cytotoxicity Assays

The human fetal lung fibroblasts (HFL1) were purchased from Procell Life Science and Technology Co., Ltd (Cat No.: CL-0106 Wuhan, China). Cells were cultured in Ham's F-12K medium (PM150910, Procell Life Science and Technology, Wuhan) supplemented with 10% fetal bovine serum (FBS) (#10270-106, GIBCO, Invitrogen, Carlsbad, CA, United States) and 1% penicillin-streptomycin in an incubator at 37°C with 5% CO_2. According to the manufacturer's protocol, the cell viability was measured using the Cell Counting Kit-8 (CCK8). The cells were seeded in 96-well plates at a density of 5×10^3 cells/well. After incubating for 24 h, the cells were treated with a medium containing 10 μM compounds **1**-**3**, **5**-**25**, pirfenidone (TargetMol, United States) for 48 h. Following incubation, each well was incubated at 37°C for 2 h with 10 μL of CCK8 solution. After that, a full function microplate reader (BioTek, United States) was used to measure the solution's absorbance at 450 nm. Survival rate = (A value, Administration)/(A value, Control) × 100%. All assays were repeated in triplicate.

Inhibition of Collagen Accumulation Rate *in vitro*

The antifibrosis activities of the compounds were investigated in HFL1 cells seeded in 96-well plates at a density of 2×10^4 cells/well. After incubation for 24 h, the cells were treated with a medium containing TGF-β1 (5 ng/mL) and 10 μM compounds **1**-**3**, **5**-**25**, pirfenidone for 48 h. Afterward, the supernatant was removed, and the cells were fixed for 30 min with 4% paraformaldehyde. After washing twice with PBS, the cells were added the 0.1% Sirius red dye with saturated picric acid. After 4 h of staining protected from light, the collagenous fiber was dyed red. Then, the cells were washed three times with 0.1% acetic acid and visualized under the microscope cell imaging system (EVOS FL Auto, Life Technologies, United States). For the quantitative determinations of the accumulated collagen, the stained cells were destained with 0.1M NaOH (100 μL/well) for 10 min. Then, the absorbance was measured at 540 nm with a spectrophotometer. Total collagen accumulation inhibition = 1 - (Administration A value - control A value)/(model A value - control A value) × 100%. All assays were repeated in triplicate (Xue et al., 2020).

Western Blot Analysis

Western blot analysis was performed as previously described methods (Hao et al., 2020). The primary antibodies: anti-α-SMA (Cat No. Ab7817), anti-fibronectin (Cat No. 15613-1-AP), anti-PCNA (Cat No. 10205-2-AP), anti-phospho-Smad2^{Ser255} (Cat No. Ab188334), anti-phospho-Smad3$^{Ser423/425}$ (Cat No. Ab52903), anti-Smad2 (Cat No. Ab40855), anti-Smad3 (Cat No. Ab40854) and anti-GAPDH (Cat No. 10494-1-AP).

Statistical Analysis

Data are expressed as the means ± SEM. The GraphPad Prism 6.0 software (San Diego, CA, United States) was used to perform statistical analysis. The one-way analysis of variance (ANOVA) and *post-hoc* test (LSD) were used to analyze the significant differences between groups. All differences were considered statistically significant at $P < 0.05$.

RESULTS

Isolation and Structure Elucidation

To induce the production of secondary metabolites in the MCCC 3A01244 strain, we employed the amino acid–directed strategy (Huang et al., 2017). The fungus was grown in GYP medium supplemented with L-Trp 2 g/L, L-Ser 2 g/L, L-Thr 2 g/L, L-Lys 2 g/L, L-Phe 2 g/L, L-Val 2 g/L, and L-Met 2 g/L. The culture was statically incubated at 28 °C for 30 days, at which point the mycelia and the culture broth were separated by filtration and extracted exhaustively with MeOH and EtOAc, respectively. The extracts were subsequently subjected to successive column chromatography and HPLC. Consequently, 25 structurally diverse natural products were identified from the extracts (**Figure 1**), including four β-carbolines, trichocarbolines A, B [(+)- and (–)-enantiomers], and C (**1**-**4**).

Trichocarboline A (**1**) was isolated as a light-yellow powder. The molecular formula of **1** was established as $C_{16}H_{16}N_2O_3$ according to the HR(-)ESIMS ion at *m*/*z* 283.1089 $[M\text{-}H]^-$ (calcd 283.1088 for $C_{16}H_{15}N_2O_3$), indicating ten degrees of unsaturation. The ^{13}C NMR spectrum, in combination with DEPT-135 and HSQC spectra (**Table 1**), showed resonances for three sp^3 methylenes (including one oxygenated methylene), six sp^2 methines, one oxygenated sp^3 methine, five non-protonated sp^2 carbons, and one carbonyl carbon. The ^1H NMR spectrum of **1** showed resonances at δ_H 8.18 (1H, d, J = 7.6 Hz, H-5), 7.27 (1H, dd, J = 7.6, 7.2 Hz, H-6), 7.55 (1H, dd, J = 8.0, 7.2 Hz, H-7), and 7.66 (1H, d, J = 8.0 Hz, H-8) in the ^1H NMR spectrum, which along with the ^1H-^1H COSY correlations of H-5/H-6/H-7/H-8 revealed the presence of an *ortho*-substituted benzene ring. Additionally, the COSY spectrum also indicated the presence of a pair of aromatic protons at δ_H 8.42 (1H, d, J = 4.8 Hz, H-3) and 8.26 (1H, d, J = 4.8 Hz, H-4). The HMBC correlations from H-3 to C-1 (δ_C 137.1) and C-11 (δ_C 133.2), from H-4 to C-10 (δ_C 136.2) and C-12 (δ_C 121.7), from H-5 to C-11 and C-13 (δ_C 143.4), and from H-8 to C-12 established a β-carboline moiety. Moreover, from the $^1H - {}^1H$ COSY correlations of H-2′ (δ_H 3.46, t)/H-3′ (δ_H 2.04, m; 1.83, m), H-3′/H-4′ (δ_H 3.72, m) and H-4′/H-5′ (δ_H 3.52, m), the fragment of $–CH_2CH_2CH(OH)CH_2OH$ was postulated. The HMBC correlations from H-2′/H-3′ to C-1′ (δ_C 204.9) demonstrated that the carbonyl group is linked with C-2′ (δ_C 35.0). Although no HMBC correlation was observed to connect C-1 with C-1′, the overall NMR data for **1** as well as direct comparisons of the ^1H and ^{13}C NMR spectra of **1** with those of **2** and **3** (see below), strongly suggest that the side chain is connected to C-1. The absolute configuration of the hydroxy group at C-4′ was determined to be *S*, as the calculated optical rotation value of 4′*S*-**1** (-32.9) fitted well with the experimental data for **1** (-29.0). Accordingly, the structure of trichocarboline A (**1**) was established as shown in **Figure 1**.

(–)- and (+)-Trichocarbolines B (**2** and **3**, respectively) were initially obtained as a mixture of enantiomers (a yellow powder) and their molecular formula was established as $C_{14}H_{14}N_2O$ based on HR(-)ESIMS ion at *m*/*z* 225.1034 $[M\text{-}H]^-$ (calcd 225.1033 for $C_{14}H_{13}N_2O$), corresponding to nine degrees of unsaturation. The ^{13}C NMR and DEPT-135 spectra of **2** and **3** displayed resonances for 11 aromatic carbons similar to those of **1** (**Table 1**), suggesting the presence of a β-carboline skeleton. The key HMBC correlations from H-4 (1H, δ_H 7.99,

TABLE 1 | ^1H (400 MHz) and ^{13}C NMR (101 MHz) data for compounds **1**, **2/3**, and **4** (δ in ppm, *J* in Hz).

	1 (in CD_3OD)		**2/3 (in CD_3OD)**		**4 (in $CDCl_3$)**	
Position	δ_C, type	δ_H, mult. (*J* in Hz)	δ_C, type	δ_H, mult. (*J* in Hz)	δ_C, type	δ_H, mult. (*J* in Hz)
1	137.1, C		148.5, C		135.1, C	
3	138.5, CH	8.42, d (4.8)	137.3, CH	8.21, d (5.6)	138.5, CH	8.01, d (4.8)
4	120.1, CH	8.26, d (4.8)	114.8, CH	7.99, d (5.6)	118.1, CH	8.47, d (4.8)
5	122.7, CH	8.18, d (7.6)	122.4, CH	8.17, d (8.0)	123.1, CH	7.97, d (8.4)
6	121.6, CH	7.27, dd (7.6, 7.2)	120.7, CH	7.25, dd (8.0, 7.2)	110.6, CH	6.85, d (8.4)
7	130.3, CH	7.55, dd (8.0, 7.2)	129.6, CH	7.55, dd (8.0, 7.2)	157.8, C	
8	113.5, CH	7.66, d (8.0)	113.0, CH	7.63, d (8.0)	97.7, CH	6.98, s
9	NH		NH		NH	10.21, brs
10	136.2, C		134.5, C		136.0, C	
11	133.2, C		131.2, C		131.9, C	
12	121.7, C		122.1, C		114.4, C	
13	143.4, C		142.6, C		143.1, C	
1’	204.9, CO		76.5, CH	5.09, t (6.4)	206.0, CO	
2’	35.0, CH_2	3.46, t (7.6)	31.0, CH_2	2.01, m	31.2, CH_2	3.42, q (7.2)
3’	29.0, CH_2	1.83, m 2.04, m	10.2, CH_3	0.99, t (7.2)	8.3, CH_3	1.30, t (7.2)
4’	72.8, CH	3.72, m				
5’	67.4, CH_2	3.52, m				

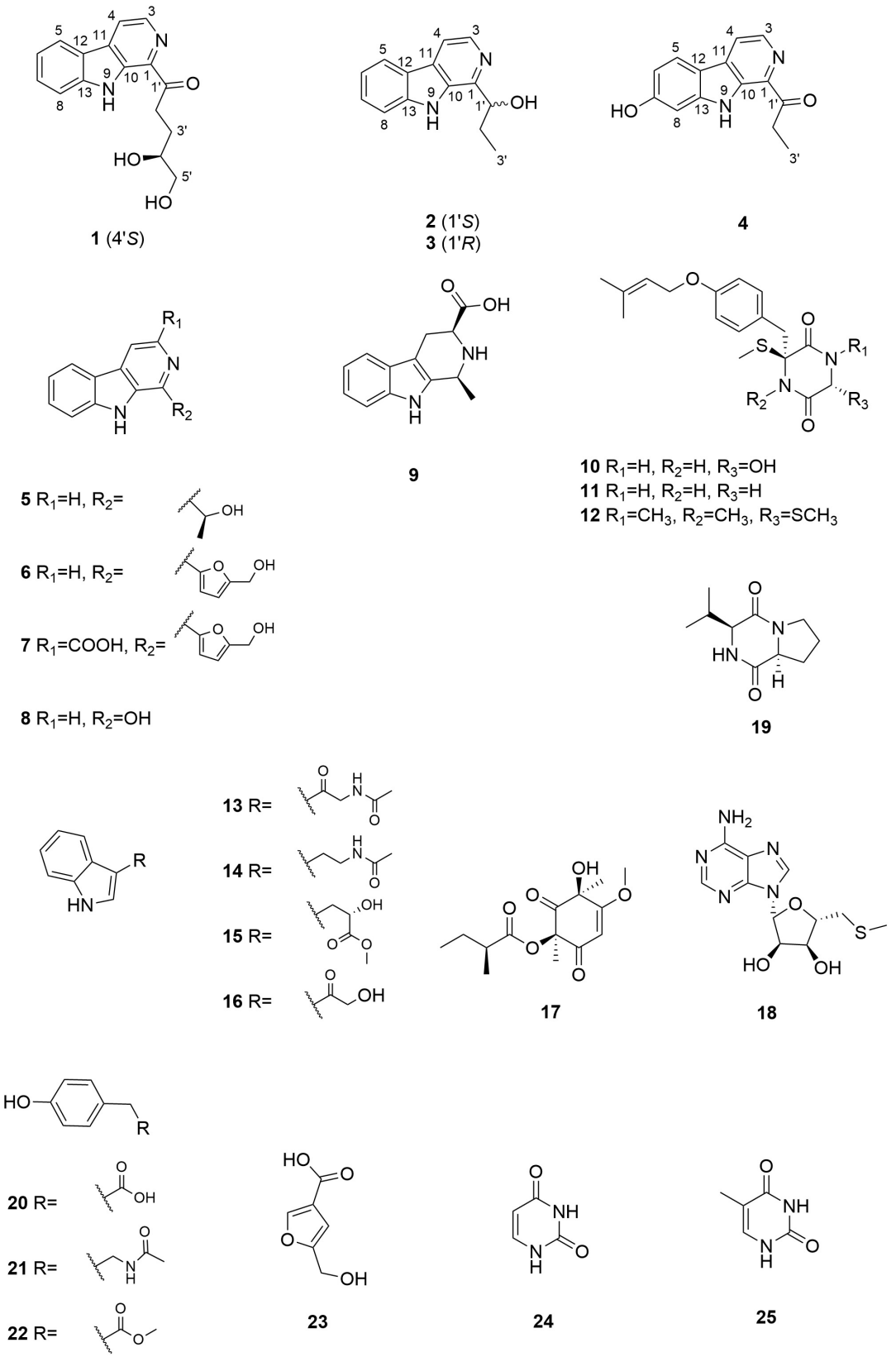

FIGURE 1 | Chemical structures of compounds **1**–**25**.

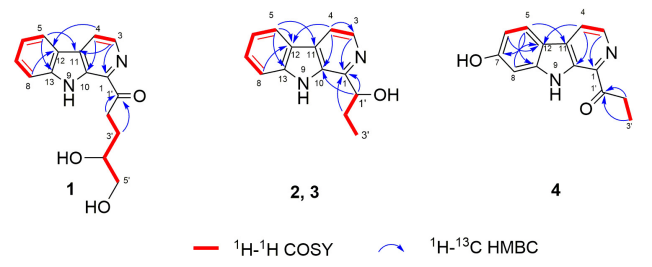

FIGURE 2 | Key COSY and HMBC correlations of compounds **1**–**4**.

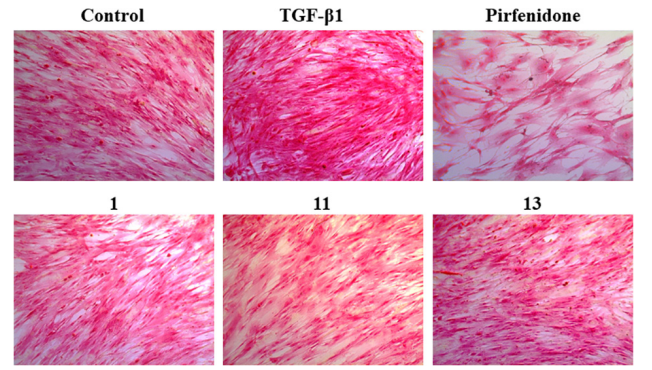

FIGURE 3 | Picro-Sirius Red (PSR) staining for the total collagen accumulation induced by TGF-β1 in HFL1 cells. The representative pictures are the cells induced by TGF-β1 and treated with 10 μM compounds **1**, **11**, and **13** pirfenidone, and the control group (untreated normal cells).

d, J = 5.6 Hz) to C-10 (δ_C 134.5) and C-12 (δ_C 122.1), and from H-5 (1H, δ_H 8.17, d, J = 7.6 Hz) to C-11 (δ_C 131.2) and C-13 (δ_C 142.6) along with the ^{1}H-^{1}H COSY correlations between H-3 (1H, δ_H 8.21, d, J = 5.6 Hz) and H-4, between H-5 and H-6 (1H, δ_H 7.25, dd, J = 7.6, 7.2 Hz), between H-6 and H-7 (1H, δ_H 7.54, dd, J = 8.0, 7.2 Hz), and between H-7 and H-8 (1H, δ_H 7.63, d, J = 8.0 Hz) further corroborated the structure of a β-carboline moiety (**Figure 2**). The ^{1}H−^{1}H COSY cross-peaks of H-1′ (1H, δ_H 5.09, t, J = 6.4 Hz) and H-2′ (2H, δ_H 2.01, m), H-2′ and H-3′ (3H, δ_H 0.99, t, J = 7.2 Hz) and the HMBC correlations of H-1′/C-1 and H-2′/C-1 (δ_C 148.8) (**Figure 2**) revealed the presence of a –CH(OH)CH_2CH_3 side chain, which is connected to C-1. Based on these data, the enantiomeric mixture was identified as 1-(9*H*-pyrido[3,4-*b*]indol-1-yl)propane-1-ol, which was reported recently as a synthetic product (Szepesi Kovács et al., 2021), but no enantiomeric purity was determined. Since the enantiomers often have disparate pharmacological activities and even metabolic pathways (Jiao et al., 2015), we decided to separate the enantiomers for further biological evaluation. After several attempts using a diverse set of chiral LC columns, we were able to separate the two enantiomers (–)-trichocarboline B (**2**) and (+)-trichocarboline B (**3**) and assigned their absolute configurations by comparing their optical rotations with the calculated values for the 2′*S* and 2′*R* isomers. The experimental optical rotation value of the faster eluting enantiomer (**2**) was -106.0 and the calculated optical rotation value of 2′*S* was -97.4, suggesting that the absolute configuration of **2** is 2′*S*. The calculated optical rotation for 2′*R* was + 97.3, which matched well with the experimental value of the second eluting enantiomer **3** (+100.0).

Compound **4**, named trichocarboline C, was found as a red powder. The molecular formula of **4** was determined to be $C_{14}H_{12}N_2O_2$ based on the HR(+)ESIMS protonated ion peak at m/z 241.0978 $[M + H]^+$ (calcd for $C_{14}H_{13}N_2O_2$, 241.0972). The ^{13}C NMR spectrum, in conjunction with DEPT and HSQC spectra (**Table 1**), showed fourteen carbon signals including one sp^3 methyl (δ_C 8.3), one sp^3 methylene (δ_C 31.2), five sp^2 methines (δ_C 97.7, 110.6, 118.1, 123.1, 138.5), six non-protonated sp^2 carbons (δ_C 114.4, 131.9, 135.1, 136.0, 138.5, 143.1), and one carbonyl carbon (δ_C 206.0). The ^{1}H − ^{1}H COSY correlations between H-3 (1H, δ_H 8.01, d, J = 4.8 Hz) and H-4 (1H, δ_H 8.47, d, J = 4.8 Hz), between H-5 (1H, δ_H 7.97, d, J = 8.4 Hz) and H-6 (1H, δ_H 6.85, d, J = 8.4 Hz) and between H-2′ (2H, δ_H 3.42, q, J = 7.2 Hz) and H-3′ (3H, δ_H 1.30, t, J = 7.2 Hz), as well as HMBC correlations from H-3 to C-1 (δ_C 135.1), from H-4 to C-12 (δ_C 114.4) and C-10 (δ_C 136.0), from H-5 to C-11 (δ_C 131.9), C-7 (δ_C 157.8) and C-13 (δ_C 143.1) and from H-6 and H-8 (δ_H 6.98, s) to C-12 (δ_C 114.4) (**Figure 2**) indicated that **4** possesses the same β-carboline core structure as trichocarboline A (**1**). Moreover, the ^{1}H−^{1}H COSY correlation between H-2′ and H-3′ and HMBC correlations from H-2′/H-3′ to C-1′ (δ_C 206.0) indicated the presence of a propionyl group, which, based on comparisons of its NMR data with those of compounds **1**–**3**, was postulated to be connected to C-1 (**Figure 2**). Furthermore, the assignment of a hydroxyl group at C-7 (δ_C 157.8) was based on a combination of the ^{1}H−^{1}H COSY and HMBC correlations shown in **Figure 2**. Consequently, the chemical structure of **4** was elucidated as depicted in **Figure 1**.

In addition to the four compounds described above, we also isolated 21 known compounds, i.e., cordysinin C (**5**) (Yang et al., 2006), perlolyrine (**6**) (Santhanam et al., 2020), flazine (**7**) (Santhanam et al., 2020), 3-hydroxy-β-carboline (**8**) (Jiao et al., 2010), 1,2,3,4-tetrahydro-1-methyl-β-carboline-3-carboxylic acid (**9**) (Kicha et al., 2003), 6-hydroxy-3-methylthio-3-[4′-(3′′-methyl-2′′-butenoxy) phenylmethyl]-2,5-piperazinedione (**10**) (Ayer et al., 1990), 3-thiomethyl-3-[4′′-(3′′-methyl-2′′-butenoyl)phenylmethyl]-2,5-piperazinedione (**11**) (Ayer et al., 1990), bis(methylthio)silvatin (**12**) (Wang et al., 1998), *N*-acetyl-β-oxotryptamine (**13**) (Yang et al., 2013), *N*-[2-(1*H*-indol-3-yl)ethyl]acetamide (**14**) (Häring et al., 2017), indole-3-lactic acid methyl ester (**15**) (Nguyen et al., 2010), 3-(2-hydroxyacetyl)indole (**16**) (Pettit et al., 2006), phomaligol A (**17**) (Li et al., 2003), 5′-deoxy-5′-methylthioadenosine (**18**) (Jiao et al., 2019), cyclo-L-prolyl-L-valine (**19**) (Begum Ahil et al., 2019), *N*-acetyltyramine (**20**) (Lee et al., 2017), 4-hydroxyphenylacetate (**21**) (Davis et al., 2011), methyl 4-hydroxyphenylacetate (**22**) (Qiu et al., 2017), 5-(hydroxymethyl)-3-furancarboxylic acid (**23**) (Evidente et al., 2009), uracil (**24**) (Kan et al., 2011), and thymine (**25**) (Kuchkarova et al., 2020). All of these compounds were identified by comparing their ^{1}H and ^{13}C NMR

TABLE 2 | Collagen accumulation inhibition rate (IR) and cell survival rate (SR) of **1**–**3**, **5**–**25**.

Compounds	Inhibition rate (%)	Survival rate (%)	Compounds	Inhibition rate (%)	Survival rate (%)
1	85.21 ± 3.15	80.01 ± 0.15	**15**	12.99 ± 7.07	96.64 ± 3.08
2	29.98 ± 2.04	96.84 ± 0.66	**16**	33.25 ± 1.50	93.68 ± 1.73
3	21.16 ± 1.50	80.76 ± 1.19	**17**	47.96 ± 2.47	98.19 ± 0.54
5	25.41 ± 0.57	86.47 ± 3.83	**18**	5.15 ± 3.53	87.37 ± 3.54
6	8.42 ± 0.57	92.83 ± 3.78	**19**	1.55 ± 1.50	94.09 ± 1.94
7	27.04 ± 3.71	91.33 ± 6.49	**20**	37.83 ± 1.50	91.13 ± 0.66
8	43.38 ± 1.96	84.37 ± 2.60	**21**	5.47 ± 3.44	86.12 ± 2.59
9	21.16 ± 2.71	93.69 ± 0.52	**22**	1.88 ± 1.13	87.08 ± 3.83
10	26.39 ± 5.74	94.79 ± 2.62	**23**	5.47 ± 3.00	93.84 ± 3.86
11	62.66 ± 2.04	96.29 ± 3.35	**24**	47.63 ± 4.63	89.88 ± 3.46
12	35.21 ± 3.00	87.38 ± 0.84	**25**	3.51 ± 2.47	85.52 ± 1.14
13	73.77 ± 3.40	91.89 ± 0.45	**pirfenidone**	87.83 ± 8.34	69.64 ± 0.80
14	36.85 ± 1.50	97.54 ± 1.52			

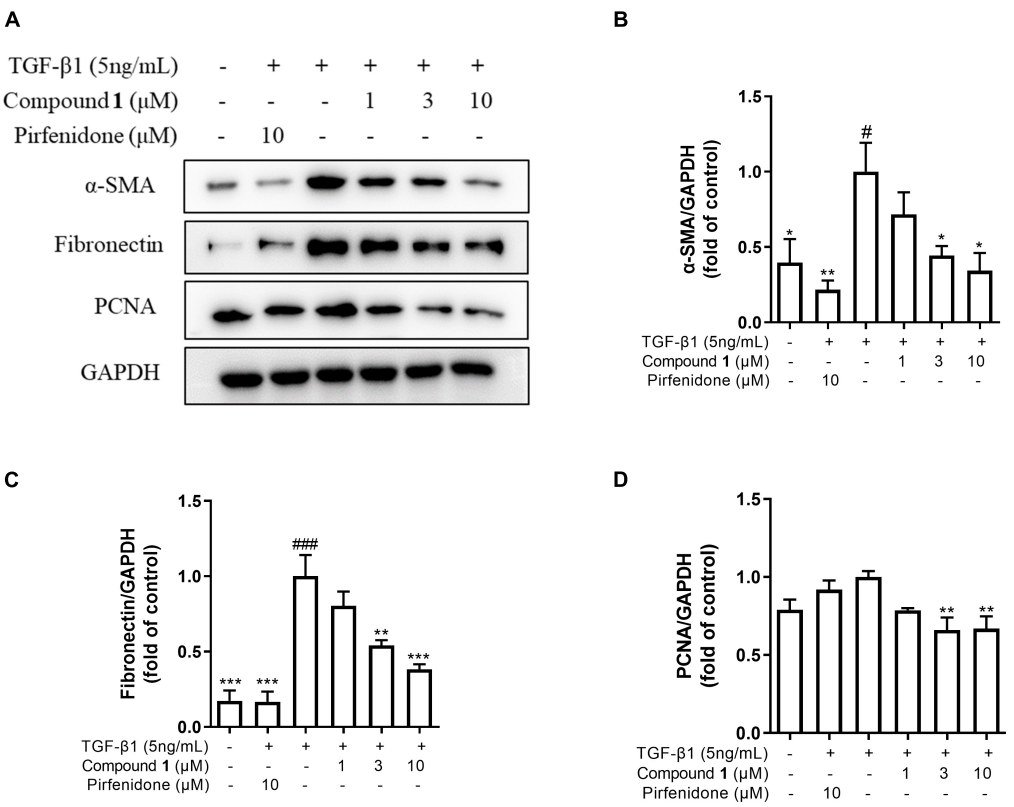

FIGURE 4 | Trichocarboline A (**1**) inhibited extracellular matrix (ECM) deposition induced by transforming growth factor (TGF)-β1 in HFL1 cells. **(A–D)** HFL1 cells were treated with various concentrations of compound **1** (0, 1, 3, 10 μM) or pirfenidone in the presence or absence of TGF-β1 (5 ng/mL) stimulation for 48 h. The protein expression of **(B)** alpha smooth muscle actin (α-SMA), **(C)** fibronectin (FN), and **(D)** proliferating cell nuclear antigen (PCNA) was analyzed by Western blot. $n = 3$. Data were presented as the mean ± SEM. $^{*}P < 0.05$, $^{**}P < 0.01$, $^{***}P < 0.001$ vs. the TGF-β1 group. $^{\#}P < 0.05$, $^{\#\#}P < 0.01$, $^{\#\#\#}P < 0.001$ vs. the control group.

data (**Supplementary Figures 22–63**) with those reported in the literatures.

Proposed Biosynthetic Pathway

The putative biosynthetic pathway for β-carboline alkaloids has been described in the previous paper published by our team (Qiu et al., 2020). Briefly, compound **1** was supposed to be biosynthesized *via* the McbB enzymatic Pictet-Spengler reaction with tryptamine and glucose, using the negatively charged Glu97 to complete the aromatization, followed by consecutive decarboxylation and oxidation (Chen et al., 2013; Chen et al., 2018; Qiu et al., 2020). Similarly, compounds **2**-**5** were also generated from tryptophan and corresponding aldehydes. Detailed descriptions of the hypothetical biosynthetic pathway

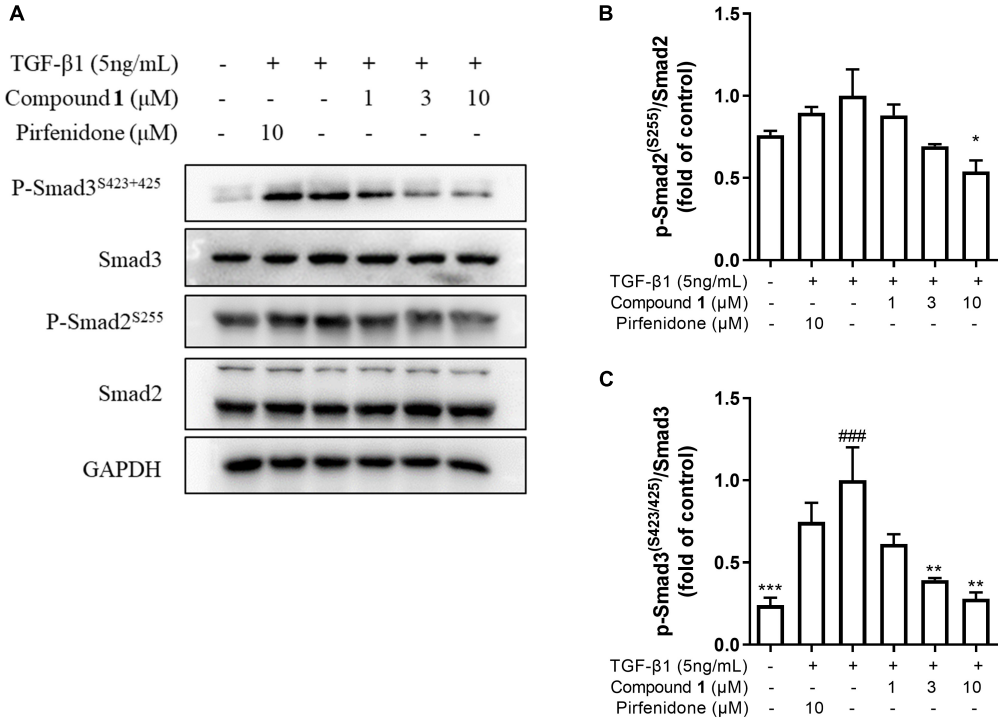

FIGURE 5 | Effect of trichocarboline A (**1**) on Smad signaling pathway. **(A–C)** HFL1 cells were treated with various concentrations of compound **1** (0, 1, 3, 10 μM) or pirfenidone in the presence or absence of transforming growth factor TGF-β1 (5 ng/mL) stimulation for 30 min. The protein expression of **(B)** p-Smad2^{Ser255}, and **(C)** p-Smad3$^{Ser423/425}$ was analyzed by Western blotting. $n = 3$. Data were presented as the mean ± SEM. $^{*}P < 0.05$, $^{**}P < 0.01$, $^{***}P < 0.001$ vs. the TGF-β1 group. $^{\#}P < 0.05$, $^{\#\#}P < 0.01$, $^{\#\#\#}P < 0.001$ vs. the control group.

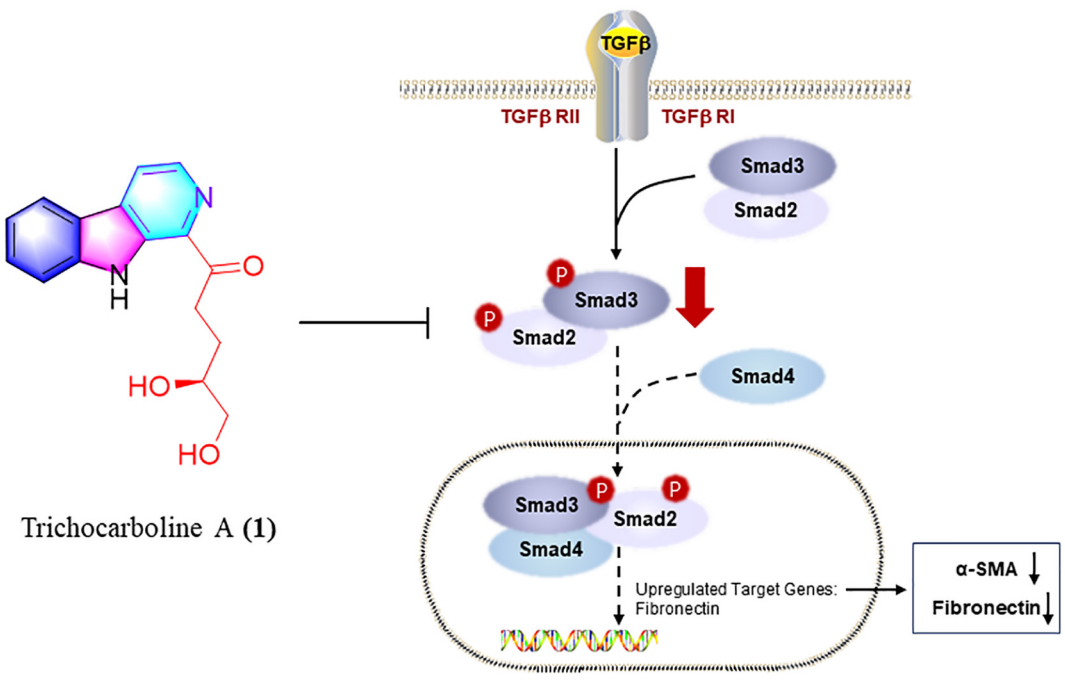

FIGURE 6 | Trichocarboline A (**1**) suppressed the phosphorylation of Smad2/3 in TGF-β/Smad signaling. Trichocarboline A (**1**) was a TGF-β/Smad signaling inhibitor, making it a promising lead compound for the development of agents to treat pulmonary fibrosis disease.

for compounds **6**-**7** have been disclosed in a previous study (Zhao et al., 2017).

Preliminary Screening of Compounds 1–25 for Inhibiting Collagen Accumulation

The pathological marker of fibrosis is the abnormal deposition of excessive extracellular matrix (ECM) with collagen as the main component. Therefore, the detection of collagen synthesis, which can be directly correlated to the degree of fibrosis, is an effective indicator for evaluating fibrotic diseases. Trichocarboline A (**1**), (–)- and (+)-trichocarbolines B (**2** and **3**), together with 21 compounds (**5**–**25**) were preliminarily screened for their cytotoxicity in HFL1 cells at a concentration of 10 μM using a Cell Counting Kit-8 (CCK8)-based assay. Trichocarboline D (**4**) was not evaluated for its activity due to insufficient quantity. The Sirius red dye staining, which has been accepted to be an effective and convenient method for the anti-fibrotic screening model *in vitro* (Deng et al., 2020; Xue et al., 2020), was then used to evaluate compound inhibitory activity on total collagen accumulation induced by TGF-β1. Pirfenidone was used as a positive control. As illustrated in **Table 2**, compounds **1**, **11**, and **13** displayed significant inhibition of collagen accumulation with weak cytotoxicity in HFL1 cells. Trichocarboline A (**1**) stood out to be the most active compound for further examination, inhibiting collagen accumulation to 85.21 ± 3.2% at 10 μM. Although pirfenidone exhibited a slightly higher inhibition rate compared to **1**, it exerted more cytotoxicity effects on HFL1 cells, which was consistent with microscopic observations (**Figure 3**).

Trichocarboline A (1) Suppressed the Expressions of Fibrotic Biomarkers

To investigate the mechanism of the anti-fibrotic activity of trichocarboline A (**1**), it was evaluated for its ability to inhibit TGF-β1-induced fibronectin (FN) and α-smooth muscle actin (α-SMA) expression in HFL1 cells. FN and α-SMA have been commonly considered fibrotic markers, as they are overexpressed in fibrotic diseases. TGF-β1 can also upregulate the expression of proliferating cell nuclear antigen (PCNA), which is a component of the replication and repair machinery (Kelman, 1997). Therefore, the ability of trichocarboline A (**1**) to inhibit the expression of PCNA was also evaluated. Trichocarboline A (**1**) also reduced the TGF-β1-induced PCNA protein level in a dose-dependent manner, indicating that trichocarboline A (**1**) can inhibit the excessive proliferation of cells. As shown in **Figure 4**, trichocarboline A (**1**) reduced TGF-β1-induced FN and α-SMA expression in HFL1 cells, which is consistent with its ability to reduce ECM deposition, suggesting that trichocarboline A (**1**) was a potential anti-fibrotic agent.

Trichocarboline A (1) Inhibited Extracellular Matrix Deposition *via* Inhibition of TGF-β/Smad Signaling

TGF-β/Smad signaling pathway mainly involves intracellular phosphorylation cascade of Smad-2/3 transcription factors. Phosphorylated Smad-2/3 complex with Smad-4, and translocate to the nucleus, then complex drive the expression of target matrix genes, finally activating the expressions of ECM proteins (Walton et al., 2017). To determine whether trichocarboline A (**1**) could inhibit this signaling pathway, the protein levels of phosphorylated Smad2 and Smad3 (p-Smad2/3) in TGF-β1-induced HFL1 cells were investigated. As anticipated, the expressions of p-Smad2 and p-Smad3 were markedly increased by TGF-β1 stimulation, whereas trichocarboline A (**1**) down-regulated their expressions in a dose-dependent manner (**Figure 5**). During this process, the total expressions of Smad2 and Smad3 had no significant changes. These evidences suggested that trichocarboline A (**1**) suppressed the phosphorylation Smad2/3 in TGF-β/Smad signaling.

DISCUSSION

Lung damage caused by pulmonary fibrosis cannot be repaired, and current options for drugs and therapies are limited. For critically ill patients, lung transplantation is the only option. Two drugs, nintedanib and pirfenidone, are currently on the market for the prevention of mild pulmonary fibrosis. A review concluded that pirfenidone appears to improve progression-free survival in patients with idiopathic pulmonary fibrosis, but has a lesser effect on lung function (Spagnolo et al., 2010). Nintedanib has been shown to slow the decline in forced vital capacity, but not improve survival in patients with fibrosis (Dimitroulis, 2014). Discovery of new anti-pulmonary fibrosis therapies remains a key challenge.

Trichoderma species have been demonstrated as a promising source of secondary metabolites with significant bioactivities, including antimicrobial sesquiterpenes, antioxidant mycotoxin, antibiotic peptaibols, antiviral trichokonins, and cytotoxic terpenes (Li M.-F. et al., 2019). However, to the best of our knowledge, there have been no reports on the secondary metabolites from the genus *Trichoderma* as anti-pulmonary fibrosis agents. This study lays the foundation for the use of β-carbolines in the treatment of pulmonary fibrosis.

In summary, chemical investigations of the deep-sea fungus *Trichoderma* sp. MCCC 3A01244 led to the isolation of 25 compounds, including two new β-carbolines, trichocarbolines A and C (**1** and **4**). Trichocarboline B [(+)- and (–)-enantiomers] are reported for the first time as naturally occurring metabolites. Compounds **1**, **11**, and **13** showed inhibitory activity against collagen accumulation in HFL1 cells. Furthermore, trichocarboline A (**1**) can suppress the expression of FN, α-SMA, and PCNA in TGF-β1-induced HFL1 cells, and reduce ECM deposition. Trichocarboline A (**1**) down-regulated phosphorylating Smad 2 and Smad 3. Thus, trichocarboline A (**1**) may reduce the accumulation of heteromeric Smad complex (phosphorylating Smad 2 and Smad 3 and binding to Smad 4) in the nucleus, thereby down-regulating the transcription of fibrosis genes, including α-SMA and fibronectin, which is expected further study. Mechanistic study revealed that trichocarboline A (**1**) was a TGF-β/Smad signaling inhibitor, making it a promising

lead compound for the development of drugs to treat pulmonary fibrosis disease.

DATA AVAILABILITY STATEMENT

The original contributions presented in this study are included in the article/**Supplementary Material**, further inquiries can be directed to the corresponding author.

AUTHOR CONTRIBUTIONS

W-JL conceived and designed the study and finalized the manuscript. M-JH and P-NC carried out the experiments. M-JH wrote the manuscript. W-JL, H-JL, FW, G-YZ, Z-ZS, X-PL, W-ZM, and JX guided experiments. TM revised the manuscript. All authors provided critical feedback and helped shape the research, analysis, and manuscript and generated in-house and no manuscript mill was used, and agreed to be accountable for all aspects of work ensuring integrity and accuracy.

FUNDING

This research was funded by the National Science Foundation of China (No. 81872795) and Guangdong Basic and Applied Basic Research Foundation (Nos. 2021A1515011761 and 2018A030313157).

SUPPLEMENTARY MATERIAL

The Supplementary Material for this article can be found online at: https://www.frontiersin.org/articles/10.3389/fmicb.2022.947226/full#supplementary-material

REFERENCES

Ayer, W. A., Altena, I. V., and Browne, L. M. (1990). Three piperazinediones and a drimane diterpenoid from Penicillium brevi-compactum. *Phytochemistry* 29, 1661–1665. doi: 10.1016/0031-9422(90)80141-3

Begum Ahil, S., Hira, K., Shaik, A. B., Pal, P. P., Kulkarni, O. P., Araya, H., et al. (2019). l-Proline-based-cyclic dipeptides from *Pseudomonas* sp. (ABS-36) inhibit pro-inflammatory cytokines and alleviate crystal-induced renal injury in mice. *Int. Immunopharmacol.* 73, 395–404. doi: 10.1016/j.intimp.2019.05.044

Biernacka, A., Dobaczewski, M., and Frangogiannis, N. G. (2011). TGF-β signaling in fibrosis. *Growth Factors* 29, 196–202. doi: 10.3109/08977194.2011.595714

Chen, Q., Ji, C., Song, Y., Huang, H., Ma, J., Tian, X., et al. (2013). Discovery of McbB, an Enzyme Catalyzing the β-Carboline Skeleton Construction in the Marinacarboline Biosynthetic Pathway. *Angew. Chem.-Int. Edit* 52, 9980–9984. doi: 10.1002/anie.201303449

Chen, Q., Zhang, S., and Xie, Y. (2018). Characterization of a new microbial Pictet-Spenglerase NscbB affording the β-carboline skeletons from Nocardiopsis synnemataformans DSM 44143. *J. Biotechnol.* 281, 137–143. doi: 10.1016/j.jbiotec.2018.07.007

Cottin, V., and Maher, T. (2015). Long-term clinical and real-world experience with pirfenidone in the treatment of idiopathic pulmonary fibrosis. *Eur. Respir. Rev.* 24, 58–64. doi: 10.1183/09059180.00011514

Davis, R. A., Hofmann, A., Osman, A., Hall, R. A., Mühlschlegel, F. A., Vullo, D., et al. (2011). Natural product-based phenols as novel probes for mycobacterial and fungal carbonic anhydrases. *J. Med. Chem.* 54, 1682–1692. doi: 10.1021/jm1013242

Deng, D., Pei, H., Lan, T., Zhu, J., Tang, M., Xue, L., et al. (2020). Synthesis and discovery of new compounds bearing coumarin scaffold for the treatment of pulmonary fibrosis. *Eur. J. Med. Chem.* 185:111790. doi: 10.1016/j.ejmech.2019.111790

Dimitroulis, I. A. (2014). Nintedanib: a novel therapeutic approach for idiopathic pulmonary fibrosis. *Respir. Care* 59:1450. doi: 10.4187/respcare.03023

Evidente, A., Cristinzio, G., Punzo, B., Andolfi, A., Testa, A., and Melck, D. (2009). Flufuran, an Antifungal 3,5-disubstituted furan produced by aspergillus flavus link. *Chem. Biodivers.* 6, 328–334. doi: 10.1002/cbdv.200800292

Hao, M., Guan, Z., Gao, Y., Xing, J., Zhou, X., Wang, C., et al. (2020). Huang-Qi San ameliorates hyperlipidemia with obesity rats via activating brown adipocytes and converting white adipocytes into brown-like adipocytes. *Phytomedicine* 78:153292. doi: 10.1016/j.phymed.2020.153292

Häring, A. P., Biallas, P., and Kirsch, S. F. (2017). An Unconventional Reaction of 2,2-Diazido Acylacetates with Amines. *Eur. J. Org. Chem.* 2017, 1526–1539. doi: 10.1002/ejoc.201601625

Herrera, J., Henke, C. A., and Bitterman, P. B. (2018). Extracellular matrix as a driver of progressive fibrosis. *J. Clin. Invest.* 128, 45–53. doi: 10.1172/JCI93557

Huang, L.-H., Xu, M.-Y., Li, H.-J., Li, J.-Q., Chen, Y.-X., Ma, W.-Z., et al. (2017). Amino acid-directed strategy for inducing the marine-derived fungus *Scedosporium apiospermum* F41–1 to Maximize Alkaloid Diversity. *Org. Lett.* 19, 4888–4891. doi: 10.1021/acs.orglett.7b02238

Jiao, L., Tao, Y., Wang, W., Mei, L., Shao, Y., Wang, Q., et al. (2019). Chemical Constituents of Fruit Body of Armillaria luteo-virens. *Chem. Nat. Comp.* 55, 373–375. doi: 10.1007/s10600-019-02695-7

Jiao, W.-H., Chen, G.-D., Gao, H., Li, J., Gu, B.-B., Xu, T.-T., et al. (2015). (±)-Quassidines I and J, Two Pairs of Cytotoxic Bis-β-carboline Alkaloid Enantiomers from *Picrasma quassioides*. *J. Nat. Prod.* 78, 125–130. doi: 10.1021/np500801s

Jiao, W.-H., Gao, H., Li, C.-Y., Zhou, G.-X., Kitanaka, S., Ohmura, A., et al. (2010). β-Carboline alkaloids from the stems of *Picrasma quassioides*. *Magn. Reson. Chem.* 48, 490–495. doi: 10.1002/mrc.2602

Kan, S., Chen, G., Han, C., Chen, Z., Song, X., Ren, M., et al. (2011). Chemical constituents from the roots of Xanthium sibiricum. *Nat. Prod. Res.* 25, 1243–1249. doi: 10.1080/14786419.2010.539182

Kelman, Z. (1997). PCNA: structure, functions and interactions. *Oncogene* 14, 629–640. doi: 10.1038/sj.onc.1200886

Kicha, A. A., Ivanchina, N. V., Kalinovsky, A. I., Dmitrenok, P. S., and Stonik, V. A. (2003). Alkaloidosteroids from the starfish *Lethasterias nanimensis chelifera*. *Tetrahedron Lett.* 44, 1935–1937. doi: 10.1016/S0040-4039(03)00088-1

Kuchkarova, N. N., Toshmatov, Z. O., Zhou, S., Han, C., and Shao, H. (2020). Secondary Metabolites with Plant Growth Regulator Activity Produced by an Endophytic Fungus *Purpureocillium* sp. from *Solanum rostratum*. *Chem. Nat. Compd.* 56, 775–776. doi: 10.1007/s10600-020-03147-3

Lee, W., Kim, M.-A., Park, I., Hwang, J. S., Na, M., and Bae, J.-S. (2017). Novel direct factor Xa inhibitory compounds from *Tenebrio molitor* with anti-platelet aggregation activity. *Food Chem. Toxicol.* 109, 19–27. doi: 10.1016/j.fct.2017.08.026

Li, B., Li, L., Peng, Z., Liu, D., Si, L., Wang, J., et al. (2019). Harzianoic acids A and B, new natural scaffolds with inhibitory effects against hepatitis C virus. *Bioorg. Med. Chem.* 27, 560–567. doi: 10.1016/j.bmc.2018.12.038

Li, M.-F., Li, G.-H., and Zhang, K.-Q. (2019). Non-Volatile Metabolites from *Trichoderma* spp. *Metabolites* 9:58. doi: 10.3390/metabo9030058

Li, X., Jeong, J. H., Lee, K. T., Rho, J. R., Choi, H. D., Kang, J. S., et al. (2003). γ-Pyrone derivatives, kojic acid methyl ethers from a marine-derived *fungusaltenaria* sp. *Arch. Pharm. Res.* 26, 532–534. doi:10.1007/BF02976876

Li, Y.-P., Ramirez, S., Jensen Sanne, B., Purcell Robert, H., Gottwein Judith, M., and Bukh, J. (2012). Highly efficient full-length hepatitis C virus genotype 1 (strain TN) infectious culture system. *Proc. Natl. Acad. Sci. U.S.A.* 109, 19757–19762. doi: 10.1073/pnas.1218260109

Liu, Z., Sun, Y., Tang, M., Sun, P., Wang, A., Hao, Y., et al. (2020). Trichodestruxins A–D: cytotoxic cyclodepsipeptides from the endophytic fungus *Trichoderma*

harzianum. *J. Nat. Prod.* 83, 3635–3641. doi: 10.1021/acs.jnatprod.0c00808

Lynch, J. P., and Belperio, J. A. (2012). "Idiopathic pulmonary fibrosis," in *Diffuse Lung Disease: A Practical Approach*, eds. R. P. Baughman and R. M. du Bois (New York, NY: Springer), 171–194.

Miyano, R., Matsuo, H., Mokudai, T., Noguchi, Y., Higo, M., Nonaka, K., et al. (2020). Trichothioneic acid, a new antioxidant compound produced by the fungal strain *Trichoderma virens* FKI-7573. *J. Biosci. Bioeng.* 129, 508–513. doi: 10.1016/j.jbiosc.2019.11.007

Morán-Diez, M. E., Martínez de Alba, ÁE., Rubio, M. B., Hermosa, R., and Monte, E. (2021). *Trichoderma* and the Plant Heritable Priming Responses. *J. Fungi* 7:318. doi: 10.3390/jof7040318

Nguyen, S. T., Butler, M. M., Varady, L., Peet, N. P., and Bowlin, T. L. (2010). A concise, total synthesis and antibacterial evaluation of 2-hydroxy-1-(1*H*-indol-3-yl)-4-methylpentan-3-one. *Bioorg. Med. Chem. Lett.* 20, 5739–5742. doi: 10.1016/j.bmcl.2010.08.003

Pettit, G. R., Du, J., Pettit, R. K., Richert, L. A., Hogan, F., Mukku, V. J. R. V., et al. (2006). Antineoplastic Agents. 554, The Manitoba Bacterium *Streptomyces* sp.,1. *J. Nat. Prod.* 69, 804–806. doi: 10.1021/np058087v

Qiu, C., Tong, L., Yuan, T., Wang, F., Zhao, F., and Chen, L. (2017). Constituents from *Vitex negundo* var. *heterophylla* and their inhibition of nitric oxide production. *J. Nat. Med.* 71, 292–298. doi: 10.1007/s11418-016-1032-y

Qiu, Y., Guo, Q., Ran, Y.-Q., Lan, W.-J., Lam, C.-K., Feng, G.-K., et al. (2020). Cytotoxic alkaloids from the marine shellfish-associated fungus *Aspergillus* sp, XBB-4 induced by an amino acid-directed strategy. *RSC Adv.* 10, 4243–4250. doi: 10.1039/C9RA10306F

Reino, J. L., Guerrero, R. F., Hernández-Galán, R., and Collado, I. G. (2008). Secondary metabolites from species of the biocontrol agent *Trichoderma*. *Phytochem. Rev.* 7, 89–123. doi: 10.1007/s11101-006-9032-2

Roth, G. J., Binder, R., Colbatzky, F., Dallinger, C., Schlenker-Herceg, R., Hilberg, F., et al. (2015). Nintedanib: from discovery to the clinic. *J. Med. Chem.* 58, 1053–1063. doi: 10.1021/jm501562a

Santhanam, S., Ramu, A., Baburaj, B., and Kalpatu Kuppusamy, B. (2020). Application of metal free aromatization to total synthesis of perlolyrin, flazin, eudistomin U and harmane. *J. Heterocycl. Chem.* 57, 2121–2127. doi: 10.1002/jhet.3931

Shi, Z.-Z., Liu, X.-H., Li, X.-N., and Ji, N.-Y. (2020). Antifungal and antimicroalgal trichothecene sesquiterpenes from the marine algicolous fungus *Trichoderma brevicompactum* A-DL-9-2. *J. Agric. Food Chem.* 68, 15440–15448. doi: 10.1021/acs.jafc.0c05586

Spagnolo, P., Del Giovane, C., Luppi, F., Cerri, S., Balduzzi, S., Walters, E. H., et al. (2010). Non-steroid agents for idiopathic pulmonary fibrosis. *Cochrane Database Syst. Rev.* 9:Cd003134. doi: 10.1002/14651858.CD003134.pub2

Szepesi Kovács, D., Hajdu, I., Mészáros, G., Wittner, L., Meszéna, D., Tóth, E. Z., et al. (2021). Synthesis and characterization of new fluorescent boro-β-carboline dyes. *RSC Adv.* 11, 12802–12807. doi: 10.1039/D1RA02132J

Tchameni, S. N., Cotârle?, M., Ghinea, I. O., Bedine, M. A. B., Sameza, M. L., Borda, D., et al. (2020). Involvement of lytic enzymes and secondary metabolites produced by *Trichoderma* spp. in the biological control of *Pythium myriotylum*. *Int. Microbiol.* 23, 179–188. doi: 10.1007/s10123-019-00089-x

Vasarmidi, E., Tsitoura, E., Spandidos, D. A., Tzanakis, N., and Antoniou, K. M. (2020). Pulmonary fibrosis in the aftermath of the Covid-19 era (Review). *Exp. Ther. Med.* 20, 2557–2560. doi: 10.3892/etm.2020.8980

Walton, K. L., Johnson, K. E., and Harrison, C. A. (2017). Targeting TGF-β Mediated SMAD Signaling for the Prevention of Fibrosis. *Front. Pharmacol.* 8:461. doi: 10.3389/fphar.2017.00461

Wang, G.-Y.-S., Abrell, L. M., Avelar, A., Borgeson, B. M., and Crews, P. (1998). New hirsutane based sesquiterpenes from salt water cultures of a marine sponge-derived fungus and the terrestrial fungus *Coriolus consors*. *Tetrahedron* 54, 7335–7342. doi: 10.1016/S0040-4020(98)00398-6

Xue, L., Deng, D., Zheng, S., Tang, M., Yang, Z., Pei, H., et al. (2020). Design, synthesis and discovery of 2(1H)-quinolone derivatives for the treatment of pulmonary fibrosis through inhibition of TGF-β/smad dependent and independent pathway. *Eur. J. Med. Chem.* 197:112259. doi: 10.1016/j.ejmech.2020.112259

Yang, J., Wang, N., Yuan, H.-S., Hu, J.-C., and Dai, Y.-C. (2013). A new sesquiterpene from the medicinal fungus *Inonotus vaninii*. *Chem. Nat. Comp.* 49, 261–263. doi: 10.1007/s10600-013-0576-2

Yang, M.-L., Kuo, P.-C., Damu, A. G., Chang, R.-J., Chiou, W.-F., and Wu, T.-S. (2006). A versatile route to the synthesis of 1-substituted β-carbolines by a single step Pictet–Spengler cyclization. *Tetrahedron* 62, 10900–10906. doi: 10.1016/j.tet.2006.08.081

Yu, J.-Y., Shi, T., Zhou, Y., Xu, Y., Zhao, D.-L., and Wang, C.-Y. (2021). Naphthalene derivatives and halogenate quinoline from the coral-derived fungus *Trichoderma harzianum* (XS-20090075) through OSMAC approach. *J. Asian Nat. Prod. Res.* 23, 250–257. doi: 10.1080/10286020.2020.1729752

Zhao, J.-Q., Wang, Y.-M., Yang, Y.-L., Zeng, Y., Wang, Q.-L., Shao, Y., et al. (2017). Isolation and identification of antioxidant and α-glucosidase inhibitory compounds from fruit juice of *Nitraria tangutorum*. *Food Chem.* 227, 93–101. doi: 10.1016/j.foodchem.2017.01.031

Zhou, F., Tao, M., Shang, L., Liu, Y., Pan, G., Jin, Y., et al. (2021). Assessment of sequelae of COVID-19 nearly 1 year after diagnosis. *Front. Med. (Lausanne)* 8:717194. doi: 10.3389/fmed.2021.717194

Zou, J.-X., Song, Y.-P., and Ji, N.-Y. (2021a). Deoxytrichodermaerin, a harziane lactone from the marine algicolous fungus *Trichoderma longibrachiatum* A-WH-20-2. *Nat. Prod. Res.* 35, 216–221. doi: 10.1080/14786419.2019.1622110

Zou, J.-X., Song, Y.-P., Zeng, Z.-Q., and Ji, N.-Y. (2021b). Proharziane and harziane derivatives from the marine algicolous fungus *Trichoderma asperelloides* RR-dl-6-11. *J. Nat. Prod.* 84, 1414–1419. doi: 10.1021/acs.jnatprod.1c00188

Conflict of Interest: The authors declare that the research was conducted in the absence of any commercial or financial relationships that could be construed as a potential conflict of interest.

Publisher's Note: All claims expressed in this article are solely those of the authors and do not necessarily represent those of their affiliated organizations, or those of the publisher, the editors and the reviewers. Any product that may be evaluated in this article, or claim that may be made by its manufacturer, is not guaranteed or endorsed by the publisher.

frontiers | Frontiers in Microbiology

TYPE Review
PUBLISHED 19 August 2022
DOI 10.3389/fmicb.2022.984801

OPEN ACCESS

EDITED BY
Peng Zhang,
Tobacco Research Institute (CAAS), China

REVIEWED BY
Dong-Lin Zhao,
Tobacco Research Institute (CAAS), China
Guo-Bo Xu,
Guizhou Medical University, China

*CORRESPONDENCE
Dong Wang
dwang@cdutcm.edu.cn
Yun Deng
dengyun@cdutcm.edu.cn

SPECIALTY SECTION
This article was submitted to Antimicrobials, Resistance and Chemotherapy, a section of the journal Frontiers in Microbiology

RECEIVED 02 July 2022
ACCEPTED 28 July 2022
PUBLISHED 19 August 2022

CITATION
Lei L-R, Gong L-Q, Jin M-Y, Wang R, Liu R, Gao J, Liu M-D, Huang L, Wang G-Z, Wang D and Deng Y (2022) Research advances in the structures and biological activities of secondary metabolites from *Talaromyces*. *Front. Microbiol.* 13:984801. doi: 10.3389/fmicb.2022.984801

Research advances in the structures and biological activities of secondary metabolites from *Talaromyces*

Li-Rong Lei, Lei-Qiang Gong, Meng-Ying Jin, Rui Wang, Ran Liu, Jing Gao, Meng-Dan Liu, Li Huang, Guang-Zhi Wang, Dong Wang* and Yun Deng*

State Key Laboratory of Characteristic Chinese Medicine Resource of Southwest China, School of Pharmacy, Chengdu University of Traditional Chinese Medicine, Chengdu, China

The genus *Talaromyces* belongs to the phylum Ascomycota of the kingdom Fungi. Studies have shown that *Talaromyces* species yield many kinds of secondary metabolites, including esters, terpenes, steroids, alkaloids, polyketides, and anthraquinones, some of which have biological activities such as anti-inflammatory, bacteriostatic, and antitumor activities. The chemical constituents of fungi belonging to the genus *Talaromyces* that have been studied by researchers over the past several years, as well as their biological activities, are reviewed here to provide a reference for the development of high-value natural products and innovative uses of these resources.

KEYWORDS

***Talaromyces*, secondary metabolite, biological activity, polyketides, terpenoids, nitrogen compounds**

Introduction

As new diseases have emerged in recent years in response to environmental changes, the search for new sources to develop effective and safe drugs cannot be delayed. Natural resources offer the potential to find new structural classes with unique bioactivities for disease treatment. Endophytic fungi represent a rich source of bioactive metabolites (Uzma et al., 2018). The genus *Talaromyces* is widely distributed in soil, plants, sponges, and foods. Recent findings have demonstrated that *Talaromyces* are very abundant in marine environments (Nicoletti and Vinale, 2018). This may be due to the fact that the ocean itself is rich in species resources. Moreover, the extreme living conditions of the oceans have led marine microorganisms to develop more specific metabolic patterns and *Talaromyces* can produce a number of structurally diverse active substances. Their metabolites have a wide range of biological activities, such as anti-inflammatory meroterpenoids, thioester-containing benzoate derivatives that exhibit significant α-glucosidase inhibitory activity and oxaphenalenone dimers with broad antibacterial activity. In this paper, we will summarize and describe the research on the secondary metabolites of *Talaromyces* species

and their biological activities over the past several years, to provide a reference for subsequent research on *Talaromyces*, and to provide an outlook on the problems in the isolation and analysis of fungal secondary metabolites and the prospect of *Talaromyces* species. The current problems in the isolation and analysis of fungal secondary metabolites are summarized and the prospects of their utilization are provided.

Research status of *Talaromyces* species

Talaromyces belongs to the fungal phylum, ascomycete subphylum, ascomycetes, sporangia, and fungal family, which are widely distributed in sponges, plants, and soil. The colonies started out yellow and slowly turned gray-green over the course of a week. The middle of the back is yellow, and the edges are white (Figure 1). *Talaromyces* has various species (Figure 2). *T. marneffei*, *T. funiculosum*, and *T. purpureogenus* are the most studied strains at present. In addition, new strains, such as *T. rubrifaciens*, *T. australis*, *T. kendrickii*, *T. veerkampii*, *T. fuscoviridis*, and *T. stellenboschiensi* were isolated and purified (Visagie et al., 2015; Luo et al., 2016), and the corresponding chemical constituents were studied, which greatly enriched the species of chemical constituents of the fungi. The secondary metabolites of *Talaromyces* are rich in species, have novel structures and have good biological activity, which provides a basis for the development and application of endophytes. At present, the compounds isolated from the secondary metabolites of *Talaromyces* include esters, terpenoids and steroids, alkaloids, polyketones, anthraquinones and others, and most of them have good biological activities such as anti-inflammatory, antibacterial and antitumor activities.

Related studies have shown that *Talaromyces* species have great potential in agriculture, food, cosmetics, medicine, and environmental protection. In the field of agriculture, *Talaromyces* species can inhibit pathological changes in crops and promote crop growth. *T. tratensis* can be used as a biological control agent to control brown spot and dirty panicle diseases in rice (Dethoup et al., 2018). The secondary metabolites in *T. tratensis*, such as glucanase, can effectively treat rot disease that affects the yield of cucumbers and tomatoes (Halo et al., 2019). *T. flavus* not only promotes the growth of cotton and potatoes (Naraghi et al., 2012) but also produces an enzyme that plays an important role in resisting plant diseases for their strong capacity of degrading chitin (Xian et al., 2011). Most *Talaromyces* species can produce a red pigment (Frisvad et al., 2013; Venkatachalam et al., 2018), which can be used as a natural colorant in cosmetics and foods. The thermostable enzyme produced in *T. emersonii* can effectively improve bread quality with respect to hardness, staling, and loaf

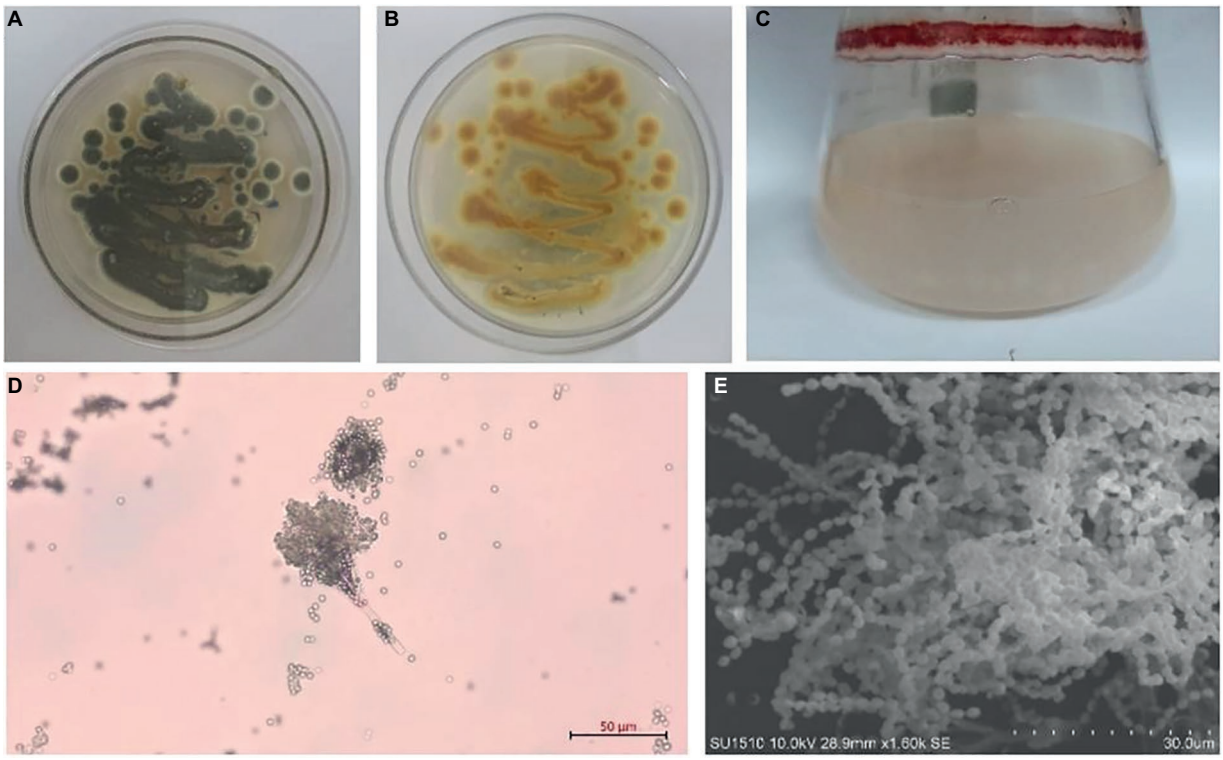

FIGURE 1
Talaromyces amestolkiae (CBS 365.48) *in vitro*. **(A,B)** Growth of *T. amestolkiae* on M1 semisolid medium at 30°C after 7 d and **(C)** in liquid M1 medium at 30°C after 7 d; **(D)** conidia, scale bar=10 µm; **(E)** *T. amestolkiae*, SEM.

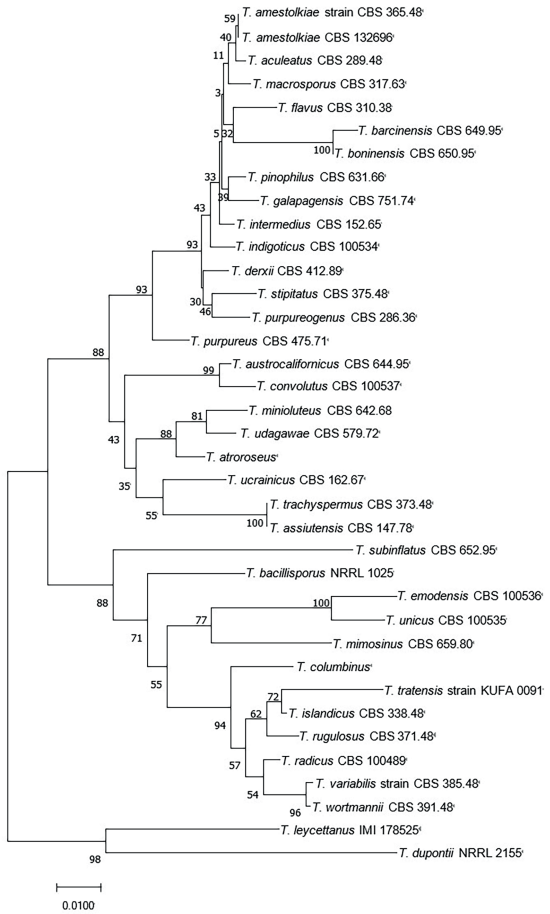

FIGURE 2
Neighbor-joining tree of *T. amestolkiae* (CBS 365.48) based on ITS rDNA.

volume (Waters et al., 2010). An aspartic protease from *T. leycettanus* has strong proteolytic activity and improves the clarity of fruit juice (Guo et al., 2019). *Talaromyces* species can produce many other bioactive secondary metabolites, and these compounds have been found to have antibacterial, anti-inflammatory, antitumor, antioxidant, nematocidal, and other effects in medical research. Secondary metabolites from an Australian Marine Tunicate-Associated Fungus *Talaromyces* sp. (CMB-TU011) exhibit certain antibacterial activities (Dewapriya et al., 2018). GH3 β-glucosidases from *T. amestolkiae* expressed in *Pichia pastoris* can transglycosylate phenolic molecules, and the resulting transglycosylation products can improve the biological activity of the original aglycones against breast cancer cells (Méndez-Líter et al., 2019). Talaraculones from a strain of *T. aculeatus* can inhibit the activity of α-glucosidase and can be used to prevent the progression of type II diabetes, as well as for the early treatment of type II diabetes (Ren et al., 2017). In the field of environmental protection, biosorption by microorganisms has been proven to be an effective technique for removing heavy metals from wastewater. A biological adsorbent formed by combining *T. amestolkiae* with a specific chitosan sponge can effectively remove trace heavy metals or high concentrations of lead from industrial wastewater (Wang et al., 2019). *Talaromyces* sp. KM-31 can remove arsenic from heavily polluted wastewater and can thus be employed in bioremediation strategies (Nam et al., 2019).

According to the classification of the chemical components, this paper will summarize and explain research carried out on secondary metabolites from *Talaromyces* species and their biological activities over the past 10 years with the aim of providing references for follow-up studies of *Talaromyces*, at the same time, the problems existing in the separation and analysis of fungal secondary metabolites and the prospect of *Talaromyces* species, as well as summarizing existing problems in the separation and analysis of fungal secondary metabolites and prospects for the use of secondary metabolites from *Talaromyces* species.

Studies on the chemical constituents and activity of *Talaromyces*

Ester-based compounds

Esters

Esters are chemical compounds derived by reacting an oxoacid with a hydroxyl compound such as an alcohol or phenol (Sparkman et al., 2011). Dinapinones AB1 and AB2 (**1** and **2**), dinapinones AC1 and AC2 (**3** and **4**), dinapinones AD1 and AD2 (**5** and **6**), and dinapinones AE1 and AE2 (**7** and **8**; Figure 3), which were isolated from the fermentation broth of *T. pinophilus* FKI-3864 in 2013 (Kawaguchi et al., 2013), were identified and characterized as ester derivatives. These dinaphthoquinones have the same backbone of aryl dihydronaphthoquinone and consist of one monapinone A and one different monapinone in a heterodimer. Compound **2** had a strong inhibitory effect on triacylglycerol synthesis in intact mammalian cells, with an IC_{50} value of 1.17 μM.

Seventeen new polyesters were isolated from the fermentation products of the wetland soil-derived fungus *T. flavus*, namely, talapolyesters A–F (**9**–**12**, **22** and **24**), 15G256ν (**13**), 15G256ν-me (**14**), 15G256π (**15**), 15G256β-2 (**16**), 15G256α-2 (**17**), 15G256α-2-me (**18**), 15G256ι (**19**), 15G256β (**20**), 15G256α (**21**), 15G256α-1 (**23**) (Figure 4), and 15G256ω (**25**) (He et al., 2014b). All macrocyclic polyesters (**19**–**25**) were cytotoxic to HL-60, SMMC-7721, A-549, MCF-7, and SW480 tumor cells, while linear polyesters (**9**–**18**) were inactive with IC_{50} > 40 mM compared to cisplatin. This suggests that a macrocyclic structure is required for cytotoxicity. Among them, **20** and **25** showed significant cytotoxic activity against MCF-7 cell lines with IC_{50} of 3.27 and 4.32 μM, respectively. The cytotoxic activity of 15G256 polyester was systematically investigated for the first time and a tight conformational relationship is presented.

Talaromycolides A–C (**26**–**28**), rubralide C (**29**), sclerotinin A (**30**), alternariol (**31**), and penicillide (**32**) were obtained from the

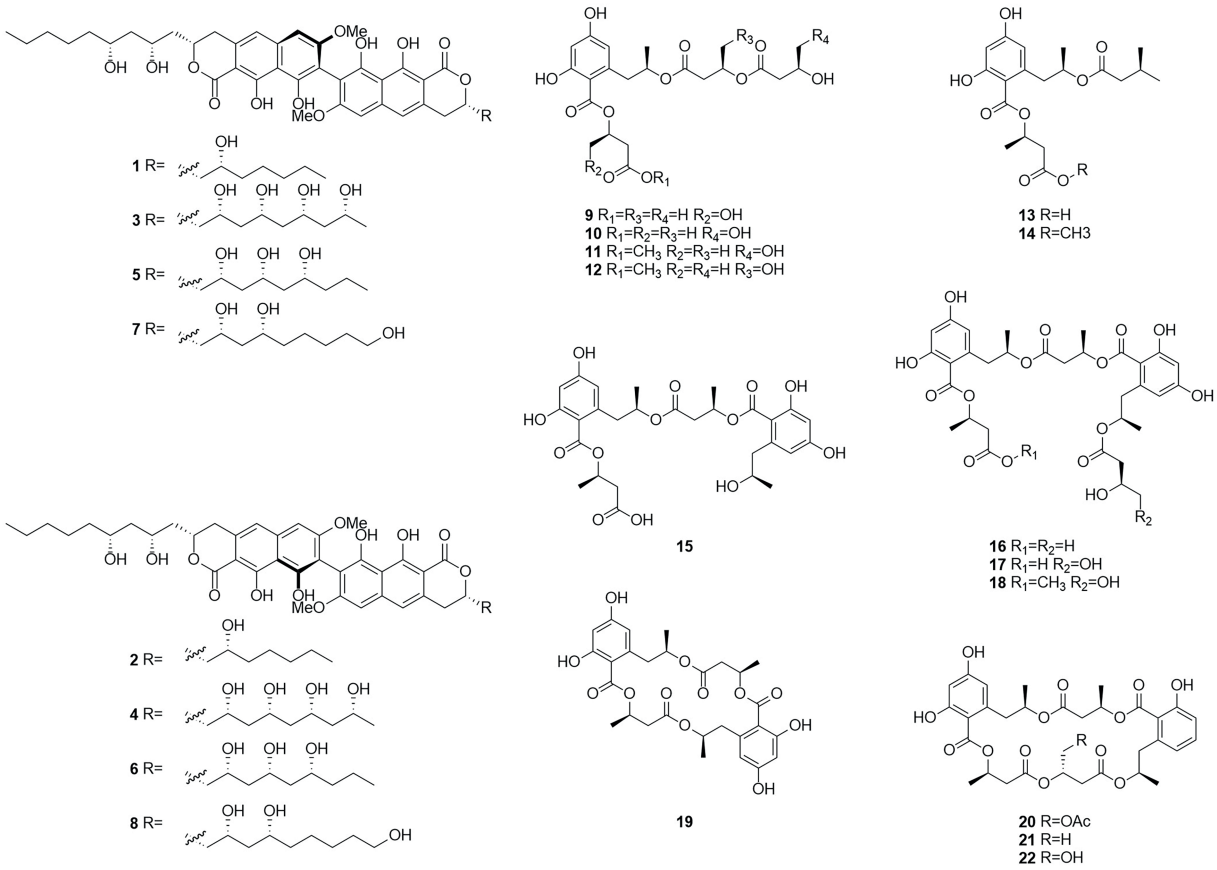

FIGURE 3
Chemical structures of compounds **1–22**.

epiphytic fungal strain *T. pinophilus* AF-02, which was isolated from green Chinese onion, in 2015 (Zhai et al., 2015). Compound **26** [minimum inhibitory concentration (MIC) = 12.5 μg/ml] showed stronger inhibitory activity against *Clostridium perfringens* than erythromycin, streptomycin, acheomycin, and ampicillin. Compound **26** (MIC = 6.25 μg/ml) showed similar inhibitory activity to acheomycin and was superior to levofloxacin, ampicillin, and streptomycin against *Bacillus subtilis*. Compound **27** (MIC = 12.5 μg/ml) showed higher inhibitory activity than erythromycin and ampicillin against *Bacillus megaterium* and higher inhibitory activity than erythromycin, ampicillin, and streptomycin against *Escherichia coli* (MIC = 25 μg/ml). Compound **28** (MIC = 25 μg/ml) was more active against *C. perfringens* than erythromycin, streptomycin, acheomycin and ampicillin.

In 2015, the structures of compounds **33** and **34** were characterized as deacetylisowortmins A and B, which were isolated from *T. wortmannii* LGT-4 derived from the leaves of a mangrove plant *Acanthus ilicifolius* (Fu et al., 2016). Four esters, talaromyones A and B (**35** and **36**), penicillide (**32**), and purpactin A (**37**), were obtained from a fermentation product of the mangrove endophytic fungus *T. stipitatus* SK-4 in 2016 (Cai et al., 2017). Compound **36** exhibited antibacterial activity against *B. subtilis* with an MIC value of 12.5 μg/ml. In the α-glucosidase inhibition assay, compounds **36** and **37** showed some inhibitory activity with an IC_{50} values of 48.4–99.8 μM.

Five butenolides (**38**–**42**), seven (3S)-resorcylide derivatives (**43**–**49**) (Figure 5), two butenolide-resorcylide dimers (**50** and **51**) were yielded by culture on a solid rice medium of *T. rugulosus* isolated from the Mediterranean sponge *Axinella cannabina* (Küppers et al., 2017). The butenolide–resorcylide dimers talarodilactones A and B (**50** and **51**) was highly cytotoxic to the L5178Y mouse lymphoma cell line with IC_{50} of 3.9 μM and 1.3 μM, respectively.

Talaromycin A (**52**) and clearanol A (**53**) were isolated from the endophytic fungus *Talaromyces* sp. MH551540 associated with *Xanthoparmelia angustiphylla* in 2018 (Yuan et al., 2018). Compound **52** and **53** had selective cytotoxicity against MDA-MB-231 cells. Compound **54**, which was identified as wortmannine F, was obtained from cultures of the endophytic fungus *T. wortmannii* LGT-4 isolated from *Tripterygium wilfordii* and has a strong phosphoinositide-3-kinase-α (PI3K-α) inhibitory activity with an IC_{50} value of 25 μM (Zhao et al., 2019b). Pentalsamonin (**55**) was isolated from submerged fermentation on Bengal gram husk (BegH) of *T. purpureogenus* CFRM-02 (Pandit et al., 2018). The MIC and MBC of pentalsamonin (**55**)

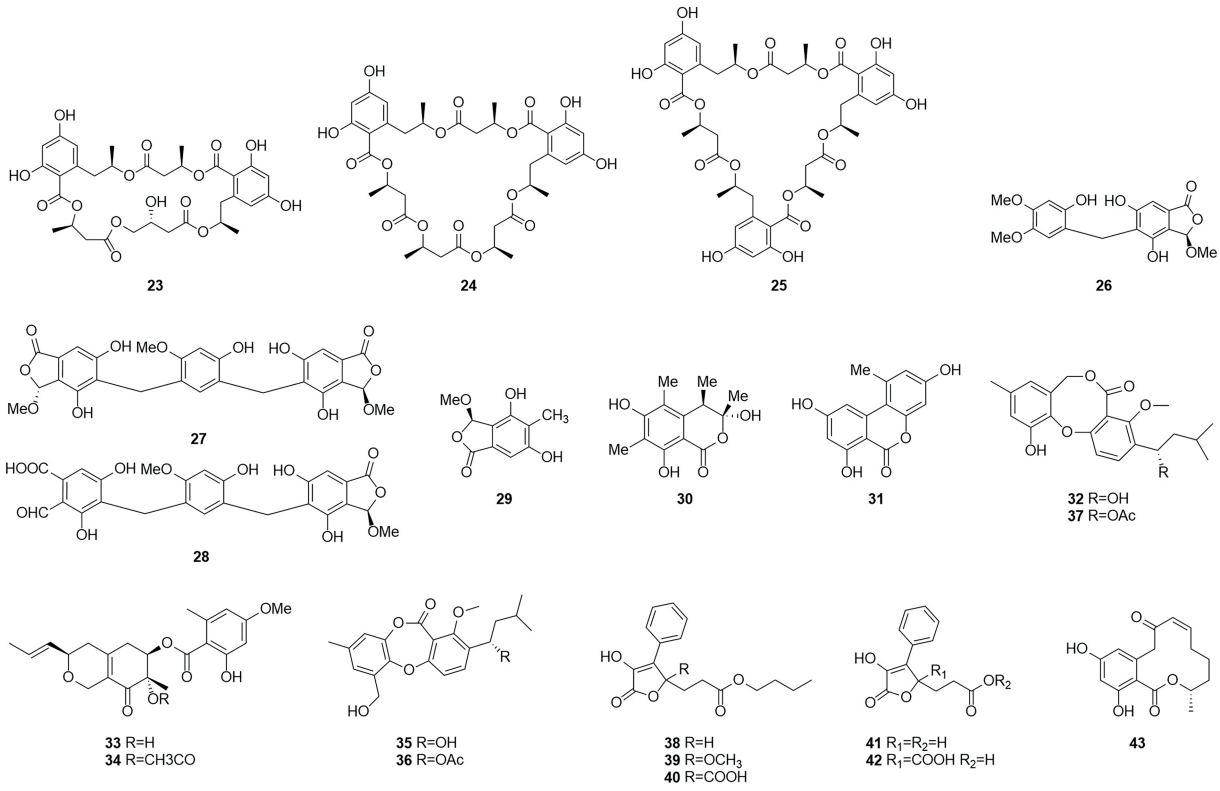

FIGURE 4
Chemical structures of compounds **23–43**.

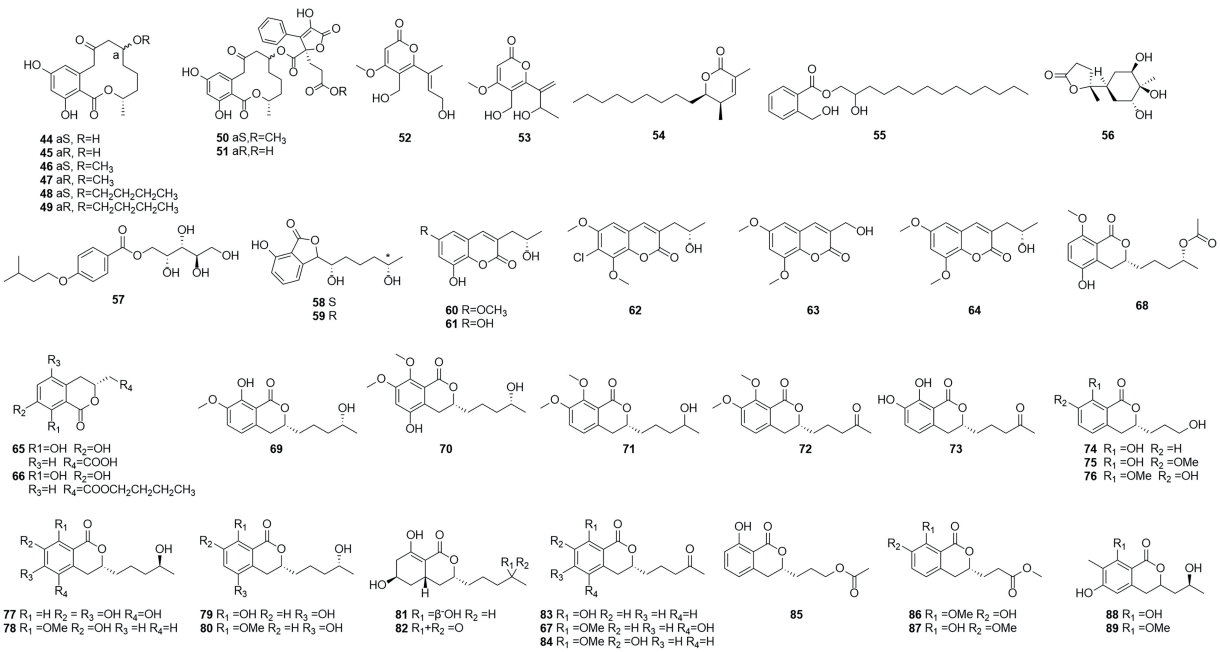

FIGURE 5
Chemical structures of compounds **44–89**.

against *B. subtilis*, *Staphylococcus aureus*, *E. coli*, and *Klebsiella pneumoniae* were 62.5–125 and 125–250 μg/ml, respectively.

Talaromarnine A (**56**) and talaromarnine B (**57**) were obtained from cultures of *T. marneffei*, an endophytic fungus of *Epilobium angustifolium* (Yang et al., 2021). Two previously undescribed phthalides, amestolkins A (**58**) and B (**59**) were isolated from *T. amestolkiae* derived from *Syngnathus acus* Linnaeus in Lingshui Li Autonomous County, Hainan Province, China, which has the same planar structure of (1,5-dihydroxyhexyl)-7-hydroxyisobenzofuran-1(3H)-one. They were shown to inhibit gene expressions of proinflammatory factors including C-C motif chemokine ligand 2 (CCL-2), tumor necrosis factor-α (TNF-α), and interleukin-6 (IL-6) as well as reducing the secretion of inducible nitric oxide synthase (iNOS) in BV2 microglia at the concentration of 30 μM (Huang et al., 2022).

Coumarins

Coumarinic compounds are lactones resulting from the fusion of a benzene ring and a α-pyrone ring (Batista et al., 2021). Talacoumarins A and B (**60** and **61**), which were characterized as coumarins, were isolated from the fermentation broth of the wetland soil fungus *T. flavus* (He et al., 2014c). Activity tests showed that compounds **60** and **61** exhibited moderate activity against the aggregation of Aβ42. This was the first report to state that a coumarin can inhibit Aβ42 aggregation. A new compound **62**, chloropestalasin A was isolated from *T. amestolkiae* derived from submerged wood collected from fresh water, along with 3-hydroxymethyl-6,8-dimethoxycoumarin (**63**) and pestalasin A (**64**) (El-Elimat et al., 2021).

Isocoumarin

Isocoumarin is the common name for 1H-2-benzopyran-1-one skeleton (Braca et al., 2012). Three dihydroisocoumarins (**65**–**67**) were yielded by culture on a solid rice medium of *T. rugulosus* isolated from the Mediterranean sponge *Axinella cannabina* (Küppers et al., 2017). Six new isocoumarin derivatives, talaromarins A-F (**68**–**73**), and 17 known analogues (**67**, **74**–**89**), were isolated from the mangrove-derived fungus *T. flavus* (Eurotiales: Trichocomaceae) TGGP35 (Cai et al., 2022). Compounds **67**, **73**–**78**, **84**–**85** and **87**–**89** showed similar or better IC_{50} values for antioxidant activity ranged from 0.009 mM to 0.27 mM, compared to the positive control trolox (IC_{50} = 0.29 mM). Compounds **77**, **84**, **87** and **89** showed strong inhibitory activity. IC_{50} values of 0.10 ~ 0.62 mM against α-glucosidase and 0.5 mM for the positive control acarbose activity at 50 μg/ml and 1 mg/ml concentrations. These results suggest that isocoumarins have important applications in the development of antioxidants and in the control of diabetes mellitus. Talaroisocoumarin A (**73**) was obtained from marine-derived *Talaromyces* sp. ZZ1616 in potato dextrose broth medium. The MIC values of talaroisocoumarin A against methicillin-resistant *S. aureus*, *E. coli* and *Candida albicans* were 36.0 μg/ml, 32.0 μg/ml and 26.0 μg/ml, respectively (Ma et al., 2022).

Polyketones

Polyketides were named in the 1890s to refer to a structurally diverse group of natural products that contained many carbonyls and alcohols, generally separated by methylene carbons. They are synthesized by a series of decarboxylative condensation reactions between small carboxylic acids and malonate using polyketide synthases (PKSs; Richardson and Khosla, 1999). Two polyketones, mitorubrin (**90**) and monascorubrin (**91**) (Figure 6), were isolated from *T. atroroseus* (Frisvad et al., 2013). Because no citrinin was found in any *Talaromyces* species, it may be a good alternative for red pigment production. Compound **92**, which was characterized as a polyketone and named talaroxanthone, was obtained from the fermentation products of an endophytic strain of a *Talaromyces* sp. isolated from the Amazonian rainforest plant *Duguetia stelechantha* root (Koolen et al., 2013). Five compounds, 9a-epi-bacillisporin E (**93**), 1-epi-bacillisporin *F* (**94**), and bacillisporins F-H (**95**–**97**) were isolated from the fermentation products of the soil fungus *T. stipitatus* (Zang et al., 2016). Compound **97** exhibited some antibacterial activity and some cytotoxicity against HeLa cells. Compounds **98**–**100**, wortmannilactones I1-I3, which were identified and characterized as three new polyketides, were purified from *T. wortmannii* using the one strain–many compounds strategy. These compounds showed selective inhibitory activity against NADH fumarate reductase (Liu et al., 2016).

The polyketone 3-O-methylfunicone (**101**) was isolated from the culture filtrate of an endophytic strain of *T. pinophilus* obtained from the strawberry tree (*Arbutus unedo*) in 2017 (Vinale et al., 2017). On water agar at a concentration of 0.1 mg/ml, it completely inhibited the growth of phytopathogenic fungi such as *Rhizoctonia solani* (De Stefano et al., 1999). Eleven polyketones, talaraculones A–F (**102**–**107**), pinazaphilone B (**108**), pinophilin B (**109**), Sch 725680 (**110**), (−)-mitorubrin (**111**), and (−)-mitorubrinol (**112**), were obtained from the fungus *T. aculeatus*, which was isolated from saline-alkali soil (Ren et al., 2017). The results of the activity tests showed that compounds **102** and **103** exhibited very high levels of inhibitory activity against α-glucosidase than the positive control acarbose (IC_{50} = 101.5 μM), with IC_{50} values of 78.6 and 22.9 μM, respectively. Compounds that were defined and characterized as six polyketones, paecillin D (**113**), secalonic acid A (**114**), blennolide G (**115**), versixanthone A (**116**) (Figure 7), penicillixanthone A (**117**), and paecillin B (**118**), were isolated from the fermentation products of three Amazonian plants endophytic strains of *T. stipitatus* in 2018 (da Silva et al., 2017). Activity tests showed that compounds **113** and **116** were active against yeasts (MICs of 15.6 μg/ml and 31.3 μg/ml, respectively).

Six new nonadride derivatives, named talarodrides A–F (**119**–**124**), were isolated from the antarctic sponge-derived fungus *Talaromyces* sp. HDN1820200. Talarodride A (**119**) and talarodride B (**120**) showed selective inhibitory effects against *Proteus mirabilis* and *Vibrio parahemolyticus* with MICs of 3.13–12.5 μM (Zhao et al., 2021b).

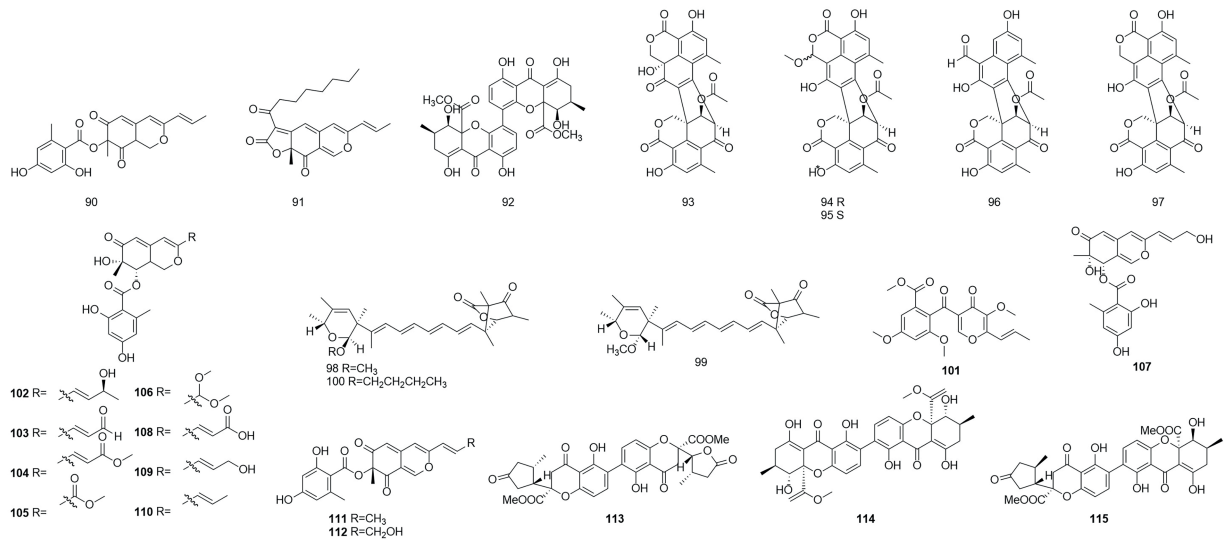

FIGURE 6
Chemical structures of compounds **90–115**.

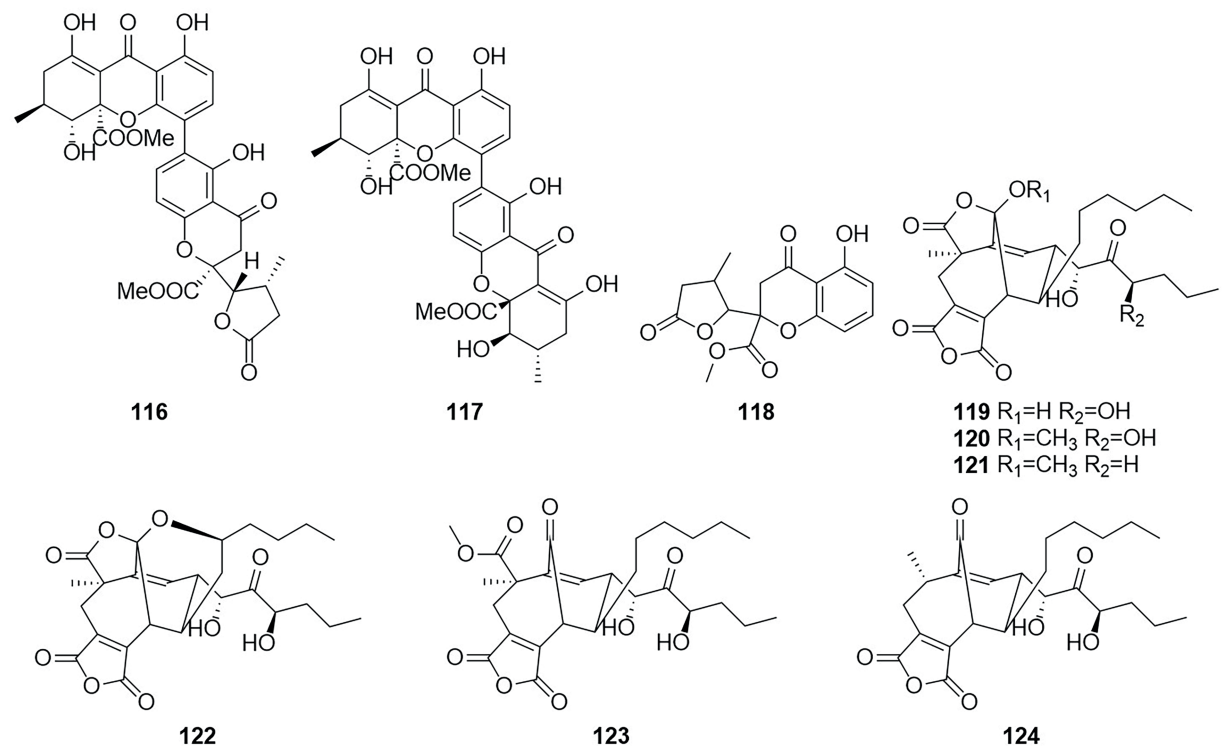

FIGURE 7
Chemical structures of compounds **116–124**.

Anthraquinone

Anthraquinones (AQs) are derived from anthracenes and have two keto groups, mostly in positions 9 and 10. The basal compound, anthraquinone (9,10-dioxoanthracene), can be substituted in various ways, resulting in a great diversity of structures (Vasil et al., 1984). Two anthraquinone compounds skyrin (**125**) and emodin (**126**) (Figure 8) were obtained from an extract of the mangrove

endophytic fungus *Talaromyces* sp. ZH-154, which was isolated from the stem bark of *Kandelia candel* (Liu et al., 2010). Both compounds exhibited moderate cytotoxic activity against KB and KBv200 cells. The anthraquinone monomer (**126**) showed higher bioactivity than the dimer dianthraquinone (**125**). A new anthraquinones biemodin (**127**) and five known anthraquinones emodic acid (**128**), skyrin (**125**), oxyskyrin (**129**), and rugulosins A and B (**130** and **131**) were isolated from cultures of the endophytic fungus *T. wortmannii* obtained from healthy inner tissues of *Aloe vera* (Bara et al., 2013a). In the same year, two anthraquinone compounds, talaromannins A and B (**132** and **133**), were obtained from *T. wortmannii* in *A. vera* (Bara et al., 2013b). Both compounds displayed moderate MICs in a comparable concentration range for *S. aureus* and **132** represented the most active congeners.

Five anthraquinones were isolated from the solid fermentation products of the endophytic fungus *Talaromyces* sp. YE3016 (Xie et al., 2016). These compounds were 3-demethyl-3-(2-hydroxypropyl)-skyrin (**134**), skyrin (**125**), oxyskyrin (**129**), emodin (**126**), and 1,3,6-trihydroxy-8-methylanthraquinone (**135**). Activity tests showed that compounds **134**, **125**, and **129** displayed moderate cytotoxic activity against the MCF-7 cell line. Six anthraquinone compounds, 2,2′-bis-(7-methyl-1,4,5-trihydroxy-anthracene-9,10-dione) (**136**), emodin (**126**), questinol (**137**), citreorosein (**138**), fallacinol (**139**), and rheoemodin (**140**), were obtained from an ethyl acetate extract of a culture of the fungus *T. stipitatus* KUFA 0207, which is derived with a marine sponge (Noinart et al., 2017). Emodin (**126**), questinol (**137**), citreorosein (**138**), fallacinol (**139**), and rheoemodin (**140**) were tested for their anti-obesity activity using the zebrafish Nile red assay. The results showed that only the anthraquinones questinol (**137**) and citreorosein (**138**) had significant anti-obesity activity. Questinol (**137**) and citreorosein (**138**) reduced >60% and > 90% of the stained lipids with the IC_{50} values of 0.95 and 0.17 μM, respectively. The positive control resveratrol (REV) had an IC_{50} value of 0.6 μM. Emodin (**140**) caused toxicity (death) for all exposed zebrafish larvae after 24 h, while fallacinol (**139**) and rheoemodin (**140**) did not have any significant effects. It is interesting to observe that questinol (**137**), citreorosein (**138**) and fallacinol (**139**) are structurally similar, all having a hydroxymethyl group on C-6 and a hydroxyl group on C-8. Replacing the hydroxyl group on C-1 by a methoxyl group, as in questinol (**137**), diminishes the activity whereas replacing the hydroxyl group on C-3 with a methoxyl group, as in fallacinol (**139**), completely removes the anti-obesity activity. Therefore, it seems that the hydroxymethyl group on C-6 and the hydroxyl groups on C-3 and C-8 are necessary for the anti-obesity activity of the polyhydroxy anthraquinones.

Terpenoids

Terpenoids otherwise known as isoprenoids are a large and diverse class of naturally occurring compounds derived from five carbon isoprene units (Reyes et al., 2018). Terpenoids are classified as hemiterpenes (C5), monoterpenes (C10), sesquiterpenes (C15), diterpenes (C20), sesterterpenes (C25), triterpenes (C30), and tetraterpenes/carotenoids (C40) (Adefegha et al., 2022).

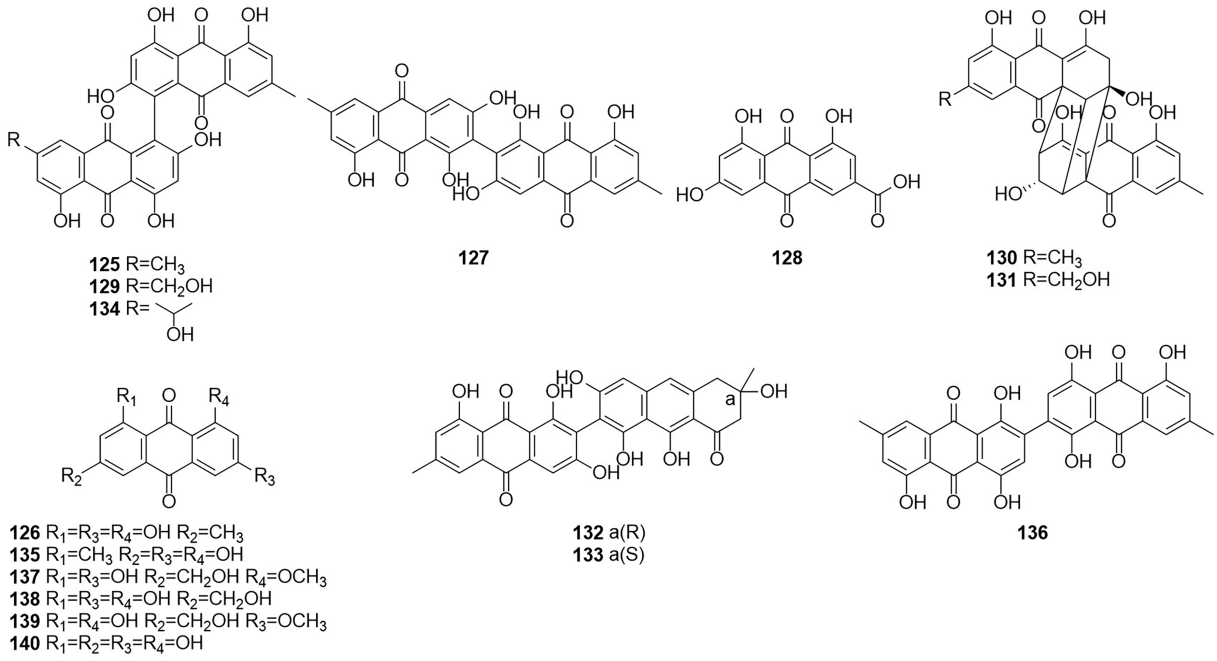

FIGURE 8
Chemical structures of compounds **125–140**.

Compound **141** (Figure 9), which was characterized as a new fusicoccane diterpene and named pinophicin A, was obtained from the endophytic fungus *T. pinophilus* collected from the aerial parts of *Salvia miltiorrhiza* in 2019 (Zhao et al., 2021a). Four new sesquiterpene peroxides, talaperoxides A–D (**142**–**145**), were isolated from the fermentation products of the mangrove endophytic fungus *T. flavus* (Li et al., 2011). Of these compounds, compounds **143** and **145** showed cytotoxicity against human cancer cell lines MCF-7 and MDA-MB-435, HepG2, HeLa and PC-3 with IC_{50} values between 0.70 and 2.78 μg/ml. Compound **146**, which was characterized as a new nardosinane-type sesquiterpene and named talaflavuterpenoid A, was isolated from the fermentation products of *T. flavus* (He et al., 2014a).

The new diterpenoid roussoellol C (**147**) was isolated from the fermentation products of *T. purpureogenus* (Wang et al., 2018). Compound **147** had an inhibitory effect on the MCF-7 cancer cell line, with an IC_{50} value of 6.5 μM. A new spiroaxane sesquiterpenoid talaminoid A (**148**) and two drimane sesquiterpenoid talaminoids B and C (**149** and **150**), together with four known compounds (**151**–**154**) were obtained from the fermentation broth of *T. minioluteus* (Nie et al., 2019). Compounds **148**, **151**, and **152** showed significant suppressive effect on the production of NO on LPS-induced BV-2 cells, with IC_{50} values ranging from 4.97 to 7.81 μM. In addition, **148**, **151**, and **152** exhibited significant anti-inflammatory activities against the production of TNF-α and IL-6. Further immunofluorescence experiments revealed the mechanism of action to be inhibitory the NF-kB-activated pathway. The structure of compound **155** was defined and characterized as sordarin, which was isolated from the Australian fungus *Talaromyces* sp. CMB-TU011, which is associated with a marine tunicate (Dewapriya et al., 2017). According to a related study, this compound exhibited antifungal activity (Domínguez et al., 1998). Four new sesquiterpene lactones (**156**–**159**) and three known compounds, purpuride (**151**), berkedrimane B (**152**) and purpuride B (**160**), were isolated from cultures of the marine fungus *T. minioluteus* (Ngokpol et al., 2015). Compounds **152, 156, 159** exhibited weak cytotoxic activity against the HepG2 cancer cell line.

Meroterpenoids

Meroterpenoids are natural products that are partially derived from terpenoid biosynthetic pathways, since the prefix "mero-" has the meanings of "part," "partial," and "fragment" (Matsuda and Abe, 2020). Four meroterpenoids talaromyolides A–D (**161**–**164**) and Talaromytin (**165**) (Figure 10) were isolated from the marine fungus *Talaromyces* sp. CX11 (Nie et al., 2019). Compound **164** exhibited potent antiviral activity against pseudorabies virus (PRV) with a IC_{50} value of 3.35 μM. Activity tests showed that this compound did not exhibit *in vitro* growth-inhibiting activity against MCF-7 breast adenocarcinoma, NCI-H460 non-small-cell lung cancer, or A375-C5 melanoma cell lines by a method based on the protein-binding dye sulforhodamine B.

A new meroterpenoid, taladrimanin A (**166**), was isolated from the marine-derived fungus *Talaromyces* sp. HM6-1-1. Compound **166** exhibited antitumor activity against MGC803 and MKN28 gastric cancer cells; it also inhibited colony formation and induced apoptosis in MGC803 cells both in a concentration-dependent manner. Additionally, **166** displayed selective antibacterial activity against *S. aureus* 6538P, and low activities toward strains of *V. parahaemolyticus* and *E. coli* (Hong et al., 2022). The structures of compounds **167**–**173**, which were obtained from the fermentation products of the soil fungus *Talaromyces* sp. YO-2 in Osaka, Japan, were defined and characterized as the seven meroterpenoids chrodrimanin A–H (Hayashi et al., 2012a,b). Chrodrimanin B (**168**) exhibited insecticidal activity with an LD_{50} value of 10 ug/g of diet. Chrodrimanins D–F (**170**–**172**) showed insecticidal activity against silkworms with respective LD_{50} values of 20, 10, and 50 ug/g of diet. Compounds 145–148, which were identified as the four meroterpenoid compounds talarolutin A–D, were isolated from the fermentation broth of a strain of the fungus *T. minioluteus* obtained from healthy surface sterilized leaves of milk thistle (Kaur et al., 2016).

Steroids

Steroids are extremely important medicinally active organic compounds with four rings constructed in a highly specific perhydrocyclopentano[α]phenanthrene orientation. In general, the steroid core structure has 17 carbon atoms connected with 4 fused rings in a specific way. Three of these are cyclohexanes (A, B, and C) and one is cyclopentane system (D ring) (Borah and Banik, 2020). Talasterone A (**174**) (Figure 11), an unprecedented 6/6/5 tricyclic 13 (14 → 8) abeo-8,14-seco-ergostane steroid, was characterized from *T. adpressus* isolated from soil collected from Yalong Bay in Sanya, Hainan (Zhang et al., 2022a). A new compound 3-acetylergosterol-5,8-endoperoxide (**175**) was obtained from the fermentation products of the sponge endophytic fungus *T. trachyspermus* KUFA 0021 (Kuml et al., 2014). In 2017, the new compound talarosterone (**176**) and cyathisterone (**177**) were obtained from the fermentation products of the sponge fungus *T. stipitatus* KUFA 0207 (Noinart et al., 2017). A new withanolide, talasteroid (**178**) was obtained from rice culture of the marine-derived fungus *T. stollii* HBU-115 (Zhang et al., 2022c). Five undescribed sterol derivatives (**179–183**), (22E,24R)-7α-methoxy-5α,6α-epoxyergosta-8(14),22-diene-3β,15β-diol, (22E,24R)-5α,6α-epoxyergosta-8(14),22-diene-3β,7β,15α-triol, (22E,24R)-3β,5α-dihydroxy-14β,15β-epoxyergosta-7,22-diene-6-one, (22E,24R)-6α-methoxy-7α,15β-dihydroxyergosta-4,8(14),22-triene-3-one, and (25S)-ergosta-7,24(28)-diene-3β,4α,6α,26-tetraol were isolated from the extract of *T. stipitatus* (Zhang et al., 2021). The antiproliferative activities of compound **179**–**183** were mainly mediated by inducing cell apoptosis.

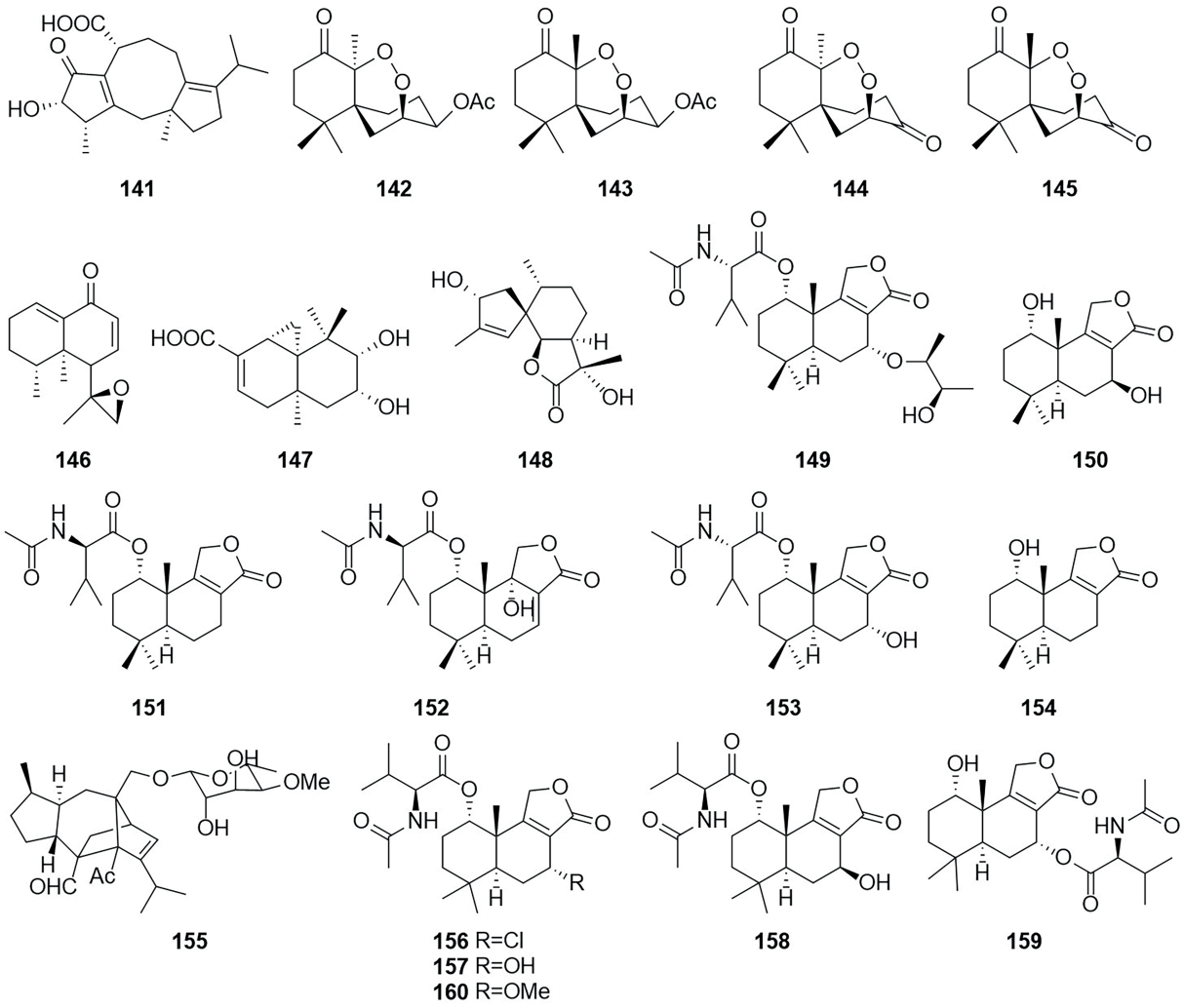

FIGURE 9
Chemical structures of compounds **141–160**.

Nitrogen-containing compound

Alkaloids

Alkaloids are structurally diverse compounds generally classified as such due to the basic character of the molecule (from Latin alkali) and a presence of at least one nitrogen atom, preferably in a heterocycle (Zotchev, 2013). The compound PP-R (**184**) (Figure 12) was isolated from *T. atroroseus* (Frisvad et al., 2013). The red pigments is of interest for the industry as they are stable and non-toxic and can be used as food colorants. Herquline B (**185**) was isolated from the culture filtrate of an endophytic strain of *T. pinophilus* obtained from the strawberry tree (*A. unedo*) (Vinale et al., 2017). In 2011, six indole alkaloids, talathermophilins A–E (**186–188**,**190–191**) and cyclo(glycyltryptophyl) (**189**), were obtained from the thermophilic fungal strain *T. thermophilus* YM3-4 (Guo et al., 2011, 3–4). ZG-1494α (**192**) was isolated from an ethyl acetate extract of a culture broth of *T. atroroseus* (Frisvad et al., 2013). According to a related study, compound **192** can be used as a novel inhibitor of platelet-activating factor acetyl-transferase (West et al., 1996). Nine alkaloids, 2-[(S)-hydroxy(phenyl) methyl]-3-methylquinazolin-4(3H)-one (**193**), 2-[(R)-hydroxy(phenyl)methyl]-3-methylquinazolin-4(3H)-one (**194**), roquefortine C (**195**), Z-roquefortine C (**196**), viridicatol (**197**), penitrem A (**198**), penijanthine A (**199**), paspaline (**200**), and 3-deoxo-4b-deoxypaxilline (**201**), were isolated from the fermentation broth of the algal endophytic fungus *Talaromyces* sp. *cf*-16 in 2014, of which compounds **196–199** could inhibit *S. aureus* (Yang et al., 2016).

Five new compounds, namely talaromanloid A (**202**), 10-hydroxy-8-demethyltalaromydine and 11-hydroxy-8-demethyltalaromydine (**203** and **204**) and ditalaromylectones A and B (**205** and **206**) were identified from the marine-derived fungus *T.* mangshanicus BTBU20211089, which was isolated

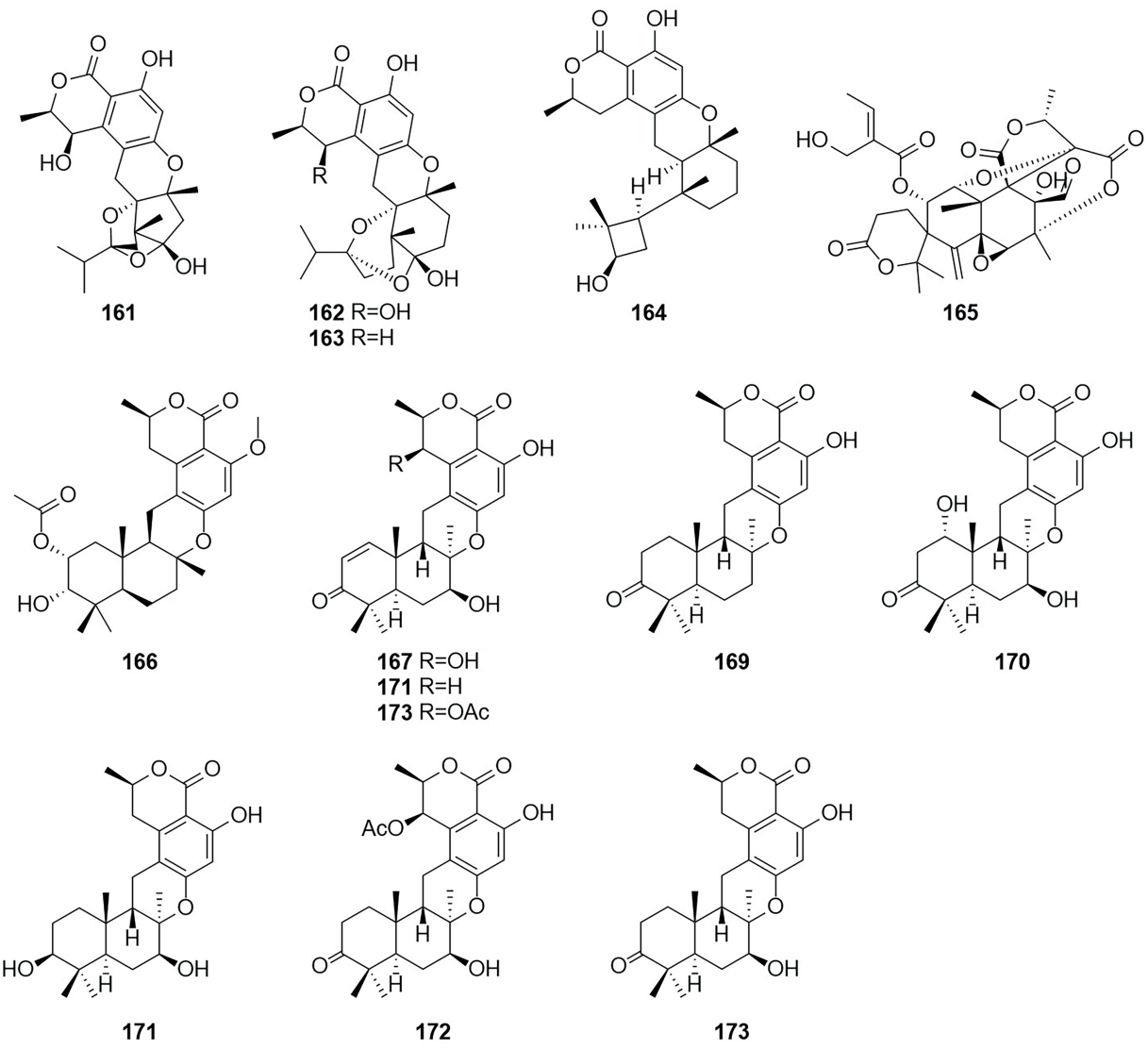

FIGURE 10
Chemical structures of compounds **161–173**.

from a sediment sample collected from the South China Sea. Compound **205** showed an inhibitory effect against *C. albicans* with an MIC value of 200 μg/ml (Zhang et al., 2022b). The endophytic fungus *T. radicus* isolated from Catharanthus roseus was cultured in M2 liquid fermentation medium and PDA fermentation medium. Vincristine (**207**) and vinblastine (**208**) were obtained from this fungus, of which HeLa cells exhibited the highest susceptibility to vincristine. In addition, the apoptosis-inducing activity of vincristine obtained from this fungus was established *via* cell cycle analysis, loss of mitochondrial membrane potential, and DNA fragmentation patterns (Palem et al., 2015). In 2017, the alkaloid talaramide A (**209**) was obtained by culturing of the mangrove endophytic fungus *Talaromyces* sp. HZ-YX1 on a solid rice medium with sea water displayed promising inhibition of the activity of mycobacterial protein kinase G, with an IC_{50} value of 55 μM. A possible biosynthetic pathway was proposed in the paper (Chen et al., 2017).

Amides

Amides are amines with a carbonyl group associated with the ammonia-associated carbon (Jackson, 2008). Six macrolides, thermolides A–F (**210**–**215**) (Figure 13), were isolated from the fermentation products of the thermophilic fungus *T. thermophilus* in 2012 (Guo et al., 2012). Of these compounds, compounds **210** and **211** exhibited strong inhibitory activity against nematodes, with LC_{50} values of 0.5–1.0 μg/ml. Two new compounds, namely talaromydene (**216**) and talaromylectone (**217**) were identified from the marine-derived fungus *T. mangshanicus* BTBU20211089, which was isolated from a

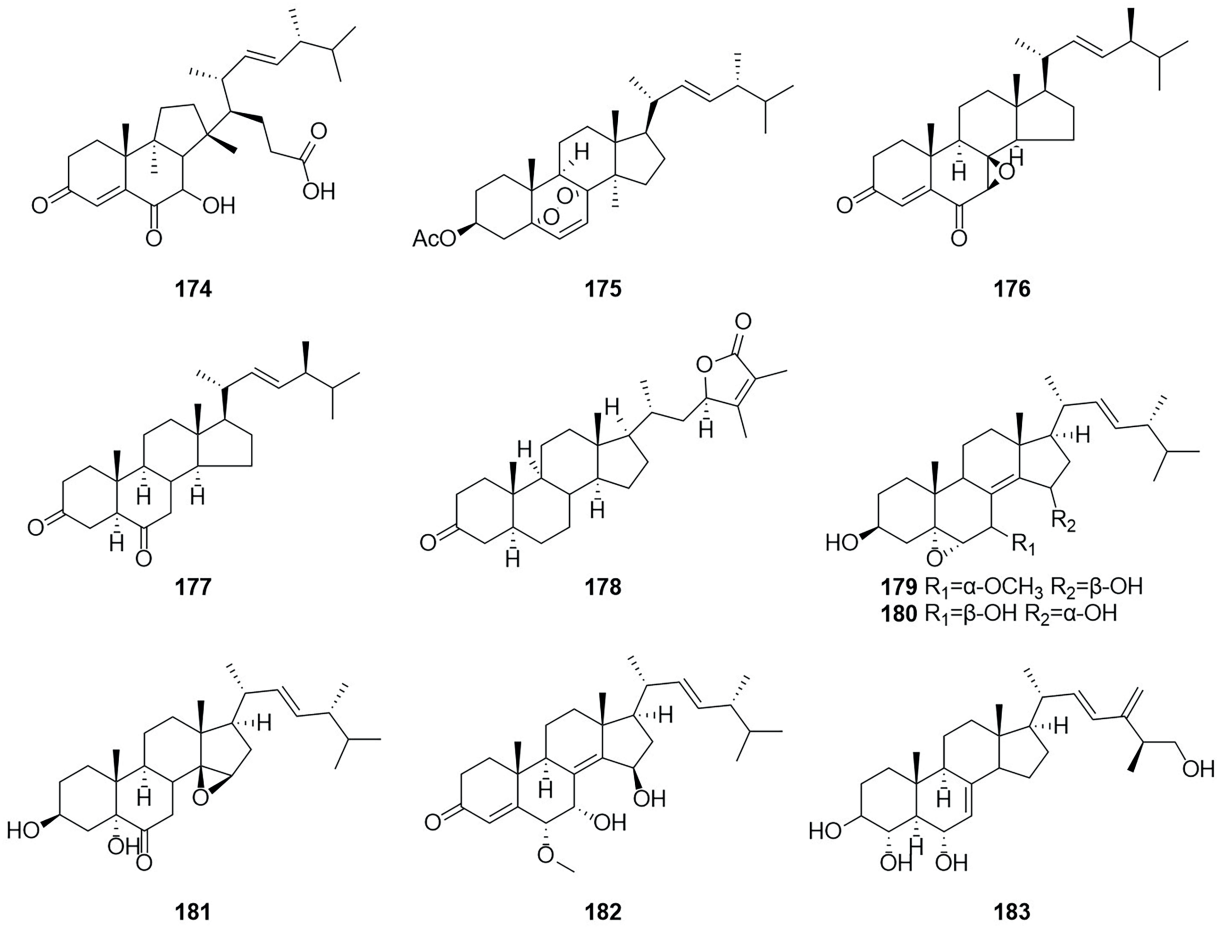

FIGURE 11
Chemical structures of compounds **174–183**.

sediment sample collected from the South China Sea (Zhang et al., 2022b). Cerebroside C (**218**) was obtained from the endophytic fungus *T. purpureogenus* hosted in *Tylophora ovate* (Zhao et al., 2020).

Acid

A compound, namely, (R)-2-[5-methoxycarbonyl-4-methyl-6-oxo-3,6-dihydro-2H-pyran-2-yl] acetic acid (61), which was obtained from cultures of the endophytic fungus *T. purpureogenus* hosted in *T. ovate*, showed some inhibitory activity against XOD at a concentration of 10 μM with the inhibition rate of 69.9% (Zhao et al., 2020). A new octadienoic acid derivative, oxoberkedienoic acid (**219**) (Figure 14), was isolated from a culture of *T. verruculosus* FKI-5393. The IC_{50} value against Jurkat cells of **219** was 6.1 μg/ml (Sakai et al., 2018). The IC_{50} value against Jurkat cells of **219** was 6.1 mg/ml. (R)-(−)-Hydroxysydonic acid (**220**) was isolated from the strain *Talaromyces* sp. C21-1 obtained from the coral Porites pukoensis collected in Xuwen, Guangdong Province (Nie et al., 2019). The compound **220** showed moderate inhibitory activities to *C. albicans* and methicillin-resistant *S. aureus* (MRSA) with the MICs at 0.075 mM and 0.2 mM, respectively. Rubratoxin acid A-E (**221**–**225**) were isolated from the endophytic fungus *T. purpureogenus* obtained from fresh leaves of the toxic medicinal plant *T. ovate* (Zhao et al., 2019a). Compound **221** showed significant inhibitory activity against NO production in LPS-induced RAW264.7 cells with an IC_{50} value of 1.9 μM. Compounds **222** showed moderate inhibitory activities toward XOD and PTP1b at 10 μM with inhibition rates of 67%. Compound **226**, which was identified as a new spiculisporic acid derivative, spic ulisporic acid E, was isolated from a culture of the fungus *T. trachyspermus* KUFA 0021, which is associated with a marine sponge (Kuml et al., 2014).

Others

The compounds 2,2',3,5'-tetrahydroxy-3'-methylbenzophenone (**227**) and 2,2',5'-trihydroxy-3-methoxy-3'-methylbenzophenone (**228**) (Figure 15), were obtained from *T. islandicus* EN-501, which is an endophytic fungus obtained from the freshly collected marine

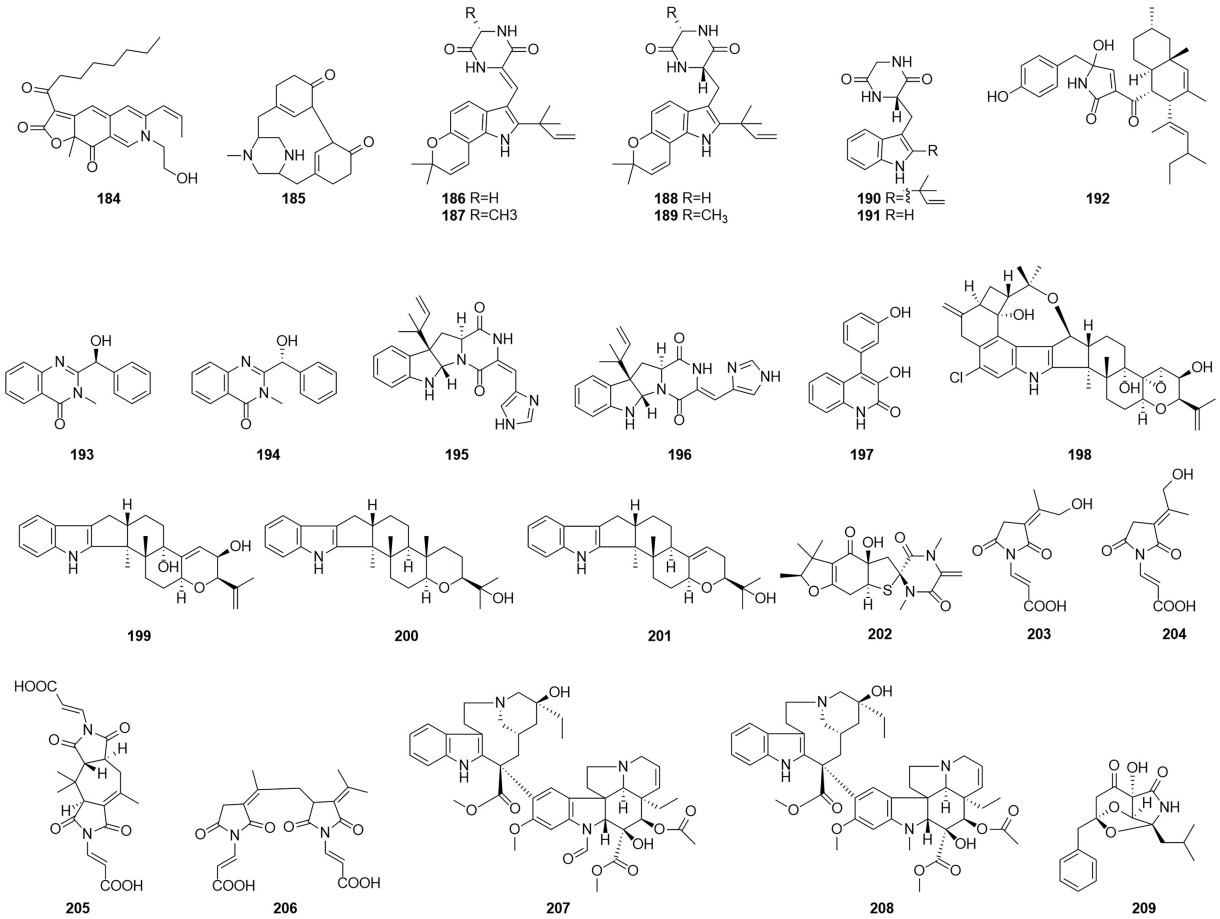

FIGURE 12
Chemical structures of compounds **184–209**.

red alga *Laurencia okamurai* (Li et al., 2016). Compounds **227–228** showed strong antioxidant activity against DPPH and ABTS radicals with IC_{50} values of 0.58 ~ 6.92 μg/ml, which were stronger than the positive controls BHT and ascorbic acid. Compounds **227** displayed potent activities against three human pathogens (*E. coli*, *Pseudomonas aeruginosa*, and *S. aureus*) and three aquatic bacteria (*V. alginolyticus*, *V. harveyi*, and *V. parahaemolyticus*) with MIC values ranging from 4 to 32 μg/ml. compound **228** showed weak activity against the tested bacteria (IC_{50} > 64 μg/ml), suggesting that methoxylation at C-3 weakened the antibacterial activities. A new phenylpentenol, wortmannine H (**229**), was isolated from *T. wortmannii* LGT-4, which is an endophytic fungus obtained from *T. wilfordii* (Li et al., 2021).

Talarodride (**230**) were isolated from the endophytic fungus *T. purpureogenus* obtained from fresh leaves of the toxic medicinal plant *T. ovate* (Zhao et al., 2019a). Compounds **230** showed moderate inhibitory activities toward XOD and PTP1b, respectively at 10 μM with inhibition rates of 76%. Four wortmannin derivative compounds, wortmannin B (**231**), wortmannin (**232**), amino adduct 3a (**233**), and wortmannin-diol (VIII) (**234**), were obtained from cultures of the aloe endophytic fungus *T. wortmannii* in 2013 (Bara et al., 2013a) Three new diphenyl ether derivatives, talaromycins A–C (**235–237**), together with a known analog (**238**), were obtained from a gorgonian-derived *Talaromyces* sp. (Chen et al., 2015). Compounds **237** showed potent antifouling activities against the larval settlement of the barnacle *Balanus amphitrite* with the EC_{50} values ranging from 2.2 to 4.8 mg/ml. Compounds **238** showed strong cytotoxicity against the human hepatoma HepG2 and Hep3B, human breast cancer MCF-7/ADR, human prostatic cancer PC-3, and human colon carcinoma HCT-116 cell lines with the IC_{50} values ranging from 4.3 to 9.8 mM.

Summary

Owing to their wide variety of species and abundance in secondary metabolites, *Talaromyces* fungi have great potential in medicine, food, cosmetics, agriculture, and environmental protection. In this paper, the secondary metabolites produced by *Talaromyces* species that have been studied over the past

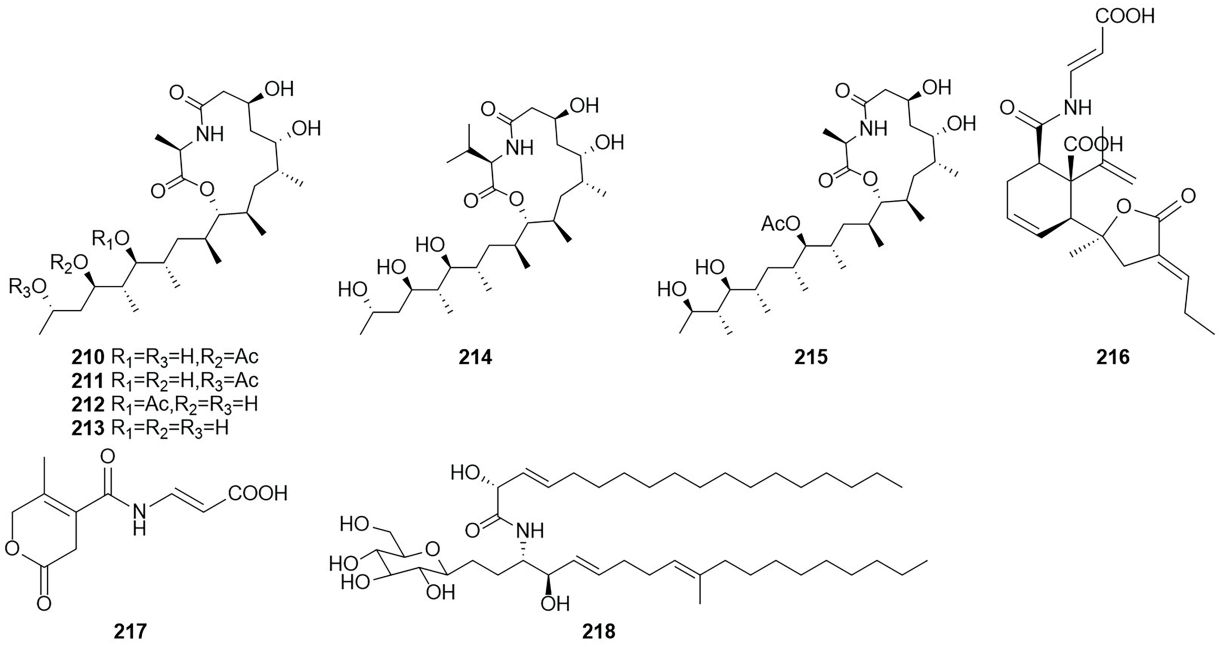

FIGURE 13
Chemical structures of compounds **210–218**.

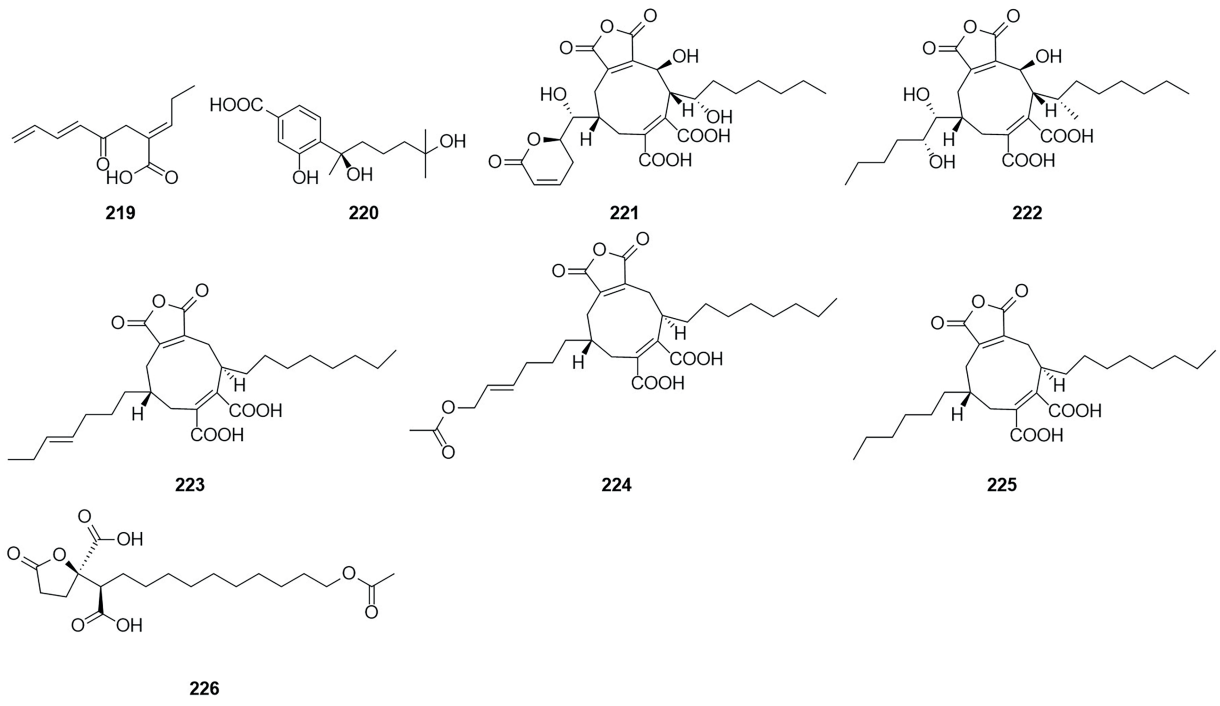

FIGURE 14
Chemical structures of compounds **219–226**.

several years are classified and summarized according to the types of compounds (Table 1). Secondary metabolites from more than ten *Talaromyces* species, including *T. wortmannii*, *T. pinophilus*, *T. flavus*, *T. stipitatus*, *T. purpureogenus*, and *T. minioluteus*, have been covered in this paper. These metabolites included 89 esters, 35 polyketones, 16

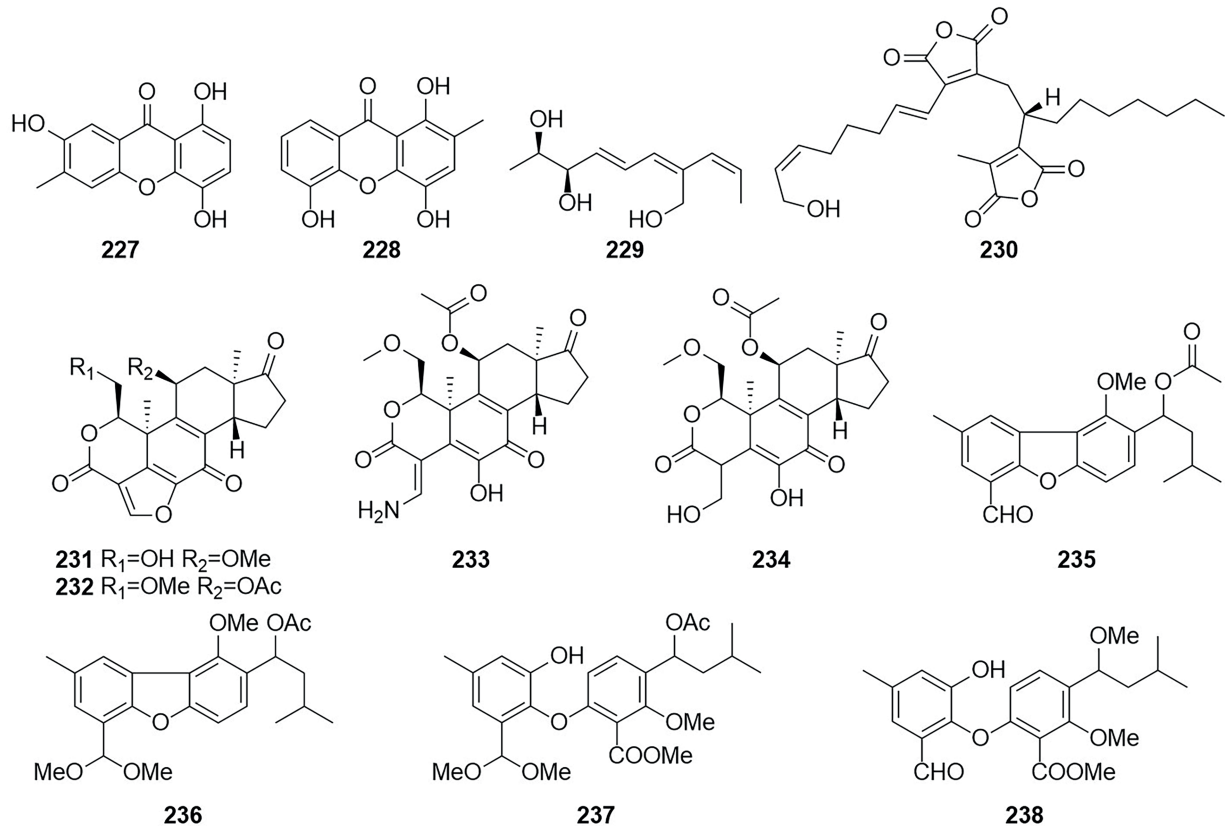

FIGURE 15
Chemical structures of compounds **227–238**.

anthraquinone, 20 terpenoids, 13 meroterpenoids, 10 steroids, 35 nitrogen compounds, 8 acids, and 12 other compounds. Most of these compounds have useful biological activities, such as anti-inflammatory, antibacterial, antitumor, hypolipidemic, or nematocidal activities or inhibition of α-glucosidase, xanthine oxidase, acetyltransferase, NADH fumarate reductase, PI3K-α, Aβ42 aggregation, or the production of NO induced by lipopolysaccharide.

Prospects

Talaromyces fungi include some of the most important species of microorganisms. The secondary metabolites from *Talaromyces* species that have unique structures and useful activities are of great value in research and development. However, there are still some problems to be solved in the study of fungal secondary metabolites. Firstly, owing to the limitations of strain isolation techniques and fungal culture conditions, some fungi cannot be isolated or do not grow well. Now often use fungal culture mediums are: PDA medium, PDB medium, BegH medium, rice solid medium and so on. Among them, rice medium is the most used (Table 1), which may be due to more fungal metabolites cultured in solid medium than liquid medium. It also reflected the problems of single nutrition and limited culture in the application of fungus synthesis medium. It is hoped that unconventional media can be used and new media can be developed. Secondly, it had been reported in available reports that the addition of epigenetic modifications to the culture medium can stimulate the expression of silenced genes thereby enabling the production of novel secondary metabolites. However, none of the literature in the study of secondary metabolites of the *Talaromyces* has investigated the effect of epigenetic modifiers. Therefore, epigenetic modifiers can be added to stimulate the expression of their silent genes. Finally, many existing studies have been done on the ethyl acetate part of the ferment, which is moderately polar and easy to separate. The aqueous part, on the other hand, has been ignored or even discarded due to its high polarity and difficulty of separation. Therefore, it is hoped that methods for the separation of compounds with high polarity will be developed as well as the development of related fillers. In a word, we should make full use of modern scientific and technological methods to carry out an in-depth study of the secondary metabolites produced by *Talaromyces* fungi and identify new active components to provide lead compounds for the research and development of innovative drugs.

TABLE 1 Name of *Talaromyces'* secondary metabolites, source strains, activity and their culture media.

Category	Compound name	Fungus	Pharmacological activity or application	Medium	References
Esters	Dinapinones AB1 (**1**)	*T. pinophilus* FKI-3864	/	Miura's medium	Kawaguchi et al., 2013
	Dinapinones AB2 (**2**)	*T. pinophilus* FKI-3864	Inhabit triacylglycerol synthesis in intact mammalian cells, with an IC_{50} value of 1.17 μM	Miura's medium	Kawaguchi et al., 2013
	Dinapinones AC1 (**3**)	*T. pinophilus* FKI-3864	/	Miura's medium	Kawaguchi et al., 2013
	Dinapinones AC2 (**4**)	*T. pinophilus* FKI-3864	/	Miura's medium	Kawaguchi et al., 2013
	Dinapinones AD1 (**5**)	*T. pinophilus* FKI-3864	/	Miura's medium	Kawaguchi et al., 2013
	Dinapinones AD2 (**6**)	*T. pinophilus* FKI-3864	/	Miura's medium	Kawaguchi et al., 2013
	Dinapinones AE1 (**7**)	*T. pinophilus* FKI-3864	/	Miura's medium	Kawaguchi et al., 2013
	Dinapinones AE2 (**8**)	*T. pinophilus* FKI-3864	/	Miura's medium	Kawaguchi et al., 2013
	Talapolyesters A (**9**)	*T. flavus*	/	potato dextrose agar (PDA); potato dextrose broth (PDB); rice solid medium	He et al., 2014b
	Talapolyesters B (**10**)	*T. flavus*	/	PDA; PDB; rice solid medium	He et al., 2014b
	Talapolyesters C (**11**)	*T. flavus*	/	PDA; PDB; rice solid medium	He et al., 2014b
	Talapolyesters D (**12**)	*T. flavus*	/	PDA; PDB; rice solid medium	He et al., 2014b
	15G256ν (**13**)	*T. flavus*	/	PDA; PDB; rice solid medium	He et al., 2014b
	15G256ν-me (**14**)	*T. flavus*	/	PDA; PDB; rice solid medium	He et al., 2014b
	15G256π (**15**)	*T. flavus*	/	PDA; PDB; rice solid medium	He et al., 2014b
	15G256β-2 (**16**)	*T. flavus*	/	PDA; PDB; rice solid medium	He et al., 2014b
	15G256α-2 (**17**)	*T. flavus*	/	PDA; PDB; rice solid medium	He et al., 2014b
	15G256α-2-me (**18**)	*T. flavus*	/	PDA; PDB; rice solid medium	He et al., 2014b
	15G256ι (**19**)	*T. flavus*	Antitumor	PDA; PDB; rice solid medium	He et al., 2014b
	15G256β (**20**)	*T. flavus*	Antitumor	PDA; PDB; rice solid medium	He et al., 2014b
	15G256α (**21**)	*T. flavus*	Antitumor	PDA; PDB; rice solid medium	He et al., 2014b
	Talapolyesters E (**22**)	*T. flavus*	Antitumor	PDA; PDB; rice solid medium	He et al., 2014b
	15G256α-1 (**23**)	*T. flavus*	Antitumor	PDA; PDB; rice solid medium	He et al., 2014b
	Talapolyesters E (**24**)	*T. flavus*	Antitumor	PDA; PDB; rice solid medium	He et al., 2014b
	15G256ω (**25**)	*T. flavus*	Antitumor	PDA; PDB; rice solid medium	He et al., 2014b
	Talaromycolides A (**26**)	*T. pinophilus* AF-02	Antibacterial	YES liquid medium	Zhai et al., 2015
	Talaromycolides B (**27**)	*T. pinophilus* AF-02	Antibacterial	YES liquid medium	Zhai et al., 2015
	Talaromycolides C (**28**)	*T. pinophilus* AF-02	Antibacterial	YES liquid medium	Zhai et al., 2015
	Rubralide C (**29**)	*T. pinophilus* AF-02	/	YES liquid medium	Zhai et al., 2015
	Sclerotinin A (**30**)	*T. pinophilus* AF-02	/	YES liquid medium	Zhai et al., 2015
	Alternariol (**31**)	*T. pinophilus* AF-02	/	YES liquid medium	Zhai et al., 2015
	Penicillide (**32**)	*T. pinophilus* AF-02	/	YES liquid medium	Zhai et al., 2015
	Deacetylisowortmins A (**33**)	*T. wortmannii* LGT-4	/	PDA	Fu et al., 2016
	Deacetylisowortmins B (**34**)	*T. wortmannii* LGT-4	/	PDA	Fu et al., 2016
	Talaromyones A (**35**)	*T. stipitatus* SK-4	/	Autoclaved wheat solid-substrate medium	Cai et al., 2017
	Talaromyones B (**36**)	*T. stipitatus* SK-4	Antibacterial; inhibitα-glucosidase	Autoclaved wheat solid-substrate medium	Cai et al., 2017
	Purpactin A (**37**)	*T. stipitatus* SK-4	Inhibit α-glucosidase	Autoclaved wheat solid-substrate medium	Cai et al., 2017

(Continued)

TABLE 1 Continued

Category	Compound name	Fungus	Pharmacological activity or application	Medium	References
	Butenolides (**38**–**42**)	*T. rugulosus*	/	Solid rice medium	Küppers et al., 2017
	(3S)-resorcylide derivatives (**43**–**49**)		/		
	Talarodilactones A and B (**50** and **51**)		Antitumor		
	Talaromycin A (**52**)	*Talaromyces* sp.	Antitumor	Co-culture with *X. angustiphylla*	Yuan et al., 2018
	Clearanol A (**53**)	MH551540	Antitumor		
	Wortmannine *F* (**54**)	*T. wortmannii* LGT-4	Antitumor	King's B Medium	Zhao et al., 2019b
	Pentalsamonin (**55**)	*T. purpureogenus* CFRM02	Antibacterial	Bengal gram husk (BegH)	Pandit et al., 2018
	Talaromarnine A (**56**)	*T. marneffei*	/	Corn medium	Yang et al., 2021
	Talaromarnine B (**57**)	*T. marneffei*	/	Corn medium	Yang et al., 2021
	Amestolkins A (**58**)	*T. amestolkiae*	Anti-inflammatory	M1 liquid medium	Huang et al., 2022
	Amestolkins B (**59**)		/		
	Talacoumarins A (**60**)	*T. flavus*	Anti-Aβ42 aggregation activity	PDA; PDB; rice	He et al., 2014c
	Talacoumarins B (**61**)	*T. flavus*	Anti-Aβ42 aggregation activity	PDA; PDB; rice	He et al., 2014c
	Chloropestalasin A (**62**)	*T. amestolkiae*	/	Solid cultures	El-Elimat et al., 2021
	3-Hydroxymethyl-6,8-dimethoxycoumarin (**63**)	*T. amestolkiae*	/	Solid cultures	El-Elimat et al., 2021
	Pestalasin A (**64**)	*T. amestolkiae*	/	Solid cultures	El-Elimat et al., 2021
	Dihydroisocoumarins (**65**–**67**)	*T. rugulosus*		Solid rice medium	Küppers et al., 2017
	Talaromarins A-F (**68**–**73**)	*T. flavus* TGGP35; *Talaromyces* sp. ZZ1616	Antioxidant; antimicrobial	PDB; rice solid medium	Cai et al., 2022; Ma et al., 2022
	Analogues (**67**,**74**–**89**)	*T. flavus* TGGP35	Antioxidant	Rice solid medium	Cai et al., 2022
Polyketons	Mitorubrin (**90**)	*T. atroroseus*	Red pigment production	Solid medium	Frisvad et al., 2013
	Monascorubrin (**91**)	*T. atroroseus*	Red pigment production	Solid medium	Frisvad et al., 2013
	Talaroxanthone (**92**)	*Talaromyces* sp.	/	ISP2-agar medium	Koolen et al., 2013
	9a-Epi-bacillisporin E (**93**)	*T. stipitatus*	/	PDA	Zang et al., 2016
	1-Epi-bacillisporin *F* (**94**)	*T. stipitatus*	/	PDA	Zang et al., 2016
	Bacillisporins F-H (**95**–**97**)	*T. stipitatus*	Antibacterial	PDA	Zang et al., 2016
	Wortmannilactones I1-I3(98–100)	*T. wortmannii*	Antioxidant	Corn plate medium	Liu et al., 2016
	Talaraculones A–F (**102**–**107**)	*T. aculeatus*	Inhibit α-glucosidase	PDA	Ren et al., 2017
	Pinazaphilone B (**108**)	*T. aculeatus*	Inhibit α-glucosidase	PDA	Ren et al., 2017
	Pinophilin B (**109**)	*T. aculeatus*	/	PDA	Ren et al., 2017
	Sch 725680 (**110**)	*T. aculeatus*	/	PDA	Ren et al., 2017
	(−)-Mitorubrin (**111**)	*T. aculeatus*	/	PDA	Ren et al., 2017
	(−)-Mitorubrinol (**112**)	*T. aculeatus*	/	PDA	Ren et al., 2017
	Paecillin D (**113**)	*T. stipitatus*	Antifungal	International streptomyces project 2 liquid medium (ISP2)	da Silva et al., 2017
	Secalonic acid A (**114**)	*T. stipitatus*	Antifungal	ISP2	da Silva et al., 2017
	Blennolide G (**115**)	*T. stipitatus*	Antifungal	ISP2	da Silva et al., 2017
	Versixanthone A (**116**)	*T. stipitatus*	Antifungal	ISP2	da Silva et al., 2017
	Penicillixanthone A (**117**)	*T. stipitatus*	/	ISP2	da Silva et al., 2017
	Paecillin B (**118**)	*T. stipitatus*	/	ISP2	da Silva et al., 2017

(Continued)

TABLE 1 Continued

Category	Compound name	Fungus	Pharmacological activity or application	Medium	References
	Talarodrides A – F (**119–124**)	*Talaromyces* sp. HDN1820200	Antimicrobial	PDB	Zhao et al., 2021b
Anthraquinone	Skyrin (**125**)	*Talaromyces* sp. ZH-154	Antitumor	PDA, PDB	Liu et al., 2010; Xie et al., 2016
	Emodin (**126**)	*Talaromyces* sp. ZH-154	Antitumor	PDA, PDB	Liu et al., 2010
	Biemodin (**127**)	*T. wortmannii*	/	Rice solid medium	Bara et al., 2013a
	Emodic acid (**128**)	*T. wortmannii*	/	Rice solid medium	Bara et al., 2013a
	Oxyskyrin (**129**)	*T. wortmannii*	Antitumor	Rice solid medium	Bara et al., 2013a; Xie et al., 2016
	Rugulosins A - B (**130–131**)	*T. wortmannii*	/	Rice solid medium	Bara et al., 2013a
	Talaromannins A-B (**132–133**)	*T. wortmannii*	Antibacterial	Rice solid medium	Bara et al., 2013b
	3-Demethyl-3-(2-hydroxypropyl)-skyrin (**134**)	*Talaromyces* sp. YE 3016	Antitumor	Rice solid medium	Xie et al., 2016
	1,3,6-Trihydroxy-8-methylanthraquinone (**135**)	*Talaromyces* sp. YE 3016	/	Rice solid medium	Xie et al., 2016
	2,2'-bis-(7-methyl-1,4,5-trihydroxy-anthracene-9,10-dione) (**136**)	*T. stipitatus* KUFA 0207	/	Rice solid medium	Noinart et al., 2017
	Questinol (**137**)	*T. stipitatus* KUFA 0207	Anti-obesity activity	Rice solid medium	Noinart et al., 2017
	Citreorosein (**138**)	*T. stipitatus* KUFA 0207	Anti-obesity activity	Rice solid medium	Noinart et al., 2017
	Fallacinol (**139**)	*T. stipitatus* KUFA 0207	/	Rice solid medium	Noinart et al., 2017
	Rheoemodin (**140**)	*T. stipitatus* KUFA 0207	/	Rice solid medium	Noinart et al., 2017
Terpenoids	Pinophicin A (**141**)	*T. pinophilus*	/	MEB medium	Zhao et al., 2021a
	Talaperoxides A–D (**142–145**)	*T. flavus*	Antitumor	Autoclaved rice solid-substrate medium	Li et al., 2011
	Talaflavuterpenoid A (**146**)	*T. flavus*	/	Rice solid medium	He et al., 2014a
	Roussoellol C (**147**)	*T. purpureogenus*	Antitumor	Rice solid medium	Wang et al., 2018
	Talaminoid A (**148**)	*T. minioluteus*	Anti-inflammatory	Rice solid medium	Chen et al., 2019
	Talaminoids B - C (**149–150**)	*T. minioluteus*	/	Rice solid medium	Chen et al., 2019
	Purpuride (**151**)	*T. minioluteus*	Anti-inflammatory	Rice solid medium	Chen et al., 2019
	Berkedrimanes B (**152**)	*T. minioluteus*	Anti-inflammatory	Rice solid medium	Chen et al., 2019
	Minioluteumide B (**153**)	*T. minioluteus*	/	Rice solid medium	Chen et al., 2019
	1αHydroxyconfertifolin (**154**)	*T. minioluteus*	/	Rice solid medium	Chen et al., 2019
	Sordarin (**155**)	*Talaromyces* sp. (CMB-TU011)	Antifungal	M1 agar plate	Domínguez et al., 1998; Dewapriya et al., 2017
	Four new sesquiterpene lactones (**156–159**)	*T. minioluteus*	Antitumor	PDB	Ngokpol et al., 2015
	Purpuride B (**160**)	*T. minioluteus*	/	PDB	Ngokpol et al., 2015
Meroterpenoid	Talaromyolides A–D (**161–164**)	*Talaromyces* sp. CX11	Antiviral	Liquid Medium	Cao et al., 2019
	Talaromytin (**165**)	*Talaromyces* sp. CX11	/	Liquid Medium	Cao et al., 2019
	Taladrimanin A (**166**)	*Talaromyces* sp. HM6-1–1	Antitumor activity; antibacterial activity	Rice solid medium	Hong et al., 2022
	Chrodrimanins A-H (**167–173**)	*Talaromyces* sp. YO-2	Antimalarial	Okara	Hayashi et al., 2012a,b
Steroids	Talasterone A (**174**)	*T. adpressus*	Anti-inflammatory	Rice solid medium	Zhang et al., 2022a

(Continued)

TABLE 1 Continued

Category	Compound name	Fungus	Pharmacological activity or application	Medium	References
	3-Acetylergosterol-5,8-endoperoxide (**175**)	*Talaromyces trachyspermus* KUFA 0021	/	GPMY	Kuml et al., 2014
	Talarosterone (**176**)	*T. stipitatus* KUFA 0207	/	Rice solid medium	Noinart et al., 2017
	Cyathisterone (**177**)		/		
	Talasteroid (**178**)	*T. stollii*	/	PDA	Zhang et al., 2022c
	(22E,24R)-7α-Methoxy-5α,6α-epoxyergosta-8(14),22-diene-3β,15β-diol (**179**)	*T. stipitatus*	Antiproliferative	Rice solid medium	Zhang et al., 2021
	(22E,24R)-5α,6α-Epoxyergosta-8(14),22-diene-3β,7β,15α-triol (**180**)	*T. stipitatus*	/	Rice solid medium	Zhang et al., 2021
	(22E,24R)-3β,5α-Dihydroxy-14β,15β-epoxyergosta-7,22-diene-6-one (**181**)	*T. stipitatus*	/	Rice solid medium	Zhang et al., 2021
	(22E,24R)-6α-Methoxy-7α,15β-dihydroxyergosta-4,8(14),22-triene-3-one (**182**)	*T. stipitatus*	/	Rice solid medium	Zhang et al., 2021
	(25S)- Ergosta-7,24(28)-diene-3β,4α,6α,26-tetraol (**183**)	*T. stipitatus*	Antiproliferative	Rice solid medium	Zhang et al., 2021
Alkaloids	PP-R (**184**)	*T. atroroseus*	Food colorants	Solid medium	Frisvad et al., 2013
	Herquline B (**185**)	*T. pinophilus*	/	Solid medium	Vinale et al., 2017
	Talathermophilins A–E (**186–188**,**190–191**)	*T. thermophilus* YM3-4	/	PDB	Guo et al., 2011
	Cyclo(glycyltryptophyl) (**189**)	*T. thermophilus* YM3-4	/	PDB	Guo et al., 2011
	ZG-1494α (**192**)	*T. atroroseus*	A novel inhibitor of platelet-activating factor acetyl-transferase	PDB	Frisvad et al., 2013
	2-[(S)-Hydroxy(phenyl) methyl]-3-methylquinazolin-4(3H)-one (**193**)	*Talaromyces* sp. *cf*-16	/	PDA	Yang et al., 2016
	2-[(R)-Hydroxy(phenyl) methyl]-3-methylquinazolin-4(3H)-one (**194**)	*Talaromyces* sp. *cf*-16	/	PDA	Yang et al., 2016
	Roquefortine C (**195**)	*Talaromyces* sp. *cf*-16	/	PDA	Yang et al., 2016
	Z-Roquefortine C (**196**)	*Talaromyces* sp. *cf*-16	Antibacterial	PDA	Yang et al., 2016
	Viridicatol (**197**)	*Talaromyces* sp. *cf*-16	Antibacterial	PDA	Yang et al., 2016
	Penitrem A (**198**)	*Talaromyces* sp. *cf*-16	Antibacterial	PDA	Yang et al., 2016
	Penijanthine A (**199**)	*Talaromyces* sp. *cf*-16	Antibacterial	PDA	Yang et al., 2016
	Paspaline (**200**)	*Talaromyces* sp. *cf*-16	/	PDA	Yang et al., 2016
	3-Deoxo-4b-deoxypaxilline (**201**)	*Talaromyces* sp. *cf*-16	/	PDA	Yang et al., 2016
	Talaromanloid A (**202**)	*T. mangshanicus* BTBU20211089	/	Rice solid medium	Zhang et al., 2022b
	10-Hydroxy-8-demethyltalaromydine (**203**)	*T. mangshanicus* BTBU20211089	/	Rice solid medium	Zhang et al., 2022b
	11-Hydroxy-8-demethyltalaromydine (**204**)	*T. mangshanicus* BTBU20211089	/	Rice solid medium	Zhang et al., 2022b

(Continued)

TABLE 1 Continued

Category	Compound name	Fungus	Pharmacological activity or application	Medium	References
	Ditalaromylectones A (**205**)	*T. mangshanicus* BTBU20211089	Antibacterial	Rice solid medium	Zhang et al., 2022b
	Ditalaromylectones A (**206**)	*T. mangshanicus* BTBU20211089	/	Rice solid medium	Zhang et al., 2022b
	Vincristine (**207**)	*T. radicus*	Antitumor	M2 liquid medium; PDA	Palem et al., 2015
	Vinblastine (**208**)		/		
	Talaramide A (**209**)	*Talaromyces* sp. HZ-YX1	Antibacterial	Solid rice medium	Chen et al., 2017
Amides	Thermolides A–F (**210–215**)	*T. thermophilus*	**210–211**: Insect resistance	PDA	Guo et al., 2012
	Talaromydene (**216**)	*T. mangshanicus* BTBU20211089	/	Rice solid medium	Zhang et al., 2022b
	Talaromylectone (**217**)	*T. mangshanicus* BTBU20211089	/	Rice solid medium	Zhang et al., 2022b
	Cerebroside C (**218**)	*T. purpurogenus*	/		Zhao et al., 2020
Acid	Oxoberkedienoic acid (**219**)	*T. verruculosus* FKI-5393	Antitumor	Rice solid medium	Sakai et al., 2018
	(R)-(−)-Hydroxysydonic acid (**220**)	*Talaromyces* sp. C21-1	Antimicrobial	Liquid medium	Nie et al., 2019
	Rubratoxin acid A-E (**221–225**)	*T. purpureogenus*	**221**: Anti-inflammatory **222**: Antioxidant	PDA	Zhao et al., 2019b
	Spic ulisporic acid E (**226**)	*T. trachyspermus* KUFA 0021	/	GPMY	Kuml et al., 2014
Others	2,2',3,5'-tetrahydroxy-3'-methylbenzophenone (**227**)	*T. islandicus* EN-501	Antioxidant; antibacterial activity	Rice solid medium	Li et al., 2016
	2,2',5'-trihydroxy-3-methoxy-3'-methylbenzophenone (**228**)	*T. islandicus* EN-501	Antioxidant; antibacterial Activity	Rice solid medium	Li et al., 2016
	Wortmannine H (**229**)	*T. wortmannii* LGT-4	/	Martin medium	Li et al., 2021
	Talarodride (**230**)	*T. purpurogenus*	Antitumor	Rice solid medium	Zhao et al., 2019b
	Wortmannin B (**231**)	*T. wortmannii*	/	Rice solid medium	Bara et al., 2013a
	Wortmannin (**232**)	*T. wortmannii*	/	Rice solid medium	Bara et al., 2013a
	Amino adduct 3a (**233**)	*T. wortmannii*	/	Rice solid medium	Bara et al., 2013a
	Wortmannin-diol (VIII) (**234**)	*T. wortmannii*	/	Rice solid medium	Bara et al., 2013a
	Talaromycins A–C (**235–237**)	*Talaromyces* sp. SBE-14 (EU236708)	Antifouling	PDA	Chen et al., 2015
	Tienilic acid A methyl ester (**238**)	Talaromyces sp. SBE-14 (EU236708)	/	PDA	Chen et al., 2015

Author contributions

L-RL, L-QG, and M-YJ wrote the paper. JG, RW, and RL cultured and identified the fungus. L-RL, M-DL, and LH collected the STM data. YD checked the paper. G-ZW and DW verified the content. All authors have read and agreed to the published version of the manuscript.

Funding

This research was funded by the National Natural Science Foundation of China (81973189, 81973460), Science and Technology Department of Sichuan Province (2021ZYD0079), Chengdu University of Traditional Chinese Medicine (CZYJC1905, 2020XSGG016, 2020JCRC006, SKL2021-19,

SKL2021-42), and National Interdisciplinary Innovation Team of Traditional Chinese Medicine (ZYYCXTD-D-202209).

Conflict of interest

The authors declare that the research was conducted in the absence of any commercial or financial relationships that could be construed as a potential conflict of interest.

Publisher's note

References

Adefegha, S. A., Oboh, G., and Oluokun, O. O. (2022). Chapter 11 – Food bioactives: the food image behind the curtain of health promotion and prevention against several degenerative diseases. *Stud. Nat. Prod. Chem.* 72, 391–421. doi: 10.1016/B978-0-12-823944-5.00012-0

Bara, R., Aly, A. H., Pretsch, A., Wray, V., Wang, B., Proksch, P., et al. (2013a). Antibiotically active metabolites from *Talaromyces wortmannii*, an endophyte of *Aloe vera*. *J. Antibiot.* 66, 491–493. doi: 10.1038/ja.2013.28

Bara, R., Zerfass, I., Aly, A. H., Goldbach-Gecke, H., Raghavan, V., Sass, P., et al. (2013b). Atropisomeric dihydroanthracenones as inhibitors of multiresistant *Staphylococcus aureus*. *J. Med. Chem.* 56, 3257–3272. doi: 10.1021/jm301816a

Batista, Â. G., Silva-Maia Da, J. K., and Maróstica, M. R. (2021). "Generation and alterations of bioactive organosulfur and phenolic compounds," in *Chemical Changes during Processing and Storage of Foods*. eds. D. B. Rodriguez-Amaya and J. Amaya-Farfan (London, UK: Elsevier). 537–577.

Borah, P., and Banik, B. K. (2020). "12 – Diverse synthesis of medicinally active steroids," in *Green Approaches in Medicinal Chemistry for Sustainable Drug Design Advances in Green and Sustainable Chemistry*. ed. B. K. Banik (London, UK: Elsevier), 449–490.

Braca, A., Bader, A., and De Tommasi, N. (2012). Plant and fungi 3,4-dihydroisocoumarins. *Stud. Nat. Prod. Chem* 37, 191–215. doi: 10.1016/B978-0-444-59514-0.00007-9

Cai, R., Chen, S., Long, Y., Li, C., Huang, X., and She, Z. (2017). Depsidones from *Talaromyces stipitatus* SK-4, an endophytic fungus of the mangrove plant *Acanthus ilicifolius*. *Phytochem. Lett.* 20, 196–199. doi: 10.1016/j.phytol.2017.04.023

Cai, J., Zhu, X. C., Zeng, W. N., Wang, B., Luo, Y. P., Liu, J., et al. (2022). Talaromarins A–F: six new isocoumarins from mangrove-derived fungus *Talaromyces flavus* TGGP35. *Mar. Drugs* 20, 361. doi: 10.3390/md20060361

Cao, X., Shi, Y., Wu, X., Wang, K., Huang, S., Sun, H., et al. (2019). Talaromyolides A-D and talaromytin: polycyclic meroterpenoids from the fungus *Talaromyces* sp. CX11. *Org. Lett.* 21, 6539–6542. doi: 10.1021/acs.orglett.9b02466

Chen, M., Han, L., Shao, C. L., She, Z. G., and Wang, C. Y. (2015). Bioactive Diphenyl ether derivatives from a gorgonian-derived fungus *Talaromyces* sp. *Chem. Biodivers.* 12, 443–450. doi: 10.1002/cbdv.201400267

Chen, S., He, L., Chen, D., Cai, R., Long, Y., Lu, Y., et al. (2017). Talaramide A, an unusual alkaloid from the mangrove endophytic fungus *Talaromyces* sp. (HZ-YX1) as an inhibitor of mycobacterial PknG. *New J. Chem.* 41, 4273–4276. doi: 10.1039/C7NJ00059F

Chen, C., Sun, W., Liu, X., Wei, M., Liang, Y., Wang, J., et al. (2019). Anti-inflammatory spiroaxane and drimane sesquiterpenoids from *Talaromyces minioluteus* (*Penicillium minioluteum*). *Bioorg. Chem.* 91:103166. doi: 10.1016/j.bioorg.2019.103166

da Silva, P., de Souza, M., Bianco, E., da Silva, S., Soares, L., Costa, E., et al. (2017). Antifungal polyketides and other compounds from amazonian endophytic *Talaromyces* fungi. *J. Braz. Chem. Soc.* 29, 622–630. doi: 10.21577/0103-5053.20170176

De Stefano, S., Nicoletti, R., Milone, A., and Zambardino, S. (1999). 3-o-Methylfunicone, a fungitoxic metabolite produced by the fungus *Penicillium pinophilum*. *Phytochemistry* 52, 1399–1401. doi: 10.1016/S0031-9422(99)00320-9

Dethoup, T., Kaewsalong, N., Songkumorn, P., and Jantasorn, A. (2018). Potential application of a marine-derived fungus, *Talaromyces tratensis* KUFA 0091 against rice diseases. *Biol. Control* 119, 1–6. doi: 10.1016/j.biocontrol.2017.11.008

Dewapriya, P., Khalil, Z. G., Prasad, P., Salim, A. A., Cruz-Morales, P., Marcellin, E., et al. (2018). Talaropeptides A-D: structure and biosynthesis of extensively N-methylated linear peptides From an Australian marine tunicate-derived *Talaromyces* sp. *Front. Chem.* 6:394. doi: 10.3389/fchem.2018.00394

Dewapriya, P., Prasad, P., Damodar, R., Salim, A. A., and Capon, R. J. (2017). Talarolide A, a cyclic heptapeptide hydroxamate from an Australian marine tunicate-associated fungus, *Talaromyces* sp. (CMB-TU011). *Org. Lett.* 19, 2046–2049. doi: 10.1021/acs.orglett.7b00638

Domínguez, J. M., Kelly, V. A., Kinsman, O. S., Marriott, M. S., Gómez de las Heras, F., and Martín, J. J. (1998). Sordarins: a new class of antifungals with selective inhibition of the protein synthesis elongation cycle in yeasts. *Antimicrob. Agents Chemother.* 42, 2274–2278. doi: 10.1128/AAC.42.9.2274

El-Elimat, T., Figueroa, M., Raja, H. A., Alnabulsi, S. M., and Oberlies, N. H. (2021). Coumarins, dihydroisocoumarins, a dibenzo-α-pyrone, a meroterpenoid, and a merodrimane from *Talaromyces amestolkiae*. *Tetrahedron Lett.* 72:153067. doi: 10.1016/j.tetlet.2021.153067

Frisvad, J. C., Yilmaz, N., Thrane, U., Rasmussen, K. B., Houbraken, J., and Samson, R. A. (2013). *Talaromyces atroroseus*, a new species efficiently producing industrially relevant red pigments. *PLoS One* 8:e84102. doi: 10.1371/journal.pone.0084102

Fu, G.-C., Yang, Z.-D., Zhou, S.-Y., Yu, H.-T., Zhang, F., and Yao, X.-J. (2016). Two new compounds, deacetylisowortmins A and B, isolated from an endophytic fungus, *Talaromyces wortmannii* LGT-4. *Nat. Prod. Res.* 30, 1623–1627. doi: 10.1080/14786419.2015.1129329

Guo, J.-P., Tan, J.-L., Wang, Y.-L., Wu, H.-Y., Zhang, C.-P., Niu, X.-M., et al. (2011). Isolation of talathermophilins from the thermophilic fungus *Talaromyces thermophilus* YM3-4. *J. Nat. Prod.* 74, 2278–2281. doi: 10.1021/np200365z

Guo, Y., Tu, T., Yuan, P., Wang, Y., Ren, Y., Yao, B., et al. (2019). High-level expression and characterization of a novel aspartic protease from *Talaromyces leycettanus* JCM12802 and its potential application in juice clarification. *Food Chem.* 281, 197–203. doi: 10.1016/j.foodchem.2018.12.096

Guo, J.-P., Zhu, C.-Y., Zhang, C.-P., Chu, Y.-S., Wang, Y.-L., Zhang, J.-X., et al. (2012). Thermolides, potent nematocidal PKS-NRPS hybrid metabolites from thermophilic fungus *Talaromyces thermophilus*. *J. Am. Chem. Soc.* 134, 20306–20309. doi: 10.1021/ja3104044

Halo, B. A., Al-Yahyai, R. A., Maharachchikumbura, S. S. N., and Al-Sadi, A. M. (2019). *Talaromyces variabilis* interferes with pythium aphanidermatum growth and suppresses pythium-induced damping-off of cucumbers and tomatoes. *Sci. Rep.* 9, 11255. doi: 10.1038/s41598-019-47736-x

Hayashi, H., Oka, Y., Kai, K., and Akiyama, K. (2012a). A new meroterpenoid, chrodrimanin C, from YO-2 of *Talaromyces* sp. *Biosci. Biotechnol. Biochem.* 76, 745–748. doi: 10.1271/bbb.110858

Hayashi, H., Oka, Y., Kai, K., and Akiyama, K. (2012b). New chrodrimanin congeners, chrodrimanins D–H, from YO-2 of *Talaromyces* sp. *Biosci. Biotechnol. Biochem.* 76, 1765–1768. doi: 10.1271/bbb.120365

He, J.-W., Liang, H.-X., Gao, H., Kuang, R.-Q., Chen, G.-D., Hu, D., et al. (2014a). Talaflavuterpenoid A, a new nardosinane-type sesquiterpene from *Talaromyces flavus*. *J. Asian Nat. Prod. Res.* 16, 1029–1034. doi: 10.1080/10286020.2014.933812

He, J.-W., Mu, Z.-Q., Gao, H., Chen, G.-D., Zhao, Q., Hu, D., et al. (2014b). New polyesters from *Talaromyces flavus*. *Tetrahedron* 70, 4425–4430. doi: 10.1016/j.tet.2014.02.060

He, J.-W., Qin, D.-P., Gao, H., Kuang, R.-Q., Yu, Y., Liu, X.-Z., et al. (2014c). Two new coumarins from *Talaromyces flavus*. *Molecules* 19, 20880–20887. doi: 10.3390/molecules191220880

Hong, X., Guan, X., Lai, Q., Yu, D., Chen, Z., Fu, X., et al. (2022). Characterization of a bioactive meroterpenoid isolated from the marine-derived fungus *Talaromyces* sp. *Appl. Microbiol. Biotechnol.* 106, 2927–2935. doi: 10.1007/s00253-022-11914-1

Huang, L.-J., Li, X.-A., Jin, M.-Y., Guo, W.-X., Lei, L.-R., Liu, R., et al. (2022). Two previously undescribed phthalides from *Talaromyces amestolkiae*, a symbiotic fungus of *Syngnathus acus*. *J. Asian Nat. Prod. Res.* 1–9. doi: 10.1080/10286020.2022.2075738

Jackson, R. S. (2008). Chemical constituents of grapes and wine. *Wine Sci.* 270–331. doi: 10.1016/B978-012373646-8.50009-3

Kaur, A., Raja, H. A., Swenson, D. C., Agarwal, R., Deep, G., Falkinham, J. O., et al. (2016). Talarolutins A-D: meroterpenoids from an endophytic fungal isolate of

Talaromyces minioluteus. *Phytochemistry* 126, 4–10. doi: 10.1016/j.phytochem.2016.03.013

Kawaguchi, M., Uchida, R., Ohte, S., Miyachi, N., Kobayashi, K., Sato, N., et al. (2013). New dinapinone derivatives, potent inhibitors of triacylglycerol synthesis in mammalian cells, produced by *Talaromyces pinophilus* FKI-3864. *J. Antibiot.* 66, 179–189. doi: 10.1038/ja.2012.127

Koolen, H. H. F., Menezes, L. S., Souza, M. P., Silva, F. M. A., Almeida, F. G. O., de Souza, A. Q. L., et al. (2013). Talaroxanthone, a novel xanthone dimer from the endophytic fungus *Talaromyces* sp. associated with *Duguetia stelechantha* (Diels) R. E. Fries. *J. Braz. Chem. Soc.* doi: 10.5935/0103-5053.20130104

Kuml, D., Dethoup, T., Buttachon, S., Singburaudom, N., Silva, A. M. S., and Kijjoa, A. (2014). Spiculisporic acid E, a new spiculisporic acid derivative and ergosterol derivatives from the marine-sponge associated fungus *Talaromyces trachyspermus* (KUFA 0021). *Nat. Prod. Commun.* 9, 1147–1150. doi: 10.1177/1934578X1400900822

Küppers, L., Ebrahim, W., El-Neketi, M., Özkaya, F., Mándi, A., Kurtán, T., et al. (2017). Lactones from the sponge-derived fungus *Talaromyces rugulosus*. *Mar. Drugs* 15, 359. doi: 10.3390/md15110359

Li, H., Huang, H., Shao, C., Huang, H., Jiang, J., Zhu, X., et al. (2011). Cytotoxic norsesquiterpene peroxides from the endophytic fungus *Talaromyces flavus* isolated from the mangrove plant *Sonneratia apetala*. *J. Nat. Prod.* 74, 1230–1235. doi: 10.1021/np200164k

Li, H.-L., Li, X.-M., Liu, H., Meng, L.-H., and Wang, B.-G. (2016). Two new diphenylketones and a new xanthone from *Talaromyces islandicus* EN-501, an endophytic fungus derived from the marine red alga *Laurencia okamurai*. *Mar. Drugs* 14. doi: 10.3390/md14120223

Li, X.-F., Yang, Z.-D., Yang, X., Yang, L.-J., Yao, X.-J., and Shu, Z.-M. (2021). Wortmannine H, a phenylpentenol isolated from an endophytic fungus, *Talaromyces wortmannii* LGT-4. *Nat. Prod. Res.* 35, 3204–3209. doi: 10.1080/14786419.2019.1690488

Liu, F., Cai, X.-L., Yang, H., Xia, X.-K., Guo, Z.-Y., Yuan, J., et al. (2010). The bioactive metabolites of the mangrove endophytic fungus *Talaromyces* sp. ZH-154 isolated from *Kandelia candel* (L.) Druce. *Planta Med.* 76, 185–189. doi: 10.1055/s-0029-1186047

Liu, W.-C., Yang, F., Zhang, R., Shi, X., Lu, X.-H., Luan, Y.-S., et al. (2016). Production of polyketides with anthelmintic activity by the fungus *Talaromyces wortmannii* using one strain-many compounds (OSMAC) method. *Phytochem. Lett.* 18, 157–161. doi: 10.1016/j.phytol.2016.10.006

Luo, Y., Lu, X., Bi, W., Liu, F., and Gao, W. (2016). *Talaromyces rubrifaciens*, a new species discovered from heating, ventilation and air conditioning systems in China. *Mycologia* 108, 773–779. doi: 10.3852/15-233

Ma, M., Yi, W., Qin, L., Lian, X.-Y., and Zhang, Z. (2022). Talaromydien a and talaroisocoumarin A, new metabolites from the marine-sourced fungus *Talaromyces* sp. ZZ1616. *Nat. Prod. Res.* 36, 460–465. doi: 10.1080/14786419.2020.1779265

Matsuda, Y., and Abe, I. (2020). Fungal meroterpenoids. *Compr. Nat. Prod. III*, 445–478. doi: 10.1016/B978-0-12-409547-2.14663-3

Méndez-Líter, J. A., Tundidor, I., Nieto-Domínguez, M., de Toro, B. F., González Santana, A., de Eugenio, L. I., et al. (2019). Transglycosylation products generated by *Talaromyces amestolkiae* GH3 β-glucosidases: effect of hydroxytyrosol, vanillin and its glucosides on breast cancer cells. *Microb. Cell Fact.* 18, 97. doi: 10.1186/s12934-019-1147-4

Nam, I. H., Murugesan, K., Ryu, J., and Kim, J. H. (2019). Arsenic (As) removal using *Talaromyces* sp. KM-31 isolated from as-contaminated mine soil. *Fortschr. Mineral.* 9, 568. doi: 10.3390/min9100568

Naraghi, L., Heydari, A., Rezaee, S., and Razavi, M. (2012). Biocontrol agent *Talaromyces flavus* stimulates the growth of cotton and potato. *J. Plant Growth Regul.* 31, 471–477. doi: 10.1007/s00344-011-9256-2

Ngokpol, S., Suwakulsiri, W., Sureram, S., Lirdprapamongkol, K., Aree, T., Wiyakrutta, S., et al. (2015). Drimane sesquiterpene-conjugated amino acids from a marine isolate of the fungus *Talaromyces minioluteus* (Penicillium Minioluteum). *Mar. Drugs* 13, 3567–3580. doi: 10.3390/md13063567

Nicoletti, R., and Vinale, F. (2018). Bioactive compounds from marine-derived *Aspergillus*, *Penicillium*, *Talaromyces* and *Trichoderma* species. *Mar. Drugs* 16, 408. doi: 10.3390/md16110408

Nie, Y., Liu, Y., Yang, W., Li, Y., Xu, M., Lei, X., et al. (2019). Bioactive secondary metabolites from the fungus *Talaromyces* sp. isolated from coral *Porites pukoensis*. *Mycosystema* 38, 585–593. doi: 10.13346/j.mycosystema.180227

Noinart, J., Buttachon, S., Dethoup, T., Gales, L., Pereira, J. A., Urbatzka, R., et al. (2017). A new ergosterol analog, a new bis-anthraquinone and anti-obesity activity of anthraquinones from the marine sponge-associated fungus *Talaromyces stipitatus* KUFA 0207. *Mar. Drugs* 15, E139. doi: 10.3390/md15050139

Palem, P. P. C., Kuriakose, G. C., and Jayabaskaran, C. (2015). An *Endophytic fungus*, *Talaromyces radicus*, isolated from *Catharanthus roseus*, produces vincristine and vinblastine, which induce apoptotic cell death. *PLoS One* 10:e0144476. doi: 10.1371/journal.pone.0144476

Pandit, S. G., Puttananjaih, M. H., Harohally, N. V., and Dhale, M. A. (2018). Functional attributes of a new molecule-2-hydroxymethyl-benzoic acid 2′-hydroxy-tetradecyl ester isolated from *Talaromyces purpureogenus* CFRM02. *Food Chem.* 255, 89–96. doi: 10.1016/j.foodchem.2018.02.034

Ren, J., Ding, S.-S., Zhu, A., Cao, F., and Zhu, H.-J. (2017). Bioactive azaphilone derivatives from the fungus *Talaromyces aculeatus*. *J. Nat. Prod.* 80, 2199–2203. doi: 10.1021/acs.jnatprod.7b00032

Reyes, B. A. S., Dufourt, E. C., Ross, J., Warner, M. J., Tanquilut, N. C., and Leung, A. B. (2018). Selected phyto and marine bioactive compounds: alternatives for the treatment of type 2 diabetes. *Stud. Natl. Prod. Chem.* 111–143. doi: 10.1016/B978-0-444-64068-0.00004-8

Richardson, M., and Khosla, C. (1999). "1.18- Structure, function, and engineering of bacterial aromatic Polyketide synthases," in *Comprehensive Natural Products Chemistry*. eds. S. D. Barton, K. Nakanishi and O. Meth-Cohn (Pergamon: Oxford), 473–494.

Sakai, K., Asami, Y., Chiba, T., Suga, T., Nonaka, K., Iwatsuki, M., et al. (2018). Oxoberkedienoic acid: a new octadienoic acid derivative isolated from *Talaromyces verruculosus* using a chemical screening system. *J. Gen. Appl. Microbiol.* 64, 136–138. doi: 10.2323/jgam.2017.09.001

Sparkman, O. D., Penton, Z., and Kitson, F. G. (2011). *Gas Chromatography and Mass Spectrometry: A Practical Guide*. *2nd Edn*. Boston, MA: Elsevier.

Uzma, F., Mohan, C. D., Hashem, A., Konappa, N. M., Rangappa, S., Kamath, P. V., et al. (2018). Endophytic fungi—alternative sources of cytotoxic compounds: a review. *Front. Pharmacol.* 9:309. doi: 10.3389/fphar.2018.00309

Vasil, I. K., Constabel, F., Bogorad, L., and Schell, J. S. (1984). *Cell Culture and Somatic Cell Genetics of Plants*. Orlando, FL: Academic Press.

Venkatachalam, M., Magalon, H., Dufossé, L., and Fouillaud, M. (2018). Production of pigments from the tropical marine-derived fungi *Talaromyces albobiverticillius*: new resources for natural red-colored metabolites. *J. Food Compos. Anal.* 70, 35–48. doi: 10.1016/j.jfca.2018.03.007

Vinale, F., Nicoletti, R., Lacatena, F., Marra, R., Sacco, A., Lombardi, N., et al. (2017). Secondary metabolites from the endophytic fungus *Talaromyces pinophilus*. *Nat. Prod. Res.* 31, 1778–1785. doi: 10.1080/14786419.2017.1290624

Visagie, C. M., Yilmaz, N., Frisvad, J. C., Houbraken, J., Seifert, K. A., Samson, R. A., et al. (2015). Five new *Talaromyces* species with ampulliform-like phialides and globose rough walled conidia resembling *T. verruculosus*. *Mycoscience* 56, 486–502. doi: 10.1016/j.myc.2015.02.005

Wang, N., Qiu, Y., Xiao, T., Wang, J., Chen, Y., Xu, X., et al. (2019). Comparative studies on Pb(II) biosorption with three spongy microbe-based biosorbents: high performance, selectivity and application. *J. Hazard. Mater.* 373, 39–49. doi: 10.1016/j.jhazmat.2019.03.056

Wang, W., Wan, X., Liu, J., Wang, J., Zhu, H., Chen, C., et al. (2018). Two new terpenoids from *Talaromyces purpurogenus*. *Mar. Drugs* 16, 150. doi: 10.3390/md16050150

Waters, D. M., Murray, P. G., Ryan, L. A., Arendt, E. K., and Tuohy, M. G. (2010). *Talaromyces emersonii* thermostable enzyme systems and their applications in wheat baking systems. *J. Agric. Food Chem.* 58, 7415–7422. doi: 10.1021/jf100737v

West, R. R., Ness, J. V., Varming, A. M., Rassing, B., Biggs, S., Gasper, S., et al. (1996). ZG-1494α, a novel platelet-activating factor acetyltransferase inhibitor from *Penicillium rubrum*, isolation, structure elucidation and biological activity. *J. Antibiot.* 49, 967–973. doi: 10.7164/antibiotics.49.967

Xian, H., Tang, W. A. L., and Li, D. (2011). Cloning and bioinformatics analysis of chitinase gene from mycoparasitic *Talaromyces flavus*. *J. Agric. Biotechnol.* 9, 1089–1098. doi: 10.3969/j.issn.16747968.2011.06.016

Xie, X.-S., Fang, X.-W., Huang, R., Zhang, S.-P., Wei, H.-X., and Wu, S.-H. (2016). A new dimeric anthraquinone from endophytic *Talaromyces* sp. YE3016. *Nat. Prod. Res.* 30, 1706–1711. doi: 10.1080/14786419.2015.1136888

Yang, H., Li, F., and Ji, N. (2016). Alkaloids from an algicolous strain of *Talaromyces* sp. *Chin. J. Ocean. Limnol.* 34, 367–371. doi: 10.1007/s00343-015-4316-2

Yang, Z.-D., Zhang, X.-D., Yang, X., Yao, X.-J., and Shu, Z.-M. (2021). A norbisabolane and an arabitol benzoate from *Talaromyces marneffei*, an endophytic fungus of *Epilobium angustifolium*. *Fitoterapia* 153:104948. doi: 10.1016/j.fitote.2021.104948

Yuan, W.-H., Teng, M.-T., Sun, S.-S., Ma, L., Yuan, B., Ren, Q., et al. (2018). Active metabolites from endolichenic fungus *Talaromyces* sp. *Chem. Biodivers* 15:e1800371. doi: 10.1002/cbdv.201800371

Zang, Y., Genta-Jouve, G., Escargueil, A. E., Larsen, A. K., Guedon, L., Nay, B., et al. (2016). Antimicrobial oligophenalenone dimers from the soil fungus *Talaromyces stipitatus*. *J. Nat. Prod.* 79, 2991–2996. doi: 10.1021/acs.jnatprod.6b00458

Zhai, M.-M., Niu, H.-T., Li, J., Xiao, H., Shi, Y.-P., Di, D.-L., et al. (2015). Talaromycolides A–C, novel phenyl-substituted phthalides isolated from the green Chinese onion-derived fungus *Talaromyces pinophilus* AF-02. *J. Agric. Food Chem.* 63, 9558–9564. doi: 10.1021/acs.jafc.5b04296

Zhang, M., Deng, Y., Liu, F., Zheng, M., Liang, Y., Sun, W., et al. (2021). Five undescribed steroids from *Talaromyces stipitatus* and their cytotoxic activities against hepatoma cell lines. *Phytochemistry* 189:112816. doi: 10.1016/j.phytochem.2021.112816

Zhang, M., Li, Q., Li, S., Deng, Y., Yu, M., Liu, J., et al. (2022a). An unprecedented ergostane with a 6/6/5 tricyclic 13(14 → 8)abeo-8,14-seco skeleton from *Talaromyces adpressus*. *Bioorg. Chem.* 127:105943. doi: 10.1016/j.bioorg.2022.105943

Zhang, K., Zhang, X., Lin, R., Yang, H., Song, F., Xu, X., et al. (2022b). New secondary metabolites from the marine-derived fungus *Talaromyces mangshanicus* BTBU20211089. *Mar. Drugs* 20, 79. doi: 10.3390/md20020079

Zhang, Y.-H., Zhao, Y.-J., Qi, L., Du, H.-F., Cao, F., and Wang, C.-Y. (2022c). Talasteroid, a new withanolide from the marine-derived fungus *Talaromyces stollii*. *Nat. Prod. Res.* 1–7. doi: 10.1080/14786419.2022.2070747

Zhao, J., Liu, Z., Sun, S., and Liu, Y. (2020). Investigation on secondary metabolites of endophytic fungus *Talaromyces purpurogenus* hosted in Tylophora ovate. *China J. Chin. Mater. Med.* 6, 1368–1373. doi: 10.19540/j.cnki.cjcmm

Zhao, W.-T., Shi, X., Xian, P.-J., Feng, Z., Yang, J., and Yang, X.-L. (2021a). A new fusicoccane diterpene and a new polyene from the plant endophytic fungus *Talaromyces pinophilus* and their antimicrobial activities. *Nat. Prod. Res.* 35, 124–130. doi: 10.1080/14786419.2019.1616727

Zhao, Y., Sun, C., Huang, L., Zhang, X., Zhang, G., Che, Q., et al. (2021b). Talarodrides A-F, nonadrides from the antarctic sponge-derived fungus *Talaromyces* sp. HDN1820200. *J. Nat. Prod.* 84, 3011–3019. doi: 10.1021/acs.jnatprod.1c00203

Zhao, J.-Y., Wang, X.-J., Liu, Z., Meng, F.-X., Sun, S.-F., Ye, F., et al. (2019a). Nonadride and Spirocyclic anhydride derivatives from the plant endophytic fungus *Talaromyces purpurogenus*. *J. Nat. Prod.* 82, 2953–2962. doi: 10.1021/acs.jnatprod.9b00210

Zhao, J.-W., Yang, Z.-D., Zhou, S.-Y., Yang, L.-J., Sun, J.-H., Yao, X.-J., et al. (2019b). Wortmannine F and G, two new pyranones from *Talaromyces wortmannii* LGT-4, the endophytic fungus of *Tripterygium wilfordii*. *Phytochem. Lett.* 29, 115–118. doi: 10.1016/j.phytol.2018.11.023

Zotchev, S. B. (2013). "Alkaloids from marine bacteria," in *Advances in Botanical Research* (Elsevier), 301–333. doi: 10.1016/B978-0-12-408061-4.00011-0

frontiers | Frontiers in Microbiology

TYPE Original Research
PUBLISHED 23 August 2022
DOI 10.3389/fmicb.2022.999996

OPEN ACCESS

EDITED BY
Peng Zhang,
Tobacco Research Institute (CAAS), China

REVIEWED BY
Boyi Fan,
Nantong University,
China
Zhenzhen Shi,
Yantai Institute of Coastal Zone Research (CAS), China

*CORRESPONDENCE
Da-Le Guo
guodale@cdutcm.edu.cn
Yun Deng
dengyun@cdutcm.edu.cn

†These authors have contributed equally to this work

SPECIALTY SECTION
This article was submitted to Antimicrobials, Resistance and Chemotherapy, a section of the journal Frontiers in Microbiology

RECEIVED 21 July 2022
ACCEPTED 01 August 2022
PUBLISHED 23 August 2022

CITATION
Huo X-Y, Lei L-R, Guo W-X, Hu Y-J, Kuang Q-X, Liu M-D, Peng W, Dai Y-F, Wang D, Gu Y-C, Guo D-L and Deng Y (2022) Trichodimerol inhibits inflammation through suppression of the nuclear transcription factor-kappaB/NOD-like receptor thermal protein domain associated protein 3 signaling pathway. *Front. Microbiol.* 13:999996. doi: 10.3389/fmicb.2022.999996

Trichodimerol inhibits inflammation through suppression of the nuclear transcription factor-kappaB/NOD-like receptor thermal protein domain associated protein 3 signaling pathway

Xue-Yan Huo[1†], Li-Rong Lei[1†], Wen-Xiu Guo[1], Yun-Jie Hu[1], Qi-Xuan Kuang[1], Meng-Dan Liu[1], Wan Peng[2], Yi-Fei Dai[3], Dong Wang[1], Yu-Cheng Gu[4], Da-Le Guo[1*] and Yun Deng[1*]

[1]State Key Laboratory of Southwestern Chinese Medicine Resources, School of Pharmacy, Chengdu University of Traditional Chinese Medicine, Chengdu, China, [2]Institute of Rare Diseases, West China Hospital of Sichuan University, Chengdu, China, [3]Department of Basic Medical Sciences, School of Medicine, Tsinghua University, Beijing, China, [4]Syngenta Jealott's Hill International Research Centre, Berkshire, United Kingdom

Excessive inflammation causes chronic diseases and tissue damage. Although there has been drug treatment, its side effects are relatively large. Searching for effective anti-inflammatory drugs from natural products has become the focus of attention. First isolated from *Trichoderma longibraciatum*, trichodimerol is a natural product with TNF inhibition. In this study, lipopolysaccharide (LPS)-induced RAW264.7 macrophages were used as a model to investigate the anti-inflammatory activity of trichodimerol. The results of nitric oxide (NO) detection, enzyme-linked immunosorbent assay (ELISA), and reactive oxygen species (ROS) showed that trichodimerol could reduce the production of NO, ROS, and the proinflammatory cytokines interleukin (IL)-6 and tumor necrosis factor (TNF)-α. Western blotting results showed that trichodimerol could inhibit the production of inflammatory mediators such as cyclooxygenase (COX)-2 and inducible nitric oxide synthase (iNOS) and the protein expression of nuclear transcription factor-kappaB (NF-κB), p-IKK, p-IκB, Toll-like receptor 4 (TLR4), NOD-like receptor thermal protein domain associated protein 3 (NLRP3), cysteinyl aspartate specific proteinase (Caspase)-1, and ASC, which indicated that trichodimerol may inhibit inflammation through the NF-κB and NLRP3 pathways. At the same time, molecular docking showed that trichodimerol can directly combine with the TLR4-MD2 complex. Hence, trichodimerol inhibits inflammation by obstructing the interaction between LPS and the TLR4-MD2 heterodimer and suppressing the downstream NF-κB and NLRP3 pathways.

KEYWORDS

trichodimerol, inflammation, NF-κB, NLRP3, molecular docking

Introduction

Excessive inflammation can lead to a series of chronic diseases and tissue damage. Due to the side effects of marketed drugs, the search for new efficacious and safe anti-inflammatory natural products with novel structures is still a focus of extensive research (Zhong and Shi, 2019). Fungi are highly rewarding resources of auspicious hit compounds for inflammation-related diseases, and many anti-inflammatory natural products with novel, complex, and compact structures have been isolated from fungi (Cao et al., 2021; Ju et al., 2021; Huang et al., 2022; Kuang et al., 2022a,b). Trichodimerol is a typical natural product isolated from *Trichoderma longibraciatum*. It has been reported that trichodimerol can inhibit the secretion of proinflammatory factors, including tumor necrosis factor (TNF-α) and nitric oxide (NO; Lee et al., 2005). However, the underlying mechanism is currently unclear.

In this study, lipopolysaccharide (LPS)-induced RAW264.7 macrophages and zebrafish were used to investigate the anti-inflammatory activity and reveal the related underlying mechanism of trichodimerol. The results showed that trichodimerol reduced the production of NO, ROS, and the proinflammatory cytokines interleukin (IL)-6 and TNF-α. Western blotting results also indicated that trichodimerol could inhibit the production of inflammatory mediators such as cyclooxygenase (COX)-2 and inducible nitric oxide synthase (iNOS) and the protein expression of nuclear transcription factor-kappa B (NF-κB), p-IKK, p-IκB, Toll-like receptor 4 (TLR4), NOD-like receptor thermal protein domain associated protein 3 (NLRP3), cysteinyl aspartate specific proteinase (Caspase)-1 and ASC, which indicated that trichodimerol may inhibit inflammation through the NF-κB and NLRP3 pathways. In addition, molecular docking indicated that TLR4 was directly combined with trichodimerol, which can provide an interpretation of the inhibition of the NF-κB and NLRP3 pathways. The details of the anti-inflammatory activity and partial underlying mechanisms of trichodimerol are reported herein.

Materials and methods

Materials

Fetal bovine serum (FBS) was purchased from Excell (FCS500, United States). Dulbecco's modified Eagle's medium (DMEM) was purchased from Gibco (C11995500BT, United States). Penicillin–streptomycin was purchased from HyClone (SV30010, United States). Phosphate buffered saline (PBS) was purchased from Boster (AR0030, Wuhan, China). Dimethyl sulfoxide (DMSO) was purchased from Gibco. Lipopolysaccharide (LPS) was purchased from Beyotime (ST1470, Shanghai, China). Radioimmunoprecipitation assay buffer (RIPA) was purchased from Beyotime (P0013B, Shanghai, China). Broad spectrum protease inhibitor cocktail and broad phosphatase inhibitor were purchased from Boster (Wuhan, China). Cell Counting Kit-8 reagent (CCK8) was purchased from MCE (HY-K0301, United States). Total RNA extraction reagent was purchased from Vazyme (R401-01, Nanjing, China). A BCA Protein Assay Kit was purchased from CWBIO (CW0014S, Beijing, China). The PAGE Gel Rapid Preparation Kit was purchased from Yamei (PG112, Shanghai, China). Omni-Easy™ Protein Sample Loading Buffer was purchased from Yamei (LT101S, Shanghai, China). The Nitric Oxide (NO) Assay Kit was purchased from Beyotime (S0021S, Shanghai, China). The Mouse TNF-α ELISA Kit was purchased from Boster (EK0527, Wuhan, China). The Mouse IL-6 ELISA Kit was purchased from Boster (EK0411, Wuhan, China). RT EasyTM II (Master Premix for first-strand cDNA synthesis for Real-Time PCR RT-01022) and Real-Time PCR EasyTM-SYBR Green I (QP-01012) were purchased from Foregene (Chengdu, China). A Reactive Oxygen Species Assay Kit was purchased from UElandy (R6033, Suzhou, China). The NF-κB Activation, Nuclear Translocation Assay Kit (rabbit polyclonal antibody) was purchased from Beyotime (SN368, Shanghai, China). A 180 kDa Prestained Protein Marker was purchased from Vazyme (MP102-02, Nanjing, China). Western Blocking Buffer was purchased from Beyotime (P0023B, Shanghai, China). Super ECL Plus Western Blotting Substrate was purchased from Biogeound (BG0001, Chongqing, China).

Cell culture

RAW264.7 macrophages were cultured in DMEM supplemented with 10% fetal bovine serum and 1% penicillin and streptomycin antibody, and the living environment was 37 °C incubator containing 5% CO_2.

Cell viability

RAW264.7 macrophages were cultured on 96-well plate with 1,000 cells per well. After 6 h, different concentrations (3.75, 7.5, 15, 30, 60, 120, and 240 μM) of trichodimerol mixed in the culture medium were added to the 96-well plate for incubation for 48 h. Afterward, 10 μl of CCK8 was added to each well for 1 h. The number of cells was detected by enzyme calibration at a wavelength of 450 nm.

Determination of NO production

RAW264.7 macrophages were cultured on 6-well plate with 10,000 cells per well overnight and then pretreated with simple trichodimerol and different concentrations of trichodimerol (5, 10, and 15 μM) for 2 h with LPS (1 μg/ml) added for 24 h. DMSO was used as a negative control. Then, the supernatant was absorbed, and the Griess reagent system was used to detect NO production.

Reverse transcription-PCR analysis

RAW264.7 macrophages were plated on six-well plate with 100,000 cells per well. After 24 h, the cells were pretreated with simple trichodimerol and different concentrations of trichodimerol (5, 10, and 15 μM) for 2 h and then with LPS (1 μg/ml) for 24 h. Then, 1 ml of TRIzol reagent was added to extract RNA. RNA purity and concentration were measured with an ultramicrospectrophotometer. After that, genomic DNA was removed with 4 × gDNA wiper Mix and reverse transcripted with 5 × HiScriptIIqRT SuperMixII, cDNA amplification was carried out with the ChamQ Universal SYBR qPCR Master Mix, in which the 2 × ChamQ Universal SYBR qPCR Master Mix was 5 μl, the DNase-free ddH_2O was 2.1 μl, the Template cDNA was 2.5 μl and the primers COX-2 (forward primer: 5′-AACCCAGGGGATCGAGTGT-3′, reverse primer: 5′-CGCAGC TCAGTGTTTGGGAT-3′), iNOS (forward primer: 5′-GAGCCACA GTCCTCTTTGCTA-3′, reverse primer: 5’-TGTCACCACCAGCA GTAGTTG-3′), IL-1β (forward primer: 5′-TGAAATGCCACC TTTTGACAG-3′, reverse primer: 5′-CCACAGCCACAATGAGTG ATAC-3′), IL-6 (forward primer: 5′-GGGACTGATGCTGGTGAC AAC-3′,reverseprimer:5′-CAACTCTTTTCTCATTTCCACGA-3′), TNF-α (forward primer: 5′-CCCTCCAGAAAAGACACCATG-3′, reverse primer: 5′-CACCCCGAAGTTCAGTAGACAG-3′), and GAPDH (forward primer: 5′-GCAAGTTCAACGGCACAG-3′, reverse primer: 5’-CGCCAGTAGACTCCACGAC-3′) was 0.2 μl.

Western blotting

RAW264.7 macrophages were plated on six-well plate with 100,000 cells per well. After 6 h, the cells were pretreated with simple trichodimerol and different concentrations of trichodimerol (5, 10, and 15 μM) for 2 h and then treated with LPS (1 μg/ml) for 24 h. The cells were removed and washed twice with phosphate buffered saline (PBS). Total protein was extracted by 1 × SDS lysis with 250 μl heated in a constant temperature metal bath at 100°C for 30 min and centrifuged at 12,000 rpm at 4°C for 15 min to obtain the supernatant. The protein concentration was detected by a BCA Protein Assay Kit. Protein sample loading buffer (1×) was used at 95°C for 10 min to prevent denaturation. The total proteins were separated by 10% sodium dodecyl sulfate–polyacrylamide gel electrophoresis (SDS-PAGE), transferred to polyvinylidene fluoride (PVDF) membranes, and incubated with primary antibody at 4°C overnight. The primary antibodies were as follows: TLR4 (1:4,000, Proteintech, 66350-1-Ig, China), NF-κB (1:1,000, CST, 8242S, United States), p-NF-κB (1:1,000, CST, 3033S), p-IκB (1:1,000, CST, 5209S), p-IKKα/β (1:1,000, CST, 2697S), NLRP3 (1:1,000, CST, 15101S), Caspase-1 (1:1,000, Proteintech, 22915-1-Ig), ASC/TMS1 (1:1,000, Proteintech, 69494-1-Ig), iNOS (1:1,000, NOVCCS, NB300-605SS, United States), COX-2 (1:1,000, Abcam, ab179800, United States), GAPDH (1:50,000, Proteintech, 60004-1-Ig), and Tubulin (1:50,000, Proteintech, 66031-1-Ig). Then, the cells were incubated with secondary antibody at room temperature for 2 h. Strips were detected by a high-sensitivity ECL chemiluminescence detection kit and analyzed by ImageJ software.

Enzyme-linked immunosorbent assay

RAW264.7 macrophages were cultured on six-well plate with 10,000 cells per well overnight and then pretreated with simple trichodimerol and different concentrations of trichodimerol (5, 10, and 15 μM) for 2 h with LPS (1 μg/ml) added for 24 h. Then, the supernatant was absorbed. The inflammatory factors TNF-α and IL-6 were assayed by ELISA kits, and then the absorbance was detected at 450 nm.

Intracellular ROS measurement

RAW264.7 macrophages were plated on 12-well plate and placed into climbing flasks at a density of 20,000 cells per well. After 6 h, the cells were pretreated with simple trichodimerol and different concentrations of trichodimerol (5, 10, and 15 μM) for 2 h with LPS (1 μg/ml) added for 24 h. The cells were stimulated with DCFH-DA reagent (10 μM) at 37°C for 30 min and washed twice with PBS. The following step was to immobilize with 5% paraformaldehyde for 15 min, wash twice with PBS dye with DAPI for 8 min with paraformaldehyde and wash twice again. Finally, the results were observed under a fluorescence microscope. Zebrafish were pretreated with 2.5 and 5 μM trichodimerol. After 1 h, 10 μg/ml LPS was cultured for 72 h. During this period, fresh trichodimerol and LPS were replaced every 24 h and then treated with DCFH-DA for 1 h and anesthetized with tricaine. Finally, the fluorescence intensity was detected by confocal microscopy (Olympus FV1200, Japan).

Nuclear transport of NF-κB/p65

RAW264.7 macrophages were plated on 12-well plate at a density of 20,000 cells per well. After 6 h, the cells were pretreated with simple trichodimerol and different concentrations of trichodimerol (5, 10, and 15 μM) for 2 h, then with LPS (1 μg/ml) added for 12 h. In cells, the NF-κB nuclear transport state was treated by the NF-κB Activation, Nuclear Translocation Assay Kit. The operation was as follows: fixation solution was added for 15 min, and the washing solution was washed three times for 5 min each time. After that, the blocking solution was blocked at room temperature for 1 h, and the NF-κB/p65 antibody was incubated at room temperature for 1 h. Then, the washing solution was washed three times for 10 min each time, and the anti-rabbit Cy3 antibody was added at room temperature for 1 h. Finally, the washing solution was washed twice. DAPI staining was performed for 5 min, and the slices were prepared. The results were presented under a fluorescence microscope (Olympus, IX73, Japan).

Molecular docking

The crystal structure of the TLR4-MD2 complex was obtained from the RCSB protein database (PDB ID: 2Z66; Berman et al., 2000). The docking analysis of trichodimerol and TLR4-MD2 was performed by Schrödinger software. Schrödinger's Maestro Molecular Modeling Apparatus was used to obtain the 3D structure, regeneration state of natural ligands, crystal structure of protein, optimization of hydrogen bond distribution, energy minimization of trichodimerol, and water removal. Finally, the best binding site was predicted by the SiteMap module (Friesner et al., 2006).

Statistical analysis

All data were analyzed by GraphPad Prism 7.0 software (San Diego, California, United States) and expressed as the mean ± SD of three repetitions of the same experiment. The data were from three independent experiments.

Results

Trichodimerol inhibited LPS-induced inflammation in RAW264.7 macrophages

Trichodimerol was extracted from *Pseudeurotium ovale* (Figure 1A). To study the anti-inflammatory effect of trichodimerol on LPS-induced RAW264.7 macrophages, a cell viability test was performed on the cells. The results showed that the cell viability was better in the range of 120 μM (Figure 1B). Concentrations of 5, 10, and 15 μM were selected for subsequent experiments. RAW264.7 macrophages were treated with trichodimerol and induced by LPS for 24 h, and the supernatant was collected to detect NO and proinflammatory cytokines. The results showed that under the influence of trichodimerol, the release of NO was inhibited (Figure 2A), and the proinflammatory cytokines TNF-α and IL-6 also showed a downward trend, which was consistent with the expression of proinflammatory factor mRNA in Reverse transcription-PCR (RT–PCR; Figures 2B,C).

Trichodimerol restrained LPS-induced expression or production of inflammatory mediators in RAW264.7 macrophages

Lipopolysaccharide-induced macrophages overexpress COX-2 and iNOS to increase prostaglandin and NO release (Miletic et al., 2006). Reactive oxygen species (ROS) are mainly generated by mitochondria (Brillo et al., 2021), and excessive release will lead to tissue and organ damage (Yang and Lian, 2020). Western blotting analysis showed that the protein levels of COX-2 and iNOS in LPS-induced RAW264.7 macrophages was significantly decreased after administration of trichodimerol (Figures 3A,B). At the same time, there was the same trend as the expression of inflammatory mediators at the mRNA level in RT–PCR (Figure 3C). Immunofluorescence showed that the green fluorescence intensity decreased after adding trichodimerol, indicating that the release of ROS decreased (Figure 3D).

Trichodimerol weakened inflammation *in vivo*

Zebrafish is a significant model system for analyzing human diseases. Studies have found that the zebrafish genome shares 60–80% homology with the human genome (Barbazuk et al., 2000). Zebrafish have the advantages of strong reproduction, fast development, and small size (Jia et al., 2019). Currently, an increasing number of zebrafish have been used in the *in vivo* study of inflammatory animals (Zanandrea et al., 2020). In this experiment, the green fluorescence intensity of zebrafish was significantly downregulated compared with that of the LPS group

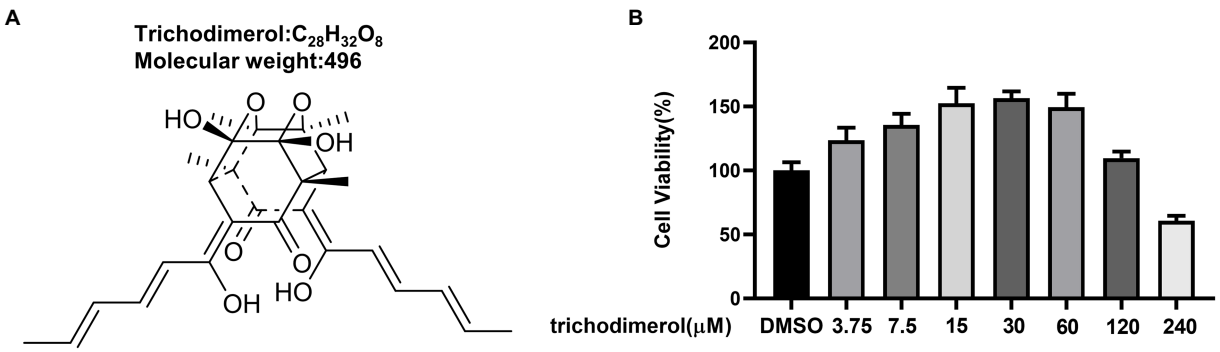

FIGURE 1
The structure and cytotoxicity of trichodimerol. **(A)** The structure of trichodimerol. **(B)** Cell viability. Cell viability was tested with CCK8 reagent 48h after RAW264.7 macrophages were administered different amounts of trichodimerol, and dimethyl sulfoxide (DMSO) was used as a blank group.

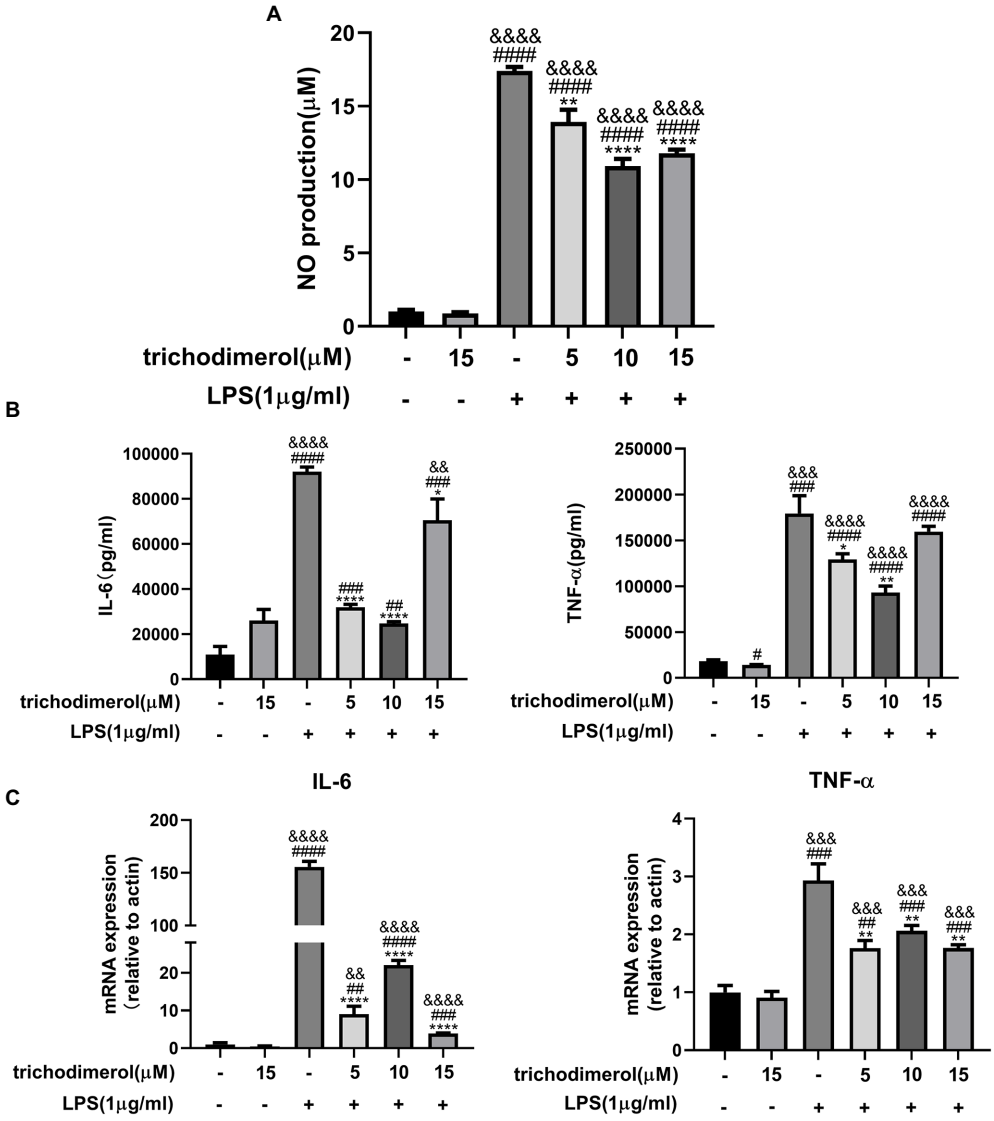

FIGURE 2
The effect of trichodimerol on inflammation. **(A)** Nitric oxide (NO) production in the supernatant of RAW264.7 macrophages after trichodimerol administration. **(B)** RAW264.7 macrophages were treated with different concentrations of trichodimerol and induced by lipopolysaccharide (LPS). The expression of tumor necrosis factor (TNF)-α and IL-6 in the supernatant was detected by ELISA. **(C)** mRNA expression levels of IL-6 and TNF-α in RAW264.7 macrophages in different treatment groups. All data are expressed as the mean±SD. $^{\#}p$ <0.05, $^{\#\#}p$ <0.01, $^{\#\#\#}p$ <0.001, and $^{\#\#\#\#}p$ <0.0001, compared with the DMSO group. $^{\&\&}p$<0.01, $^{\&\&\&}p$<0.001, and $^{\&\&\&\&}p$<0.0001, compared with the trichodimerol 15μM group. $^{*}p$<0.05, $^{**}p$<0.01, and $^{****}p$<0.0001, compared with the LPS group.

(Figures 4A,B), indicating that trichodimerol inhibited the release of ROS, which is consistent with the *in vitro* experiment.

Trichodimerol inhibited the NLRP3 pathway

Multiple pathogen-and damage-associated stresses drive inflammation by activating the multimolecular NLRP3-inflammasome complex (Seoane et al., 2020), which is composed of ASC, Caspase-1, and NLRP3. To explore the effect of trichodimerol on the NLRP3 pathway, LPS was used to induce RAW264.7 macrophages. After trichodimerol administration, compared with LPS, the protein levels of ASC, Caspase-1, and NLRP3 were downregulated (Figures 5A,B), and the mRNA expression of IL-1β downstream was significantly downregulated (Figure 5C). This result indicated that the inflammatory response may be inhibited by restraining the NLRP3 pathway.

Trichodimerol blocked the NF-κB pathway

Toll-like receptor (Toll) is an important component of the innate immune system and plays a significant role in inflammation. When

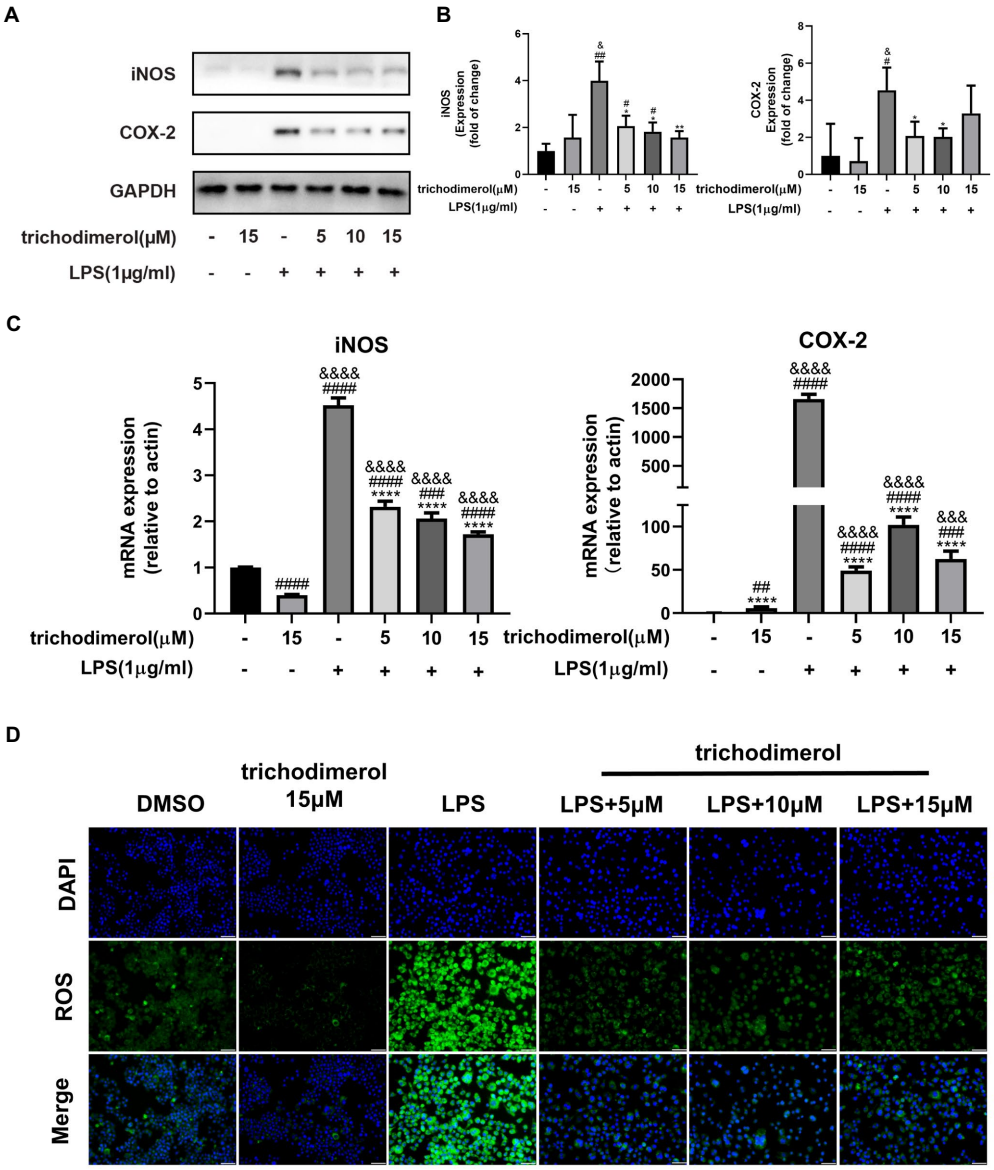

FIGURE 3
The effect of trichodimerol on the inflammatory mediators. **(A)** The protein expression of inducible nitric oxide synthase (iNOS) and cyclooxygenase (COX)-2 in RAW264.7 macrophages treated with different concentrations; GAPDH was used as an internal reference. **(B)** Quantitative statistical results of the protein expression of iNOS and COX-2. **(C)** mRNA expression levels of iNOS and COX-2 in RAW264.7 macrophages in different treatment groups. **(D)** Reactive oxygen species (ROS) production in RAW264.7 macrophages induced by LPS 24h after trichodimerol treatment. Green fluorescence represents intracellular ROS stained by DCFH-DA, blue fluorescence represents nucleus, white stripe=50μm. All data are expressed as the mean±SD. $^{\#}p<0.05$, $^{\#\#}p<0.01$, $^{\#\#\#}p<0.001$, and $^{\#\#\#\#}p<0.0001$, compared with the DMSO group. $^{\&}p<0.05$, $^{\&\&\&}p<0.001$, and $^{\&\&\&\&}p<0.0001$, compared with the trichodimerol 15μM group. $^{*}p<0.05$, $^{**}p<0.01$, and $^{****}p<0.0001$, compared with the LPS group.

TLR4 recognizes various microbial pathogens, it stimulates the activation of the NF-κB pathway (Kawai and Akira, 2007). The activation of NF-κB in macrophages can trigger the inflammatory cascade. IκBα promotes NF-κB to remain in the cytoplasm, is unable to enter the nucleus, and prevents its transcription. When IKK is activated, IκBα is phosphorylated and degraded by ubiquitination, releasing NF-κB and causing it to enter the nucleus (Baker et al., 2011). Compared with LPS-induced RAW264.7 macrophages, after administration of trichodimerol, fluorescence microscopy showed that NF-κB entered the nucleus decreased (red fluorescence; Figure 6A). At the same time, the protein levels of NF-κB, TLR4, p-IKK, p-IκB, and p-NF-κB showed a downward trend after adding trichodimerol (Figures 6B–G), which suggests that trichodimerol may inhibit inflammation by blocking the NF-κB pathway.

Trichodimerol possessed affinity for TLR4-MD2

TLR4-MD2 as the receptor of LPS is upstream molecule of NF-κB and plays an important role in inflammation, and

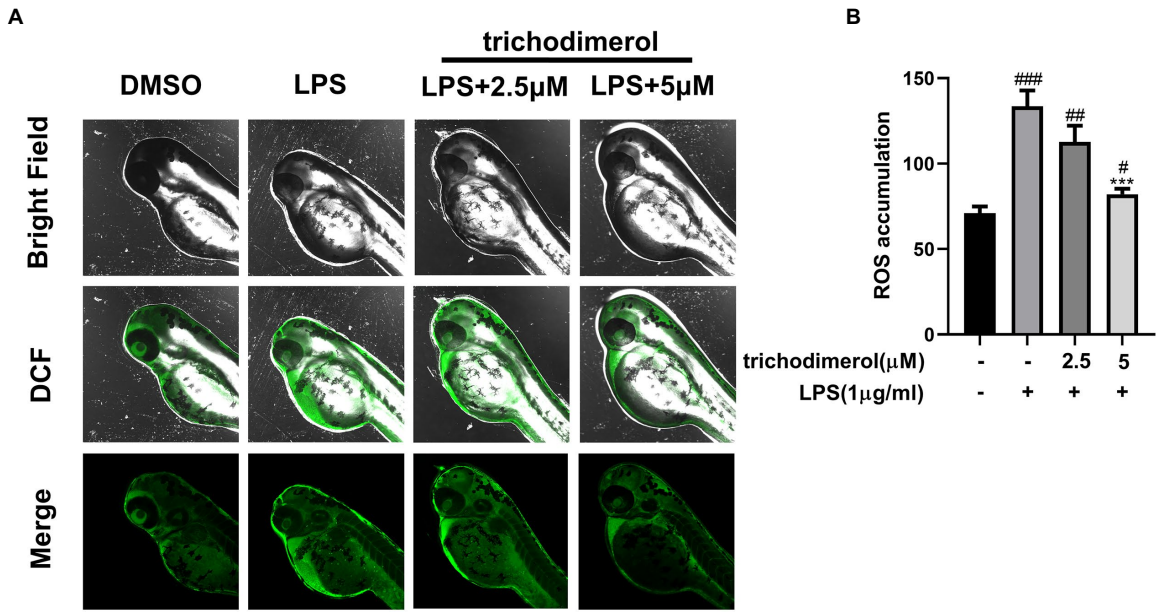

FIGURE 4
The accumulation of ROS in zebrafish. **(A)** Images of reactive oxygen species (ROS) levels in zebrafish exposed to different amounts of trichodimerol. Green fluorescence represents intracellular ROS stained by DCFH-DA. **(B)** ImageJ was used to quantify the fluorescence intensity, which was statistically analyzed. All data are expressed as the mean±SD. $^{\#}p<0.05$, $^{\#\#}p<0.01$, and $^{\#\#\#}p<0.001$, compared with the DMSO group. $^{***}p<0.001$, compared with the LPS group.

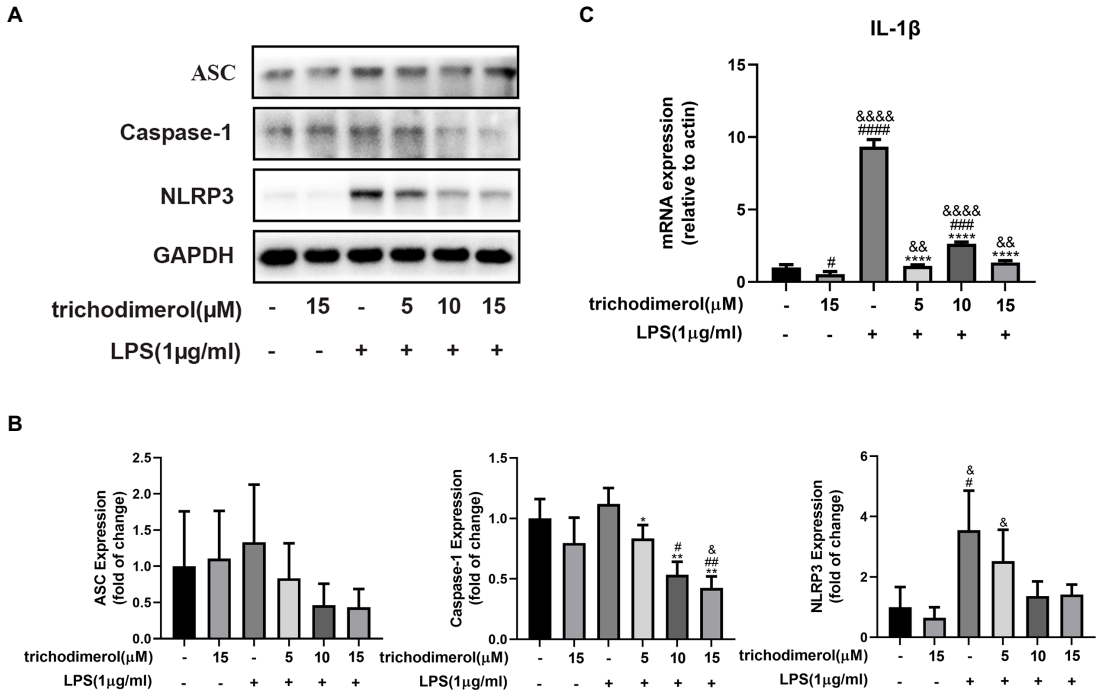

FIGURE 5
The effect of trichodimerol on the NLRP3 pathway. **(A)** RAW264.7 macrophages were treated with different concentrations of trichodimerol (5, 10, and 15μM) for 2h, followed by LPS (1μg/ml) for 24h. The protein expression of ASC, Caspase-1, and NLRP3 was detected by Western blotting; GAPDH was used as an internal reference. **(B)** Quantitative statistical results of the protein expression of ASC, Caspase-1, and NLRP3. **(C)** mRNA expression levels of IL-1β. All data are expressed as the mean±SD. $^{\#}p<0.05$, $^{\#\#}p<0.01$, $^{\#\#\#}p<0.001$, $^{\#\#\#\#}p<0.0001$, compared with the DMSO group. $^{\&}p<0.05$, $^{\&\&}p<0.01$, and $^{\&\&\&\&}p<0.0001$, compared with the trichodimerol 15μM group. $^{*}p<0.05$, $^{**}p<0.01$, and $^{****}p<0.0001$, compared with the LPS group.

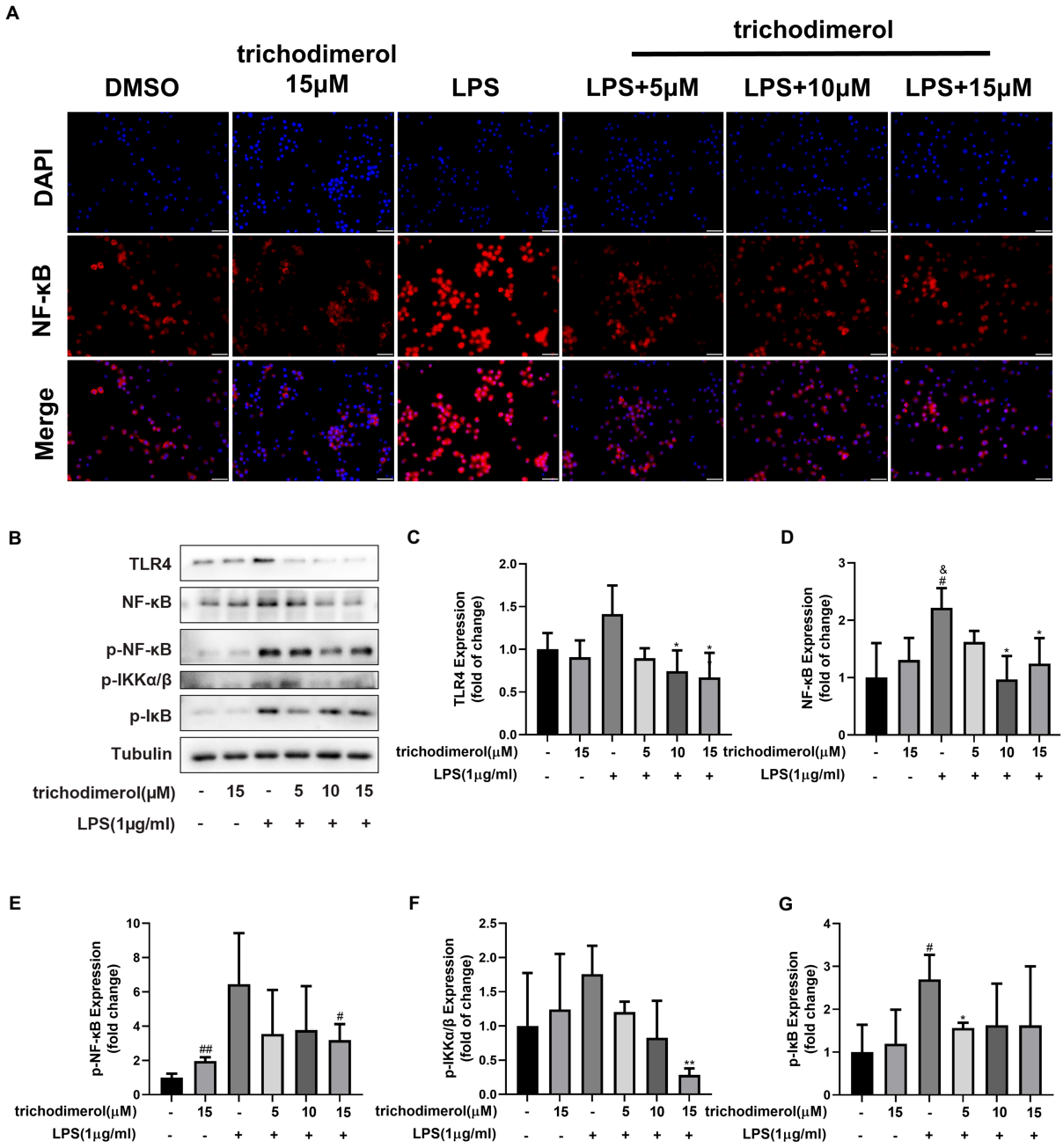

FIGURE 6
The effect of trichodimerol on the NF-κB pathway. **(A)** Nuclear translocation of RAW264.7 macrophages induced by LPS after 12h of trichodimerol treatment. Red fluorescence represents the NF-κB signal, blue fluorescence represents the nucleus, white stripe=50μm. **(B)** The protein expression of TLR4, NF-κB, p-NF-κB, p-IKKα/β, and p-IκB in RAW264.7 macrophages treated with different concentrations; Tubulin was used as an internal reference. **(C)** Quantitative statistical results of TLR4 protein expression. **(D)** Quantitative statistical results of the protein expression of NF-κB. **(E)** Quantitative statistical results of the protein expression of p-NF-κB. **(F)** Quantitative statistical results of the protein expression of p-IKKα/β. **(G)** Quantitative statistical results of the protein expression of p-IκB. All data are expressed as the mean±SD. $^{\#}p<0.05$, $^{\#\#}p<0.01$, compared with the DMSO group. $^{\&}p<0.05$, compared with the trichodimerol 15μM group. $^{*}p<0.05$, $^{**}p<0.01$, compared with the LPS group.

molecular docking was used to predict whether TLR4 can competitively bind LPS with trichodimerol. The results showed that hydrogen bonds were formed between trichodimerol and four amino acid residues at the TLR4-MD2 active site, including CYS 95, ASP 101, ARG 264, and ASN 339 (Figure 7), which indicated that trichodimerol might have the ability to modify the conformation of the TLR4-MD2 complex and obstruct the interaction between LPS and the TLR4-MD2 heterodimer. Subsequently, downstream signaling pathways might be suppressed.

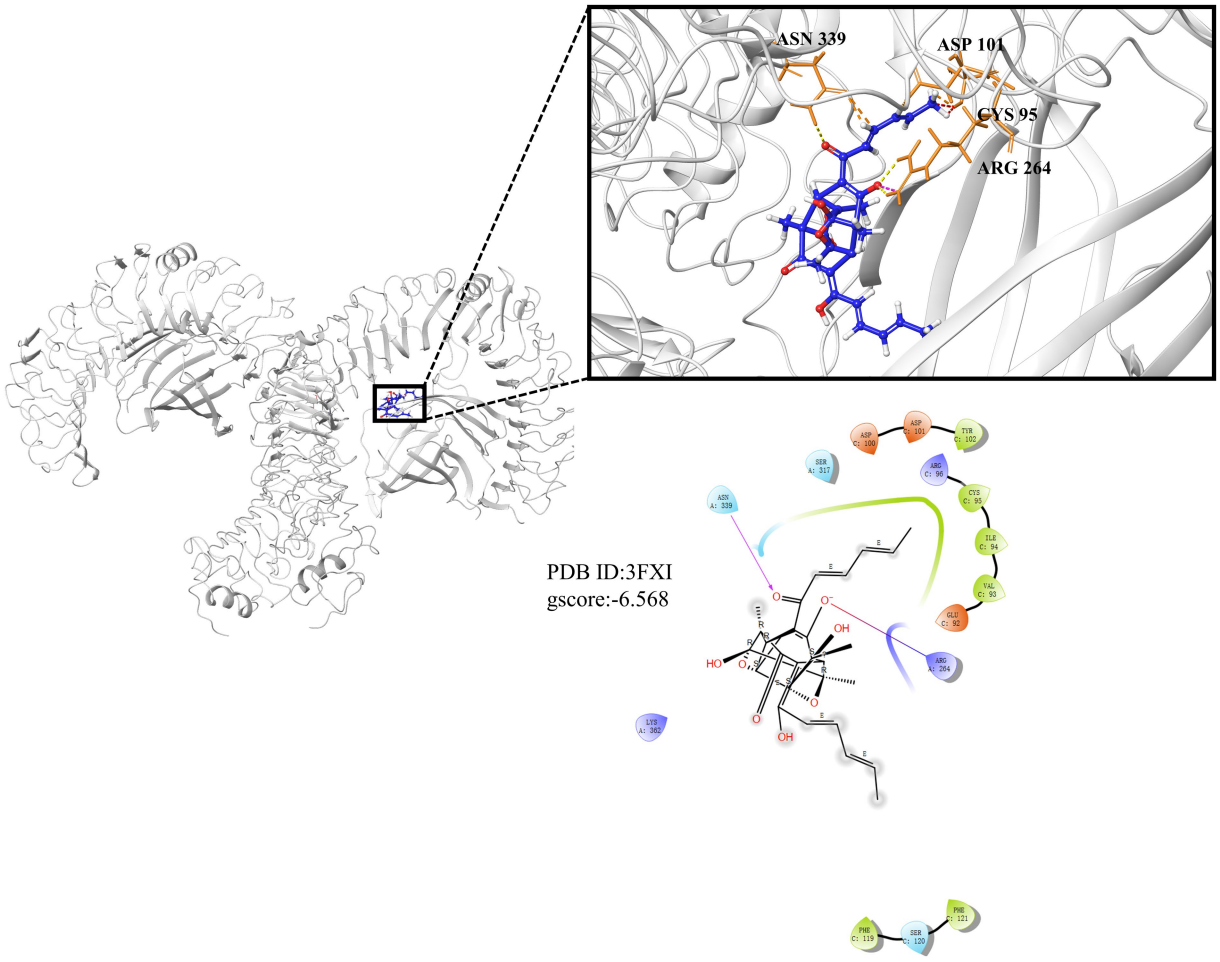

FIGURE 7
Molecular docking results of trichodimerol and TLR4-MD2. Molecular docking is simulated under the lowest energy conformation. Hydrogen bond interactions are represented by dotted lines.

Discussion

Acute inflammation is a self-defense protection produced by the human body that can subside by itself (Fredman et al., 2012). However, excessive injury time will further lead to the occurrence of chronic inflammation, such as asthma, arthritis, and cardiovascular diseases, which threaten human health (Zhong and Shi, 2019). Monocyte-derived macrophages play an active role in tissue regeneration and maintenance of tissue homeostasis (Viola et al., 2019). As an outer membrane component of Gram-negative bacteria, LPS plays an important role in inflammation (Batista et al., 2009). Induced by LPS, proinflammatory macrophages overexpress iNOS and COX-2 and produce a large number of proinflammatory cytokines, such as TNF-α, IL-1β, IL-6, and ROS (Reuter et al., 2010; Viola et al., 2019).

As a pattern recognition receptor of LPS, TLR4-MD2 plays a significant role in the development of inflammation. TLR4 receptor dimerization activates the downstream NF-κB and NLRP3 signaling pathways. The activation of NF-κB leads to the expression of proinflammatory factors, such as TNF-α, IL-1β, and IL-6 and upregulates the expression of NLRP3 (Bauernfeind et al., 2009; Rocha et al., 2016). Active NLRP3 oligomerizes and binds to the adaptor protein ASC (apoptosis-associated speck-like protein containing a caspase recruitment domain or CARD; Mezzaroma et al., 2021). Then, pro-caspase-1 is recruited and activated. Active caspase-1 cleaves its substrate pro-IL-1β to form mature IL-1β (White et al., 2017). IL-1β plays an important role in regulating the expression of adhesion molecules, mediating the inflammatory response, and immune cell infiltration (Wang et al., 1995). Based on this, we performed molecular docking of TLR4. The results showed that trichodimerol binds to TLR4-MD2 and forms hydrogen bonds with the four residues of the active site (Figure 7), suggesting that blocking TLR4-MD2 and suppressing TLR4-related downstream signaling pathways, such as the NF-κB (Figure 6) and NLRP3 (Figure 5) pathways, might be the underlying mechanism of trichodimerol's anti-inflammatory activity. In this study, we confirmed that trichodimerol inhibited inflammation and partially uncovered a related mechanism. Further studies are

needed to determine whether trichodimerol inhibits LPS binding to other sites and pathways.

Conclusion

In this study, we used LPS-induced RAW264.7 macrophages and zebrafish to confirm that trichodimerol reduces the production of ROS *in vitro* and *in vivo*, NO, and the expression of proinflammatory factors, such as IL-6, TNF-α, COX-2, and iNOS and revealed that trichodimerol is anti-inflammatory through the NF-κB and NLRP3 pathways. Molecular docking was also applied to provide a possible interpretation. These results suggested that trichodimerol may become a hit compound for the treatment of inflammation.

Data availability statement

The original contributions presented in the study are included in the article/Supplementary material; further inquiries can be directed to the corresponding authors.

Ethics statement

The animal study was reviewed and approved by Ethics Committee of Chengdu University of Traditional Chinese Medicine.

Author contributions

D-LG and YD designed and supervised the article. Q-XK performed the experiments and collected the data. X-YH, L-RL, and Y-JH analyzed and plotted the data. W-XG and M-DL isolated and purified trichodimerol. X-YH, L-RL, Y-JH, and Q-XK participated in the experiments. Y-FD and L-RL performed the molecular docking. X-YH wrote and finalized the manuscript. WP, Y-CG, D-LG, and YD contributed to the writing of this manuscript. All authors contributed to the article and approved the submitted version.

Funding

This work was supported by the National Natural Science Foundation of China (U19A2011 and 81973460), Department of Science and Technology of Sichuan Province (2021ZYD0079 and 2021YFN0134), Chengdu University of Traditional Chinese Medicine (CZYJC1905, 2020XSGG016, and 2020JCRC006), and National Interdisciplinary Innovation Team of Traditional Chinese Medicine (ZYYCXTD-D-202209).

Acknowledgments

The authors thank the analytical facilities of the Innovative Institute of Chinese Medicine and Pharmacy, Chengdu University of TCM for providing instruments.

Conflict of interest

The authors declare that the research was conducted in the absence of any commercial or financial relationships that could be construed as a potential conflict of interest.

Publisher's note

Supplementary material

The Supplementary material for this article can be found online at: https://www.frontiersin.org/articles/10.3389/fmicb.2022.999996/full#supplementary-material

References

Baker, R. G., Hayden, M. S., and Ghosh, S. (2011). NF-κB, inflammation, and metabolic disease. *Cell Metab.* 13, 11–22. doi: 10.1016/j.cmet.2010.12.008

Barbazuk, W. B., Korf, I., Kadavi, C., Heyen, J., Tate, S., Wun, E., et al. (2000). The syntenic relationship of the zebrafish and human genomes. *Genome Res.* 10, 1351–1358. doi: 10.1101/gr.144700

Batista, C. R. A., Gomes, G. F., Candelario-Jalil, E., Fiebich, B. L., and Oliveira, A. C. P. (2009). Lipopolysaccharide-induced neuroinflammation as a bridge to understand neurodegeneration. *Int. J. Mol. Sci.* 20:2293. doi: 10.3390/ijms20092293

Bauernfeind, F. G., Horvath, G., Stutz, A., Alnemri, E. S., MacDonald, K., Speert, D., et al. (2009). Cutting edge: NF-kappa B activating pattern recognition and cytokine receptors license NLRP3 inflammasome activation by regulating NLRP3 expression. *J. Immunol.* 183, 787–791. doi: 10.4049/jimmunol.0901363

Berman, H. M., Westbrook, J., Feng, Z., Gilliland, G., Bhat, T. N., Weissig, H., et al. (2000). The protein data bank. *Nucleic Acids Res.* 28, 235–242. doi: 10.1093/nar/28.1.235

Brillo, V., Chieregato, L., Leanza, L., Muccioli, S., and Costa, R. (2021). Mitochondrial dynamics, ROS, and cell signaling: a blended overview. *Lifestyles* 11:332. doi: 10.3390/life11040332

Cao, Y. M., Guo, D. L., Jin, M. Y., Tan, L., Yang, T. L., Deng, F., et al. (2021). Two new nor-sesquiterpenoids from *Fusarium tricinctum*, an endophytic fungus isolated from *Ligusticum chuanxiong*. *Nat. Prod. Res.* 35, 3535–3539. doi: 10.1080/14786419.2020.1712385

Fredman, G., Li, Y., Dalli, J., Chiang, N., and Serhan, C. N. (2012). Self-limited versus delayed resolution of acute inflammation: temporal regulation of pro-resolving mediators and microRNA. *Sci. Rep.* 2:639. doi: 10.1038/srep00639

Friesner, R. A., Murphy, R. B., Repasky, M. P., Frye, L. L., Greenwood, J. R., Halgren, T. A., et al. (2006). Extra precision glide: docking and scoring incorporating a model of hydrophobic enclosure for protein–ligand complexes. *J. Med. Chem.* 49, 6177–6196. doi: 10.1021/jm051256o

Huang, L. J., Wang, Y. M., Gong, L. Q., Hu, C., Gui, Y., Zhang, C., et al. (2022). N-acetyldopamine dimer attenuates DSS-induced ulcerative colitis by suppressing NF-κB and MAPK pathways. *Front. Pharmacol.* 13:842730. doi: 10.3389/fphar.2022.842730

Jia, Z. L., Cen, J., Wang, J. B., Zhang, F., Xia, Q., Wang, X., et al. (2019). Mechanism of isoniazid-induced hepatotoxicity in zebrafish larvae: activation of ROS-mediated ERS, apoptosis and the Nrf2 pathway. *Chemosphere* 227, 541–550. doi: 10.1016/j.chemosphere.2019.04.026

Ju, F., Kuang, Q. X., Li, Q. Z., Huang, L. J., Guo, W. X., Gong, L. Q., et al. (2021). Aureonitol analogs and orsellinic acid esters isolated from *Chaetomium elatum* and their antineuroinflammatory activity. *J. Nat. Prod.* 84, 3044–3054. doi: 10.1021/acs.jnatprod.1c00783

Kawai, T., and Akira, S. (2007). Signaling to NF-kappaB by toll-like receptors. *Trends Mol. Med.* 13, 460–469. doi: 10.1016/j.molmed.2007.09.002

Kuang, Q. X., Lei, L. R., Li, Q. Z., Peng, W., Wang, Y. M., Dai, Y. F., et al. (2022a). Investigation of the anti-inflammatory activity of fusaproliferin analogs guided by transcriptome analysis. *Front. Pharmacol.* 13:881182. doi: 10.3389/fphar.2022.881182

Kuang, Q. X., Luo, Y., Lei, L. R., Guo, W. X., Li, X. A., Wang, Y. M., et al. (2022b). Hydroanthraquinones from nigrospora sphaerica and their anti-inflammatory activity uncovered by transcriptome analysis. *J. Nat. Prod.* 85, 1474–1485. doi: 10.1021/acs.jnatprod.1c01141

Lee, D., Lee, J. H., Cai, X. F., Shin, J. C., Lee, K., Hong, Y. S., et al. (2005). Fungal metabolites, sorbicillinoid polyketides and their effects on the activation of peroxisome proliferator-activated receptor gamma. *J. Antibiot.* 58, 615–620. doi: 10.1038/ja.2005.84

Mezzaroma, E., Abbate, A., and Toldo, S. (2021). NLRP3 inflammasome inhibitors in cardiovascular diseases. *Molecules* 26:976. doi: 10.3390/molecules26040976

Miletic, A. V., Graham, D. B., Montgrain, V., Fujikawa, K., Kloeppel, T., Brim, K., et al. (2006). Vav proteins control the MyD88-dependent oxidative burst. *Blood* 109, 3360–3368. doi: 10.1182/blood-2006-07-033662

Reuter, S., Gupta, S. C., Chaturvedi, M. M., and Aggarwal, B. B. (2010). Oxidative stress, inflammation, and cancer: how are they linked? *Free Radic. Biol. Med.* 49, 1603–1616. doi: 10.1016/j.freeradbiomed.2010.09.006

Rocha, D. M., Caldas, A. P., Oliveira, L. L., Bressan, J., and Hermsdorff, H. H. (2016). Saturated fatty acids trigger the TLR4-mediated inflammatory response. *Atherosclerosis* 244, 211–215. doi: 10.1016/j.atherosclerosis.2015.11.015

Seoane, P. I., Lee, B., Hoyle, C., Yu, S., Lopez-Castejon, G., Lowe, M., et al. (2020). The NLRP3 inflammasome is a sensor of organelle dysfunction. *J. Cell Biol.* 219:e202006194. doi: 10.1083/jcb.202006194

Viola, A., Munari, F., Sánchez-Rodríguez, R., Scolaro, T., and Castegna, A. (2019). The metabolic signature of macrophage responses. *Front. Immunol.* 10:1462. doi: 10.3389/fimmu.2019.01462

Wang, X., Feuerstein, G. Z., Gu, J. L., Lysko, P. G., and Yue, T. L. (1995). Interleukin-1 beta induces expression of adhesion molecules in human vascular smooth muscle cells and enhances adhesion of leukocytes to smooth muscle cells. *Atherosclerosis* 115, 89–98. doi: 10.1016/0021-9150(94)05503-b

White, C. S., Lawrence, C. B., Brough, D., and Rivers-Auty, J. (2017). Inflammasomes as therapeutic targets for Alzheimer's disease. *Brain Pathol.* 27, 223–234. doi: 10.1111/bpa.12478

Yang, S., and Lian, G. (2020). ROS and diseases: role in metabolism and energy supply. *Mol. Cell. Biochem.* 467, 1–12. doi: 10.1007/s11010-019-03667-9

Zanandrea, R., Bonan, C. D., and Campos, M. M. (2020). Zebrafish as a model for inflammation and drug discovery. *Drug Discov. Today* 25, 2201–2211. doi: 10.1016/j.drudis.2020.09.036

Zhong, J., and Shi, G. (2019). Editorial: regulation of inflammation in chronic disease. *Front. Immunol.* 10:737. doi: 10.3389/fimmu.2019.00737

frontiers | Frontiers in Microbiology

TYPE Original Research
PUBLISHED 26 September 2022
DOI 10.3389/fmicb.2022.1033823

OPEN ACCESS

EDITED BY
Peng Zhang,
Tobacco Research Institute (CAAS),
China

REVIEWED BY
Da-Le Guo,
Chengdu University of Traditional Chinese Medicine, China
Xin Li,
Institute of Oceanology (CAS),
China

*CORRESPONDENCE
Chi Zhang
zhangchi515@126.com
Xuemian Lu
luxuemian@wmu.edu.cn

†These authors have contributed equally to this work

SPECIALTY SECTION
This article was submitted to Antimicrobials, Resistance and Chemotherapy,
a section of the journal
Frontiers in Microbiology

RECEIVED 01 September 2022
ACCEPTED 12 September 2022
PUBLISHED 26 September 2022

CITATION
Weng W, Li R, Zhang Y, Pan X, Jiang S, Sun C, Zhang C and Lu X (2022) Polyketides isolated from an endophyte *Penicillium oxalicum* 2021CDF-3 inhibit pancreatic tumor growth.
Front. Microbiol. 13:1033823.
doi: 10.3389/fmicb.2022.1033823

Polyketides isolated from an endophyte *Penicillium oxalicum* 2021CDF-3 inhibit pancreatic tumor growth

Wenya Weng[1†], Ruidian Li[1,2†], Yanxia Zhang[3], Xiaofu Pan[1], Shicui Jiang[1], Chuchu Sun[1], Chi Zhang[1*] and Xuemian Lu[1,2*]

[1]The Third Affiliated Hospital of Wenzhou Medical University, Zhejiang, China, [2]Department of Endocrinology, Ruian People's Hospital, Zhejiang, China, [3]Shandong Research Center of Engineering and Technology for Safety Inspection of Food and Drug, Shandong Institute for Food and Drug Control, Jinan, China

Fungal secondary metabolites are inherently considered valuable resources for new drugs discovery. To search for novel fungal secondary metabolites with lead compounds potential, a fungal strain *Penicillium oxalicum* 2021CDF-3, an endophyte of the marine red algae *Rhodomela confervoides*, was chemically studied. Cultivation of this fungus on solid rice medium yielded 10 structurally diverse metabolites (**1**–**10**), including two new polyketides, namely oxalichroman A (**1**) and oxalihexane A (**2**). Their structures were determined by detailed analysis of NMR and HRESIMS spectroscopic data. Oxalihexane A (**2**) was elucidated as a novel polyketide formed by a cyclohexane and cyclohexanone moiety *via* an ether bond. The stereochemistry of **2** was successfully assigned by NMR and ECD calculations. In the cytotoxic assay, the new compound **2** showed remarkable inhibitory effect on the human pancreatic cancer PATU8988T cell line. Further pharmacological study demonstrated that the expression level of Cyclin D1 was down-regulated by the treatment with **2**, which suggested that cell cyclin abnormity was involved in pancreatic tumor cell apoptosis. Moreover, the activation of Wnt5a/Cyclin D1 signaling pathway might be involved in the mechanism of panreatic tumor cell apoptosis induced by **2**.

KEYWORDS

polyketides, secondary metabolites, algal-derived fungus, *Penicillium oxalicum*, cytotoxic activity

Introduction

Filamentous fungi are well known for their capability to afford tremendous bioactive molecules, termed secondary metabolites, which possess not only diverse structures but also remarkable functions (Li et al., 2021). Although some of secondary metabolites are mycotoxins and phytotoxins that tend to be problematic for humans, foods, and crops, fungal secondary metabolites have proven to be an important source of bioactive natural

products with potential pharmaceutical and/or agricultural applications (Bills and Gloer, 2016). The discovery of penicillin as the first broad-spectrum antibiotic agent by Alexander Fleming in 1928 considered the "wonder drug" of World War II and then started the "Golden Age of Antibiotics" in the last century (Keller, 2019; Zhang et al., 2020). Subsequently, fungal secondary metabolites have attracted more and more attention due to their rich biological functionality and drugability (Greco et al., 2019; Keller, 2019; Shankar and Sharma, 2022). The intrinsic properties of fungal secondary metabolites make the study of these natural compounds of great significance (Hautbergue et al., 2018). Newman and Cragg revealed that 40% of all approved therapeutic agents from 1981 to 2019 were of natural origin and a significant number of natural product-derived drugs/leads are actually of microbial origin (Newman and Cragg, 2020). It should be noted that fungal secondary metabolites have become the nonnegligible source of many important approved pharmaceuticals, such as cephalosporin, griseofulvin, compactin, ergotamine, and echinocandin, with a variety of mechanisms of action (González-Medina et al., 2017). Therefore, in-depth exploration of fungal secondary metabolites with remarkable biological activities is an important approach for new drug discovery.

The genus *Penicillium* has been well-studied due to their high biosynthetic potential for producing bioactive secondary metabolites (Koul and Singh, 2017; Zhang et al., 2020). Our preliminary screening on the in-house fungi library afforded a targeted fungal strain, *Penicillium oxalicum* 2021CDF-3, which was isolated as an endophyte of the marine red algae *Rhodomela confervoides*. Initial cytotoxic assay of the EtOAc crude extracts of this strain revealed a certain inhibitory effect on various human tumor cell lines (Supplementary Table S1 in Supplementary Material), especially for the human pancreatic cancer PATU8988T cell line, with the inhibition rate of 83% at the concentration of 40 μg/ml. The above screening results indicated that this fungal strain may possess high biosynthetic potential to produce cytotoxic secondary metabolites. In order to characterize these active ingredients, a large-scale fermentation was conducted. Cultivation of this fungus on solid rice medium and further chromatographic separation yielded 10 structurally diverse polyketides (**1**–**10**), including two new ones, namely, oxalichroman A (**1**) and oxalihexane A (**2**). Their chemical structures were determined by a detailed analysis of NMR and HRESIMS spectroscopic data. Structurally, the new polyketide, oxalihexane A (**2**), was characterized as a novel polyketide formed by a cyclohexane and cyclohexanone moiety *via* an ether bond. The species *P. oxalicum* is a well-known producer of structurally diverse secondary metabolites, including chromones (Sun et al., 2012), *N*-containing alkaloids (Zhang et al., 2015), butyrolactones (Yuan et al., 2015), monoterpenoids (Zhao et al., 2022), phenylhydrazones, and quinazolines (Liu et al., 2020). Although polyketides such as chromones (compounds **1** and **7**), and phthalides (compounds **3**–**5**) were commonly found in *P. oxalicum*, it is the first time to report the isolation of **2** as the unique polyketide, indicating it as the characteristic secondary metabolite of *P. oxalicum* with chemotaxonomic significance. Moreover, compound **2** was found to induce apoptosis mediated by the activation of Wnt5a/Cyclin D1 signaling pathway in human pancreatic tumor cells. In the present study, we report the isolation, structural determination, and cytotoxic evaluation of these fungal metabolites.

Materials and methods

General experimental procedures

A JASCO P-1020 digital polarimeter (Tokyo, Japan) was used to detect optical rotations of the isolated compounds in MeOH. A Lambda 35 UV/Vis spectrophotometer (Perkin Elmer, Waltham, United States) was used to collect UV data of the isolated compounds. A scientific LTQ Orbitrap XL spectrometer (Thermo Scientific, Waltham, United States) was used to acquire HRESIMS. An Agilent DD2 500 MHz spectrometer (Agilent Technologies, Santa Clara, United States; 500 and 125 MHz for ^{1}H and ^{13}C, respectively) with tetramethylsilane (TMS) as an internal standard was used to obtain NMR spectra. HPLC was conducted on an Agilent 1,260 system using an RP-C18 column (5 mm, 10 × 250 mm, flow rate 2 ml/min, YMC, Kyoto, Japan) with MeOH (HPLC grade) as mobile phase. Silica gel (100–200 mesh and 200–300 mesh, Qingdao Marine Chemical Factory, Qingdao, China), octadecylsilyl (ODS) reversed-phase gel (30–50 μm, YMC CO., LTD., Japan), and Sephadex LH-20 (GE Healthcare, United States) were used for chromatographic separation.

Fungal material

The fungal strain *P. oxalicum* 2021CDF-3 was isolated from the marine red algae *Rhodomela confervoides*, which was collected from Lianyungang, Jiangsu province, China. This fungus was obtained from the inner tissue of *R. confervoides* with strict surface sterilizing procedures (suffered from 75% ethyl alcohol and 2.5% sodium hypochlorite). Therefore, this obtained fungus was considered as endophyte. The fungal strain was successfully identified by morphological character and sequencing of the internal transcribed spacer (ITS) of the rRNA locus. The ITS region was amplified using the ITS1 primer (TCCGTAGGTGAACCTGCGG). Then, the ITS sequence, which showed 99% identical to that of *P. oxalicum* (GenBank accession, KY400080.1), has been submitted to GenBank with the accession number of OP349593. To clarify the evolutionary position of the producing strain 2021CDF-3, a phylogenetic analysis based on the ITS sequence, together with those from other *Penicillium* species, has been performed. Results indicated that the strain 2021CDF-3 was located at the basal position of the whole tree with high confidence (100%, Figure 1). A voucher specimen of this fungus was stored at −80°C at School of Food and Pharmacy, Zhejiang Ocean University.

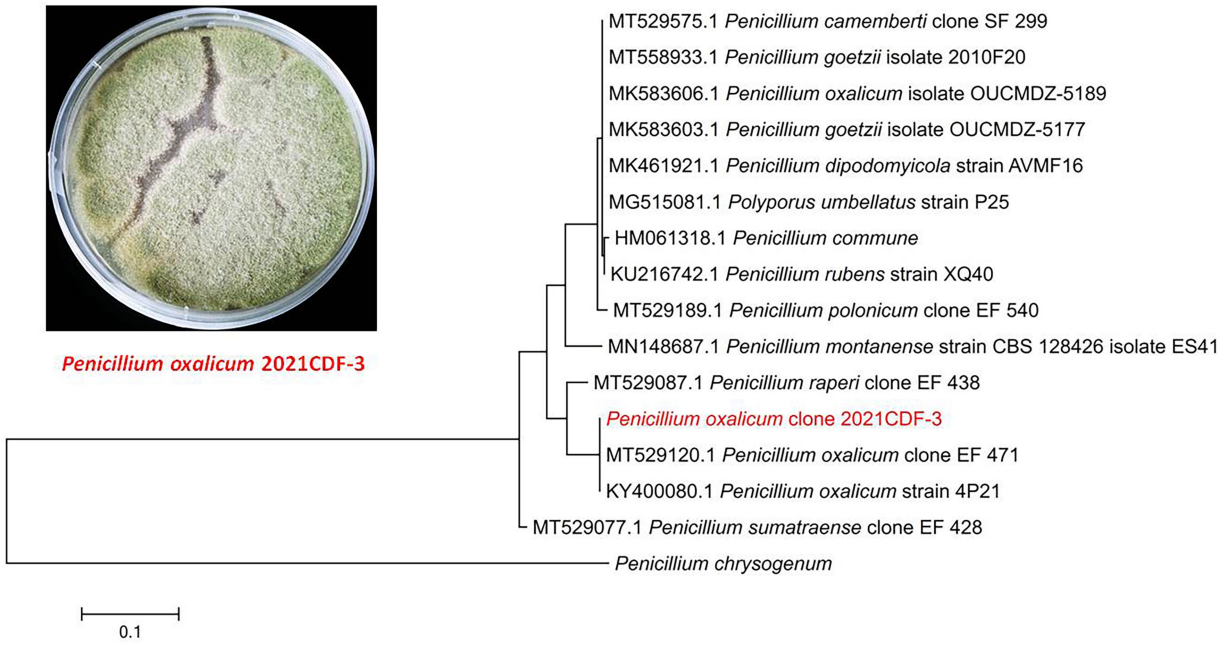

FIGURE 1
Morphology of *Penicillium oxalicum* 2021CDF-3 on PDA medium and neighbor-joining tree based on ITS nucleotide sequences.

Fermentation, extraction, and isolation

The producing strain was fermented in solid rice medium (*ca.* 100 g) that was previously sterilized by 100 ml of distilled seawater in a 500 ml Erlenmeyer flask. A total of 50 flasks were fermented statically with natural conditions (room temperature and sunlight) for 40 days. Afterwards, the wole cultures were extracted with EtOAc for three times. Then the EtOAc solution was collected and evaporated to dryness, which finally gave 22.6 g of brown extracts.

The extracts were subjected to open silica gel vacuum liquid chromatography column (CC, 15 × 6 cm i.d.), using mixed solvents in a gradient of increasing polarity (CH_2Cl_2-MeOH mixed system, from 100:1 to 10:1, v/v). Six fractions in total were obtained. Fraction 2, which was eluted with CH_2Cl_2-MeOH 80:1, was afforded to silica gel CC (CH_2Cl_2-MeOH, from 80:1 to 20:1) to yield three subfractions 2.1–2.3. Compounds **9** (2.5 mg, t_R 10.5 min) and **10** (7.8 mg, t_R 14.3 min) were isolated from subfractions 2.1 and 2.2, respectively, by semi-preparative HPLC (65% MeOH-H_2O). Compound **8** (12.0 mg) was isolated from subfraction 2.3 by Sephadex LH-20 CC (MeOH). Fraction 3, which was eluted with CH_2Cl_2-MeOH 60:1, was fractionated by ODS reversed-phase CC (MeOH-H_2O, from 10 to 100%) to give five subfractions 3.1–3.5. Compound **1** (7.0 mg) was isolated from subfraction 3.2 by preparative TLC (CH_2Cl_2-MeOH, 20:1), while compounds **4** (11.5 mg, t_R 9.0 min) and **7** (11.2 mg, t_R 12.3 min) were isolated from subfractions 3.3 and 3.5, respectively, by semi-preparative HPLC (55% MeOH-H_2O). Compound **2** (26.5 mg) was isolated from Fraction 4 (eluted with CH_2Cl_2-MeOH 40:1) by silica gel CC (CH_2Cl_2-MeOH, 20:1) and followed by Sephadex LH-20 CC (MeOH). Separation of Fraction 5, which was eluted with CH_2Cl_2-MeOH 20:1, was found to yield compounds **3** (5.8 mg) and **5** (16.2 mg) by silica gel CC (CH_2Cl_2-MeOH, from 30:1 to 10:1). Finally, compound **6** (7.4 mg) was obtained from Fraction 6 by preparative TLC (CH_2Cl_2-MeOH-acetic acid, 10:1:0.4).

Oxalichroman A (**1**): amorphous power; $[\alpha]^{25}_D$ −19.1 (*c* 0.10, MeOH); UV (MeOH) λ_{max} (log ε) 215 (4.05), 253 (3.62), 326 (3.20) nm; ECD (1 mg/ml, MeOH) λ_{max} ($\Delta\varepsilon$) 212 (+7.40), 252 (−0.32), 274 (+0.17), 317 (−1.54), 354 (+0.44) nm; ^{1}H and ^{13}C NMR data, see Table 1; HRESIMS *m/z* 245.0790 $[M+Na]^+$ (calcd for $C_{12}H_{14}O_4Na$, 245.0788).

Oxalihexane A (**2**): colorless gum; $[\alpha]^{25}_D$ −42.6 (*c* 0.12, MeOH); UV (MeOH) λ_{max} (log ε) 220 (3.89), 280 (3.96), 320 (4.08) nm; ECD (0.5 mg/ml, MeOH) λ_{max} ($\Delta\varepsilon$) 214 (−7.26), 241 (−2.37), 265 (−1.11), 289 (−2.28), 326 (−0.33) nm ^{1}H and ^{13}C NMR data, see Table 1; HRESIMS *m/z* 309.1697 $[M+H]^+$ (calcd for $C_{17}H_{25}O_5$, 309.1702).

Computational section

Computational details were shown in Supplementary Material.

Cytotoxic assay

Cell culture

The human pancreatic cancer PATU8988T cell line was purchased from Shanghai Fuheng Biotechnology Co., LTd. The cells were cultured in RPMI 1640 medium containing 10% fetal

TABLE 1 ^{1}H NMR (500MHz, δ in ppm) and ^{13}C NMR Data (125MHz, δ in ppm) of 1 and 2.

Postion	Compound1[a]		Postion	Compound2[b]	
	δ_H (J in Hz)	δ_C, type		δ_H (J in Hz)	δ_C, type
1		192.5, C	1		205.2, C
2	2.95, d (16.6) 2.61, d (16.6)	44.0, CH_2	2	2.89, dd (13.9, 3.8) 2.41, m	46.6, CH_2
3		82.2, C	3	4.44, m	69.9, CH
4		159.0, C	4	2.14, m 1.71, m	28.7, CH_2
5	6.94, d (8.4)	118.3, CH	5	2.24, m 2.03, m	34.1, CH_2
6	7.47, dd (8.4, 2.2)	135.2, CH	6		83.3, C
7		135.2, C	7	1.48, s	20.8, CH_3
8	7.66, d (2.2)	123.9, CH	8		130.7, C
9		119.9, C	9	2.61, m 2.15, m	31.2, CH_2
10	4.44, d (5.2)	62.6, CH_2	10	4.06, m	65.8, CH
11	3.55, dd (11.6, 5.4) 3.47, dd (11.6, 5.4)	66.9, CH_2	11	1.88, m 1.76, m	29.6, CH_2
12	1.27, s	21.4, CH_3	12	2.50, m 2.32, m	31.8, CH_2
10-OH	5.19, overlap		13		155.4, C
11-OH	5.19, overlap		14	2.19, s	18.0, CH_3
			15	10.16, s	190.8, CH
			16		170.3, C
			17	2.11, s	21.2, CH_3

[a]measured in DMSO-d_6.
[b]measured in $CDCl_3$.

bovine serum (Gibco, Gaithersburg, MD, United States). All cells were cultured in a humidified atmosphere of 5% CO_2 incubator at 37°C. The medium was changed every 2 days and subcultured once they reached ~80% confluence. Cells were treated with the tested compounds in the dose of 40 μM for 24 h.

Western blot analysis

Protein lysates of the cells were prepared in RIPA buffer (Beyotime Biotechnology, China) containing protease inhibitors (Beyotime Biotechnology). Protein concentration was measured by the Bradford assay. After being diluted in loading buffer and denatured at 95°C for 5 min, the samples were separated in 10% SDS-PAGE gel followed by being transferred into nitrocellulose membranes for separation. After blocking with 5% dried non-fat milk solution for 1 h at room temperature, the membrane was incubated with these primary antibodies, including Bax, Bcl-2, MMP-3, p53, β-Catenin, Wnt5a, and Cyclin D1 (purchased from ABclone), cleaved-Caspase3 and β-Actin (purchased from Abcam). Membranes were incubated with appropriate secondary antibodies for 1 h at room temperature following three washes with Tris-buffered saline (pH7.2) containing 0.05% Tween 20. Antigen–antibody complexes were visualized with ECL substrate (Bio-Rad Laboratories).

Flow cytometry

Cell appoptosis was evaluated by flow cytometry using Annexin V-FITC Apoptosis Detection Kit (Beyotime Biotechnology) according to the manufacturer's allowed to attach over night. Then the cells were treated with or without compounds at the indicated concentration for 24 h. After that, the cells were incubated with 200 ml binding buffffer and stained with Annexin V-FITC and PI in the dark for 40 min. Then, the cells were assessed by flow cytometry (Agilent, United States).

Results and discussion

Structural elucidation

Oxalichroman A (**1**; Figure 2) was isolated as amorphous power. Its molecular formula $C_{12}H_{14}O_4$ was established by HRESIMS (Supplementary Figure S1 in Supplementary Material). The NMR spectra of **1** (Table 1) showed one ketone carbonyl carbon at δ_C 192.5 (C-1), signals of a 1,3,4-trisubstituted benzene ring at δ_C 118.3–159.0 (C-4 – C-9) and at δ_H 6.94 (1H, d, J = 8.4 Hz, H-5), 7.47 (1H, dd, J = 8.4, 2.2 Hz, H-6), and 7.66 (1H, d, J = 2.2 Hz, H-7), one oxygenated quaternary carbon at δ_C 82.2 (C-3), three methylene groups including two oxygenated at δ_C 62.6 (C-10) and at δ_H 4.44 (2H, d, J = 5.2 Hz, H-10), at δ_C 66.9 (C-11) and at δ_H 3.55 (1H, dd, J = 11.6, 5.4 Hz, H-11) and δ_H 3.47 (1H, dd, J = 11.6, 5.4 Hz, H-11), and one methyl group at δ_C 21.4 (C-12) and at δ_H 1.27 (3H, s, H-12). Moreover, two exchangeable OH groups were observed at δ_H 5.19 (2H, overlapped, 10-OH and 11-OH). Compound **1** possessed a benzopyrone skeleton (Kashiwada et al., 1984), which can be deduced by the key HMBC correlations from H-8 to C-1 and C-4, from H-5 to C-4 and C-9, and from H_2-2 to C-1 (Figure 3). The location of the oxymethylene group C-10 was confirmed by the HMBC correlations from these protons to C-6, C-7, and C-8. In addition, the other oxymethylene group C-11 and the methyl group C-12 were located at C-3 due to the presence of clear HMBC correlations from H_2-2 to C-11 and C-12, and from

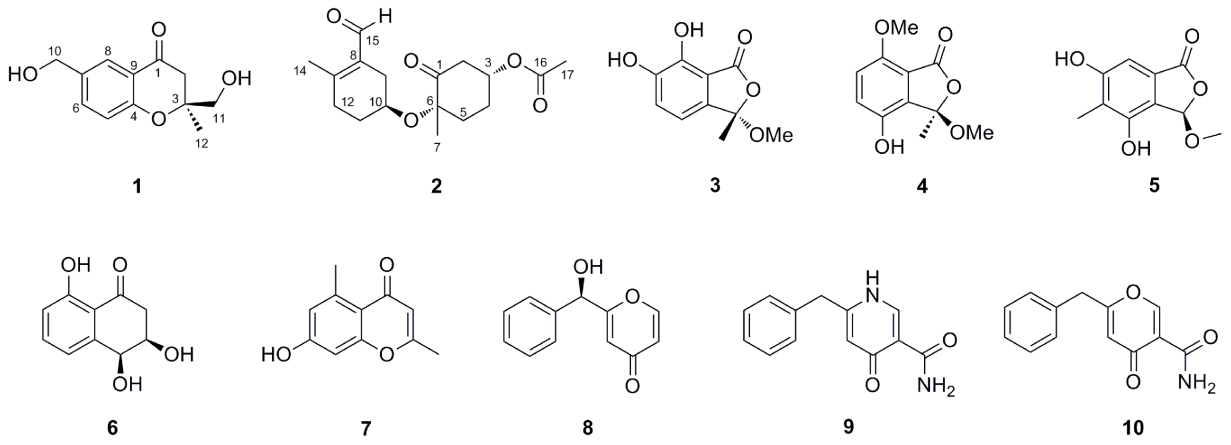

FIGURE 2
Structures of compounds 1–10.

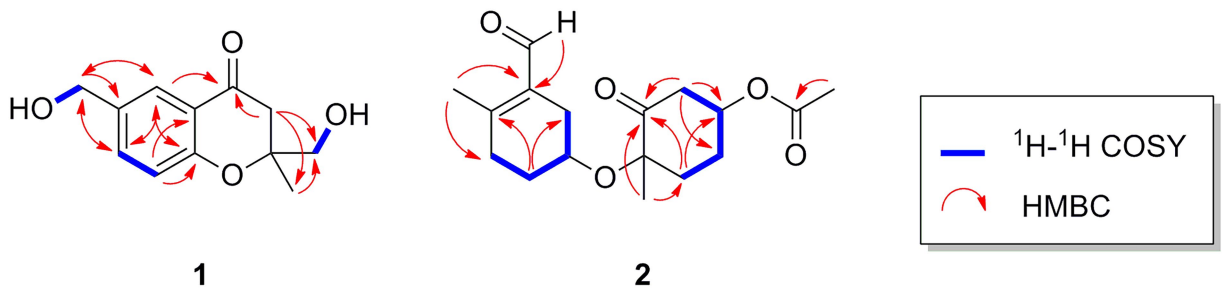

FIGURE 3
Important 1H-1H COSY and HMBC correlations of compounds 1 and 2.

H_3-12 to C-11. Thus, compound **1** was elucidated as shown in Figure 2 and was named as oxalichroman A. TDDFT calculation of the ECD spectrum of **1** at Cam-B3LYP/Def2SVP level suggested the stereochemistry of C-3 as *S*, as evidenced by the theoretical ECD curve that matched with the experimental one (Figure 4).

Oxalihexane A (**2**) was isolated as colorless gum. On the basis of the HRESIMS data, the molecular formula of **2** was determined as $C_{17}H_{24}O_5$. Inspection of ^{1}H NMR spectrum of **2** (Table 1) revealed the presence of one aldehyde group at δ_H 10.16 (1H, s, H-15), two oxygenated methine groups at δ_H 4.44 (1H, m, H-3) and δ_H 4.06 (1H, s, H-10), a set of methylene groups ranging from δ_H 1.71 to δ_H 2.89, and three methyl groups at δ_H 1.48 (3H, s, H_3-7), 2.19 (3H, s, H_3-14), and 2.11 (3H, s, H_3-17). The ^{13}C NMR and DEPT spectra evidenced one ketone carbonyl at δ_C 205.2 (C-1), one aldehyde group at δ_C 190.8 (C-15), one ester carbonyl at δ_C 170.3 (C-16), three methyls at δ_C 20.8 (C-7), 18.0 (C-14), and 21.2 (C-17), six methylenes (δ_C 28.7, 29.6, 31.2, 31.8, 34.1, and 46.6), two oxygenated methines at δ_C 69.9 (C-3) and 65.8 (C-10), and three quaternary carbons including two sp^2 at δ_C 130.7 (C-8) and 155.4 (C-13) and one oxygenated sp^3 at δ_C 83.3 (C-6). The ^{1}H-^{1}H COSY cross peaks of H_2-9/H-10/H_2-11/H_2-12 constructed a $-CH_2CHCH_2CH_2-$ spin system (Figure 3). Further important

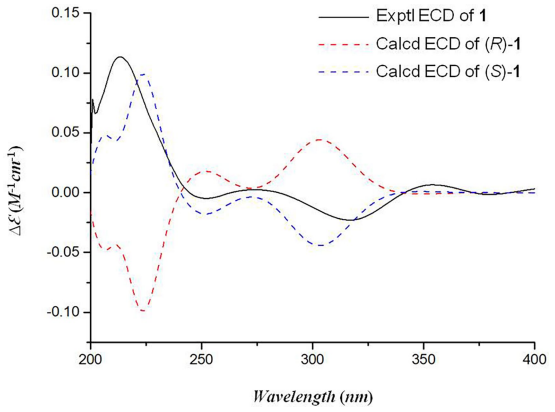

FIGURE 4
The experimental and calculated ECD spectra of compound 1.

HMBC correlations, including HMBCs from H_3-14 to C-8 and C-12, from H_2-11 to C-9 and C-13, and from H-15 to C-8 (Figure 3) indicated the presence of a cyclohexane moiety. Moreover, COSY correlations between H_2-2/H-3, H-3/H_2-4, and

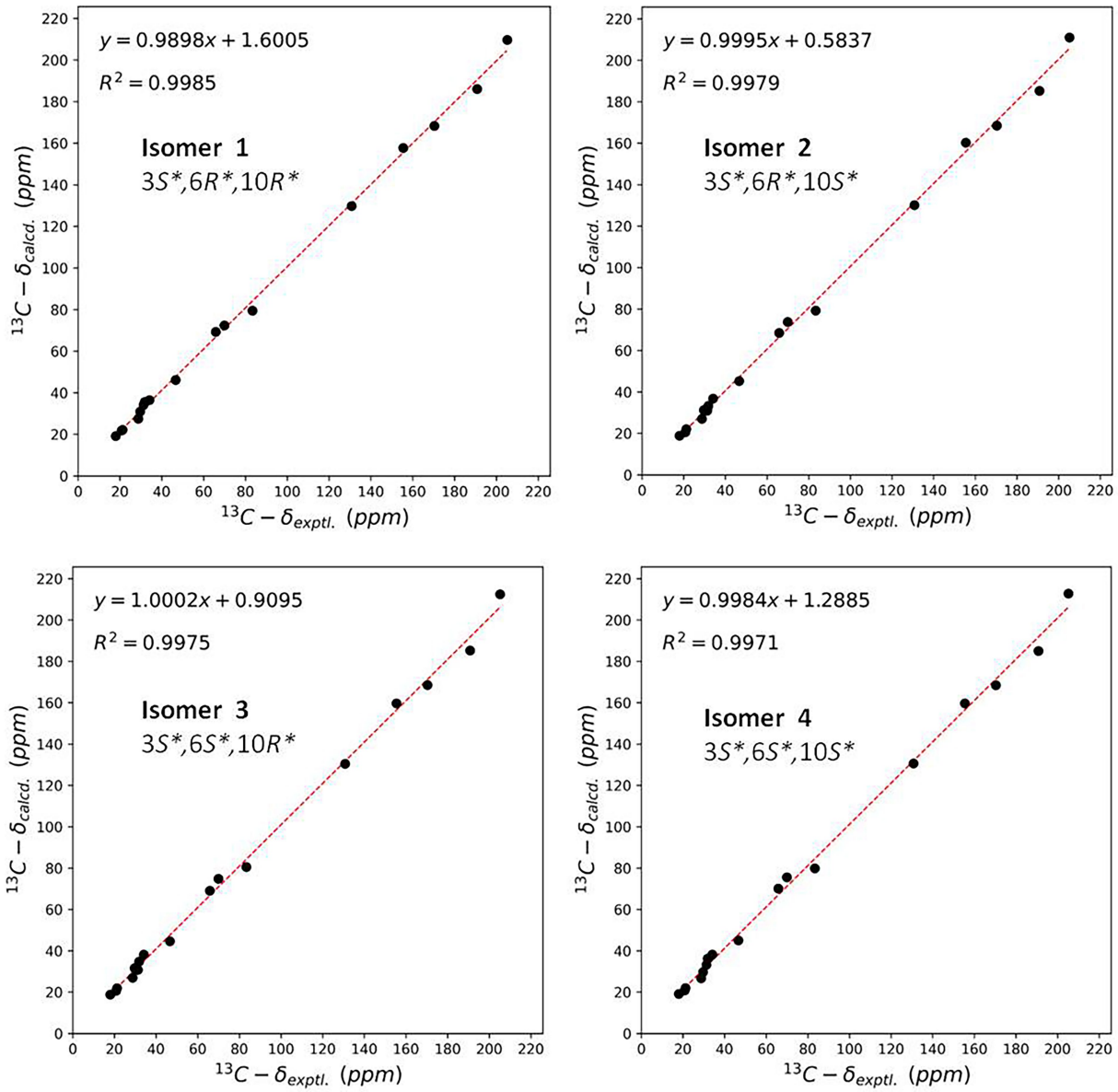

FIGURE 5
Linear regression analysis between the experimental and calculated NMR data of conformers of isomer 1–isomer 4.

H_2-4/H_2-5 and key HMBCs from H_2-2 to C-1, from H_2-5 to C-1 and C-3, and from H_3-7 to C-1 and C-5 revealed a cyclohexanone moiety (Figure 3). The above cyclohexane and cyclohexanone moieties were connected *via* an ether bond based on detailed analysis of HRESIMS and chemical shifts of C-6 and C-10. In addition, the acetyl group was attached to C-3 based on the HMBC correlation from H-3 to C-16. The structure of **2** was thus determined accordingly.

The NOE correlations gave useless information to determine the relative configuration of **2** (Supplementary Figure S13 in Supplementary Material). To establish the relative stereochemistry of **2**, (3*S**,6*R**,10*R**)-**2**, (3*S**,6*R**,10*S**)-**2**, (3*S**,6*S**,10*R**)-**2**, and (3*S**,6*S**,10*S**)-**2** were subjected to quantum chemical calculation of chemical shifts under the theory level of MPW1PW91-SCRF/6–31 + G(d,p)//B3LYP/6-31G(d) with the IEFPCM solvent model. As a result, the calculated ^{13}C NMR data of (3*S**,6*R**,10*R**)-**2** were found to be in better agreement with their experimental counterparts, as indicated by R^2 and supported by DP4+ probability analysis (Figure 5). Thus, the relative configuration of **2** was assigned as 3*S**,6*R**,10*R**, and subsequent TDDFT ECD calculation at the Cam-B3LYP/Def2SVP, which was run on one of the two possible enantiomers, (3*S*,6*R*,10*R*)-**2** and (3*R*,6*S*,10*S*)-**2**, succeeded in the establishment of the absolute configuration of **2** as 3*R*,6*S*,10*S* (Figure 6).

In addition, eight previously reported compounds (**3**–**10**) were also isolated from this fungus. They were finally

characterized as 6,7-dihydroxy-3-methoxy-3-methylphthalide (**3**) (Wang et al., 2013), chrysoalide B (**4**) (Ge et al., 2021), rubralide C (**5**) (Kimura et al., 2007), *cis*-(3*RS*,4*SR*)-3,4-dihydro-3,4,8-trihydroxynaphthalen-1(2*H*)-one (**6**) (Couché et al., 2009), 2,5-dimethyl-7-hydroxychromone (**7**) (Kashiwada et al., 1984), (7*R*)-(hydroxy(phenyl)methyl)-4*H*-pyran-4-one (**8**) (Xu et al., 2019), 6-benzyl-4-oxo-1,4-dihydropyridine-3-carboxamide (**9**) (Ye et al., 2005), and carbonarone A (**10**) (Zhang et al., 2007), respectively, by comparison of their spectroscopic data with literatures.

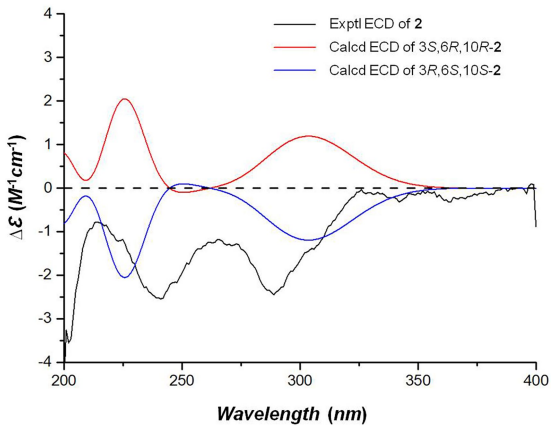

FIGURE 6
The experimental and calculated ECD spectra of compound 2.

Cytotoxic activity

The new compounds **1** and **2** were evaluated for their cytotoxicity against the human pancreatic cancer PATU8988T cell line. Compound **2** was found to possess promising activity with the inhibition rate of 93% at the concentration of 20 μM. In order to explore whether the proliferation inhibition of PATU8988T cells was related to the cell apoptosis, we detected apoptosis indicators. After the cells were treated with **2** at the concentration of 40 μM for 24 h, cell number reduction and cell morphology abnormity including pyknosis, shrinkage and dissociated from the plate were observed in both doxorubicin and **2** treated groups under a light microscope. While in contrast, the cells in the control group grew well (Figure 7A), suggesting compound **2** as well as doxorubicin might induce tumor cell death. In addition, Annexin V-FITC/PI assay was performed to detect apoptosis percentatge by flow cytometry. As shown in Figure 7B, both doxorubicin and **2** remarkbly increased the proportion of apoptotic cells. Additionally, western blotting was applied to further detect whether apoptosis related indicators were altered in the cells treated with **2**. As shown in Figures 7C,D **2**

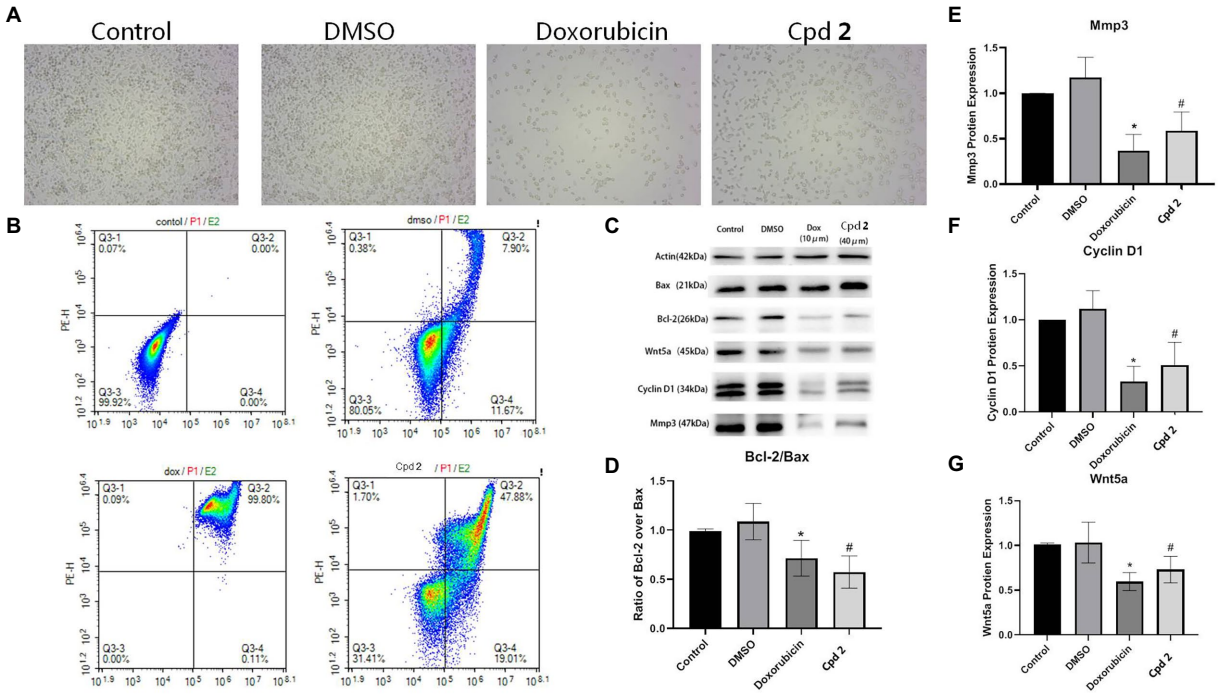

FIGURE 7
Compound **2** (Cpd **2**) alleviated the apoptosis induced in human pancreatic cancer cells. **(A)** Morphological changes of human pancreatic cancer cell (PATU8988T). **(B)** Functions of **2** in cell apoptosis in human pancreatic cancer cell (PATU8988T). Annexin V/PI double staining with flow cytometry analysis was applied for cell apoptosis. **(C)–(G)** Western blotting of Bcl-2/Bax, Mmp3, Cyclin D1 and Wnt5a. **p*<0.05, doxorubicin group vs. DMSO group; #*p*<0.05, test group vs. DMSO group.

significantly down-regulated the ratio of Bcl-2/Bax, indicating that cell apoptosis occurred after treated with **2**. In addition, we also detected the expression level of MMP-3. Figures 7C,E showed that **2** decreased the expression level of MMP-3, a tumor indicator. To investigate whether Wnt5a/Cyclin D1 pathway was involved in the **2**-induced apoptosis, the expression levels of Wnt5a and Cyclin D1 in cells treated with the doxorubicin and **2** were both evaluated. The results demonstrated that the expression levels of Cyclin D1 and Wnt5a were both dramatically down-regulated by doxorubicin as well as **2** (Figures 7C,F,G). The above results suggested that compound **2** might induce the apoptosis of pancreas cancer cells through Wnt5a/Cyclin D1 signaling pathway.

Conclusion

In summary, chemical examination of the endophytic fungus *P. oxalicum* 2021CDF-3 resulted in the isolation of 10 diverse polyketides. Among them, compounds **1** and **2** were characterized as new compounds. Oxalihexane A (**2**), elucidated as a novel polyketide formed by a cyclohexane and cyclohexanone moiety, showed remarkable inhibitory effect on the human pancreatic cancer PATU8988T cell line. Apoptosis is involved in the regulation of tumor cell proliferation. Compound **2** induced remarkable apoptosis in human pancreatic tumor cells, characterized by the morphologies abnormity, the decrease in cell number and the ratio of Bcl-2 to Bax, in the **2**-treated group compared with the control group. Understanding of underlying mechanism is of significance to explore more effective therapeutic strategy for pancreatic tumor treatment. In this work, the result demonstrated that the expression level of Cyclin D1 was down-regulated by **2**, suggesting that cell cyclin abnormity was involved in pancreatic tumor cell apoptosis. Furthermore, we found that the activation of Wnt5a/Cyclin D1 signaling pathway might be involved in the mechanism of pancreatic tumor cell apoptosis induced by **2**.

Data availability statement

The datasets presented in this study can be found in online repositories. The names of the repository/repositories and accession number(s) can be found in the article/Supplementary material.

Author contributions

WW and XL: conception or design. RL, WW, YZ, XP, SJ, and CS: acquisition, analysis, or interpretation of data. WW, XL, and CZ: drafting the work or revising. WW, CZ, and XL: final approval of the manuscript. All authors reviewed the manuscript. All authors contributed to the article and approved the submitted version.

Funding

This study was supported by grant from the Ruian Bureau of Science and Technology (MS2022004, to WW).

Conflict of interest

All authors declare that the research was conducted in the absence of any commercial or financial relationships that could be construed as a potential conflict of interest.

Publisher's note

All claims expressed in this article are solely those of the authors and do not necessarily represent those of their affiliated organizations, or those of the publisher, the editors and the reviewers. Any product that may be evaluated in this article, or claim that may be made by its manufacturer, is not guaranteed or endorsed by the publisher.

Supplementary material

The Supplementary material for this article can be found online at: https://www.frontiersin.org/articles/10.3389/fmicb.2022.1033823/full#supplementary-material

References

Bills, G. F., and Gloer, J. B. (2016). Biologically active secondary metabolites from the fungi. *Microbiol. Spectr.* 4, 1–32. doi: 10.1128/microbiolspec.FUNK-0009-2016

Couché, E., Fkyerat, A., and Tabacchi, R. (2009). Stereoselective synthesis of *cis*- and *trans*-3,4-dihydro-3,4,8-trihydroxynaphthalen-1(2*H*)-one. *Helv. Chim. Acta* 92, 903–917. doi: 10.1002/hlca.200800380

Ge, Y., Tang, W. L., Huang, Q. R., Wei, M. L., Li, Y. Z., Jiang, L. L., et al. (2021). New enantiomers of a nor-Bisabolane derivative and two new Phthalides produced by the marine-derived fungus *Penicillium chrysogenum* LD-201810. *Front. Microbiol.* 12:727670. doi: 10.3389/fmicb.2021.727670

González-Medina, M., Owen, J. R., El-Elimat, T., Pearce, C. J., Oberlies, N. H., Figueroa, M., et al. (2017). Scaffold diversity of fungal metabolites. *Front. Pharmacol.* 8:180. doi: 10.3389/fphar.2017.00180

Greco, C., Keller, N. P., and Rokas, A. (2019). Unearthing fungal chemodiversity and prospects for drug discovery. *Curr. Opin. Microbiol.* 51, 22–29. doi: 10.1016/j.mib.2019.03.002

Hautbergue, T., Jamin, E. L., Debrauwer, L., Puel, O., and Oswald, I. P. (2018). From genomics to metabolomics, moving toward an integrated strategy for the discovery of fungal secondary metabolites. *Nat. Prod. Rep.* 35, 147–173. doi: 10.1039/C7NP00032D

Kashiwada, Y., Nonaka, G. I., and Nishioka, I. (1984). Studies on rhubarb (Rhei Rhizoma). V. Isolation and characterization of Chromone and Chromanone derivatives. *Chem. Pharm. Bull.* 32, 3493–3500. doi: 10.1248/cpb.32.3493

Keller, N. P. (2019). Fungal secondary metabolism: regulation, function and drug discovery. *Nat. Rev. Microbiol.* 17, 167–180. doi: 10.1038/s41579-018-0121-1

Kimura, Y., Yoshinari, T., Koshino, H., Fujioka, S., Okada, K., and Shimada, A. (2007). Rubralactone, rubralides a, B and C, and rubramin produced by *Penicillium rubrum*. *Biosci. Biotechnol. Biochem.* 71, 1896–1901. doi: 10.1271/bbb.70112

Koul, M., and Singh, S. (2017). *Penicillium* spp.: prolific producer for harnessing cytotoxic secondary metabolites. *Anti-Cancer Drugs* 28, 11–30. doi: 10.1097/CAD.0000000000000423

Li, X. D., Su, J. C., Jiang, B. Z., Li, Y. L., Guo, Y. Q., and Zhang, P. (2021). Janthinoid a, an unprecedented tri-normeroterpenoid with highly modified bridged 4a,1-(epoxymethano)phenanthrene scaffold, produced by the endophyte of *Penicillium janthinellum* TE-43. *Org. Chem. Front.* 8, 6196–6202. doi: 10.1039/D1QO01066B

Liu, Y. P., Fang, S. T., Shi, Z. Z., Wang, B. G., Li, X. N., and Ji, N. Y. (2020). Phenylhydrazone and Quinazoline derivatives from the cold-seep-derived fungus *Penicillium oxalicum*. *Mar. Drugs* 19:9. doi: 10.3390/md19010009

Newman, D. J., and Cragg, G. M. (2020). Natural products as sources of new drugs over the nearly four decades from 01/1981 to 09/2019. *J. Nat. Prod.* 83, 770–803. doi: 10.1021/acs.jnatprod.9b01285

Shankar, A., and Sharma, K. K. (2022). Fungal secondary metabolites in food and pharmaceuticals in the era of multi-omics. *Appl. Microbiol. Biotechnol.* 106, 3465–3488. doi: 10.1007/s00253-022-11945-8

Sun, Y. L., He, F., Liu, K. S., Zhang, X. Y., Bao, J., Wang, Y. F., et al. (2012). Cytotoxic dihydrothiophene-condensed chromones from marine-derived fungus *Penicillium oxalicum*. *Planta Med.* 78, 1957–1961. doi: 10.1055/s-0032-1327874

Wang, M. H., Li, X. M., Li, C. S., Ji, N. Y., and Wang, B. G. (2013). Secondary metabolites from Penicillium pinophilum SD-272, a marine sediment-derived fungus. *Mar. Drugs* 11, 2230–2238. doi: 10.3390/md11062230

Xu, K., Guo, C., Shi, D., Meng, J., Tian, H., and Guo, S. (2019). Discovery of natural Dimeric Naphthopyrones as potential cytotoxic agents through ROS-mediated apoptotic pathway. *Mar. Drugs* 17:207. doi: 10.3390/md17040207

Ye, Y. H., Zhu, H. L., Song, Y. C., Liu, J. Y., and Tan, R. X. (2005). Structural revision of aspernigrin a, reisolated from *Cladosporium herbarum* IFB-E002. *J. Nat. Prod.* 68, 1106–1108. doi: 10.1021/np050059p

Yuan, L., Huang, W., Zhou, K., Wang, Y., Dong, W., Du, G., et al. (2015). Butyrolactones derivatives from the fermentation products of a plant entophytic fungus *Penicillium oxalicum*. *Nat. Prod. Res.* 29, 1914–1919. doi: 10.1080/14786419.2015.1013473

Zhang, P., Li, X. M., Liu, H., Li, X., and Wang, B. G. (2015). Two new alkaloids from *Penicillium oxalicum* EN-201, an endophytic fungus derived from the marine mangrove plant *Rhizophora stylosa*. *Phytochem. Lett.* 13, 160–164. doi: 10.1016/j.phytol.2015.06.009

Zhang, P., Wei, Q., Yuan, X., and Xu, K. (2020). Newly reported alkaloids produced by marine-derived *Penicillium* species (covering 2014-2018). *Bioorg. Chem.* 99:103840. doi: 10.1016/j.bioorg.2020.103840

Zhang, Y., Zhu, T., Fang, Y., Liu, H., Gu, Q., and Zhu, W. (2007). Carbonarones a and B, new bioactive γ-pyrone and α-pyridone derivatives from the marine-derived fungus *Aspergillus carbonarius*. *J. Antibiot.* 60, 153–157. doi: 10.1038/ja.2007.15

Zhao, W. Y., Luan, Z. L., Sun, C. P., Zhang, B. J., Jin, L. L., Deng, S., et al. (2022). Metabolites isolated from the human intestinal fungus *Penicillium oxalicum* SL2 and their agonistic effects on PXR and FXR. *Phytochemistry* 193:112974. doi: 10.1016/j.phytochem.2021.112974

frontiers | Frontiers in Microbiology

TYPE Original Research
PUBLISHED 04 October 2022
DOI 10.3389/fmicb.2022.1038487

OPEN ACCESS

EDITED BY
Peng Zhang,
Tobacco Research Institute (CAAS), China

REVIEWED BY
Jianlong Zhang,
Ludong University,
China
Xiao-Long Yuan,
Chinese Academy of Agricultural Sciences (CAAS), China

*CORRESPONDENCE
Guan-Yi Cao
cheerychy@163.com
Zi-Xiang Zhang
zhangzxz66@163.com

SPECIALTY SECTION
This article was submitted to Antimicrobials, Resistance and Chemotherapy, a section of the journal Frontiers in Microbiology

RECEIVED 07 September 2022
ACCEPTED 20 September 2022
PUBLISHED 04 October 2022

CITATION
Chen Y, Xu L-C, Liu S, Zhang Z-X and Cao G-Y (2022) Halometabolites isolated from the marine-derived fungi with potent pharmacological activities. *Front. Microbiol.* 13:1038487. doi: 10.3389/fmicb.2022.1038487

Halometabolites isolated from the marine-derived fungi with potent pharmacological activities

Yu Chen[1], Lian-Cheng Xu[1], Shan Liu[1], Zi-Xiang Zhang[2]* and Guan-Yi Cao[1]*

[1]Department of General Surgery, Suqian First Hospital, Suqian, China, [2]Department of General Surgery, The First Affiliated Hospital of Soochow University, Suzhou, China

Halometabolites, usually produced in marine environment, are an important group of natural halogenated compounds with rich biological functionality and drugability and thus play a crucial role in pharmaceutical and/or agricultural applications. In the exploration of novel halometabolites from marine microorganisms, the growing number of halogenated compounds makes it necessary to fully present these metabolites with diverse structures and considerable bioactivities. This review particularly focuses on the chemodiversity and bioactivities of halometabolites from marine-derived fungi. As a result, a total of 145 naturally halogenated compounds, including 118 chlorinated, 23 brominated, and four iodinated compounds, were isolated from 17 genera of marine-derived fungi. Interestingly, many of halometabolites, especially for the brominated and iodinated compounds, are generated by the substitution of bromide and iodide ions for the chloride ion in cultivation process. In addition, these compounds possess diverse structural types, which are classified into polyketides (62.7%), phenols (16.6%), alkaloids (14.5%), and terpenoids (6.2%). Their cytotoxic, antibacterial, and anti-inflammatory activities indicate the high potential of these halogenated compounds as lead compounds for drug discovery.

KEYWORDS

halometabolites, natural products, marine fungi, chemical diversity, biological activities

Introduction

Halometabolites are a group of natural halogen-containing (Cl, Br, I, F) compounds which possess rich biological functionality and drugability. It is estimated that more than 5,000 halogenated compounds have been reported (Liao et al., 2016). Among them, chlorination is the predominant occurance, and then followed by bromination, while iodination and fluorination are extremely rare (Neumann et al., 2008). Halometabolites are generally produced from abiogenic and biogenic pathways. Biogenic halometabolites are formed by microorganisms (fungi and bacteria), plants, algae, and marine invertebrates

(sponges and corals) (Kasanah and Triyanto, 2019). Biosynthetically, enzymatic halogenation through halogenases such as flavin adenine dinucleotide-dependent halogenases (FDHs) and non-heme Fe^{II}/α-ketoglutarate halogenases is the most common way to these compounds (Neumann et al., 2008; Liao et al., 2016). Halometabolites possess high diversity in structure, ranging in complexity from simple halogenated indoles, terpenes, and phenols to miscellaneous polypeptides and polyketides.

Apart from their novel structures, the presence of halogens in natural products significantly enhances their biological activities. The halogen substituents are responsible for the bioactivity, bioavailability, and stability of the compounds (Kasanah and Triyanto, 2019). Halometabolites also play an important role in pharmaceutical and agricultural applications. Many of them have been used for decades as pharmaceuticals and agrochemicals. It is worth mentioning that natural products have benefited significantly from the growth of the pharmaceutical industry, especially of pharmacologically attractive lead drugs and potential clinical therapeutic drugs. Among them, approximately 25% of clinically therapeutic drugs are halogenated, indicating halogen substituents as remarkable contributors to pharmacological applications. A large number of halogenated natural products-inspired pharmaceuticals are either FDA or EMEA approved. Representative examples of them include the antibiotics chloramphenicol and vancomycin, the anticancer drugs salinosporamide A, spongistatin, rebeccamycin, and calicheamicin (Supplementary Figure S1; Niu et al., 2021). Therefore, in this sense, halometabolites bioprospecting is a considerable approach to discover new innovative drugs.

Compared to those from terrestrial plants, halometabolites derived from marine environment are relatively unexplored. The marine environment is a crucial source of halotolerant microorganisms (Wang et al., 2011). Microorganisms living in marine extreme environment are suffered from low temperature, high pressure, high salinity, and low oxygen concentration, and have evolved extraordinary metabolic pathways to produce novel secondary metabolites (Xu et al., 2020). Marine-derived fungi have been largely explored due to their ability to generate structurally novel secondary metabolites with remarkable biological activities. Given the crucial role that halogen substituents can play in the bioactivity of these metabolites, high metabolic potential of halometabolites production can be expected from the marine-derived fungi. This present review illustrates the chemistry and biological activities of halometabolites produced by marine-derived fungi. A total of 145 naturally halogenated compounds, including 118 chlorinated, 23 brominated, and four iodinated compounds, were isolated in the past decades. Crucial insights into their chemical diversity and biological activities are provided herein. This review will reveal these halogenated compounds as lead compounds for the development of innovative drugs.

Chemical diversity and biological activity

Halogenated polyketides from marine-derived fungi

Azaphilones

Thirty-nine halogenated azaphilones featured an oxabicyclic core were isolated from marine-derived fungi (Figures 1, 2; Table 1). Ten chlorinated azaphilones (**1**–**10**) including eight new nitrogenated azaphilones (**1**–**8**) were isolated from the deep-sea-derived fungus *Chaetomium globosum* MP4-S01-7 (Wang et al., 2020). Compounds **1**–**4** belong to *N*-(3,7-dimethyl-2,6-octadienyl) azaphilone polyketides, while compounds **5**–**8** are *N*-(3-methyl-2-butenyl) azaphilones. Most of them showed strong cytotoxic activity against the human gastric cancer MGC803 and AGS cell lines with IC_{50} values ranging from 0.12 to 10 μM. Importantly, compounds **1**, **2**, and **5**, in particularly, demonstrated the strongest activity at a nanomole level. In-depth mechanism study revealed that **2** arrested gastric cancer MGC803 and AGS cells in the G1 phase, while **1** and **2** induced apoptosis of both cells in a concentration-dependent manner. Eight chlorinated azaphilones, including five new ones **11**–**15** as well as three known analogs **16**–**18** were isolated from the deep-sea-derived fungus *Phomopsis tersa* FS441 (Chen et al., 2021). It should be pointed out that, compound **12**, which featured a cleaved tetrahydrofuranyl ring, possesses the novel 6/6–6 carbon framework. Moreover, compounds **14** and **15** are characterized as a pair of diastereomers with a characteristic epoxide ring, which are uncommon in azaphilones. In the cytotoxic assay, the new compounds **14** and **15** showed potent cytotoxicity against MCF-7, SF-268, and A549 cell lines with the IC_{50} values of 5.4–8.3 μM (compared with the positive control cisplatin, IC_{50} of 1.6–3.3 μM). Chemical investigations of *Chaetomium* sp. NA-S01-R1, which was isolated from the deep-sea seawater sample, yielded four new chlorinated azaphilone pigments (**19**–**22**) and two known ones (**23**–**24**; Wang et al., 2018). Compound **19** is a novel azaphilone bearing a fused tetrahydrofuran and *δ*-lactone moiety. The new azaphilones **20** and **21** exhibited antibacterial activities against aquatic pathogenic bacteria *Vibrio rotiferianus* and *V. vulnificus*, with MIC values of 7.3 and 7.4 μg/ml, respectively, while compounds **19**, **21** and **22** were found to possess anti-methicillin resistant *Staphylococcus aureus* activity with MIC values ranging from 7.3 to 7.8 μg/ml (chloramphenicol as the positive control with an MIC value of 7.6 μg/ml). Moreover, compound **20** showed cytotoxic activity against the HepG2 cell line with an IC_{50} value of 3.9 μM. The marine-derived fungus *Aspergillus falconensis*, when cultured on solid rice medium containing 3.5% NaCl, yielded two new chlorinated azaphilones **25** and **26** as well as four known derivatives **27**–**30** (El-Kashef et al., 2020). Then, replacing NaCl with 3.5% NaBr induced accumulation of two additional brominated azaphilones **31** and **32** and a known analog **33**. All of these compounds were examined for their nuclear factor kappa B (NF-κB) inhibitory activity in the triple negative breast cancer cell

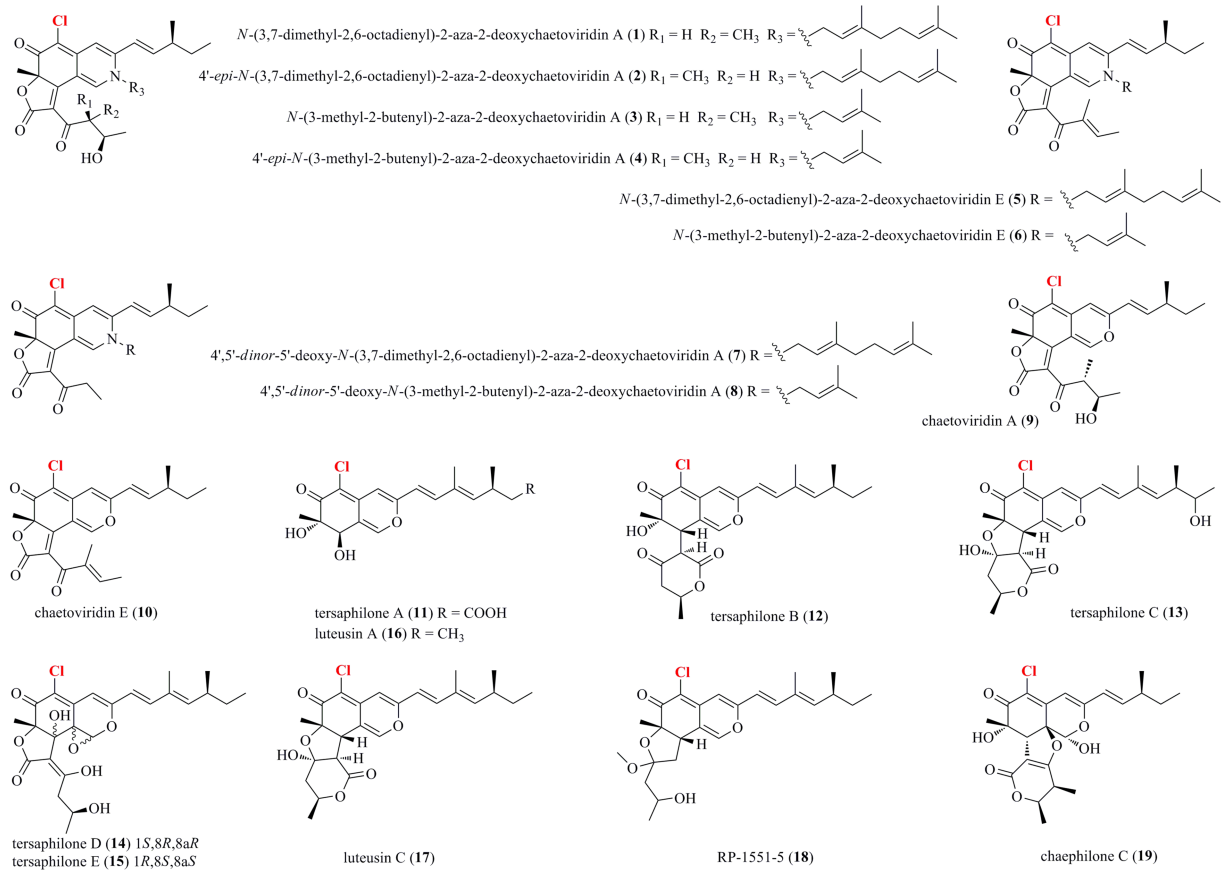

FIGURE 1
Halogenated azaphilones from marine-derived fungi (**1**–**19**).

line MDA-MB-231. As a result, compounds **25** and **27**–**32** showed NF-κB inhibitory activity against the MDA-MB-231 cell line with IC_{50} values ranging from 11.9 to 72.0 μM. The mangrove rhizosphere soil-derived fungus *Penicillium janthinellum* HK1-6 was found to produce chlorinated azaphilones **36** and **37** (Chen et al., 2019). Cultivation of this fungal strain with NaBr instead of sea salt led to the isolation of two new brominated azaphilones **34** and **35**. Structurally, compounds **34**–**37** have a 7-*O*-2′,4′-dimethyldec-2′-enoyl side chain. The NaBr-induced brominated azaphilones **34** and **35** possess the opposite configuration at C-7 to the chlorinated analogs **36** and **37**. The brominated **35** exhibited antibacterial activity against the Gram-positive bacteria including both antibiotic-resistant (methicillin-resistant *Staphylococcus aureus* and vancomycin-resistant *Enterococcus faecium*) and antibiotic-susceptible (*S. aureus* and *E. faecalis*) strains with MIC values of 3.13–12.5 μg/ml. Fermentation of the fungus *P. canescens* 4.14.6a obtained from the Mediterranian sponge *Agelas oroides* with the addition of 5% NaBr yielded two new brominated azaphilones **38** and **39** (Frank et al., 2019). Compounds **38** and **39**, which represent the first azaphilones with a benzene moiety and the pyranoquinone skeleton *via* a methylene group, were exclusively produced when the fungus was cultivated with NaBr. Compound **39** exerted mild cytotoxicity against the mouse lymphoma cell line L5178Y (IC_{50} = 8.9 μM) and the human ovarian cancer cell line A2780 (IC_{50} = 2.7 μM), while its epimer **38** was relatively less active.

Benzophenones

As shown in Figure 3, 25 halogenated benzophenones (**40**–**64**) were isolated from marine-derived fungi. A chemical survey of the sponge-associated fungus *Pestalotiopsis colombiensis* yielded eight chlorinated benzophenone derivatives **40**–**47**, which were isolated from this fungal species for the first time (Lei et al., 2020). These compounds, exclusively isolated from the genus *Pestalotiopsis* and never found in other genus, possess a great significance in the chemotaxonomic study of *Pestalotiopsis*. Therefore, they could be regarded as important chemotaxonomic markers for the genus of *Pestalotiopsis*. A new chlorinated benzophenone derivative **48** was isolated from the soft coral-derived fungus *Pestalotiopsis* sp. (Wei et al., 2013). Compound **48** demonstrated antibacterial activities against *Escherichia coli*, *V. anguillarum*, and *V. parahaemolyticus* with MIC values of 5.0, 10.0 and 20.0 μM, respectively. A new chlorinated xanthone **49** substituted with a tetrahydropyran ring was isolated from the marine-derived fungus *Chaetomium* sp. (Pontius et al., 2008). Compound **49** showed moderate antiprotozoal activity against *Trypanosoma cruzi* with

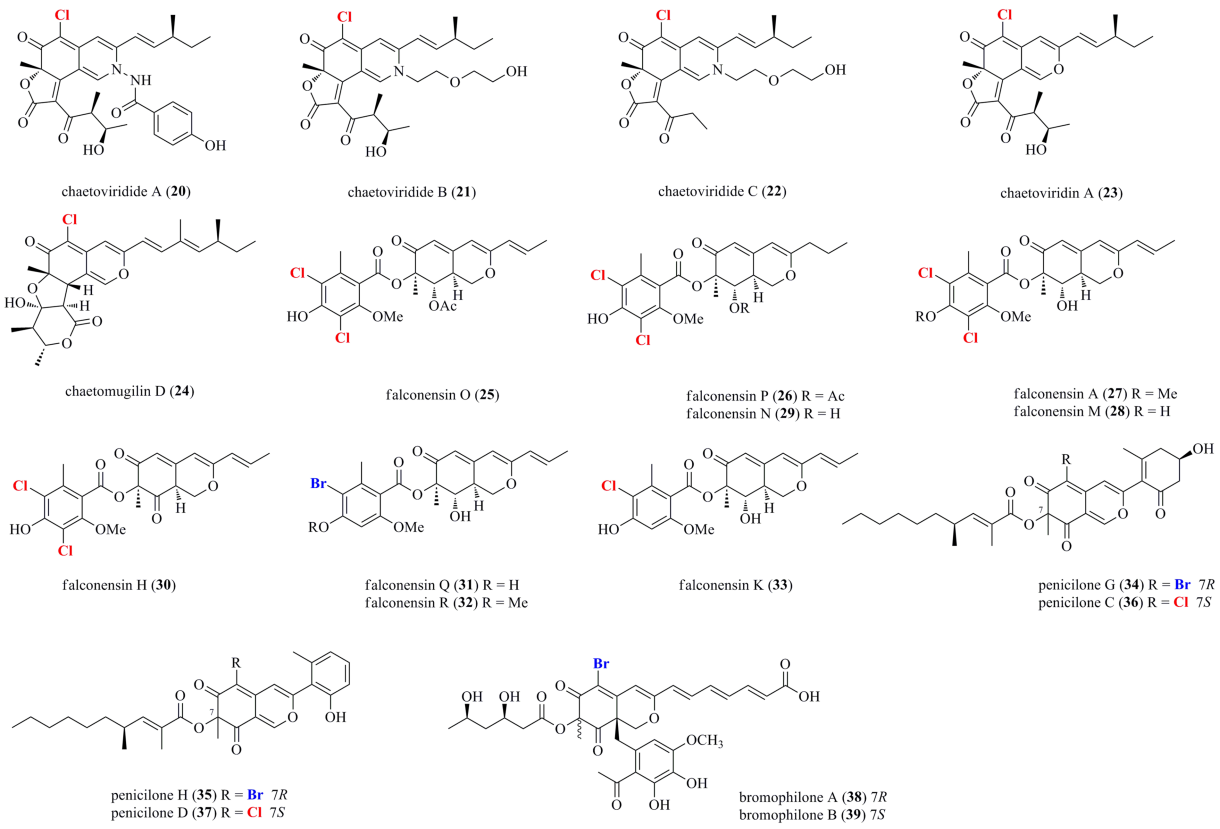

FIGURE 2
Halogenated azaphilones from marine-derived fungi (Continue) (**20–39**).

an IC_{50} value of 1.5 μg/ml. Metabolomic investigations on the marine-derived fungus *Aspergillus* sp. SCSIO F063 unveiled seven new chlorinated anthraquinones **50**–**56** (Huang et al., 2012). Futhermore, when the fungus was fermented with 3% NaBr, two new brominated anthraquinones **57** and **58** were additionally isolated. Interestingly, no iodinated secondary metabolites were observed when the fungus was fermented with NaI. Among these metabolites, only compound **51** moderately inhibited the growth of three human tumor cell lines, SF-268, MCF-7, and NCI-H460, with IC_{50} values of 7.11, 6.64, and 7.42 μM, respectively. The above-mentioned fungal strain *P. canescens* 4.14.6a cultured in sea salt produced compounds **59** and **60** (Frank et al., 2019). Metabolic studies on two different developmental stages, the vegetative stage (asexual morph) and the sexual stage (sclerotial morph), of the marine algal-derived fungus *A. alliaceus* were performed (Mandelare et al., 2018). As a result, the asexual morph of *A. alliaceus* produced a chlorinated anthraquinone **61**, whereas three chlorinated bianthrones **62**–**64** were generated by the coculture of the asexual and sclerotial morph of *A. alliaceus*. Compound **62** was active against the HCT-116 colon carcinoma and SK-Mel-5 skin cancer cell lines with IC_{50} values of 9.0 and 11.0 μM, respectively.

Coumarin-/chromone/pyran-/furan-derived polyketides

Diverse coumarin-/chromone/pyran-/furan-derived polyketides (**65**–**85**) isolated from marine-derived fungi are shown in Figure 4. Two chlorinated dihydro-isocoumarin derivatives **65** and **66** were isolated from the marine-derived fungus *Phoma* sp. 135 (Elsebai and Ghabbour, 2016). Two new chlorinated isocoumarins **67** and **68** with an exomethylene group at C-3 were isolated from a deep-sea-derived fungus *Spiromastix* sp. MCCC 3A00308 (Niu et al., 2021). The dichlorinated isocoumarin **68** showed higher antibacterial activity (*Bacillus thuringiensis* and *B. subtilis*, with an MIC value of 4 μg/ml) than the monochlorinated **67**. The addition of metal bromides, NaBr and $CaBr_2$, to the medium of marine-mudflat-derived fungus *A. niger* induced the production of a new brominated naphthopyranone **69** (Leutou et al., 2016), while the addition of NaBr to a marine-derived *A. ochraceus* led to the induced production of a new brominated isocoumarin **70** (Yun et al., 2013). Compounds **69** and **70** displayed strong radical scavenging activity against DPPH with IC_{50} values of 21 and 24 μM, respectively. Two new chlorinated benzofuran derivatives, **71** and **72**, were isolated from the marine starfish-derived fungus

TABLE 1 Halometabolites isolated from marine-derived fungi (1–145).

Compounds	Fungus	Source	Biological activities	Reference
1–10	*Chaetomium globosum* MP4-S01-7	Deep-sea water sample (4,300 m)	Cytotoxic activity	Wang et al. (2020)
11–18	*Phomopsis tersa* FS441	Deep-sea sediment sample (3,000 m)	Cytotoxic activity	Chen et al. (2021)
19–24	*Chaetomium* sp. NA-S01-R1	Deep-sea seawater sample (4,050 m)	Antimicrobial and cytotoxic activities	Wang et al. (2018)
25–33	*Aspergillus falconensis*	Marine sediment	Anti-inflammatory activity	El-Kashef et al. (2020)
34–37	*Penicillium janthinellum* HK1-6	Mangrove rhizosphere soil	Antimicrobial activity	Chen et al. (2019)
38–39	*P. canescens* 4.14.6a	Sponge *Agelas oroides*	Cytotoxic activity	Frank et al. (2019)
40–47	*Pestalotiopsis colombiensis*	Sponge *Axinella* sp.	-	Lei et al. (2020)
48	*Pestalotiopsis* sp.	Soft coral *Sarcophyton* sp.	Antibacterial activity	Wei et al. (2013)
49	*Chaetomium* sp.	Marine algae	Antiprotozoal activity	Pontius et al. (2008)
50–58	*Aspergillus* sp. SCSIO F063	Marine sediment sample (1,451 m)	Cytotoxic activity	Huang et al. (2012)
59–60	*P. canescens* 4.14.6a	Sponge *Agelas oroides*	No cytotoxic activity	Frank et al. (2019)
61–64	*A. alliaceus*	Marine algae	Cytotoxic activity	Mandelare et al. (2018)
65–66	*Phoma* sp. 135	Sponge *Ectyplasia perox*	-	Elsebai and Ghabbour (2016)
67–68	*Spiromastix* sp. MCCC 3A00308	Marine sediment (2,869 m)	Antibacterial activity	Niu et al. (2021)
69	*A. niger*	Marine mudflat	Antioxidant activity	Leutou et al. (2016)
70	*A. ochraceus*	Marine red alga *Chondria crassicualis*	Antioxidant activity	Yun et al. (2013)
71–72	*Pseudallescheria boydii*	Marine starfish *Acanthaster planci*	-	Yan et al. (2015)
73	*P. canescens* 4.14.6a	Sponge *Agelas oroides*	No cytotoxic activity	Frank et al. (2019)
74	*Pleosporales* sp. HDN1811400	Marine sediment	Antibacterial activity	Han et al. (2021)
75	*Cladosporium cladosporioides* HDN14-342	Deep-sea sediment (3,471 m)	Cytotoxic activity	Zhang et al. (2016)
76	*C. cladosporioides* 8–1	Cold-seep	Antimicroalgal activity	Li et al. (2022)
77–78	*A. sydowii*	Marine alga *Acanthophora spicifera*	-	Teuscher et al. (2006)
79	*Roussoella* sp. DLM33	Source ungiven	-	Ferreira et al. (2015)
80–81	*P. terrestre*	Marine sediments	No cytotoxic activity	Li et al. (2011)
82	*Trichoderma harzianum* (XS-20090075)	Soft coral	No antifouling activity	Yu et al. (2021)
83–85	*Phoma* sp.135	Sponge *Ectyplasia perox*	Antibacterial activity	Elsebai et al. (2018)
86–87	*P. terrestre*	Marine sediments	Cytotoxic activity	Li et al. (2011)
88–89	*Cochliobolus lunatus* (TA26-46)	Sea anemone *Palythoa haddoni*	No cytotoxic activity	Zhang W. et al. (2014)
90–91	Unidentified	Marine alga *Gracillaria verrucosa*	-	Li et al. (2004)
92	*Tryblidiopycnis* sp. 4,275	Mangrove Kandelia	-	Huang et al. (2006)
93	*Penicillium* sp. MMS351	Seawater sample	Cytotoxic activity	Vansteelandt et al. (2013)
94–97	*Penicillium* sp. PR19N-1	Marine sludge	Cytotoxic activity	Wu et al. (2013)
98	*T. harzianum* (XS-20090075)	Soft coral	No antimicrobial activity	Shi et al. (2020)
99–100	*Penicillium* sp. SCS-KFD09	Marine worm *Sipunculus nudus*	Antiviral activity	Kong et al. (2017)
101	*A. nidulans* EN-330	Marine alga *Polysiphonia scopulorum*	Antimicrobial activity	Zhang et al. (2015)
102–107	*Malbranchea aurantiaca*	Marine invertebrate	-	Watts et al. (2011)
108–110	*Phomopsis* sp. QYM-13	Mangrove *Kandelia candel*	Cytotoxic activity	Chen et al. (2022)
111–115	*Trichoderma* sp. TPU199	Marine alga	-	Yamazaki et al. (2020)
116	*A. alliaceus*	Marine alga	-	Mandelare et al. (2018)
117–119	*A. flavipes* 164,013	Sponge	Enzyme inhibitory activity	Jiao et al. (2020)
120	*T. harzianum* (XS-20090075)	Soft coral	No antifouling activity	Yu et al. (2021)
121	*Graphostroma* sp. MCCC 3A00421	Deep-sea hydrothermal sulfide	No antifood allergic activity	Niu et al. (2018)
122–123	*P. canescens* 4.14.6a	Sponge *Agelas oroides*	No cytotoxic activity	Frank et al. (2019)
124–130	*A. unguis* GXIMD 02505	Coral *Pocillopora damicornis*	Anti-osteoclastogenic and antibacterial activity	Zhang et al. (2022)

(Continued)

TABLE 1 (Continued)

Compounds	Fungus	Source	Biological activities	Reference
131–133	*Spiromastix* sp. MCCC 3A00308	Marine sediment (2,869 m)	Antibacterial activity	Niu et al. (2021)
134–135	*A. unguis*	Seaweed	Antimicrobial and larvicidal activity	Zhang Y. et al. (2014)
136	*P. citreonigrum* XT20-134	Deep-sea sediment (2,910 m)	Cytotoxic activity	Tang et al. (2019)
137–143	*Acremonium sclerotigenum* GXIMD 02501	Coral *Pocillopora damicornis*	Anti-osteoclastogenic activity	Lu et al. (2022)
144–145	*Aspergillus* sp.	Marine alga *Ishige okamurae*	Antioxidant activity	Leutou et al. (2013)

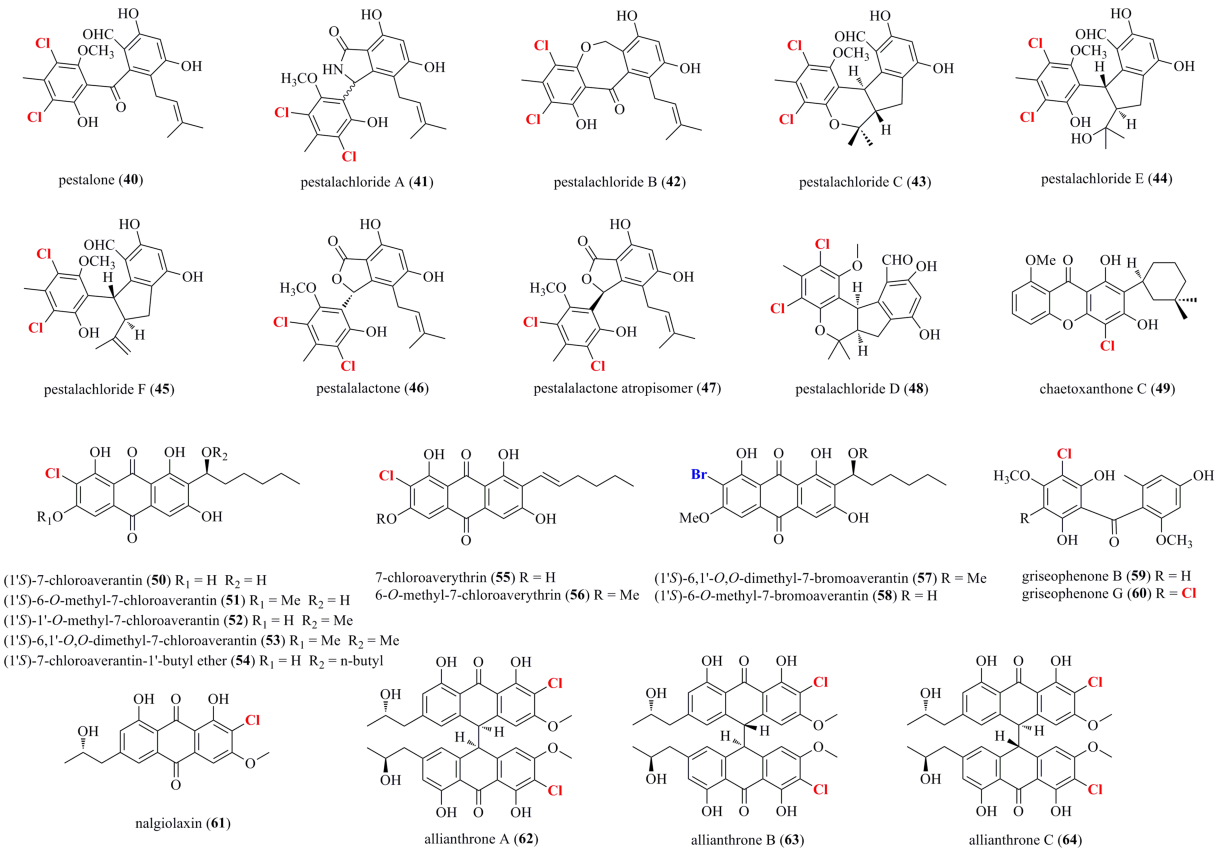

FIGURE 3
Halogenated benzophenones from marine-derived fungi (**40–64**).

Pseudallescheria boydii (Yan et al., 2015). A chlorinated griseofulvin-type spirocyclic polyketide **73** was isolated from *P. canescens* 4.14.6a (Frank et al., 2019). A new phenalenone **74**, representing the first example of chlorinated acenaphthenquinone derivative, was characterized from the marine sediment-derived fungus *Pleosporales* sp. HDN1811400 (Han et al., 2021). Compound **74** displayed higher inhibitory activity against MRCNS (MIC = 25.0 μM) and MRSA (MIC = 12.5 μM) than the positive control ciprofloxacin (MICs of 25.0 and > 50 μM, respectively), suggesting the high potential of these heptaketide phenalenones as lead compounds for drug-resistant pathogens. A new naturally occurring 8–4′ linkage 1-tetralone dimeric derivative **75** was isolated from the deep-sea derived fungus *Cladosporium cladosporioides* HDN14-342 (Zhang et al., 2016). Compound **75**, which represents the first halogenated cladosporol derivatives, showed cytotoxicity against HeLa, K562, and HCT-116 cell lines with IC_{50} values of 3.9, 8.8, and 19.4 μM. An unexpected iodinated dimeric naphtho-γ-pyrone **76** was obtained from the marine cold-seep fungus *C. cladosporioides* 8–1 (Li et al., 2022). Compared to chlorine- and bromine-containing compounds, iodine-bearing metabolites are rarely encountered. Compound **76** displayed potent antimicroalgal activity against the

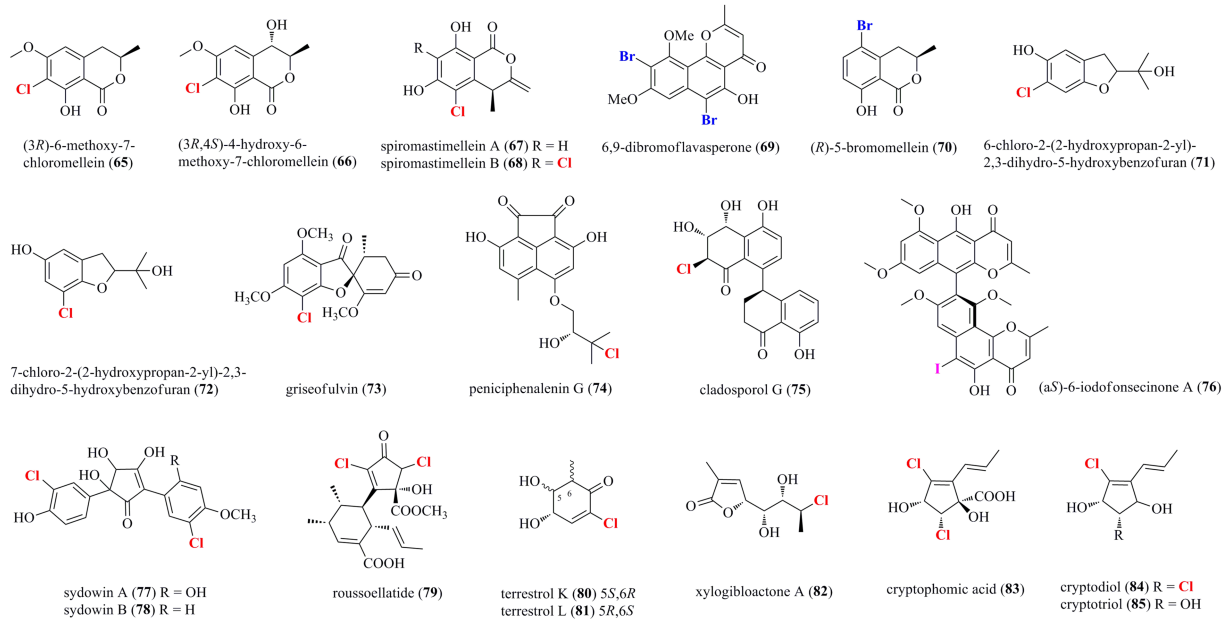

FIGURE 4
Halogenated coumarin–/chromone/pyran–/furan-derived polyketides from marine-derived fungi (**65–85**).

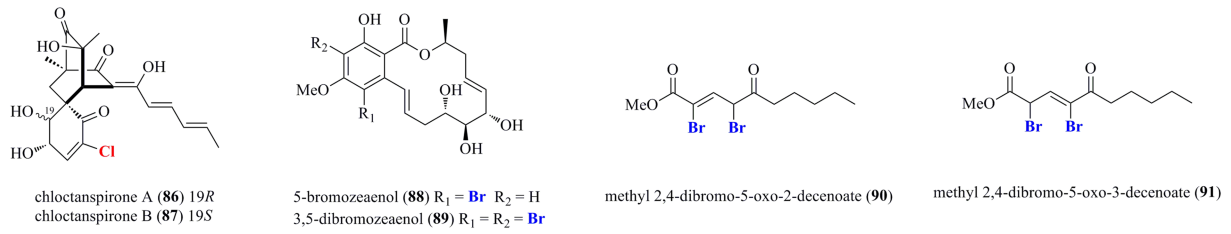

FIGURE 5
Other halogenated polyketides from marine-derived fungi (**86–91**).

marine microalgae *Prorocentrum minimum* with an IC_{50} value being 0.61 μg/ml, compared with the positive control $CuSO_4$ (IC_{50} = 2.4 μg/ml). Two new chlorinated cyclopentanoids **77** and **78** were isolated from *A. sydowii*, an endophyte associated with the marine alga *Acanthophora spicifera* (Teuscher et al., 2006). Both compounds are structurally related hydroxylated 2,5-diarylcyclopentenones, which have hitherto only been isolated from higher basidiomycetes. A novel dichlorinated compound **79** having an unprecedented polyketide skeleton was isolated from the marine-derived fungus *Roussoella* sp. DLM33 (Ferreira et al., 2015). Stable isotope feeding experiments revealed a complicated biosynthetic origin of **79** by Favorskii rearrangements in individual pentaketides before being linked *via* an intermolecular Diels–Alder reaction. Two new chlorinated quasi-precursors of sorbicillinoid-type polyketides, **80** and **81**, were isolated from the marine sediment-derived fungus *P. terrestre* (Li et al., 2011). A furan lactone **82** was isolated from the soft coral-derived fungus *Trichoderma harzianum* (XS-20090075) cultured with rice medium (Yu et al., 2021). Chromatographic separation of the marine-derived fungus *Phoma* sp.135 resulted in the characterization of three new chlorinated cyclopentene derivatives **83–85** (Elsebai et al., 2018). Compounds **83–85** showed weak antimicrobial activity against *E. coli*, *Bacillus subtilis*, *Mycobacterium phlei*, and *S. aureus*, with MIC values ranging from 10 to 35 μM.

Other polyketides

As shown in Figure 5, compounds **86** and **87**, two novel chlorinated sorbicillinoids possessing an unprecedented bicyclo[2.2.2]octane-2-spiro cyclohexane skeleton, were isolated from *P. terrestre* (Li et al., 2011). Compounds **86** and **87** are identified as the first occurrence of spiro cyclohexane-containing and chlorinated sorbicillinoids. Interestingly, **86** was more active against HL-60 cell line with an IC_{50} value of 9.2 μM than **87**

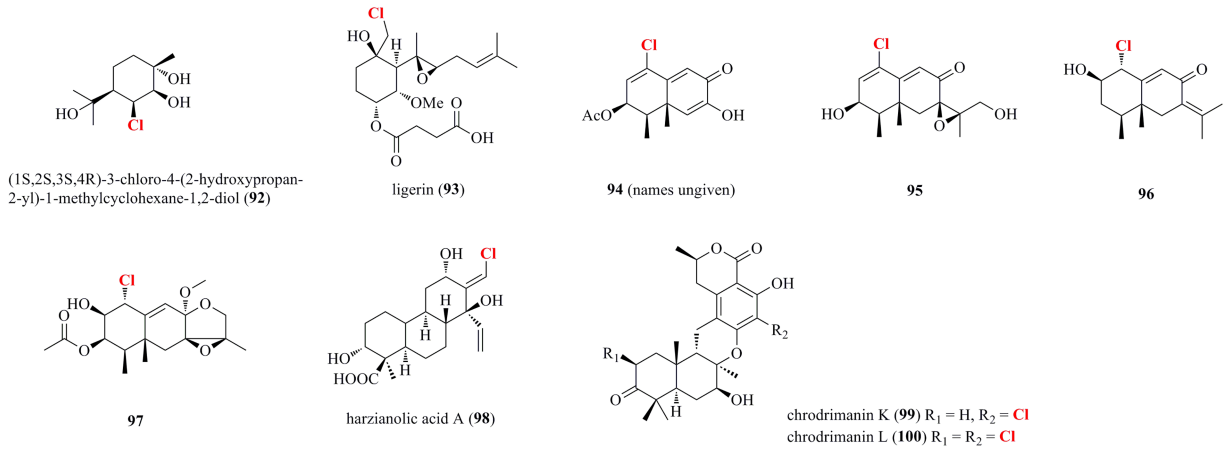

FIGURE 6
Halogenated terpenoids from marine-derived fungi (**92–100**).

(IC_{50} = 37.8 μM), indicating that the stereochemistry may influence the cytotoxic activity. Chemical epigenetic modification, a promising approach to manipulate the silent fungal genes, was used to the marine-derived fungus *Cochliobolus lunatus* (TA26-46) with histone deacetylase inhibitors, led to the isolation and identification of two new brominated 14-membered resorcylic acid lactones **88** and **89** (Zhang W. et al., 2014). It should be noted that both compounds, which were identified as the first examples of brominated resorcylic acid lactones, were exclusively isolated *via* epigenetic modifying agents. Finally, two new dibrominated alkenoates **90** and **91** were isolated from an unidentified fungus (Li et al., 2004).

Halogenated terpenoids from marine-derived fungi

Diverse halogenated terpenoids isolated from marine-derived fungi, including one monoterpene **92**, five sesquiterpenoids **93–97**, one diterpenoid **98**, and two meroterpenoids **99–100**, are shown in Figure 6. A new chloro-monoterpene **92** was isolated from the mangrove-sourced endophytic fungal strain *Tryblidiopycnis* sp. 4,275 (Huang et al., 2006). A new chlorinated sesquiterpenoid **93** was obtained from the marine-derived *Penicillium* strain MMS351 (Vansteelandt et al., 2013). **93** is elucidated as an analog of fumagillin, a sesquiterpene esterified by a deca-2,4,6,8-tetraenedioic acid and functionalized by a spiro-epoxide fused with the cyclohexane ring. Compound **93** showed potent antiproliferative activity against the osteosarcoma cell line POS1 with an IC_{50} value of 117 nM. Four new chlorinated eremophilane-type sesquiterpenes **94–97** were obtained from the deep-sea derived fungus *Penicillium* sp. PR19N-1 (Wu et al., 2013). Compound **94**, which is identified as a trinor-eremophilene core with an 8-oxo-1(2),9(10)-diene unit, was found to possess modest cytotoxic activity against HL-60 and A549 cell lines with IC_{50} values of 11.8 and 12.2 μM, respectively. A new chlorinated cleistanthane-type diterpenoid **98** was isolated from the soft coral-derived fungus *T. harzianum* (XS-20090075) cultured with 10 μM sodium butyrate (Shi et al., 2020). The cleistanthane-type diterpenoid, arisen owing to chemical epigenetic modification, was discovered from genus *Trichoderma* for the first time. Isolation of the marine worm (*Sipunculus nudus*)-derived fungus *Penicillium* sp. SCS-KFD09 afforded two new previously unreported chlorinated meroterpenoids **99** and **100** (Kong et al., 2017). Both meroterpenoids possess a drimane-type sesquiterpenoid substructure fused with an isochromanone moiety. Compound **99** showed strong antiviral activity against influenza A virus (H1N1) with an IC_{50} value of 74 μM (ribavirin as positive control with an IC_{50} of 103 μM).

Halogenated alkaloids from marine-derived fungi

A total of 21 halogenated alkaloids (**101–121**, Figure 7) were isolated from marine-derived fungi. A new chlorinated indole-diterpenoid **101** was isolated from the algal-endophytic fungus *A. nidulans* EN-330 (Zhang et al., 2015). Compound **101** inhibited the growth of brine shrimp (*Artemia salina*) with an LD_{50} value of 3.2 μM. Moreover, it also displayed antimicrobial activities against human- (*E. coli* and *S. aureus*) and aqua- (*Edwardsiella tarda* and *V. anguillarum*) pathogens with MIC values of 16–64 μg/ml. The chlorine-substitution may enhance bioactivities to some degree. Prenylated indole alkaloids possessing a characteristic bicyclo[2.2.2]diazaoctane or diketopiperazine ring are a diverse group of fungal secondary metabolites for biosynthetic investigations (Zhang et al., 2019). A systematic isolation of *Malbranchea aurantiaca*, obtained from an unidentified marine invertebrate, provided six new halogenated prenylated indole alkaloids **102–107** (Watts et al., 2011). Structurally, all of the

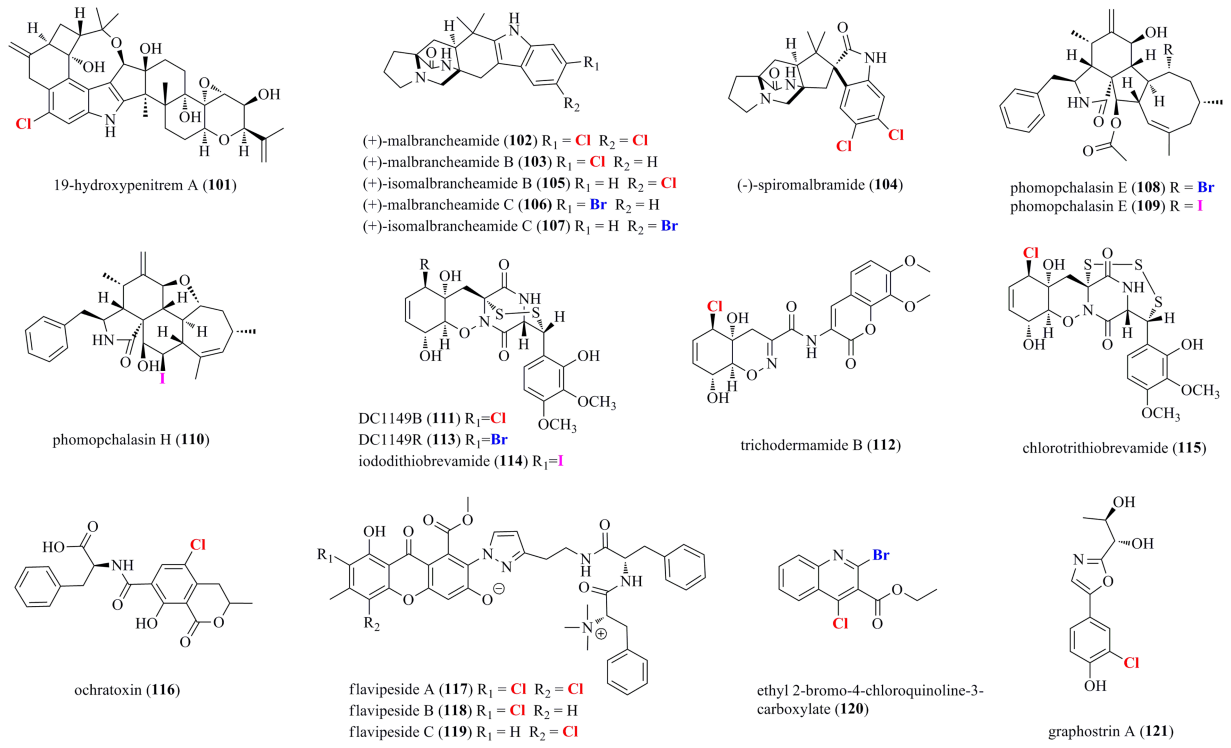

FIGURE 7
Halogenated alkaloids from marine-derived fungi (**101–121**).

isolated compounds are identified as prenylated indole alkaloids containing a halogenated indole ring and the bicyclo[2.2.2] diazaoctane skeleton. Compounds **102–105** were isolated in normal artificial seawater medium, while two brominated **106** and **107** were produced by modifying the solid growth medium with NaBr. Inspired by OSMAC approach, the mangrove-derived fungus *Phomopsis* sp. QYM-13 was cultured with the addition of NaBr or KI to afford halogen-substituted metabolites. As a result, a new brominated cytochalasin **108** and two new iodinated cytochalasins **109** and **110** were isolated from this strain treated with 3% NaBr and 3% KI, respectively (Chen et al., 2022). Compounds **109** and **110** represent the first iodinated cytochalasins. The brominated **108** displayed selective cytotoxicity to MDA-MB-435 cell line with an IC_{50} value of 7.4 μM. Research into the fungus *Trichoderma* sp. TPU199 derived from a red alga yielded a series of new epipolythiodiketopiperazines **111–115** with a sulfide bridge (–S–, –SS–, –SSS–, or –SSSS–) between the α- and β-positions of two amino acid residues (Yamazaki et al., 2020). This fungal strain afforded the halogenated **111**, **113**, and **114**, when fermented with 3% NaCl, NaBr, and NaI, respectively. Moreover, compound **115**, the first trisulfide derivative, was induced by cultivation of this strain with DMSO. A chlorinated mycotoxin **116** was isolated from sclerotial morph of *A. alliaceus* (Mandelare et al., 2018). Three unprecedented chlorinated PKS-NRPS hybrid metabolites **117–119** were isolated from the marine sponge symbiotic fungus *A. flavipes* 164,013 (Jiao et al., 2020). These compounds consisting of a chlorinated xanthone, an aminoethyl-modified pyrazol, and a methylated dipeptide represent a new structural family of PKS-NRPS hybrid metabolites. Compounds **117–119** showed significant inhibitory activity on pancreatic lipase with IC_{50} values of 0.23, 0.07, and 0.14 μM, respectively, which were 6–21 times more potent than that of the positive control kaempferol (IC_{50} = 1.50 μM). A new brominated chloroquinoline **120** was isolated from the fungus *T. harzianum* (Yu et al., 2021). **120** was isolated as the first halogenated quinoline derivative from the genus *Trichoderma*. A novel chlorinated alkaloid **121** featuring a rare oxazole moiety was isolated from the hydrothermal fungus *Graphostroma* sp. MCCC 3A00421 (Niu et al., 2018).

Halogenated phenolic derivatives from marine-derived fungi

Figure 8 presents a total of 24 halogenated phenolic derivatives (**122–145**) isolated from marine-derived fungi. Two chlorinated diphenyl ethers, **122** and **123**, were isolated from the sponge-associated fungus *P. canescens* 4.14.6a (Frank et al., 2019). Seven chlorinated phenolic derivatives, including two diphenyl ethers (**124** and **125**), four depsidones (**126–129**), and one depside (**130**), were isolated from the coral-derived fungus *A. unguis* GXIMD 02505 (Zhang et al., 2022). Compounds **124–128** and **130** were

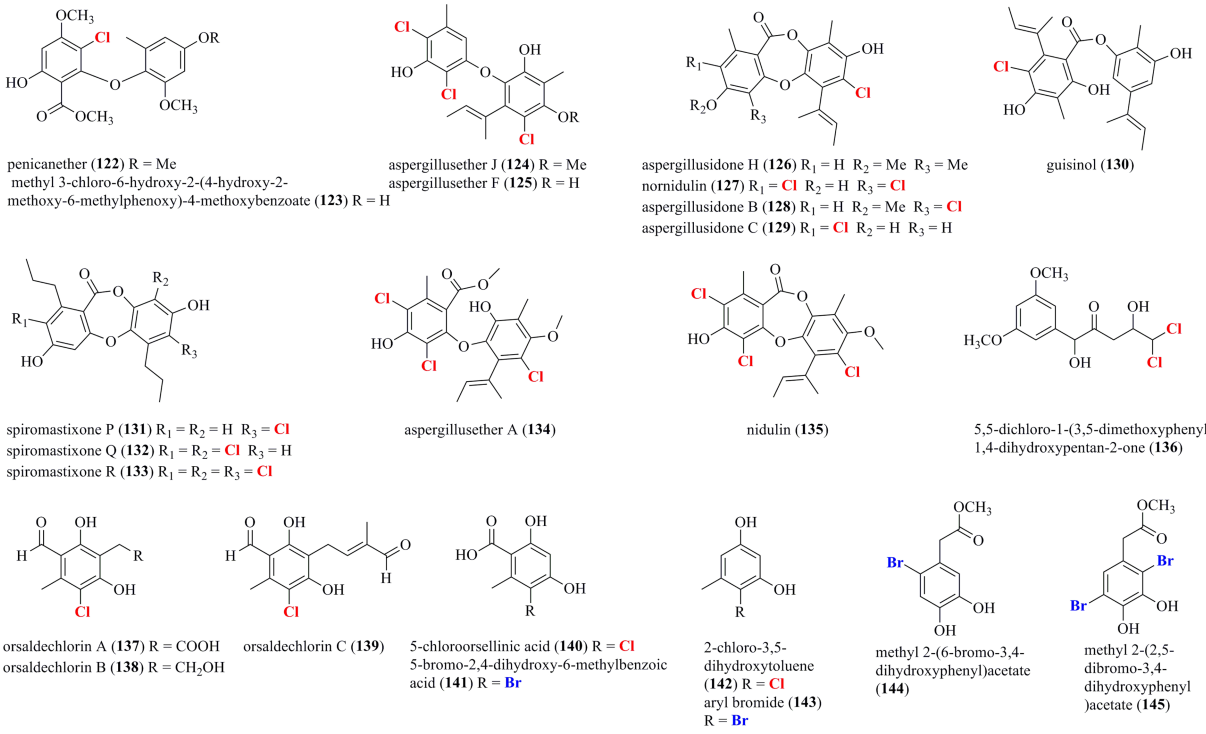

FIGURE 8
Halogenated phenolic derivatives from marine-derived fungi (**122–145**).

found to inhibit lipopolysaccharide (LPS)-induced NF-κB in RAW 264.7 macrophages at a concentration of 20 μM. Most importantly, compounds **125** and **130**, acted as the most potent inhibitors, dose-dependently suppressed RANKL-induced osteoclast differentiation. In addition, compounds **124**, **125**, **127**, **129**, and **130** displayed moderate antibacterial activities against methicillin-resistant *S. aureus*, *Microbulbifer variabilis*, *Marinobacterium jannaschii*, and *V. pelagius* with the MIC values ranging from 2 to 64 μg/ml. Three new chlorinated depsidone-type compounds (**131**–**133**) were isolated from the deep-sea-derived *Spiromastix* fungus (Niu et al., 2021). Compound **133** was characterized as a tri-chlorinated derivative and possessed remarkable antibacterial activities against *S. aureus*, *Bacillus thuringiensis*, and *B. subtilis*, with MIC values of 0.5–1.0 μg/ml. Two tri-chlorinated depsidones **134** and **135** were isolated from a seaweed-derived *A. unguis* strain (Zhang Y. et al., 2014). Compound **135** strongly inhibited methicillin-resistant *S. aureus* (MIC = 4 μg/ml) and brine shrimp *Artemia larva* (LC_{50} = 2.8 μg/ml). A new dichlorinated compound **136** was isolated from the deep-sea sediment-derived fungus *P. citreonigrum* XT20-134 (Tang et al., 2019). Compound **136** possessed promising cytotoxicities against the human hepatoma tumor cell Bel7402 and the human fibrosarcoma tumor cell HT1080, with IC_{50} values of 13.14 and 16.53 μM, respectively. Seven halogenated phenolic derivatives, including three new chlorinated orsellinic aldehyde derivatives **137**–**139**, two orsellinic acids (chlorinated **140** and brominated **141**), and two phenols (chlorinated **142** and brominated **143**), were isolated from the coral-associated fungus *Acremonium sclerotigenum* GXIMD 02501 (Lu et al., 2022). Compounds **137**, **138**, **140**, and **143** showed certain inhibition of LPS-induced NF-κB activation in RAW 264.7 cells at 20 μM. Two new potent inhibitors (**137** and **138**) strongly suppressed RANKL-induced osteoclast differentiation. Finally, the addition of NaBr and $CaBr_2$ in the fermentation of the marine-derived fungus *Aspergillus* sp. induced the production of two new brominated dihydroxyphenylacetic acid derivatives **144** and **145** (Leutou et al., 2013). Both compounds exerted strong DPPH scavenging activity with IC_{50} values of 14.2 and 12.1 μM.

Induced production of halometabolites with different cultural conditions

In order to expand the structural diversity of the halometabolites from the marine-derived fungi, OSMAC (One Strain MAny Compounds) strategy was used to remodel the fungal metabolome and activate the cryptic biosynthetic pathways. Of all the isolated halometabolites from the marine-derived fungi, most of them are chlorinated (81.4%), then followed by brominated (15.9%), while iodinated compounds are rather rare (2.7%). It should be pointed out that the occurrence of halogenated metabolites depends on halogen salts in the fermentation of the producing fungi. It seems that most of the brominated and iodinated compounds are generated by the substitution of bromide and iodide ions for the chloride ion in

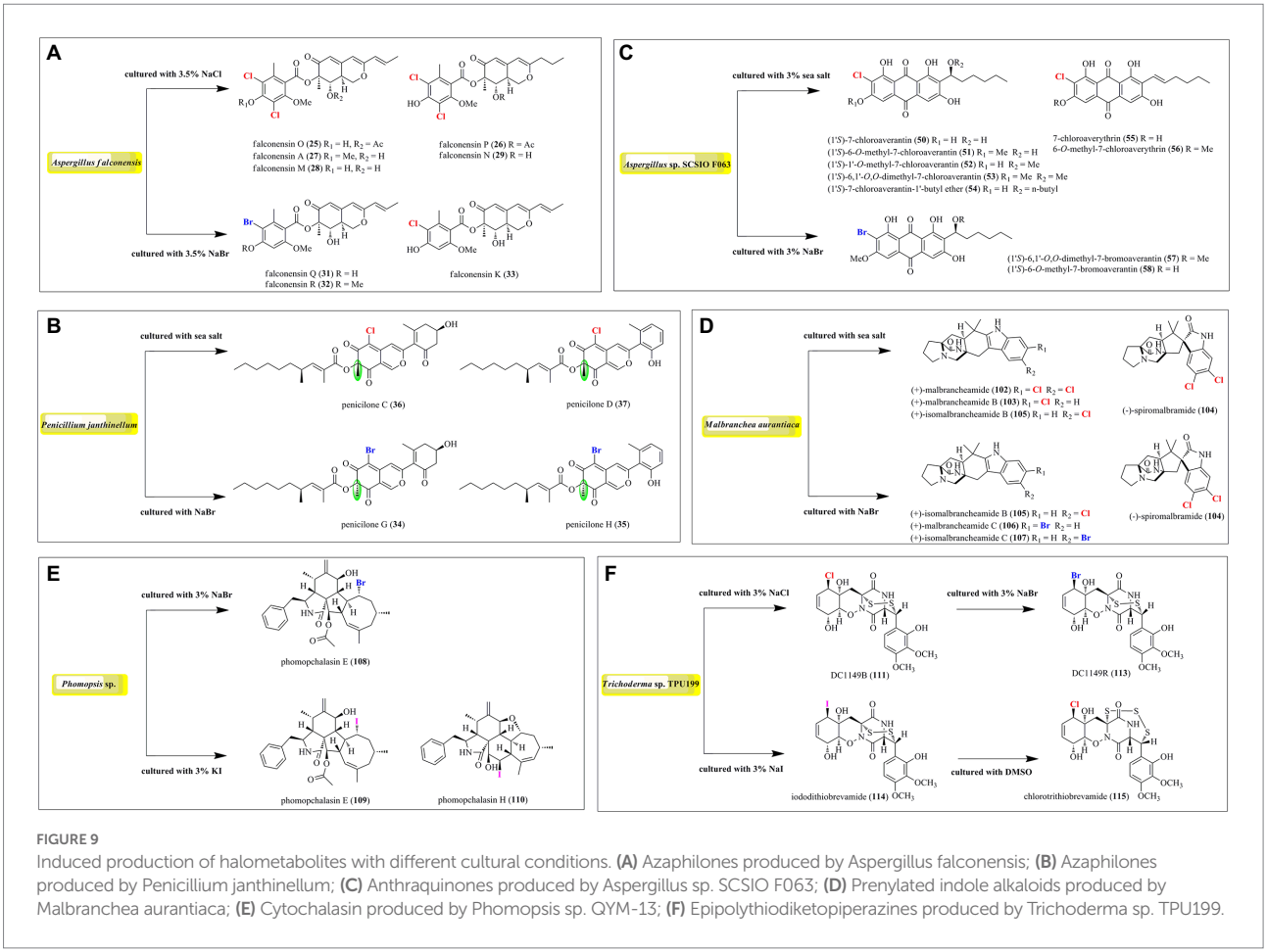

FIGURE 9
Induced production of halometabolites with different cultural conditions. **(A)** Azaphilones produced by Aspergillus falconensis; **(B)** Azaphilones produced by Penicillium janthinellum; **(C)** Anthraquinones produced by Aspergillus sp. SCSIO F063; **(D)** Prenylated indole alkaloids produced by Malbranchea aurantiaca; **(E)** Cytochalasin produced by Phomopsis sp. QYM-13; **(F)** Epipolythiodiketopiperazines produced by Trichoderma sp. TPU199.

cultivation (Figure 9). For example, fermentation of *A. falconensis* with 3.5% NaCl afforded chlorinated azaphilones **25**–**30**, while replacing NaCl with 3.5% NaBr induced the production of additional brominated azaphilones **31** and **32** (El-Kashef et al., 2020). Cultivation of *P. janthinellum* HK1-6 with sea salt and NaBr yielded chlorinated azaphilones **36**–**37** and brominated **34**–**35**, respectively (Chen et al., 2019). Interestingly, the NaBr-induced brominated **34**–**35** possess the opposite configuration at C-7 compared to the chlorinated analogs **36**–**37** cultured with normal sea salt condition. In addition to the chlorinated anthraquinones **50**–**56**, two brominated anthraquinones **57** and **58** were obtained from *Aspergillus* sp. SCSIO F063 by the substitution of 3% NaBr for sea salt (Huang et al., 2012). The authors also fermented the fungus with NaI; however, no iodinated metabolites were observed. The fungus *M. aurantiaca* produced chlorinated prenylated indole alkaloids **102**–**105**, when fermented in normal artificial seawater medium, while the brominated **106** and **107** were isolated from its culture broth in NaBr-containing medium (Watts et al., 2011). The fungus *Phomopsis* sp. QYM-13 cultured with the addition of 3% NaBr or 3% KI was found to produce a brominated cytochalasin **108** and two new iodinated cytochalasins **109** and **110**, respectively (Chen et al., 2022). Finally, the fungus *Trichoderma* sp. TPU199 afforded the halogenated **111**, **113**, **114**, and **115** when induced by cultivation of this fungal strain with 3% NaCl, 3% NaBr, 3% NaI, and DMSO, respectively (Yamazaki et al., 2020). These results indicated that the substitution of bromide or iodide ions for sea salt in the fermentation of the producing fungi may be an effective way to afford more intriguing halometabolites, expecially brominated and iodinated compounds, from the marine-derived fungi.

Conclusions and future perspectives

Halometabolites are mainly produced by marine organisms due to the presence of chloride, bromine, and iodine ions in seawater. As previously discussed, among all of the halometabolites described herein, chlorination is the predominant modification, and then followed by bromination, while iodination is extremely rare. In this review, a total of 118 chlorinated (accounting for 81.4%), 23 brominated (15.9%), and four iodinated (2.7%) metabolites isolated from marine-derived fungi were summarized (Figure 10A). Marine fungi may possess the capability to oxidize chlorine more easily than bromide and iodine in the biosynthesis of these metabolites, thus the number of chlorinated compounds is quite higher than brominated and

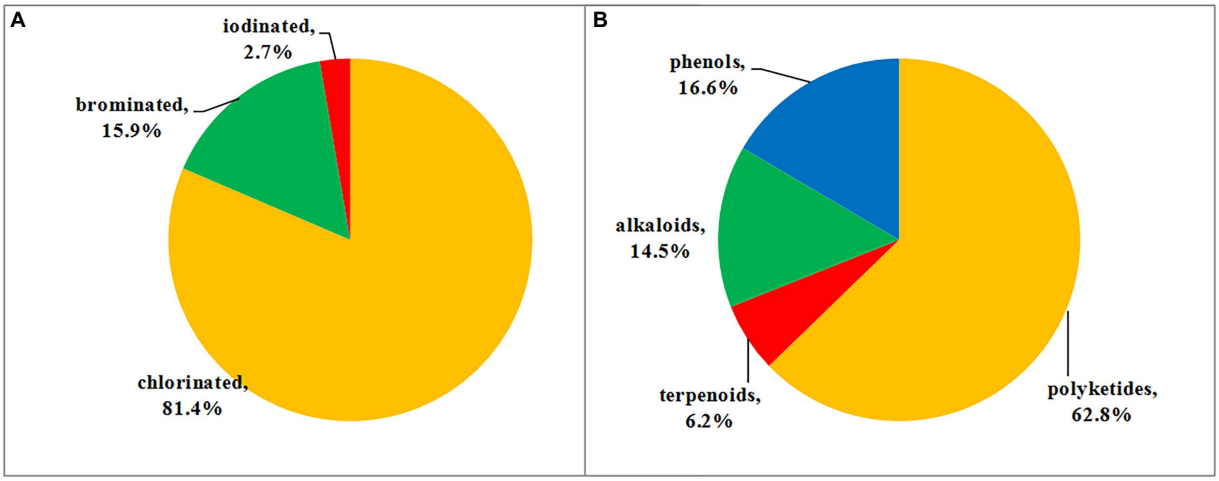

FIGURE 10
(A) Proportion of halometabolites from marine-derived fungi; **(B)** Structural classes of halometabolites.

iodinated compounds. Moreover, these halometabolites possess a high structural diversity. The reported 145 halometabolites, shown in this review, are categorized into polyketides (**1**–**91**; including azaphilones **1**–**39**, benzophenones **40**–**64**, coumarin−/chromone/pyran−/furan-derived polyketides **65**–**85**, and other types of polyketides **86**–**91**), terpenoids (**92**–**100**), alkaloids (**101**–**121**), and phenolic derivatives (**122**–**145**). Structural classification of compounds based on biogenetic categories is unprecise, as many compounds are derived from mixed biosynthetic pathways. For example, compounds **1**–**6** are clearly classified as nitrogen-containing compounds. However, we categorize them as polyketides based on the biosynthetic origin of azaphilones. It is estimated that 62.8% of the reported halometabolites are polyketides (Figure 10B), especially azaphilones, which accounted for 42.9% of the reported halogenated polyketides. As for the halogenated alkaloids, a series of halogenated prenylated indole alkaloids **102**–**107** and epipolythiodiketopiperazines **111**–**115** were isolated and induced by the addition of additional halogen salts. Changing the cultural conditions will help to increase the chemical diversity of halometabolites produced by marine-derived fungi.

Halometabolites isolated from marine microorganisms are relatively unexplored compared with those from marine macroorganisms, such as algae, sponges, and soft corals. Marine-derived fungi have proven to be a precious house of bioactive secondary metabolites with novel structures. Table 1 shows a total of 17 genera of marine-derived fungi as producers of these halometabolites. Among them, the species belonging to genera *Aspergillus*, *Penicillium*, *Chaetomium*, *Phomopsis*, *Pestalotiopsis*, *Trichoderma*, *Acremonium*, *Malbranchea*, *Phoma*, and *Spiromastix* are the Top 10 producers, with 42, 23, 17, 11, 9, 8, 7, 6, 5, and 5 halometabolites being isolated, respectively (Figure 11A). In addition, the distribution of these fungal producers is shown in Figure 11B. These fungal producers were obtained from a wide range of marine habitats, such as marine sediments (including mudflats and sludges), marine invertebrates (including sponges, soft corals, starfishes, and anemones), and marine plants (algae and mangroves). Marine sediments, marine sponges, marine algae, seawater, soft corals, and mangroves are dominating origins of these fungal strains, with 43, 23, 21, 19, 18, and 8 of the reported compounds characterized (Figure 11B).

Halometabolites are vital sources for new drugs discovery given to their high diversity in structures and bioactivities. It is considered that the presence of halogen substituents profoundly enhances the bioactivity of natural compounds, as it is obvious that halometabolites often possess higher biological activity than that non-halogen substituted natural compounds. However, it lacks solid evidence that compounds with two or more halogen substituents, such as compounds **25**–**27** with two chlorine groups, **40**–**48** with two chlorine groups, and **134**–**135** with three chlorine groups, exhibit better activity than those with single substituent. The reported halometabolites derived from marine fungi demonstrated pronounced biological activities, including cytotoxic, antimicrobial, anti-inflammatory, antioxidant, and enzyme inhibitory properties (Figure 12). 31.3% of the isolated halometabolites were found to possess certain cytotoxicities. More importantly, some of them showed even higher activity than the positive controls. For example, the chlorinated azaphilones **1**, **2**, and **5** showed significant cytotoxic activity against the human gastric cancer MGC803 and AGS cell lines at a nanomole level (Wang et al., 2020), while compounds **19**, **21** and **22** were found to possess anti-methicillin resistant *S. aureus* activity with MICs of 7.3–7.8 μg/ml (the positive control chloramphenicol, MIC = 7.6 μg/ml) (Wang et al., 2018). The phenalenone **74**

displayed higher activity against MRCNS (MIC = 25.0 μM) and MRSA (MIC = 12.5 μM) than the positive control ciprofloxacin (MICs of 25.0 and > 50 μM, respectively), indicating the high potential of these heptaketide phenalenones as lead compounds for drug-resistant pathogens (Han et al., 2021). The iodinated dimeric naphtho-γ-pyrone **76** displayed potent antimicroalgal activity against the marine microalgae *Prorocentrum minimum* with an IC_{50} value of 0.61 μg/ml, compared with the positive control $CuSO_4$ (IC_{50} = 2.4 μg/ml) (Li et al., 2022). It is well-known that some halometabolites have been on the market for decades as pharmaceuticals, as exemplified of antibiotic chloramphenicol and pyrrolnitrin and antitumor rebeccamycin. The promising bioactivities indicate that searching for new halometabolites is an important way to develop new drugs and agrochemicals.

In conclusion, in the exploration of bioactive natural compounds, we focus on the potential of marine-derived fungi as producers of halometabolites. This comprehensive review illustrates the chemistry and biological activities of halometabolites produced by marine-derived fungi. 145 halogenated compounds, including 118 chlorinated, 23 brominated, and 4 iodinated, which are classified into polyketides (62.7%), phenols (16.6%), alkaloids (14.5%), and terpenoids (6.2%), were isolated from 17 genera of marine-derived fungi. Their pronounced biological activities, such as cytotoxic, antimicrobial, anti-inflammatory, antioxidant, and

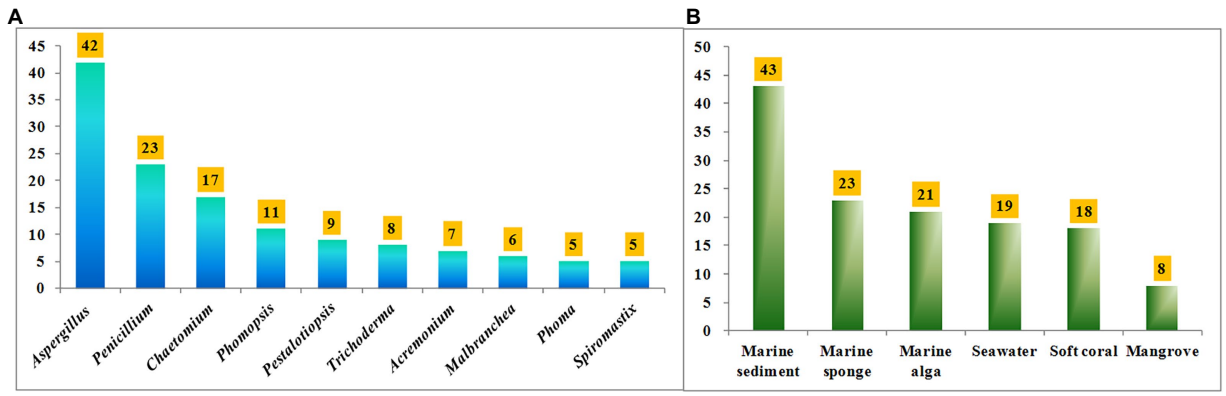

FIGURE 11
(A) Numbers of halometabolites from different marine-derived fungi; **(B)** Numbers of halometabolites from different sources of marine origins.

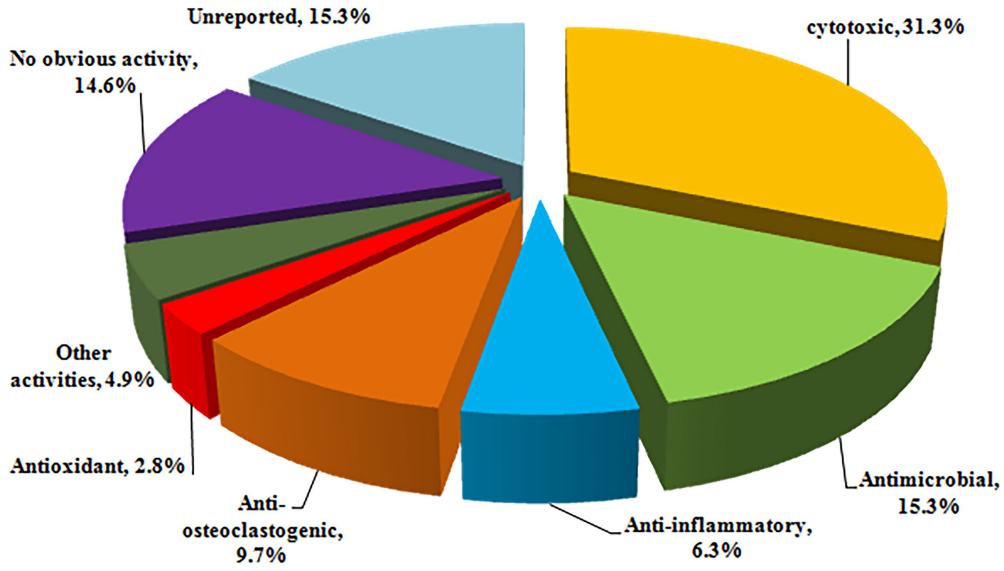

FIGURE 12
Percentages of bioactivities of halometabolites.

enzyme inhibitory properties, revealed a high potential of these halogenated compounds as lead compounds for drug discovery. It should be pointed out that despite a large number of new halometabolites have been characterized; those halogenated compounds are relatively unexplored. Further OSMAC method by changing the cultural conditions will induce the production of more halometabolites.

Data availability statement

The original contributions presented in the study are included in the article/Supplementary material, further inquiries can be directed to the corresponding authors.

Author contributions

YC, L-CX, and SL: collected and reorganized the literature data. YC: wrote this manuscript. Z-XZ and G-YC: conceived the ideas and revised this manuscript. All authors contributed to the article and approved the submitted version.

Conflict of interest

The authors declare that the research was conducted in the absence of any commercial or financial relationships that could be construed as a potential conflict of interest.

Publisher's note

All claims expressed in this article are solely those of the authors and do not necessarily represent those of their affiliated organizations, or those of the publisher, the editors and the reviewers. Any product that may be evaluated in this article, or claim that may be made by its manufacturer, is not guaranteed or endorsed by the publisher.

Supplementary material

The Supplementary material for this article can be found online at: https://www.frontiersin.org/articles/10.3389/fmicb.2022.1038487/full#supplementary-material

References

Chen, S., Liu, Z., Chen, Y., Tan, H., Liu, H., and Zhang, W. (2021). Tersaphilones A-E, cytotoxic chlorinated azaphilones from the deep-sea-derived fungus *Phomopsis tersa* FS441. *Tetrahedron* 78:131806. doi: 10.1016/j.tet.2020.131806

Chen, Y., Yang, W., Zou, G., Wang, G., Kang, W., Yuan, J., et al. (2022). Cytotoxic bromine- and iodine-containing cytochalasins produced by the mangrove endophytic fungus *Phomopsis* sp. QYM-13 using the OSMAC approach. *J. Nat. Prod.* 85, 1229–1238. doi: 10.1021/acs.jnatprod.1c01115

Chen, M., Zheng, Y. Y., Chen, Z. Q., Shen, N. X., Shen, L., Zhang, F. M., et al. (2019). NaBr-induced production of brominated azaphilones and related tricyclic polyketides by the marine-derived fungus *Penicillium janthinellum* HK1-6. *J. Nat. Prod.* 82, 368–374. doi: 10.1021/acs.jnatprod.8b00930

El-Kashef, D. H., Youssef, F. S., Hartmann, R., Knedel, T. O., Janiak, C., Lin, W., et al. (2020). Azaphilones from the red sea fungus *Aspergillus falconensis*. *Mar. Drugs* 18:204. doi: 10.3390/md18040204

Elsebai, M. F., and Ghabbour, H. A. (2016). Isocoumarin derivatives from the marine-derived fungus *Phoma* sp. 135. *Tetrahedron Lett.* 57, 354–356. doi: 10.1016/j.tetlet.2015.12.024

Elsebai, M. F., Ghabbour, H. A., Legrave, N., Fontaine-Vive, F., and Mehiri, M. (2018). New bioactive chlorinated cyclopentene derivatives from the marine-derived fungus *Phoma* sp. *Med. Chem. Res.* 27, 1885–1892. doi: 10.1007/s00044-018-2201-1

Ferreira, E. L., Williams, D. E., Ióca, L. P., Morais-Urano, R. P., Santos, M. F., Patrick, B. O., et al. (2015). Structure and biogenesis of roussoellatide, a dichlorinated polyketide from the marine-derived fungus *Roussoella* sp. DLM33. *Org. Lett.* 17, 5152–5155. doi: 10.1021/acs.orglett.5b02060

Frank, M., Hartmann, R., Plenker, M., Mándi, A., Kurtán, T., Özkaya, F. C., et al. (2019). Brominated Azaphilones from the sponge-associated fungus *Penicillium canescens* strain 4.14.6a. *J. Nat. Prod.* 82, 2159–2166. doi: 10.1021/acs.jnatprod.9b00151

Han, Y., Sun, C., Li, C., Zhang, G., Zhu, T., Li, D., et al. (2021). Antibacterial phenalenone derivatives from marine-derived fungus *Pleosporales* sp. HDN1811400. *Tetrahedron Lett.* 68:152938. doi: 10.1016/j.tetlet.2021.152938

Huang, H., Wang, F., Luo, M., Chen, Y., Song, Y., Zhang, W., et al. (2012). Halogenated anthraquinones from the marine-derived fungus *Aspergillus* sp. SCSIO F063. *J. Nat. Prod.* 275, 1346–1352. doi: 10.1021/np3002699

Huang, H. R., Xia, X. K., She, Z. G., Lin, Y. C., Vrijmoed, L. L., and Gareth Jones, E. B. (2006). A new chloro-monoterpene from the mangrove endophytic fungus *Tryblidiopycnis* sp. (4275). *J. Asian Nat. Prod. Res.* 8, 609–612. doi: 10.1080/10286020500208493

Jiao, W. H., Xu, Q. H., Ge, G. B., Shang, R. Y., Zhu, H. R., Liu, H. Y., et al. (2020). Flavipesides A-C, PKS-NRPS hybrids as pancreatic lipase inhibitors from a marine sponge symbiotic fungus *Aspergillus flavipes* 164013. *Org. Lett.* 22, 1825–1829. doi: 10.1021/acs.orglett.0c00150

Kasanah, N., and Triyanto, T. (2019). Bioactivities of halometabolites from marine *Actinobacteria*. *Biomol. Ther.* 9:225. doi: 10.3390/biom9060225

Kong, F. D., Ma, Q. Y., Huang, S. Z., Wang, P., Wang, J. F., Zhou, L. M., et al. (2017). Chrodrimanins K-N and related meroterpenoids from the fungus *Penicillium* sp. SCS-KFD09 isolated from a marine worm, *Sipunculus nudus*. *J. Nat. Prod.* 80, 1039–1047. doi: 10.1021/acs.jnatprod.6b01061

Lei, H., Niu, H., Song, C., Fu, X., Luo, Y., Chen, S., et al. (2020). Chlorinated benzophenone derivatives as chemotaxonomic markers for the genus of pestalotiopsis. *Biochem. Syst. Ecol.* 91:104072. doi: 10.1016/j.bse.2020.104072

Leutou, A. S., Yun, K., Kang, J. S., and Son, B. W. (2013). Induced production of methyl bromodihydroxyphenyl acetates by the marine-derived fungus *Aspergillus* sp. *Chem. Pharm. Bull.* 61, 483–485. doi: 10.1248/cpb.c12-01048

Leutou, A. S., Yun, K., and Son, B. W. (2016). Induced production of 6,9-dibromoflavasperone, a new radical scavenging naphthopyranone in the marine-mudflat-derived fungus *Aspergillus niger*. *Arch. Pharm. Res.* 39, 806–810. doi: 10.1007/s12272-016-0764-2

Li, D., Chen, L., Zhu, T., Kurtán, T., Mándi, A., Zhao, Z., et al. (2011). Chloctanspirones A and B, novel chlorinated polyketides with an unprecedented skeleton, from marine sediment derived fungus *Penicillium terrestre*. *Tetrahedron* 67, 7913–7918. doi: 10.1016/j.tet.2011.08.037

Li, X., Kim, S. K., Kang, J. S., Choi, H. D., and Son, B. W. (2004). Polyketide and sesquiterpenediol metabolites from a marine-derived fungus. *Bull. Kor. Chem. Soc.* 25, 607–608.

Li, C. P., Song, Y. P., Wang, B. G., and Ji, N. Y. (2022). Sulfurated and iodinated metabolites from the cold-seep fungus *Cladosporium cladosporioides* 8-1. *Tetrahedron Lett.* 93:153689. doi: 10.1016/j.tetlet.2022.153689

Liao, L., Chen, R., Jiang, M., Tian, X., Liu, H., Yu, Y., et al. (2016). Bioprospecting potential of halogenases from arctic marine actinomycetes. *BMC Microbiol.* 16:34. doi: 10.1186/s12866-016-0662-2

Lu, H., Tan, Y., Zhang, Y., Li, Z., Chen, J., Gao, C., et al. (2022). Osteoclastogenesis inhibitory phenolic derivatives produced by the beibu gulf coral-associated fungus *Acremonium sclerotigenum* GXIMD 02501. *Fitoterapia* 159:105201. doi: 10.1016/j.fitote.2022.105201

Mandelare, P. E., Adpressa, D. A., Kaweesa, E. N., Zakharov, L. N., and Loesgen, S. (2018). Coculture of two developmental stages of a marine-derived *Aspergillus alliaceus* results in the production of the cytotoxic bianthrone allianthrone A. *J. Nat. Prod.* 81, 1014–1022. doi: 10.1021/acs.jnatprod.8b00024

Neumann, C. S., Fujimori, D. G., and Walsh, C. T. (2008). Halogenation strategies in natural product biosynthesis. *Chem. Biol.* 15, 99–109. doi: 10.1016/j.chembiol.2008.01.006

Niu, S., Liu, D., Shao, Z., Huang, J., Fan, A., and Lin, W. (2021). Chlorinated metabolites with antibacterial activities from a deep-sea-derived *Spiromastix* fungus. *RSC Adv.* 11, 29661–29667. doi: 10.1039/D1RA05736G

Niu, S., Liu, Q., Xia, J. M., Xie, C. L., Luo, Z. H., Shao, Z., et al. (2018). Polyketides from the deep-sea-derived fungus *Graphostroma* sp. MCCC 3A00421 showed potent antifood allergic activities. *J. Agric. Food Chem.* 66, 1369–1376. doi: 10.1021/acs.jafc.7b04383

Pontius, A., Krick, A., Kehraus, S., Brun, R., and König, G. M. (2008). Antiprotozoal activities of heterocyclic-substituted xanthones from the marine-derived fungus *Chaetomium* sp. *J. Nat. Prod.* 71, 1579–1584. doi: 10.1021/np800294q

Shi, T., Shao, C. L., Liu, Y., Zhao, D. L., Cao, F., Fu, X. M., et al. (2020). Terpenoids from the coral-derived fungus *Trichoderma harzianum* (XS-20090075) induced by chemical epigenetic manipulation. *Front. Microbiol.* 11:572. doi: 10.3389/fmicb.2020.00572

Tang, X. X., Liu, S. Z., Yan, X., Tang, B. W., Fang, M. J., Wang, X. M., et al. (2019). Two new cytotoxic compounds from a deep-sea *Penicillum citreonigrum* XT20-134. *Mar. Drugs* 17:509. doi: 10.3390/md17090509

Teuscher, F., Lin, W., Wray, V., Edrada, R., Padmakumar, K., Proksch, P., et al. (2006). Two new cyclopentanoids from the endophytic fungus *Aspergillus sydowii* associated with the marine alga *Acanthophora spicifera*. *Nat. Prod. Comm.* 1, 927–933. doi: 10.2174/138955706775197794

Vansteelandt, M., Blanchet, E., Egorov, M., Petit, F., Toupet, L., Bondon, A., et al. (2013). Ligerin, an antiproliferative chlorinated sesquiterpenoid from a marine-derived *Penicillium* strain. *J. Nat. Prod.* 76, 297–301. doi: 10.1021/np3007364

Wang, W., Liao, Y., Chen, R., Hou, Y., Ke, W., Zhang, B., et al. (2018). Chlorinated azaphilone pigments with antimicrobial and cytotoxic activities isolated from the deep sea derived fungus *Chaetomium* sp. NA-S01-R1. *Mar. Drugs* 16:61. doi: 10.3390/md16020061

Wang, Y., Lu, Z., Sun, K., and Zhu, W. (2011). Effects of high salt stress on secondary metabolite production in the marine-derived fungus *Spicaria elegans*. *Mar. Drugs* 9, 535–542. doi: 10.3390/md9040535

Wang, W., Yang, J., Liao, Y. Y., Cheng, G., Chen, J., Cheng, X. D., et al. (2020). Cytotoxic nitrogenated azaphilones from the deep-sea-derived fungus *Chaetomium globosum* MP4-S01-7. *J. Nat. Prod.* 83, 1157–1166. doi: 10.1021/acs.jnatprod.9b01165

Watts, K. R., Loveridge, S. T., Tenney, K., Media, J., Valeriote, F. A., and Crews, P. (2011). Utilizing DART mass spectrometry to pinpoint halogenated metabolites from a marine invertebrate-derived fungus. *J. Org. Chem.* 76, 6201–6208. doi: 10.1021/jo2009593

Wei, M. Y., Li, D., Shao, C. L., Deng, D. S., and Wang, C. Y. (2013). (±)-Pestalachloride D, an antibacterial racemate of chlorinated benzophenone derivative from a soft coral-derived fungus *Pestalotiopsis* sp. *Mar. Drugs* 11, 1050–1060. doi: 10.3390/md11041050

Wu, G., Lin, A., Gu, Q., Zhu, T., and Li, D. (2013). Four new chloro-eremophilane sesquiterpenes from an antarctic deep-sea derived fungus, *Penicillium* sp. PR19N-1. *Mar. Drugs* 11, 1399–1408. doi: 10.3390/md11041399

Xu, K., Wei, X. L., Xue, L., Zhang, Z. F., and Zhang, P. (2020). Antimicrobial meroterpenoids and erythritol derivatives isolated from the marine-algal-derived endophytic fungus *Penicillium chrysogenum* XNM-12. *Mar. Drugs* 18:578. doi: 10.3390/md18110578

Yamazaki, H., Takahashi, O., Kirikoshi, R., Yagi, A., Ogasawara, T., Bunya, Y., et al. (2020). Epipolythiodiketopiperazine and trichothecene derivatives from the NaI-containing fermentation of marine-derived *Trichoderma* cf. *brevicompactum*. *J. Antibiot.* 73, 559–567. doi: 10.1038/s41429-020-0314-5

Yan, D. F., Lan, W. J., Wang, K. T., Huang, L., Jiang, C. W., and Li, H. J. (2015). Two chlorinated benzofuran derivatives from the marine fungus *Pseudallescheria boydii*. *Nat. Prod. Commun.* 10, 621–622. doi: 10.1177/1934578X1501000421

Yu, J. Y., Shi, T., Zhou, Y., Xu, Y., Zhao, D. L., and Wang, C. Y. (2021). Naphthalene derivatives and halogenate quinoline from the coral-derived fungus *Trichoderma harzianum* (XS-20090075) through OSMAC approach. *J. Asian Nat. Prod. Res.* 23, 250–257. doi: 10.1080/10286020.2020.1729752

Yun, K., Feng, Z., Choi, H. D., Kang, J. S., and Son, B. W. (2013). New production of (*R*)-(−)-5-bromomellein, a dihydroisocoumarin derivative from the marine-derived fungus *Aspergillus ochraceus*. *Chem. Nat. Compd.* 49, 24–26. doi: 10.1007/s10600-013-0496-1

Zhang, Z., He, X., Liu, C., Che, Q., Zhu, T., Gu, Q., et al. (2016). Clindanones A and B and cladosporols F and G, polyketides from the deep-sea derived fungus *Cladosporium cladosporioides* HDN14-342. *RSC Adv.* 6, 76498–76504. doi: 10.1039/C6RA14640F

Zhang, Y., Li, Z., Huang, B., Liu, K., Peng, S., Liu, X., et al. (2022). Anti-osteoclastogenic and antibacterial effects of chlorinated polyketides from the beibu gulf coral-derived fungus *Aspergillus unguis* GXIMD 02505. *Mar. Drugs* 20:178. doi: 10.3390/md20030178

Zhang, P., Li, X. M., Li, X., and Wang, B. G. (2015). New indole-diterpenoids from the algal-associated fungus *Aspergillus nidulans*. *Phytochem. Lett.* 12, 182–185. doi: 10.1016/j.phytol.2015.03.017

Zhang, Y., Mu, J., Feng, Y., Wen, L., and Han, J. (2014). Four chlorinated depsidones from a seaweed-derived strain of *Aspergillus unguis* and their new biological activities. *Nat. Prod. Res.* 28, 503–506. doi: 10.1080/14786419.2013.879305

Zhang, W., Shao, C. L., Chen, M., Liu, Q. A., and Wang, C. Y. (2014). Brominated resorcylic acid lactones from the marine-derived fungus *Cochliobolus lunatus* induced by histone deacetylase inhibitors. *Tetrahedron Lett.* 55, 4888–4891. doi: 10.1016/j.tetlet.2014.06.096

Zhang, P., Yuan, X. L., Du, Y. M., Zhang, H. B., Shen, G. M., Zhang, Z. F., et al. (2019). Angularly prenylated indole alkaloids with antimicrobial and insecticidal activities from an endophytic fungus *Fusarium sambucinum* TE-6L. *J. Agric. Food Chem.* 67, 11994–12001. doi: 10.1021/acs.jafc.9b05827

frontiers | Frontiers in Microbiology

TYPE Original Research
PUBLISHED 11 October 2022
DOI 10.3389/fmicb.2022.1034779

OPEN ACCESS

EDITED BY
Peng Zhang,
Tobacco Research Institute (CAAS), China

REVIEWED BY
Yin Chen,
University of Warwick, United Kingdom
Guangyi Wang,
Tianjin University, China

*CORRESPONDENCE
Hai-Yan Cao
haiyancao92@126.com
Xiao-Yan Song
xysong@sdu.edu.cn

†These authors have contributed equally to this work

SPECIALTY SECTION
This article was submitted to Antimicrobials, Resistance and Chemotherapy, a section of the journal Frontiers in Microbiology

RECEIVED 02 September 2022
ACCEPTED 23 September 2022
PUBLISHED 11 October 2022

CITATION
Zhang Y-Q, Zhang S, Sun M-L, Su H-N, Li H-Y, Kun-Liu, Zhang Y-Z, Chen X-L, Cao H-Y and Song X-Y (2022) Antibacterial activity of peptaibols from *Trichoderma longibrachiatum* SMF2 against gram-negative *Xanthomonas oryzae* pv. *oryzae*, the causal agent of bacterial leaf blight on rice. *Front. Microbiol.* 13:1034779. doi: 10.3389/fmicb.2022.1034779

Antibacterial activity of peptaibols from *Trichoderma longibrachiatum* SMF2 against gram-negative *Xanthomonas oryzae* pv. *oryzae*, the causal agent of bacterial leaf blight on rice

Yu-Qiang Zhang[1†], Shan Zhang[1†], Mei-Ling Sun[2], Hai-Nan Su[1], Hao-Yang Li[1], Kun-Liu[1], Yu-Zhong Zhang[1,2,3], Xiu-Lan Chen[1,3], Hai-Yan Cao[1*] and Xiao-Yan Song[1*]

[1]State Key Laboratory of Microbial Technology, Marine Biotechnology Research Center, Shandong University, Qingdao, China, [2]College of Marine Life Sciences & Frontiers Science Center for Deep Ocean Multispheres and Earth System, Ocean University of China, Qingdao, China, [3]Laboratory for Marine Biology and Biotechnology, Pilot National Laboratory for Marine Science and Technology, Qingdao, China

Bacterial leaf blight caused by Gram-negative pathogen *Xanthomonas oryzae* pv. *oryzae* (*Xoo*) is one of the most destructive bacterial diseases on rice. Due to the resistance, toxicity and environmental issues of chemical bactericides, new biological strategies are still in need. Although peptaibols produced by *Trichoderma* spp. can inhibit the growth of several Gram-positive bacteria and plant fungal pathogens, it still remains unclear whether peptaibols have anti-*Xoo* activity to control bacterial leaf blight on rice. In this study, we evaluated the antibacterial effects of Trichokonins A (TKA), peptaibols produced by *Trichoderma longibrachiatum* SMF2, against *Xoo*. The *in vitro* antibacterial activity analysis showed that the growth of *Xoo* was significantly inhibited by TKA, with a minimum inhibitory concentration of 54 μg/mL and that the three TKs in TKA all had remarkable anti-*Xoo* activity. Further inhibitory mechanism analyses revealed that TKA treatments resulted in the damage of *Xoo* cell morphology and the release of intracellular substances, such as proteins and nucleic acids, from *Xoo* cells, suggesting the damage of the permeability of *Xoo* cell membrane by TKA. Pathogenicity analyses showed that the lesion

length on rice leaf was significantly reduced by 82.2% when treated with 27 μg/mL TKA. This study represents the first report of the antibacterial activity of peptaibols against a Gram-negative bacterium. Thus, TKA can be of a promising agent in controlling bacterial leaf blight on rice.

KEYWORDS

***Trichoderma longibrachiatum* SMF2, Trichokonins A, *Xanthomonas oryzae* pv. *oryzae*, biological control, bacterial leaf blight (BLB)**

Introduction

Rice (*Oryza sativa*) is one of the most important staple food crops, serving for more than half of the population in the world (Hutin et al., 2016; Laborte et al., 2017). However, its production is severely affected by plant diseases caused by bacteria, fungi, viruses, nematodes and insects. Bacterial leaf blight caused by *Xanthomonas oryzae* pv. *oryzae* (*Xoo*) is one of the most destructive bacterial diseases on rice, which is prevalent in southeast Asia, west Africa, USA and northern Australia, resulting in up to 50% losses of rice production and representing a threat for food security (Niño-Liu et al., 2006; Quibod et al., 2020). *Xoo*, a rod-shaped Gram-negative bacterium, infects any growth stage of rice through hydathodes or wound sites on leaves and then colonizes in the space of epidermis to utilize the nutritional sources, leading to rice tissue necrosis and wilting (González et al., 2012; Ji et al., 2016; Timilsina et al., 2020).

Various management strategies have been used to minimize the loss of rice production caused by bacterial leaf blight. Chemical bactericides, including thiodiazole copper, thiazole zinc, phenazine-1-carboxamide, niclosamide 1,2,3,4-tetrahydro - β-carboline, S-thiazol-2-yl-furan-2-carbothioate, benzothiadiazole and bismerthiazol, were commonly used to control this disease (Shanmugaiah et al., 2010; Fan et al., 2017; Liang et al., 2018; Sahu et al., 2018; Jiang et al., 2019; Liu et al., 2020). In recent years, nano-technological products were considered as alternative strategies to control this disease, such as ZnO, MgO and MnO_2 nanoparticles (Ogunyemi et al., 2020). Moreover, metal nanoparticles biosynthesized with chitosan, *Trichoderma* spp. or *Bacillus cereus* SZT1 also exhibited remarkable anti-*Xoo* activity (Abdallah et al., 2020; Ahmed et al., 2020; Shobha et al., 2020). However, the overuse of chemical bactericides and metal nanoparticles has resulted in environment pollution, increased resistance of pathogens and potential toxin to animals and humans. Therefore, the environmentally friendly and low-toxicity biological strategies have been contemplated as one of the most effective strategies to replace chemical bactericides and metal nanoparticles (Raaijmakers and Mazzola, 2012). To date, some bacterial strains, including *Pesudomonas* spp., *Streptomyces* spp. and *Paenibacillus polymyxa*, have been used as biological control agents to control this disease. Antibiotics produced by these bacterial strains played key roles in controlling this disease, such as phenazine-1-carboxamide from *P. aeruginosa* MML2212, pyoverdine from *P. chlororaphis* YL-1, carbazomycin B from S. roseoverticillatus 63 and fusaricidins P from *P. polymyxa* Sx3 (Shanmugaiah et al., 2010; Abdallah et al., 2019; Liu et al., 2021; Shi et al., 2021). However, effective strategies to control this disease by using biological control fungus is still lacking.

Trichoderma spp. are important fungal biological control agents, frequently living in root, soil, rotten wood and other environments with highly opportunistic potential and adaptability (Druzhinina et al., 2011). Many *Trichoderma* strains, including *T. harzianum*, *T. atroviride* and *T. reesei*, were effective to control soil-borne diseases caused by plant fungal pathogens (Green et al., 1999; Martinez et al., 2008; Seidl et al., 2009). The antimicrobial secondary metabolites (SMs) from *Trichoderma* spp., such as anthraquinones, stigmasterol, koninginins, harzianopyridone, pyrone and peptaibols, played key roles in controlling plant fungal diseases (Schirmböck et al., 1994; Vinale et al., 2006; Khan et al., 2020). Peptaibols are linear peptide antibiotics containing 5 to 20 amino acid residues with an acetylated N-terminus, a C-terminal amino alcohol and a high content of α-amino isobutyric acid (Aib) (Wiest et al., 2002). Antimicrobial activity analysis has revealed that peptaibols, including Trichorzianines, Trichorzins, Harzianines, Tricholongins and Trichotoxins, could effectively inhibit the growth of fungi, Gram-positive bacteria, viruses and nematodes (Bertelsen et al., 2007; Tamandegani et al., 2020). However, no peptaibol has been reported to inhibit Gram-negative bacteria till now.

Trichoderma longibrachiatum SMF2 (*Tl*SMF2) has been reported to produce peptaibols designated as Trichokonins (TKs), including Trichokonins A (TKA) with 20 amino acid residues and Trichokonins B (TKB) with 12 amino acid residues (Xiao-Yan et al., 2006; Zhou et al., 2019). Genome sequencing and gene deletion analysis revealed that the two non-ribosomal peptide synthetase (NRPS) encoding genes, *tlx1* and *tlx2*, are responsible for the biosynthesis of TKA and TKB, respectively (Xie et al., 2015; Zhou et al., 2019). TKs displayed broad-spectrum antimicrobial activity against several Gram-positive

bacteria and plant fungal pathogens, but not against the analyzed Gram-negative bacteria, including *P. aeruginosa*, *Ralstonia solanacearum*, *Erwinia carotovora* and *Escherichia coli* (Xiao-Yan et al., 2006). In addition, although TKs could induce the resistance of Chinese cabbage against the infection caused by the Gram-negative bacterium *Pectobacterium carotovorum* subsp. *carotovorum*, TKs showed no antibacterial activity against this pathogen *in vitro* (Li et al., 2014).

In this study, we reported the antibacterial activity of TKA produced by *Tl*SMF2 against the Gram-negative bacterium *Xoo*. We found that *Tl*SMF2 could significantly inhibit the growth of *Xoo*, but the *tlx1*-deletion mutant strain could not. The purified TKA and its three components all showed remarkable anti-*Xoo* activity. Investigation of the inhibitory mechanism showed that TKA treatments led to the damage of the cell morphology of *Xoo* and the release of intracellular substances, such as proteins and nucleic acids, suggesting the damage of the permeability of cell membrane by TKA. Moreover, the pathogenicity analysis indicated that TKA had significant effect on controlling bacterial leaf blight caused by *Xoo* on rice, suggesting that TKA has the potential to be developed as an effective bio-bactericide to control this disease.

Materials and methods

Strains and culture conditions

The strains used in this study were listed in **Table 1**. *Xoo* and GFP tagged *Xoo* were grown on nutrient agar medium (Bacto^{TM} Peptone 5 g/L, Yeast Extract 1 g/L, Sucrose 10 g/L, Beef extract 3 g/L and agar 15 g/L) at 28°C, or in the nutrient broth medium (Qian et al., 2013). The strains of WT, Δ*tlx1*, Δ*tlx2* and Δ*tlx1*&*tlx2* were grown on potato dextrose agar medium (fresh potato 200 g/L, Glucose 20 g/L and 15 g/L) at 28°C, or in the potato dextrose broth medium (Xiao-Yan et al., 2006). The mutants of *Tl*SMF2, Δ*tlx1*, Δ*tlx2* and Δ*tlx1*&*tlx2* were previously constructed (Zhou et al., 2019). The GFP tagged *Xoo* was previously constructed (Zhang et al., 2019).

Extraction of secondary metabolites produced by *Tl*SMF2 and purification of Trichokonins A and its components

In order to extract the SMs, 0.25 cm2 plate of the mycelium margin of the WT, Δ*tlx1*, Δ*tlx2* or Δ*tlx1*&*tlx2* strain of *Tl*SMF2 was grown on the plate containing 15 mL potato dextrose agar medium for 12 days, and then the potato dextrose agar medium was dipped into 200 mL ethanol for 24 h. The mixture was centrifuged at 10,000 g, and the supernatant was collected and was dried by using freeze-drying. The dried SMs were dissolved with 2 mL methanol, which were used for the analysis of the anti-*Xoo* activity.

TKA and Trichokonin VI (TK VI), Trichokonin VII (TK VII) and Trichokonin VIII (TK VIII) were purified and identified as previously described (Xiao-Yan et al., 2006; Zhou et al., 2019). Briefly, approximately 2×10^7 spores of the WT strain were inoculated into 100 mL potato dextrose broth medium in a 500 mL flask, which were cultured at 28°C with shaking at 180 rpm for 12 days. Then the potato dextrose broth culture was centrifuged at 10,000 *g*, and the collected supernatant (40 mL) was loaded on a Cleanert C18 SPE Cartridge, and the TKA was eluted by 2 mL methanol. The eluted TKA was furtuer purified by using HPLC on a reversed phase analytical column (Shimadzu, Japan) that were eluted with methanol/ddH_2O (84:16, v/v) at a flow rate of 1.0 mL/min. The chromatogram was monitored at 203 nm. TKs VI, VII and VIII were collected together as purified TKA, or collected separately as purified TKs VI (retention time 17.35 min), VII (retention time 20 min) and VIII (retention time 22.5 min) according to previous identification (Xiao-Yan et al., 2006). The purified TKA and each TKA component (TKs VI, VII or VIII) were dried by using freeze-drying. The purified TKA and each component were dissolved in methanol at a concentration of 10 mg/mL as stock solution. The stock solution was filter-sterilized (0.22 μm) and then used for the analysis of their anti-*Xoo* activities.

Analysis of the anti-*Xoo* activity

The anti-*Xoo* activity of *Tl*SMF2 was analyzed by using the method described previously by Dos et al. with some modification (Dos Santos et al., 2015). Briefly, 0.25 cm^2 plate of the mycelium margin of the WT, Δ*tlx1*, Δ*tlx2* or Δ*tlx1*&*tlx2* was transferred to the center of a test plate containing 15 mL nutrient agar medium or to a 250 mL flask containing 50 mL nutrient broth medium, both of which contained *Xoo* at 1×10^7 CFU/mL. The co-cultures were incubated at 28°C with (for nutrient broth medium) or without (for nutrient agar medium) shaking at 180 rpm for 2 to 6 days. The antagonistic circle around the colony of *Tl*SMF2 or its mutants on the test plate was observed, and the OD_{600} of the lens cleaning tissue filtered liquid culture was recorded.

The anti-*Xoo* activities of SMs, TKA and TKs VI, VII and VIII were analyzed using agar well-diffusion assay as described previously with some modification (Nanda and Saravanan, 2009). Briefly, *Xoo* was cultured in nutrient broth medium to 1×10^7 CFU/mL, and 200 μL suspension of *Xoo* was spread on nutrient agar medium in a test plate containing 15 mL nutrient agar medium by using a sterile triangular glass coating rod. Then, the wells of 5 mm diameter were loaded on the surface of the test plate and the extracted SMs (20 μL, 40 μL, 60 μL, and 80 μL), 80 μg of TKA and TKs VI, VII and VIII were poured into the wells. The test plate was incubated

TABLE 1 Strains used in this study.

Strains	Function	References
*Tl*SMF2	Wild type strain	Xiao-Yan et al., 2006
Δ*tlx1*	The *tlx1* gene deletion mutant strain of *Tl*SMF2	Zhou et al., 2019
Δ*tlx2*	The *tlx2* gene deletion mutant strain of *Tl*SMF2	Zhou et al., 2019
Δ*tlx1*&*tlx2*	The *tlx1* and *tlx2* gene double deletion mutant strain of *Tl*SMF2	Zhou et al., 2019
Xoo PXO99^{A}	Philippine race 6	Salzberg et al., 2008
Xoo-GFP	*Xoo* PXO99^{A} harboring plasmid pUFZ75 (GFP-tagged strain), Km^{R}	Zhang et al., 2019

Km^{R}, kanamycin resistance.

at 28°C for 3 days, and the diameter of the inhibition zone was recorded. Moreover, 5 × 10^8 *Xoo* cells were inoculated into 250 mL flask containing 50 mL nutrient broth medium containing the extracted SMs (0.2%, 0.4%, 0.6%, and 0.8%, v/v), and were incubated with shaking (180 rpm) at 28°C for 48 h, and the OD_{600} of the culture was recorded every 2 h. Methanol (0.8%, v/v) was used as the negative control. Three replicates were performed in each treatment, and the experiment was repeated three times.

Determination of minimum inhibitory concentration

The MICs of TKA and TKs VI, VII and VIII against *Xoo* were determined using the method as described previously with some modification (Du et al., 2020). Briefly, 2 × 10^6 *Xoo* cells were inoculated into the column of a 96-well plate containing 200 μL nutrient broth medium, and different concentration (0 to 100 μg/mL) of TKA or TKs VI, VII or VIII was added to the 200 μL nutrient broth medium. The 96-well plate was incubated at 28°C for 2 days. The OD_{600} of the culture was recorded every 2 h using Bioscreen C optical growth analyzer (Bioscreen, Finland) to assess the growth of *Xoo*. The lowest concentration of TKA or TKs VI, VII or VIII that completely inhibited the growth of *Xoo* was regarded as the MIC. The results were further confirmed by repeating the experiment in 30 mL bottles containing with 8 × 10^7 *Xoo* cells in 8 mL nutrient broth medium with different concentrations (0 to 100 μg/mL) of TKA or TKs VI, VII or VIII at 28°C for 2 days. Methanol (1.2%, v/v) was used as the negative control. Three replicates were performed in each treatment, and the experiment was repeated three times.

Transmission electron microscopy observation of *Xoo*

The cell morphology of *Xoo* was observed using transmission electron microscopy as described previously with some modification (Erdmann et al., 2017). *Xoo* was cultured in nutrient broth medium to 1 × 10^9 CFU/mL. The cells were collected by centrifugation at 6,000 *g* for 5 min, and then were washed with sterile ddH_2O for three times. The cells were suspended in sterile ddH_2O, and were treated with 54 μg/mL TKA at 28°C for 24 h. After treatment, 5 μL cell preparation was adsorbed onto the carbon-coated copper grids for 1.5 min, and then the cells were stained with 2% uranyl acetate for 30 s. Images were pictured by using transmission electron microscopy (JEOL, Japan). Methanol (0.3%, v/v) treatment was used as the negative control. At least 50 *Xoo* cells were detected in each treatment. Three replicates were performed in each treatment, and the experiment was repeated three times.

Atomic force microscopy observation of *Xoo*

The cell morphology of *Xoo* was observed using atomic force microscopy with a previously described method with some modification (Tang et al., 2020). Cell preparations with 1 × 10^9 CFU/mL were obtained as described in the method of TEM observation. After treated with 54 μg/mL TKA at 28°C for 24 h, 2.5 μL cell preparation was deposited onto freshly cleaved mica and was dried in a chamber at room temperature. Atomic force microscopy was performed using a Multimode VIII AFM with Nanoscope V controller (Bruker AXS, Germany), and images were pictured in the scanasyst mode under air condition. Methanol (0.3%, v/v) treatment was used as the negative control. At least 50 *Xoo* cells were detected in each treatment. Three replicates were performed in each treatment, and the experiment was repeated three times.

Detection of the release of intracellular substances from *Xoo* cells treated by Trichokonins A

The method to detect the release of intracellular substances from cells was carried out as previously described with

some modification (Liang et al., 2020). Cell preparations with 1×10^9 CFU/mL were obtained as described in the method of TEM observation. After treated with 54 μg/mL TKA at 28°C for 24 h, the OD_{600} of the culture was recorded, and the supernatant was collected by centrifugation at 8,000 *g* for 5 min. The concentration of nucleic acids in the supernatant was measured by recording the absorbance of the supernatant at 260 nm using NanoDrop™ One (Thermo Scientific, USA). The supernatant was concentrated (1:20) by using a 3, 000 Da ultrafilter tube (Merck Millipore, USA), and then the concentration of protein in the concentrated supernatant was measured by using Pierce BCA Protein Assay Kit (Thermo Scientific, USA) with bovine serum albumin as the standard.

The GFP tagged *Xoo* cells were prepared and treated with TKA using the same method as WT *Xoo*. The concentration of released GFP protein in the supernatant of GFP tagged *Xoo* cells was detected by Western blot using the method described previously with some modification (Shi et al., 2019). Proteins were separated by SDS-PAGE at 90 V for 30 min, and then at 120 V for 90 min. Proteins in the gel were transferred onto PVDF membrane at 120 mA for 60 min. The PVDF membrane was incubated in the blocking buffer for 1 h, and then in a new blocking buffer containing the primary antibody (GFP-Tag Mouse mAb, 1: 5000, Abmart, China) for 2 h, followed by an incubation in a new blocking buffer containing the secondary antibody (Goat Anti-Rabbit$Mouse IgG-HRP, 1: 5000, Abmart, China) for 1 h. After that, the PVDF membrane was stained with the Super ECL Plus kit and imaged using FluorChem M (Alpha Innotech, USA). Methanol (0.3%, v/v) treatment was used as the negative control. Three replicates were performed in each treatment, and the experiment was repeated three times.

Pathogenicity analysis

The pathogenicity of *Xoo* on rice was analyzed with the method as described previously with some modification (Zhang et al., 2019). Briefly, the susceptible rice cultivar IR24 was planted in greenhouse under a cycle of light at 28°C for16 h and dark at 25°C for 8 h. The 4 weeks old rice seedlings were dipped into water containing TKA at the concentration of 13.5 μg/mL, 27 μg/mL or 54 μg/mL for 2 days. After that, the rice leaves were inoculated with *Xoo* cells suspension in sterile distilled water (OD_{600} = 0.5) by the method of leaf-clipping. Moreover, TKA at the concentration of 13.5 μg/mL, 27 μg/mL or 54 μg/mL also was sprayed to the *Xoo*-inoculated rice leaves on the 5^{th} and the 10^{th} day. Lesion lengths on the rice leaves were measured after 14 days from the inoculation. Methanol (0.3%, v/v) was used as the negative control. At least 50 rice leaves were inoculated in each treatment. Three replicates were performed in each treatment, and the experiment was repeated three times.

Data analysis

All analysis was conducted by using SPSS 14.0 (SPSS Inc., Chicago, IL, USA). Significant differences were determined *via* the hypothesis test of percentages (*t*-test) (** $p < 0.01$).

Results

*Tl*SMF2 and its secondary metabolites exhibited anti-*Xoo* bacterial activity

To investigate whether *Tl*SMF2 has anti-*Xoo* activity, they were co-cultured on nutrient agar medium. An antagonistic circle could be clearly observed around the margin of *Tl*SMF2 after co-cultured for 2 to 6 days (**Figure 1A**), indicating that *Tl*SMF2 likely produced SMs to inhibit the growth of *Xoo*. Then, the SMs produced by *Tl*SMF2 were extracted and the anti-*Xoo* activity of the SMs extract was analyzed. Compared with the negative control of methanol, inhibition zones could be clearly seen on the test plate and their diameter ranged from 2.19 to 2.99 cm when *Xoo* was treated with the SMs extract from 20 to 80 μL (**Figure 1B**). Correspondingly, the growth of *Xoo* in nutrient broth liquid medium was severely inhibited by the addition of 0.2 to 0.6% (v/v) SMs extract, and almost complete inhibited by the addition of 0.8% (v/v) (**Figure 1C**). These results indicated that one or more SMs produced by *Tl*SMF2 had anti-*Xoo* activity.

The anti-*Xoo* activity of *Tl*SMF2 was attributed to Trichokonins A

Because TKs have been shown to be a kind of antimicrobial peptides in the SMs produced by *Tl*SMF2 (Xiao-Yan et al., 2006), we speculated that the TKs produced by *Tl*SMF2, TKA and/or TKB, may have anti-*Xoo* activity. To test this hypothesis, we analyzed the anti-*Xoo* activities of the wild-type strain of *Tl*SMF2 and its gene-deletion strains Δ*tlx1*, Δ*tlx2,* and Δ *tlx1*&*tlx2* previously constructed (Zhou et al., 2019). On potato dextrose agar plates, the three mutant strains displayed similar growth rate to wild-type *Tl*SMF2 (**Figure 2A**), suggesting that gene deletion had little impact on the growth of these mutants. On the co-culture plates containing nutrient agar medium, Δ*tlx2* formed an antagonistic circle with a size similar to that of WT, but Δ*tlx1* and Δ*tlx1*& *tlx2* both formed a negligible one, indicating that Δ*tlx1* and Δ*tlx1*& *tlx2* almost completely lost the anti-*Xoo* activity, but Δ*tlx2* still retained this activity (**Figure 2B**). This was further supported by co-culture in nutrient broth liquid medium. After 48 h co-culture of *Xoo* with WT or its mutants, the OD_{600} of the control (containing only *Xoo*) and the co-cultures of *Xoo* with Δ*tlx1*

10.3389/fmicb.2022.1034779

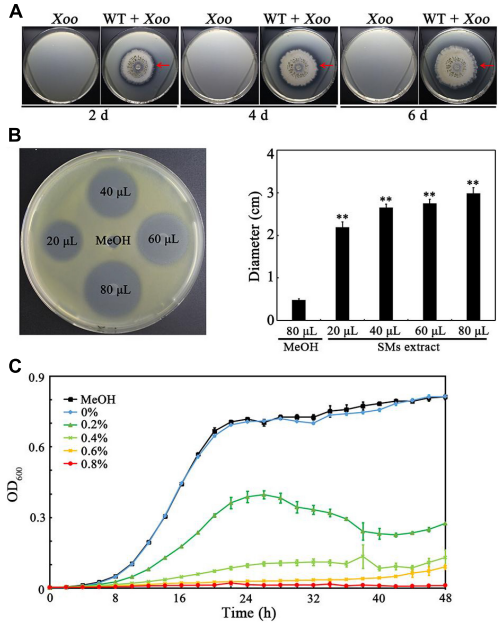

FIGURE 1

Determination of the anti-*Xoo* activities of *Tl*SMF2 and its SMs. **(A)** The representative anti-*Xoo* activity of *Tl*SMF2 on the test plates containing nutrient agar medium after co-cultured for 2, 4 and 6 days. **(B)** The representative *Xoo*-inhibition zones of the SMs extracted from *Tl*SMF2 on the test plate containing nutrient agar medium (left) and the diameters of the zones (right). The diameters were data from three repeats (mean ± S.D.). Asterisk indicates significant difference compared with the control of MeOH (** means $P < 0.01$). **(C)** The growth of *Xoo* in nutrient broth medium containing different volume of the SMs (0%, 0.2%, 0.4%, 0.6%, and 0.8%, v/v) extracted from *Tl*SMF2. MeOH, the nutrient broth medium containing methanol (0.8%, v/v). The graph shows data from triplicate experiments.

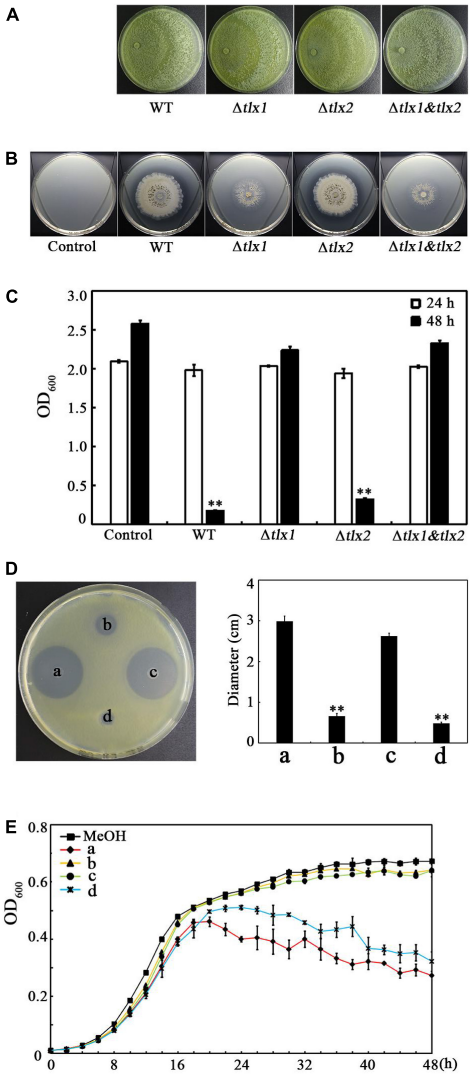

FIGURE 2

Effect of the gene *tlx1* and *tlx2* deletion on the anti-*Xoo* activity of *Tl*SMF2. **(A)** Growth of the WT *Tl*SMF2 and its mutants on the test plates containing potato dextrose agar medium after cultured for 4 days. The picture shows a representative of three repeats. **(B)** The representative anti-*Xoo* activities of the WT *Tl*SMF2 and its mutants on the test plates containing nutrient agar medium after co-cultured for 6 days. **(C)** The OD_{600} of the co-cultures with the WT *Tl*SMF2 and its mutants after 24 and 48 h. Control: *Xoo* cultured without WT *Tl*SMF2 or its mutants. WT, the co-culture of *Xoo* with WT *Tl*SMF2. Δ*tlx1*, Δ*tlx2* and Δ*tlx1*&*tlx2*, the co-cultures of *Xoo* with the mutant strains Δ*tlx1*, Δ*tlx2* and Δ*tlx1*& *tlx2*, respectively. **(D)** The representative *Xoo*-inhibition zones of the SMs extracted from WT *Tl*SMF2 and its mutants on the test plate containing nutrient agar medium (left) and the diameters of the zones (right). a, b, c and d represent the SMs produced by strains WT *Tl*SMF2 (a), Δ*tlx1*(b), Δ*tlx2* (c) and Δ*tlx1*&*tlx2* (d), respectively. The diameters were data from three repeats (mean ± S.D.). Asterisk indicates significant difference compared with the control of MeOH (** means $P < 0.01$). **(E)** The growth of *Xoo* in nutrient broth medium containing the SMs (0.8%, v/v) extracted from the WT *Tl*SMF2 and its mutants. MeOH, the nutrient broth medium containing methanol (0.8%, v/v). The graphs show data from triplicate experiments.

or Δ*tlx1*&*tlx2* all reached to approximately 2.5, but those of the co-cultures of *Xoo* with WT and Δ*tlx2* were only 0.18 and 0.32, respectively (Figure 2C), indicating that the growth of *Xoo* was significantly inhibited by WT or Δ*tlx2*, but not by Δ*tlx1* or Δ*tlx1*&*tlx2*. Because gene *tlx1* encodes TKA and gene *tlx2* encodes TKB in *Tl*SMF2 (Zhou et al., 2019), these results suggested that the anti-*Xoo* activity of *Tl*SMF2 was mainly attributed to the production of TKA in its SMs. This was also supported by analyzing the anti-*Xoo* activities of the SMs from WT and its mutants in solid and liquid culture. On the test plate containing nutrient agar medium, the SMs from WT and Δ*tlx2* showed noticeable inhibition zones, but those from Δ*tlx1* or Δ*tlx1*&*tlx2* did not (Figure 2D). In nutrient broth liquid culture, the SMs from WT and Δ*tlx2* both showed a noticeable inhibitory effect on the growth of *Xoo*, but those from Δ*tlx1* or Δ*tlx1*&*tlx2* did not (Figure 2E).

To confirm the anti-*Xoo* activity of TKA, we purified TKA (Figure 3A) and analyzed its anti-*Xoo* activity. The purified TKA showed remarkable anti-*Xoo* activity on the test

10.3389/fmicb.2022.1034779

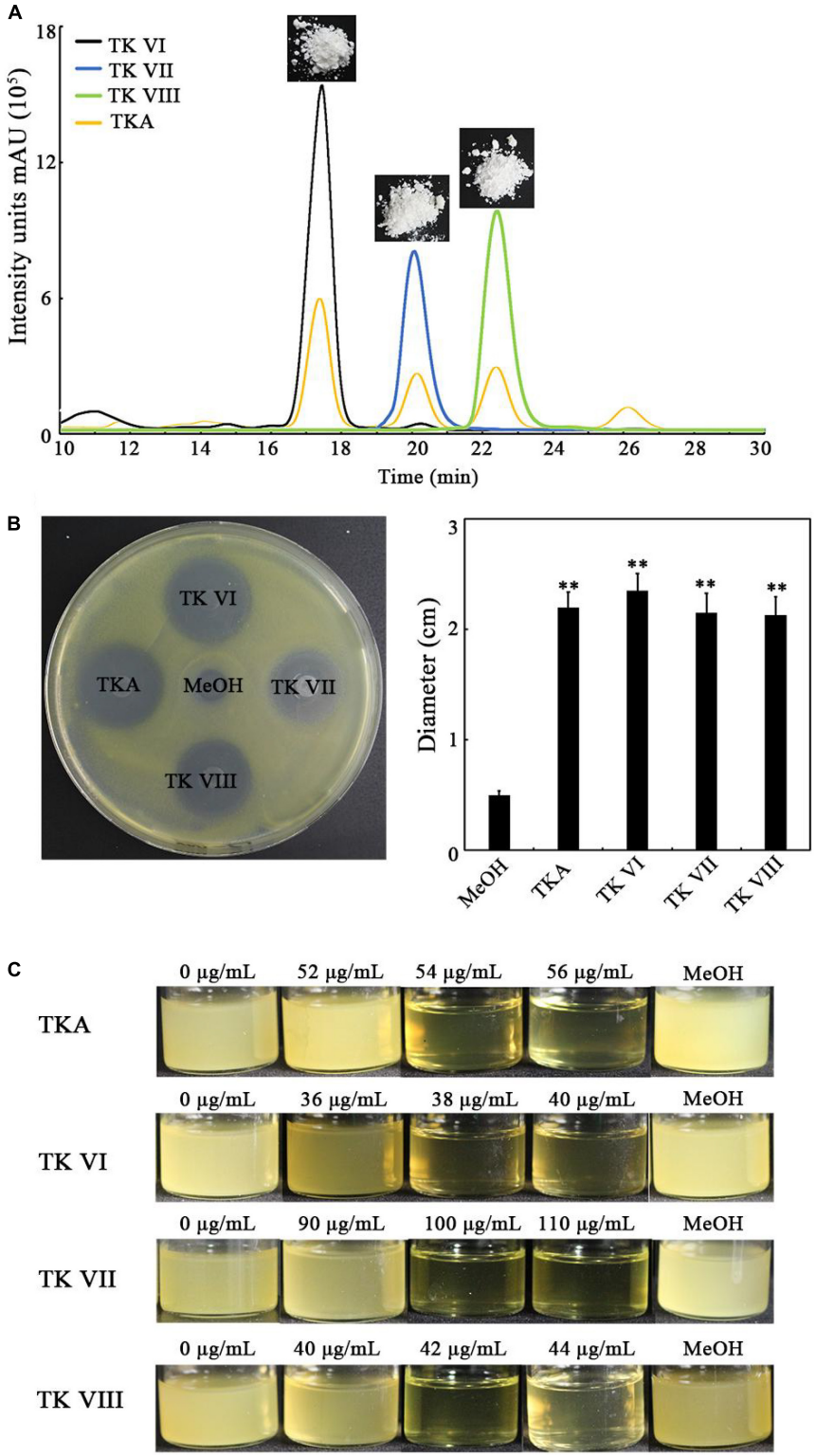

FIGURE 3
Determination of the anti-*Xoo* activities of TKA and TKs VI, VII and VIII. **(A)** The representative purified TKA and TKs VI, VII and VIII detected by using HPLC. **(B)** The representative *Xoo*-inhibition zones of 80 μg TKA and TKs VI, VII and VIII on the test plate containing nutrient agar medium (left) and the diameters of the zones (right). The diameters were data from triplicate experiments (mean ± S.D.). Asterisk indicates significant difference compared with the control of MeOH (** means $P < 0.01$). **(C)** The growth of *Xoo* in 8 mL nutrient broth medium containing different concentrations (0 to 110 μg/mL) of TKA or TKs VI, VII or VIII, respectively. MeOH, the nutrient broth medium containing methanol (1.2%, v/v).

plate (Figure 3B). It has been reported the TKA produced by *Tl*SMF2 contained three TKs, that is, TKs VI, VII and VIII (Xiao-Yan et al., 2006). We then purified the three TKs of TKA separately (Figure 3A) and tested their anti-*Xoo* activities. As shown in Figure 3B, the three TKs all showed remarkable anti-*Xoo* activity. To further compare their anti-*Xoo* activities, we determined the MIC of TKA and TKs VI, VII and VIII against *Xoo* by monitoring their inhibitory effects on the growth of *Xoo* under different concentrations. The MIC of TKA against *Xoo* was 54 μg/mL. Compared with TKA, both TKs VI and VIII showed a stronger anti-*Xoo* activity, with the MICs at 38 μg/mL and 42 μg/mL, respectively, but the anti-*Xoo* activity of TK VII was much weaker, with the MIC at 100 μg/mL (Figure 3C). Thus, TK VI had the strongest anti-*Xoo* activity among the three components of TKA.

Trichokonins A treatment led to the damage of the *Xoo* cell morphology and the release of intracellular substances

Cell morphology is fundamental for the cellular functions (Fukuda et al., 2021). To investigate whether TKA affects the cell morphology of *Xoo, Xoo* cells treated with TKA or methanol (as a negative control) was observed by using transmission electron microscopy and atomic force microscopy. The result of transmission electron microscopy observation showed that, after treated with 54 μg/mL TKA for 24 h, 96% *Xoo* cells displayed distorted and irregular morphology, with separated cell membrane from the cell envelop and intracellular permeated uranyl acetate, suggesting the damage

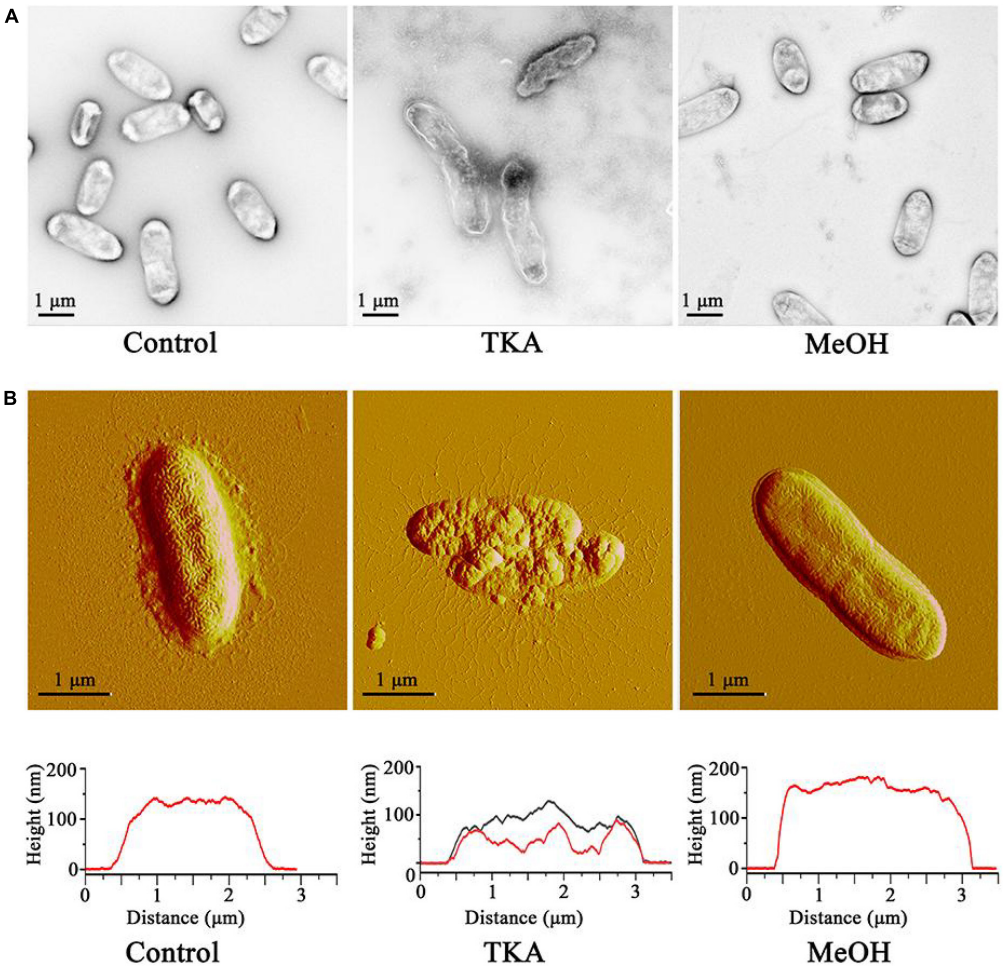

FIGURE 4
Effect of TKA on the cell morphology of *Xoo*. **(A)** Morphology of representative *Xoo* cells observed by using transmission electron microscopy. **(B)** Morphology (up) and height (down) of representative *Xoo* cells observed by using atomic force microscopy. Control, a representative of *Xoo* cells untreated with methanol or TKA. TKA, two representative of *Xoo* cells treated with 54 μg/mL TKA for 24 h. MeOH, a representative of *Xoo* cells treated with methanol (0.3%, v/v) for 24 h. Fifty *Xoo* cells were observed in each treatment. Each treatment was repeated three times.

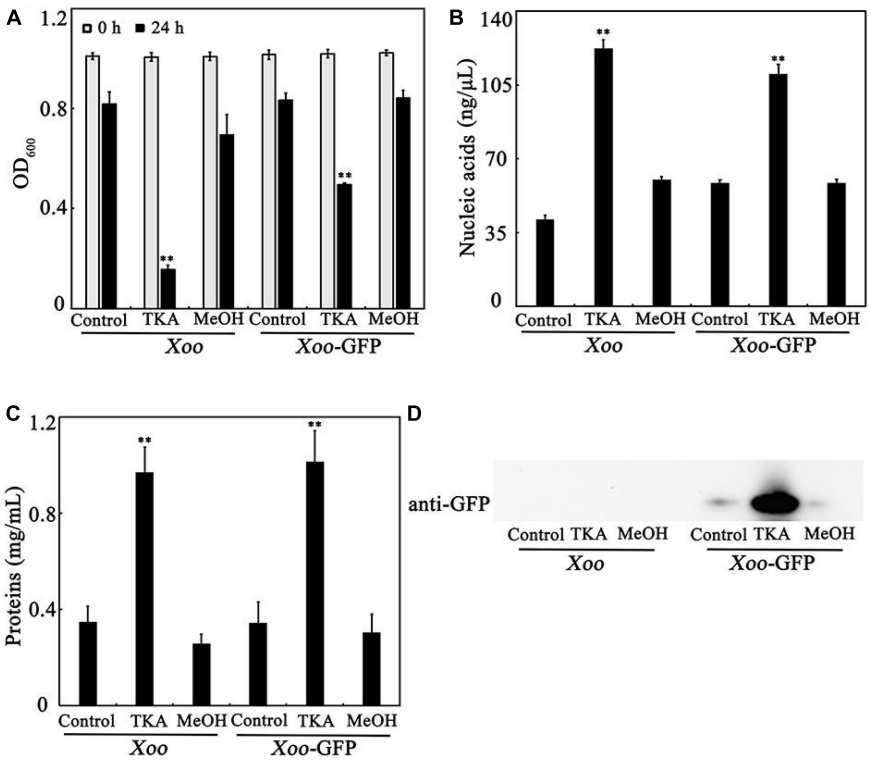

FIGURE 5
Effect of TKA on the release of intracellular substances from *Xoo* cells. **(A)** The OD_{600} of the cultures of WT *Xoo* and GFP tagged *Xoo* (*Xoo*-GFP) in ddH_2O incubated at 28°C with or without TKA for 0 and 24 h. **(B)** The concentration of nucleic acids in the supernatants of the cultures of WT *Xoo* and GFP tagged *Xoo* incubated with or without TKA for 24 h. **(C)** The concentration of total proteins in the supernatants of the cultures of WT *Xoo* and GFP tagged *Xoo* incubated with or without TKA for 24 h. **(D)** Western blot detection of the GFP protein in the supernatants of the cultures of WT *Xoo* and GFP tagged *Xoo* incubated with or without TKA for 24 h. Control, WT *Xoo* and GFP tagged *Xoo* incubated without methanol or TKA. TKA, WT *Xoo* and GFP tagged *Xoo* incubated with 54 μg/mL TKA. MeOH, WT *Xoo* and GFP tagged *Xoo* incubated with methanol (0.3%, v/v). The graphs show data from triplicate experiments (mean ± S.D.). The picture in D is a representative of three repeats. Asterisk indicates significant difference compared with the control (** means $P < 0.01$).

of the cell membrane permeability. In contrast, the cells treated with methanol all displayed intact, normal morphology, with uranyl acetate being attached on the cell surface (Figure 4A). Correspondingly, the atomic force microscopy observation showed that the *Xoo* cells untreated and those treated with methanol displayed similar intact and smooth surfaces and height, but those treated with 54 μg/mL TKA for 24 h were clearly destroyed, with roughed surfaces and significantly decreased height (Figure 4B). In addition, it seemed that intracellular substances were released from the *Xoo* cells treated with 54 μg/mL TKA based on the atomic force microscopy observation (Figure 4B).

To confirm the effects of TKA treatment on the intracellular substances, *Xoo* cells were treated with 54 μg/mL TKA for 24 h, and then the cell density (OD_{600}) and the concentrations of nucleic acids and proteins in the supernatant were determined and compared to those untreated or treated with methanol. After TKA treatment, the OD_{600} of the cell suspension reduced 84.4%, but that treated with methanol reduced only 19.2%, similar to that untreated with TKA or methanol (Figure 5A), which indicated the damage of *Xoo* cells by TKA. The concentration of both nucleic acids and proteins in the supernatant of *Xoo* cells treated with TKA were significantly higher (approximately 3 folds and 5 folds, respectively) than those in the supernatant of *Xoo* cells untreated or treated with methanol (Figures 5B,C), suggesting that TKA treatment led to much more release of intracellular nucleic acids and proteins from *Xoo* cells. To further confirm the effects of TKA, the endogenously expressed GFP protein was used as an indicator to investigate the leakage of intracellular substances. Similar to the case in WT *Xoo,* TKA treatment led to significant decrease in the cell number of GFP tagged *Xoo* and significant increase in the release of intracellular nucleic acids and proteins (Figures 5A–C). Moreover, a large concentration of GFP protein was detected by western blot in the supernatant of the GFP tagged *Xoo* cells treated with TKA for 24 h, but only trace concentration of GFP protein was detected in the supernatant of the GFP tagged *Xoo* cells untreated or treated with methanol (Figure 5D), indicating the severe leakage of intracellular GFP protein

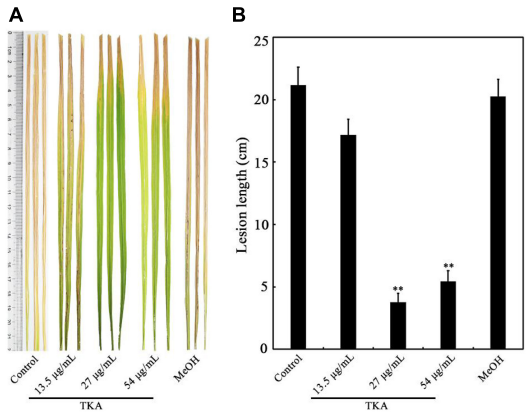

FIGURE 6
Effect of TKA on the pathogenicity of *Xoo* on rice. **(A)** The representative lesion lengths on the leaves of the *Xoo*-inoculated rice seedlings of cultivar IR24 treated with different concentration of TKA (13.5 μg/mL, 27 μg/mL and 54 μg/mL) in greenhouse for 14 days. At least 50 rice leaves were recorded in each treatment. Each treatment was repeated three times. **(B)** The lesion lengths on the leaves of the *Xoo*-inoculated rice seedlings of cultivar IR24 treated with different concentration of TKA (13.5 μg/mL, 27 μg/mL and 54 μg/mL) in greenhouse for 14 days. The graph shows data from triplicate experiments (mean ± S.D.). Asterisk indicates significant difference compared with the control of MeOH (** means $P < 0.01$). Control, the *Xoo*-inoculated rice seedling leaves of cultivar IR24 untreated with methanol or TKA. MeOH, the *Xoo*-inoculated rice seedling leaves of cultivar IR24 treated with methanol (0.3%, v/v).

from *Xoo* cells treated with TKA. Altogether, these results demonstrated that TKA treatment led to the severe release of intracellular substances from *Xoo* cells, suggesting that the permeability of the cell membrane of *Xoo* was likely destroyed by TKA.

Trichokonins A reduced the pathogenicity of *Xoo* on rice

Because TKA showed remarkable anti-*Xoo* activity, the role of TKA in controlling bacterial leaf blight on rice caused by *Xoo* was further evaluated by pathogenicity analysis. The lesion length on the leaf of rice untreated with TKA or methanol was approximately 21.2 cm, which was approximately 20.3 cm on that treated with methanol. In contrast, when the rice was treated with 13.5 μg/mL, 27 μg/mL and 54 μg/mL TKA, the lesion length on rice leaf was reduced to approximately 17.2 cm, 3.8 cm and 5.4 cm, respectively. The calculated protective efficiency was approximately 18.8%, 82.2% and 74.3% when the rice was treated with 13.5 μg/mL, 27 μg/mL and 54 μg/mL TKA, respectively (**Figure 6**). This result showed that TKA could reduce the pathogenicity of *Xoo* on rice, and that 27 μg/mL TKA had the best protective efficiency.

Discussion

Peptaibols are a class of linear peptides mainly produced by *Trichoderma* and *Emericellopsis* (Daniel and Filho, 2007). Studies have shown that peptaibols exhibited broad-spectrum antimicrobial activity against several Gram-positive bacteria and plant fungal pathogens. For example, TKs exhibited broad-spectrum antimicrobial activity against *B. subtilis*, *S. aureus* and *Fusarium oxysporum* (Xiao-Yan et al., 2006). Trichotoxins showed antibacterial activity against *B. stearothermophilus* (Chutrakul et al., 2008). Emericellipsin A showed significant inhibitory activity against *Aspergillus niger* ATCC 16404 and *Candida albicans* ATCC 14053 (Kuvarina et al., 2021). A recent study found that water-soluble trichogin GA IV-derived peptaibols inhibited the growth of plant fungal pathogens, such as *Botrytis cinerea*, *F. graminearum*, *Penicillium expansum* and *Pyricularia oryzae* (Baccelli et al., 2022). However, there has been no peptaibol being shown to have antibacterial activity against Gram-negative bacteria. In this study, we found that TKA from *Tl*SMF2 showed significant antibacterial activity against the Gram-negative bacterium *Xoo*. Moreover, the three Trichokonins in TKA, including TKs VI, VII and VIII, all showed remarkable anti-*Xoo* activity. Notably, the MIC of TK VII against *Xoo* was much higher than those of TKs VI and VIII, which may be caused by the amino acid difference in their sequences. The 17^{th} amino acid residue is Iva in TK VII, but is Aib in TK VI and VIII. Further study needs to be conducted to decipher this difference. In addition, whether TKA has antibacterial activity against other Gram-negative bacterial pathogens awaits further investigation.

Most peptaibols are membrane-active compounds with the ability to form multimeric ion channels in lipid bilayer membranes (Chugh et al., 2002; Marik et al., 2019). This is considered to be the main antimicrobial mechanism of peptaibols. The pore formation in the membranes eventually results in the leakage of intracellular substances (Milov et al., 2016). For example, emericellipsin A disrupted the cells membrane of *Staphylococcus aureus*, resulting in the influx of propidium iodide into cells (Rogozhin et al., 2018). In our previous studies, TK VI could induce the autophagy through an influx of Ca^{2+} to inhibit the growth of HepG2 cancer cells (Shi et al., 2012). Moreover, TK VI could change the cell morphology of plant fungal pathogen *F. oxysporum* and induce the production of reactive oxygen species to inhibit its growth (Shi et al., 2010). In this study, consistent with the effect of emericellipsin A, we found the application of TKA led to clearly changed cell morphology of *Xoo* and significant release of intracellular substances from *Xoo* cells, such as nucleic acids and proteins. Thus, TKA likely adopts the similar antimicrobial strategy against *Xoo* as other peptaibols against Gram-positive bacteria, fungi and mammal cells, which rupture the integrity of *Xoo* cell membrane and promotes the cell leakage, thereby leading to the morphology change and the cell death.

In our previous study, we found that TKs from *Tl*SMF2 controlled the tobacco mosaic virus by increasing the production of reactive oxygen species and phenolic compounds, as well as enhancing the expression of pathogenesis-related genes (Luo et al., 2010). Moreover, TKs from *Tl*SMF2 also could enhance the resistance of Chinese cabbage against the infection of pathogen through inducing the production of reactive oxygen species and the expression of pathogenesis-related genes (Li et al., 2014). In addition, Viterbo et al. (2007) found that the application of two synthetic 18-amino-acid peptaibol isoforms (TvBI and TvBII) from *T. virens* strain Gv29-8 induced the expression of plant resistance related enzymes, including hydroxyperoxide lyase, phenylalanine ammonia lyase and peroxidase, to against the infection of *P. syringae* pv. *lachrymans* on cucumber seedlings. Therefore, the induced plant resistance against pathogens also plays an important role in the control of plant diseases by peptaibols. In this study, we found the pathogenicity of *Xoo* on rice significantly reduced after the application of TKA at the concentration of 27 μg/ml, only half of the MIC of TKA against *Xoo*. It would be an interesting topic for the future investigation to understand the underlined molecular mechanisms of TKA eliciting resistance response in rice. In recent years, some microbial SMs have been used to against *Xoo* and to decrease the incidence of bacterial leaf blight on rice. For example, staurosporine produced by *Streptomyces* sp. MJM4426 inhibited the growth of *Xoo* with the MIC at 200 μg/mL (Cheng et al., 2016). Difficidin and bacilysin produced by *B. amyloliquefaciens* FZB42 also exhibited anti-*Xoo* activity, and the protective rates to bacterial leaf blight reached to 58.82% and 72.31% with the concentration at 50 μg/mL, respectively (Wu et al., 2015). Decyl alcohol and 3,5,5-trimethylhexanol produced by *Bacillus* strain D13 inhibited the growth of *Xoo* with the MIC at 480 μg/mL and 2.4 mg/mL, respectively (Xie et al., 2018). In this study, we found the MIC of TKA produced by *Tl*SMF2 against *Xoo* was 54 μg/mL, and that 82.2% protective rate could be achieved with TKA at the concentration of 27 μg/mL. However, the protective rate decreased to 74.3% at the concentration of 54 μg/mL, suggesting that the excess of TKA may be toxic to rice. The high protective rate indicates that TKA can be of a promising agent in controlling bacterial leaf blight on rice.

Data availability statement

The original contributions presented in this study are included in the article/supplementary material, further inquiries can be directed to the corresponding authors.

Author contributions

X-YS and H-YC: conceptualization. H-YL: extraction of SMs. Kun-Liu: purification of TKs. M-LS: TEM observation. H-NS: AEM observation. Y-QZ: analysis of anti-*Xoo* activity and pathogenicity and writing – original draft preparation. SZ, X-LC, and Y-ZZ: writing – review and editing. All authors have read and agreed to the published version of the manuscript.

Funding

This work was supported by grants from the National Natural Science Foundation of China (Grant Nos. 31971535 and 31961133016), and the China Postdoctoral Science Foundation (Grant No. 2021M691960).

Conflict of interest

The authors declare that the research was conducted in the absence of any commercial or financial relationships that could be construed as a potential conflict of interest.

Publisher's note

All claims expressed in this article are solely those of the authors and do not necessarily represent those of their affiliated organizations, or those of the publisher, the editors and the reviewers. Any product that may be evaluated in this article, or claim that may be made by its manufacturer, is not guaranteed or endorsed by the publisher.

References

Abdallah, Y., Liu, M., Ogunyemi, S. O., Ahmed, T., Fouad, H., Abdelazez, A., et al. (2020). Bioinspired Green Synthesis of Chitosan and Zinc Oxide Nanoparticles with Strong Antibacterial Activity against Rice Pathogen *Xanthomonas oryzae* pv. *oryzae*. *Molecules* 25:4795. doi: 10.3390/molecules25204795

Abdallah, Y., Yang, M., Zhang, M., Masum, M., Ogunyemi, S. O., Hossain, A., et al. (2019). Plant growth promotion and suppression of bacterial leaf blight in rice by *Paenibacillus polymyxa* Sx3. *Lett. Appl. Microbiol.* 68, 423–429.

Ahmed, T., Shahid, M., Noman, M., Niazi, M., Mahmood, F., Manzoor, I., et al. (2020). Silver Nanoparticles Synthesized by Using *Bacillus cereus* SZT1 Ameliorated the Damage of Bacterial Leaf Blight Pathogen in Rice. *Pathogens* 9:160. doi: 10.3390/pathogens9030160

Baccelli, I., Luti, S., Bernardi, R., Favaron, F., De Zotti, M., and Sella, L. (2022). Water-Soluble Trichogin GA IV-Derived peptaibols protect tomato plants from *Botrytis cinerea* infection with limited impact on plant defenses. *Front. Plant Sci.* 13:881961. doi: 10.3389/fpls.2022.881961

Bertelsen, K., Pedersen, J. M., Rasmussen, B. S., Skrydstrup, T., Nielsen, N. C., and Vosegaard, T. (2007). Membrane-bound conformation of peptaibols with methyl-deuterated alpha-amino isobutyric acids by ^{2}H magic angle spinning solid-state NMR spectroscopy. *J. Am. Chem. Soc.* 129, 14717–14723. doi: 10.1021/ja0749690

Cheng, J., Park, S. B., Kim, S. H., Yang, S. H., Suh, J. W., Lee, C. H., et al. (2016). Suppressing activity of staurosporine from *Streptomyces* sp. MJM4426 against rice bacterial blight disease. *J. Appl. Microbiol.* 120, 975–985. doi: 10.1111/jam.13034

Chugh, J. K., Brückner, H., and Wallace, B. A. (2002). Model for a helical bundle channel based on the high-resolution crystal structure of trichotoxin_A50E. *Biochemistry* 41, 12934–12941. doi: 10.1021/bi026150z

Chutrakul, C., Alcocer, M., Bailey, K., and Peberdy, J. F. (2008). The production and characterisation of trichotoxin peptaibols, by *Trichoderma asperellum*. *Chem. Biodivers.* 5, 1694–1706. doi: 10.1002/cbdv.200890158

Daniel, J. F., and Filho, E. R. (2007). Peptaibols of *trichoderma*. *Nat. Prod. Rep.* 24, 1128–1141. doi: 10.1039/b618086h

Dos Santos, I. P., da Silva, L. C., da Silva, M. V., de Araújo, J. M., Cavalcanti, M., and Lima, V. L. (2015). Antibacterial activity of endophytic fungi from leaves of *Indigofera suffruticosa* Miller (Fabaceae). *Front. Microbiol.* 6:350. doi: 10.3389/fmicb.2015.00350

Druzhinina, I. S., Seidl-Seiboth, V., Herrera-Estrella, A., Horwitz, B. A., Kenerley, C. M., and Monte, E. (2011). *Trichoderma*: The genomics of opportunistic success. *Nat. Rev. Microbiol.* 9, 749–759. doi: 10.1038/nrmicro2637

Du, F. Y., Li, X. M., Sun, Z. C., Meng, L. H., and Wang, B. G. (2020). Secondary metabolites with agricultural antagonistic potentials from *Beauveria felina*, a marine-derived entomopathogenic Fungus. *J. Agric. Food Chem.* 68, 14824–14831. doi: 10.1021/acs.jafc.0c05696

Erdmann, S., Tschitschko, B., Zhong, L., Raftery, M. J., and Cavicchioli, R. (2017). A plasmid from an Antarctic haloarchaeon uses specialized membrane vesicles to disseminate and infect plasmid-free cells. *Nat. Microbiol.* 2, 1446–1455. doi: 10.1038/s41564-017-0009-2

Fan, S., Tian, F., Li, J., Hutchins, W., Chen, H., Yang, F., et al. (2017). Identification of phenolic compounds that suppress the virulence of *Xanthomonas oryzae* on rice *via* the type III secretion system. *Mol. Plant Pathol.* 18, 555–568. doi: 10.1111/mpp.12415

Fukuda, S., Yamamoto, R., Yanagisawa, N., Takaya, N., Sato, Y., Riquelme, M., et al. (2021). Trade-off between plasticity and velocity in mycelial growth. *mBio* 12:e3196–e3120. doi: 10.1128/mBio.03196-20

González, J. F., Degrassi, G., Devescovi, G., De Vleesschauwer, D., Höfte, M., Myers, M. P., et al. (2012). A proteomic study of *Xanthomonas oryzae* pv. *oryzae* in rice xylem sap. *J. Proteomics* 75, 5911–5919. doi: 10.1016/j.jprot.2012.07.019

Green, H., Larsen, J., Olsson, P. A., Jensen, D. F., and Jakobsen, I. I. (1999). Suppression of the biocontrol agent *Trichoderma harzianum* by mycelium of the arbuscular mycorrhizal fungus glomus intraradices in root-free soil. *Appl. Environ. Microbiol.* 65, 1428–1434. doi: 10.1128/AEM.65.4.1428-1434.1999

Hutin, M., Césari, S., Chalvon, V., Michel, C., Tran, T. T., Boch, J., et al. (2016). Ectopic activation of the rice NLR heteropair RGA4/RGA5 confers resistance to bacterial blight and bacterial leaf streak diseases. *Plant J.* 88, 43–55. doi: 10.1111/tpj.13231

Ji, Z., Ji, C., Liu, B., Zou, L., Chen, G., and Yang, B. (2016). Interfering TAL effectors of *Xanthomonas oryzae* neutralize R-gene-mediated plant disease resistance. *Nat. Commun.* 7:13435. doi: 10.1038/ncomms13435

Jiang, S., He, M., Xiang, X. W., Adnan, M., and Cui, Z. N. (2019). Novel S-Thiazol-2-yl-furan-2-carbothioate derivatives as potential T3SS inhibitors against *Xanthomonas oryzae* on rice. *J. Agric. Food Chem.* 67, 11867–11876. doi: 10.1021/acs.jafc.9b04085

Khan, R., Najeeb, S., Hussain, S., Xie, B., and Li, Y. (2020). Bioactive secondary metabolites from *Trichoderma* spp. against phytopathogenic Fungi. *Microorganisms* 8:817. doi: 10.3390/microorganisms8060817

Kuvarina, A. E., Gavryushina, I. A., Kulko, A. B., Ivanov, I. A., Rogozhin, E. A., Georgieva, M. L., et al. (2021). The Emericellipsins A-E from an alkalophilic fungus *Emericellopsis alkalina* show potent activity against multidrug-resistant pathogenic fungi. *J. Fungi* 7:153. doi: 10.3390/jof7020153

Laborte, A. G., Gutierrez, M. A., Balanza, J. G., Saito, K., Zwart, S. J., Boschetti, M., et al. (2017). RiceAtlas, a spatial database of global rice calendars and production. *Sci. Data* 4:170074. doi: 10.1038/sdata.2017.74

Li, H. Y., Luo, Y., Zhang, X. S., Shi, W. L., Gong, Z. T., Shi, M., et al. (2014). Trichokonins from *Trichoderma pseudokoningii* SMF2 induce resistance against Gram-negative *Pectobacterium carotovorum* subsp. *carotovorum* in Chinese cabbage. *FEMS Microbiol. Lett.* 354, 75–82. doi: 10.1111/1574-6968.12427

Liang, H., He, K., Li, T., Cui, S., Tang, M., Kang, S., et al. (2020). Mechanism and antibacterial activity of vine tea extract and dihydromyricetin against *Staphylococcus aureus*. *Sci. Rep.* 10:21416. doi: 10.1038/s41598-020-78379-y

Liang, X., Yu, X., Pan, X., Wu, J., Duan, Y., Wang, J., et al. (2018). A thiadiazole reduces the virulence of *Xanthomonas oryzae* pv. *oryzae* by inhibiting the histidine utilization pathway and quorum sensing. *Mol. Plant Pathol.* 19, 116–128. doi: 10.1111/mpp.12503

Liu, H. W., Ji, Q. T., Ren, G. G., Wang, F., Su, F., Wang, P. Y., et al. (2020). Antibacterial functions and proposed modes of action of novel 1,2,3,4-Tetrahydro-β-carboline derivatives that possess an attractive 1,3-Diaminopropan-2-ol pattern against rice bacterial blight, kiwifruit bacterial canker, and citrus bacterial canker. *J. Agric. Food Chem.* 68, 12558–12568. doi: 10.1021/acs.jafc.0c02528

Liu, Y., Dai, C., Zhou, Y., Qiao, J., Tang, B., Yu, W., et al. (2021). Pyoverdines are essential for the antibacterial activity of *Pseudomonas chlororaphis* YL-1 under low-iron conditions. *Appl. Environ. Microbiol.* 87:e2840–e2820. doi: 10.1128/AEM.02840-20

Luo, Y., Zhang, D. D., Dong, X. W., Zhao, P. B., Chen, L. L., Song, X. Y., et al. (2010). Antimicrobial peptaibols induce defense responses and systemic resistance in tobacco against tobacco mosaic virus. *FEMS Microbiol. Lett.* 313, 120–126. doi: 10.1111/j.1574-6968.2010.02135.x

Marik, T., Tyagi, C., Balázs, D., Urbán, P., Szepesi, Á, Bakacsy, L., et al. (2019). Structural diversity and bioactivities of peptaibol compounds from the longibrachiatum clade of the filamentous fungal genus *Trichoderma*. *Front. Microbiol.* 10:1434. doi: 10.3389/fmicb.2019.01434

Martinez, D., Berka, R. M., Henrissat, B., Saloheimo, M., Arvas, M., Baker, S. E., et al. (2008). Genome sequencing and analysis of the biomass-degrading fungus *Trichoderma reesei* (syn. *Hypocrea jecorina*). *Nat. Biotechnol.* 26, 553–560. doi: 10.1038/nbt1403

Milov, A. D., Tsvetkov, Y. D., Raap, J., De Zotti, M., Formaggio, F., and Toniolo, C. (2016). Conformation, self-aggregation, and membrane interaction of peptaibols as studied by pulsed electron double resonance spectroscopy. *Biopolymers* 106, 6–24. doi: 10.1002/bip.22713

Nanda, A., and Saravanan, M. (2009). Biosynthesis of silver nanoparticles from *Staphylococcus aureus* and its antimicrobial activity against MRSA and MRSE. *Nanomedicine* 5, 452–456. doi: 10.1016/j.nano.2009.01.012

Niño-Liu, D. O., Ronald, P. C., and Bogdanove, A. J. (2006). *Xanthomonas oryzae* pathovars: Model pathogens of a model crop. *Mol. Plant Pathol.* 7, 303–324. doi: 10.1111/j.1364-3703.2006.00344.x

Ogunyemi, S. O., Zhang, M., Abdallah, Y., Ahmed, T., Qiu, W., Ali, M. A., et al. (2020). The bio-synthesis of three metal oxide nanoparticles (ZnO, MnO_2 and MgO) and their antibacterial activity against the bacterial leaf blight pathogen. *Front. Microbiol.* 11:588326. doi: 10.3389/fmicb.2020.588326

Qian, G., Liu, C., Wu, G., Yin, F., Zhao, Y., Zhou, Y., et al. (2013). AsnB, regulated by diffusible signal factor and global regulator Clp, is involved in aspartate metabolism, resistance to oxidative stress and virulence in *Xanthomonas oryzae* pv. *oryzicola*. *Mol. Plant Pathol.* 14, 145–157. doi: 10.1111/j.1364-3703.2012.00838.x

Quibod, I. L., Atieza-Grande, G., Oreiro, E. G., Palmos, D., Nguyen, M. H., Coronejo, S. T., et al. (2020). The green revolution shaped the population structure of the rice pathogen *Xanthomonas oryzae* pv. *oryzae*. *ISME J.* 14, 492–505. doi: 10.1038/s41396-019-0545-2

Raaijmakers, J. M., and Mazzola, M. (2012). Diversity and natural functions of antibiotics produced by beneficial and plant pathogenic bacteria. *Annu. Rev. Phytopathol.* 50, 403–424. doi: 10.1146/annurev-phyto-081211-172908

Rogozhin, E. A., Sadykova, V. S., Baranova, A. A., Vasilchenko, A. S., Lushpa, V. A., Mineev, K. S., et al. (2018). A novel lipopeptaibol emericellipsin A with antimicrobial and antitumor activity produced by the extremophilic fungus *Emericellopsis alkalina*. *Molecules* 23:2785. doi: 10.3390/molecules23112785

Sahu, S. K., Zheng, P., and Yao, N. (2018). Niclosamide blocks rice leaf blight by inhibiting biofilm formation of *Xanthomonas oryzae*. *Front. Plant Sci.* 9:408. doi: 10.3389/fpls.2018.00408

Salzberg, S. L., Sommer, D. D., Schatz, M. C., Phillippy, A. M., Rabinowicz, P. D., Tsuge, S., et al. (2008). Genome sequence and rapid evolution of the rice pathogen *Xanthomonas oryzae* pv. *oryzae* PXO99^{A}. *BMC Genomics* 9:204. doi: 10.1186/1471-2164-9-204

Schirmböck, M., Lorito, M., Wang, Y. L., Hayes, C. K., Arisan-Atac, I., Scala, F., et al. (1994). Parallel formation and synergism of hydrolytic enzymes and peptaibol antibiotics, molecular mechanisms involved in the antagonistic action of *Trichoderma harzianum* against phytopathogenic fungi. *Appl. Environ. Microbiol.* 60, 4364–4370. doi: 10.1128/aem.60.12.4364-4370.1994

Seidl, V., Song, L., Lindquist, E., Gruber, S., Koptchinskiy, A., Zeilinger, S., et al. (2009). Transcriptomic response of the mycoparasitic fungus *Trichoderma*

atroviride to the presence of a fungal prey. *BMC Genomics* 10:567. doi: 10.1186/1471-2164-10-567

Shanmugaiah, V., Mathivanan, N., and Varghese, B. (2010). Purification, crystal structure and antimicrobial activity of phenazine-1-carboxamide produced by a growth-promoting biocontrol bacterium, *Pseudomonas aeruginosa* MML2212. *J. Appl. Microbiol*. 108, 703–711. doi: 10.1111/j.1365-2672.2009.04466.x

Shi, D., Zhao, S., Jiang, W., Zhang, C., Liang, T., and Hou, G. (2019). TLR5: A prognostic and monitoring indicator for triple-negative breast cancer. *Cell Death Dis*. 10:954. doi: 10.1038/s41419-019-2187-8

Shi, M., Chen, L., Wang, X. W., Zhang, T., Zhao, P. B., Song, X. Y., et al. (2012). Antimicrobial peptaibols from *Trichoderma pseudokoningii* induce programmed cell death in plant fungal pathogens. *Microbiology* 158, 166–175. doi: 10.1099/mic.0.052670-0

Shi, M., Wang, H. N., Xie, S. T., Luo, Y., Sun, C. Y., Chen, X. L., et al. (2010). Antimicrobial peptaibols, novel suppressors of tumor cells, targeted calcium-mediated apoptosis and autophagy in human hepatocellular carcinoma cells. *Mol. Cancer* 9:26. doi: 10.1186/1476-4598-9-26

Shi, T., Guo, X., Zhu, J., Hu, L., He, Z., and Jiang, D. (2021). Inhibitory effects of Carbazomycin B produced by *Streptomyces roseoverticillatus* 63 against *Xanthomonas oryzae* pv. *oryzae*. *Front. Microbiol*. 12:616937. doi: 10.3389/fmicb.2021.616937

Shobha, B., Lakshmeesha, T. R., Ansari, M. A., Almatroudi, A., Alzohairy, M. A., Basavaraju, S., et al. (2020). Mycosynthesis of ZnO nanoparticles using *Trichoderma* spp. isolation from rhizosphere soils and its synergistic antibacterial effect against *Xanthomonas oryzae* pv. *oryzae*. *J. Fungi* 6:181. doi: 10.3390/jof6030181

Tamandegani, P. R., Marik, T., Zafari, D., Balázs, D., Vágvölgyi, C., Szekeres, A., et al. (2020). Changes in peptaibol production of *Trichoderma* species during *in vitro* antagonistic interactions with fungal plant pathogens. *Biomolecules* 10:730. doi: 10.3390/biom10050730

Tang, B. L., Yang, J., Chen, X. L., Wang, P., Zhao, H. L., Su, H. N., et al. (2020). A predator-prey interaction between a marine *Pseudoalteromonas* sp. and Gram-positive bacteria. *Nat. Commun*. 11:285. doi: 10.1038/s41467-019-14133-x

Timilsina, S., Potnis, N., Newberry, E. A., Liyanapathiranage, P., Iruegas-Bocardo, F., White, F. F., et al. (2020). *Xanthomonas* diversity, virulence and plant-pathogen interactions. *Nat. Rev. Microbiol*. 18, 415–427. doi: 10.1038/s41579-020-0361-8

Vinale, F., Marra, R., Scala, F., Ghisalberti, E. L., Lorito, M., and Sivasithamparam, K. (2006). Major secondary metabolites produced by two commercial *Trichoderma* strains active against different phytopathogens. *Lett. Appl. Microbiol*. 43, 143–148. doi: 10.1111/j.1472-765X.2006.01939.x

Viterbo, A., Wiest, A., Brotman, Y., Chet, I., and Kenerley, C. (2007). The 18mer peptaibols from *Trichoderma virens* elicit plant defence responses. *Mol. Plant Pathol*. 8, 737–746. doi: 10.1111/j.1364-3703.2007.00430.x

Wiest, A., Grzegorski, D., Xu, B. W., Goulard, C., Rebuffat, S., Ebbole, D. J., et al. (2002). Identification of peptaibols from *Trichoderma virens* and cloning of a peptaibol synthetase. *J. Biol. Chem*. 277, 20862–20868. doi: 10.1074/jbc.M201654200

Wu, L., Wu, H., Chen, L., Yu, X., Borriss, R., and Gao, X. (2015). Difficidin and bacilysin from *Bacillus amyloliquefaciens* FZB42 have antibacterial activity against *Xanthomonas oryzae* rice pathogens. *Sci. Rep*. 5:12975. doi: 10.1038/srep12975

Xiao-Yan, S., Qing-Tao, S., Shu-Tao, X., Xiu-Lan, C., Cai-Yun, S., and Yu-Zhong, Z. (2006). Broad-spectrum antimicrobial activity and high stability of Trichokonins from *Trichoderma koningii* SMF2 against plant pathogens. *FEMS Microbiol. Lett*. 260, 119–125. doi: 10.1111/j.1574-6968.2006.00316.x

Xie, B. B., Li, D., Shi, W. L., Qin, Q. L., Wang, X. W., Rong, J. C., et al. (2015). Deep RNA sequencing reveals a high frequency of alternative splicing events in the fungus *Trichoderma longibrachiatum*. *BMC Genomics* 16:54. doi: 10.1186/s12864-015-1251-8

Xie, S., Zang, H., Wu, H., Uddin Rajer, F., and Gao, X. (2018). Antibacterial effects of volatiles produced by *Bacillus* strain D13 against *Xanthomonas oryzae* pv. *oryzae*. *Mol. Plant Pathol*. 19, 49–58. doi: 10.1111/mpp.12494

Zhang, Y., Wu, G., Palmer, I., Wang, B., Qian, G., Fu, Z. Q., et al. (2019). The role of a host-induced Arginase of *Xanthomonas oryzae* pv. *oryzae* in promoting virulence on rice. *Phytopathology* 109, 1869–1877. doi: 10.1094/PHYTO-02-19-0058-R

Zhou, Y. R., Song, X. Y., Li, Y., Shi, J. C., Shi, W. L., Chen, X. L., et al. (2019). Enhancing peptaibols production in the biocontrol fungus *Trichoderma longibrachiatum* SMF2 by elimination of a putative glucose sensor. *Biotechnol. Bioeng*. 116, 3030–3040. doi: 10.1002/bit.27138

frontiers | Frontiers in Microbiology

TYPE Original Research
PUBLISHED 14 November 2022
DOI 10.3389/fmicb.2022.1046099

OPEN ACCESS

EDITED BY
Peng Zhang,
Tobacco Research Institute (CAAS), China

REVIEWED BY
Wen-Bo Han,
Northwest A&F University, China
Yongbo Xue,
Sun Yat-sen University, China

*CORRESPONDENCE
Fei He
hefei8131@smu.edu.cn

†These authors have contributed equally to this work

SPECIALTY SECTION
This article was submitted to Antimicrobials, Resistance and Chemotherapy, a section of the journal Frontiers in Microbiology

RECEIVED 16 September 2022
ACCEPTED 20 October 2022
PUBLISHED 14 November 2022

CITATION
Shi H, Jiang J, Zhang H, Jiang H, Su Z, Liu D, Jie L and He F (2022) Antibacterial spirooxindole alkaloids from *Penicillium brefeldianum* inhibit dimorphism of pathogenic smut fungi. *Front. Microbiol.* 13:1046099. doi: 10.3389/fmicb.2022.1046099

Antibacterial spirooxindole alkaloids from *Penicillium brefeldianum* inhibit dimorphism of pathogenic smut fungi

Huajun Shi[1†], Jinyan Jiang[1,2†], Hang Zhang[1†], Haimei Jiang[1], Zijie Su[1], Dandan Liu[3], Ligang Jie[1,3] and Fei He[1,3*]

[1]School of Traditional Chinese Medicine, Southern Medical University, Guangzhou, China, [2]Department of Applied Biological Chemistry, Graduate School of Agricultural and Life Sciences, The University of Tokyo, Tokyo, Japan, [3]Zhujiang Hospital, Southern Medical University, Guangzhou, China

Three new antibacterial spirooxindole alkaloids, spirobrefeldins A–C (1–3), together with four known analogs, spirotryprostatin M (4), spirotryprostatin G (5), 12β-hydroxyverruculogen TR-2 (6), and 12α-hydroxyverruculogen TR-2 (7), were isolated from terrestrial fungus *Penicillium brefeldianum*. All the new compounds were elucidated extensively by the interpretation of their NMR (1D and 2D) spectra and high-resolution mass data, and their absolute configurations were determined by computational chemistry and CD spectra. The absolute configurations of spiro carbon C-2 in spirotryprostatin G (5) and spirotryprostatin C in literature were reported as *S*, which were revised to *R* based on experimental and calculated CD spectra. All the compounds were evaluated for their antimicrobial activities toward *Pseudomonas aeruginosa* PAO1, *Dickeya zeae* EC1, *Staphylococcus epidermidis*, *Escherichia coli*, and *Sporisorium scitamineum*. Compound 7 displayed moderate inhibitory activity toward dimorphic switch of pathogenic smut fungi *Sporisorium scitamineum* at 25 μM. Compounds 3 and 6 showed weak antibacterial activities against phytopathogenic bacterial *Dickeya zeae* EC1 at 100 μM.

KEYWORDS

***Penicillium brefeldianum*, spirooxindole diketone piperazine, absolute configuration, antibacterial activities, fungal secondary metabolites**

Introduction

Microbes have been considered to be a significant source of bioactive secondary metabolites for drugs (Demain and Sanchez, 2009; Newman, 2021). Fungi as one of the widest phyla of organisms spread all over the world inhabiting all substrates and climate conditions. It is estimated that at least 18,000 species of fungi have been described (Marin-Felix et al., 2017). Fungi are also well known to produce secondary metabolites, such as terpenoids, alkaloids, macrolides, polyketides, and pigments, with diverse significant biological activities such as anti-tumor, antioxidant, anti-inflammatory, antimicrobial, and anticancer, which could be widely used

in the pharmaceutical and agricultural industries (Bills and Gloer, 2016; Keller, 2019; Steele et al., 2019; Adeleke and Babalola, 2021; Tiwari and Bae, 2022; Wen et al., 2022). Penicillin is probably the best known β-lactam antibiotic drug made by fungi strains. Besides, Lovastatin, which is used to lower LDL cholesterol, and Cyclosporine, which suppresses the immune system activity and treats some autoimmune diseases, are both well-known fungal secondary metabolite-derived drugs (Schueffler and Anke, 2014).

Spirooxindole ring is widely distributed in various bioactive natural products and has been used as a promising pharmacophore in drug discovery (Rottmann et al., 2010; Ye et al., 2016). These structures feature a spiro ring at the C-2 or C-3 position of the oxindole core with a heterocyclic skeleton. Interestingly, spirooxindole alkaloids with both *R* and *S* absolute configurations at the C-3 position were reported in the literature, such as paraherquamide N (3*R*) (Blanchflower et al., 1993), notoamide B (3*R*) (Kato et al., 2007), cyclopiamine A (3*R*) (Bond et al., 1979), and brevianamide X (3*S*) (Paterson et al., 1987), chrysogenamide A (3*S*) (Lin et al., 2008), citrinalin A (3*S*) (Tsuda et al., 2004), and citrinadin C (3*S*) (Jiang et al., 2022), while the absolute configurations of spiro carbon at C-2 position showed only *S* absolute configuration, such as spirotryprostatin M (Lin et al., 2020), spirotryprostatin G (Zhang et al., 2019), and spirotryprostatin C (Wang et al., 2008). Many spirooxindole alkaloids have been found to show significant biological activity, including anticancer, insecticidal, cytotoxic, and antibacterial activities (Tsukamoto et al., 2010; Kagiyama et al., 2016; Klas et al., 2018). The unique structural features and diverse biological activities of spirooxindole alkaloids have brought great interest and challenge to chemists for total synthesis and biosynthesis (Greshock et al., 2007; Bian et al., 2013; Mercado-Marin et al., 2014; Liu et al., 2021).

In our continuing investigation for new pharmacologically active secondary metabolites from microbes (He et al., 2012, 2013a,b; Zhang et al., 2016; Wu et al., 2017; Jiang et al., 2022), the bioactive natural products of *Penicillium brefeldianum* have been studied. Three new spirooxindole alkaloids, sprirobrefeldins A–C (1–3), together with four known ones, spirotryprostatin M (4) (**Supplementary Figures S28, S29**), spirotryprostatin G (**5**), 12β-hydroxyverruculogen TR-2 (6) (**Supplementary Figures S32, S33**) (Li et al., 2012), and 12α-hydroxyverruculogen TR-2 (7) (**Supplementary Figures S34, S35**) (Li et al., 2012), were isolated (**Figure 1**). The absolute configurations of spiro carbon at C-2 position in spirotryprostatin G (5) and spirotryprostatin C in literature were reported as *S*, which were revised to *R* based on experimental and calculated CD spectra. This is the first report of spirooxindoles with spiro carbon at the C-2 position that have both *S* and *R* configurations. All the compounds were evaluated for their antimicrobial activities toward *Pseudomonas aeruginosa* PAO1, *Dickeya zeae* EC1, *Staphylococcus epidermidis*, *Escherichia coli,* and *Sporisorium scitamineum*. Compound 7 displayed moderate inhibitory activity toward dimorphic switch of *Sporisorium scitamineum*, with an MIC value of 25 μM. Around 100 M, compounds 3 and 6 showed weak antibacterial activities against phytopathogenic bacterial *Dickeya zeae*.

Materials and methods

General experimental procedures

FT-IR spectrometer (Affinity-1, Shimadzu) was used to measure IR spectra. Optical rotations were measured in a polarimeter (MCP 300, Anton Paar) at 25°C. U-2910 spectrometer (Hitachi) was used to record UV spectra. Advance 600 spectrometer (Bruker) was used to measure ^{1}H NMR (600 MHz) and ^{13}C NMR (150 MHz). Esquire 3000 plus spectrometer (Bruker) was used to measure ESIMS spectra. A micro TOF-QII mass spectrometer (Bruker) was used to record HRESIMS data. Sephadex LH-20 gel (Amersham Pharmacia) and silica gel (100–200 mesh and 200–300 mesh; Qingdao Marine Chemicals) were used in column chromatography. Analytical and preparative HPLC was performed on a Shimadzu Prominence system. Circular Dichroism Spectrometer (V100) was used to measure CD spectra.

Fungal materials

The strain *P. brefeldianum* used in this project was isolated from soil samples collected in the Tengchong forest of Yunnan province, China. The isolate was identified by Miss Jinyan Jiang based on the morphology and sequence analysis of the ITS region of the rDNA (GenBank Accession Number is 138263), and a voucher specimen (*Penicillium brefeldianum* SMU008) was stored in the School of Chinese Medicine, Southern Medical University.

Fermentation and extraction

The fresh mycelia of *Penicillium brefeldianum* were initially grown on the PDA medium at 28°C (72 h). Small pieces of Agar plugs were selected to inoculate 10 Erlenmeyer flasks (500 mL) each containing 200 mL of PDB, and were cultured for 5 days (shake, 150 rpm, 28°C). The seed culture was then inoculated into 50 × 500 mL conical flasks on rice solid medium (80 g rice, 120 mL of filtered water) for 28 days at room temperature. The fermented solid cultures were then extracted fully with ethyl acetate to yield 12-gram crude extract.

Isolation and purification

The crude extract had been chromatographed on silica using elution system with $CHCl_3$/MeOH (v/v, 100:0, 95:5, 9:1, 8:2,

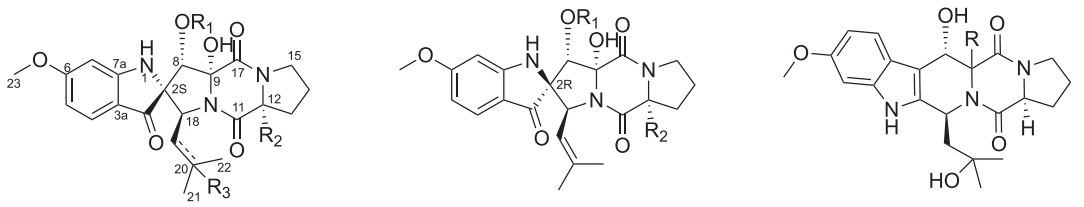

1 R_1= H, R_2=H, R_3=OH
2 R_1= H, R_2=OH, R_3=H, $\Delta^{19,20}$
3 R_1= H, R_2=H, R_3=H, $\Delta^{19,20}$
4 R_1=isopentanyl, R_2=H, R_3=OH

5 R_1= H, R_2=OH (revised)
spirotryprostatin C R_1= H, R_2=OH (revised)

6 R= α OH
7 R= β OH

FIGURE 1
Compounds 1–7 isolated and identified from *Penicillium brefeldianum* and revised structures of compounds 5 and spirotryprostatin C.

1:1, and 0:100) to give six crude parts (Fraction A–Fraction F). Fr.D was further purified to afford five subfractions (Fr.D-1 to Fr.D-5) using silica column chromatography eluting with CH_2Cl_2/MeOH. Fr.D-1 was isolated by Sephadex LH-20 using CH_2Cl_2/MeOH (v/v, 1:1) to obtain five subfractions. Then Fr. D-1-2 was separated on ODS column with MeOH/H_2O (10%, 30%, 50%, 70%, 80%, 100%) to obtain six fractions (Fr.D-1-2-1 to Fr.D-1-2-6). Eight fractions (Fr.D-1-2-4-1 to Fr.D-1-2-4-8) were obtained from Fr.D-1-2-4 by p-TLC ($CHCl_3$-acetone, 2:1 v/v). 1 (5 mg), 2 (5 mg), and 3 (6 mg) were separated from Fr.D-1-2-4-7 by p-HPLC (v/v, 45% MeOH/H_2O, 3.0 mL/min with retention time of 20 min, 25 min, 29 min, respectively. Fr.D-1-2-4-4 was further isolated by p-HPLC (v/v, 50% MeOH/H_2O, 3.0 mL/min) to obtain 5 (4 mg) with retention time of 18 min. Fr. D-1-2-4-5 was further purified by HPLC (v/v, 30% ACN/H_2O, 3.0 mL/min) to obtain 6 (12 mg) with a retention time of 19 min. Fr.D-1-2-4-6 was purified by HPLC (v/v, 40% MeOH/H_2O, 3.0 mL/min) to obtain 7 (5 mg) with a retention time of 29 min. Fr.C was further purified by silica C.C. with hexane/EtOAc system to afford five subfractions (Fr.C-1 to Fr.C-5). Then Fr.C-5 was separated by CH_2Cl_2/MeOH to afford seven subfractions (Fr.C-5-1 to Fr.C-5-7). Seven fractions (Fr.C-5-3-1 to Fr.C-5-3-7) were obtained from Fr.C-5-3 by p-TLC (v/v, $CHCl_3$/acetone, 4:1). 4 (10 mg) was obtained from Fr.D-5-3-5 by p-HPLC (v/v, 60% MeOH/H_2O, 3.0 mL/min) with a retention time of 30 min.

Spirobrefeldin A (1): pale yellow powder; UV (MeOH) λ_{max} (log ε) 203 (4.08), 224 (4.12), 249 (4.08), 281 (3.87), 374 (3.39) nm. CD (MeOH) λ_{max} (Δε) 200 (+ 21.2), 227 (− 27.4), 283 (+ 6.0), 320 (− 4.7), 353 (+ 0.8), 390 (− 2.9) nm; HRESIMS *m/z* 444.1772 $[M - H]^-$, (calculated for $C_{22}H_{25}N_3O_7$, 444.1776); IR (neat) ν_{max} 3,432, 2,941, 1,668, 1,662, 1,614, 1,456, 1,303, 1,215, and 1,024 cm^{-1}; [α]25 D − 81.2 (*c* 0.09, MeOH) (**Supplementary Figures S1–S9**).

Spirobrefeldin B (2): amorphous yellow powder; UV (MeOH) λ_{max} (log ε) 203 (4.04), 225 (3.97), 248 (3.83), 284 (3.69), 374 (3.16) nm; CD (MeOH) λ_{max} (Δε) 200 (+ 15.8), 231 (− 64.6), 256 (+ 16.3), 282 (+ 6.5), 313 (− 20.2), 366 (+ 4.3) nm; HRESIMS *m/z* 442.1615 $[M - H]^-$, (calculated for $C_{22}H_{24}N_3O_7$, 442.1620); IR (neat) ν_{max} 3,344, 3,334, 1,681, 1,662, 1,614, 1,456, 1,396, 1,213, and 1,024 cm^{-1}; [α]25 D − 69.1 (*c* 0.08, MeOH) (**Supplementary Figures S10–S18**).

Spirobrefeldin C (3): amorphous yellow powder; UV (MeOH) λ_{max} (log ε) 204 (4.23), 227 (4.23), 248 (4.15), 284 (4.01), 375 (3.50) nm; CD (MeOH) λ_{max} (Δε) 229 (− 32.3), 255 (+ 8.9), 282 (+ 2.5), 315 (− 10.1), 361 (+ 2.2) nm; HRESIMS *m/z* 426.1671 $[M - H]^-$, (calculated for $C_{22}H_{24}N_3O_6$, 426.1671); IR (neat) ν_{max} 3,344, 3,334, 1,670, 1,610, 1,456, 1,309, 1,213, and 1,022 cm^{-1}; [α]25 D − 151.1 (*c* 0.08, MeOH) (**Supplementary Figures S19–S27**).

Spirotryprostatin G (5): amorphous yellow powder; CD (MeOH) λ_{max} (Δε) 201 (+ 34.8), 223 (− 9.1), 252 (− 15.8), 283 (− 3.2), 307 (+ 6.4), 387 (+ 3.7) nm; ESIMS *m/z* 442.10 $[M - H]^-$; [α]25 D + 60.9 (*c* 0.1, MeOH) (**Supplementary Figures S30, S31, S36–S38** and **Supplementary Tables S1–S8**).

Antibacterial assay

The plant pathogenic smut fungi used in this assay is *Sporisorium scitamineum*, and tested compounds were dissolved in DMSO in different concentrations. MAT-1 and MAT-2 colonies were cultured in 5 mL of YEPSA overnight (28°C, 200 rpm), respectively. Then 1 mL of YEPSA medium (agar) with different concentrations of compounds was added to a 24-well plate. After that, 1 μL of the mixture of MAT-1 and MAT-2 was added to each well. The well without compounds was used as a negative control. The 24-well plate was incubated in a 28°C incubator for 2 days by observing hypha formation. MPA was used as a positive control in this assay (Zhong et al., 2018).

The bacterial strains used in this work (*Pseudomonas aeruginosa* PAO1, *Dickeya zeae* EC1, *Staphylococcus epidermidis,* and *Escherichia coli.*) were grown in LB medium at 30°C. Luria–Bertani (LB) medium (1 L contains 10 g trypeptone, 5 g yeast extract, and 10 g NaCl) was used to isolate biocontrol agents. Vancomycin and imipenem were used as positive control. Overnight cultured bacterial strains were diluted in fresh LB

media to an OD_{600} of 0.1 in the absence or presence of compounds at different concentrations. The bacterial cells were grown in each well of a 96-well polystyrene plate at 37°C for 12 h with shaking. Then, a microplate reader was used to measure the absorbance of each well at 600 nm.

Electronic circular dichroism calculations

The Gaussian 09 software was used to determine the absolute configurations of compounds 1, 2, and 5. Briefly, random conformational analyses were conducted on the basis of MMFF94 force fields before the relative configurations of compounds were determined by the NOESY spectra initially. The obtained conformers were optimized at the B3LYP/6-31G(d) level of time-dependent density functional theory (TDDFT) and followed by ECD calculations *via* TDDFT [B3LYP/6-31 + G(d), CPCM model = MeOH]. The ECD curves were generated by SpecDisv1.51 (Huo et al., 2018).

Nuclear magnetic resonance calculation

The theoretical calculations were performed using Gaussian 16. The systematic random conformational analysis was performed in the Sybyl-X 2.0 program by using MMFF94s molecular force field and a global minima energy cutoff of 6 kcalmol-1. All the obtained conformers were further optimized using DFT at the B3LYP/6-31 G(d) level in the gas phase by using Gaussian 16 software. Harmonic vibrational frequencies were also performed to confirm no imaginary frequencies of the finally optimized conformers. On basis of the energies, conformers with a Boltzmann distribution > 1% were chosen. Gauge-independent atomic orbital (GIAO) calculations of 1H- and 13C-NMR chemical shifts were accomplished by DFT at the mPW1PW91/6-31 + G level in DMSO with the PCM solvent model in Gaussian 16 software. After Boltzmann weighing of the predicted chemical shift of each isomer, the linear correlation coefficients (R2), mean absolute deviation

TABLE 1 ^{1}H and ^{13}C NMR data (δ in ppm, *J* in Hz) for compounds 1, 2, and 3[a].

NO.	1		2		3	
	δ_H[b]	δ_C[c]	δ_H	δ_C	δ_H	δ_C
1-NH	7.09, s		7.19, s		7.16, s	
2		73.4 C		75.3 C		75.5 C
3		196.9 C		195.3 C		195.3 C
3a		114.4 C		113.3 C		113.4 C
4	7.26, d (8.6)	124.9 CH	7.27, d (8.6)	124.9 CH	7.26, d (8.6)	124.8 CH
5	6.26, dd (8.6, 2.2)	107.3 CH	6.28, dd (8.6, 2.2)	107.5 CH	6.28, dd (8.6, 2.2)	107.5 CH
6		166.8 C		167.1 C		166.9 C
7	6.44, d (2.2)	94.4 CH	6.46, d (2.2)	94.6 CH	6.46, d (2.2)	94.7 CH
7a		163.5 C		163.8 C		163.9 C
8	4.38, s	74.4 CH	4.43, s	74.4 CH	4.47, s	74.1 CH
9		85.2 C		85.1 C		85.4 C
11		169.5 C		167.0 C		168.6 C
12	4.43, dd (8.7, 6.8)	59.8 CH		88.8 C	4.40, dd (9.0, 7.2)	59.7 CH
13	1.90, m; 2.23, m	27.8 CH_2	2.07, m	35.8 CH_2	2.19, t (2.2); 1.83, m	27.8 CH_2
14	1.85, m; 1.93, m	22.7 CH_2	1.93, m	20.2 CH_2	1.86, m	22.6 CH_2
15	3.34, dt (11.6, 7.7)	44.6 CH_2	3.48, m	44.5 CH_2	3.46, m	44.5 CH_2
17		164.6 C		165.6 C		164.8 C
18	4.14, dd (7.6, 1.8)	58.8 CH	4.63, d (9.5)	61.0 CH	4.61, d (9.6)	60.7 CH
19	1.37, dd (14.4, 1.8) 2.60, dd (14.4, 7.6)	38.5 CH_2	4.99, m	120.9 CH	4.93, dt (9.6, 1.4)	121.1 CH
20		68.3 C		133.7 C		133.6 C
21	0.99, s	30.2 CH_3	1.30, s	18.0 CH_3	1.38, d (1.4)	17.9 CH_3
22	0.84, s	29.1 CH_3	1.58, s	25.4 CH_3	1.57, d (1.4)	25.4 CH_3
23	3.78, s	55.4 CH_3	3.80, s	55.4 CH_3	3.79, s	55.4 CH_3
8-OH	5.63, s				5.64, s	
9-OH	6.95, s				7.05, s	
20-OH	4.06, s					

[a]Recorded in DMSO-d_6. [b]Recorded at 600 MHz. [c]Recorded at 150 MHz.

(MAD), root-mean-square deviation (RMSD), and corrected mean absolute deviation (CMAD) were calculated for the evaluation of the results. Moreover, the DP4 + parameters were calculated using the excel file provided by Grimblat et al. (2015) and Marcarino et al. (2022).

Results and discussion

Structure elucidation

Spirobrefeldin A (1) was isolated as an amorphous yellow powder and exhibited $[M - H]^-$ ion peak at *m/z* 444.1772 (calcd. 444.1776) in the HRESIMS, associated with a molecular formula of $C_{22}H_{26}N_3O_7$, requiring 11 degrees of unsaturation. The IR spectrum of 1 showed absorption bands at 3344 (OH), 1670 (C = O), and 1610 (C = C) in the functional group region. The ^{1}H NMR data of 1 (Table 1) showed signals of three aromatic protons at δ_H 7.26 (d, J = 8.6, H-4), 6.44 (d, J = 2.2, H-7), and 6.26 (dd, J = 8.5, 2.1, H-5), as well as one methoxyl group (δ_H 3.78), two methyl groups (δ_H 0.84, 0.99), and three methane protons at δ_H 4.14 (H-18), 4.38 (H-8), and 4.43 (H-12). The ^{13}C and DEPT135 NMR spectra showed signals of 22 carbons, including three carbonyl carbons (δ_C 196.9, 169.5, 164.6), three sp^2 quaternary carbons (δ_C 166.8, 163.5, 114.4), three sp^2 methines (δ_C 124.9, 107.3, 94.4), three sp^3 quaternary carbons (δ_C 85.2, 73.4, 68.3), three sp^3 methines (δ_C 74.4, 59.8, 58.8), four sp^3 methylene (δ_C 44.6, 38.5, 27.8, 22.7), and three methyl groups (δ_C 29.1, 30.2, 55.4). From the above observations and by comparison with NMR data from closely related structures, it was evident that 1 was similar to those of spirotryprostatin M (4), which suggested that 1 was spirooxindole diketone piperazine alkaloids. The above deduction was further confirmed by correlations from H-8 to C-2/C-3, N1-H to C-3/C-3a, H-18 to C-9/C-11/C-20, H-15 to C-12/C-13, and H-19 to C-21/C-22 in the HMBC spectrum, together with the ^{1}H-^{1}H COSY correlations, confirmed the connectivity of H-12/H-13/H-14/H-15 (Figure 2). Owing to the HRESIMS and ^{13}C NMR data, it showed that the isopentenyl at C-18 in 4 disappeared and was substituted by a hydroxyl group in 1. Therefore, the planner structure of 1 was established.

Correlations between OH-9 and H-18/OH-8/H-12, H-8, and H-19, and N1-H and H-7/H-18 in the NOESY experiment (Figure 3) suggested that the relative configurations of C-8,

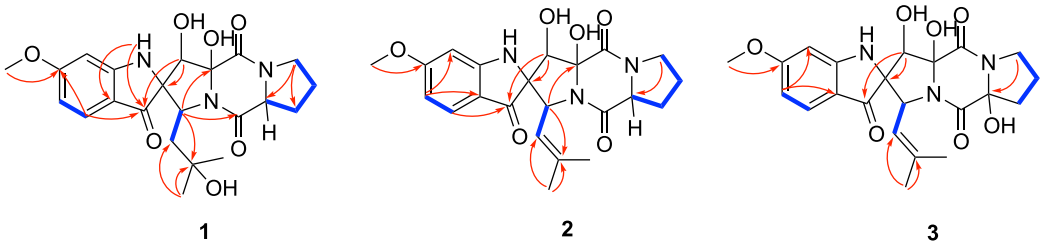

FIGURE 2
Key HMBC and COSY correlations of compounds 1–3.

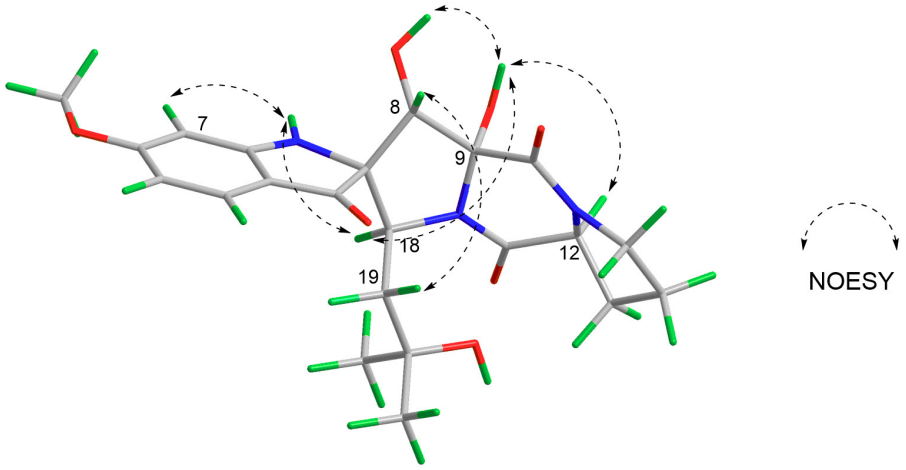

FIGURE 3
Key NOESY correlations of compound 1.

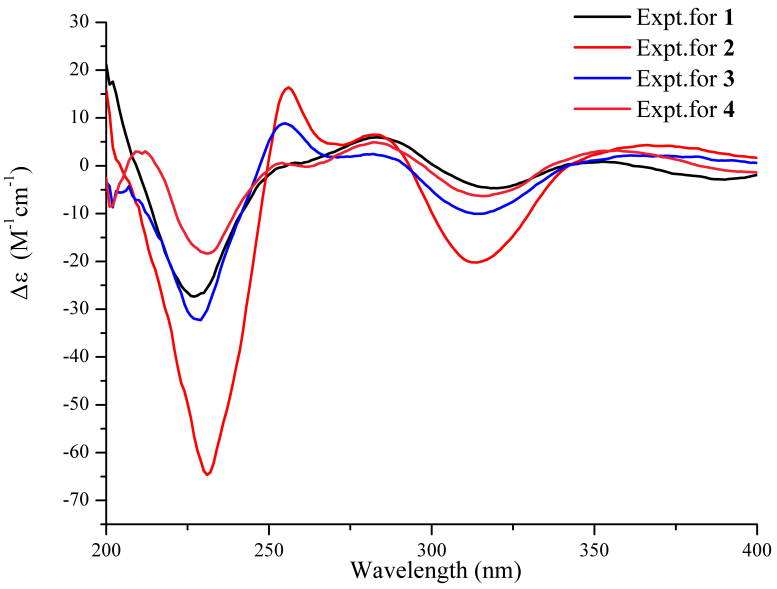

FIGURE 4
Comparisons of experimental CD (MeOH) spectra between compounds 1–4.

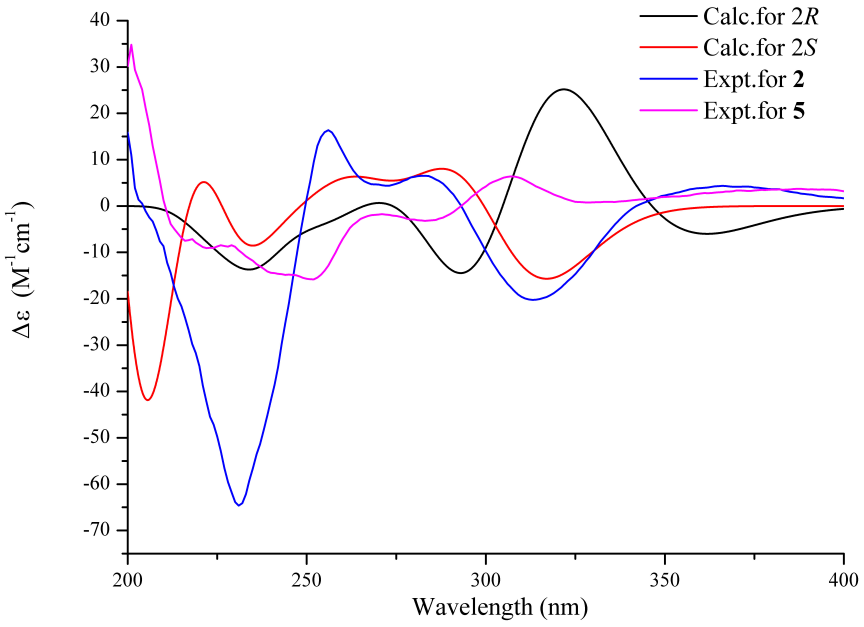

FIGURE 5
Experimental CD spectra of compounds 2 and 5 (MeOH) and ECD calculations of 2*R* and 2*S* configurations.

C-9, and C-12 were the same as those of 4. The absolute configurations of 1 were finally confirmed to be 2*S*, 8*S*, 9*R*, 12*S*, 18*S* by CD spectrum, which showed almost identical cotton effect curves compared to that of 4, demonstrating positive cotton effect at 283/353 nm and negative cotton effect at 227/320/390 nm (**Figure 4**).

Compound 2 was isolated as an amorphous yellow powder, and the molecular formula was assigned as $C_{22}H_{24}N_3O_7$ by HRESIMS (*m/z* 442.1615, $[M-H]^-$, calcd. 442.1620), requiring 12 degrees of unsaturation. The ^{1}H NMR data of 2 showed signals of three aromatic protons at δ_H 6.28 (dd, J = 8.6, 2.2, H-5), 6.46 (d, J = 2.2, H-7), and 7.27 (d, J = 8.6, H-4), one methoxy group (δ_H 3.80), and two methyl groups (δ_H 1.30, 1.58). The ^{13}C and DEPT135 NMR spectra showed 22 carbons, including three carbonyl carbons (δ_C 195.3, 167.0, 165.6), four sp^2 quaternary carbons (δ_C 167.1, 163.8, 137.7, 113.3), four sp^2

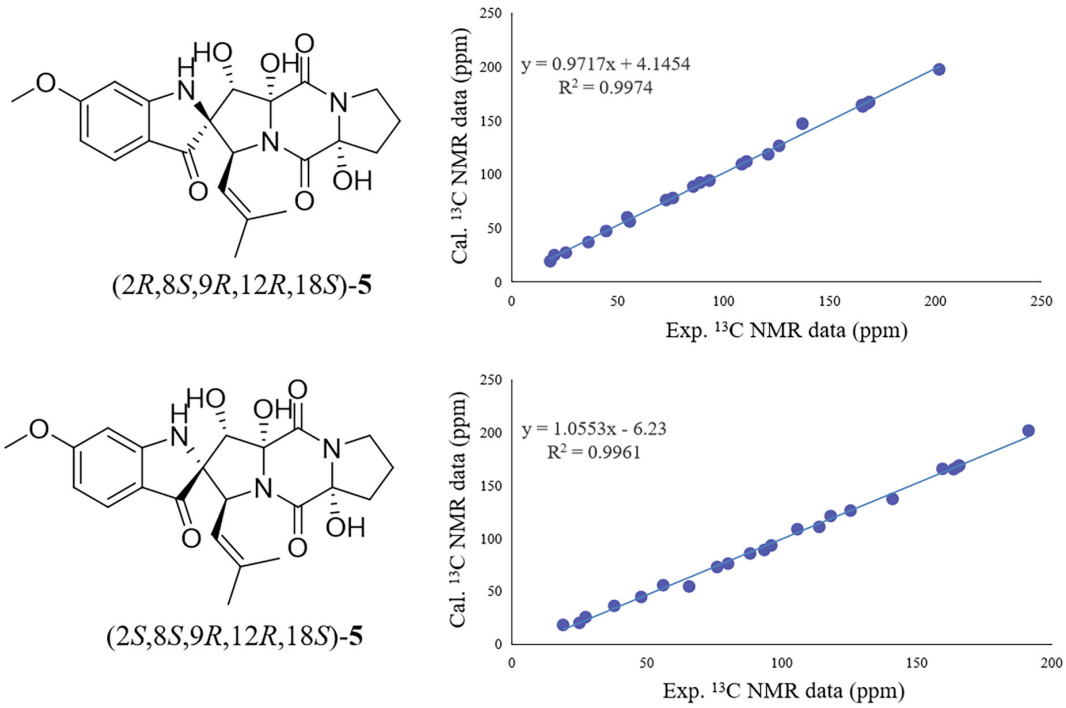

FIGURE 6
Regression analysis of experimental vs. calculated ^{13}C NMR chemical shifts of 5 with 2*R*, 8*S*, 9*R*, 12*R*, 18*S* and 2*R*, 8*S*, 9*R*, 12*R*, 18*S* configurations at the mPW1PW91/6-31 + G(d,p) level.

methines (δ_C 124.9, 120.9, 107.5, 94.6), three sp^3 quaternary carbons (δ_C 88.8, 85.1, 75.3), two sp^3 methines (δ_C 74.4, 61.0), three sp^3 methylenes (δ_C 44.5, 35.8, 20.2), one methoxyl group (δ_C 55.4), and two methyl groups (δ_C 25.4, 18.0). The ^{1}H NMR and ^{13}C NMR data showed similarities with those of spirotryprostatin G (5), indicating a similar planner structure (Table 1). Furthermore, the value of specific optical rotation $[\alpha]_D^{25}$ − 69.1 (*c* 0.08, MeOH) for 2 was negative which was in agreement with that of 1 ($[\alpha]_D^{25}$ − 81.2), and the experimental CD spectrum of 2 also showed similar cotton effect as that of 1. The above-mentioned evidence strongly supported the absolute configurations of 2 as 2*S*, 8*S*, 9*R*, 12*R*, 18*S*.

On the contrary, the value of specific optical rotation for spirotryprostatin G (5) was positive ($[\alpha]_D^{25}$ + 60.9), which is opposite to that of 1, 2, and 4, indicating the differences of absolute configurations. Also, further analysis of NOESY correlations of 5 showed the key correlations between N1-H and H-19 and between H-8 and H-7/N1-H/H-19, suggesting that H-7/N1-H/H-8/H-19 were on the same side. The above-mentioned data illustrated that the configuration of spiro carbon at the C-2 position of 5 might be different from that of 1, 2, and 4. The experimental and computational calculation CD spectra of 5 were then applied to elucidate the absolute configurations. It showed that the experimental CD spectrum of 5 was quite different from that of 2. ECD calculations of 2*S* and 2*R* configurations of 5 were also applied consequently comparing with experimental CD spectra. It showed that the calculated ECD spectrum of 2*R* matched well with the experimental ECD spectrum of 5, while the calculated ECD spectrum of 2*S* matched well with the experimental ECD spectrum of 2 (Figure 5). Moreover, the ^{13}C NMR chemical shifts of proposed structures for compound 5 with 2*R*, 8*S*, 9*R*, 12*R*, 18*S* and 2*S*, 8*S*, 9*R*, 12*R*, 18*S* configurations were subjected to calculate at the level of MPW1PW91/6-31G(d) with the PCM solvent model for DMSO. As a result, the calculated NMR values of (2*R*, 8*S*, 9*R*, 12*R*, 18*S*) of compound 5 was predicted to be the correct one with a DP4 + probability of 100% (using both H and C data) *via* comparing the data of candidate and experimental structures (Figure 6 and Supplementary Table S1). In addition, the values of the higher linear correlation coefficients (R^2), the lower RMSD, MAD, and CMAD also support the assigned absolute configuration as 2*R*, 8*S*, 9*R*, 12*R*, 18*S* (Supplementary Table S2). Thus, the absolute configurations of 2 and 5 (spirotryprostatin G) were finally confirmed to be 2*S*, 8*S*, 9*R*, 12*R*, 18*S*, and 2*R*, 8*S*, 9*R*, 12*R*, 18*S*, respectively (Supplementary Tables S3–S8).

Compound 3, a pale yellow powder, exhibited the molecular formula $C_{22}H_{25}N_3O_6$, as determined from the HRESIMS (*m/z* 426.1671, $[M - H]^-$, calcd. 426.1671), requiring 12 degrees of unsaturation. The ^{1}H NMR spectrum showed three aromatic protons at δ_H 7.26 (d, *J* = 8.6, H-4), 6.46 (d, *J* = 2.1, H-7), and 6.28 (dd, *J* = 8.6, 2.2, H-5), one methoxy group (δ_H 3.79), and two methyl groups (δ_H1.38, 1.57). The ^{13}C NMR

and DEPT135 NMR spectra showed signals for 22 carbons, including three carbonyl carbons (δ_C 195.3, 168.6, 164.8), four sp^2 quaternary carbons (δ_C 166.09, 163.9, 133.6, 113.4), four sp^2 methines (δ_C 124.8, 121.1, 107.5, 94.7), two sp^3 quaternary carbons (δ_C 85.4, 75.5), three sp^3 methine (δ_C 74.1, 60.7, 59.7), three sp^3 methylene (δ_C 44.5, 27.8, 22.6), and three methyl groups (δ_C 55.4, 25.4, 17.9). The ^{1}H NMR and ^{13}C NMR data of 3 showed similarity to those of 2 and differed only in the absence of the hydroxyl group of 2 (**Table 1**). The planner structure of 3 was further determined by HSQC, COSY, and HMBC correlations. In the NOESY spectrum of 3, the obvious correlation signals between N-H and H-7/H-18, H-8 and H_2-19, 8-OH, and H-12/9-OH were observed, indicating that these protons of H-7/N-H/8-OH/9-OH/H-12 were on the same side. Thus, the relative stereochemistry of 3 was determined. Further study showed that the specific optical rotation $[\alpha]_D^{25}$ − 151.1 (*c* 0.08, MeOH) for 3 was consistent with those of compounds 1, 2, and 4, which was opposite compared to that of the reported known compound spirotryprostatin C $[\alpha]_D^{25}$ + 147.2 (*c* 0.10, MeOH). The experimental ECD spectrum was then applied to determine the absolute configuration of 3. It showed that the experimental ECD spectrum of 3 had a similar Cotton effect curve with those of 2, suggesting 2*S* configurations, while the absolute configuration of spirotryprostatin C should be revised to 2*R* (**Figure 4**).

Bioassay

All the compounds were evaluated for their antimicrobial activities toward *Pseudomonas aeruginosa* PAO1, *Dickeya zeae* EC1, *Staphylococcus epidermidis*, *Escherichia coli,* and *Sporisorium scitamineum*. Compound 7 displayed moderate inhibitory activity toward dimorphic switch of pathogenic smut fungi *Sporisorium scitamineum* at 25 μM. Compounds 3 and 6 showed weak antibacterial activities against phytopathogenic bacterial *Dickeya zeae* EC1 at 100 μ M.

Conclusion

In this study, we described that three new spirooxindole diketone piperazine derivatives, named spirobrefeldins A–C (1–3), together with four known indole diketone piperazine analogs were isolated from *Penicillium brefeldianum*. The absolute configurations of compounds 1–5 were determined by CD spectra together with ECD calculations. The absolute configurations of C-2 chiral carbon in spirotryprostatin G (5) and spirotryprostatin C were revised accordingly. After preliminary antimicrobial inhibitory bioassays of them, compound 7 displayed moderate inhibitory activity toward the dimorphic switch of pathogenic smut fungi *Sporisorium scitamineum* at 25 μM. Compounds 3 and 6 showed weak antibacterial activities against phytopathogenic bacterial *Dickeya zeae* EC1 at 100 μ M.

Data availability statement

The original contributions presented in this study are included in the article/**Supplementary material**, further inquiries can be directed to the corresponding author.

Author contributions

HS and JJ did the experiments. JJ wrote the draft. HZ calculated the ECD spectra and determined the absolute structures. HJ measured and analyzed the NMR data. ZS did the fermentation and got crude extract. DL purified the strain from soil samples. LJ gave some advices on writing. FH designed the experiment, got the fundings, and wrote the manuscript. All authors contributed to the article and approved the submitted version.

Acknowledgments

We are thankful to the National Natural Science Foundation of China (41206130) and Guangdong Marine Economy Development Special Project No. GDNRC (2022) 35 and Research Funding of SMU for financial support.

Conflict of interest

The authors declare that the research was conducted in the absence of any commercial or financial relationships that could be construed as a potential conflict of interest.

Publisher's note

Supplementary material

The Supplementary Material for this article can be found online at: https://www.frontiersin.org/articles/10.3389/fmicb.2022.1046099/full#supplementary-material

References

Adeleke, B. S., and Babalola, O. O. (2021). The plant endosphere-hidden treasures: A review of fungal endophytes. *Biotechnol. Genet. Eng. Rev.* 37, 154–177. doi: 10.1080/02648725.2021.1991714

Bian, Z. G., Marvin, C. C., and Martin, S. (2013). Enantioselective total synthesis of (-)-citrinadin A and revision of its stereochemical structure. *J. Am. Chem. Soc.* 135, 10886–10889.

Bills, G., and Gloer, J. B. (2016). Biologically active secondary metabolites from the fungi. *Microbiol. Spectr.* 4, 1–32. doi: doi:10.1128/microbiolspec.FUNK-0009-2016

Blanchflower, S. E., Banks, R. M., Everett, J. R., and Reading, C. (1993). Further novel metabolites of the paraherquamide family. *J. Antibiot.* 46, 1355–1363. doi: 10.7164/antibiotics.46.1355

Bond, R. F., Boeyens, J. C. A., Holzapfel, C. W., and Steyn, P. S. (1979). Cyclopiamines A and B, novel oxindole metabolites of *Penicillium cyclopium* westling. *J. Chem. Soc. Perkin. Trans. I* 1, 1751–1761.

Demain, A. L., and Sanchez, S. (2009). Microbial drug discovery: 80 years of progress. *J. Antibiot.* 62, 5–16.

Greshock, T. J., Grubbs, A. W., Tsukamoto, S., and Williams, R. M. (2007). Total synthesis of stephacidin A and notoamide B. *Angew. Chem. Int. Ed.* 46, 2662–2665.

Grimblat, N., Zanardi, M. M., and Sarotti, A. M. (2015). Beyond DP4: An improved probability for the stereochemical assignment of isomeric compounds using quantum chemical calculations of NMR shifts. *J. Org. Chem.* 80, 12526–12534. doi: 10.1021/acs.joc.5b02396

He, F., Bao, J., Zhang, X. Y., Tu, Z. T., Shi, Y. M., and Qi, S. H. (2013a). Asperterrestide A, a cytotoxic cyclic tetrapeptide from the marine-derived fungus *Aspergillus terreus* SCSGAF0162. *J. Nat. Prod.* 76, 1182–1186. doi: 10.1021/np300897v

He, F., Han, Z., Peng, J., Qian, P. Y., and Qi, S. H. (2013b). Antifouling indole alkaloids from two marine derived strains. *Nat. Prod. Commun.* 8, 329–332.

He, F., Liu, Z., Yang, J., Fu, P., Peng, J., Zhu, W. M., et al. (2012). Novel antifouling alkaloid from halotolerant fungus *Penicillium* sp. OUCMDZ-776. *Tetrahedron. Lett.* 53, 2280–2283.

Huo, H. X., Zhu, Z. X., Song, Y. L., Shi, S. P., Sun, J., Sun, H., et al. (2018). Anti-inflammatory Dimeric 2- (2-Phenylethyl) chromones from the Resinous Wood of *Aquilaria sinensis*. *J. Nat. Prod.* 81, 543–553. doi: 10.1021/acs.jnatprod.7b00919

Jiang, J. Y., Jiang, H. M., Shen, D. N., Chen, Y. C., Shi, H. J., and He, F. (2022). Citrinadin C, a new cytotoxic pentacyclic alkaloid from marine-derived fungus *Penicillium citrinum*. *J. Antibiot.* 75, 301–303. doi: 10.1038/s41429-022-00516-8

Kagiyama, I., Kato, H., Nehira, T., Frisvad, J. C., Sherman, D. H., Williams, R. M., et al. (2016). Taichunamides. Prenylated indole alkaloids from *Aspergillus taichungensis* (IBT 19404). *Angew. Chem. Int. Ed. Engl.* 55, 1128–1132.

Kato, H., Yoshida, T., Tokue, T., Nojiri, Y., Hirota, H., Ohta, T., et al. (2007). Notoamides A–D: Prenylated indole alkaloids isolated form a marine-derived fungus, *Aspergillus* sp. *Angew. Chem. Int. Ed. Engl.* 46, 2254–2256. doi: 10.1002/anie.200604381

Keller, N. P. (2019). Fungal secondary metabolism: Regulation, function and drug discovery. *Nat. Rev. Microbiol.* 17, 167–180.

Klas, K. R., Kato, H., Frisvad, J. C., Yu, F., Newmister, S. A., Fraley, A. E., et al. (2018). Structural and stereochemical diversity in prenylated indole alkaloids containing the bicyclo [2.2.2] diazaoctane ring system from marine and terrestrial fungi. *Nat. Prod. Rep.* 35, 532–558. doi: 10.1039/c7np00042a

Li, X. J., Zhang, Q., Zhang, A. L., and Gao, J. M. (2012). Metabolites from *Aspergillus fumigatus*, an endophytic fungus associated with *Melia azedarach*, and their antifungal, antifeedant, and toxic activities. *J. Agric. Food Chem.* 60, 3424–3431. doi: 10.1021/jf300146n

Lin, S., He, Y., Li, F. L., Yang, B. Y., Liu, M. T., Zhang, S. T., et al. (2020). Structurally diverse and bioactive alkaloids from an insect-derived fungus *Neosartorya fischeri*. *Phytochem* 17:112374. doi: 10.1016/j.phytochem.2020.112374

Lin, Z. J., Wen, J. N., Zhu, T. J., Fang, Y. C., Gu, Q. Q., and Zhu, W. M. (2008). Chrysogenamide A from an endophytic fungus associated with *Cistanche deserticola* and its neuroprotective effect on SH-SY5Y cells. *J. Antibiot.* 61, 81–85. doi: 10.1038/ja.2008.114

Liu, Z. W., Zhao, F. L., Zhao, B. Y., Yang, J., Ferrara, J., Sankaran, B., et al. (2021). Structural basis of the stereoselective formation of the spirooxindole ring in the biosynthesis of citrinadins. *Nat. Commun.* 12:4158. doi: 10.1038/s41467-021-24421-0

Marcarino, M. O., Cicetti, S., Zanardi, M. M., and Sarotti, A. M. (2022). A critical review on the use of DP4+ in the structural elucidation of natural products: The good, the bad and the ugly. A practical guide. *J. Nat. Prod.* 39, 58–76. doi: 10.1039/d1np00030f

Marin-Felix, Y., Groenewald, J. Z., and Cai, L. (2017). Genera of phytopathogenic fungi: GOPHY 1. *Stud. Mycol.* 86, 99–216.

Mercado-Marin, E. V., Garcia-Reynaga, P., Romminger, S., Pimenta, E. F., Romney, D. K., Lodewyk, M. W., et al. (2014). Total synthesis and isolation of citrinalin and cyclopiamine congeners. *Nature* 509, 318–324. doi: 10.1038/nature13273

Newman, D. J. (2021). Natural product based antibody drug conjugates: Clinical status as of November 9, 2020. *J. Nat. Prod.* 84, 917–931. doi: 10.1021/acs.jnatprod.1c00065

Paterson, R. R. M., Simmonds, M. S. J., and Blaney, W. M. (1987). Mycopesticidal effects of characterized extracts of *Penicillium* isolates and purified secondary metabolites (including mycotoxins) on drosophila melanogaster and *Spodoptora littoralis*. *J. Invertebr. Pathol.* 50, 124–133.

Rottmann, M., McNamara, C., Yeung, B. K., Lee, M. C., Zou, B., Russell, B., et al. (2010). Spiroindolones, a potent compound class for the treatment of malaria. *Science* 329, 1175–1180.

Schueffler, A., and Anke, T. (2014). Fungal natural products in research and development. *Nat. Prod. Rep.* 31, 1425–1448.

Steele, A. D., Teijaro, C. N., Yang, D., and Shen, B. (2019). Leveraging a large microbial strain collection for natural product discovery. *J. Biol. Chem.* 45, 16567–16576. doi: 10.1074/jbc.REV119.006514

Tiwari, P., and Bae, H. (2022). Endophytic fungi: Key insights, emerging prospects, and challenges in natural product drug discovery. *Microorganisms* 10:360. doi: 10.3390/microorganisms10020360

Tsuda, M., Kasai, Y., Komatsu, K., Sone, T., Tanaka, M., Mikami, Y., et al. (2004). Citrinadin A, a novel pentacyclic alkaloids from marine-derived fungus *Penicillium citrinum*. *Org. Lett.* 6, 3087–3089. doi: 10.1021/ol048900y

Tsukamoto, S., Umaoka, H., Yoshikawa, K., Ikeda, T., and Hirota, H. (2010). Notoamide O a structurally unprecedented prenylated indole alkaloid, and notoamides P-R from a marine-derived fungus. *Aspergillus* sp. *J. Nat. Prod.* 73, 1438–1440. doi: 10.1021/np1002498

Wang, F. Z., Fang, Y. C., Zhu, T. J., Zhang, M., Lin, A. Q., Gu, Q. Q., et al. (2008). Seven new prenylated indole diketopiperazine alkaloids from holothurian-derived fungus *Aspergillus fumigatus*. *Tetrahedron* 64, 7986–7991.

Wen, J., Okyere, S. K., Wang, S., Wang, J. C., Xie, L., Ran, Y. N., et al. (2022). Endophytic fungi: An effective alternative source of plant-derived bioactive compounds for pharmacological studies. *J. Fungi* 20:205. doi: 10.3390/jof8020205

Wu, Y. H., Zhang, Z. H., Huang, J. J., Zhong, Y., Li, X. X., Deng, Y. Y., et al. (2017). Sumalactones A–D, four new curvularin-type macrolides from a marine deep-sea fungus *Penicillium sumatrense*. *RSC Adv.* 7, 40015–40019.

Ye, N., Chen, H., Wold, E. A., Shi, P. Y., and Zhou, J. (2016). Therapeutic potential of spirooxindoles as antiviral agents. *ACS Infect. Dis.* 2, 382–392.

Zhang, Y. H., Geng, C., Zhang, X. W., Zhu, H. J., Shao, C. L., Cao, F., et al. (2019). Discovery of bioactive indole-diketopiperazines from the marine-derived fungus *Penicillium brasilianum* aided by genomic information. *Mar. Drugs* 17:514. doi: 10.3390/md17090514

Zhang, Z. H., Min, X. T., Huang, J. J., Zhong, Y., Wu, Y. H., Li, X. X., et al. (2016). Cytoglobosins H and I, new antiproliferative cytochalasans from deep-sea-derived fungus *Chaetomium globosum*. *Mar. Drugs* 14:233. doi: 10.3390/md14120233

Zhong, Y., Yan, M. X., Jiang, J. Y., Zhang, Z. H., Huang, J. J., Zhang, L. H., et al. (2018). Mycophenolic acid as a promising fungal dimorphism inhibitor to control sugar cane disease caused by *Sporisorium scitamineum*. *J. Agric. Food Chem.* 67, 112–119. doi: 10.1021/acs.jafc.8b04893

frontiers | Frontiers in Microbiology

TYPE Original Research
PUBLISHED 13 December 2022
DOI 10.3389/fmicb.2022.1099592

OPEN ACCESS

EDITED BY
Peng Zhang,
Tobacco Research Institute (CAAS), China

REVIEWED BY
Fengyu Du,
Qingdao Agricultural University, China
Xiao-Dong Li,
Yantai Institute of Coastal Zone Research (CAS), China

*CORRESPONDENCE
Xuemian Lu
luxuemian@wmu.edu.cn
Chi Zhang
zhangchi515@126.com

†These authors have contributed equally to this work

SPECIALTY SECTION
This article was submitted to Antimicrobials, Resistance and Chemotherapy, a section of the journal Frontiers in Microbiology

RECEIVED 16 November 2022
ACCEPTED 29 November 2022
PUBLISHED 13 December 2022

CITATION
Weng W, Jiang S, Sun C, Pan X, Xian L, Lu X and Zhang C (2022) Cytotoxic secondary metabolites isolated from *Penicillium* sp. YT2019-3321, an endophytic fungus derived from *Lonicera Japonica*. *Front. Microbiol.* 13:1099592. doi: 10.3389/fmicb.2022.1099592

Cytotoxic secondary metabolites isolated from *Penicillium* sp. YT2019-3321, an endophytic fungus derived from *Lonicera Japonica*

Wenya Weng[1,2†], Shicui Jiang[1†], Chuchu Sun[1], Xiaofu Pan[1], Li Xian[3], Xuemian Lu[1,2*] and Chi Zhang[1*]

[1]Department of Scientific Research, The Third Affiliated Hospital of Wenzhou Medical University, Zhejiang, China, [2]Department of Endocrinology, Ruian People's Hospital, Zhejiang, China, [3]College of Life Sciences, Ludong University, Yantai, China

Introduction: Endophytic fungi associated with medicinal plants have proven to possess a high potential to produce structurally diverse metabolites, some of which are valuable for medicinal applications. In this study, *Penicillium* sp. YT2019-3321, an endophytic fungus derived from traditional Chinese medicine Lonicera japonica, was chemically studied.

Methods: The chemical structures of the isolated compounds were established by a correlative interpretation of HRESIMS and NMR spectroscopic data. The optical resolution of (±)-**1** by chiral HPLC yielded individual enantiomers (+)-**1** and (−)-**1**, and their stereochemistry were solved by X-ray diffraction crystallography, respectively.

Results and discussion: Eight structurally diversified secondary metabolites, including two previously unreported polyketides, named (±)-chrysoalide B (**1**) and penicidone E (**2**), were isolated and identified from Penicillium sp. YT2019-3321. Compound 2 possessed the γ-pyridone nucleus, which is rarely found in natural products. Cytotoxic assay revealed that the new compound 2 demonstrated a dose-dependent cytotoxicity against the human pancreatic tumor cells PATU8988T with the IC_{50} value of 11.4 μM. Further studies indicated that **2** significantly induced apoptosis of PATU8988T cell lines, characterized by the morphologies abnormity, the reduction of cell number, the upregulation of proportion of apoptotic cells, and the ratio of Bcl-2 to Bax. Our study demonstrates that fungal secondary metabolites may have important significance in the discovery of drug leads.

KEYWORDS

polyketides, secondary metabolites, *Penicillium*, endophytic fungus, cytotoxic activity

1 Introduction

Filamentous fungi from both marine and terrestrial sources are inherently regarded as a treasure house of structurally diversified secondary metabolites with potent pharmacological activity (Bills and Gloer, 2016; Zhang et al., 2016; Deshmukh et al., 2018). Fungi possess a well-developed secondary metabolism, which hold unique biosynthetic pathways to produce these fungal metabolites with a staggering variation in chemical structures and biological activities (Yu and Keller, 2005; Fox and Howlett, 2008; Ortega et al., 2021). Fungal metabolites have developed many important pharmaceuticals. The success of the β-lactam antibiotics including penicillins and cephalosporins effectively aroused the enthusiasm of the development of microbial medicines and contributed significantly in the establishment of the modern pharmaceutics (Zhang et al., 2020; Li et al., 2021). Subsequently, a large number of fungal-sourced pharmaceuticals with various mode of action, such as fusidic acid, griseofulvin, pneumocandin, lovastatin, cyclosporin A, and ergometrine, have been on the market (Bills and Gloer, 2016). It is estimated that an appreciable portion of natural-derived approved therapeutic agents were actually sourced from microorganisms, especially from fungi (Newman and Cragg, 2020). Moreover, many agricultural chemicals, including the existing fungicides, insecticides, and herbicides, are also fungal-derived (Sparks et al., 2017; Xu et al., 2021).

Endophytic fungi are recognized as microorganisms that spend the whole or part of their lifetime colonizing inter-and/or intra-cellularly plant tissues without causing any apparent disease symptoms (Aly et al., 2011). Endophytic fungi associated with medicinal plants have proven to possess a high potential to produce structurally diverse metabolites, some of which are valuable for medicinal and agricultural applications (Gouda et al., 2016). For example, chemical investigation of *Alternaria* sp. YUD20002, an endophytic fungus derived from the tubers of *Solanum tuberosum*, yielded five previously undescribed epoxy octa-hydronaphthalene polyketides altereporenes A-E (Xia et al., 2022). Acrocalysterols A and B, two new steroids were isolated from an endophytic fungus *Acrocalymma* sp. derived from the stems of *Sinomenium acutum* (Yang et al., 2022). Acrocalysterol B demonstrated strong cytotoxicity against HeLa, HCC-1806, and RKO cell lines with IC_{50} values of 18.37-19.64 μM (Yang et al., 2022). It should be pointed out that the genus belonging to *Penicillium* is considered as a rich resource of bioactive metabolites. In this study, chemical studies and chromatographic separation on *Penicillium* sp. YT2019-3321, an endophytic fungus derived from traditional Chinese medicine *Lonicera Japonica*, resulted in the isolation and identification of eight structurally diversified secondary metabolites, including two previously unreported polyketides, named (±)-chrysoalide B (**1**) and penicidone E (**2**) (Figure 1). The optical resolution of (±)-**1** by chiral HPLC yielded individual enantiomers (+)-**1** and (−)-**1**, and their stereochemistry were solved by X-ray diffraction crystallography. The new compound **2** possessed the γ-pyridone nucleus, which is rarely found in natural products. In addition to the structural elucidation, the cytotoxic activity of the isolated compounds is also described herein.

2 Materials and methods

2.1 General experimental procedures

Optical rotations were measured with a JASCO P-1020 digital polarimeter (Tokyo, Japan). UV spectra were obtained on a Lambda 35 UV/Vis spectrophotometer (Perkin Elmer, Waltham, United States). HRESIMS data were acquired with a scientific LTQ Orbitrap XL spectrometer (Thermo Scientific, Waltham, United States). 1D (500 and 125 MHz for ^{1}H and ^{13}C, respectively) and 2D (HSQC, COSY, and HMBC) NMR spectra were performed by an Agilent DD2 500 MHz spectrometer (Agilent Technologies, Santa Clara, United States). X-ray diffraction data were collected on an Agilent Xcalibur Gemini E diffractometer equipped with Eos charge-coupled device (CCD) detector with graphite monochromated Cu Kα radiation (λ = 1.54178 Å). Column chromatography was undertaken by using various packing materials including silica gel (100-200/200-300 mesh, Qingdao Marine Chemical Factory, Qingdao, China), octadecylsilyl (ODS) reversed-phase gel (30-50 μm, YMC CO., Ltd., Japan), and Sephadex LH-20 (GE Healthcare, United States).

2.2 Fungal material and fermentation

The fungal strain *Penicillium* sp. YT2019-3321 was previously isolated from the traditional Chinese medicine *Lonicera Japonica*. The taxonomic identification of this fungus was performed based on a molecular protocol by DNA amplification and sequencing of the internal transcribed spacer (ITS) of the rRNA locus. The ITS sequence showed 99% identical to that of *P. oxalicum* (GenBank accession no. KY400080.1). A voucher specimen of this fungal strain was stored at −80°C at the Third Affiliated Hospital of Wenzhou Medical University. This fungus was cultured on potato dextrose agar medium (PDA, Solarbio Life Sciences CO., Ltd., Beijing, China) at 28°C for 5 days. Then all of agar plugs were cut into small pieces (0.5 × 0.5 cm^2). Each piece was inoculated in a 1 L Erlenmeyer flask containing 250 mL of potato dextrose broth (PDB) medium (Solarbio). A total of 100 flasks were statically fermented at room temperature for 30 days.

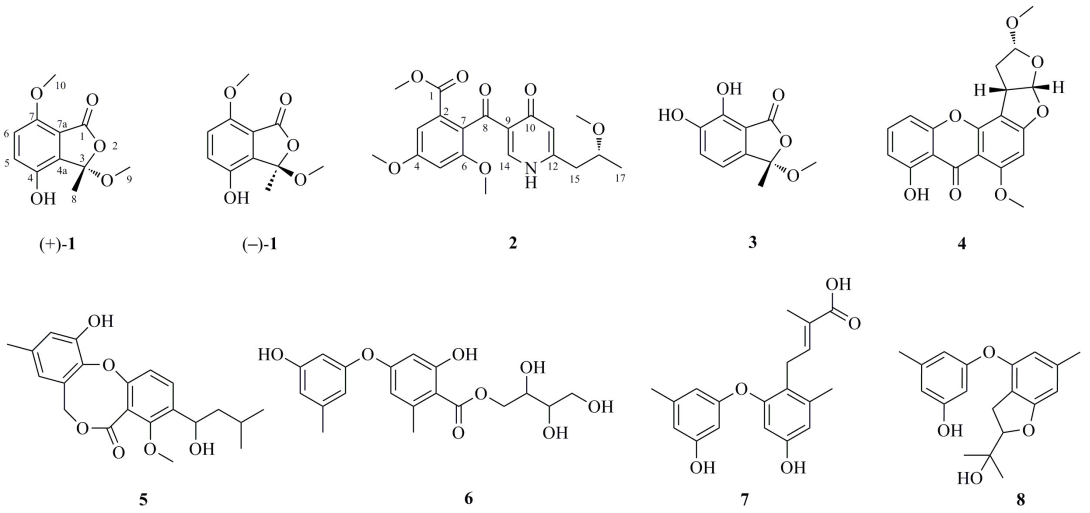

FIGURE 1
Structures of the isolated compounds **1–8**.

2.3 Extraction and isolation

The fermentation materials were adequately extracted with EtOAc (3 × 25 L), and the organic solvent was evaporated in vacuum to yield ca. 20 g of crude extracts. The crude extracts were subjected to a silica gel vacuum liquid chromatography column, which was eluted with an increasing gradient of EtOAc/petroleum ether (from 30:1 to 1:1) to afford six fractions (Fr. 1-Fr. 6). Fr. 4 (3.2 g), eluting with EtOAc/petroleum ether 5:1, was further fractionated over an ODS reversed-phase silica gel with a mixed solvent system of MeOH/H_2O (from 10 to 100%, v/v). This afforded a total of eight subfractions (Fr. 4.1-Fr. 4.8). Fr. 4.6 was further purified over an open silica gel column chromatography by using the solvent system CH_2Cl_2 and MeOH with the ratio 20:1 to afford 16 mg of compound **2**. Fr. 5 (2.5 g), eluting with EtOAc/petroleum ether 2:1, was applied to ODS silica gel with gradient elution of MeOH/H_2O (from 10 to 100%, v/v) to yield eight subfractions (Fr. 5.1-Fr. 5.8). Compound **1** (10.2 mg) was isolated from a two-step purification process, first from Fr. 5.3 over an open silica gel column chromatography using the solvent system CH_2Cl_2 and MeOH with the ratio 20:1, followed by preparative TLC (CH_2Cl_2/MeOH, 15:1, v/v). Compound **1** was further resolved into the pure enantiomers (+)-**1** (4.9 mg, t_R = 9.6 min) and (−)-**1** (4.7 mg, t_R = 10.9 min) by chiral HPLC using a (*R*,*R*). Whelk-O1 chiral column (10 mm; 4.6 × 250 mm; *n*-hexane-ethanol eluent 6:4, v/v; 1.0 mL/min). Compound **3** (10.2 mg, t_R 7.7 min) was isolated from Fr. 5.4 by semipreparative HPLC (YMC-pack ODS-A, 5 μm; 10 × 250 mm; 55% MeOH/H_2O; flow rate 2 mL/min). Compound **7** (5.6 mg) was isolated from Fr. 5.5 by preparative TLC (CH_2Cl_2/MeOH/acetic acid, 15:1:0.4, v/v). Compound **6** (11.3 mg) was isolated from Fr. 5.6 by preparative TLC (CH_2Cl_2/MeOH/acetic acid, 20:1:0.4, v/v). Fr. 6 (4.0 g), eluting with EtOAc/petroleum ether 1:1, was fractionated by Sephadex LH-20 column chromatography in MeOH to give subfractions Fr. 6.1-Fr. 6.3. Fr. 6.1 was subjected to semipreparative HPLC (65% MeOH/H_2O) to give compounds **4** (20.2 mg, t_R 6.9 min) and **5** (6.2 mg, t_R 8.8 min), respectively. Finally, compound **8** (4.9 mg) was obtained by preparative TLC (CH_2Cl_2/MeOH, 20:1, v/v) from Fr. 6.3.

(±)-Chrysoalide B (**1**): white amorphous powder; $[\alpha]^{20}_D$ + 9.6 (*c* 0.10, MeOH) for (+)-**1** and $[\alpha]^{20}_D$ −10.2 (*c* 0.10, MeOH) for (−)-**1**; UV (MeOH) λ_{max} (log ε) 213 (2.16), 239 (1.60), 331 (1.49) nm; ^{1}H and ^{13}C NMR data (measured in DMSO-d_6) (see Table 1); HRESIMS *m/z* 223.0644 [M - H]$^-$ (calcd for $C_{11}H_{11}O_5$, 223.0606).

Penicidone E (**2**): colorless oil; $[\alpha]^{20}_D$ + 13.5 (*c* 0.10, MeOH); UV (MeOH) λ_{max} (log ε) 220 (3.88), 254 (3.26), 309 (2.98); ^{1}H and ^{13}C NMR data (measured in DMSO-d_6) (see Table 1); HRESIMS *m/z* 390.1547 [M + H]$^+$ ($C_{20}H_{24}NO_7$) and 412.1369 [M + Na]$^+$ ($C_{20}H_{23}NO_7Na$).

2.4 X-ray crystallographic analysis of (+)-1 and (−)-1

Suitable crystals of (+)-**1** and (−)-**1** were obtained by slowly evaporating the solvent mixture of MeOH and H_2O. Single-crystal X-ray diffraction data were obtained on an Agilent Xcalibur Gemini E diffractometer equipped with Eos CCD detector with graphite monochromated Cu Kα radiation (λ = 1.54178 Å). Structures were solved by direct methods using the SHELXTL software package (Sheldrick, 1997a). All non-hydrogen atoms were refined anisotropically. H atoms were located by geometrical calculations, and their positions and

TABLE 1 NMR data for compounds (±)-1 and 2 in DMSO-d_6 (^{1}H at 500 MHz and ^{13}C at 125 MHz).

No.	Compound (±)-1		No.	Compound 2	
	δ_H (mult, *J* in Hz)	δ_C, type		δ_H (mult, *J* in Hz)	δ_C, type
1		165.1, C	1		166.3, C
3		106.8, C	2		129.6, C
4		146.6, C	3	6.93 (s)	105.3, CH
4a		132.2, C	4		160.0, C
5	7.13 (d, 8.8)	123.5, CH	5	6.80 (s)	103.2, CH
6	7.05 (d, 8.8)	115.2, CH	6		157.6, C
7		150.2, C	7		127.9, C
7a		115.2, C	8		192.4, C
8	1.75 (s)	23.6, CH_3	9		124.5, C
9	2.94 (s)	50.7, CH_3	10		175.8, C
10	3.80 (s)	55.9, CH_3	11	6.00 (s)	121.3, CH
			12		148.5, C
			14	8.12 (s)	142.2, CH
			15	2.60 (m)	39.2, CH_2
			16	3.62 (m, overlap)	75.3, CH
			17	1.11 (d, 6.1)	19.1, CH_3
			1-OMe	3.64 (s)	52.5, CH_3
			4-OMe	3.84 (s)	56.0, CH_3
			6-OMe	3.66 (s)	56.5, CH_3
			16-OMe	3.23 (s)	56.0, CH_3

thermal parameters were fixed during structure refinement. Structure was refined by full-matrix least-squares techniques (Sheldrick, 1997b).

Crystal data for (+)-**1**: $C_{22}H_{26}O_{11}$ (2 $C_{11}H_{12}O_5$ + H_2O), F.W. = 466.43, monoclinic space group $P2_1$, unit cell dimensions a = 7.3590 (9) Å, b = 14.4044 (16) Å, c = 10.4189 (12) Å, $\alpha = \beta = \gamma = 90°$, V = 1103.9 (2) Å^3, Z = 2, d_{calcd} = 1.403 mg/m^3. Crystal size: 0.08 × 0.05 × 0.04 mm^3, μ = 0.967 mm^{-1}, F (000) = 492.0. Reflections collected/unique: 19,174/4,377 [R (int) = 0.0438]. Final indices resulted in R_1 = 0.0424 and wR_2 = 0.1067 [$I > 2\sigma(I)$] Flack parameter = 0.13 (6).

Crystal data for (−)-**1**: $C_{22}H_{26}O_{11}$ (2 $C_{11}H_{12}O_5$ + H_2O), F.W. = 466.43, monoclinic space group $P2_1$, unit cell dimensions a = 7.3638 (2) Å, b = 14.3632 (4) Å, c = 10.4176 (3) Å, $\alpha = \beta = \gamma = 90°$, V = 1101.11 (5) Å^3, Z = 2, d_{calcd} = 1.407 mg/m^3. Crystal size: 0.12 × 0.07 × 0.04 mm^3, μ = 0.970 mm^{-1}, F (000) = 492.0. Reflections collected/unique: 25,073/4,450 [R (int) = 0.0590]. Final indices resulted in R_1 = 0.0358 and wR_2 = 0.0827 [$I > 2\sigma(I)$] Flack parameter = 0.05 (10).

2.5 Cytotoxic bioassay

2.5.1 Cell culture

The human pancreatic cancer cell line PATU8988T was acquired from Shanghai Fuheng Biotechnology Co., Ltd., RPMI 1640 medium containing 10% fetal bovine serum (Gibco, Gaithersburg, MD, USA) was used. The cells were cultured in 5% CO_2 at 37°C. Cells were treated with the positive control doxorubicin (dox) at the dose of 10 μM and the test compounds at the dose of 20 μM, respectively, for 48 h when they reached ∼80% confluence.

2.5.2 Cell viability assay

CCK-8 (Solarbio) was applied to detect the cell viability according to the manufacturer's instruction as previously described (Yuan et al., 2020). In brief, cells were treated with test compounds at the gradient concentration of 1, 5, 10, 20, 30, 40, and 50 μM for 24 and 48 h, respectively. Doxorubicin (dox) at the concentration of 10 μM was applied as the positive control. Then the media of the cells was changed with 10% CCK-8 solution followed by indcubating 5% CO_2 at 37°C. Cell viability was detected at absorbance of 450 nm.

2.5.3 Flow cytometry

Cell apoptosis was examined by flow cytometry using Annexin V-FITC Apoptosis Detection Kit (Beyotime Biotechnology, China) according to the manufacturer's instruction. Cells were incubated with or without test compounds at 20 μM for 48 h, followed by being treated with 200 mL binding buffer and stained with Annexin V-FITC and PI for 40 min in the dark. After that, the cells were assessed by flow cytometry (Agilent, United States).

2.5.4 Western blot analysis

RIPA buffer (Beyotime Biotechnology, China) containing protease inhibitors (Beyotime Biotechnology, China) was applied to extract protein lysates of the cells. The concentration of protein was examined by the Bradford assay. The samples

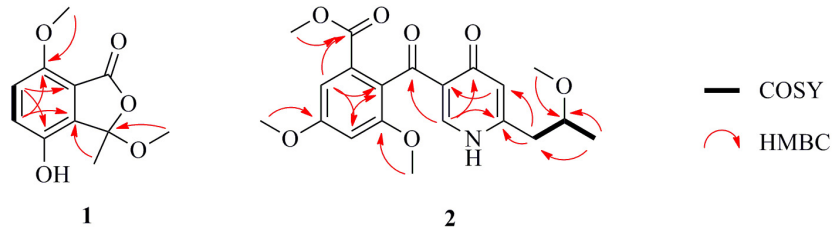

FIGURE 2
Key COSY and HMBC correlations for **1** and **2**.

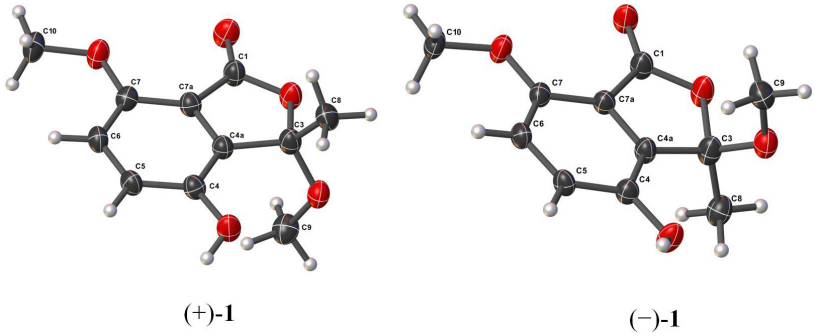

FIGURE 3
Molecular structures of (+)-**1** and (−)-**1** from single-crystal X-ray diffractometry.

were diluted in loading buffer and denatured at 95°C for 5 min. Then they were separated in SDS PAGE gel followed by being transferred into nitrocellulose membranes for next steps. After being treated with blocking solution for 1 h at room temperature, the membranes were incubated with the following primary antibodies: Bax and Bcl-2 purchased from ABclone. After that, membranes were washed with Tris-buffered saline (pH 7.2) containing 0.05% Tween 20 for 15 min for three times followed by being treated with secondary antibodies for 1 h at room temperature. Bands were visualized with ECL substrate (Bio-Rad Laboratories).

2.6 Computational details

The conformer rotamer ensemble sampling tool (crest) (Pracht et al., 2020) was used to afford candidate conformers for *S*-**2** and DFT calculations were performed with the Gaussian 16 program (Frisch et al., 2016). The conformers within an energy window of 10 kcal/mol were optimized at B3LYP/6-31G (d) level of theory with Grimme's D3 dispersion correction ("EmpiricalDispersion = GD3" key words in input files). Frequency analysis of all optimized conformations was undertaken at the same level of theory to ensure they were true local minima on the potential energy surface. Then, energies of all optimized conformations were evaluated by M062X/6-311 + G (2d,p) with D3 dispersion correction. Gibbs free energies of each conformers were calculated by adding "Thermal correction to Gibbs Free Energy" obtained by frequency analysis to electronic energies obtained at M062X/6-311 + G (2d,p). Room-temperature (298.15 K) equilibrium populations were calculated according to Boltzmann distribution law. Those conformers accounting for over 2% population were subjected to subsequent calculations. Calculation of optical rotations of different conformers were carried out using the TDDFT method at CAM-B3LYP/6-311 + g (2d,p) level in methanol (λ = 589 nm). Detailed computational data have shown in **Supplementary material**.

3 Results and discussion

3.1 Structural elucidation

(±)-Chrysoalide B (**1**) was isolated as white amorphous powder. Its molecular formula, $C_{11}H_{12}O_5$, was established by HRESIMS at *m/z* 223.0644 $[M\text{-}H]^-$ (calcd for $C_{11}H_{11}O_5$, 223.0606). Observation of the ^{1}H NMR data of **1** (Table 1) revealed the presence of three methyl groups including two methoxy groups at δ_H 2.94 (s, H_3-9) and 3.80 (s, H_3-10) as well as two coupled aromatic methines at δ_H 7.13 (d, J = 8.8 Hz, H-5) and 7.05 (d, J = 8.8 Hz, H-6). The ^{13}C spectroscopic data of **1** (Table 1) displayed 11 carbon resonances, including an ester carbonyl at δ_C 165.1 (C-1), five quaternary carbons including

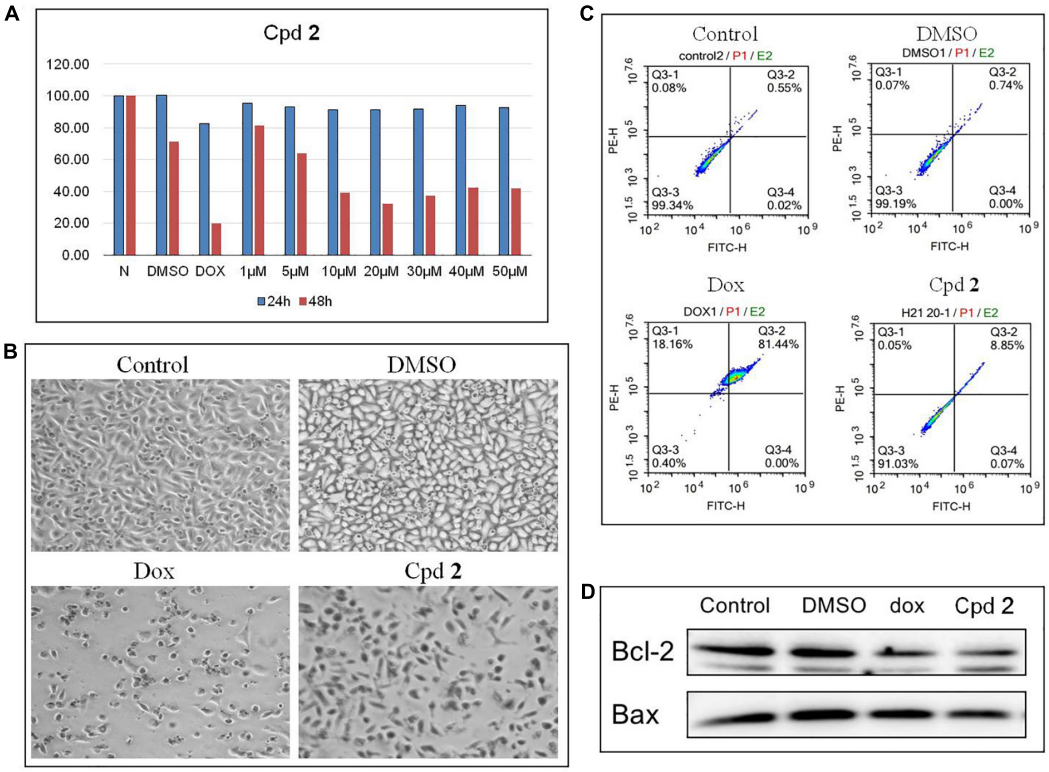

FIGURE 4
Compound **2** (Cpd **2**) induced human pancreatic cancer cells apoptosis. **(A)** Cytotoxic effect of Cpd **2** on PATU8988T measured by CCK-8. Cells were treated with Cpd **2** at the gradient concentrations from 1 to 50 μM for 24 and 48 h, respectively. **(B)** Morphological results of PATU8988T treated with Cpd **2**. **(C)** Annexin V/PI double staining with flow cytometry analysis was used for the detection of cell apoptosis. **(D)** Western blotting of Bcl-2 and Bax.

one oxygenated sp^3 at δ_C 106.8 (C-3), two aromatic methines at δ_C 123.5 (C-5) and 115.2 (C-6), and three methyl groups including two methoxy groups at δ_C 50.7 (C-9) and 55.9 (C-10). Considering the functional groups observed for compound **1** as well as the characteristic UV absorption peaks at 213, 239, and 331 nm (Saetang et al., 2021), the presence of an isobenzofuran core framework was deduced. HMBC correlations (**Figure 2**) from H-5 to C-4a and C-7 as well as from H-6 to C-4 and C-7a deduced the presence of a 1,2,3,4-tetrasubstituted benzene group. Finally, HMBC correlations from H_3-9 to C-3 and from H_3-10 to C-7 led to the location of two methoxy groups at C-3 and C-7, respectively. The planar structure of **1** was thus determined as shown in **Figure 1**.

Compound **1** possessed the same planar structure as chrysoalide B, a new phthalide produced by the marine-derived fungus *Penicillium chrysogenum* LD-201810 (Ge et al., 2021). Surprisingly, the specific rotation value of **1** was found to be zero. Considering its baseline ECD curve, compound **1** was existed as racemic enantiomers. Compound **1** was then subjected to chiral HPLC separation, which successfully afforded two individual enantiomers (+)-**1** and (−)-**1** with a ratio of 1:1. Both (+)-**1** and (−)-**1** were cultured into suitable single crystals in MeOH/H_2O mixed solution. Single-crystal X-ray diffraction of (+)-**1** and (−)-**1** (**Figure 3**) not only confirmed the proposed structure but also the absolute configurations of (+)-**1** and (−)-**1**. It should be pointed out that Ge et al. (2021) reported the new compound chrysoalide B with the optical rotation of + 15.8° and established the absolute configuration of C-3 to be *R* based on ECD calculations. However, in our study, the absolute configuration of (+)-chrysoalide B (**1**) was revised as 3*S* by single-crystal X-ray diffraction.

Penicidone E (**2**), isolated as colorless oil, was found to possess the molecular formula of $C_{20}H_{23}NO_7$ on the basis of HRESIMS (*m/z* 390.1547 $[M + H]^+$ for $C_{20}H_{24}NO_7$ and 412.1369 $[M + Na]^+$ for $C_{20}H_{23}NO_7Na$). Overall inspection of the ^1H and ^{13}C NMR spectra of **2** (**Table 1**) indicated that it contained two carbonyls at δ_C 192.4 (C-8) and 175.8 (C-10), one ester carbonyl at δ_C 166.3 (C-1), ten sp^2-hybridized carbons which resonated between δ_C 103.2 and 160.0, one methylene at δ_C 39.2 (C-15), one oxygenated sp^3 methine at δ_C 75.3 (C-16), and five methyls including four methoxy groups at δ_C 52.5 (1-OMe), 56.0 (4-OMe), 56.5 (6-OMe), and 56.0 (16-OMe). The ^1H and ^{13}C NMR spectra of **2** were partially similar to that of penicidone C, a cytotoxic alkaloidal metabolite isolated from

an endophytic *Penicillium* sp. (Ge et al., 2008). However, the resonances at δ_C 125.3 and 134.2 ascribable to the two sp^2 methine groups in penicidone C were replaced by a methylene (C-15) and an oxygenated sp^3 methine (C-16). Moreover, an extra methoxyl signal at δ_H 3.23 and δ_C 56.0 (16-OMe) appeared in the ^1H and ^{13}C NMR spectra of **2**. The observation could be explained by assuming that **2** was an oxidative derivative of penicidone C at the location of C-15 and C-16. This assumption was reinforced by the HMBC correlations from H_3-17 to C-15 and C-16, from H_2-15 to C-11 and C-12, and from 16-OMe to C-16 (**Figure 2**). Compound **2** was named as penicidone E. The γ-pyridone nucleus found in **2** is rare in natural products, with only four analogs, penicidones A-D, possessing similar structures (Liu et al., 2015). Calculation of optical rotations of different conformers 16*R* and 16*S* were carried out using the TDDFT method at CAM-B3LYP/6-311 + g (2d,p) level in methanol (λ = 589 nm). The calculated optical rotation was −24.4, which was of the opposite sign to the experimental value ($[\alpha]^{20}_D$ + 13.5). Therefore, the absolute configuration of **2** was established as 16*R*.

In addition to the new compounds **1** and **2**, the structures of the remaining six known compounds were established based on their spectroscopic data, as well as by comparison with the literatures. These compounds were identified as 6,7-dihydroxy-3-methoxy-3-methylphthalide (**3**) (Wang et al., 2013), oxisterigmatocystin C (**4**) (Cai et al., 2011), penicillide (**5**) (Jeon and Shim, 2020), a diphenyl ether **6** (Wu et al., 2018), diorcinol L (**7**) (Li et al., 2018), and 3-[2-(1-hydroxy-1-methyl-ethyl)-6-methyl-2,3-dihydrobenzofuran-4-yloxy]-5-methylphenol (**8**) (Zhuravleva et al., 2013).

3.2 Cytotoxic activity

The isolated compounds **1**-**8** were detected for their cytotoxicity against human pancreatic cancer cell line PATU8988T by using the CCK-8 method (Yuan et al., 2020). The results of CCK-8 showed that only the new compound **2** showed a promising activity (**Supplementary Table 6**). **2** demonstrated a dose-dependent cytotoxicity against the cells treated for 48 h, with the IC_{50} value of 11.4 μM (**Figure 4A**). Cell apoptosis might inhibit tumor cell proliferation. Therefore, compounds which could aggravate tumor cell apoptosis might possess application prospect for the anti-tumor therapy. To further study whether the inhibition of PATU8988T cells proliferation was caused by cell apoptosis, we examined apoptosis-related indicators. After treated with compound **2** at the concentration of 20 μM for 48 h, PATU8988T cell number reduction and cell morphology abnormity occurred in both doxorubicin (dox) and **2**-treated groups while the cells in the control group and DMSO group performed normally (**Figure 4B**), suggesting **2** as well as dox induced PATU8988T cell death. Additionally, Annexin V-FITC/PI assay was used to examine apoptosis percentage by flow cytometry. As shown in **Figure 4C**, dox significantly up-regulated the proportion of apoptotic cells with a percentage of 81.44% while **2** increased the proportion of apoptotic cells with a percentage of 8.85% in comparison with 0.55% in the control group and 0.74% in DMSO group. In addition, Bcl-2 family members including Bcl-2 and Bax can regulate apoptosis. The result of western blotting demonstrated that both dox and **2** markedly decreased the ratio of Bcl-2/Bax, indicating that **2** might induce pancreatic tumor cell apoptosis (**Figure 4D**). The above results proved that **2** might kill pancreas tumor cells by inducing the cell apoptosis.

4 Conclusion

Eight structurally diversified secondary metabolites, including two previously unreported polyketides, named (±)-chrysoalide B (**1**) and penicidone E (**2**), were isolated from *Penicillium* sp. YT2019-3321, an endophytic fungus derived from traditional Chinese medicine *Lonicera Japonica*. The optical resolution of (±)-**1** by chiral HPLC yielded individual enantiomers (+)-**1** and (−)-**1**, and their stereochemistry were solved by X-ray diffraction crystallography, respectively. The γ-pyridone nucleus found in **2** is rare in natural products, with only four analogs having similar structures. Tumor cell proliferation might be inhibited by cell apoptosis. Our study demonstrated that the new compound **2** significantly induced apoptosis in human pancreatic tumor cells (PATU8988T), characterized by the morphologies abnormity, the reduction of cell number, the upregulation of proportion of apoptotic cells, and decrease in the ratio of Bcl-2 to Bax.

Data availability statement

The datasets presented in this study can be found in online repositories. The names of the repository/repositories and accession number(s) can be found in the article/**Supplementary material**.

Author contributions

CZ and XL: conception or design. SJ, WW, CS, XP, and LX: acquisition, analysis, and interpretation of data. WW: drafting the work and revising. CZ, XL, and WW: final approval of the manuscript. All authors contributed to the article and approved the submitted version.

Funding

This study was supported by grants from the National Science Foundation of China (Grant no. 82073843), and the Ruian Bureau of Science and Technology (Grant no. MS2022004 to WW).

Conflict of interest

The authors declare that the research was conducted in the absence of any commercial or financial relationships that could be construed as a potential conflict of interest.

Publisher's note

All claims expressed in this article are solely those of the authors and do not necessarily represent those of their affiliated organizations, or those of the publisher, the editors and the reviewers. Any product that may be evaluated in this article, or claim that may be made by its manufacturer, is not guaranteed or endorsed by the publisher.

Supplementary material

The Supplementary Material for this article can be found online at: https://www.frontiersin.org/articles/10.3389/fmicb.2022.1099592/full#supplementary-material

References

Aly, A., Debbab, A., and Proksch, P. (2011). Fungal endophytes: Unique plant inhabitants with great promises. *Appl. Microbiol. Biotechnol.* 90, 1829–1845. doi: 10.1007/s00253-011-3270-y

Bills, G., and Gloer, J. (2016). Biologically active secondary metabolites from the fungi. *Microbiol. Spectr.* 4, 1–32. doi: 10.1128/microbiolspec.FUNK-0009-2016

Cai, S., Zhu, T., Du, L., Zhao, B., Li, D., and Gu, Q. (2011). Sterigmatocystins from the deep-sea-derived fungus *Aspergillus versicolor*. *J. Antibiot.* 64, 193–196. doi: 10.1038/ja.2010.154

Deshmukh, S., Prakash, V., and Ranjan, N. (2018). Marine fungi: A source of potential anticancer compounds. *Front. Microbiol.* 8:2536. doi: 10.3389/fmicb.2017.02536

Fox, E., and Howlett, B. (2008). Secondary metabolism: Regulation and role in fungal biology. *Curr. Opin. Microbiol.* 11, 481–487. doi: 10.1016/j.mib.2008.10.007

Frisch, M. J., Trucks, G. W., Schlegel, H. B., Scuseria, G. E., Robb, M. A., Cheeseman, J. R., et al. (2016). *Gaussian 16 Rev. C.01*. Wallingford, CT: Gaussian Inc.

Ge, H., Shen, Y., Zhu, C., Tan, S., Ding, H., Song, Y., et al. (2008). Penicidones A-C, three cytotoxic alkaloidal metabolites of an endophytic *Penicillium* sp. *Phytochemistry*. 69, 571–576. doi: 10.1016/j.phytochem.2007.07.014

Ge, Y., Tang, W., Huang, Q., Wei, M., Li, Y., Jiang, L., et al. (2021). New enantiomers of a nor-bisabolane derivative and two new phthalides produced by the marine-derived fungus *Penicillium chrysogenum* LD-201810. *Front. Microbiol.* 12:727670. doi: 10.3389/fmicb.2021.727670

Gouda, S., Das, G., Sen, S., Shin, H., and Patra, J. (2016). Endophytes: A treasure house of bioactive compounds of medicinal importance. *Front. Microbiol.* 7:1538. doi: 10.3389/fmicb.2016.01538

Jeon, H., and Shim, S. (2020). Chemical constituents of the endophyte *Penicillium* sp. isolated from *Artemisia princeps*. *Chem. Nat. Compd.* 2020, 122–124. doi: 10.1007/s10600-020-02959-7

Li, X., Su, J., Jiang, B., Li, Y., Guo, Y., and Zhang, P. (2021). Janthinoid A, an unprecedented *tri*-normeroterpenoid with highly modified bridged 4a,1-(epoxymethano)phenanthrene scaffold, produced by the endophyte of *Penicillium janthinellum* TE-43. *Org. Chem. Front.* 8:6196. doi: 10.1039/D1QO01066B

Li, Z., Wang, X., Ren, G., Yuan, X., Deng, N., Ji, G., et al. (2018). Prenylated diphenyl ethers from the marine algal-derived endophytic fungus *Aspergillus tennesseensis*. *Molecules* 23:2368. doi: 10.3390/molecules23092368

Liu, Y., Yang, Q., Xia, G., Huang, H., Li, H., Ma, L., et al. (2015). Polyketides with α-glucosidase inhibitory activity from a mangrove endophytic fungus, *Penicillium* sp. HN29-3B1. *J. Nat. Prod.* 78, 1816–1822. doi: 10.1021/np500885f

Newman, D., and Cragg, G. (2020). Natural products as sources of new drugs over the nearly four decades from 01/1981 to 09/2019. *J. Nat. Prod.* 83, 770–803. doi: 10.1021/acs.jnatprod.9b01285

Ortega, H., Torres-Mendoza, D., Caballero, E. Z., and Cubilla-Rios, L. (2021). Structurally uncommon secondary metabolites derived from endophytic fungi. *J. Fungi* 7:570. doi: 10.3390/jof7070570

Pracht, P., Bohle, F., and Grimme, S. (2020). Automated exploration of the low-energy chemical space with fast quantum chemical methods. *Phys. Chem. Chem. Phys.* 22, 7169–7192. doi: 10.1039/C9CP06869D

Saetang, P., Rukachaisirikul, V., Phongpaichit, S., Preedanon, S., Sakayaroj, J., Hadsadee, S., et al. (2021). Antibacterial and antifungal polyketides from the fungus *Aspergillus unguis* PSU-MF16. *J. Nat. Prod.* 84, 1498–1506. doi: 10.1021/acs.jnatprod.0c01308

Sheldrick, G. (1997a). *SHELXTL, structure determination software programs*. Madison, WI: Bruker Analytical X-ray System Inc.

Sheldrick, G. (1997b). *SHELXL-97 and SHELXS-97, program for X-ray crystal structure solution and refinement*. Göttingen: University of Göttingen.

Sparks, T., Hahn, D., and Garizi, N. (2017). Natural products, their derivatives, mimics and synthetic equivalents: Role in agrochemical discovery. *Pest. Manag. Sci.* 73, 700–715. doi: 10.1002/ps.4458

Wang, M., Li, X., Li, C., Ji, N., and Wang, B. (2013). Secondary metabolites from *Penicillium pinophilum* SD-272, a marine sediment-derived fungus. *Mar. Drugs* 11, 2230–2238. doi: 10.3390/md11062230

Wu, Y., Chen, Y., Huang, X., Pan, Y., Liu, Z., Yan, T., et al. (2018). α-Glucosidase Inhibitors: Diphenyl ethers and phenolic bisabolane sesquiterpenoids from the mangrove endophytic fungus *Aspergillus flavus* QQSG-3. *Mar. Drugs* 16:307. doi: 10.3390/md16090307

Xia, D., Duan, H., Xie, F., Xie, T., Zhang, Y., Sun, Y., et al. (2022). Altereporenes A-E, five epoxy octa-hydronaphthalene polyketides produced by an endophytic fungus *Alternaria* sp. YUD20002. *RSC Adv.* 12, 22295–22301. doi: 10.1039/D2RA03917F

Xu, K., Li, X., Zhao, D., and Zhang, P. (2021). Antifungal secondary metabolites produced by the fungal endophytes: Chemical diversity and potential use in the development of biopesticides. *Front. Microbiol.* 12:689527. doi: 10.3389/fmicb.2021.689527

Yang, T., Liu, J., Lin, L., Hu, J., Wu, G., Fan, P., et al. (2022). Acrocalysterols A and B, two new steroids from endophytic fungus *Acrocalymma* sp. *Phytochem. Lett.* 48, 77–80. doi: 10.1016/j.phytol.2022.02.003

Yu, J., and Keller, N. (2005). Regulation of secondary metabolism in filamentous fungi. *Annu. Rev. Phytopathol.* 43, 437–458. doi: 10.1146/annurev.phyto.43.040204.140214

Yuan, X. L., Li, X. Q., Xu, K., Hou, X. D., Zhang, Z. F., Xue, L., et al. (2020). Transcriptome profiling and cytological assessments for identifying regulatory pathways associated with diorcinol N-induced autophagy in A3 cells. *Front. Pharmacol.* 11:570450. doi: 10.3389/fphar.2020.570450

Zhang, P., Li, X., and Wang, B. (2016). Secondary metabolites from the marine algal-derived endophytic fungi: Chemical diversity and biological activity. *Planta Med.* 82, 832–842. doi: 10.1055/s-0042-103496

Zhang, P., Wei, Q., Yuan, X., and Xu, K. (2020). Newly reported alkaloids produced by marine-derived *Penicillium* species (covering 2014-2018). *Bioorg. Chem.* 99:103840. doi: 10.1016/j.bioorg.2020.103840

Zhuravleva, O., Afiyatullov, S. S., Yurchenko, E., Denisenko, V., Kirichuk, N., and Dmitrenok, P. (2013). New metabolites from the algal associated marine-derived fungus *Aspergillus carneus*. *Nat. Prod. Commun.* 8, 1071–1074. doi: 10.1177/1934578X1300800809

frontiers | Frontiers in Microbiology

TYPE Review
PUBLISHED 06 January 2023
DOI 10.3389/fmicb.2022.1085666

OPEN ACCESS

EDITED BY
Peng Zhang,
Tobacco Research Institute (CAAS), China

REVIEWED BY
Xuefeng Zhou,
South China Sea Institute of Oceanology (CAS), China
Lixin Duan,
Guangzhou University of Chinese Medicine, China

*CORRESPONDENCE
Xiliang Yang
yxlyxl117@163.com

†These authors have contributed equally to this work and share first authorship

SPECIALTY SECTION
This article was submitted to Antimicrobials, Resistance and Chemotherapy, a section of the journal Frontiers in Microbiology

RECEIVED 31 October 2022
ACCEPTED 17 November 2022
PUBLISHED 06 January 2023

CITATION
Zhao S, Li J, Liu J, Xiao S, Yang S, Mei J, Ren M, Wu S, Zhang H and Yang X (2023) Secondary metabolites of *Alternaria*: A comprehensive review of chemical diversity and pharmacological properties. *Front. Microbiol.* 13:1085666. doi: 10.3389/fmicb.2022.1085666

Secondary metabolites of *Alternaria*: A comprehensive review of chemical diversity and pharmacological properties

Shiqin Zhao[1†], Juan Li[2†], Jinping Liu[1], Shaoyujia Xiao[1], Sumei Yang[1], Jiahui Mei[1], Mengyao Ren[1], Shuzhe Wu[1], Hongyuan Zhang[1] and Xiliang Yang[1]*

[1]Hubei Province Key Laboratory of Occupational Hazard Identification and Control, Department of Pharmacy, Institute of Infection, Immunology and Tumor Microenvironments, Institute of Pharmaceutical Process, Medical College, Wuhan University of Science and Technology, Wuhan, China, [2]Department of Pharmacy, Tongji Hospital Affiliated to Tongji Medical College, Huazhong University of Science and Technology, Wuhan, China

Fungi are considered to be one of the wealthiest sources of bio-metabolites that can be employed for yielding novel biomedical agents. *Alternaria*, including parasitic, saprophytic, and endophytic species, is a kind of dark fungi that can produce a broad array of secondary metabolites (SMs) widely distributed in many ecosystems. These are categorized into polyketides, nitrogen-containing compounds, quinones, terpenes, and others based on the unique structural features of the metabolites. New natural products derived from *Alternaria* exhibit excellent bioactivities characterized by antibacterial, antitumor, antioxidative, phytotoxic, and enzyme inhibitory properties. Thus, the bio-metabolites of *Alternaria* species are significantly meaningful for pharmaceutical, industrial, biotechnological, and medicinal applications. To update the catalog of secondary metabolites synthesized by *Alternaria* fungi, 216 newly described metabolites isolated from *Alternaria* fungi were summarized with their diverse chemical structures, pharmacological activity, and possible biosynthetic pathway. In addition, possible insights, avenues, and challenges for future research and development of *Alternaria* are discussed.

KEYWORDS

fungi, *Alternaria*, metabolites, bioactivity, biosynthesis, application

1. Introduction

Fungi are vital microorganisms that reside in various environments where they play a significant role in protecting eco-balance and diversity (Keller, 2019; Noor et al., 2020; Ibrahim et al., 2021). Fungi have attracted considerable attention in the fields of natural product chemistry, medicine, and agriculture (Al-Obaidi et al., 2021;

Ibrahim et al., 2022). *Alternaria* fungus is a widespread dark fungus, belonging to classes Ascomycota, Dothideomycetes, Pleosporales, and Pleosporaceae (Feng and Sun, 2020). The fungal genus *Alternaria* is a ubiquitous group growing in diverse ecosystems worldwide as a parasitic, saprophytic, or endophytic species (Wang et al., 2022). Of these, *Alternaria alternata*, *Alternaria brassicicola*, *Alternaria penicillata*, *Alternaria cetera*, *Alternaria alternantherae*, and another 28 groups are ubiquitous (Feng and Sun, 2020; Li et al., 2021; Wang et al., 2022). *Alternaria* species can produce a variety of secondary metabolites. These metabolites mainly include polyketides, nitrogen-containing compounds, quinones, terpenes, and other compounds (Yamada et al., 2019; Li et al., 2020a; Tian et al., 2021). A large number of potentially bioactive molecules have been found, with intriguing structural skeletons and remarkable activities (Lou et al., 2013; Wang et al., 2022). Bioactive metabolites secreted by *Alternaria* fungi often exhibit excellent pharmacological potential, such as anticancer, antibacterial, antioxidant, and enzyme inhibitory effects (Wang J. et al., 2015; Dalinova et al., 2020; Mahmoud et al., 2021; Tian et al., 2021). For example, the world's first plant immune protein biological insecticide, ATailing, has been successfully developed by enhancing the broad-spectrum resistance of plants (Sheng et al., 2017). In addition, bio-metabolites of *Alternaria* fungi also have the efficacy of weeding and insecticide, and enhance the role of plant immunity in agricultural and food applications (Shi et al., 2017, 2018b; Tan et al., 2019; Li et al., 2021).

Furthermore, continuous studies on *Alternaria* metabolites have been carried out on the production, isolation, chemical complexity, culture conditions, plant disease mechanisms and toxicokinetics of toxin metabolomics (Figure 1) (Brian et al., 1951; Bemmann, 1986; Pinto and Patriarca, 2017; Sheng et al., 2017; Meena and Samal, 2019; Chen et al., 2021). A recent review focused on the 80 *Alternaria* phytotoxins with their classification, chemical structure, occurrence, bioactivity, and biosynthesis (Wang et al., 2022). These metabolites have an important but less-explored application value in the microorganism, where the chemical industry and fields of medicine, biological control, etc. have endeavored to discover structurally novel natural products. In this study, we summarize the new *Alternaria*-derived metabolites and give a general overview of the occurrence, chemical structure, and pharmacological properties of secondary metabolites as seen in research from 2014 to 2022. In addition, biosynthetic pathways with some biologically important metabolites are also discussed, which provide new research opportunities for the discovery of drug compounds and practical production technology in the future. Related literature can be found on various databases, including Science Direct, PubMed, Elsevier, Google Scholar, Baidu Scholar, CNKI, and Springer.

2. Secondary metabolites of *Alternaria* fungi

2.1. Polyketides

Polyketides are potential virulence factors and immunosuppressants. Pathogenic fungi, which can be synthesized from simple acyl building blocks, exhibit a high degree of structural diversity (Miyanaga, 2017). Polyketides are important natural metabolites that have attracted considerable attention. Simple phenylpropanoids and pyranones are the major groups of the polyketide family secreted by *Alternaria* sp. A total of 96 polyketides, 9 simple phenylpropanoids (**1**–**9**) (Figure 2), 76 pyranones (**10**–**85**) (Figures 3, 4), and 11 other polyketides (**86**–**96**) (Figure 5) are summarized. Most pyranones have intriguing stereoisomeric frameworks, which are described in detail in this article.

Simple phenylpropanoids are also common in *Alternaria* endophytes (Figure 2). A total of nine novel phenylpropanoid derivatives, namely alternaritins B–C (**1**–**2**), (2S, 3R)-2-hydroxy-3-(4-hydroxyphenyl) butanoic acid (**3**), and alternarias A–F (**4**–**9**), were isolated from the *Alternaria* species (Lu et al., 2021; Tian et al., 2021). Notably, alternaritin C (**2**), composed of hydrogenated pyran and tetrasubstituted benzene, is a rare carbon skeleton with double-ring units (Tian et al., 2021). In addition, compound **3** was a new natural product consisting of a p-substituted phenol moiety and a 2-hydroxybutyric acid fragment (Tian et al., 2021).

Pyranones, also known as pyrones, include α-, β-, and γ-pyranones. Most pyranones isolated from *Alternaria* fungi belong to α-pyranones, and most of these have enantiomeric structures, including dibenzo-α-pyranone derivatives (Tang et al., 2019), aromatic polyketone dimers (Yang C. L. et al., 2019), cyclopentane isochromone derivatives (Lu et al., 2018), and biphenyl structure derivatives (Kong et al., 2020). Of these, three pairs of unprecedented α-enantiomers of pyrone derivatives (**10**–**12**) were derived from *Alternaria brassicicola*, along with five diastereomeric structures, alterpyrones D-H (**13**–**17**) (Li et al., 2021). Structurally, two pyranone derivatives, alternariol (**18**) and alternariol-9-methyl ether (**19**), isolated from the marine endophytic *Alternaria*, have the same tricyclic skeleton as the alternates A–C (**20**–**22**) (Mahmoud et al., 2021; Wang et al., 2021). In addition, alternatiol (**23**) was reported as a new altenusin metabolite separated from *Vitex rotundifolia Alternaria alternata* JS0515 (Lee et al., 2019). Alternatains A–D (**24**–**27**) were obtained from the solid substrate cultures of *Alternaria alternata* MT-47 (Yang H. et al., 2019). It can be inferred that it is mainly composed of acetyl coenzyme A and polyketone synthase according to structural characteristics (Yang H. et al., 2019). The enantiomer (+)- and (−)- alternarilactone A (**28**) was identified as a dibenzo-α-pyranone derivative, possessing a diepoxy-cage-like

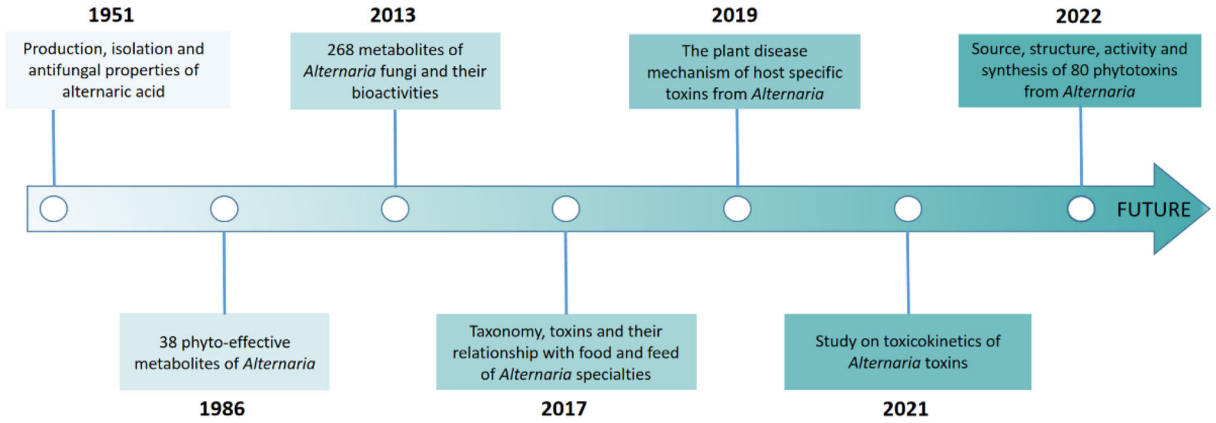

FIGURE 1
Timeline of related studies on the bio-metabolites of *Alternaria* fungi.

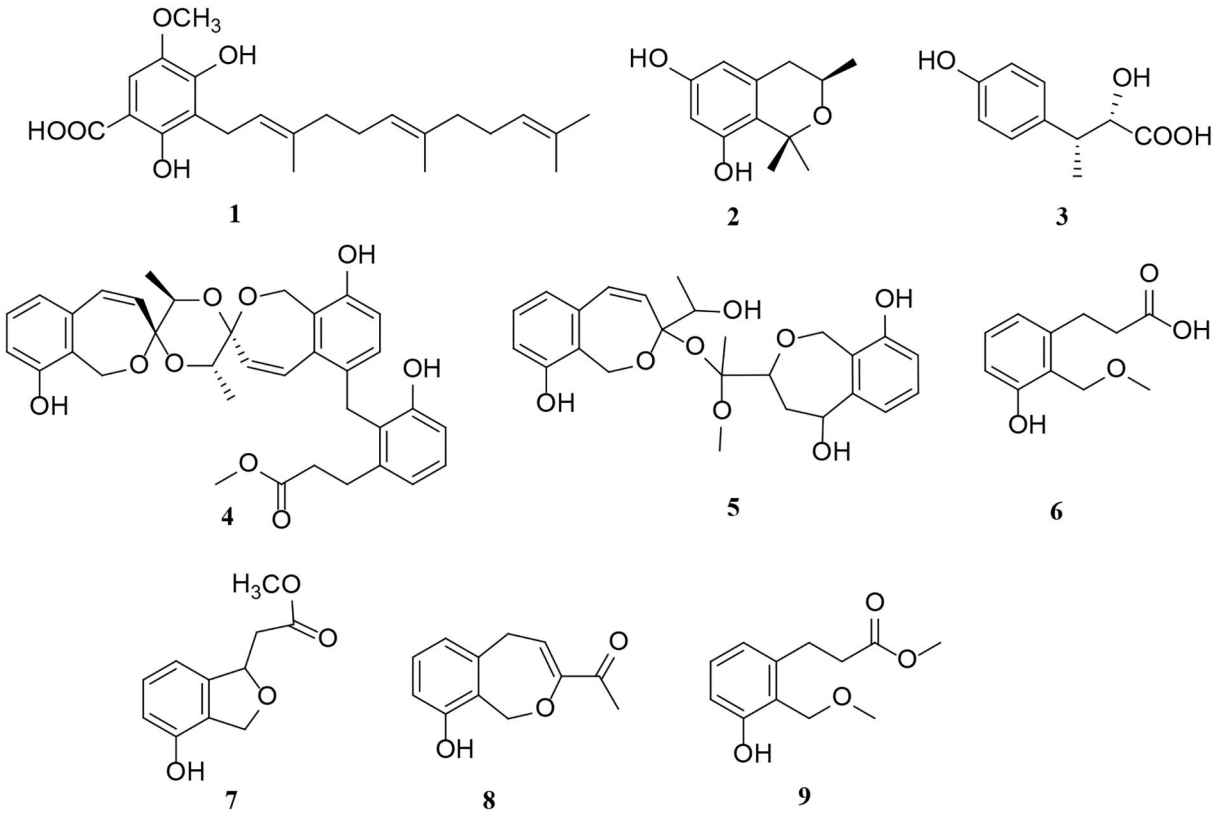

FIGURE 2
Simple phenylpropanoid derivatives (**1**–**9**) from *Alternaria* fungi.

moiety isolated from *Alternaria* sp. Hh930. (Tang et al., 2019). Interestingly, (+)- and (–)-alternamgin (**29**) is also an enantiomeric pyranone derivative with an unprecedented 6/6/6/6/5/6/6 seven-ring framework from *Vitis quinquangularis* (Wu J. C. et al., 2019). A new example of aromatic polyketone dimer metabolite, bialternacins E-F (**30**–**31**), was produced by *Alternaria* sp. NF2128 from the stem of *Maianthemum bifolium* fungus (Yang C. L. et al., 2019). Notably, indandione B (**32**), featuring an extremely rare indole ketone moiety, was found in the *Morinda officinalis* fungus *Alternaria* sp. A744 (Wang et al., 2017). The absolute configuration of compound **33** was determined as a pair of new cyclopentane isochromone

10.3389/fmicb.2022.1085666

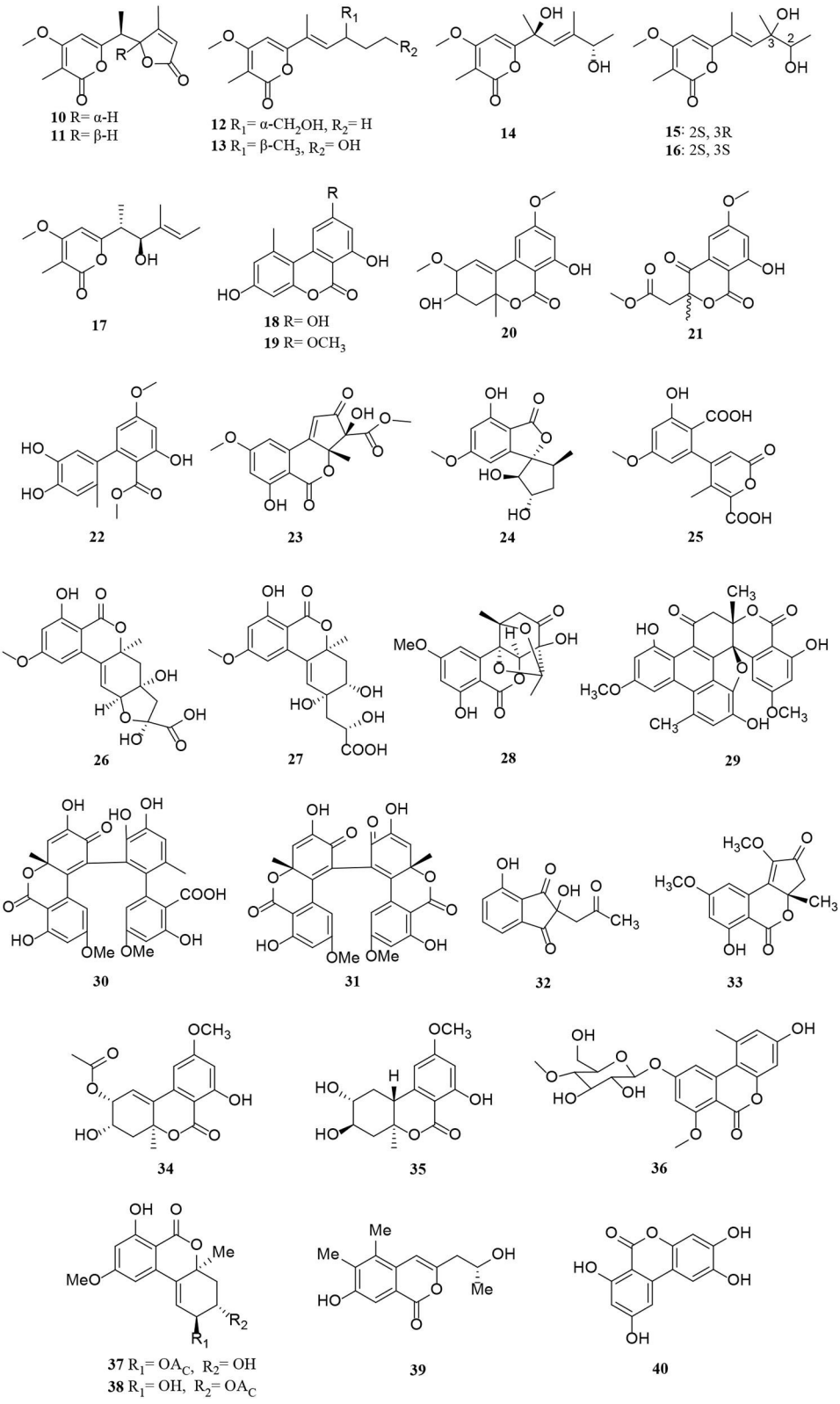

FIGURE 3
Pyranone derivatives (**10**–**40**) from *Alternaria* fungi.

10.3389/fmicb.2022.1085666

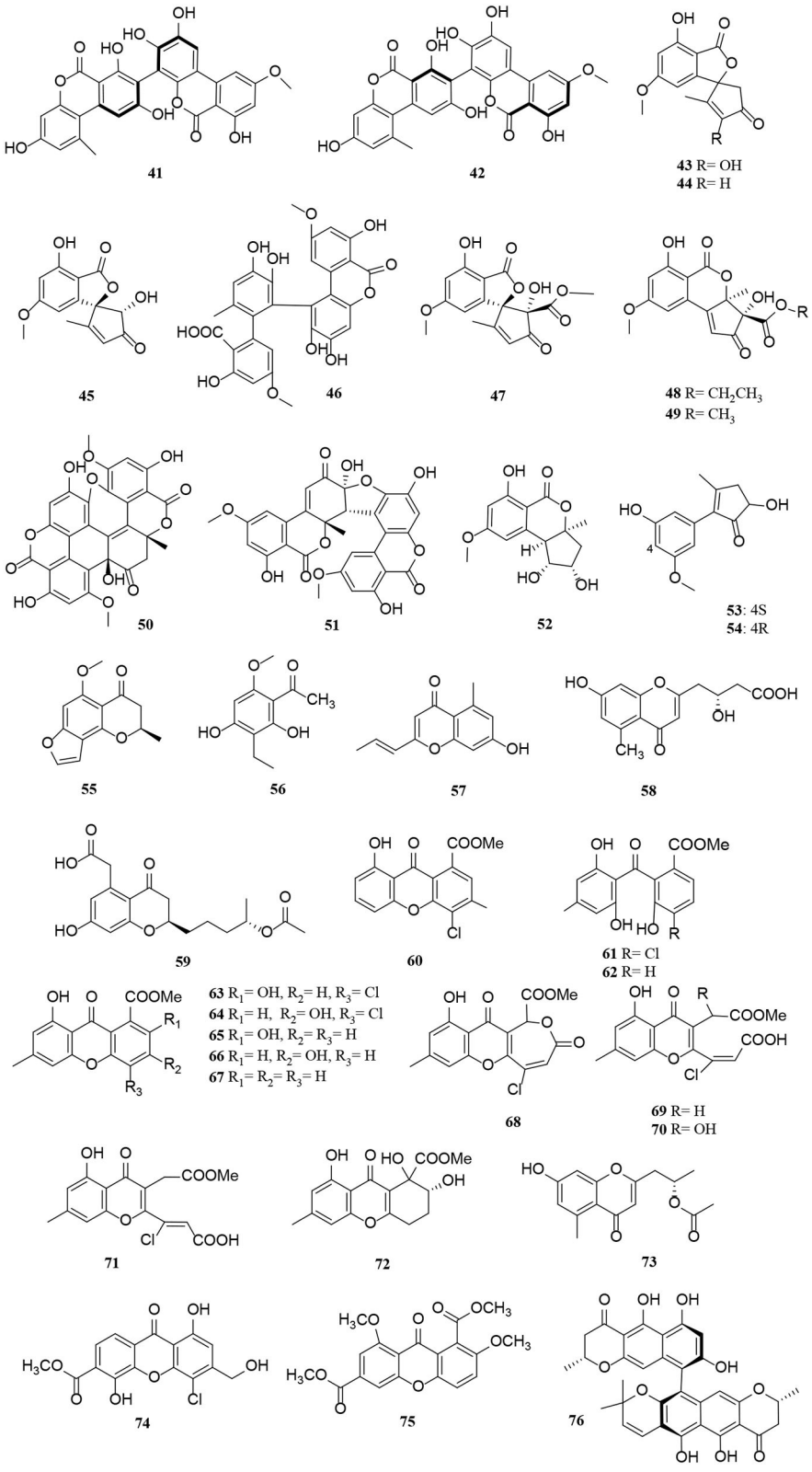

FIGURE 4
Pyranone derivatives (**41**–**76**) from *Alternaria* fungi.

10.3389/fmicb.2022.1085666

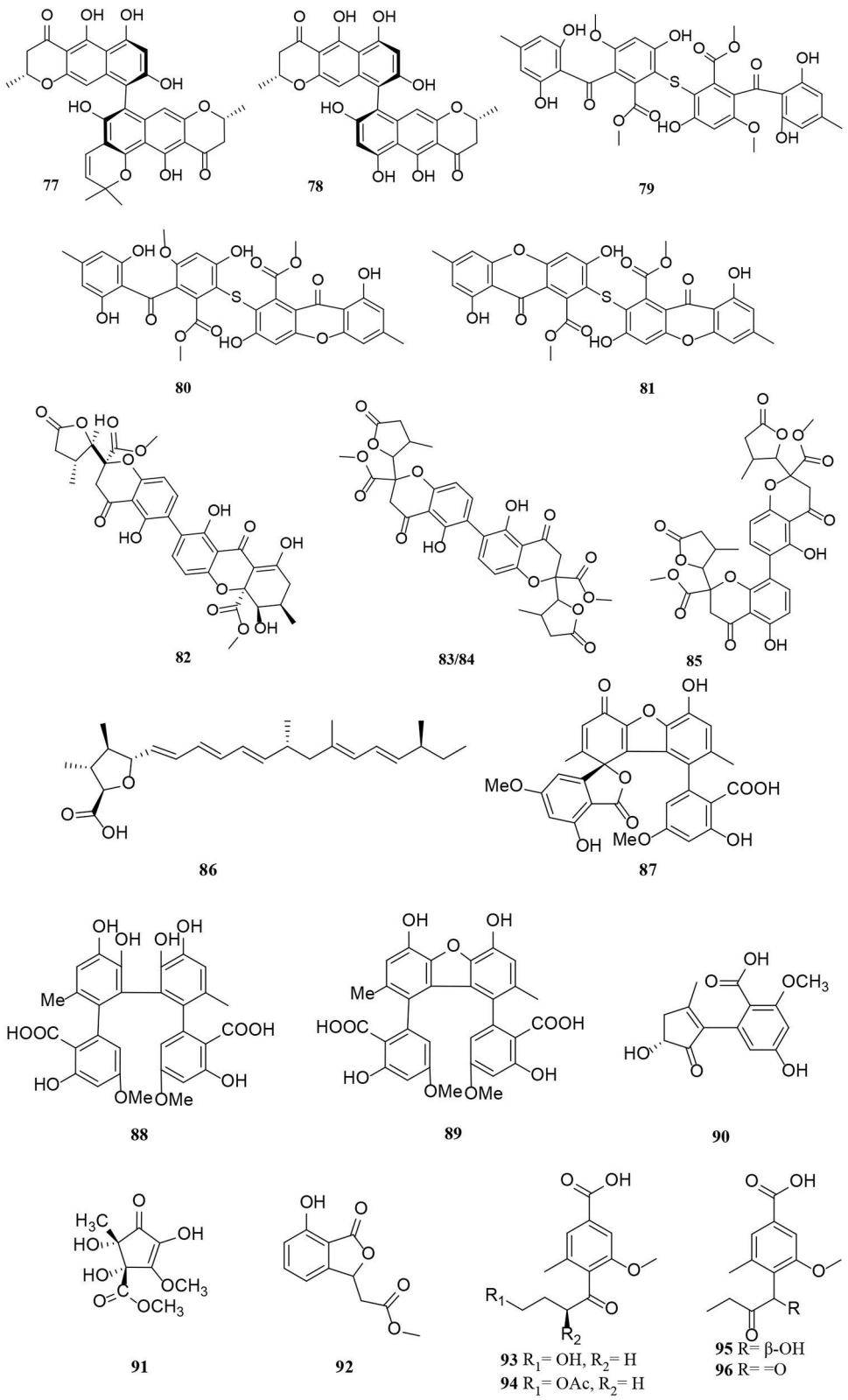

FIGURE 5
Polyketide derivatives (**77**–**96**) from *Alternaria* fungi.

enantiomers by 2D-nuclear magnetic resonance (2D-NMR) and high-resolution electrospray ionization mass spectroscopy (HRESIMS) (Lu et al., 2018). Compounds **34**–**42** possess a similar three-ring system, formed an ester bond between a six-membered ring and phenol. Interestingly, the third ring of **39** is open, and both **41** and **42** are dimers (Wang et al., 2014; Xu et al., 2015; Tian et al., 2017; Kong et al., 2020). The *Alternaria alternata* ZHJG5 produced a series of compounds (**43**–**49**), including five novel polyketide derivatives (**43**–**46**) and three pairs of dibenzo-α-pyrone derivatives (**47**–**49**) (Zhao et al., 2020, 2021). In this study, (±) alternarlactones A (**50**) and B (**51**) were two new isolated dimers, which were formed by the C-O- and C-C-bond between dehydroaltenusin and alternariol from *Halophyte Salicornia* sp. fungus *Alternaria alternata* P1210 (Shi et al., 2019). In addition, the isolation of the same marine fungi *Alternaria* sp. SCSIO41014 yielded three new α-pyranone derivatives (**52**–**54**) (Pang et al., 2018). Compounds **53** and **54** were proved to be two stereoisomeric configurations isolated from marine sponge (Pang et al., 2018).

Two new phomalone derivatives, phomalichenones E-F (**55**–**56**), were isolated from a deep-sea-derived fungus, *Alternaria* sp. MCCC 3A00467 (Zhong et al., 2022). **56** is an open γ-pyranone ring with an acetyl group at C-1 compared with **55**. Alterchromanone A (**59**) is a new chromanone derivative, also isolated from marine *Alternaria longipes* (Liu et al., 2021). Structurally, alternate D (**57**) and alternaritin D (**58**) have similar benzo-γ-pyranone moiety (Tian et al., 2021; Wang et al., 2021). A total of 13 compounds (**60**–**72**) were isolated from *Alternaria sonchi*, including chromones, xanthones, and benzophenones (Dalinova et al., 2020). Among them, **60** and **61** represent two new derivatives of chlorinated anthrone and benzophenone, respectively, which were determined by spectroscopy (mainly through 2D-NMR and MS). And compounds **62**, **64**–**67**, **71**, and **72** were first reported for *Alternaria sonchi* (Dalinova et al., 2020). In addition, (2′S)-2-(2-acetoxypropyl)-7-hydroxy-5-methylchromone (**73**) was isolated from the *Vitex rotundifolia* endophytic fungus *Alternaria brassicae* JS959 (Kim et al., 2019). Compounds (**74**–**75**) with xanthone moiety were isolated from the marine *Alternaria* sp. R6 (Wang J. et al., 2015). 4-chloro-1,5-dihydroxy-3-hydroxymethyl-6-methoxycarbonyl-xanthen-9-one (**74**) bearing a chlorine atom was also named 4-chlorofischexanthone. Two new cephalochromin derivatives, prenylcephalochromin A (**76**) and prenylcephalochromin B (**77**), along with cephalochromin (**78**), were isolated from the *Dasymaschalon rostratum* fungus *Alternaria* sp. ZG22 (Song et al., 2021). Notably, **76** were elucidated by comprehensive spectroscopic methods, indicating that **76** bears a bis-naphtho-γ-pyrone skeleton. Polluxochrin (**79**) and dioscin (**80**), two new dimers of sulochrin linked by thioether bonds, as well as another five compounds (**81**–**85**), were purified from an *Alternaria* sp. isolate obtained from Hawaiian soil (Cai et al., 2014). Compounds **80**–**81** were produced by intramolecular cyclization of **82**, and metabolites **82**–**85** were four secalonic acid analogs (Cai et al., 2014). Compound **83** is a symmetrical dimer. Overall, the planar structure of **83,** especially the C-6–C-6′ linkage, was established by the HMBC correlation spectrum. Subsequently, **84** was determined to share the same planar structure as **83**. However, the presence of two distinct sets of resonances representing the two monomeric portions of **84** denoted it was an asymmetric diastereomer of **83**.

Other polyketides include aliphatic polyketone (**86**), aromatic polyketone dimer (**87**–**89**), and alternative acid B (**90**) (Ding et al., 2017; Xu et al., 2019; Yang C. L. et al., 2019). One new cyclohexanone derivative with unsaturated ketone groups was (±)-(4S*,5S*)-2,4,5-trihydroxy-3-methoxy-4-methoxycarbonyl-5-methyl-2-cyclopentene-1-one (**91**), which was characterized to originate from the mangrove *Alternaria* strain (Wang J. et al., 2015). Isobenzofuranone A (**92**) bearing isobenzofuranone moiety was isolated from the *Morinda officinalis* fungus *Alternaria* sp. A744 (Wang et al., 2017). Finally, four new pyrenochaetic acid derivatives (**93**–**96**) isolated from soil samples have the same carbon skeleton by analysis of the ^{1}H and ^{13}C NMR data (Cai et al., 2014).

2.2. Nitrogen-containing compounds

Nitrogen-containing compounds, isolated from *Alternaria*, include amides, peptides, and alkaloids. A total of 35 nitrogen-containing compounds, 16 amides (**97**–**112**) (Figure 6), 5 peptides (**113**–**117**) (Figure 7), and 14 alkaloids (**118**–**131**) (Figure 8) have been summarized and are described in detail as follows.

A pair of enantiomeric nitrogen-containing compounds, alternaritin A [(±)-**97**], is composed of the amide bond and γ-pyranone composition isolated from *Alternaria* sp. MG1 (Tian et al., 2021). Structurally, two new anthraquinones named anthrininones B-C (**98**–**99**) with a 4,5-disubstituted butylaminolate unit were obtained from the marine fungus *Alternaria tenuissima* DFFSCS013 (Pan et al., 2019). In addition, alteamide (**100**) bearing oxygenated prenyl group was obtained from *Alternaria alternata* (Wang et al., 2021). 2-(N-vinylacetamide)-4-hydroxymethyl-3-ene-butyrolactone (**101**) and chrysogeside F (**102**) were isolated from a marine-derived fungus *Alternaria* sp. NH-F6 bearing 3-ene-butyrolactone moiety and methyl D-glucopyranoside moiety structures, respectively (Ding et al., 2017). Compounds **103**–**106** were amide derivatives extracted from marine microorganisms (Li et al., 2015; Wang J. et al., 2015). Of these, (±)-(4R*,5S*,6S*)-3-amino-4,5,6-trihydroxy-2-methoxy-5-methyl-2-cyclohexen-1-one (**106**) is a new cyclohexenone derivative isolated from the marine *Nerium indicum Alternaria* sp. SPS-04 (Wang J. et al., 2015). Five new decalin derivatives, altercrasins A-E (**107**–**111**), contain lactam-ring structures from a sea-urchin-derived *Alternaria*

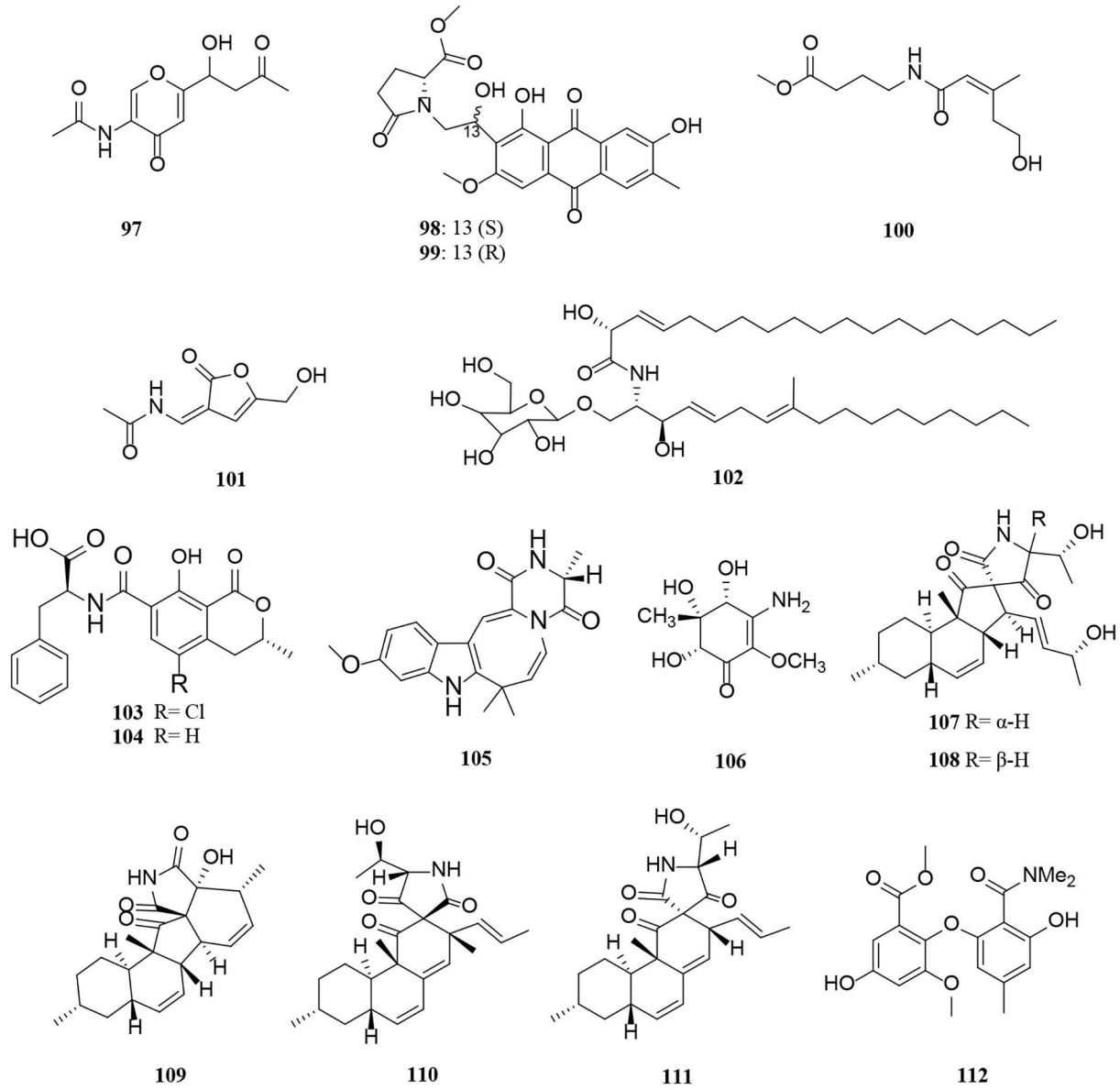

FIGURE 6
Amide derivatives (**97**–**112**) from *Alternaria* fungi.

sp. (Yamada et al., 2019). The absolute stereostructure of altercrasins A (**107**) was determined by NMR chemical shifts, NOESY correlations, and electronic circular dichroism (ECD) spectral analyses, and furthermore deduced by chemical transformation and the modified Mosher's method. As a result, the compound pairs of **107/108** and **110/111** were ascertained to be stereoisomers, deduced by the aforementioned methods respectively (Yamada et al., 2019). Dimethylamide asterrate (**112**), one new asterric acid analog with two new methyl groups, was obtained from an *Alternaria* sp. isolate (Cai et al., 2014).

Diketopiperazines (DKPs) consisting of two α-amino acids and cyclic dipeptides are amino acid peptides (He et al., 2019). Five new diketopiperazine derivatives (**113**–**117**) were isolated from the marine *Alternaria alternate* HK-25 (He et al., 2019). In comparison with conventional column chromatography with either C18 or C8 columns, compounds **114** and **116** were successfully separated from crude samples by a new high-speed counter-current chromatography (HSCCC) elution method with high efficiency and recovery (He et al., 2019).

Most alkaloids have heterocyclic structures, such as swainsonine (**118**), 2H-benzindazole derivative (**119**), indole

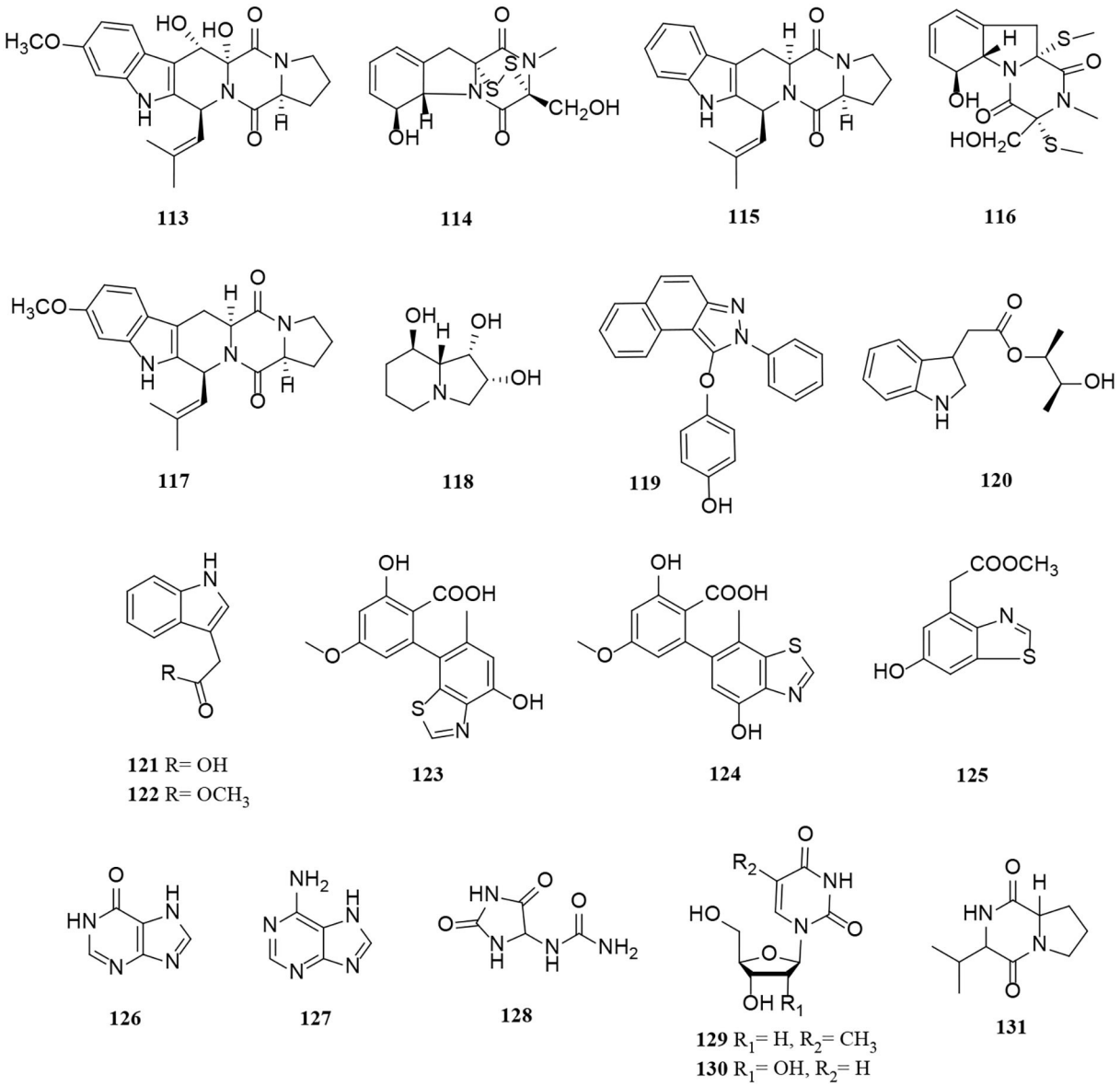

FIGURE 7
Peptide and alkaloid derivatives (**113**–**131**) from *Alternaria* fungi.

derivatives (**120**–**122**), and thiazoles (**123**–**125**) (Chen et al., 2018; Tan et al., 2019; Wu J. C. et al., 2019; Xu et al., 2019). Alterindazolin A (**119**) is a rare heterocyclic aromatic compound, containing indazole from *Alternaria alternata* Shm-1 (Wu X. et al., 2019). Similarly, altenusinoide A (**123**) and altenusinoide B (**124**) have an unusual altenusin-thiazole-fused skeleton core (6/6/5) (Chen et al., 2018). Moreover, compound **125** was identified as the first benzothiazole secondary metabolite from the marine sponge-derived fungus *Alternaria* sp. SCSIOS02F49 (Chen et al., 2018). Compounds (**126**–**130**) were purine and pyrimidine derivatives from different *Alternaria* strains (Miao et al., 2017). Compound (**131**) was a maculosin derivative isolated from *Alternaria alternata* (Hawas et al., 2015).

2.3. Quinones

So far, there are two groups of quinones among *Alternaria* metabolites that have been isolated, perylenequinones and anthraquinones. In this part of the research, 14 perylenequinones (**132**–**145**) (Figure 8) and 10 anthraquinones (**146**–**155**) (Figure 9) were produced. Perylenequinones are a class of highly conjugated pentacyclic nuclear aromatic

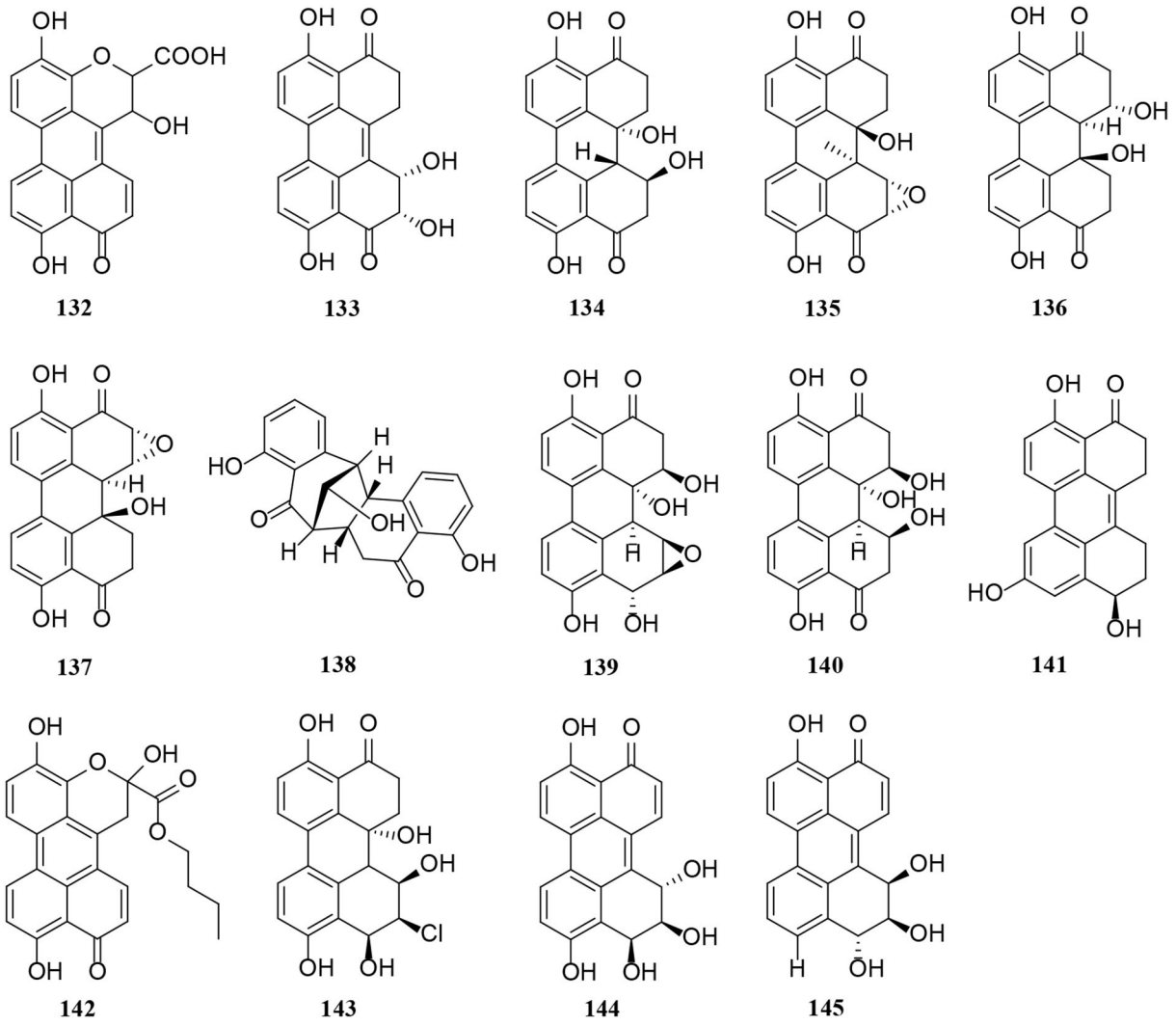

FIGURE 8
Perylene quinone derivatives (**132**–**145**) from *Alternaria* fungi.

polyketones, which are described in detail as follows (Zhao et al., 2019).

Perylenequinone is generally a dark-colored pigment characterized by an oxidized pentacyclic nuclear skeleton and has been widely used in traditional Chinese herbal medicine (Tantry et al., 2018). Four compounds (**132**–**135**) also have the structural skeleton of perylene quinone, namely isoxanalteric acid I (**132**), altertoxin VII (**133**), altertoxin I (**134**), and altertoxin II (**135**) (Kong et al., 2020; Mahmoud et al., 2021; Tian et al., 2021). In addition, altertoxin I (**136**) and altertoxin II (**137**) are two perylene quinone cytotoxins from *Alternaria alternata* (Hohenbichler et al., 2020). A novel perylenequinone-related derivative, known as alternatone A (**138**), was isolated from the marine *Alternaria alternata* L3111′, which possessed an unprecedented tricyclo [6.3.1.0] dodecane skeleton (Zhao et al., 2019). Furthermore, two new perylenequinones (**139**–**140**) were isolated from the *Pinus ponderosa* endophytic *Alternaria* sp. (Tantry et al., 2018). Compared with compound **140**, compound **139** has a significantly epoxide ring. Notably, altertoxin VII (**141**) and butyl xanalterate (**142**) are two new polyketides from the sponge-derived fungus *Alternaria* sp. SCSIO41014. And **141** is the first example to bear a novel 4,8-dihydroxy-substituted perylenequinone structure, while the phenolic hydroxy groups be commonly substituted at C-4 and C-8 (Pang et al., 2018). Moreover, two new perylenequinones (**143**–**144**) have a similar structure to deep-sea sediment fungus *Alternaria* sp. NH-F6, which is characterized as a tetrahydroperylenone (Ding et al., 2017). Altertoxin IV (**145**) is also a new tetrahydroperylene ketone derivative from

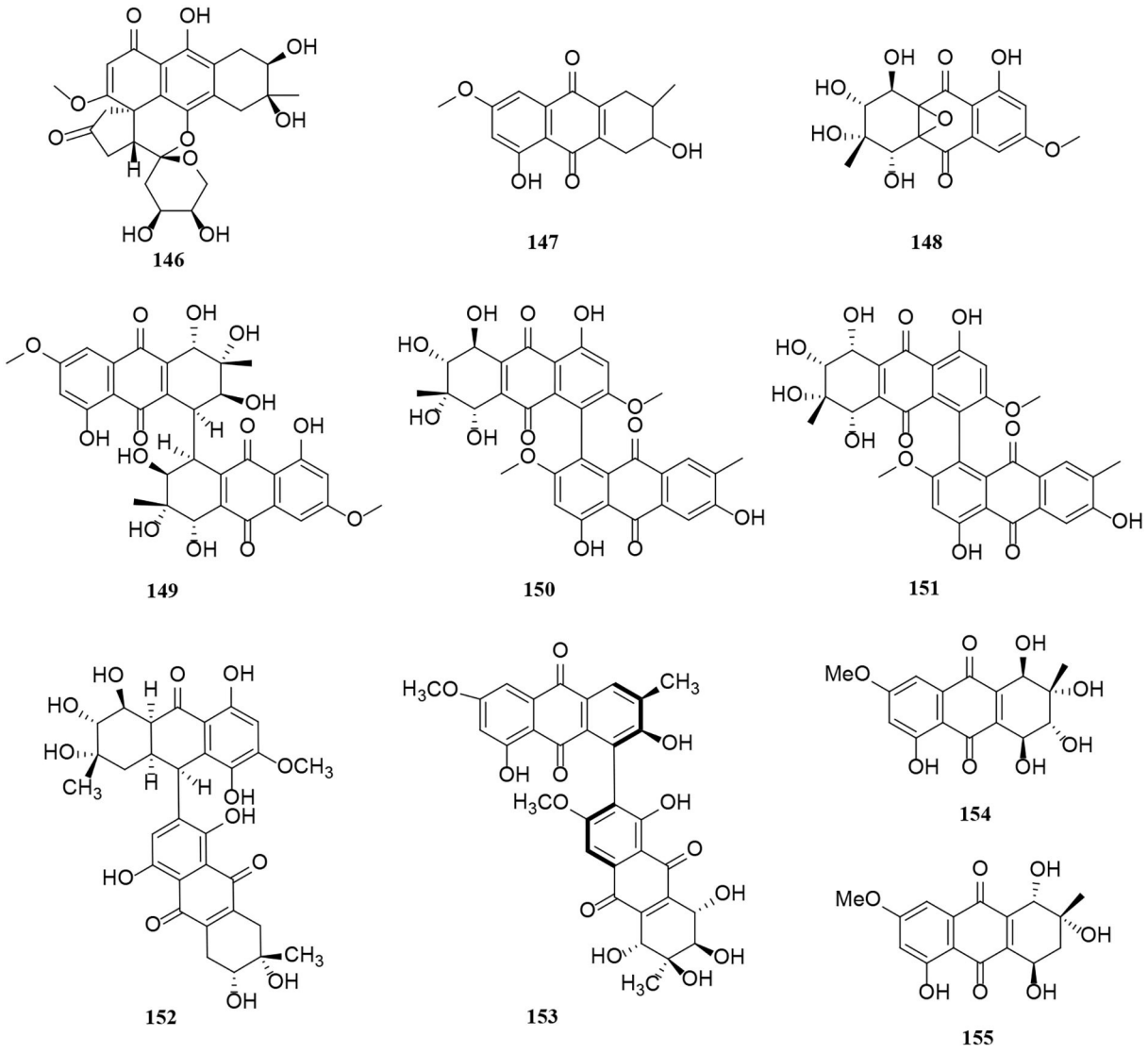

FIGURE 9
Anthraquinone derivatives (**146**–**155**) from *Alternaria* fungi.

the *Broussonetia papyrifera* fungus *Alternaria* species G7 (Zhang et al., 2016).

A novel hydroanthraquinone, anthrininone A (**146**), possessing an unprecedented hexacyclic spiro-fused ring skeleton, was isolated from the marine fungus *Alternaria tenuissima* DFFSCS013 (Pan et al., 2019). In addition, macrosporin (**147**) is an anthraquinone from marine *Alternaria* species (Wang Y. N. et al., 2015). Four new anthraquinone derivatives, compounds (**148**–**151**), were isolated from the saline lake *Alternaria* sp. XZSBG-1 (Chen et al., 2014). In this study, altersolanol O (**148**) and alterporriol S (**149**) are relatively rare compounds, representing a novel tetrahydroanthraquinone bearing an epoxy ether bond between C-4a and C-9a and a tetrahydroanthraquinone dimer bearing a C-4-C-4' linkage, respectively (Chen et al., 2014). Alterporriol S (**152**) and (+)-aS-alterporriol C (**153**) were also obtained from the marine *Alternaria* sp. SK11 (Xia et al., 2014). A novel alterporriol-type anthranoid dimer, alterporriol S (**152**), was represented as the first member of the alterporriol family to possess a unique C-10–C-2′ linkage (Xia et al., 2014). In addition, two anthraquinones (**154**–**155**) were isolated from the endophyte *Alternaria* sp. in *Erythrina variegata* (Pompeng et al., 2013).

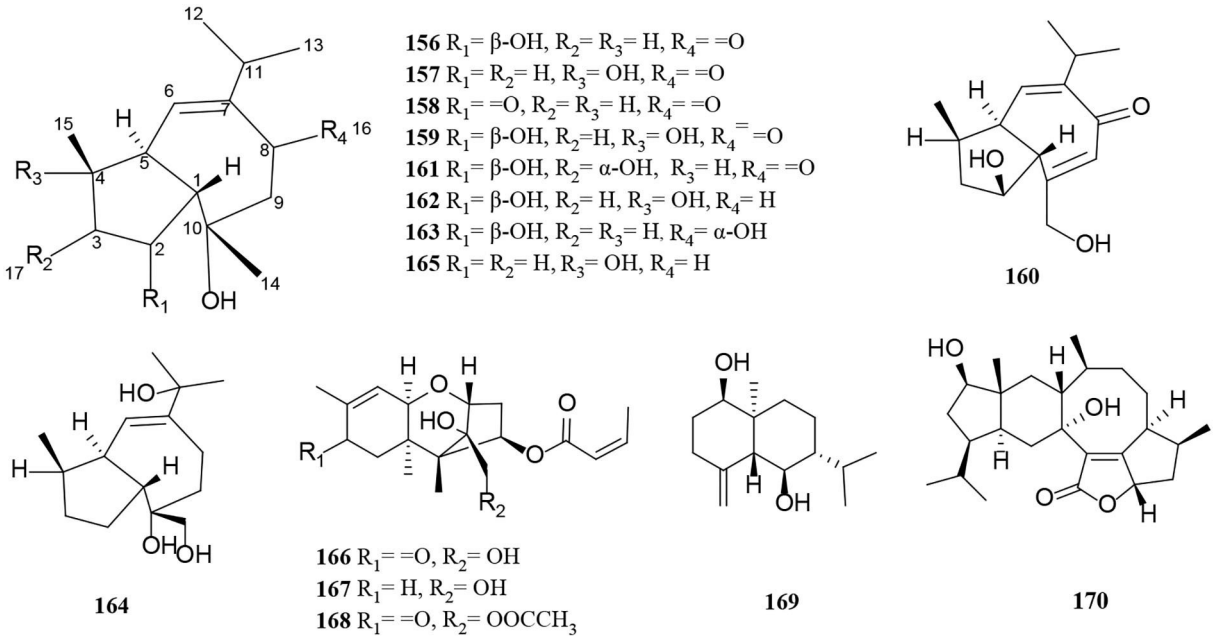

FIGURE 10
Sesquiterpene derivatives (**156**–**170**) from *Alternaria* fungi.

2.4. Terpenes

Terpenoids from *Alternaria* fungi include sesquiterpenes, diterpenes, and meroterpenoids. In this section, a total of 60 terpenoids, comprising 15 sesquiterpenes (**156**–**170**) (Figure 10), 16 diterpenes (**171**–**186**) (Figure 11), and 29 meroterpenoids (**187**–**215**) (Figure 12), are summarized. The specific description is as follows.

Oxytropiols A-J (**156**–**165**) were found in 10 undescribed guaiane-type sesquiterpenoids isolated from *Alternaria oxytropis* (Tan et al., 2019). Their typical structural feature is that they construct a seven-membered ring and fuse a five-membered ring, indicating a guaiacol-type sesquiterpene skeleton. New trichothecene derivatives with a 1, 2-diol moiety at C-12 and C-13, alterchothecenes A-C (**166**–**168**), were isolated from *Alternaria* sp. sb23 bearing a 12, 13-epoxytrichothec-9-ene ring moiety (Gao et al., 2020). Spectra data analysis of NMR, DEPT, and HSQC suggested that **167** is 8-dihydrogeneated derivatives and **168** is 13-acetylated derivatives of **166** respectively (Gao et al., 2020). Similarly, (1R,5R,6R,7R,10S)-1,6-Dihroxyeudesm-4(15)-ene (**169**) is a new sesquiterpenoid isolated from *Alternaria alternate* (Xu et al., 2019). In addition, sesteralterin (**170**) represents the first nitidasane sesterterpene obtained from the marine *Alternaria alternata* strain (k21-1) (Shi et al., 2017).

Compounds (**171**–**177**) were new fusicoccane-like diterpenoids isolated from modified rice cultures medium of *Alternaria brassicicola*, among which compounds (**171**–**173**) possess a rare 16-nor-dicyclopenta [a, d] cyclooctane structure, compounds **172** and **174** feature two previously new tetracyclic 5/6/6/5 ring systems that represent the typical examples of fusicoccane-type diterpenoids, and compound **175** features a new tetracyclic 5/8/5/3 ring system (Li et al., 2020a). Interestingly, four unprecedented diterpene dimers, alterbrassinoids A-D (**178**–**181**), were obtained in the same manner as above (Li et al., 2019a). Compounds (**178**–**181**) are the first examples of fusicoccane-derived diterpenoid dimers furnished by forming an undescribed C-12–C-18′ linkage, in which **178** and **179** represent unprecedented heterodimers, whereas **180** and **181** represent unprecedented homodimers (Li et al., 2019a). This suggests that the production of new compounds can be achieved by modifying the medium (Li et al., 2019a, 2020a). Three new rearranged fusicoccane diterpenoids, alterbrassicenes B–D (**182**–**184**) bearing a rare bridgehead double-bond-containing tricyclo [9.2.1.0] tetradecane core skeleton found from *Alternaria brassicicola* (Li et al., 2020b). A highly functionalized diterpenoid, alterbrassicicene A (**185**), with a new monocyclic carbon skeleton bearing unique dihydro-2(3H)-furanone and 2-cyclopenten1-one motifs, was obtained from *Alternaria brassicicola* (Li et al., 2018). Alterbrassicene A (**186**) was characterized as a fusicoccane-derived diterpenoid, possessing an undescribed 5/9/4-fused carbocyclic framework bearing a rare 2-cyclobuten-1-one motif, which were obtained from *Alternaria brassicicola* (Hu et al., 2018).

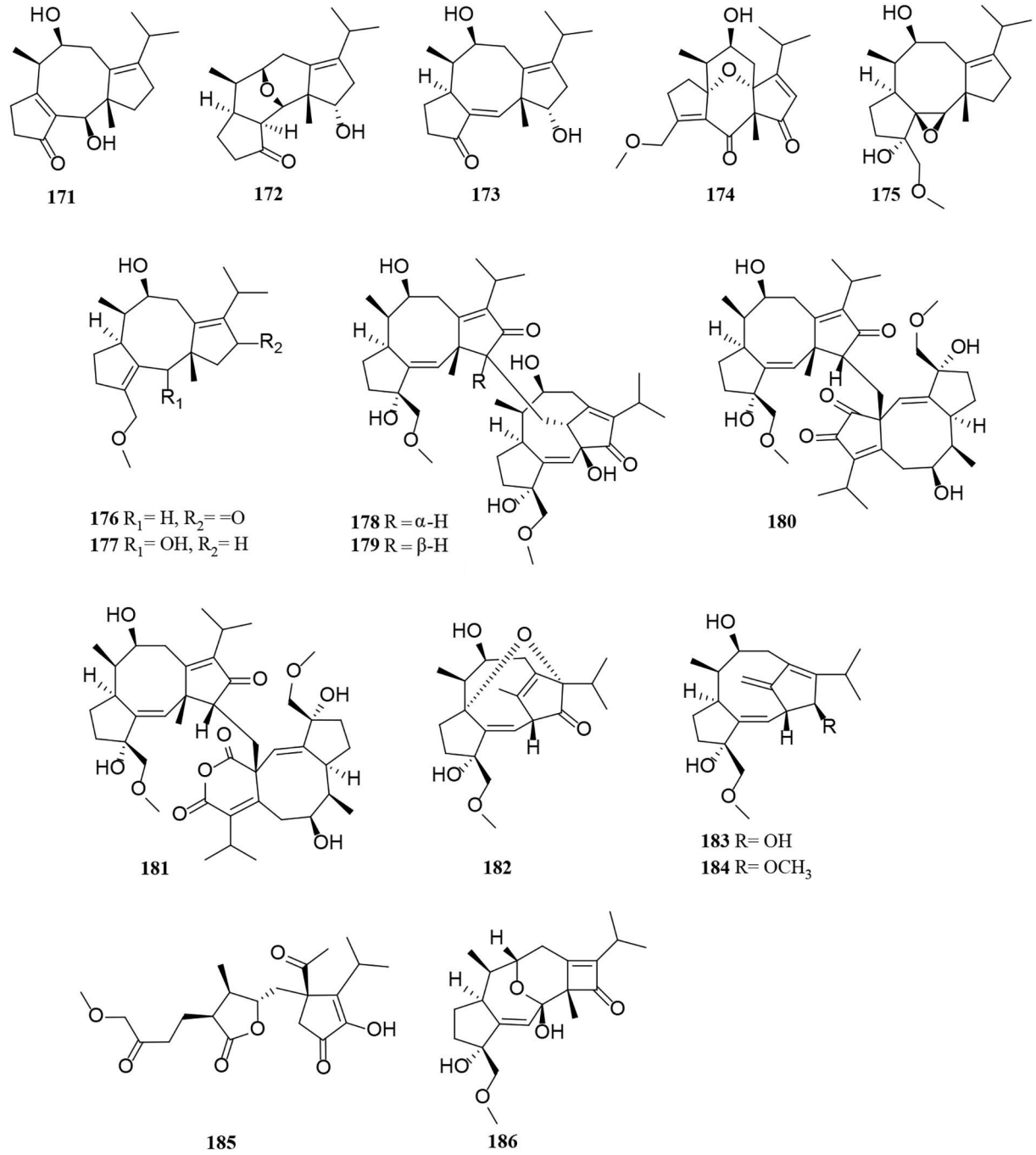

FIGURE 11
Diterpene derivatives (**171**–**186**) from *Alternaria* fungi.

The new compounds (**187–196**) have a similar tricycloalternarene structure to each other (Shen et al., 2018; Shi et al., 2018a; Li et al., 2019b). Of these, tricycloalternarenes Q-W (**187–193**) were characterized as seven unprecedented metabolites from *Alternaria brassicicola* (Li et al., 2019b). Four new meroterpenes, tricycloalterfurenes A-D (**197–200**), rarely occur in tricycloalternarenes and bear a tetrahydrofuran unit obtained from an *Alternaria alternata* strain (k21-1). Compound **199** represents the first hydroperoxy-containing tricycloalternarene (Shi et al., 2017).

10.3389/fmicb.2022.1085666

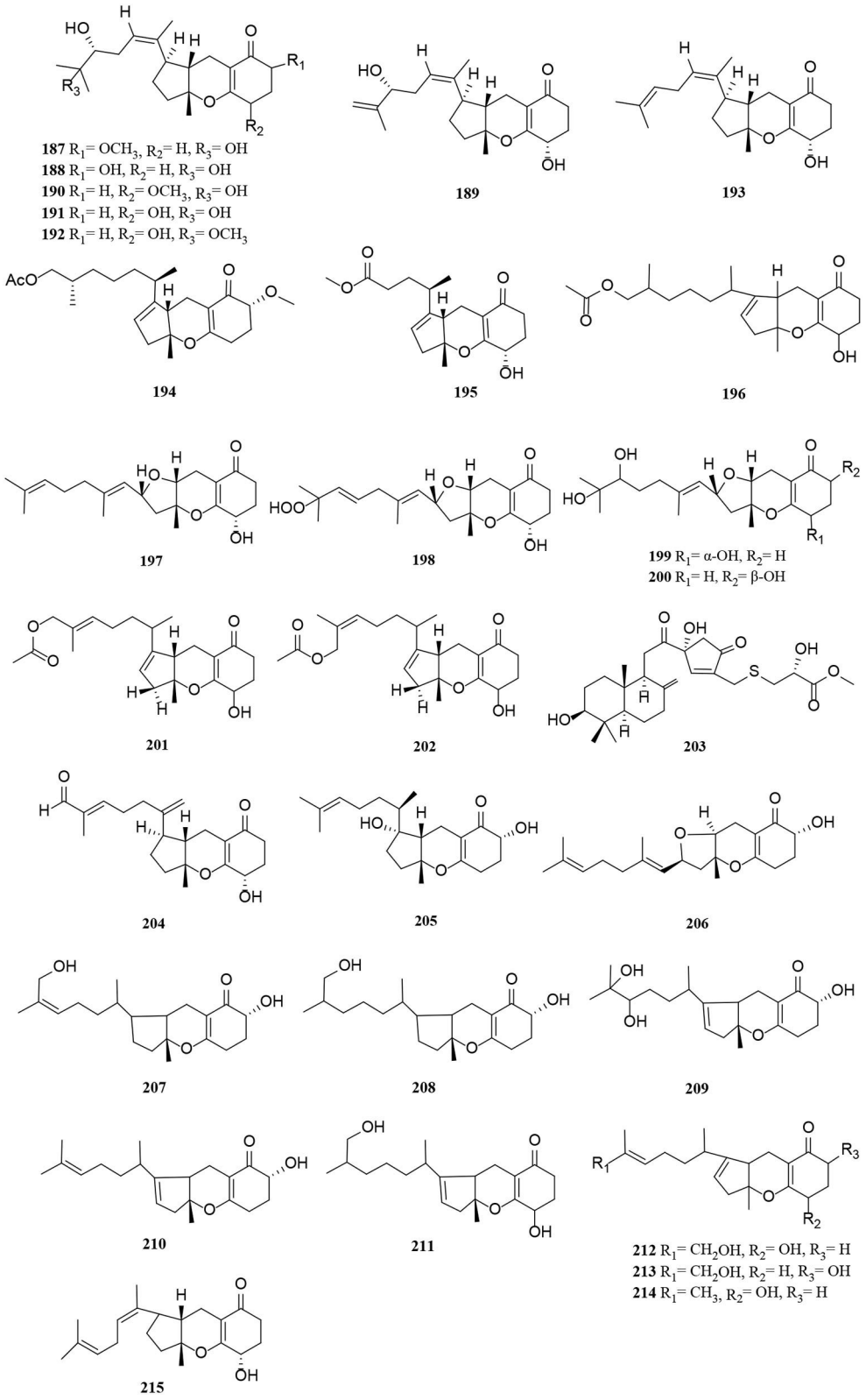

FIGURE 12
Meroterpenoid derivatives (**187**–**215**) from *Alternaria* fungi.

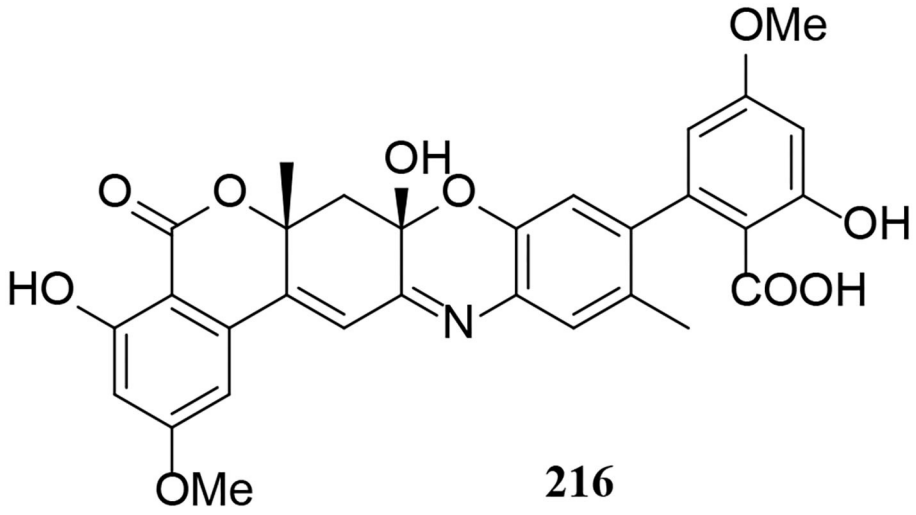

FIGURE 13
Other derivative (**216**) from *Alternaria* fungi.

Two new 15-hydroxytricycloalternarenes (**201–202**) represent a pair of E and Z isomers, possessing a double bond linked by an acetoxymethylene group (Shi et al., 2018a). A rearranged drimane meroterpenoid with a thioglycerate moiety, alternarin A (**203**), was obtained from the marine fungi *Alternaria* sp. ZH-15 (Wang H. L. et al., 2020). Tricycloalternarenes X-Y (**204–205**) and metabolites (**206–211**) were meroterpenoid compounds isolated similarly from the marine fungi (Pan et al., 2018; Wang L. et al., 2020). Compounds **212–215** were mixed terpenoids isolated from the endophyte *Alternaria* sp. Be-1 of the insect Pierisrapae Linne (Zhang et al., 2015).

2.5. Other classes

One miscellaneous metabolite **216** was isolated from *Alternaria* fungi (Figure 13). Notably, bialternacins A (**216**) is a racemic mixture of aromatic polyketone dimer with an unprecedented 6/6/6/6/6/6-hexacyclic scaffold (Yang C. L. et al., 2019).

3. Biological activity

The biological activities of secondary metabolites of *Alternaria* fungi are listed in Table 1. As shown in Table 1, antitumor, antibacterial, and antioxidant properties were characterized as the main indexes to assess the biological activity of these natural products (Zhang et al., 2021). Detailed descriptions of the compounds with excellent biological activities are provided as follows.

3.1. Antibacterial activity

Pyranones (**37–39**, **43**, **47**) can effectively inhibit fungal growth and have a great impact in the application of biofungicide. Of these, (+)-**37** and (+)-**38** showed a productive inhibitory effect on *Candida albicans* with IC_{50} of 19.5 ± 1.5 and 24.0 ± 1.0 μg/ml, while (–)-**37** and (–)-**38** were less active, suggesting different antifungal abilities between enantiomers (Wang et al., 2014). Notably, pyranone (**43**) showed significant activities toward the phytopathogenic bacteria *Xoo*, *Xanthomonas oryzae pv. oryzicola* (*Xoc*), and *Rs* with minimal inhibitory concentration (MIC) value of 0.5–64 μg/ml, indicating the potential of **43** for the development of novel bactericides (Zhao et al., 2021). Similarly, enantiomeric dibenzo-α-pyrone derivative (**47**) exhibited moderate antibacterial activities on phytopathogenic bacteria *Xoo* and *Xoc* with MIC value of 32–100 μg/ml (Zhao et al., 2020). Pyranone (**63**) exhibited antimicrobial activity toward *Bacillus subtilis* and *Candida tropicalis* with MIC of 0.5–5 μg/disk, which proved that they may be effective biological probes for antibacterial agents (Dalinova et al., 2020). γ-pyranones **79–81** inhibited methicillin-resistant *Staphylococcus aureus* (MRSA) with an MIC of 2.9, 3.2, and 2.0 μg/ml, respectively (Cai et al., 2014). The structure–activity relationship (SAR) of **79–81** indicated that the possible intramolecular cyclization caused by sulfur atom was necessary. Pyranones **74** and **91** showed antibacterial activity against *Fusarium graminearum* with MIC values of 107.14 and 215.52 μM, respectively (Wang J. et al., 2015). Compared with **91**, **74** showed better activity, probably due to the presence of chlorine atoms in molecular. Moreover, perylenequinone (**133**) showed antibacterial activity against *Streptococcus agalactiae*, with an MIC of 17.3 μg/ml

TABLE 1 Bioactivities and sources of secondary metabolites from *Alternaria* fungi.

Compounds	*Alternaria* species	Source of strain	Biological activities	References
Polyketides				
Alternaritins B–C (**1**–**2**)	*Alternaria* sp. MG1	*Vitis quinquangularis*	Moderate inhibition of COX-2	Tian et al., 2021
Alternaria A (**4**), Alternaria C (**6**), Alternaria F (**9**)	*Alternaria* sp. HJT-Y7	*Rhodiola tibetica*	Anti-SARS-CoV- 2 virus	Lu et al., 2021
(4S,5S)-Alterpyrone A (**10**a), (4R,5R)-Alterpyrone A (**10**b)	*A. brassicicola*	*Siegesbeckia pubescens* Makino	Herbicidal activity	Li et al., 2021
Alternariol-9-methyl ether (**19**)	*Alternaria* sp. LV52	*Cystoseira tamariscifolia*	Significant cytotoxicity	Mahmoud et al., 2021
Alternate (**22**)	*A. alternata*	*Paeonia lactiflora*	Moderate cytotoxicity	Wang et al., 2021
Alternatain D (**27**)	*A. alternata* MT-47	*Huperzia serrata*	Inhibition of platelet ATP release	Yang H. et al., 2019
(+)- and (−)-Alternamgin (**29**)	*Alternaria* sp. MG1	*Vitis quinquangularis*	Moderate cytotoxicity	Wu J. C. et al., 2019
Bialternacin E (**30**)	*Alternaria* sp. NF2128	*Maianthemum bifolium*	Inhibition of acetylcholinesterase	Yang C. L. et al., 2019
(+)-(S)-6-hydroxy-1,8-dimethoxy-3a-methyl-3,3a-dihydrocyclopenta[c]-isochromene-2,5-dione (**33**a), (−)-(R)-6-hydroxy-1,8-dimethoxy-3a-methyl-3,3a-dihydrocyclopenta[c] isochromene-2,5-dione (**33**b)	*Alternaria* sp. TNXY-P-1	*Arisaema heterophyllum*	Significant selective antitumor	Lu et al., 2018
3-epi-dihydroaltenuene A (**35**)	*Alternaria* sp. Samif01	*Salvia miltiorrhiza* Bunge	Significant antioxidant	Tian et al., 2017
Altenuene-2-acetoxy ester (**37**), Altenuene-3-acetoxy ester (**38**), (+)-(10R)-7-hydroxy-3-(2-hydroxy-propyl)-5, 6-dimethyl-isochromen-1-one (**39**)	*A. alternata*	*Camellia sinensis*	Moderate antibacterial	Wang et al., 2014
Isotalaroflavone (**43**)	*A. alternata* ZHJG5	*Cercis chinensis*	Significant antibacterial	Zhao et al., 2021
(±)-Alternaone A (**47**)	*A. alternata* ZHJG5	*Cercis chinensis*	Moderate antibacterial	Zhao et al., 2020
(±) alternarlactones A (**50**) and B (**51**)	*A. alternata* P1210	*Salicornia* sp.	Antiparasitic	Shi et al., 2019
Phomalichenone F (**56**)	*Alternaria* sp. MCCC 3A00467	Deep-sea sediments	Cytotoxicity	Zhong et al., 2022
Alterchromanone A (**59**)	*A. longipes*	Mangrove	Antioxidant	Liu et al., 2021
5-chloromoniliphenone (**61**), methyl 3,8-dihydroxy-6-methyl-9-oxo-9H-xanthene-1-carboxylate (**65**)	*A. sonchi*	_	Selective inhibition of carboxylesterase	Dalinova et al., 2020
Methyl 3,8-dihydroxy-6-methyl-4-chloro-9-oxo-9H-xanthene-1-carboxylate (**63**), chloromonilinic acid B (**69**)	*A. sonchi*	_	Antibacterial, insecticidal	Dalinova et al., 2020
(2'S)-2-(2-acetoxypropyl)-7-hydroxy-5-methylchromone (**73**)	*A. brassicae* JS959	*Vitex rotundifolia*	Lipoprotein oxidation inhibitory	Kim et al., 2019
4-chloro-1,5-dihydroxy-3-hydroxymethyl-6-methoxycarbonyl-xanthen-9-one (**74**)	*Alternaria* sp. R6	Mangrove	Antibacterial	Wang J. et al., 2015

(Continued)

TABLE 1 (Continued)

Compounds	*Alternaria* species	Source of strain	Biological activities	References
Prenylcephalochromin A (**76**), prenylcephalochromin B (**77**), cephalochromin (**78**)	*Alternaria* sp. ZG22	*Dasymaschalon rostratum*	Inhibition of α-Glucosidase	Song et al., 2021
Polluxochrin (**79**), dioschrin (**80**), castochrin (**81**)	*Alternaria* sp.	Soil sample	Antibacterial, weak cytotoxicity	Cai et al., 2014
(±)- (4S*,5S*)-2,4,5-trihydroxy-3-methoxy-4-methoxycarbonyl-5-methyl-2-cyclopenten-1-one (**91**)	*Alternaria* sp.	Mangrove	Significant ABTS scavenging, antibacterial	Wang J. et al., 2015
Nitrogen-containing metabolites				
Anthrininones B–C (**98**–**99**)	*A. tenuissima* DFFSCS013	Deep-sea sediments	Significant inhibition of IDO1 and of protein tyrosine phosphatase	Pan et al., 2019
3R, 14S-ochratoxin A (**103**)	*A. brassicae* 93	*Comanthina schlegeli*	Significant cytotoxicity	Li et al., 2015
(±)-(4R*,5S*,6S*)-3-amino-4,5,6-trihydroxy-2-methoxy-5-methyl-2-cyclohexen-1-one (**106**)	*Alternaria* sp.	Mangrove	Significant ABTS scavenging	Wang J. et al., 2015
Altercrasins D–E (**110**–**111**)	*Alternaria* sp.OUPS-117D-1	*Anthocidaris crassispina*	Significant cytotoxicity	Yamada et al., 2019
Swainsonine (**118**)	*A. oxytrop*	Lockfeed	Cytotoxicity	Tan et al., 2019
Indole-3-methylethanoate (**122**)	*A. alternate*	*Psidium littorale*	Neuroprotection	Xu et al., 2019
Adenine (**127**), allantoin (**128**)	*Alternaria* sp.	*Nerium indicum*	Antioxidant and antibacterial	Miao et al., 2017
Quinones				
Isoxanalteric acid I (**132**)	*Alternaria* sp. MG1	*Vitis quinquangularis*	Moderate COX-2 inhibition and antibacterial	Tian et al., 2021
Altertoxin VII (**133**)	*Alternaria* sp. PfuH1	*Pogostemon cablin*	Antibacterial	Kong et al., 2020
Altertoxin II (**135**)	*Alternaria* sp. LV52	*Cystoseira tamariscifolia*	Cytotoxicity	Mahmoud et al., 2021
Altertoxin I (**136**), altertoxin II (**137**)	*A. alternata*	Potato and rice	Cytotoxicity	Hohenbichler et al., 2020
3,6,6a,9,10-pentahydroxy-7,8-epoxy-4-oxo-4,5,6,6a,6b,7,8,9-octahydroperylene (**139**), 3,6,6a,7,10-pentahydroxy-4,9-dioxo-4,5,6,6a,6b,7,8,9-octahydroperylene (**140**)	*Alternaria* sp.	*Pinusponderosa*	Insecticidal, antimalarial, and cytotoxicity	Tantry et al., 2018
Altertoxin VII (**141**)	*Alternaria* sp. SCSIO41014	*Callyspongia* sp. sponge	Cytotoxicity	Pang et al., 2018
3,11α,12β,13β,16-Pentahydroxy-11,12-dihydroperylen-6(13H)-one (**144**)	*Alternaria* sp. NH-F6	Deep-sea sediments	Inhibition of BRD4 protein	Ding et al., 2017
Anthrininone A (**146**)	*A. tenuissima* DFFSCS013	Deep sea sediments	Effect of calcium ion level and IDO1	Pan et al., 2019

(Continued)

TABLE 1 (Continued)

Compounds	*Alternaria* species	Source of strain	Biological activities	References
Macrosporin (**147**)	*Alternaria* sp. WZL003	Gorgonian *Echinogorgia rebekka*	Significant antibacterial	Wang Y. N. et al., 2015
Alterporriol T (**150**)	*Alternaria* sp. XZSBG-1	Carbonate saline lake	Cytotoxicity	Chen et al., 2014
(+)-aS-alterporriol C (**153**)	*Alternaria sp.* SK11	Mangrove	Anti-mycobacterium tuberculosis	Xia et al., 2014
Altersolanol (**154**)	*Alternaria* sp.	*Erythrina variegata*	Antiangiogenic	Pompeng et al., 2013
Terpenoids				
Oxytropiol A (**156**)	*A. oxytropis*	*Oxytropis glabra*	Cytotoxicity	Tan et al., 2019
Sesteralterin (**170**)	*A. alternata* k21-1	*Lomentaria hakodatensis*	Phytotoxicity	Shi et al., 2017
Alterbrassicicene B (**172**), 3-Ketobrassicicene W (**173**), 1β,2β-Epoxybrassicicene I (**175**), Alterbrassicicene E (**177**)	*A. brassicicola*	*Siegesbeckia pubescens Makino*	Weak cytotoxicity, moderate anti-inflammatory effect	Li et al., 2020a
Alterbrassinoids A–D (**178–181**)	*A. brassicicola*	_	Cytotoxicity	Li et al., 2019a
Alterbrassicenes B–D (**182–184**)	*A. brassicicola*	*Siegesbeckia pubescens Makino*	Moderate cytotoxicity	Li et al., 2020b
Alterbrassicicene A (**185**)	*A. brassicicola*	*Siegesbeckia pubescens Makino*	PPAR- γ agonist	Li et al., 2018
Alterbrassicene A (**186**)	*A. brassicicola*	_	IKK β inhibitory	Hu et al., 2018
Tricycloalternarenes Q–W (**187–193**)	*A. brassicicola*	*Siegesbeckia pubescens* Makino	Selective cytotoxicity	Li et al., 2019b
17-O-methyltricycloalternarene D (**194**), methyl nortricycloalternarate (**195**)	*Alternaria* sp. k21-1	A marine red alga-epiphyte	Inhibition of marine plankton growth	Shi et al., 2018a
2H-(2E)-tricycloalternarene 12a (**196**)	*Alternaria* sp. W-1	*Laminaria japonica*	Cytotoxicity	Shen et al., 2018
Tricycloalterfurenes A–D (**197–200**)	*A. alternata* k21-1	*Lomentaria hakodatensis*	Inhibition of marine plankton growth	Shi et al., 2017
15-hydroxytricycloalternarenes (**201–202**)	*A. alternata* k23-3	Marine alga	Inhibition of marine plankton growth	Shi et al., 2018a
Alternarin A (**203**)	*Alternaria sp.* ZH-15	Lobophytum crassum	Neuroprotective	Wang H. L. et al., 2020
Tricycloalternarene X (**204**)	*Alternaria* sp. JJY-32	*Callyspongia* sp.	Cytotoxicity	Wang L. et al., 2020
Tricycloalternarene 3b (**210**)	*A. tenuissma* DFFSCS013	The deep sea	Antibacterial	Pan et al., 2018
Tricycloalternarene 3a (**214**), Tricycloalternarene F (**215**)	*Alternaria* sp. Be-1	*Pierisrapae Linne*	Significant tyrosine kinase inhibitory	Zhang et al., 2015

(Kong et al., 2020). Moreover, anthraquinone (**147**) had a strong inhibitory effect on *Vibrio anguillarum* with an MIC value of 17.6 μmol/L, which can destroy the cell wall and cell membrane, and its effect was equivalent to that of streptomycin at the same concentration (Wang Y. N. et al., 2015). In antimicrobial and antifungal activity tests, meroterpenoid (**210**) showed a significant inhibitory effect on *E. coli* and *B. subtilis* (Pan et al., 2018). Ethyl acetate (EA) fraction of endophytic *A. tenuissima* OE7 had an inhibitory effect on *C. albicans* (Chatterjee et al., 2020). Two fractions that could inhibit α-glucosidase activity were obtained from *Alternaria destruens*, which showed broad-spectrum antibacterial activity (Kaur et al., 2020). The *Alternaria* extracts with excellent antibacterial activity provide an important direction for future research on antibacterial drugs and will guide bioactivity isolation.

3.2. Antioxidant activity

Antioxidants acknowledged as "free-radical scavengers" have been widely connected to the treatment of aging, cancer, diabetes, etc., (Neha et al., 2019). Pyranone (**59**) showed scavenging activity of 1,1-diphenyl-2-picrylhydrazyl (DPPH) radical, with an IC_{50} of 56.3 μg/ml (Liu et al., 2021). Compounds **91** and **106** showed strong free-radical scavenging efficiency for 2,2′-azino-bis (3-ethylbenzthiazoline-6-sulphonic acid) (ABTS)

with EC_{50} values of 8.19 ± 0.15 and 16.09 ± 0.01 μM, respectively, which were stronger than that of the positive control ascorbic acid (EC_{50}, 17.14 ± 0.11 μM) (Wang J. et al., 2015). A free-radical scavenging test showed that pyranone (**35**) and nitrogenous metabolites (**127**–**128**) also had significant antioxidant activity (Miao et al., 2017; Tian et al., 2017). The discovery of antioxidant compounds is of great significance to various nutraceuticals and cosmetic medicine industries, which has been widely considered as a promising source of new therapeutics.

3.3. Enzyme-inhibitory metabolites

Inhibitory enzymes are often used as biocatalysts to participate in the catalysis of various metabolism activities in living organisms. They attach to the enzyme's active site and reduce the its activity, which can be used as medicine, pathogens, or insecticides in biotechnological applications. Pyranones (**1**–**2**) and perylene quinone (**132**) showed a moderate inhibitory effect on cyclooxygenase-2 (COX-2), with IC_{50} of 1.50, 7.00, and 7.00 μM. For comparison, celecoxib showed IC_{50} values of 0.06 μM as a positive control, demonstrating their potential for pharmaceutical uses in antipyretic analgesic and anti-inflammatory drugs (Tian et al., 2021). Pyranone (**27**) showed antiplatelet and anticoagulant effects after intracoronary tent implantation, with an IC_{50} of 57.6 ± 3.2 μM (Yang H. et al., 2019). Pyranone (**30**) showed an inhibitory effect on acetylcholinesterase with an IC_{50} of 15.5 μM (Yang C. L. et al., 2019). Huperzine can also inhibit acetylcholinesterase activity, which can be a prospective therapeutic drug candidate for Alzheimer's disease (Zaki et al., 2019). In addition, compounds **61** and **65** displayed selective carboxylesterase inhibition activity at a concentration of 100 μg/ml as a key serine hydrolase with potential applications in the treatment of hypertriglyceridemia, obesity, and type 2 diabetes (Zou et al., 2018; Dalinova et al., 2020). Pyranones (**76**–**78**) and anthraquinone (**150**) showed inhibitory activity on α-glucosidase activity with IC_{50} values of 2.9, 2.8, 3.1, and 7.2 μM, respectively, indicating that they have potential in the treatment of diabetes (Chen et al., 2014; Ruiz-Vargas et al., 2019; Song et al., 2021). Notably, anthrinones A-C (**146**, **98**–**99**) showed significant inhibitory activity on indoleamine 2,3-dioxygenase 1 (IDO1), and amides (**98**–**99**) had selective inhibitory activity on different protein tyrosine phosphatases (Pan et al., 2019). Comparatively, anthraquinone (**153**) showed strong inhibitory activity against *Mycobacterium tuberculosis* protein tyrosine phosphatase B (MptpB), with IC_{50} of 8.70 μM (Xia et al., 2014). Similarly, meroterpenoids (**214**–**215**) showed strong inhibitory activity on three tyrosine kinase (EGFR, VEGFR-1, and c-Met) with an inhibition rate of 28.4–56.2%, indicating stronger activity than that of the positive control erlotinib, pazopanib, and bms-777607 (inhibition rate, 100.2, 98.5, and 99.1%, respectively) (Zhang et al., 2015). However, alternative monomer ether (AME) showed selective inhibitory activity on monoamine oxidase A (MAO-α), which may be related to dibenzo of α-pyranone (Lee et al., 2017). The cytotoxin produced by *Alternaria* can also inhibit topoisomerase (Jarolim et al., 2017).

3.4. Antitumor activity

Some *Alternaria* metabolites that have been identified as cytotoxic are considered potential sources of cancer chemo-preventive agents. Pyranone **19** and perylene quinone **135** on A549 (EC_{50}, 0.73, 0.40 μg/ml) and PC3 (EC_{50}, 0.17, 0.12 μg/ml) cells exhibited potential cytotoxicity *in vitro* (Mahmoud et al., 2021). Pyranones **22** and **29** exhibited moderate cytotoxicity against different tumor cells (MDA-MB-231, MCF-7, HeLa, and HepG2), where compound **22** was the most active in MDA-MB-231 and MCF-7 with IC_{50}s of 20.1 and 32.2 μM, respectively (Wu J. C. et al., 2019; Wang et al., 2022). Notably, one pair of new cyclopentaisochromenone enantiomers, (+)-**33**a and (−)-**33**b from *Alternaria* sp. TNXY-P-1, showed distinct selective antitumor activities against HL-60 cell lines with IC_{50} values of >200 and 75.3 μM, respectively (Lu et al., 2018). Pyranone (**56**) exhibited cytotoxicity to human myeloma cancer U266, with an IC_{50} of 24.99 μg/ml (Zhong et al., 2022). However, γ-pyranones **79**–**81** exhibited weak cytotoxicity to pancreatic cancer cells (MIA PaCa-2), with IC_{50}s of 50.8, 30.3, and 29.3 μM, respectively (Cai et al., 2014). Amide **103** has certain cytotoxicity, strong nephrotoxicity, neurotoxicity, immunotoxicity, carcinogenicity, teratogenicity, and mutagenicity (Li et al., 2015). In comparison, the cytotoxicity of amides (**110**–**111**) was equivalent to that of 5-fluorouracil (Yamada et al., 2019). Alkaloid (**118**) was merely cytotoxic to A549 and HeLa, with IC_{50}s of 10.93 ± 0.80 and 66.69 ± 1.58 μM, respectively (Tan et al., 2019). Antitumor activity of **118** to A549 is equivalent to the positive control cis-platinum (IC_{50} values of 8.73 ± 1.77) (Tan et al., 2019). Two variants of an extract from cultured *Alternaria alternata*, quinones **136**–**137**, displayed dose-dependent enhancements of cytochrome P450 (CYP) activity by testing singularly the 7-ethoxy-resorufin-O-deethylase (EROD) assay in MCF-7 breast cancer cells (Hohenbichler et al., 2020). In addition, perylenequinone (**141**) had cytotoxicity to K562, SGC-7901, and BEL-7402 with IC_{50}s are 26.58 ± 0.80, 8.75 ± 0.13, and 13.11 ± 0.95 μg/ml, respectively (Pang et al., 2018). Diterpenes **172**, **173**, **175**, and **177** were active against certain human tumor cell lines, with IC_{50} values ranging from 25.0 to 38.2 μM, but had no obvious toxicity to the normal LO2 cells (Li et al., 2020a). Interestingly, terpenoids **178**–**184**, **187**, **188**, **191,** and **193** all had antitumor activity, of which diterpenes **178**–**181** exhibited moderate cytotoxicity to OCvar, MDA-MB-231, HeLa, and HT-29, while being non-toxic to normal

cells (Li et al., 2019a). Diterpenes **182**–**184** exhibited moderate cytotoxic activity against certain human tumor cell lines, with IC_{50} values in the range of 15.87–36.85 μM, but no obvious cytotoxicity to human normal cell LO2 (Li et al., 2020b). Meroterpenoids **187**, **188**, **191**, and **193** exhibited selective cytotoxicity to some human cancer cells, with IC_{50}s ranging from 12.83 to 32.87 μM; meanwhile, they had no obvious effect on normal human LO2 cells, indicating their significant potential as selective cancer chemo-preventive agents (Li et al., 2019b). Meroterpenoid **196** displayed inhibitory activity against the growth of SMMC-7721 cells with an IC_{50} of 49.7 ± 1.1, which is comparable with that of the positive control, cisplatin (IC_{50} = 6.5 ± 0.5 μg/ml) (Shen et al., 2018). Similarly, meroterpenoid **204** showed cytotoxicity to HL-60 and HO8910 cells, with IC_{50} of 7.54 and 20.32 μM (Wang L. et al., 2020). The emergence of a large number of metabolites with antitumor activities provides more opportunities for the development of cancer-treatment drugs.

3.5. Phytotoxicity

Partial metabolites of *Alternaria* fungi have exhibited pathogenicity that causes damage to plants and possess the potential to be as herbicides on account of excellent phytotoxicity (Meena and Samal, 2019; Leyte-Lugo et al., 2020). In phytotoxicity assays, pyranone **10**a and **10**b showed a significant inhibition rate on the germination of monocotyledonous weed seeds (*E. crusgalli* and *S. viridis*), with inhibitory ratios ranging from 68.6 ± 6.4 to 84.2 ± 5.1%, which was equivalent to that of the positive control, glyphosate, at a concentration of 100 μg/ml (Li et al., 2021). At 1 mg/ml, pyranone **69** showed contact insecticidal activity against wheat aphids (*Schizaphis graminum*), indicating its use as a potential agricultural insecticide (Dalinova et al., 2020). In addition, sesquiterpenoid **156** showed an inhibition of the root growth of *Arabidopsis thaliana* but no remarkable effect on leaf growth (Tan et al., 2019). Sesquiterpene (**170**) and meroterpenoids **194**–**195** and **197**–**202** showed weak or moderate inhibition of the growth of marine algae and plankton (Shi et al., 2017, 2018a). Among the three tested marine phytoplankton (*Chattonella marina*, *Heterosigma akashiwo*, and *Prorocentrum donghaiense*), compounds **170** and **197**–**200** appeared more sensitive to *C. marina* (Shi et al., 2017). Compounds **170** and **197** showed inhibition of these three phytoplanktons but were inactive to the zooplankton *A. salina*, indicating that the hydroxy group positions on ring C had almost no effect on their activities. Hydroxylation at C-2 and C-3 (**199** and **200**) slightly reduced the inhibition of the three phytoplankton (17–56% inhibition) (Shi et al., 2017). Taking structure into account, α-pyranones and terpenoids have great potential as biological control candidates in the application of herbicide, insecticide and marine protection.

3.6. Other activities

The various activity of *Alternaria* metabolites is of great significance for research. Pyranones **4**, **6**, and **9** exhibited inhibitory activities related to the SARS-CoV-2 virus (EC_{50} = 0.02, 0.3, 0.07 μM), which is conducive for the development of antiviral drugs (Lu et al., 2021). In addition, pyranones **50**–**51** exhibited a specific inhibitory effect on *L. donovani* and *P. falciparum* (Shi et al., 2019). Interestingly, compounds **139** and **140** have insect-resistant activity, and **139** showed antibacterial activity against *Leishmania donovani* with IC_{50} = 2.55 μg/ml (Tantry et al., 2018). In the study of biological mechanisms, **73** inhibited the oxidation of human plasma high-density lipoprotein (HDL) and low-density lipoprotein (LDL) induced by Cu^{2+}, which is of great significance for Cardiovascular and cerebrovascular drugs development (Kim et al., 2019). Compound **144** exhibited a potent inhibition rate of 88.1% at a concentration of 10 μM, which provides new bromodomain protein 4 (BRD4) inhibitors possessing potential antitumoral, antiviral and anti-inflammatory pharmaceutical effects (Ding et al., 2017). In addition, anthraquinone (**154**) was further characterized to have good anti-angiogenic activity *in vivo* and *in vitro* by aortic-sprouting assay in rats, related to inhibited proliferation, tube formation, and migration in endothelial cells (Pompeng et al., 2013). Compounds **122** and **177** exhibited neuroprotective effects and moderate anti-inflammatory effects, respectively (Shi et al., 2017; Tian et al., 2021). Diterpene (**185**) was the first fusicoccane-derived diterpenoid to function as a potent peroxisome proliferator-activated receptor (PPAR-γ) agonist (EC_{50} = 744.1 nM) (Li et al., 2018). In addition, diterpenes (**186**) can inhibit IKKβ in the NF-κB signal pathway and have obvious anti-inflammatory activity (Hu et al., 2018). Meroterpenoid **203** can inhibit neuronal excitation due to its unique cyclopentanone structure, which will be applied in antiepileptic drugs development (Wang H. L. et al., 2020).

4. Possible biosynthesis mechanism of secondary metabolites

Biosynthesis is indispensable in the application of natural products. The diversity of endophytic biosynthesis often depends on the diversity of the host and the complexity of its metabolism, which provide a new way for the biosynthesis of various novel compounds (Lin et al., 2019; He et al., 2021). The study of biosynthetic pathways in pharmaceutical chemistry contributes to the discovery of novel drugs and provides new research opportunities for the sustainable development and utilization of natural drugs (Lin et al., 2019; He et al., 2021).

Polyketones have a variety of structural types and corresponding biosynthetic pathways. Three metabolic pathways of polyketones from *Alternaria* fungi are briefly described, and eight important metabolites are involved

10.3389/fmicb.2022.1085666

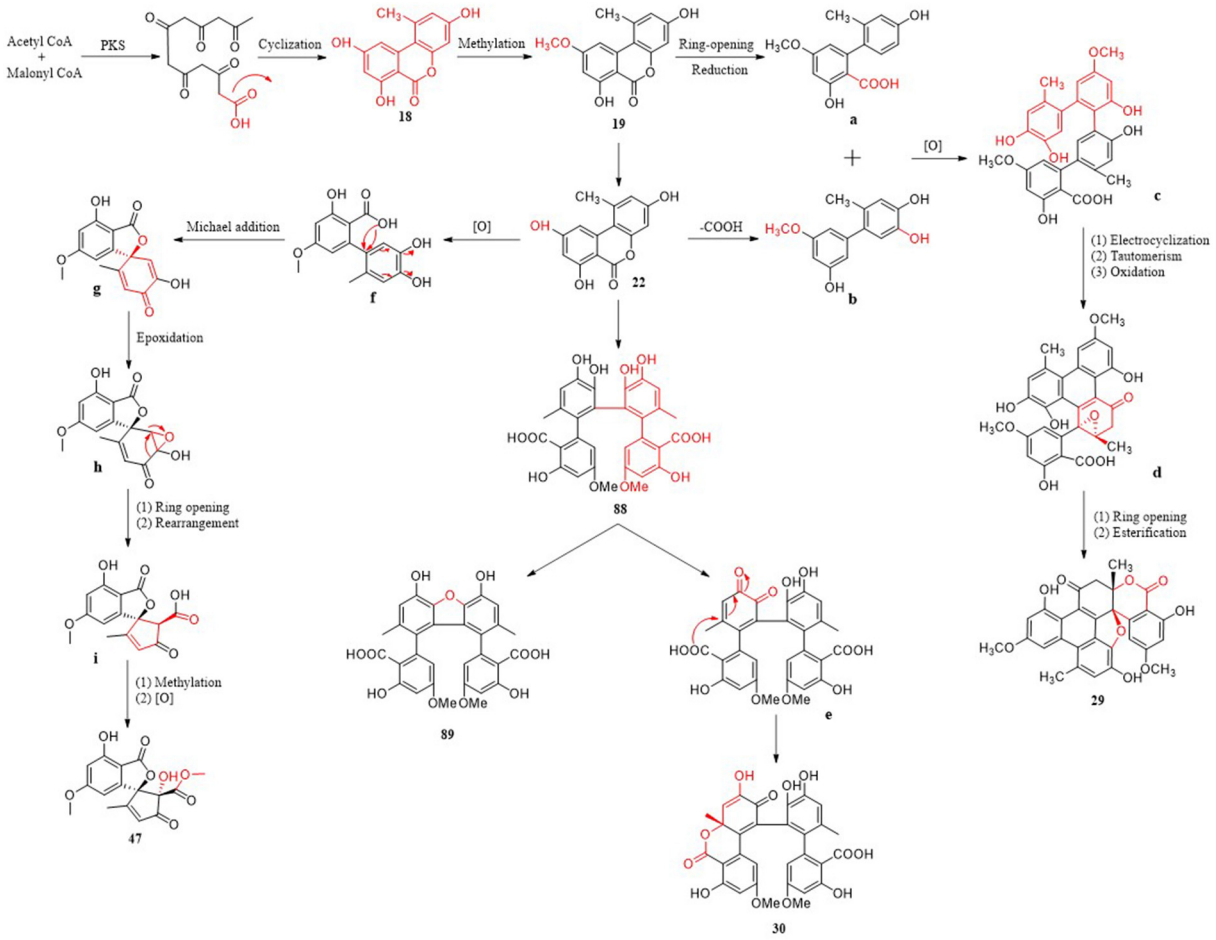

FIGURE 14
Possible biosynthetic pathway of polyketones.

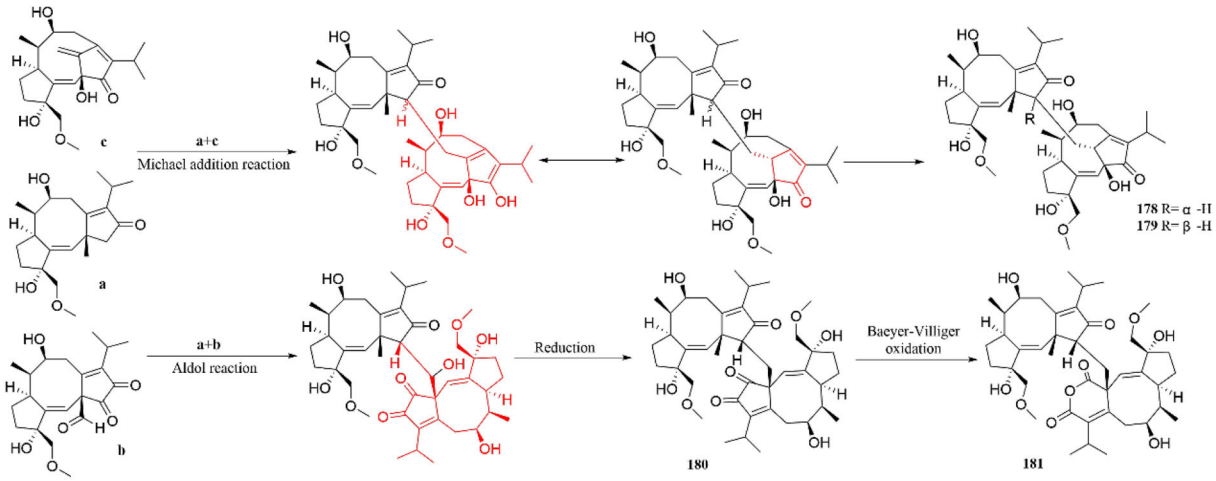

FIGURE 15
Possible biosynthetic pathway of terpenoid dimer.

(Figure 14). The cinnamic acid–shikimic pathway, a familiar biosynthetic pathway, emerged as the basis of various biosynthetic pathways. Firstly, a heptapeptide intermediate can be produced by iterative condensation of acetyl-CoA(starter) with six molecules of malonyl-CoA (extenders) by polyketide synthase (PKS). Subsequently, the heptapeptide intermediate is cyclized to obtain compound **18**, followed by methylation to obtain **19**. The key intermediate molecule **22** is obtained from the loop-opened of **19**, and then the carboxyl group is removed to form intermediate molecule **b** (Wu J. C. et al., 2019). Finally, compound **29** featuring an unprecedented seven-ring backbone, which was obtained from two molecular intermediates **a** and **b** through oxidative coupling, electrocyclization, tautomerism, oxidation, ring opening, and esterification (Wu J. C. et al., 2019). Complex compounds **30**, **91**, and **92** are also polymerized from two molecules with simple structures. Compound **22** can be dimerized *via* a C–C bond to form compound **88** through intermolecular oxidative phenol coupling, catalyzed most likely by a P450 monooxygenase or laccase. Dehydration of **88** gives compound **89** (Yang C. L. et al., 2019). Oxidation, regioselective intramolecular Michael additions, and Ketone–enol tautomerization of catechol in **88** afforded a new compound, **30,** with a lactone ring (Yang C. L. et al., 2019). It is worth noting that a third possible biosynthetic pathway generates two five-membered rings, which are completely different from the first two pathways. **f** as an ortho-quinone intermediate is formed *via* oxidization of the catechol moiety in **22**, followed by regioselective Michael additions that give intermediate **g**. Intermediate **i** was obtained after epoxidation and stereospecific acid-catalyzed rearrangement of intermediate **g**, indicating that the carbon skeleton of **47** was formed by the key epoxy-rearrangement step (Zhao et al., 2020). Then, compound **47** yielded the methylation and oxidization of **i**. As the starting materials of various metabolic pathways, compound **22** plays an important role in the biosynthesis and transformation of new compounds. This provides a new synthetic route for obtaining the novel structure of *Alternaria* fungi metabolites. In addition, the polyketide metabolites may also have a variety of metabolic pathways to be discovered, which is worthy of deep research.

Furthermore, the possible biosynthetic pathways of terpenoid dimers are also described (Figure 15). Brassicicene A synthesizes three intermediates (a\b and **c**) through dehydrogenation, oxidation, and Wagner–Meerwein rearrangement. Intermediates **a** and **c** are formed through Michael addition reaction to produce **178** and **179**. Interestingly, they are a pair of unprecedented heterodimers, bearing dicyclopentane [a, d], cyclooctane, and tricyclo [9.2.1.0] tetradecane diterpenoid subunits (Li et al., 2019a). In addition, compounds **180** and **181** are obtained by a series of aldol and reduction reactions, containing two dicyclopentadiene [a, d] cyclooctane diterpene subunits (Li et al., 2019a).

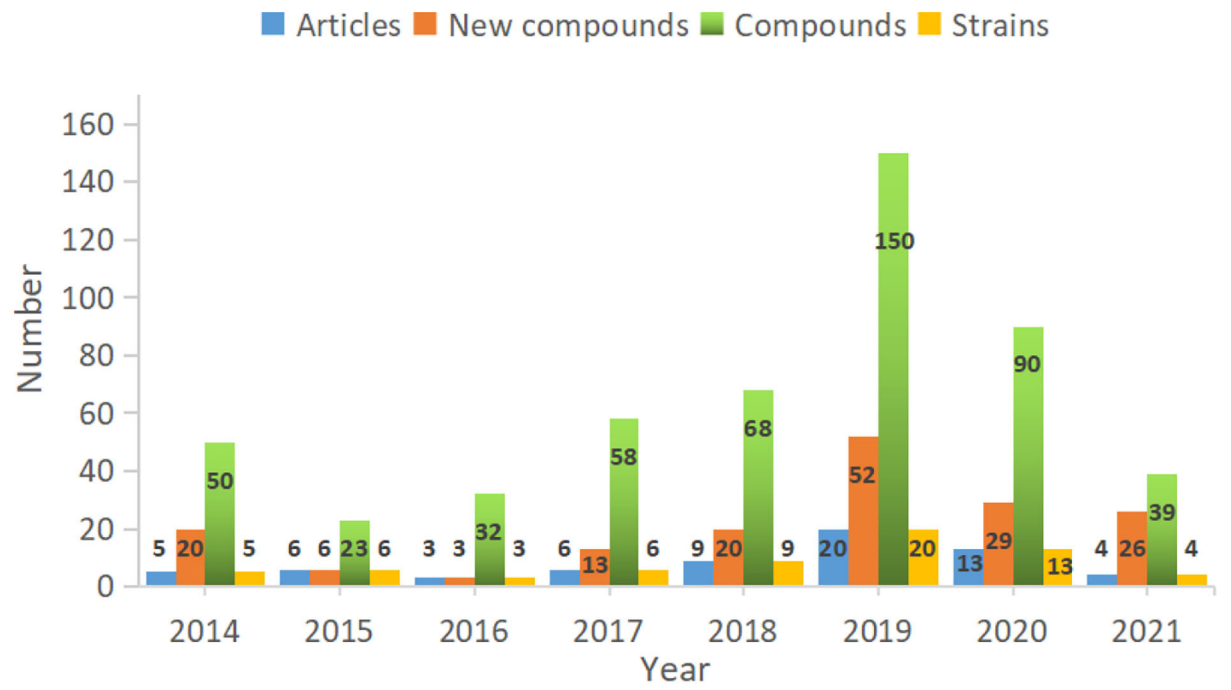

FIGURE 16
The number of articles, compounds, and strains reported from *Alternaria* fungi in recent years.

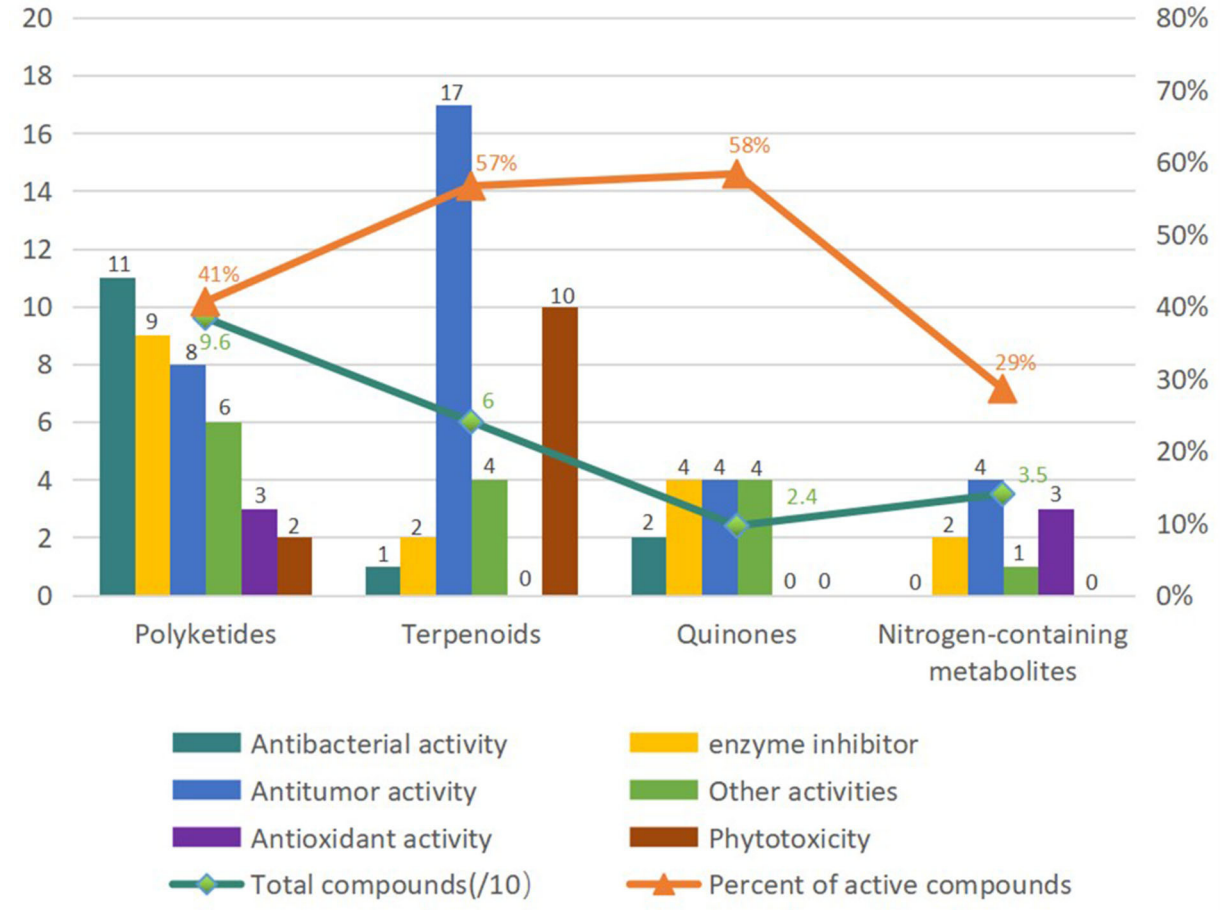

FIGURE 17
Classification of diverse chemicals of *Alternaria* fungi based on the pharmacological activities.

5. Conclusion and prospects

Fungi are ubiquitous in nature with their tenacious vitality and serve as a wealthy reservoir of structurally diverse metabolites. *Alternaria* fungi occupy a wide spectrum of habitats in diverse ecosystems worldwide. Remarkable progress has been made in the characterization of *Alternaria* fungi metabolites. Data showed that the number of articles published, the number of strains discovered, the number of new compounds, and the total compounds all increased dramatically from 2014 to 2019 (Figure 16). Numerous chemical studies suggest that *Alternaria* fungi are one of the prolific sources of functional biomolecules, including polyketides, terpenoids, quinones, and nitrogen-containing compounds. In this study, 216 metabolites from *Alternaria* species with diverse chemical structures and bioactivities were reviewed based on research from 2014 to 2022 (Figure 17). Polyketones, as the largest number of bio-metabolites, have immense potential in various fields of agriculture and the food and medical industries, considering their characteristics as being antibacterial and enzyme-inhibitory, as well as having antitumor, antioxidant, and phytotoxic properties, amongst others. Remarkably, terpenoids and quinones provided a higher proportion of active compounds. Additionally, the basic biosynthetic pathways of polyketones and terpenoid dimers have also been discussed, which would allow production for industrial purposes.

Unfortunately, the study of secondary metabolites has decreased in the past 2 years. Many metabolites remain to be discovered. Therefore, the construction and breeding of strains, as well as optimization of cultivation and fermentation processes, should be intensively conducted to accelerate the development of valuable products. In addition, a better understanding of the evaluation of bioactivities and pharmacological mechanisms would assist in ascertaining underlying therapeutic potential. Moreover, studying the molecular basis of biosynthetic pathways would be necessary for industrial production. More efforts should be made to explore further sources for the isolation of new *Alternaria* strains and to manufacture novel functional biomolecules using new

strategies, such as the "one strain many compounds" (OSMAC) approach, genetic mining (phylogenomic analyses), combined with metabolic engineering.

Finally, we believe the therapeutic potential and chemical diversity of *Alternaria* fungi will provide new avenues for drug discovery with deep research.

Author contributions

JLi, SY, XY, and JM: conceptualization. SZ, SX, and MR: discussion of the contents. JM, MR, SW, and HZ: writing—original draft preparation. SZ, JLiu, SX, SY, JM, MR, and XY: writing—review and editing. All authors have read and approved the final manuscript.

Funding

This research was funded by the National Natural Science Foundation of China, Grant Numbers 31900286 to XY and 81703380 to JLi and the Research and Innovation Fund of Wuhan Asia General Hospital, Grant Number 2022KYCX1-A02.

Conflict of interest

The authors declare that the research was conducted in the absence of any commercial or financial relationships that could be construed as a potential conflict of interest.

Publisher's note

All claims expressed in this article are solely those of the authors and do not necessarily represent those of their affiliated organizations, or those of the publisher, the editors and the reviewers. Any product that may be evaluated in this article, or claim that may be made by its manufacturer, is not guaranteed or endorsed by the publisher.

References

Al-Obaidi, J. R., Jambari, N. N., and Ahmad-Kamil, E. I. (2021). Mycopharmaceuticals and nutraceuticals: promising agents to improve human well-being and life quality. *J. Fungi.* 7, 503. doi: 10.3390/jof7070503

Bemmann, W. (1986). Phytoeffective alternaria-metabolite phytoeffective metabolites of *Alternaria*. *Zentralbl. Mikrobiol.* 141, 49–66. doi: 10.1016/S0232-4393(86)80085-3

Brian, P. W., Curtis, P. J., Hemming, H. G., Jefferys, E. G., Unwin, C. H., and Wright, J. M. (1951). Alternaric acid; a biologically active metabolic product of *Alternaria solani* (Ell. and Mart.) Jones and Grout; its production, isolation and antifungal properties. *J. Gen. Microbial.* 5, 619–632. doi: 10.1099/00221287-5-4-619

Cai, S., King, J. B., Du, L., Powell, D. R., and Cichewicz, R. H. (2014). Bioactive sulfur-containing sulochrin dimers and other metabolites from an *Alternaria* sp. isolate from a Hawaiian soil sample. *J. Nat. Prod.* 77, 2280–2287. doi: 10.1021/np5005449

Chatterjee, S., Ghosh, R., and Mandal, N. C. (2020). Inhibition of biofilm- and hyphal- development, two virulent features of *Candida albicans* by secondary metabolites of an endophytic fungus *Alternaria tenuissima* having broad spectrum antifungal potential. *Microbiol Res.* 232, 126386. doi: 10.1016/j.micres.2019.126386

Chen, A., Mao, X., Sun, Q., Wei, Z., Li, J., You, Y., et al. (2021). *Alternaria* mycotoxins: an overview of toxicity, metabolism, and analysis in food. *J. Agric. Food Chem.* 69, 7817–7830. doi: 10.1021/acs.jafc.1c03007

Chen, B., Shen, Q., Zhu, X., and Lin, Y. (2014). The anthraquinone derivatives from the fungus *Alternaria* sp. XZSBG-1 from the saline lake in Bange, Tibet, China. *Molecules* 19, 16529–16542. doi: 10.3390/molecules191016529

Chen, Y., Chen, R., Xu, J., Tian, Y., Xu, J., and Liu, Y. (2018). Two new altenusin/thiazole hybrids and a new benzothiazole derivative from the marine sponge-derived fungus *Alternaria* sp. SCSIOS02F49. *Molecules* 23, 2844. doi: 10.3390/molecules23112844

Dalinova, A., Chisty, L., Kochura, D., Garnyuk, V., Petrova, M., Prokofieva, D., et al. (2020). Isolation and bioactivity of secondary metabolites from solid culture of the fungus, *Alternaria sonchi*. *Biomolecules* 10, 81. doi: 10.3390/biom10010081

Ding, H., Zhang, D., Zhou, B., and Ma, Z. (2017). Inhibitors of BRD4 protein from a marine-derived fungus *Alternaria* sp. NH-F6. *Mar. Drugs* 15, 76. doi: 10.3390/md15030076

Feng, Z. H., and Sun, G. Y. (2020). Advances in the classification of *Alternaria* and related genera. *J. Fungal Res.* 18, 294–303. doi: 10.13341/j.jfr.2020.8010

Gao, Y., Zhou, J., and Ruan, H. (2020). Trichothecenes from an Endophytic Fungus *Alternaria* sp. sb23. *Planta Med.* 86, 976–982. doi: 10.1055/a-1091-8831

Hawas, U. W., El-Desouky, S., Abou El-Kassem, L., and Elkhateeb, W. (2015). Alternariol derivatives from *Alternaria alternata*, an endophytic fungus residing in red sea soft coral, inhibit HCV NS3/4A protease. *Appl. Biochem. Microbiol.* 51, 579–584. doi: 10.1134/S0003683815050099

He, T., Bao, J., Leng, Y., Snow, D., Kong, S., Wang, T., et al. (2021). Biotransformation of doxycycline by Brevundimonas naejangsanensis and Sphingobacterium mizutaii strains. *J. Hazard. Mater.* 411, 125126. doi: 10.1016/j.jhazmat.2021.125126

He, X., Ding, L., Yi, M., Xu, J., Zhou, X., Zhang, W., et al. (2019). Separation of five diketopiperazines from the marine fungus *Alternaria* alternate HK-25 by high-speed counter-current chromatography. *J. Sep. Sci.* 42, 2510–2516. doi: 10.1002/jssc.201801284

Hohenbichler, J., Aichinger, G., Rychlik, M., Del Favero, G., and Marko, D. (2020). *Alternaria alternata* toxins synergistically activate the aryl hydrocarbon receptor pathway *in vitro*. *Biomolecules* 10, 1018. doi: 10.3390/biom10071018

Hu, Z., Sun, W., Li, F., Guan, J., Lu, Y., Liu, J., et al. (2018). Fusicoccane-derived diterpenoids from *Alternaria brassicicola*: investigation of the structure-stability relationship and discovery of an IKKβ inhibitor. *Org. Lett.* 20, 5198–5202. doi: 10.1021/acs.orglett.8b02137

Ibrahim, S., Choudhry, H., Asseri, A. H., Elfaky, M. A., Mohamed, S., and Mohamed, G. A. (2022). *Stachybotrys chartarum*-A hidden treasure: secondary metabolites, bioactivities, and biotechnological relevance. *J. Fungi* 8, 504. doi: 10.3390/jof8050504

Ibrahim, S., Sirwi, A., Eid, B. G., Mohamed, S., and Mohamed, G. A. (2021). Bright side of *Fusarium oxysporum*: secondary metabolites bioactivities and industrial relevance in biotechnology and nanotechnology. *J. Fungi* 7, 943. doi: 10.3390/jof7110943

Jarolim, K., Del Favero, G., Ellmer, D., Stark, T. D., Hofmann, T., Sulyok, M., et al. (2017). Dual effectiveness of *Alternaria* but not Fusarium mycotoxins against human topoisomerase II and bacterial gyrase. *Arch. Toxicol.* 91, 2007–2016. doi: 10.1007/s00204-016-1855-z

Kaur, J., Sharma, P., Kaur, R., Kaur, S., and Kaur, A. (2020). Assessment of alpha glucosidase inhibitors produced from endophytic fungus *Alternaria destruens* as antimicrobial and antibiofilm agents. *Mol. Biol. Rep.* 47, 423–432. doi: 10.1007/s11033-019-05145-3

Keller, N. P. (2019). Fungal secondary metabolism: regulation, function and drug discovery. *Nat Rev Microbiol* 17, 167–180. doi: 10.1038/s41579-018-0121-1

Kim, J. W., Kim, J. Y., Li, W., Ryu, J. Y., Kim, S., and Shim, S. H. (2019). Chromones with lipoprotein oxidation inhibitory activity from an endophytic fungus *Alternaria brassicae* JS959 derived from *Vitex rotundifolia*. *J. Antibiot.* 72, 709–713. doi: 10.1038/s41429-019-0198-4

Kong, F. D., Yi, T. F., Ma, Q. Y., Xie, Q. Y., Zhou, L. M., Chen, J. P., et al. (2020). Biphenyl metabolites from the patchouli endophytic fungus *Alternaria* sp. PfuH1. *Fitoterapia* 146, 104708. doi: 10.1016/j.fitote.2020.104708

Lee, C., Li, W., Bang, S., Lee, S. J., Kang, N. Y., Kim, S., et al. (2019). Secondary metabolites of the endophytic fungus *Alternaria alternata* JS0515 isolated from *Vitex rotundifolia* and their effects on pyruvate dehydrogenase activity. *Molecules* 24, 4450. doi: 10.3390/molecules24244450

Lee, H. W., Kim, Y. J., Nam, S. J., and Kim, H. (2017). Potent selective inhibition of monoamine oxidase a by alternariol monomethyl ether isolated fROM *Alternaria brassicae*. *J. Microbiol. Biotechnol.* 27, 316–320. doi: 10.4014/jmb.1610.10053

Leyte-Lugo, M., Richomme, P., Poupard, P., and Peña-Rodriguez, L. M. (2020). Identification and quantification of a phytotoxic metabolite from *Alternaria dauci*. *Molecules* 25, 4003. doi: 10.3390/molecules25174003

Li, F., Lin, S., Zhang, S., Hao, X., Li, X. N., Yang, B., et al. (2019a). Alterbrassinoids A–D: fusicoccane-derived diterpenoid dimers featuring different carbon skeletons from *Alternaria brassicicola*. *Org. Lett.* 21, 8353–8357. doi: 10.1021/acs.orglett.9b03133

Li, F., Lin, S., Zhang, S., Pan, L., Chai, C., Su, J. C., et al. (2020a). Modified fusicoccane-type diterpenoids from *Alternaria brassicicola*. *J. Nat. Prod.* 83, 1931–1938. doi: 10.1021/acs.jnatprod.0c00165

Li, F., Pan, L., Lin, S., Zhang, S., Li, H., Yang, B., et al. (2020b). Fusicoccane-derived diterpenoids with bridgehead double-bond-containing tricyclo[9.2.1.0(3,7)]tetradecane ring systems from *Alternaria brassicicola*. *Bioorg. Chem.* 100, 103887. doi: 10.1016/j.bioorg.2020.103887

Li, F., Sun, W., Guan, J., Lu, Y., Zhang, S., Lin, S., et al. (2018). Alterbrassicicene A, a highly transformed fusicoccane-derived diterpenoid with potent PPAR-γ agonistic activity from *Alternaria brassicicola*. *Org. Lett.* 20, 7982–7986. doi: 10.1021/acs.orglett.8b03553

Li, F., Tang, Y., Sun, W., Guan, J., Lu, Y., Zhang, S., et al. (2019b). New cytotoxic tricycloalternarenes from fungus *Alternaria brassicicola*. *Bioorg. Chem.* 92, 103279. doi: 10.1016/j.bioorg.2019.103279

Li, F., Ye, Z., Huang, Z., Chen, X., Sun, W., Gao, W., et al. (2021). New α-pyrone derivatives with herbicidal activity from the endophytic fungus *Alternaria brassicicola*. *Bioorg. Chem.* 117, 105452. doi: 10.1016/j.bioorg.2021.105452

Li, Y. F., Wang, H. W., Xu, J. Y., Li, J., and Liu, L. (2015). The secondary metabolites of the crinoid (*Comanthina schlegeli*) epipsymbiosis fungus *Alternaria brassicae* 93. *Acta Scientiarum Naturalium Universitatis Sunyatseni* 54, 75–78. doi: 10.13471/j.cnki.acta.snus.2015.04.014

Lin, H. C., Hewage, R. T., Lu, Y. C., and Chooi, Y. H. (2019). Biosynthesis of bioactive natural products from basidiomycota. *Org. Biomol. Chem.* 17, 1027–1036. doi: 10.1039/C8OB02774A

Liu, G., Niu, S., and Liu, L. (2021). Alterchromanone A, one new chromanone derivative from the mangrove endophytic fungus *Alternaria longipes*. *J. Antibiot.* 74, 152–155. doi: 10.1038/s41429-020-00364-4

Lou, J., Fu, L., Peng, Y., and Zhou, L. (2013). Metabolites from *Alternaria* fungi and their bioactivities. *Molecules* 18, 5891–5935. doi: 10.3390/molecules18055891

Lu, X., Tang, X. Y., Wang, H. X., Huang, W. J., Feng, W. X., and Feng, B. M. (2021). Polyketone metabolites isolated from Rhodiola tibetica endohytic fungus *Alternaria* sp. HJT-Y7 and their SARS-CoV-2 virus inhibitory activitives. *Bioorg. Chem.* 116, 105309. doi: 10.1016/j.bioorg.2021.105309

Lu, X. J., Chen, S. F., Xu, X. W., Zhao, D., Wang, H. F., Bai, J., et al. (2018). One pair of new cyclopentaisochromenone enantiomer from *Alternaria* sp. TNXY-P-1 and their cytotoxic activity. *J. Asian Nat. Prod. Res.* 20, 328–336. doi: 10.1080/10286020.2017.1336164

Mahmoud, M. M., Abdel-Razek, A. S., Soliman, H., Ponomareva, L. V., Thorson, J. S., Shaaban, K. A., et al. (2021). Diverse polyketides from the marine endophytic *Alternaria* sp. LV52: Structure determination and cytotoxic activities. *Biotechnol. Rep.* 33, e00628. doi: 10.1016/j.btre.2021.e00628

Meena, M., and Samal, S. (2019). *Alternaria* host-specific (HSTs) toxins: an overview of chemical characterization, target sites, regulation and their toxic effects. *Toxicol. Rep.* 6, 745–758. doi: 10.1016/j.toxrep.2019.06.021

Miao, Z., Ma, Y. M., Kong, Y., Yan, M. R., and Wang, J. (2017). Study on alkaloid metabolites of a strain of *Alternaria* fungi. *Jiangsu Agric. Sci.* 45, 314–316. doi: 10.15889/j.issn.1002-1302.2017.22.081

Miyanaga, A. (2017). Structure and function of polyketide biosynthetic enzymes: various strategies for production of structurally diverse polyketides. *Biosci. Biotechnol. Biochem.* 81, 2227–2236. doi: 10.1080/09168451.2017.1391687

Neha, K., Haider, M. R., Pathak, A., and Yar, M. S. (2019). Medicinal prospects of antioxidants: a review. *Eur. J. Med. Chem.* 178, 687–704. doi: 10.1016/j.ejmech.2019.06.010

Noor, A. O., Almasri, D. M., Bagalagel, A. A., Abdallah, H. M., Mohamed, S., Mohamed, G. A., et al. (2020). Naturally occurring isocoumarins derivatives from endophytic fungi: sources, isolation, structural characterization, biosynthesis, and biological activities. *Molecules* 25, 395. doi: 10.3390/molecules25020395

Pan, D., Zhang, X., Zheng, H., Zheng, Z., Nong, X., Liang, X., et al. (2019). Novel anthraquinone derivatives as inhibitors of protein tyrosine phosphatases and indoleamine 2,3-dioxygenase 1 from the deep-sea derived fungus *Alternaria tenuissima* DFFSCS013. *Org. Chem. Front.* 6, 3252–3258. doi: 10.1039/C9QO00775J

Pan, D. Y., Huang, Z. H., Liang, X., Ma, X., and Qi, S. H. (2018). Study of tricycloalternarenes from the deep-sea derived fungus *Alternaria tenuissma* DFFSCS013 and their antimicrobial activity. *Nat. Prod. Res. Dev.* 30, 1166–1169. doi: 10.16333/j.1001-6880.2018.7.012

Pang, X., Lin, X., Wang, P., Zhou, X., Yang, B., Wang, J., et al. (2018). Perylenequione derivatives with anticancer activities isolated from the marine sponge-derived fungus, *Alternaria* sp. SCSIO41014. *Mar. Drugs* 16, 280. doi: 10.3390/md16080280

Pinto, V. E., and Patriarca, A. (2017). *Alternaria* species and their associated mycotoxins. *Methods Mol. Biol.* 1542, 13–32. doi: 10.1007/978-1-4939-6707-0_2

Pompeng, P., Sommit, D., Sriubolmas, N., Ngamrojanavanich, N., Matsubara, K., and Pudhom, K. (2013). Antiangiogenetic effects of anthranoids from *Alternaria* sp., an endophytic fungus in a Thai medicinal plant Erythrina variegata. *Phytomed. Int. J. Phytotherapy Phytopharmacol.* 20, 918–922. doi: 10.1016/j.phymed.2013.03.019

Ruiz-Vargas, J. A., Morales-Ferra, D. L., Ramírez-Ávila, G., Zamilpa, A., Negrete-León, E., Acevedo-Fernández, J. J., et al. (2019). α-Glucosidase inhibitory activity and *in vivo* antihyperglycemic effect of secondary metabolites from the leaf infusion of Ocimum campechianum mill. *J. Ethnopharmacol.* 243, 112081. doi: 10.1016/j.jep.2019.112081

Shen, L., Tian, S. J., Song, H. L., Chen, X., Guo, H., Wan, D., et al. (2018). Cytotoxic tricycloalternarene compounds from endophyte *Alternaria* sp. W-1 associated with *Laminaria japonica*. *Mar. Drugs* 16, 402. doi: 10.3390/md16110402

Sheng, S. Y., Zhou, Q., Qiu D. W., and Yang, X. F. (2017). Effects and mechanism of disease resistance and yield improvement induced by plant immune protein preparation atailing in wheat. *Chinese J. Biol. Control* 33, 213–218. doi: 10.16409/j.cnki.2095-039x.2017.02.011

Shi, Y. N., Pusch, S., Shi, Y. M., Richter, C., Maciá-Vicente, J. G., Schwalbe, H., et al. (2019). (±)-Alternarlactones A and B, two antiparasitic alternariol-like dimers from the fungus *Alternaria alternata* P1210 isolated from the halophyte *Salicornia* sp. *J. Org. Chem.* 84, 11203–11209. doi: 10.1021/acs.joc.9b01229

Shi, Z. Z., Fang, S. T., Miao, F. P., and Ji, N. Y. (2018a). Two new tricycloalternarene esters from an alga-epiphytic isolate of *Alternaria alternata*. *Nat. Prod. Res.* 32, 2523–2528. doi: 10.1080/14786419.2017.1423312

Shi, Z. Z., Miao, F. P., Fang, S. T., Liu, X. H., Yin, X. L., and Ji, N. Y. (2017). Sesteralterin and tricycloalterfurenes A–D: terpenes with rarely occurring frameworks from the marine-alga-epiphytic fungus *Alternaria alternata* k21-1. *J. Nat. Prod* 80, 2524–2529. doi: 10.1021/acs.jnatprod.7b00478

Shi, Z. Z., Yin, X. L., Fang, S. T., Miao, F. P., and Ji, N. Y. (2018b). Two new isomeric tricycloalternarenes from the marine alga-epiphytic fungus *Alternaria alternata* k23-3. *Magnet. Resonance Chem. MRC* 56, 210–215. doi: 10.1002/mrc.4676

Song, X. M., Zhou, X. M., Li, Y. L., Huang, L. B., Chen, C. C., Gao, Y., et al. (2021). Two new cephalochromin derivative from the *Alternaria* sp. ZG22. *Nat. Prod. Res.* 35, 3370–3375. doi: 10.1080/14786419.2019.1700248

Tan, X., Zhang, X., Yu, M., Yu, Y., Guo, Z., Gong, T., et al. (2019). Sesquiterpenoids and mycotoxin swainsonine from the locoweed endophytic fungus *Alternaria oxytropis*. *Phytochemistry* 164, 154–161. doi: 10.1016/j.phytochem.2019.05.012

Tang, J. W., Xu, H. C., Wang, W. G., Hu, K., Zhou, Y. F., Chen, R., et al. (2019). (+)- and (–)-Alternarilactone A: enantiomers with a diepoxy-cage-like scaffold from an endophytic *Alternaria* sp. *J. Nat. Prod.* 82, 735–740. doi: 10.1021/acs.jnatprod.8b00571

Tantry, M. A., Idris, A. S., Williamson, J. S., Shafi, T., Dar, J. S., Malik, T. A., et al. (2018). Perylenequinones from an endophytic *Alternaria* sp. of *Pinus ponderosa*. *Heliyon* 4, e01046. doi: 10.1016/j.heliyon.2018.e01046

Tian, J., Fu, L., Zhang, Z., Dong, X., Xu, D., Mao, Z., et al. (2017). Dibenzo-α-pyrones from the endophytic fungus *Alternaria* sp. Samif01: isolation, structure elucidation, and their antibacterial and antioxidant activities. *Nat. Prod. Res.* 31, 387–396. doi: 10.1080/14786419.2016.1205052

Tian, L. L., Ren, H., Xi, J. M., Fang, J., Zhang, J. Z., and Wu, Q. X. (2021). Diverse anti-inflammation and anti-cancer polyketides isolated from the endophytic fungi *Alternaria* sp. MG1. *Fitoterapia* 153, 105000. doi: 10.1016/j.fitote.2021.105000

Wang, H., Guo, Y., Luo, Z., Gao, L., Li, R., Zhang, Y., et al. (2022). Recent advances in *Alternaria* phytotoxins: a review of their occurrence, structure, bioactivity, and biosynthesis. *J. Fungi* 8, 168. doi: 10.3390/jof8020168

Wang, H. L., Li, R., Li, J., He, J., Cao, Z. Y., Kurtán, T., et al. (2020). Alternarin A, a drimane meroterpenoid, suppresses neuronal excitability from the coral-associated fungi *Alternaria* sp. ZH-15. *Org. Lett.* 22, 2995–2998. doi: 10.1021/acs.orglett.0c00746

Wang, J., Ding, W., Wang, R., Du, Y., Liu, H., Kong, X., et al. (2015). Identification and bioactivity of compounds from the mangrove endophytic fungus *Alternaria* sp. *Mar. Drugs* 13, 4492–4504. doi: 10.3390/md13074492

Wang, J. T., Ma, Z. H., Wang, G. K., Xu, F. Q., Yu, Y., Wang, G., et al. (2021). Chemical constituents from plant endophytic fungus *Alternaria alternata*. *Nat. Prod. Res.* 35, 1199–1206. doi: 10.1080/14786419.2019.1639699

Wang, L., Jiao, J., Liu, D., Zhang, X., Li, J., Che, Q., et al. (2020). Cytotoxic meroterpenoids from the fungus *Alternaria* sp. JJY-32. *Chem. Biodivers.* 17, e2000226. doi: 10.1002/cbdv.202000226

Wang, Y., Liu, H. X., Chen, Y. C., Sun, Z. H., Li, H. H., Li, S. N., et al. (2017). Two new metabolites from the endophytic fungus *Alternaria* sp. A744 derived from morinda officinalis. *Molecules* 22, 765. doi: 10.3390/molecules22050765

Wang, Y., Yang, M. H., Wang, X. B., Li, T. X., and Kong, L. Y. (2014). Bioactive metabolites from the endophytic fungus *Alternaria alternata*. *Fitoterapia* 99, 153–158. doi: 10.1016/j.fitote.2014.09.015

Wang, Y. N., Zeng, C. J., Shao, C. L., Wang, and C. Y. (2015). Isolation of antibacterial macrosporin from gorgonian-derived fungus *Alternaria* sp. and preliminary study on its antimicrobial mechanism. *Chinese J. Marine Drugs* 34, 10–16. doi: 10.13400/j.cnki.cjmd.2015.02.002

Wu, J. C., Hou, Y., Xu, Q., Jin, X. J., Chen, Y., Fang, J., et al. (2019). ($\pm$)-Alternamgin, a pair of enantiomeric polyketides, from the endophytic fungi *Alternaria* sp. MG1. *Org. Lett.* 21, 1551–1554. doi: 10.1021/acs.orglett.9b00475

Wu, X., Wang, S., Liu, C., Zhang, C., Guo, J., and Shang, X. (2019). A new 2H-benzindazole compound from *Alternaria alternata* Shm-1, an endophytic fungus isolated from the fresh wild fruit of *Phellinus igniarius*. *J. Nat. Med.* 73, 620–626. doi: 10.1007/s11418-019-01291-x

Xia, G. Li, J., Li, H., Long, Y., Lin, S., Lu, Y., He, L., et al. (2014). Alterporriol-type dimers from the mangrove endophytic fungus, *Alternaria* sp. (SK11), and their MptpB inhibitions. *Mar. Drugs* 12, 2953–2969. doi: 10.3390/md12052953

Xu, G. B., Pu, X., Bai, H. H., Chen, X. Z., and Li, G. Y. (2015). A new alternariol glucoside from fungus *Alternaria alternate* cib-137. *Nat. Prod. Res.* 29, 848–852. doi: 10.1080/14786419.2014.990905

Xu, J., Hu, Y. W., Qu, W., Chen, M. H., Zhou, L. S., Bi, Q. R., et al. (2019). Cytotoxic and neuroprotective activities of constituents from *Alternaria alternate*, a fungal endophyte of *Psidium littorale*. *Bioorg. Chem.* 90, 103046. doi: 10.1016/j.bioorg.2019.103046

Yamada, T., Tanaka, A., Nehira, T., Nishii, T., and Kikuchi, T. (2019). Altercrasins A?E, decalin derivatives, from a sea-urchin-derived *Alternaria* sp.: isolation and structural analysis including stereochemistry. *Mar. Drugs* 17, 218. doi: 10.3390/md17040218

Yang, C. L., Wu, H. M., Liu, C. L., Zhang, X., Guo, Z. K., Chen, Y., et al. (2019). Bialternacins A–F, aromatic polyketide dimers from an endophytic *Alternaria* sp. *J. Nat. Prod.* 82, 792–797. doi: 10.1021/acs.jnatprod.8b00705

Yang, H., Qi, B., Ding, N., Jiang, F., Jia, F., Luo, Y., et al. (2019). Polyketides from *Alternaria alternata* MT-47, an endophytic fungus isolated from *Huperzia serrata*. *Fitoterapia* 137, 104282. doi: 10.1016/j.fitote.2019.104282

Zaki, A. G., El-Shatoury, E. H., Ahmed, A. S., and Al-Hagar, O. (2019). Production and enhancement of the acetylcholinesterase inhibitor, huperzine A, from an endophytic *Alternaria brassicae* AGF041. *Appl. Microbiol. Biotechnol.* 103, 5867–5878. doi: 10.1007/s00253-019-09897-7

Zhang, J. L., Tang, W. L., Huang, Q. R., Li, Y. Z., Wei, M. L., Jiang, L. L., et al. (2021). *Trichoderma*: a treasure house of structurally diverse secondary metabolites with medicinal importance. *Front. Microbiol.* 12, 723828. doi: 10.3389/fmicb.2021.723828

Zhang, N., Zhang, C., Xiao, X., Zhang, Q., and Huang, B. (2016). New cytotoxic compounds of endophytic fungus *Alternaria* sp. isolated from *Broussonetia papyrifera (L.) Vent. Fitoterapia* 110, 173–180. doi: 10.1016/j.fitote.2016.03.014

Zhang, Q. Q., Guo, L. Z., Chen, J. F., Zou, K., and Gou, Z. Y. (2015). Secondary metabolites from insect-derived endophytic fungus *Alternaria* sp. *J. China Three Gorges Univ.* 37, 110–112. doi: 10.13393/j.cnki.issn.1672-948X.2015.05.025

Zhao, D. L., Cao, F., Wang, C. Y., Yang, L. J., Shi, T., Wang, K. L., et al. (2019). Alternatone A, an unusual perylenequinone-related compound from a soft-coral-derived strain of the fungus *Alternaria alternata*. *J. Nat. Prod.* 82, 3201–3204. doi: 10.1021/acs.jnatprod.9b00905

Zhao, S., Tian, K., Li, Y., Ji, W., Liu, F., Khan, B., et al. (2020). Enantiomeric dibenzo-α-pyrone derivatives from *Alternaria alternata* ZHJG5 and their potential as agrochemicals. *J. Agric. Food Chem.* 68, 15115–15122. doi: 10.1021/acs.jafc.0c04106

Zhao, S., Wang, B., Tian, K., Ji, W., Zhang, T., Ping, C., et al. (2021). Novel metabolites from the Cercis chinensis derived endophytic fungus *Alternaria alternata* ZHJG5 and their antibacterial activities. *Pest Manag. Sci.* 77, 2264–2271. doi: 10.1002/ps.6251

Zhong, T. H., Zeng, X. M., Feng, S. B., Zhang, H. T., Zhang, Y. H., Luo, Z. H., et al. (2022). Three new phomalone derivatives from a deep-sea-derived fungus *Alternaria* sp. MCCC 3A00467. *Nat. Prod. Res.* 36, 414–418. doi: 10.1080/14786419.2020.1771706

Zou, L. W., Jin, Q., Wang, D. D., Qian, Q. K., Hao, D. C., Ge, G. B., et al. (2018). Carboxylesterase inhibitors: an update. *Curr. Med. Chem.* 25, 1627–1649. doi: 10.2174/0929867325666171204155558

Frontiers in Microbiology

Explores the habitable world and the potential of microbial life

The largest and most cited microbiology journal which advances our understanding of the role microbes play in addressing global challenges such as healthcare, food security, and climate change.

Discover the latest Research Topics

See more →

Frontiers

Avenue du Tribunal-Fédéral 34
1005 Lausanne, Switzerland
frontiersin.org

Contact us

+41 (0)21 510 17 00
frontiersin.org/about/contact